E1.28:DOE/NASA/4396-4

DOE/NASA/4396-4
NASA CR-159836

AUTOMOTIVE STIRLING ENGINE DEVELOPMENT PROGRAM

Ernest W. Kitzner
Ford Motor Company

March 1980

NOTICE

AUTOMOTIVE STIRLING ENGINE DEVELOPMENT PROGRAM

Ernest W. Kitzner
Ford Motor Company
Dearborn, Michigan 48121

March 1980

TABLE OF CONTENTS

TABLE OF CONTENTS

TABLE OF CONTENTS

TABLE OF CONTENTS

TABLE OF CONTENTS

TABLE OF CONTENTS

TABLE OF CONTENTS

TABLE OF CONTENTS

TABLE OF CONTENTS

FINAL REPORT — STIRLING ENGINE PROGRAM

LIST OF FIGURES

FOREWORD

This report summarizes the results of the first year of effort under Department of Energy Contract No. EC-77-C-02-4396 which was performed by Ford Motor Company's Engineering and Research Staff under the technical direction of the National Aeronautic and Space Administration's Lewis Research Center. The performance of technical work under the contract started September 19, 1977.

For many years Ford Motor Company has been active in a variety of programs to investigate the potential of using engines other than conventional reciprocating piston engines in automotive applications.

In 1970 a meeting between Ford Motor Company and N. V. Philips Gloeilampenfabrieken of the Netherlands was held to discuss Philips' progress in their development of Stirling cycle engines. Philips originally started work on Stirling engines to develop a power source for electrical generator sets in 1938. Development of Stirling engines has continued since that time with a variety of applications ranging from torpedo propulsion to space power.

Until recent years, it had appeared that the Stirling engine was too heavy and complex for passenger car application, and that NOx emissions were excessive. Philips Laboratories had been working actively to solve these problems and, at the time of the 1970 meetings, sufficient evidence was provided to suggest that resolution was possible. A joint technical program was undertaken by Ford and Philips to investigate the applicability of a Stirling engine designed specifically to replace the 351 cubic inch displacement (cid) internal combustion (I.C.) engine in the Ford Torino intermediate size passenger car. Subsequent to the completion of the investigation, a decision was made to continue with a design, build and development program, which commenced in August, 1972.

In June 1975 a contract between Ford Motor Company and the U.S. Energy Research and Development Administration was initiated to conduct studies of an automotive Stirling engine. The contract included two tasks. Task I was to report information obtained from the Ford funded development program of a 170 horsepower Stirling engine powered intermediate size vehicle; and Task II of the contract was an initial design study of an 80 to 100 horsepower Stirling engine for a compact vehicle and funded by ERDA.

The baseline vehicle for the ERDA study was a 1976 Pinto 3-door equipped with a 2.3L I.C. engine with California emission control package and an automatic transmission. From this feasibility study, a number of conclusions were made, and are summarized as follows (the 4-98 engine is the designation given the engine designed to replace the 2.3L I.C. engine):

- The Stirling engine can be downsized from the present 4-215 size for smaller automobiles such as the Pinto, but the swashplate drive concept tends to result in a long engine compared to an internal combustion engine of equivalent power.

- The 4-98 Stirling engine can be packaged into a 1976 Pinto with changes to the sheet metal, and no major changes to the front suspension, steering, and drivetrain.

• Other drive concepts, although only explored on a preliminary basis, seem to offer packaging advantages over the swashplate design.

• The projected weight of the 4-98 engine installation is approximately 76 pounds heavier than the 2.3 liter I.C. engine installation. It is believed that this difference could be reduced through a weight reduction program.

• The low mileage emission objective of one half of the level included in the Clean Air Act (0.20 g/mile HC, 1.7 g/mile CO, .20 g/mile NOx) could be obtained.

• The projected performance, 0-60 MPH acceleration time, is equivalent to the I.C. engine vehicle performance.

• The projected metro-highway fuel economy with the 1976 state of art design restraints for the Stirling engine, was the same or approximately 3% better than the 1976 2.3 liter Pinto, depending upon the emission calibration. However, this equivalent fuel economy is at a much lower emission level than 1976 standards. (This report contains economy information that supercedes these projections.)

For further information regarding the 80-100 HP engine study, see DOE report COO-2631-22.

The present contract Statement of Work was divided into twelve tasks. Four of these tasks were directed toward the iterative development of the Stirling Engine System (SES) via a series of engine "generations." Work during the first year was devoted to completion of Task I — Fuel Economy Assessment.

This report represents an effort to present the reader with all of the relevant information resulting from the performance of work under Task I of the Statement of Work for Contract EC-77-C-02-4396. If additional information is required, copies of the quarterly reports submitted during the contract performance period (i.e., NASA CR 135331-CONS/4396-1, NASA CR 159435-CONS/4396-2 and NASA CR 159436-CONS/4396-3) are available upon request through the National Technical Information Service, Springfield, Virginia 22161.

At the conclusion of Task I, Ford Motor Company officially notified (in accordance with the contract provisions) the Federal government agencies and private firms that it intended to withdraw from active participation in the development of the Stirling engine as an automotive powerplant. This action was taken because Ford had concluded that there was a need to use existing personnel and facilities to comply with government standards, rather than continuing work in this area.

ACKNOWLEDGMENT

E. W. Kitzner, Manager
Alternate Engines Research Dept.
Ford Motor Company
Technical Manager, Stirling
Engine Program

R. C. Ronzi, Director
Engines & Emissions Research Office
Ford Motor Company
Program Manager, Stirling
Engine Program

EXECUTIVE SUMMARY

TASK I, FUEL ECONOMY ASSESSMENT

Automotive Stirling Engine Development Program
DOE Contract No. EC-77-02-C-4396

Introduction

This report summarizes the results of the first year of effort under Department of Energy Contract No. EC-77-C-02-4396 which was performed by Ford Motor Company's Engineering and Research Staff under the technical direction of the National Aeronautic and Space Administration's Lewis Research Center. The performance of technical work under the contract started September 19, 1977.

The total contractual effort was divided into twelve tasks. Four of these tasks were directed toward the iterative development of an automotive Stirling Engine System (SES) via a series of engine "generations" over a seven-year developmental program. The engine generations ranged from the First Generation SES, which consisted of the existing Ford-Philips 4-215 Stirling engine, to a manufacturable Fourth Generation SES which could meet the following program objectives:

. At least 30% improvement in EPA metro-highway fuel economy (miles per gallon) for the Stirling Powered Automobile (SPA) compared to the equivalent 1977 spark-ignition (S.I.) engine powered automobile calibrated to 49 states emission standards, utilizing identical fuels and at identical inertia weights and performance levels. (To be based on the EPA composite driving cycle as applicable to 1977 model automobiles.)

. Exhaust emissions of prototype automobiles low enough to meet or better the following limits after 50,000 miles of AMA durability. (To be based on the EPA composite driving cycle as applicable to 1977 model automobiles.)

HC	0.41 gm/mile
CO	3.4 gm/mile
NOx	0.4 gm/mile

. Exterior noise no greater than 70 dba when tested according to the SAE J986a test procedure.

. Warm-up time (key-on to drive-away) no greater than 15 sec. at 65°F ambient temperature.

. Driveability to average at least 6.0 when tested according to the Ford specified jury rating system.

. Durability, maintenance requirements and safety equal to or better than the projected equivalent S.I. engine powered vehicle system.

. Reasonable initial and life cycle cost of ownership competitive with the projected equivalent S.I. engine powered automobile.

Work during the first year was devoted to completion of Task I — Fuel Economy Assessment. The primary objective of Task I was to predict the fuel economy potential of the Fourth Generation SES with a high degree of confidence. The program to accomplish this objective included:

. use of available First Generation SES hardware for engine mapping to optimize air flow, fuel flow, and exhaust gas recirculation,

. upgrading the durability of existing engines to provide the required engine test capability,

. component testing and development to substantiate improvements which result in fuel economy gains, and

. detailed analyses of the Stirling cycle and other engine-related parameters.

This report is divided into two Sections. Section I consists of this Executive Summary of the Task I accomplishments, and a description of the existing Stirling engine. Section II describes the work performed in each of the 13 engineering sub-tasks into which the Task I Statement of Work was divided. These detailed sub-task reports in Section II are arranged as follows.

1. Sub-tasks which were directly related to fuel economy are reported as follows.

No.	Subject Matter
2.1	Mapping and Optimization
2.2	Burner System
2.3	Preheater Development
2.4	Engine Drive Study
2.5	External Heat and Blower System
2.6	Power Control
2.7	Air/Fuel Control
2.8	Cycle Analysis
2.9	Other Fuel Economy Improvements
2.10	Cooling System Analysis
2.11	Fuel Economy Analysis

2. Other sub-tasks which were an integral part of the Task I effort:

No.	Subject Matter
3.1	Engine Durability Upgrading
3.2	Reference Engine

Results

The baseline First Generation engine used for the efforts of Task I was the Ford-Philips 4-215 engine shown in Figure 1.1-1. The 4-215 is a double-acting four cylinder swashplate drive engine having a displacement of 215 cc/cylinder and a maximum horsepower rating of 170 HP at 4000 RPM (for additional detail, see Section 4.2).

At the beginning of Task I on September 19, 1977 the metro-highway (M-H) fuel economy of the existing First Generation SES was calculated to be between 12.9 and 14.0 MPG in a 4500 lb. inertia weight test vehicle. These calculations were based on data from dynamometer and in-vehicle tests conducted by Ford Motor Company during 1976 and 1977. The 12.9 and 14.0 MPG fuel economy data were selected as the minimum and maximum figures to which improvements identified in the course of Task I would be added.

The baseline vehicle selected for comparison purposes was a 1977 Ford LTD II equipped with a 351 CID engine and C4 automatic transmission. At an inertia test weight of 4500 lb., the baseline fuel economy was 15.5 MPG (M-H).

As a result of the Task I studies, potential improvements in the fuel economy of an automotive Stirling engine were identified; these are discussed in detail in Section II of the report. A summary of the improvements from the various sub-tasks is given in Table 1.1-1. From this activity major potential improvements were identified resulting in the following recommended design actions:

. Air preheater; change to an engine driven preheater and use a ceramic core with a thin-wall matrix.

. Engine drive system; redesign piston crossheads to reduce friction, change to engine driven fuel and atomizing air pumps, and reduce piston friction.

. Power control system; change from a variable pressure control system to a hybrid system in which both pressure and dead volume are varied; replace internal hydrogen compressor pistons with an external hydrogen compressor.

. Cycle analysis; reoptimize engine for maximum efficiency at part load (the present First Generation SES was optimized for maximum efficiency at full load).

. Other; a number of other potential improvements were identified, such as the use of thin walls to minimize heat transfer from the hot to the cold sections of the engine, higher heater head temperatures, etc.

The potential fuel economy improvement associated with each of the identified design changes was calculated and, in some cases, verified in whole or in part by component

and engine testing. In most cases, the calculations and tests resulted in a range of improvements that were considered possible; the minimum and maximum of this range was then added to the calculated fuel economy of the First Generation SES to obtain the projected fuel economy potential of the Fourth Generation SES.

Table 1.1-1

IMPROVEMENTS SUMMARY

	Metro-Highway MPG	
	Minimum	Maximum
Estimated First Generation SES	12.9	14.0
Projected Improvements:		
. Air preheater system	0.4	0.6
. Engine drive system	1.2	1.9
. Power control system	2.3	3.1
. Cycle analysis (reoptimization)	3.0	3.4
. All other	1.6	5.1
Sub-total	8.5	14.1
Projected Fourth Generation SES	21.4	28.1

A confidence weighting factor was assigned to each of the identified potential improvements, and the projected fuel economy of the Fourth Generation SES was then compared with the baseline 1977 production vehicle:

	Fourth Generation SES Fuel Economy (MPG)	Improvement Over Baseline		Confidence Level
		MPG	%	%
Minimum	21.4	5.9	38%	73%
Maximum	28.1	12.6	81%	52%

All of the fuel economy projections assume the use of gasoline as a fuel. If diesel fuel were used, the MPG projections would increase by 11%.

The first hardware problem which had to be resolved was that of engine durability. Prior to September 19, 1977 the largest total of running hours accumulated on any one (4-215) engine build was 58. The major contributor to engine failures up to this time was the sealing system which was employed to contain the working gas (H_2) in the gas side of the engine. Two alternative types of sealing systems were employed: (1) the rollsock system and (2) the sliding seal system (refer to section 3.1, Engine Durability Upgrading, for a complete description of these systems). A dual approach was implemented to resolve this problem. First, a rollsock protection device was designed, built, and installed on the 4-215 engine to increase the durability of the existing rollsock system (refer to section 2.1, Mapping and optimization). The protection device was successful in that engine 3X17 (which was equipped with the device) accumulated 220 hours of variable speed running. With increased durability, mapping could be con-

tinued without interruption, increasing the credibility of the projections. Secondly, a program was initiated to investigate an existing sliding seal system and to redesign the system and select materials for future seals which could withstand the severe conditions of that application (refer to section 3.1, Engine Durability Upgrading). This program resulted in recommendations for consideration for any future sliding seal programs.

At the conclusion of Task I, a series of Transfer of Knowledge Meetings were conducted by Ford for the benefit of the participants in the second Automotive Stirling Engine Development Program being funded by the Department of Energy (Mechanical Technologies, Inc., United Stirling of Sweden, and American Motors General). In addition to MTI, USS, and AMG personnel, the meetings were attended by representatives of the National Aeronautic and Space Administration and N. V. Philips. A total of twelve half-day sessions were held over the three-day period of November 7 through November 9, 1978. During these meetings, the results of Ford's Task I studies were reviewed in detail. Ford's experiences with the Stirling engine prior to the start of Task I were also reviewed, to the extent that such experiences were considered relevant to the on-going DOE/NASA Stirling engine programs.

Conclusion

Results of the two major tasks in this one year effort identified opportunities for improvement of the Stirling engine M-H fuel economy of 38 to 81% over a given spark ignition baseline. Durability of the engine has increased from approximately 50 hours of running before a major failure to over 200 hours and still running at the end of the program primarily as the result of a fail safe test rig operating change.

Recommendations

The present 4-215 Stirling engine hardware would require extensive redesign to incorporate most of the fuel economy improvements identified in this study. Thus, little could be done to substantiate the fuel economy gains using the present hardware. Therefore, it is recommended that the information contained in this report be made available to organizations that are engaged in Stirling engine work, so that the report can be used as a textbook for methods to improve fuel economy in their own particular engine design.

AIR INLET

REGENERATOR

COOLER TUBES

OUTPUT SHAFT

IGNITOR

CROSSHEAD AND SLIDERS

ATOMIZER

ROLL SOCK

EXHAUST

PISTON ROD

DOUBLE ACTING PISTON

BURNER

HEATER TUBES

ROTARY PREHEATER
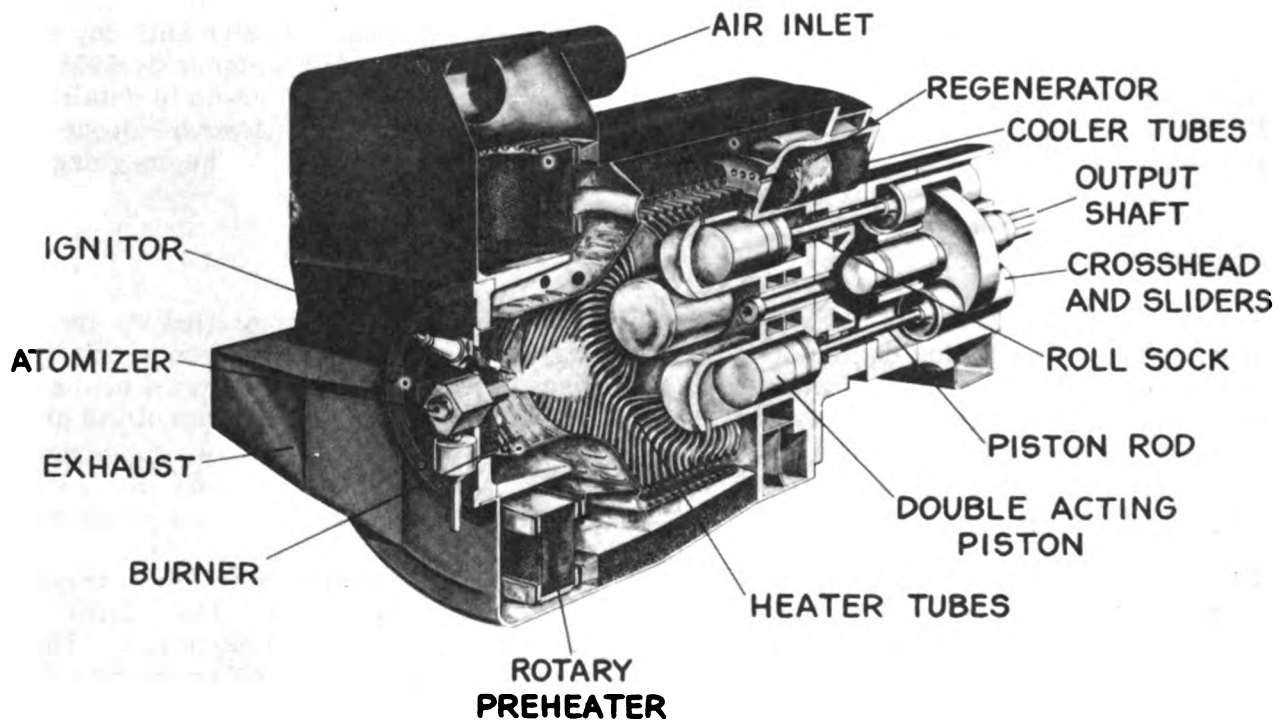
CUTAWAY VIEW OF STIRLING ENGINE

Figure 1.1-1

2.1 Mapping and Optimization

2.1.1 Summary — The objective of this section was to use engine mapping techniques to optimize engine operating parameters such as exhaust gas recirculation, air fuel ratio and heater head gas temperature. Also to determine fuel economy and emissions resulting from redesigned components from other sub-tasks.

Mapping is a procedure by which engine parameters are varied at different speed-load points to determine optimum engine calibration and emissions. The parameters varied were air/fuel ratio, EGR (exhaust gas recirculation) levels, and the working gas temperature in the heater head. The engine speed and load points were selected by an engine mapping methodology prepared by R. E. Baker and E. E. Daby of Ford Motor Company (Fig. 2.1-1). Engine mapping was performed at ten speed-load points which, when combined with the proper time weighting factor at each point gives an accurate representation of vehicle fuel economy and emissions for metro and highway driving cycles. With three variables and four tests for each variable at ten simulation points, i.e., heater head gas temperature, EGR level, and air/fuel ratio, a total of over 600 mapping test runs must be made for complete mapping. Because of questionable 4-215 engine durability, priorities were established for the sequence of simulation point mapping. (Refer to section 5.2 for a description of the 4-215 engine.)

From Figure 2.1-2 it is noted that four vehicle simulation points (1, 4, 5, and 6) accounted for approximately 60 percent of the total fuel usage on the city cycle, and therefore were given first priority. The next priority was given points 7 and 9 which were large contributors to the highway cycle. Points 2, 8 and 10 were low priority because the fuel flow is very close to that of points number 1, 6, and 7 and therefore the same trend would continue. At each of these vehicle simulation points, the burner computer program was used to calculate trends of air/fuel ratio and EGR; however, emissions, soot, and the ability of the engine to hold hydrogen temperature were not considered in theoretical projections. Therefore, tests were run to determine what levels could be tolerated before these parameters exceeded the objectives.

2.1.2 Work Performed — Prior to the initiation of the mapping, baseline and repeatability tests were performed to assure the accuracy of the data. During the contract the following engines were run:

Engine	Purpose of test	Reason test stopped
1 x 16	Mapping	Hydrogen leak
1 x 17	Mapping	Drive failure
3 x 16	Mapping	Hydrogen leak
3 x 17	Mapping	Data completed
3 x 17A	Regenerator evaluation	Data completed
1 x 18	Component test	Rollstock seal failure
1 x 19	Component test	Test cell problem
1 x 20	Hydrogen compressor evaluation	Data completed
1 x 20	Redesigned Preheater	Data completed

1

Engine numbers were designated as follows:

$$\frac{1X}{\text{Engine Number}} \qquad \frac{16}{\substack{\text{Number of Builds on} \\ \text{Engine IX}}}$$

Engines 1 x 16, 1 x 17, 1 x 18, 1 x 19 & 3 x 16 failed prior to completion of baseline data.

2.1.3 Summary of Tests — All mapping data was obtained using an absorption dynamometer. It was the first installation of the 4-215 Stirling engine in a dynamometer cell in the U.S.A. (See Figure 2.1-3 & Figure 4.2-2).

2.1.3.1 Engine 1X16 — Dynamometer testing of engine 1X16 with sliding seals (see section 3.1 for description) began on August 30, 1977. The engine accumulated 40.2 hours of testing before it was removed from the dynamometer on October 3, 1977 because of a severe working gas leak in the high pressure crankcase caused by a poor braze joint.

Because of a tolerance stacking error which restricted air flow, the preheater insulation bush was revised to provide more air to the burner swirler. After this revision, simulation points 1 through 8 and 10 were run on the engine. However, before point 9 could be run the hydrogen leak developed, and the engine was removed from the dynamometer.

No conclusions can be drawn from these test runs because the sliding seals allowed oil into the hydrogen gas side of the engine. This caused contamination of the regenerator-coolers, reducing their efficiency, thereby possibly affecting the fuel economy of the engine.

2.1.3.2 Engine 1X17 — Dynamometer testing of engine 1X17 began on October 27, 1977. This engine was equipped with a rollsock seal system and a 3-valve rollsock protection back-up system (see Figure 2.1-4). The engine accumulated 23.3 hours of operation before a failure in the slider retaining ring groove occurred on the number 3 crosshead (see Figure 2.1-5). The engine was stopped in time to prevent further major damage. However, there was galling of the outer rear edge of the swashplate, and the rear sliders were damaged because of the swashplate galling.

The functions of the 3-valve rollsock protection system were to add nitrogen at low rollsock Δ P (60 psi), to dump oil at excessively low Δ P (20 psi), and to dump hydrogen at excessively high Δ P (100 psi).

Due to sporadic electrical surges from an unknown origin to the Δ P transducer, nitrogen was added to the engine every time the engine was run. This problem was solved by lowering the low rollsock Δ P trip point from 60 psi to 36 psi.

The engine had very poor combustion and soot plugged the preheater. The preheater was removed and cleaned and the fuel nozzle flow checked. The nozzle displayed an uneven flow pattern with many large streaks of unatomized fuel. A new Excello designed fuel nozzle (see section 2.2) was flow

tested and revealed a uniform flow pattern. The cone angle was slightly less than the Philips nozzle and the spray angle decreased with decreasing fuel flow.

Four tests were conducted with the Excello fuel nozzle and the normal 15 in. Hg air assist pressure. Combustion flame-out occurred regularly as indicated by very loud combustion "rumble" at re-ignition. Four tests were then conducted at 7.5 in. Hg air assist pressure which reduced the flame-out problem.

No conclusions can be drawn from these few test runs. The various problems with the combustor indicate that additional testing is required to develop the combustor for a more stable and uniform combustion pattern.

2.1.3.3 Engine 3X16 — Dynamometer testing of engine 3X16 began on November 28, 1977. This engine was also equipped with a rollsock seal system and the rollsock protection back-up system. The engine had accumulated 24.2 hours of testing when a large hydrogen leak developed allowing hydrogen into the cooling water system. Water was found throughout the heater head and high pressure crankcase. Therefore, the engine was removed from the dynamometer cell.

Prior to the hydrogen leak, testing had revealed a problem in the power control system as indicated by an inability of the engine to change speeds. The problem was found to be a failure of the "O" ring seals for the control valve pivot shafts. The problem was corrected by tapering the shaft ends for more reliable assembly.

Excessive heater head temperature differences were recorded during two runs. The temperature instrumentation was recalibrated and found to be approximately 40°C high (actual temperature was lower than indicated).

On two occasions, water (exhaust condensation) contaminated the emission measuring equipment. After the second occurrence, testing was suspended while the CO detector was replaced and recalibrated.

Projections of emissions and fuel economy from the test results are:

HC	=	0.0008 g/mile	CVS-H	=	13.4 MPG
CO	=	5.31 g/mile	HWY	=	17.56 MPG
NO_x	=	0.376 g/mile			

Definition of Symbols:

HC	Hydrocarbons
CO	Carbon Monoxide
NOx	Nitrogen Oxides
CVS-H	Constant Volume Sampling — Hot start
HWY	Highway cycle

3

Constant Volume Sampling — Cold start (CVS-C) which completes the city cycle cannot be obtained directly from the engine dynamometer tests. CO levels were much higher than those recorded in previous runs. Discounting possible measurement error due to CO detector contamination, the higher CO levels indicated poor mixing and distribution within the combustor chamber.

2.1.3.4 Engine 3X17 — Engine 3X17 was the first engine to accumulate significant running time (220 hours). It was assembled with oversize "O" rings on the regenerator-coolers, and was also equipped with rollsock seals and a rollsock protection system.

Dynamometer testing of engine 3X17 began on January 18, 1978. By February 2, 1978 the engine had accumulated 28.7 hours of running time while establishing baseline and repeatability data. The base data was established at ten Stirling engine vehicle simulation points. Repeatability was confirmed by re-running the ten simulation points.

Emission and fuel economy measurements at the simulation points are presented in Figures 2.1-6 and 2.1-7. The summations for the driving cycle are:

	Test 1 (base)	Test 2
HC (gm/mi)	0.020	0.008
CO (gm/mi)	3.22	2.70
NOx (gm/mi)	0.447	0.382
CVS-H (MPG)	12.95	12.81
HWY (MPG)	17.28	17.34

These results show, overall, good correlation between test 1 and 2. The CVS-H fuel economy differed by 0.14 MPG or 1.08%. When each simulation point was examined, the maximum fuel flow difference was 8.4% at point number 9. The average of all of the simulation points' fuel flow differences was 3.2% between test 1 and 2.

The hydrocarbons differed by 0.012 gm/mile. Considering percentage, this difference was very large (60%) but was considered insignificant because of the very low values. The objective for HC was .41 gm/mile.

The carbon monoxide variance of .52 gm/mile (16.1%) was considered somewhat significant. However, the difference was partly accounted for in the slightly higher air/fuel ratios in test 2 (averages of 21.07 vs. 20.72).

Nitrogen oxides differed by .065 gm/mile from test 1 to test 2. Again, this difference was due to the higher air/fuel ratios and the overall higher levels of NOx in test 2.

A graph showing comparisons of fuel flows and mean cycle pressures for tests 1 and 2 is given in Figure 2.1-8.

A graph showing comparison of fuel flows and mean cycle pressures for test 1 and theoretical results is shown in Figure 2.1-9. The theoretical results were

4

calculated with an alternator load of 50 amps. A major difference between the theoretical engine and the dynamometer engine were:

An auxiliary oil pump for the rollsock seals was included on the dynamometer engine. The power required to drive this pump was not included in the theoretical calculations.

The theoretical engine calculations included a negative (6.8 Nm) net torque for simulation point number 3. The engine dynamometer was an absorption type, and could not operate at negative torque. Therefore, simulation point 3 was run at zero torque.

The theoretical engine had a constant inside heater tube temperature of 750°C or approx. gas temperature of 700°C. The mean hot gas temperature of the dynamometer engine was about 720°C.

These facts accounted for some of the differences between the theoretical projections and test results.

2.1.3.4.1 Mapping of Engine 3X17 — Mapping of engine 3X17 was initiated after baseline data and repeatability were established.

Due to the durability problems experienced with previous engine builds, it was decided engine 3X17 would be tested at vehicle simulation points 1, 4, 5, and 6 first. Summaries of the test data for the four simulation points are given in Figure 2.1-10 through 2.1-19.

Tests at the first four vehicle simulation points indicated that a fuel economy improvement of no more than 1% can be expected for an optimum EGR and air/fuel setting, when compared with the baseline settings. If this trend held true for all ten (10) vehicle simulation points, the fuel economy improvement over the CVS cycle will be about 0.13 MPG.

The improvement in fuel economy due to temperature scheduling was less than 2.5% when fuel economy at optimum heater head gas temperature was compared with the baseline setting of about 720°C. Using this analysis for the remaining vehicle simulation points, fuel economy improvement over the CVS cycle was expected to be no more than 0.32 MPG. The effects of transient conditions on heater head gas temperatures over CVS cycle, which were expected to be detrimental, were not included in this analysis.

Fuel consumption at various hydrogen temperatures from 680°C to 800°C was measured with the exhaust emissions held at an approximately constant level. The results are shown graphically in Figure 2.1-20. Total variation in fuel flows in this temperature range was approximately 5% for each simulation point. The minimum fuel flow for each point, however, occurred at different temperatures. These are tabulated below:

Simulation Point No.	Min. Fuel Flow Temp. (C°)
1 (600 RPM, 5.4 kg-m)	680

Simulation Point No.	Min. Fuel Flow Temp. (C°)
4 (1000 RPM, 619 kg-m)	730
5 (1100 RPM, 11.1 kg-m)	764
6 (1300 RPM, 15.9 kg-m)	780

Because of a drop in hydrogen temperature during rapid acceleration, 700°C was established as a minimum controlled temperature at idle.

Fuel consumption and exhaust emissions (HC-CO-NOx) were measured for various air/fuel ratios and EGR levels at a constant hydrogen temperature for the four simulation points. The results are shown graphically in Figures 2.1-21 through 2.1-42.

All test points (with the exception of point number 4) were run more than once to verify or check the results of the original run.

Fuel flow, except at simulation point number 1, varied directly with EGR and air/fuel ratio. The fuel flow within the range of air/fuel ratios and EGR levels tested varied about 3% at point number 1 to 8% at point number 6. When emission constraints (maximum CO and NOx values) are considered, the total fuel flow variation is 1% to 5% for points 1 and 6.

Carbon monoxide varied indirectly with air/fuel ratio and EGR had very little effect on CO emissions. A graph showing the relationship between CO emissions and air/fuel ratio at a nominal EGR setting (about 90%) for the four VS points is shown in Figure 2.1-43.

A graph showing air/fuel ratio versus fuel flow for 500, 600, and 700 PPM CO is shown in Figure 2.1-44. A constant level of 500, 600, and 700 PPM CO yielded about 2.3, 2.8 and 3.3 grams per mile CO emission respectively not including cold start.

Burner emission levels were measured at four points around the heater head as shown in the following figure.

Emission data from the four probes was used in determining preheater leakage and to give an indication of air/fuel distribution within the burner. Figures 2.1-45 through 2.1-52 are graphs of distribution of excess air and CO which existed around the burner at the four VS points. The air inlet was located near region 1, and the exhaust near region 4. Regions 1 and 4 were regions of low excess air and high CO concentration. The lowest CO concentration and highest excess air was in region 3. Region 3 was directly opposite the inlet (region 1). These results indicated a critically skewed air velocity and/or fuel distribution within the burner, with maximum velocity and/or minimum fuel in region 3 and minimum velocity and/or maximum fuel in region 4.

Oxides of nitrogen varied primarily with EGR, but also with air/fuel ratio. Higher EGR yielded lower NOx and lower A/F ratio yielded lower NOx.
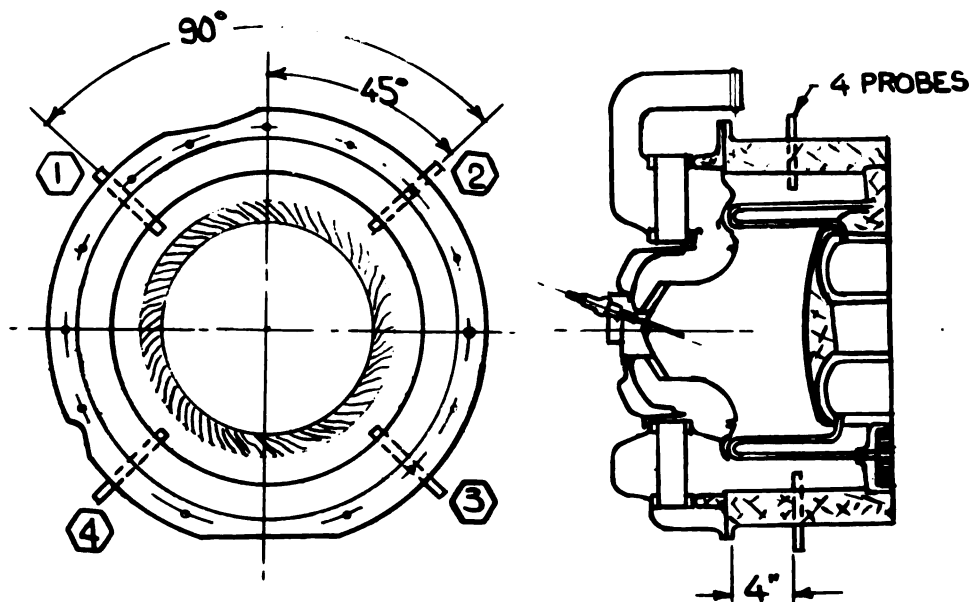
Changes in EGR at values less than 110% had a great effect on NOx, i.e., a change in EGR of 10 percentage units caused a change in NOx of about 2-5 PPM.

Small changes in air/fuel ratio did not have significant effect on NOx concentration, however, a decrease of 30% excess air (A/F ratio) caused about a 10-20 PPM decrease in NOx.

Hydrogen (heater) temperature also effected NOx concentration in the exhaust. As indicated from the temperature schedule data (Figures 2.1-12, -14, -16, and -19) a 10°C change in hydrogen temperature required a 2 to 5 percentage unit change in EGR to maintain a constant NOx level.

Hydrocarbon concentration was extremely small (1-10 PPM) at all conditions and was therefore ignored in mapping and optimization evaluation.

Vehicle simulation points 7 and 9 were also run on engine 3X17. A total of 96 hours were accumulated on the engine during the mapping of these two points.

Fuel consumption of points 7 and 9 at various temperatures from 700°C to 780°C was measured with the exhaust emissions held at approximately constant levels. These results, along with the results of the first four simulation points (1, 4, 5, and 6) are shown in Figure 2.1-53. Total variation in fuel flows in the temperature range tested was about 5% for each simulation point. The temperature at which minimum fuel flow occurred for each point is as

7

follows:

Simulation Point No.	Min. Fuel Flow Temp. (°C)
1 (600 RPM, 5.9 kg-m)	680
4 (1000 RPM, 6.9 kg-m)	730
5 (1100 RPM, 11.1 kg-m)	764
6 (1300 RPM, 15.9 kg-m)	780
7 (1600 RPM, 20.7 kg-m)	780
9 (1800 RPM, 22.1 kg-m)	780

Fuel flows at various air/fuel ratios and EGR settings, for vehicle simulation points 7 and 9, are shown in Figures 2.1-54 and 2.1-55. These fuel flows were not measured with sufficient accuracy to make conclusions as to absolute effect of EGR and air/fuel ratio on fuel flow. These figures do indicate, however that a lower EGR setting resulted in lower fuel flows.

Data from vehicle simulation points 7 and 9 indicated that fuel economy improvement for optimum EGR and air/fuel setting and for improvement for temperature scheduling was the same as reported earlier i.e., .13 and .32 MPG respectively.

Carbon monoxide varied indirectly with air/fuel ratio. EGR had little effect on CO emissions at equivalence ratios (λ) greater than 1.35. These results are shown graphically in Figures 2.1-56 and 2.1-57. A graph showing the relationship between CO emissions and air/fuel ratios at a nominal EGR setting of about 90% for vehicle simulation points 7, 9 and the four points tested earlier is shown in Figure 2.1-58.

Oxides of nitrogen varied primarily with EGR. Lower air/fuel ratios yielded lower NOx concentration. NOx concentration varied greatly at EGR levels less than 55% and little at levels about 55% for all air/fuel ratios tested. These results are shown graphically in Figures 2.1-59 and 2.1-60.

Mapping of engine 3X17 was discontinued after 220 engine running hours to allow the test cell to be used for component evaluation. Operation of the test cell which was originally selected for component evaluation was delayed due to cell problems.

2.1.3.4.2 Conclusions — Changes in air/fuel ratio and EGR of the external combustion Stirling engine had a minimal effect on fuel consumption. The effect on fuel consumption was due primarily to changes in the combustion blower power. The major consideration for air/fuel and EGR variations should have been for control of CO and NOx. NOx tended to have the same concentration from vehicle simulation point to vehicle simulation point for a specific EGR value. However, CO levels changed drastically from vehicle simulation point to vehicle simulation point for a given air/fuel ratio.

8

It was observed that when the fuel was shut off, HC emissions increased to a value in excess of the 6000 PPM. Also, during deceleration, CO emissions exceeded the full scale reading of 6900 PPM and smoke increased to a visible level. Because of these detrimental emission effects, and the tendency of CO to increase when fuel flow decreased, the following changes were suggested for the air/fuel control system:

- The air/fuel ratio control should be changed from a constant setting to one that varies with fuel flow to more closely simulate optimal engine operating conditions.

- Idle air holes should be added to the throttle plate to prevent the shut-off of air at the minimum fuel flow of .4 g/s. This will prevent extremely rich mixtures on decels and idle.

- The minimum fuel flow should be lowered from .4 g/s to .2 g/s or the smallest value at which the fuel will atomize. This would prevent rich mixtures on decels.

- The fuel shut-off temperature should be raised from 800°C to 840°C. Over temps occur on decel shutting off fuel and cause a lean mixture on relight.

It was observed that CO readings occasionally doubled for a particular EGR and air/fuel setting from one run to a recheck of that same vehicle simulation point. It was found that the high CO values were due to combustion pressure fluctuation causing a fluctuation in fuel flow through the nozzle. The problem was corrected by installing a checkvalve in the fuel line.

It was projected that mapping would yield a 0.15 to 0.45 MPG fuel economy improvement opportunity on the chassis rolls. The wide range is due to the inability to predict the transient effects of the varied EGR, air/fuel ratio, and heater head gas temperature as all parameters were measured on steady state conditions on the dynamometer.

2.1.4 Component Evaluation — Work on the component test cell was initiated on schedule. This test cell was to be similar to the cell being used for engine mapping with the following exceptions:

- A Programmable Analog Computer (PAC 500) was installed to enable engine functions to be easily changed.

- The dynamometer in this cell was a double-ended, water-cooled, motoring type rated at 725 HP when used as a generator for speeds of 1500 to 3000 RPM. As a motor, it was rated at 600 HP. The dynamometer could be controlled by either speed or torque.

Cell preparation fell behind schedule because the emissions measurement equipment was one month late in arriving and required extensive rebuilding before it could function properly. Because of this delay, no testing in this cell was accomplished during Task I, although component evaluation was performed in the mapping test cell. Component evaluation was initiated as follows:

9

2.1.4.1 Component Testing — All components tested on the engine are reported in their own respective section. The tests were as follows:

	Test	Engine	Section
1.	Hydrogen compressor losses	1X20	2.8
2.	New design preheater cover	1X20	2.3
3.	Thin wall preheater core	1X20	2.3
4.	Regenerator coolers	3X17A	2.1

Regenerator Coolers — During the assembly of engine 1X16 in August of 1977 the protective gauze separated from the regenerator, revealing the fine gauze and substantial rust colored deposits, later analyzed as iron oxide. The cleaning process was believed to be the cause, making all regenerators suspect to the same contamination. New regenerators were then tested for cycle efficiency comparison with the contaminated ones. Following is a summary of a test comparing the contaminated regenerators in engine build 3X17 with new regenerators run in engine 3X17A.

. Dynamometer engine tests of fuel economy revealed little difference between new and contaminated regenerators. These tests, run at the same emissions levels, resulted in a marginal improvement in the CVS-H fuel economy for the new regenerators.

. The highway fuel economy decreased with new regenerators, 0.55 MPG (3%). Fuel flow on the average was 0.15 g/sec (1%) greater for metro-highway points #7-10. The lower highway fuel economy reflects the weighting of the HWY cycle toward these points. The following table shows the fuel flow difference between contaminated and new regenerators.

PT No.	CONTAMINATED FUEL FL. g/s	NEW FUEL FL. g/s
1	0.60	0.64
2	0.70	0.61
3	0.52	0.43
4	1.03	0.97
5	1.40	1.33
6	2.00	1.97
7	2.84	3.16
8	2.10	2.17

PT No.	CONTAMINATED FUEL FL. g/s	NEW FUEL FL. g/s
9	3.57	3.67
10	2.57	2.67

CVS-H=12.95mpg   CVS-H=13.11mpg

HWY=17.28mpg   HWY=16.73mpg

Flow tests which were conducted on the regenerators showed a higher pressure drop across the new regenerator which explains the decreased efficiency at the higher speed points. The cause of this increased pressure drop was not determined due to lack of time and parts. The pressure drop on 8 new and 8 contaminated regenerators with an air flow of 16.8 g/sec was as follows:

No	New $P(cmH_2O)$	No	Contaminated $P(cmH_2O)$
1	734.2	11	730.8
2	788.6	12	786.8
3	747.8	21	761.9
4	761.4	22	697.5
5	761.4	31	761.9
6	761.4	32	707.4
7	761.4	41	692.2
8	761.6	42	725.8

Prior to removing engine 1X20 from the test cell a test was run on the air fuel control system to determine the air fuel ratio change from .4 g per second fuel flow to maximum fuel flow of approximately 12 g per second. During this test the engine was run at 4200 RPM and 160 Kg/cm^2 mean cycle pressure for 3 to 5 minutes and produced approximately 177 HP. A tear down of the preheater after this test revealed that the burner was badly distorted and several holes burned through, however no other damage was evident on the engine.

SPEED LOAD POINT	ENGINE SPEED RPM	ENGINE TORQUE Kg-m
1	600	5.32
2	.800	4.07
3	900	-6.8
4	1000	6.78
5	1100	10.85
6	1300	15.59
7	1600	20.34
8	1700	10.85
9	1800	21.69
10	2000	12.20

Figure 2.1-1   CVS Vehicle Simulation Points

Metro-Highway Fuel Economy Summary For 4-215 Engine Prepared On 12 SEP 1978 BY T. DUNLAP
BASED ON ENGINE MAP DATA FILE TDEMBLVT AND M-H DATA FILE MH2.5-10 (4500 LB. IWC VEH.)
THESE RESULTS ARE BASED ON A DYNAMOMETER ENGINE WITH STEERING AND FAN LOSSES EQUAL TO ZERO

M-H PT	SPEED RPM	TORQUE NM	POWER KW	PRESS ATM	FUEL G/S	CITY SEC	CITY GRAM	% TOT CITY	HIWAY SEC	HIWAY GRAM	% TOT HIWAY	BSFC # /HP HR
1	600.000	53.200	3.343	33.015	0.552	362.338	199.881	14.406	10.253	5.656	0.401	0.977
2	800.000	40.700	3.410	27.997	0.598	272.141	162.663	11.723	5.235	3.129	0.222	1.037
3	900.000	-6.000	-0.641	12.092	0.410	74.000	30.325	2.186	52.000	21.310	1.511	0.
4	1000.000	67.800	7.100	37.120	0.842	167.184	140.773	10.146	29.131	24.529	1.740	0.702
5	1100.000	108.500	12.498	51.490	1.160	185.672	215.290	15.516	32.763	37.989	2.694	0.549
6	1300.000	155.900	21.224	69.614	1.706	147.190	251.097	18.097	45.847	78.212	5.547	0.476
7	1600.000	203.400	34.080	90.239	2.583	58.349	150.701	10.861	72.734	187.854	13.322	0.449
8	1700.000	108.500	19.316	54.332	1.733	57.496	99.615	7.179	331.356	574.091	40.713	0.531
9	1800.000	216.900	40.885	97.123	3.087	36.123	111.530	8.038	76.840	237.243	16.825	0.447
10	2000.000	122.000	25.552	61.528	2.226	11.509	25.622	1.847	107.842	240.082	17.026	0.516

TOTAL CVS-H FUEL CONSUMPTION   = 1387.4964 GRAMS
CVS-H FUEL ECONOMY   = 15.1499 MPG
COLD START FUEL PENALTY   = 148.9000 GRAMS
TOTAL CVS-CH FUEL CONSUMPTION = 1536.3964 GRAMS
CVS-CH FUEL ECONOMY   = 13.6816 MPG
TOTAL EPA HWY FUEL CONSUMPTION = 1410.0952 GRAMS
EPA HWY FUEL ECONOMY   = 20.3573 MPG

TOTAL M-H FUEL ECONOMY   =   16.0501 MPG

Figure 2.1-2   Vehicle Simulation Points
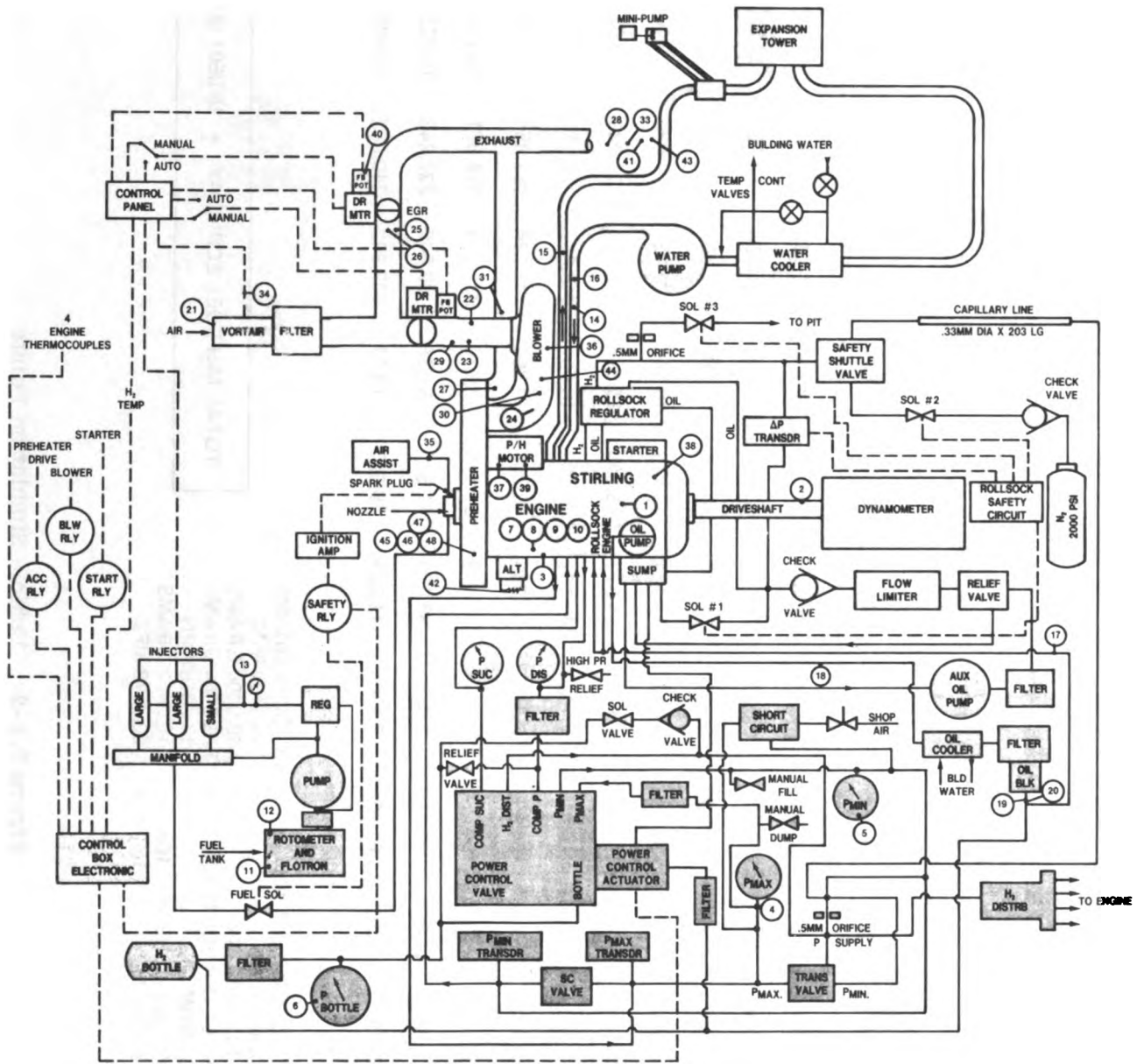
Figure 2.1-3   Test Cell Schematic Stirling Engine

PARAMETER	INSTRUMENT	RANGE	ACCURACY
1. ENGINE SPEED	MAGNETIC PROBE	0-10,000 RPM	±1 RPM
2. ENGINE TORQUE	STRAIN GAGE	0-25 KG-M	±0.15%
3. MEAN ENGINE PRESSURE	GAGE	0-210 ATM	±½% OF FULL SCALE
4. MAX ENGINE PRESSURE	GAGE	0-350 ATM	"
5. MIN ENGINE PRESSURE	GAGE	0-140 ATM	"
6. BOTTLE PRESSURE	GAGE	0-350 ATM	"
7. ENGINE GAS TEMPERATURE T_1 IN	THERMOCOUPLE	0-1200°C	±4°C
8. ENGINE GAS TEMPERATURE T_1 OUT	"	"	"
9. ENGINE GAS TEMPERATURE T_2 IN	"	"	"
10. ENGINE GAS TEMPERATURE T_2 OUT	"	"	"
11. FUEL FLOW-FLOWTRON	ELEC. MASS FLOWMETER	0-119 LBS/HR	±½% OF READING + .01% OF F.S.
12. FUEL FLOW-ROTOMETER	FLOAT	0.4-48g/s	±1% OF READING
13. FUEL PRESSURE	GAGE	0-7 KG/CM²	±½% OF FULL SCALE
14. COOLING WATER IN	RTD	−20 TO 78°C	±0.1°C
15. COOLING WATER OUT	RTD	−20 TO 78°C	±0.1°C
16. COOLING WATER FLOW RATE	TURBINE METER	2-225 GPM	±½% OF FULL SCALE
17. OIL TEMPERATURE IN	THERMOCOUPLE	0-600°F	±1½% OF READING
18. OIL TEMPERATURE OUT	"	"	"
19. OIL FLOW RATE	TURBINE METER	½-25 GPM	±½% OF FULL SCALE
20. OIL PRESSURE	GAGE	0-11 KG/CM²	±½% OF FULL SCALE
21. AIR INLET TEMPERATURE	THERMOCOUPLE	0-600°C	±1½% OF READING
22. BLOWER TEMPERATURE IN-TOP	"	"	"
23. BLOWER TEMPERATURE IN-BOTTOM	"	"	"
24. BLOWER TEMPERATURE OUT	"	"	"
25. E.G.R. TEMPERATURE TOP	"	"	"
26. E.G.R. TEMPERATURE BOTTOM	"	"	"
27. EXHAUST PREHEATER TEMPERATURE	"	"	"
28. EXHAUST PIPE TEMPERATURE	"	"	"
29. BLOWER PRESSURE IN	WATER MANOMETER	0-100 IN.	±½% OF READING
30. BLOWER PRESSURE OUT	"	"	"
31. PREHEATER PRESSURE OUT	"	"	"
32. E.G.R. PRESSURE	"	"	"
33. EXHAUST PIPE PRESSURE	"	"	"
34. VORTAIR	FREQUENCY COUNTER	0-80,000,000	±1 COUNT
35. AIR ASSIST PRESSURE	GAGE	0-120" HG.	±0.066% OF FULL SCALE
36. BLOWER SPEED	MAGNETIC PROBE	0-100,000	±1 COUNT
37. PREHEATER MOTOR CURRENT	AMMETER	0-5 AMP	±2% OF FULL SCALE
38. ACCESSORY SHAFT TORQUE	STRAIN GAGE	0-40 FT-LBS	±½% OF FULL SCALE
39. PREHEATER TORQUE	STRAIN GAGE	0-100 IN OZ	±1½% OF FULL SCALE
40. E.G.R. VALVE POSITION	AMMETER	0-90°	±2 OF FULL SCALE
41. EXHAUST VALVE POSITION	AMMETER	0-90°	±2% OF FULL SCALE
42. ALTERNATOR LOAD	AMETER	0-100 AMPS	±2% OF FULL SCALE
43. EXHAUST EMISSIONS	(HC) CARBON ANALYZER	0-4000 PPM	±1% OF FULL SCALE
44. INLET EMISSIONS	(NOx) PHOTONS ANALYZER	0-10,000 PPM	±½% OF FULL SCALE
45. PREHEATER EMISSIONS NO-1	(O₂) POLARGRAPHIC ANALYZER	0-25%	±0.7% OF FULL SCALE
46. PREHEATER EMISSIONS NO-2	(CO₂) INFARRED ANALYZER	0-16%	±1% OF FULL SCALE
47. PREHEATER EMISSIONS NO-3	(CO) INFARRED ANALYZER	0-2000 PPM	±1% OF FULL SCALE
48. PREHEATER EMISSIONS NO-4			

ORIGINAL SYSTEM — BOLD LINES
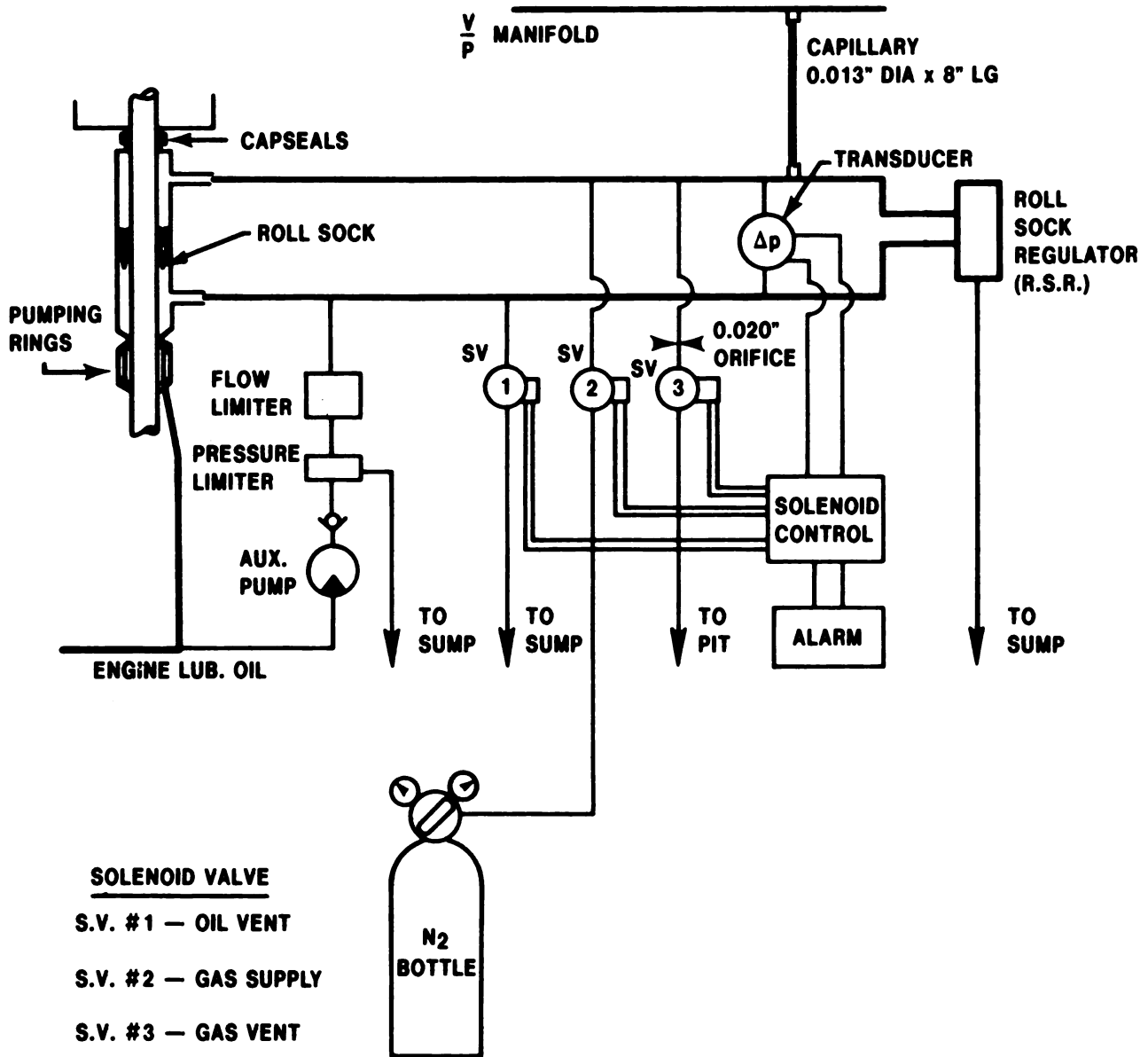
Figure 2.1-4   Rollsock Gas and Oil Circuitry with Protection Devices
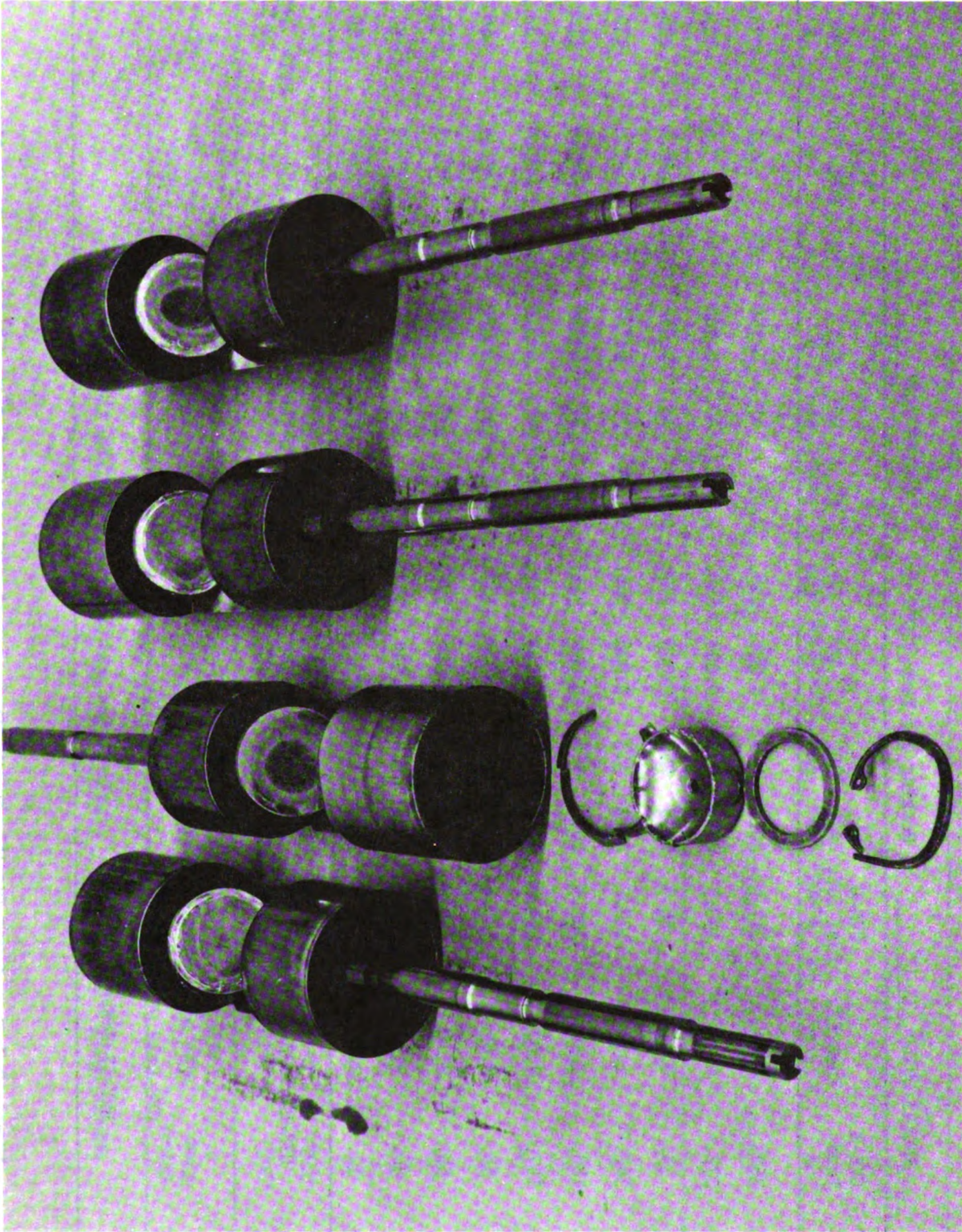
Figure 2.1-5   Slider Retaining Ring Groove Failure

ENGINE BUILD 3X-17   Working Gas Temp 720°C   ENGINE TEST 1

Sim. Pt. No.	CVS-H Time s	Fuel Fl. g/s	CVS-H Fuel Tot. g	A/F	HC ppm	HC g	CO ppm	CO g	NOX ppm	NOX g	HWY. TIME s	HWY. FUEL TOT. g	EGR %
1	362.	0.60	217.4	20.8	4.8	0.011	648.	2.975	47.	0.355	10.	6.2	93.
2	272.	0.70	190.5	21.1	4.2	0.008	648.	2.643	40.	0.268	5.	3.6	105.
3	74.	0.52	38.5	20.5	2.0	0.005	277.	0.222	35.	0.046	52.	27.0	126.
4	167.	1.03	172.2	20.3	3.3	0.006	455.	1.617	29.	0.169	29.	30.0	130.
5	188.	1.40	262.5	20.3	3.6	0.010	435.	2.356	38.	0.338	33.	45.9	112.
6	147.	2.00	294.4	20.9	4.2	0.013	931.	5.816	61.	0.626	46.	91.8	83.
7	58.	2.84	165.6	20.7	3.2	0.023	1117.	3.888	105.	0.600	73.	206.5	66.
8	58.	2.10	120.8	21.0	1.6	0.028	594.	1.529	73.	0.309	331.	695.9	84.
9	36.	3.57	128.9	20.8	3.0	0.044	931.	2.534	125.	0.559	77.	274.2	56.
10	12.	2.57	29.6	20.8	9.6	0.003	896.	0.559	82.	0.084	108.	277.0	80.

CVS-H= 1620.2   HC TOTAL= 0.150   CO TOTAL= 24.14   NOX TOTAL- 3.354   HWY= 1658.2

HC= 0.020g/mile   CO=3.22g/mile   NOX=0.447g/mile

CVS-H=12.95mpg

HWY=17.28mpg

Figure 2.1-6   4-215 Stirling Engine Dynamometer Emission and Fuel Economy Projections

ENGINE BUILD   X-17   Working Gas Temp 720°C   ENGINE TEST   2

Sim. Pt. No.	CVS-H Time s	Fuel Fl. g/s	Fuel Tot. g	A/F	HC ppm	HC g	CO ppm	CO g	NOX ppm	NOX g	Hwy. Time s	Hwy. Fuel Tot. g	Egr. %
1	362.	0.61	221.0	21.0	2.4	0.006	569.	2.680	37.	0.286	10.	6.3	97.
2	272.	0.74	201.4	21.0	5.4	0.011	569.	2.442	34.	0.240	5.	3.8	104.
3	74.	0.53	39.2	21.2	4.2	0.002	190.	0.160	22.	0.030	52.	27.6	176.
4	167.	1.04	173.9	21.1	2.4	0.004	569.	2.119	27.	0.165	29.	30.3	140.
5	188.	1.37	256.9	21.0	1.8	0.005	594.	3.252	38.	0.342	33.	44.9	108.
6	147.	2.00	294.4	21.0	1.8	0.006	569.	3.571	54.	0.557	46.	91.8	90.
7	58.	3.00	174.9	21.1	2.4	0.004	734.	2.749	83.	0.511	73.	218.1	72.
8	58.	2.00	115.0	21.2	3.9	0.005	521.	1.289	58.	0.236	331.	662.8	82.
9	36.	3.60	130.0	21.0	7.2	0.010	569.	1.576	93.	0.423	77.	276.5	68.
10	12.	2.70	31.0	21.1	9.2	0.006	676.	0.449	67.	0.073	108.	291.1	81.

CVS-H= 1637.7   HC TOTAL= 0.059   CO TOTAL= 20.29   NOX TOTAL= 2.863   HWY= 1653.1

HC= 0.008g/mile   CO=2.70g/mile   NOX=0.382g/mile

CVS-H=12.81mpg

HWY=17.34mpg

Figure 2.1-7   4-215 Stirling Engine Dynamometer Emission and Fuel Economy Projections

19
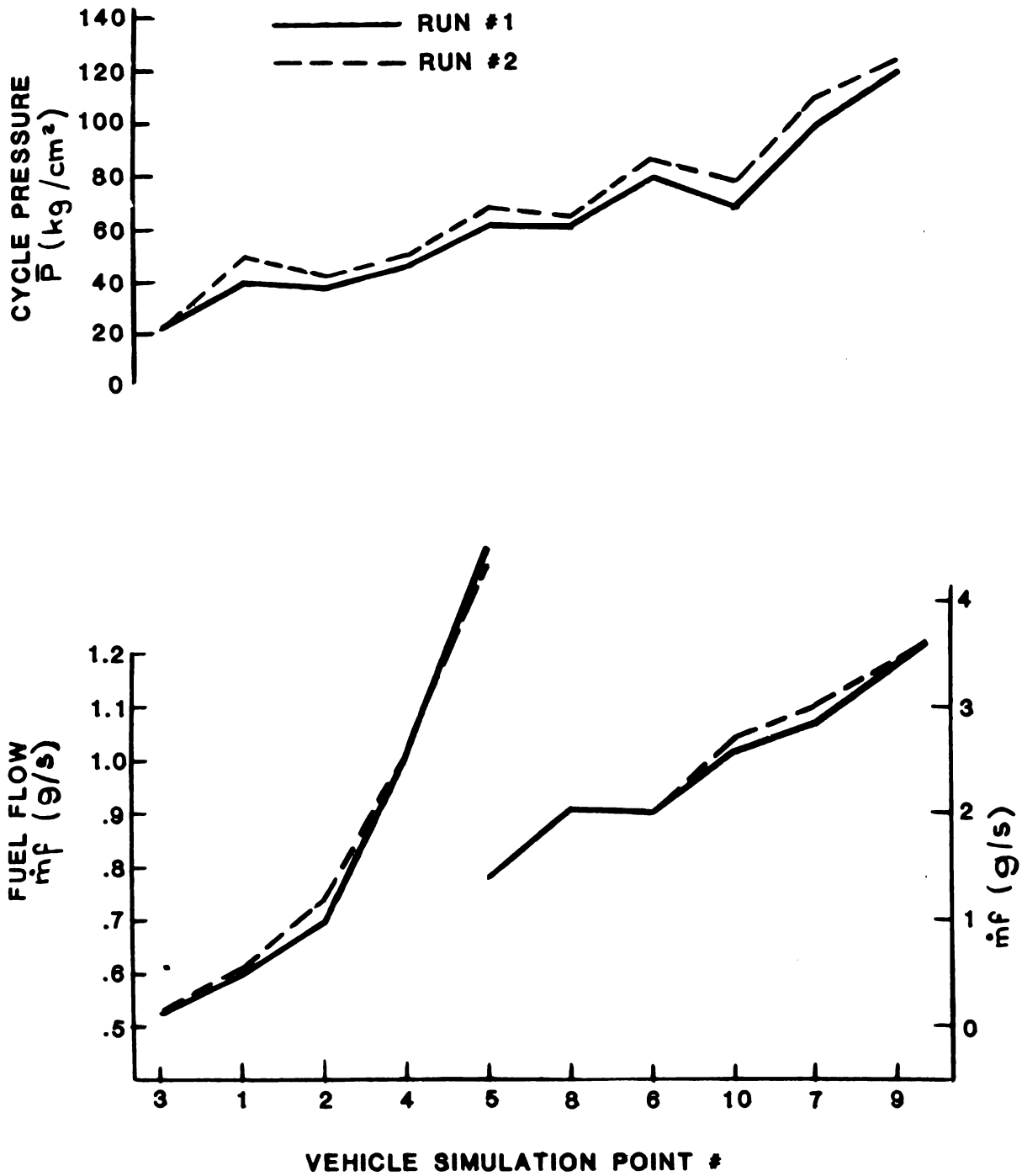
Figure 2.1-8   Engine 3X17 Fuel Flow and Mean Cycle Pressure of Run 1 and 2
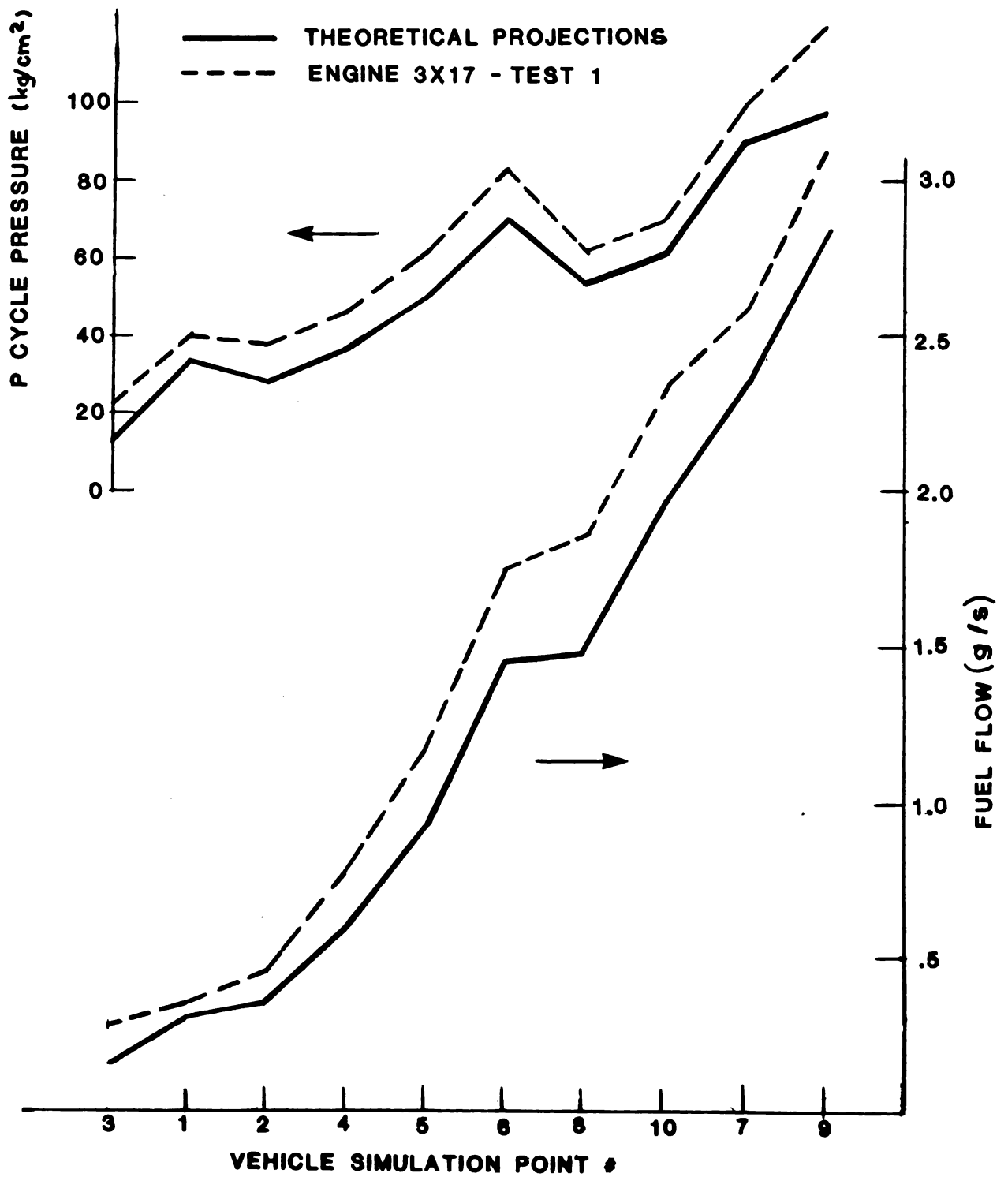
Figure 2.1-9   Dynamometer Test Evaluation

Simulation Point No. I

(600 RPM, 5.4 kg-m Torque)

Equiv. * Ratio	EGR (%)	Fuel Flow (g/s)	Exhaust Emissions			H_2 Mean Temp. (°C)
			HC (PPM)	CO (PPM)	NOx (PPM)	
1.63	133	.621	2.4	397	29	698
1.58	100	.620	4.2	594	40	701
1.62	74	.620	3.6	455	65	702
1.48	123	.625	10.8	1197	25	700
1.49	95	.622	6.0	1041	37	701
1.50	73	.621	4.8	1041	63	704
1.37	122	.639	4.2	2594	27	701
1.40	98	.637	2.4	2310	40	700
1.42	67	.632	1.2	1409	70	701
1.64	135	.626	1.8	310	33	702
1.64	110	.630	1.5	326	42	703
1.64	74	.624	1.2	277	68	700

* Equivalance ratio is measured air/fuel ratio divided by stoichiometric air/fuel ratio (14.7).

Figure 2.1-10   Mapping and Optimization Summary

Simulation Point No. I (Re-Run)

(600 RPM, 5.4 kg-m Torque)

Equiv. Ratio	EGR (%)	Fuel Flow (g/s)	Exhaust Emissions			H₂ Mean Temp. (°C)
			HC (PPM)	CO (PPM)	NOx (PPM)	
1.75	133	.603	1.8	277	26	696
1.76	116	.598	1.8	260	34	702
1.76	84	.598	1.2	260	53	702
1.55	140	.618	1.8	343	23	709
1.57	110	.604	1.2	397	36	701
1.56	74	.603	.6	476	52	712
1.47	136	.586	10.6	621	21	703
1.47	105	.582	7.2	931	29	700
1.47	78	.583	.6	1409	49	697
1.37	171	.606	3.6	1409	15	706
1.37	142	.550	3.0	2062	19	705
1.37	105	.586	1.8	2377	29	698

Figure 2.1-11   Mapping and Optimization Summary

Simulation Point No. I

(600 RPM, 5.4 kg-m Torque)

Temperature Affect on Fuel for Constant Emissions

Equiv. Ratio	EGR (%)	Fuel Flow (g/s)	Exhaust Emissions			H_2 Mean Temp. (°C)
			HC (PPM)	CO (PPM)	NOx (PPM)	
1.52	144	.645	0	209	40	772
1.33	136	.630	2.4	569	37	771
1.20	125	.621	1.2	476	38	759
1.47	95	.613	1.2	594	41	739
1.49	114	.623	1.2	569	39	720
1.56	110	.608	1.8	498	40	700
1.59	109	.603	2.4	521	39	679
1.63	105	.595	2.4	521	40	659

Figure 2.1-12   Mapping and Optimization Summary

Simulation Point No. 4

(1000 RPM, 6.9 kg-m Torque)

Equiv. Ratio	EGR (%)	Fuel Flow (g/s)	Exhaust Emissions			H_2 Mean Temp. (°C)
			HC (PPM)	CO (PPM)	NOx (PPM)	
1.68	168	1.077	1.8	260	31	732
1.67	128	1.002	1.8	293	41	729
1.69	75	.982	1.8	361	84	729
1.48	170	1.053	1.5	343	27	730
1.49	126	1.011	1.8	397	38	729
1.50	81	1.006	1.8	435	65	730
1.33	170	1.023	.6	862	22	731
1.33	131	.996	4.8	1197	31	730
1.35	82	.990	4.2	1322	60	730
1.67	167	1.087	2.4	260	30	730
1.69	138	1.051	1.8	277	39	730
1.69	70	1.015	1.8	378	81	730

Figure 2.1-13   Mapping and Optimization Summary

Simulation Point No. 4

(1000 RPM, 6.9 kg-m Torque)

.Temperature Affect for Constant Emission Level

Equiv. Ratio	EGR (%)	Fuel Flow (g/s)	Exhaust Emissions			H$_2$ Mean Temp. (°C)
			HC (PPM)	CO (PPM)	NOx (PPM)	
1.42	141	1.01	6.6	931	15	708
1.24	172	1.036	6.0	545	30	783
1.30	165	1.004	4.2	569	29	761
1.35	147	.991	3.6	521	30	743
1.43	136	.991	3.6	569	29	720
1.48	131	.994	4.2	569	30	699

Figure 2.1-14   Mapping and Optimization Summary

Simulation Point No. 5
(1100 RPM, 11.1 kg-m Torque)

Equiv. Ratio	EGR (%)	Fuel Flow (g/s)	Exhaust Emissions			H_2 Mean Temp. (°C)
			HC (PPM)	CO (PPM)	NOx (PPM)	
1.63	130	1.45	1.2	171	52	767
1.63	86	1.39	1.2	151	87	763
1.63	69	1.36	.3	277	120	758
1.47	141	1.43	.6	260	35	763
1.42	103	1.38	.6	243	52	761
1.42	71	1.35	.6	260	91	753
1.3	148	1.41	.4	435	28	761
1.3	103	1.37	.6	435	47	761
1.3	73	1.36	.6	476	75	758
1.3	128	1.436	4.8	594	36	762
(RE-RUN)						
1.31	158	1.440	2.4	676	30	761
1.30	115	1.394	3.6	1117	42	759
1.32	80	1.380	.6	1689	67	760
1.31	92	1.383	3.6	1157	54	758
1.42	141	1.425	2.4	455	37	759
1.43	107	1.398	1.8	277	52	759
1.47	82	1.376	1.8	621	77	759
1.59	133	1.415	1.8	277	44	761
1.60	103	1.422	1.2	277	57	760
1.68	72	1.387	1.2	226	88	759

Figure 2.1-15   Mapping and Optimization Summary

Simulation Point No. 5

(1100 RPM, 11.1 kg-m Torque)

Temperature Affect For Constant Emission Level

Equiv. Ratio	EGR (%)	Fuel Flow (g/s)	Exhaust Emissions			H_2 Mean Temp. (°C)
			HC (PPM)	CO (PPM)	NOx (PPM)	
1.43	111	1.40	.6	521	34	726
1.37	120	1.36	.3	521	32	746
1.43	112	1.40	6.0	1117	38	724
1.42	102	1.30	1.8	545	43	723
1.42	112	1.34	1.8	648	39	722
1.35	124	1.34	2.4	569	40	744
1.30	116	1.29	1.2	521	40	762
1.28	117	1.26	2.4	521	40	780
1.28	133	1.29	1.2	476	40	783
1.49	107	1.31	1.2	545	40	715
1.42	132	1.44	3.0	521	33	722
1.37	147	1.44	4.8	521	33	743
1.30	148	1.37	1.2	521	32	762
1.24	178	1.42	4.8	521	32	783
1.43	141	1.44	4.2	521	32	724
1.47	136	1.44	3.6	521	31	702

Figure 2.1-16   Mapping and Optimization Summary

Simulation Point No. 6

(1300 RPM, 15.9 kg-m Torque)

Equiv. Ratio	EGR (%)	Fuel Flow (g/s)	Exhaust Emissions			H_2 Mean Temp. ($^\circ$C)
			HC (PPM)	CO (PPM)	NOx (PPM)	
1.44	90	2.0	3.6	545	54	726
1.43	48	1.94	3.6	797	120	725
1.45	59	1.91	.6	705	84	726
1.31	61	1.94	1.8	1197	78	724
1.30	39	1.91	7.2	1949	132	720
1.32	104	1.96	.6	931	39	725
1.44	98	2.0	.6	931	50	727
1.44	62	2.0	3.3	1003	88	724
1.57	64	2.07	2.4	662	95	727
1.6	41	1.96	3.0	648	150	727
1.61	116	2.08	3.0	498	460	718

Figure 2.1-17   Mapping and Optimization Summary

Simulation Point No. 6 (Re-Run)

(1300 RPM, 15.9 kg-m Torque)

Equiv. Ratio	EGR (%)	Fuel Flow (g/s)	Exhaust Emissions			H₂ Mean Temp. (°C)
			HC (PPM)	CO (PPM)	NOx (PPM)	
1.33	108	1.969	1.8	498	53	759
1.33	72	1.922	1.8	734	85	758
1.33	140	1.956	1.2	476	38	758
1.46	118	1.949	1.2	343	39	759
1.46	98	1.900	.9	361	60	753
1.46	69	1.876	1.2	397	97	750
1.67	105	1.978	1.2	243	59	757
1.69	101	1.973	1.2	243	63	754
1.71	78	1.921	1.2	243	89	752

Figure 2.1-18   Mapping and Optimization Summary

Simulation Point No. 6

(1300 RPM, 15.9 kg-m Torque)

Temperature Affect on Fuel Flow

Equiv. Ratio	EGR (%)	Fuel Flow (g/s)	HC (PPM)	CO (PPM)	NOx (PPM)	Mean Temp. (°C)
1.42	91	2.02	1.5	862	53	724
1.43	90	2.01	.6	734	57	740
1.43	88	1.99	.6	676	62	743
1.35	91	1.97	.06	648	60	765
1.34	91	1.97	.09	734	60	783
1.52	74	2.07	.9	765	60	704
RECHECK						
1.44	96	2.14	2.4	594	48	726
1.32	86	1.99	.6	569	63	767

Figure 2.1-19   4-215 Stirling Engine Mapping and Optimization Summary

4-215 STIRLING ENGINE
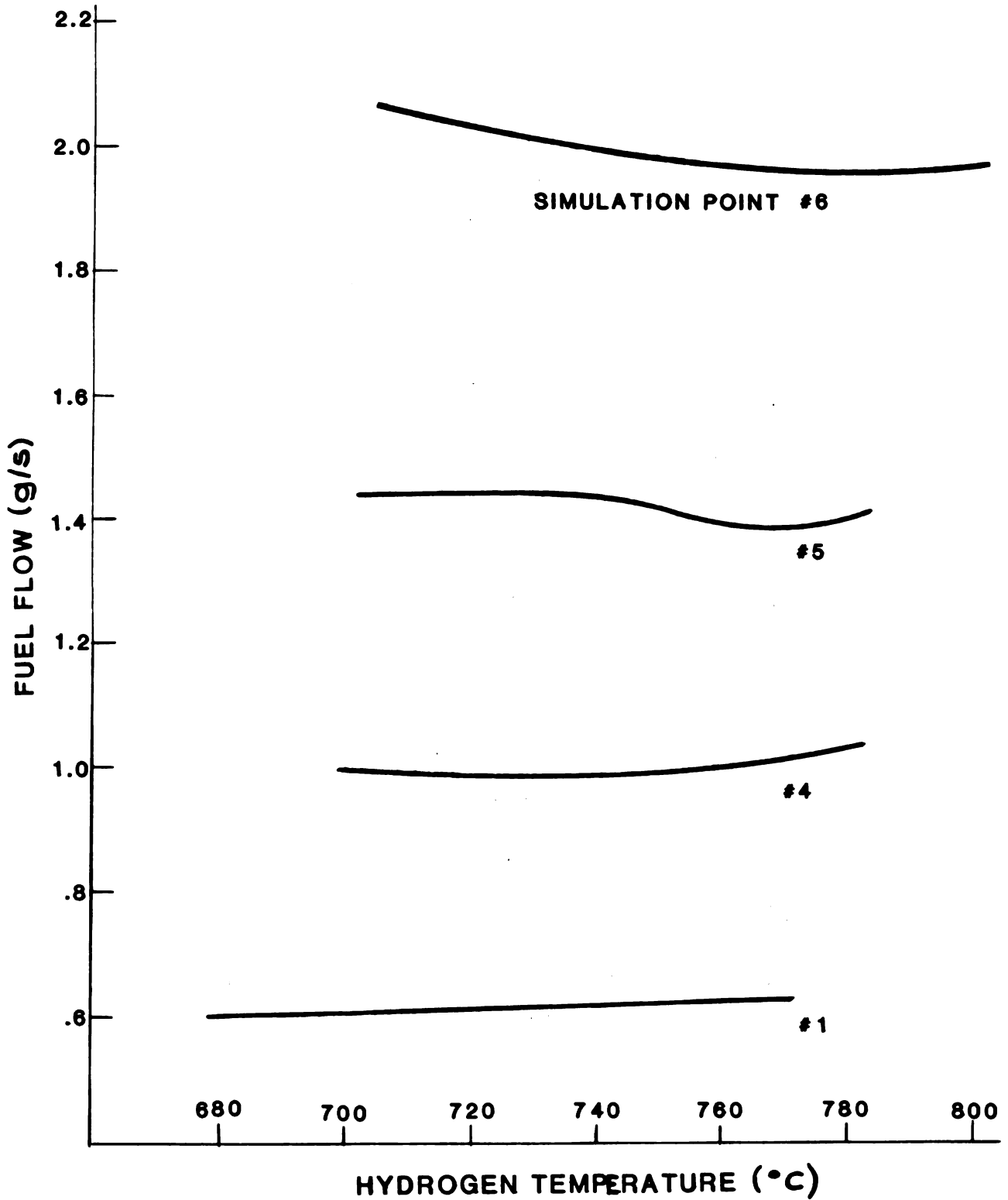
Figure 2.1-20   Fuel Flow vs. Hydrogen Temperature
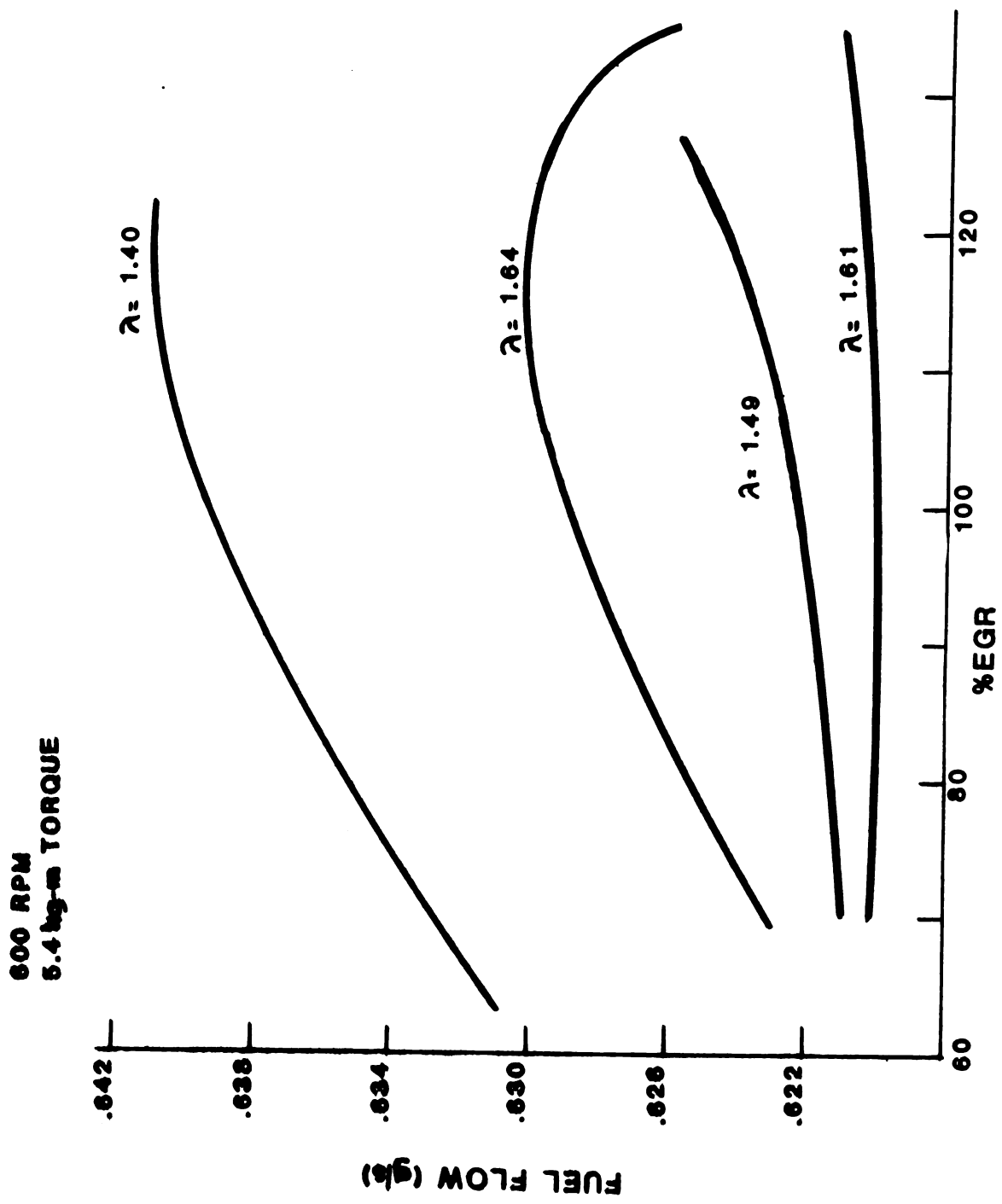
Figure 2.1-21   Vehicle Simulation Point #1

BURNER λ SHOWN IN PARENTHESES

600 RPM

5.4 KG-M TORQUE FUEL FLOW

λ = 1.56 (1.38)

λ = 1.76 (1.53)

λ = 1.37 (1.19)

λ = 1.47 (1.28)

%EGR

FUEL FLOW (g/s)
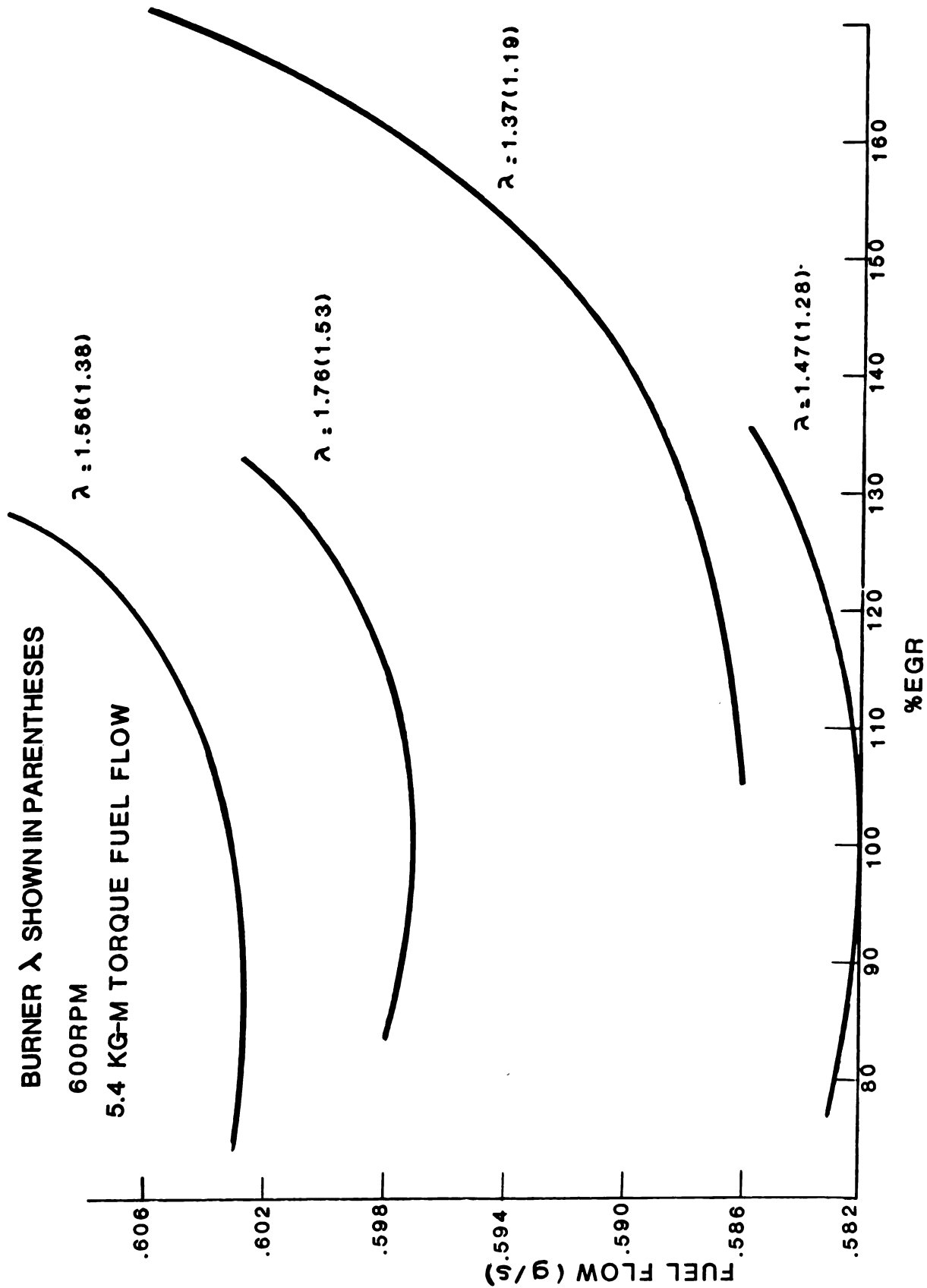
Figure 2.1-22   Vehicle Simulation Point #1 (2nd run)

34
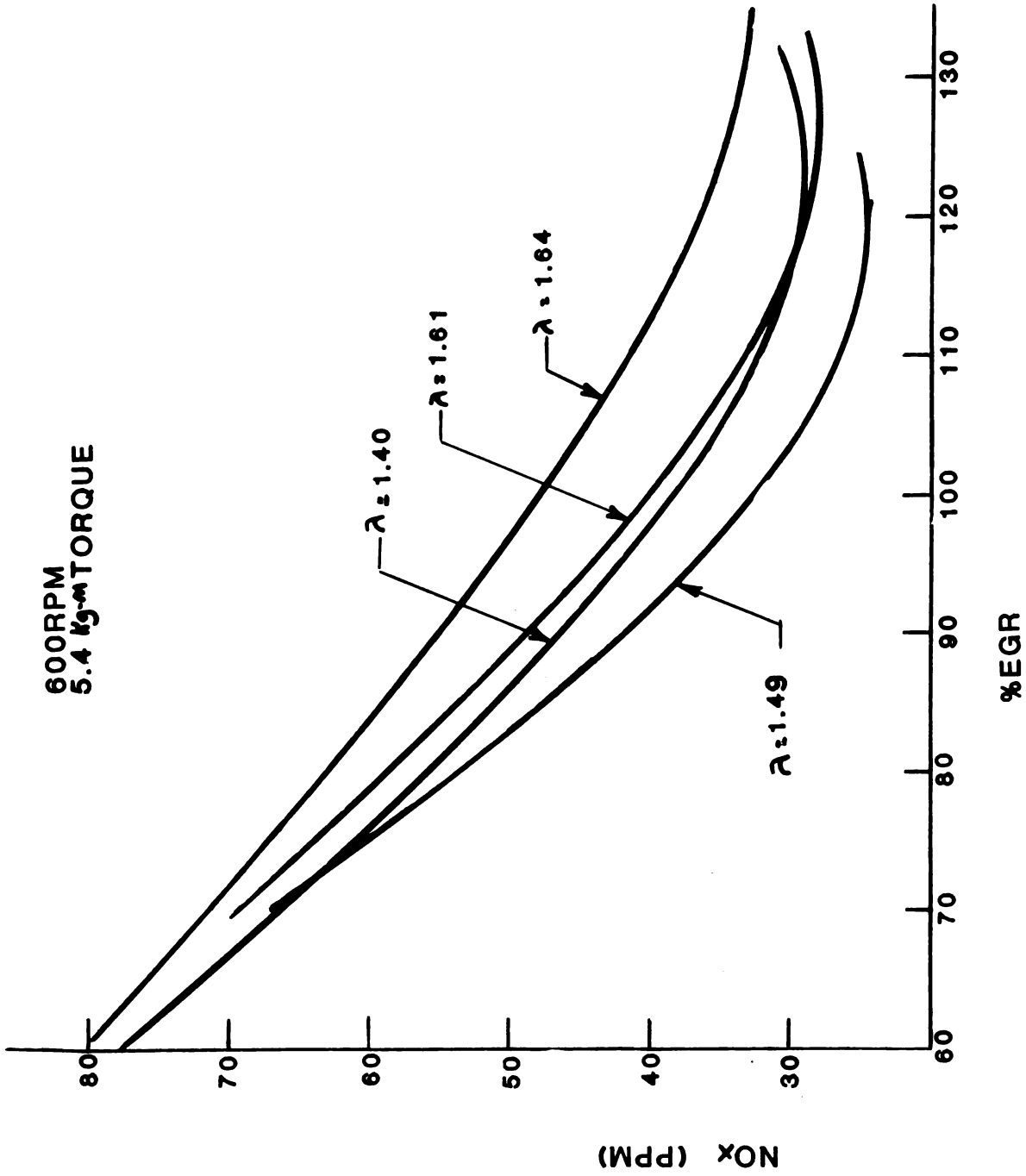
Figure 2.1-23 Vehicle Simulation Point #1
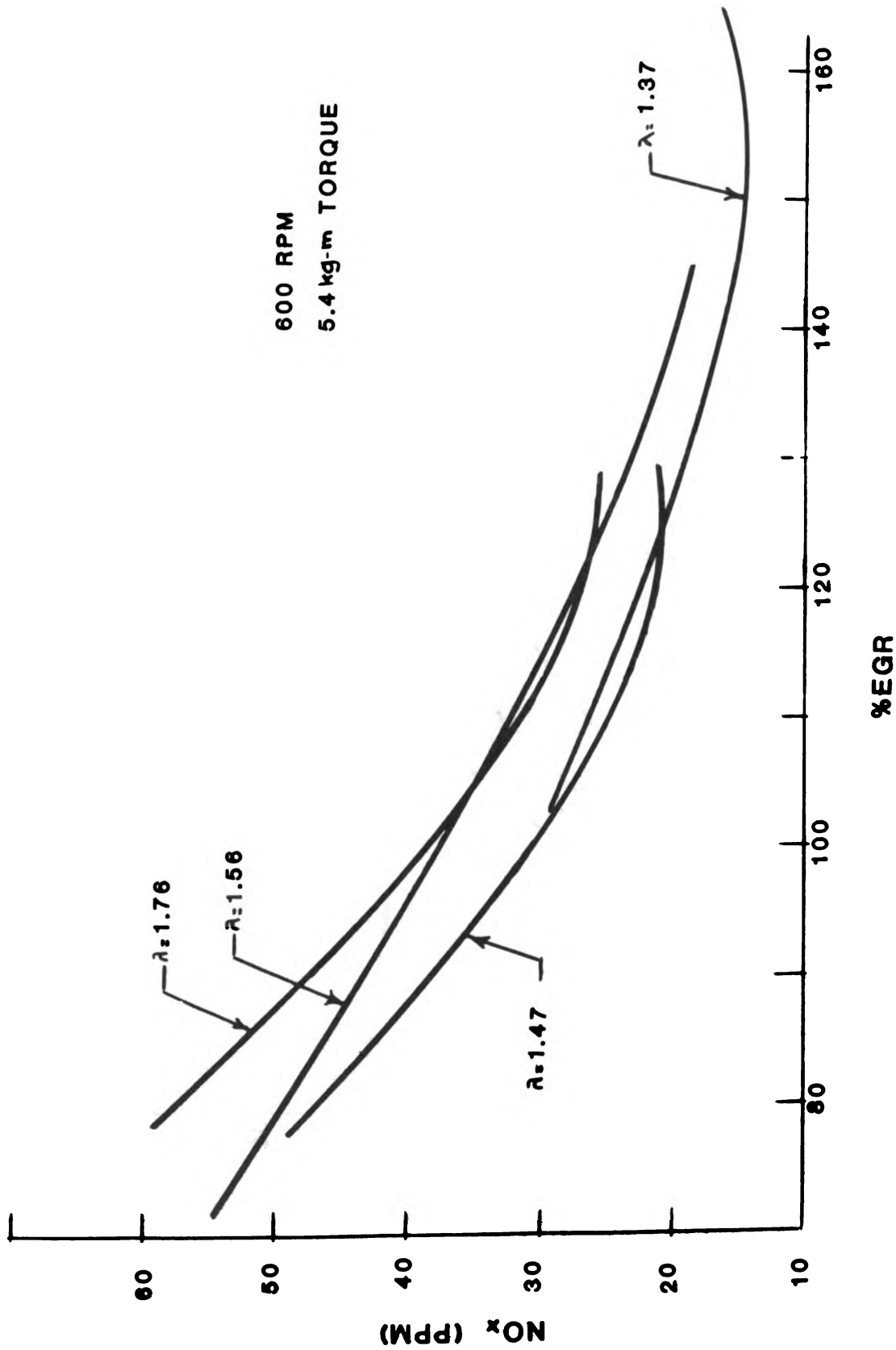
Figure 2.1-24   Vehicle Simulation Point #1 (2nd run)

36

600 RPM
5.4 kg-m TORQUE
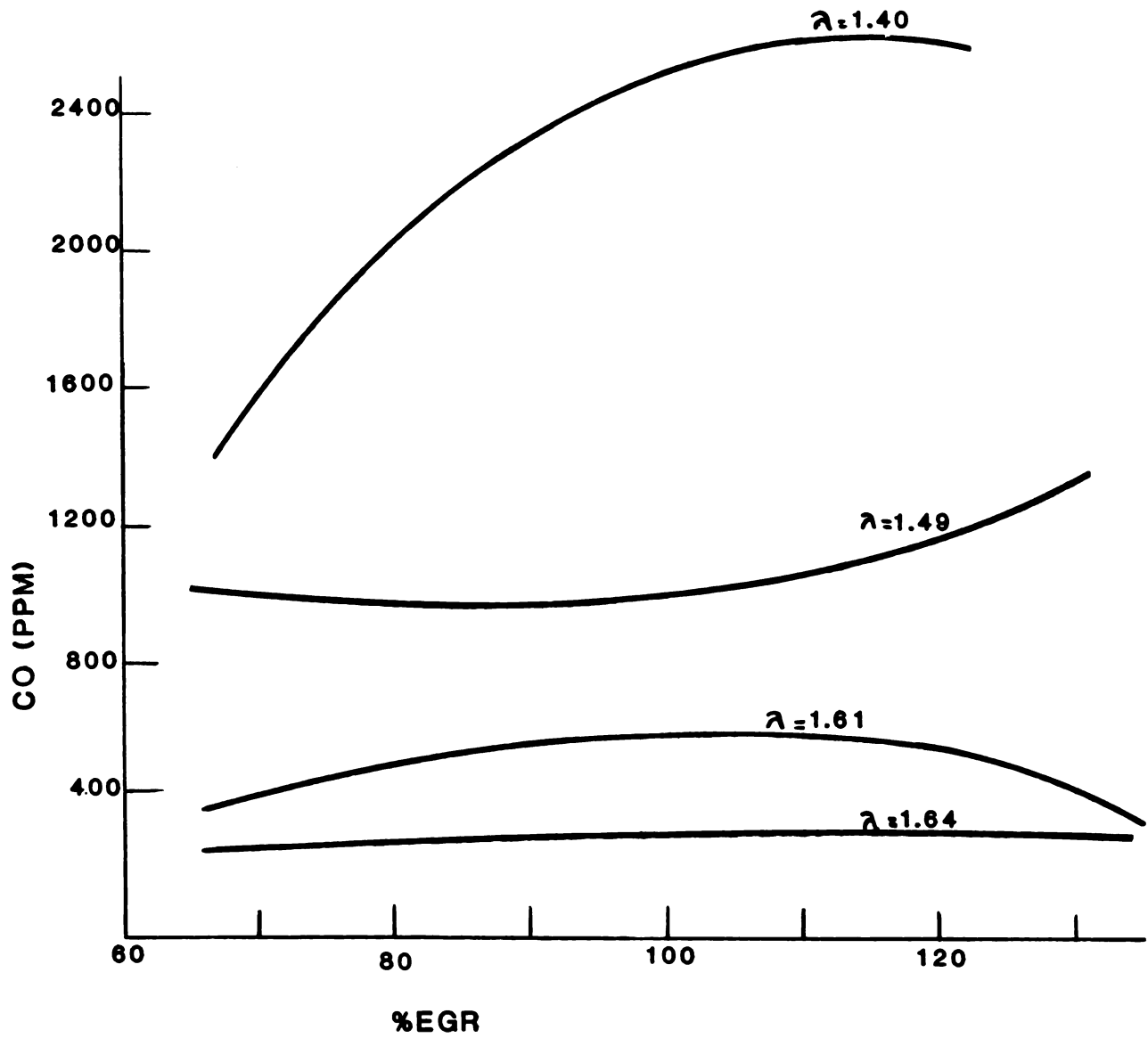
Figure 2.1-25   Vehicle Simulation Point #1
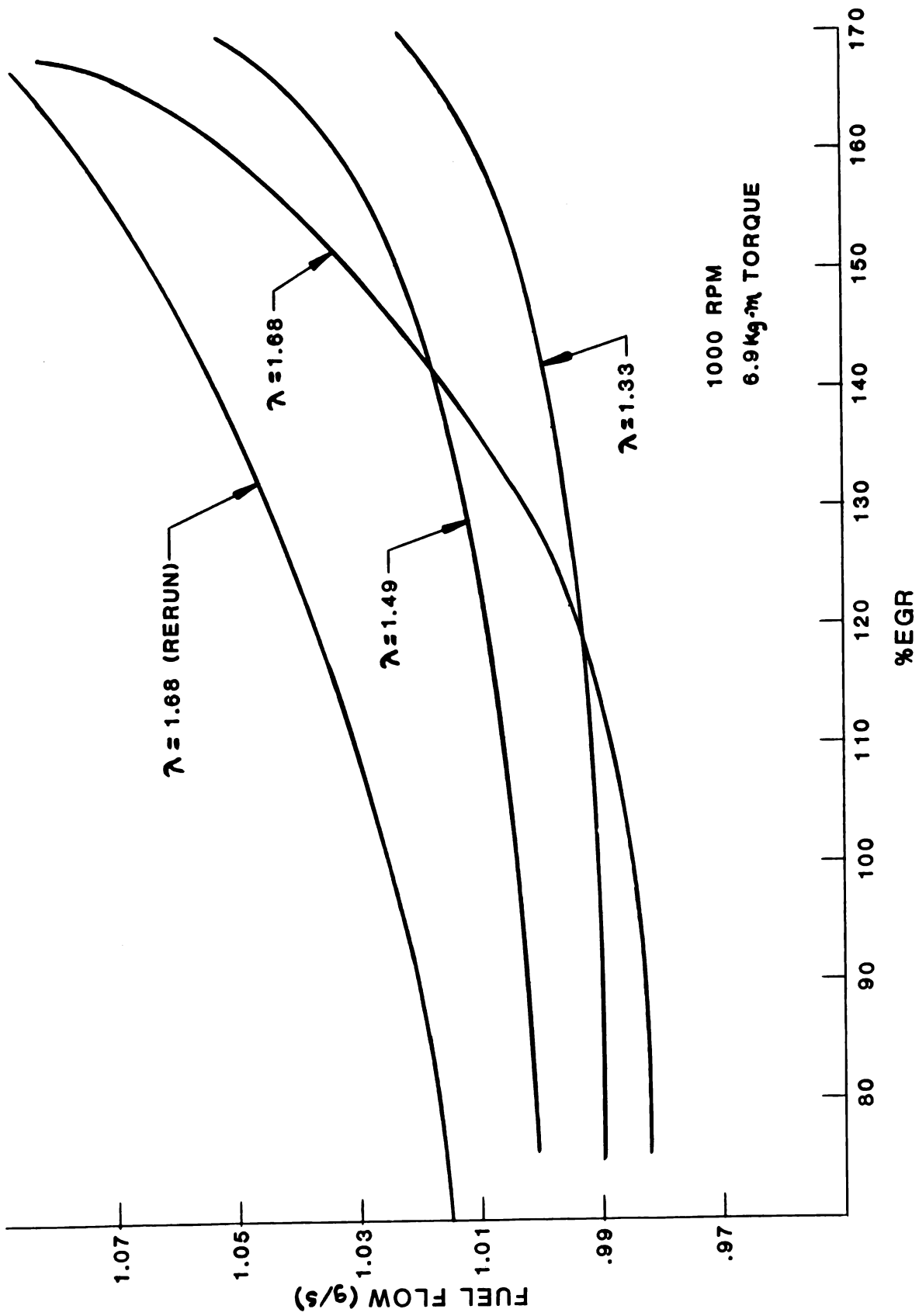
Figure 2.1-26   Vehicle Simulation Point #4

FUEL FLOW (g/s)

%EGR

1000 RPM
6.9 kg·m TORQUE

λ = 1.68 (RERUN)

λ = 1.68

λ = 1.49

λ = 1.33

38

1000RPM
6.9 kg-m TORQUE

$\lambda = 1.68$

$\lambda = 1.49$

$\lambda = 1.33$

NO$_x$ (PPM)

%EGR
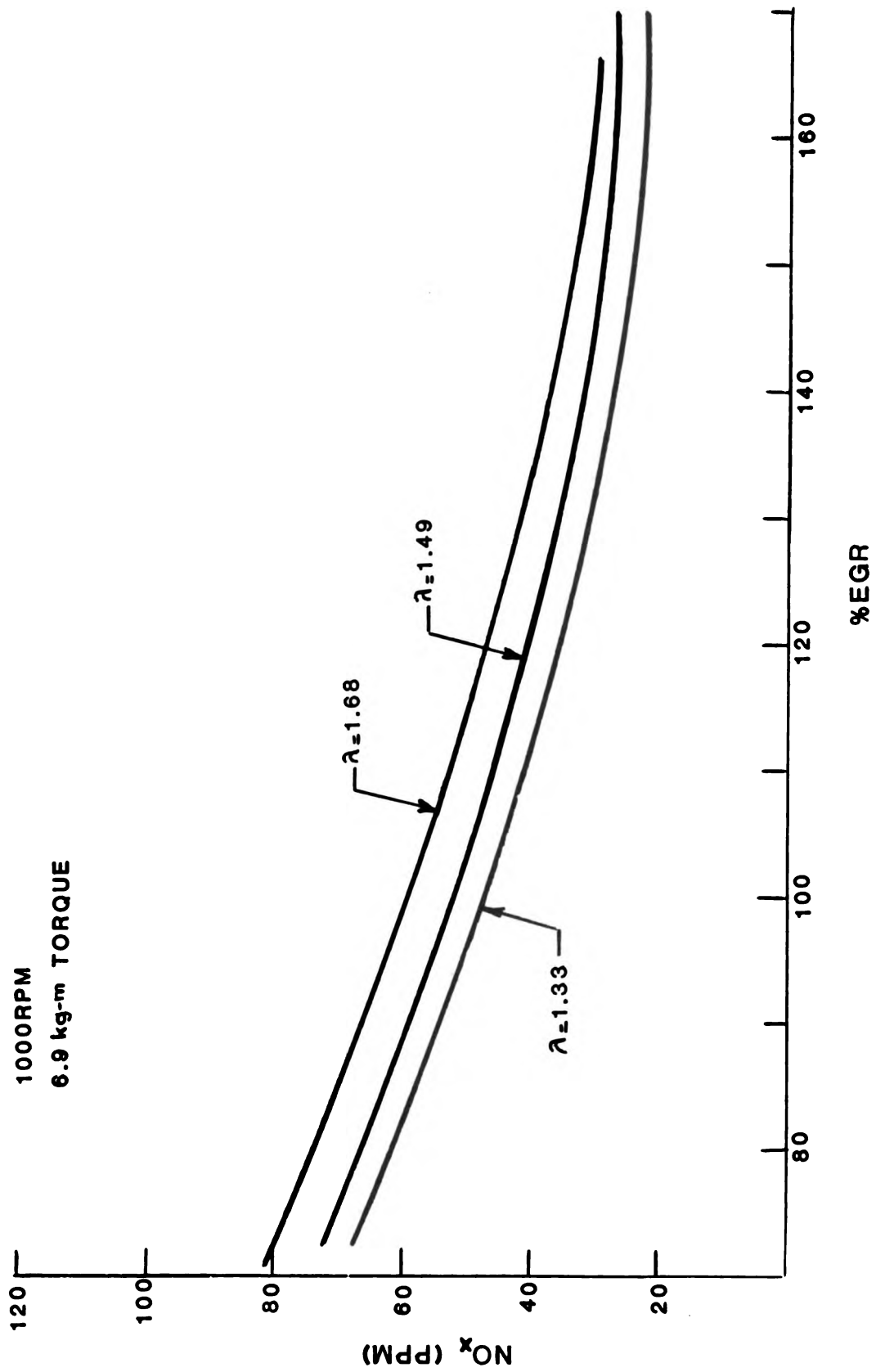
Figure 2.1-27   Vehicle Simulation Point #4

39
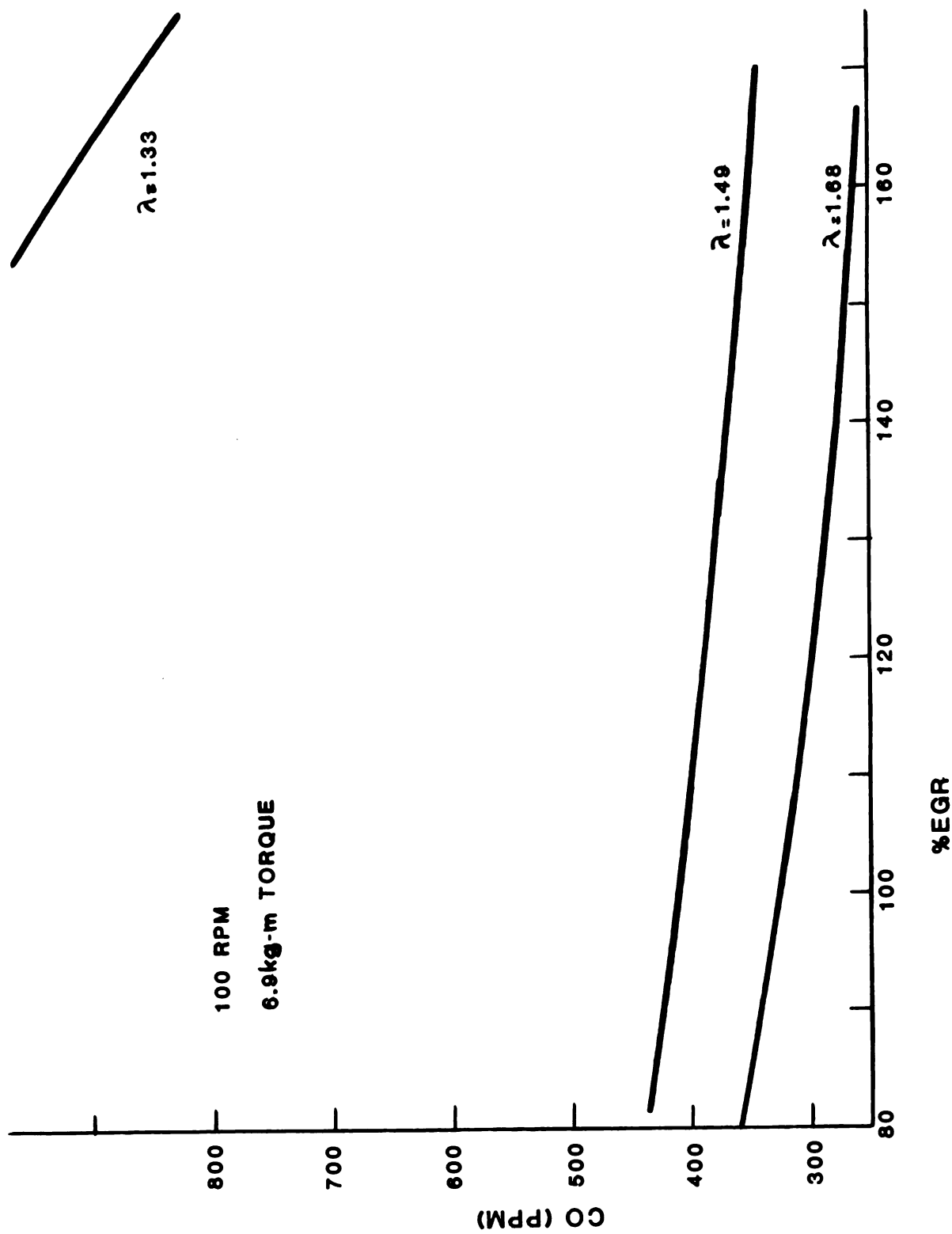
Figure 2.1-28   Vehicle Simulation Point #4

40
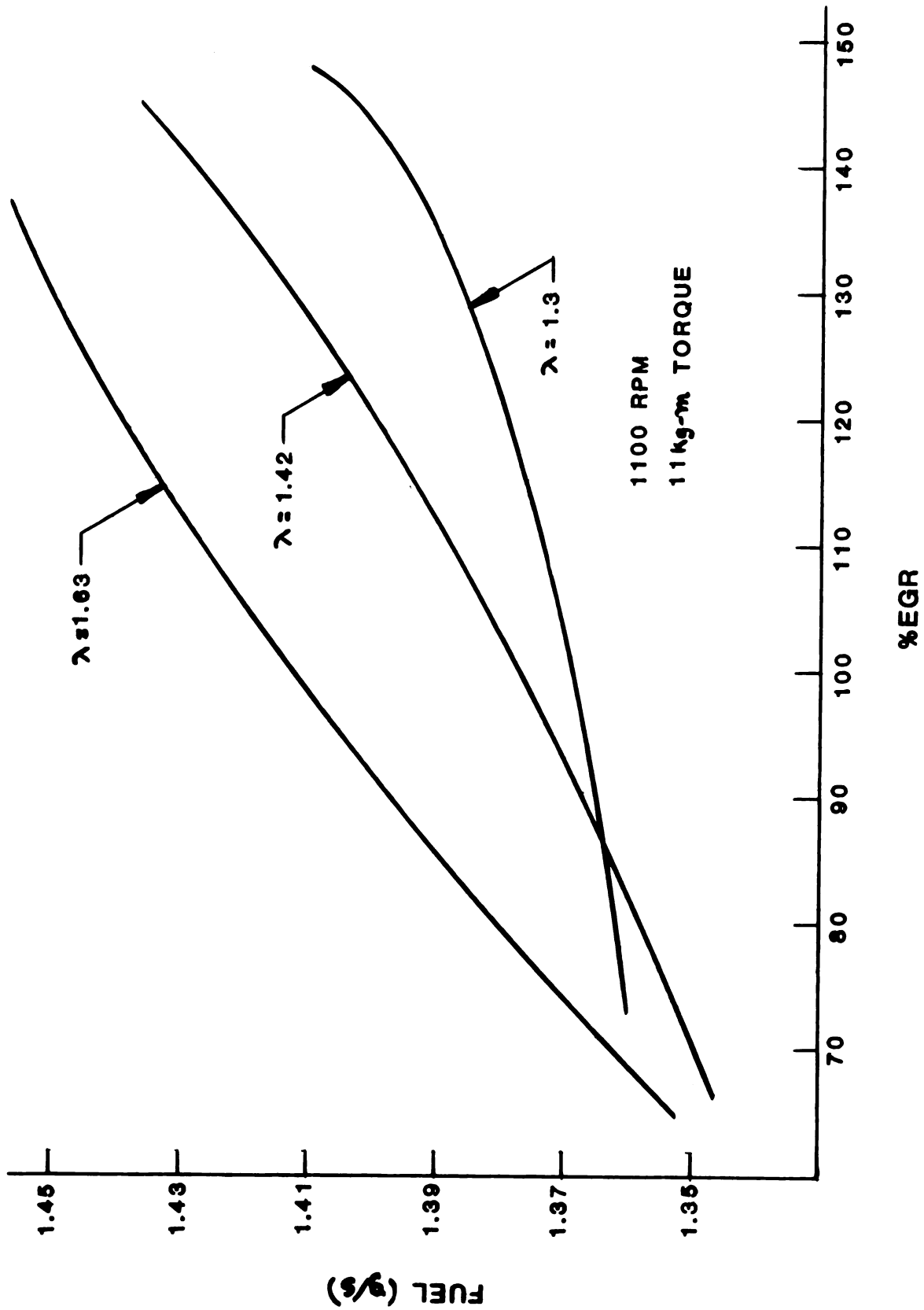
Figure 2.1-29   Vehicle Simulation Point #5
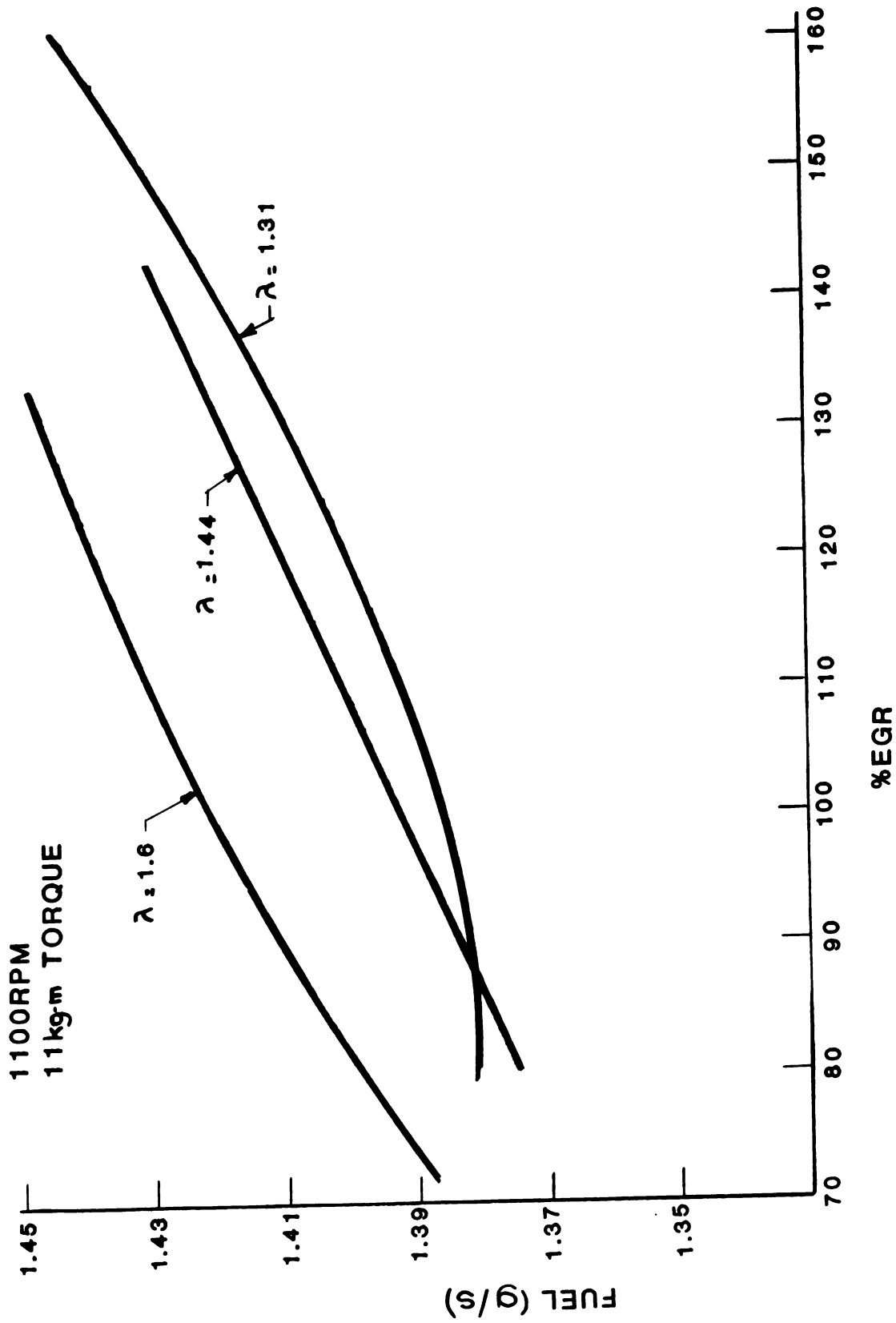
Figure 2.1-30   Vehicle Simulation Point #5 (2nd run)
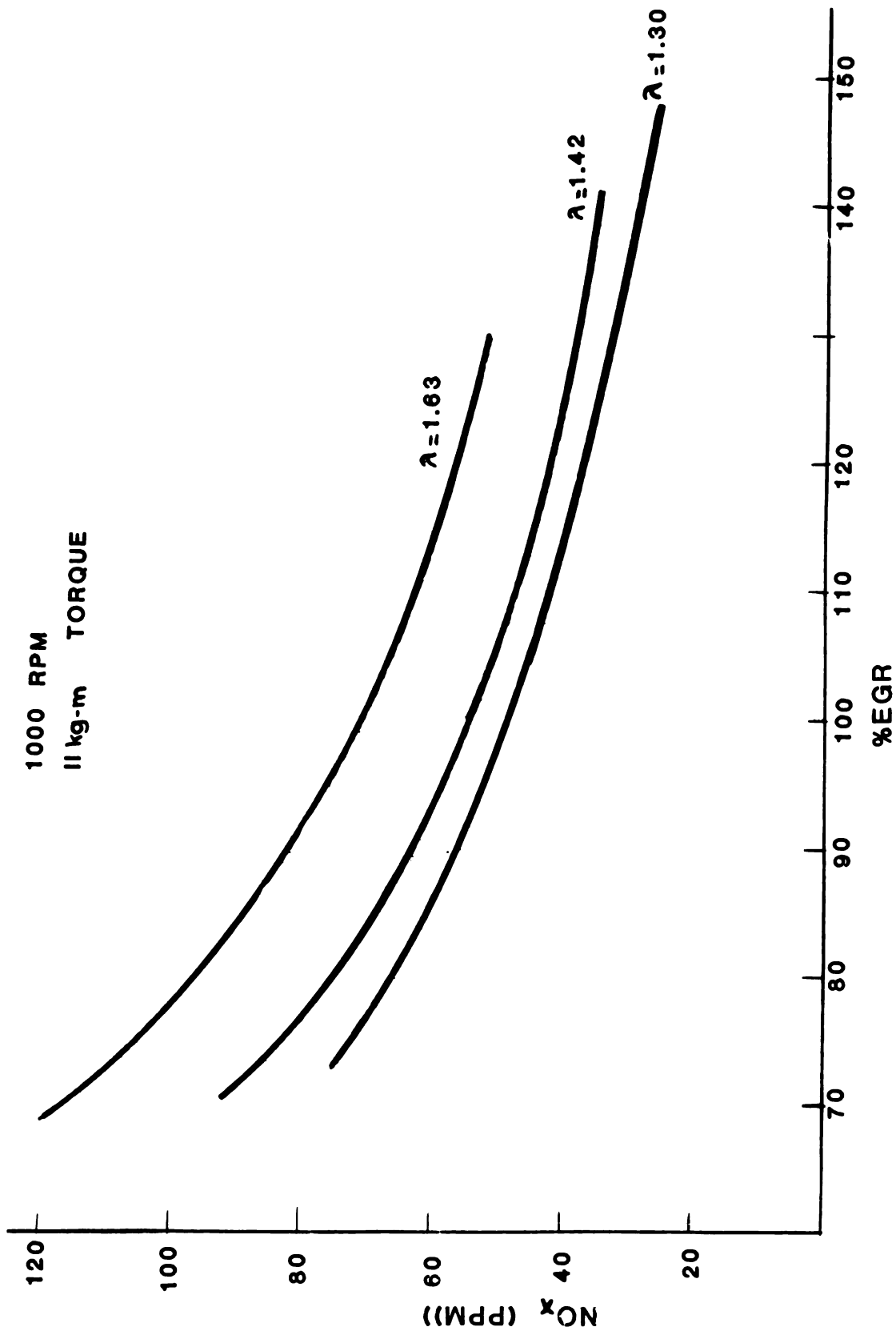
Figure 2.1-31   Vehicle Simulation Point #5 (2nd run)

43
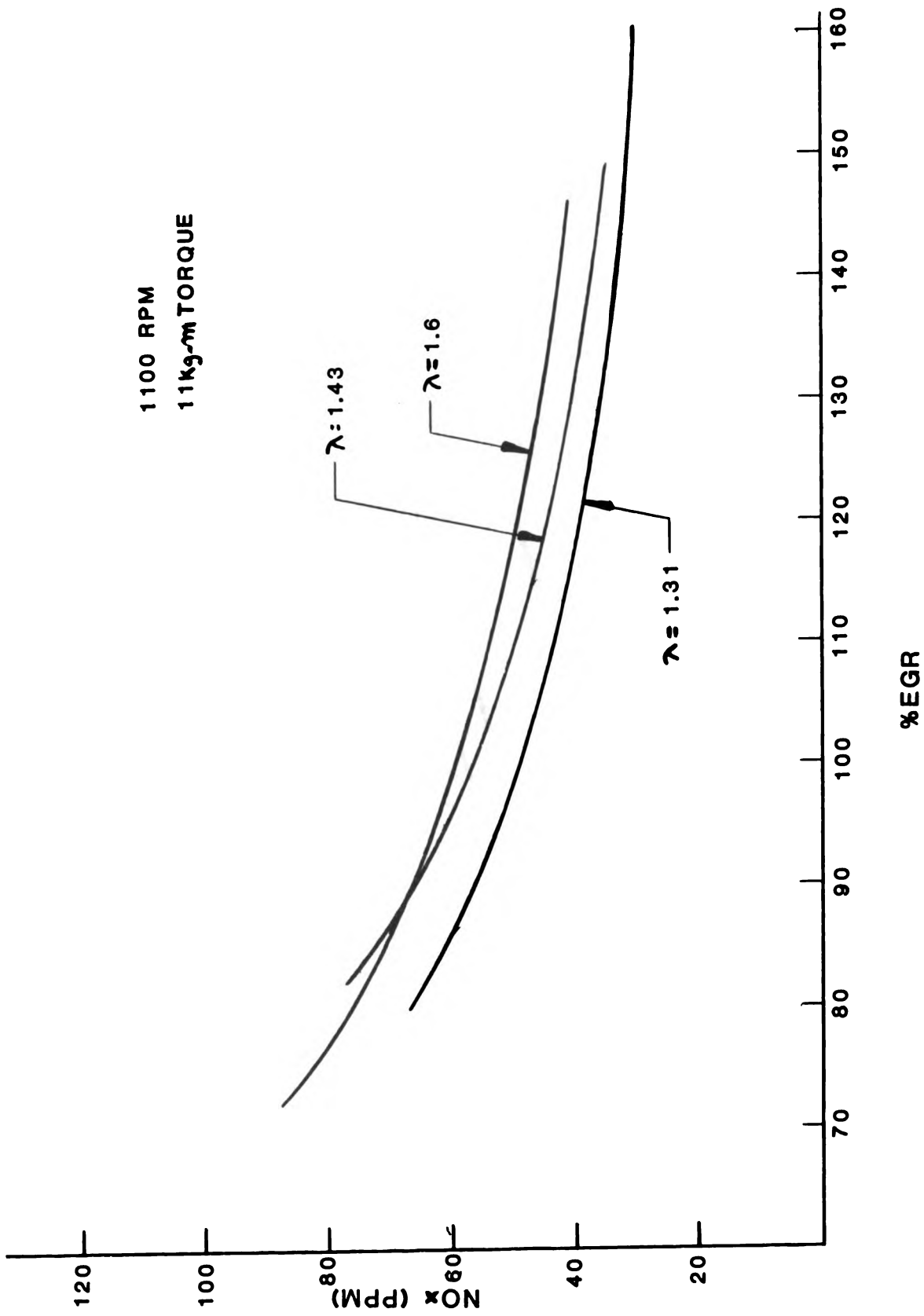
Figure 2.1-32   Vehicle Simulation Point #5
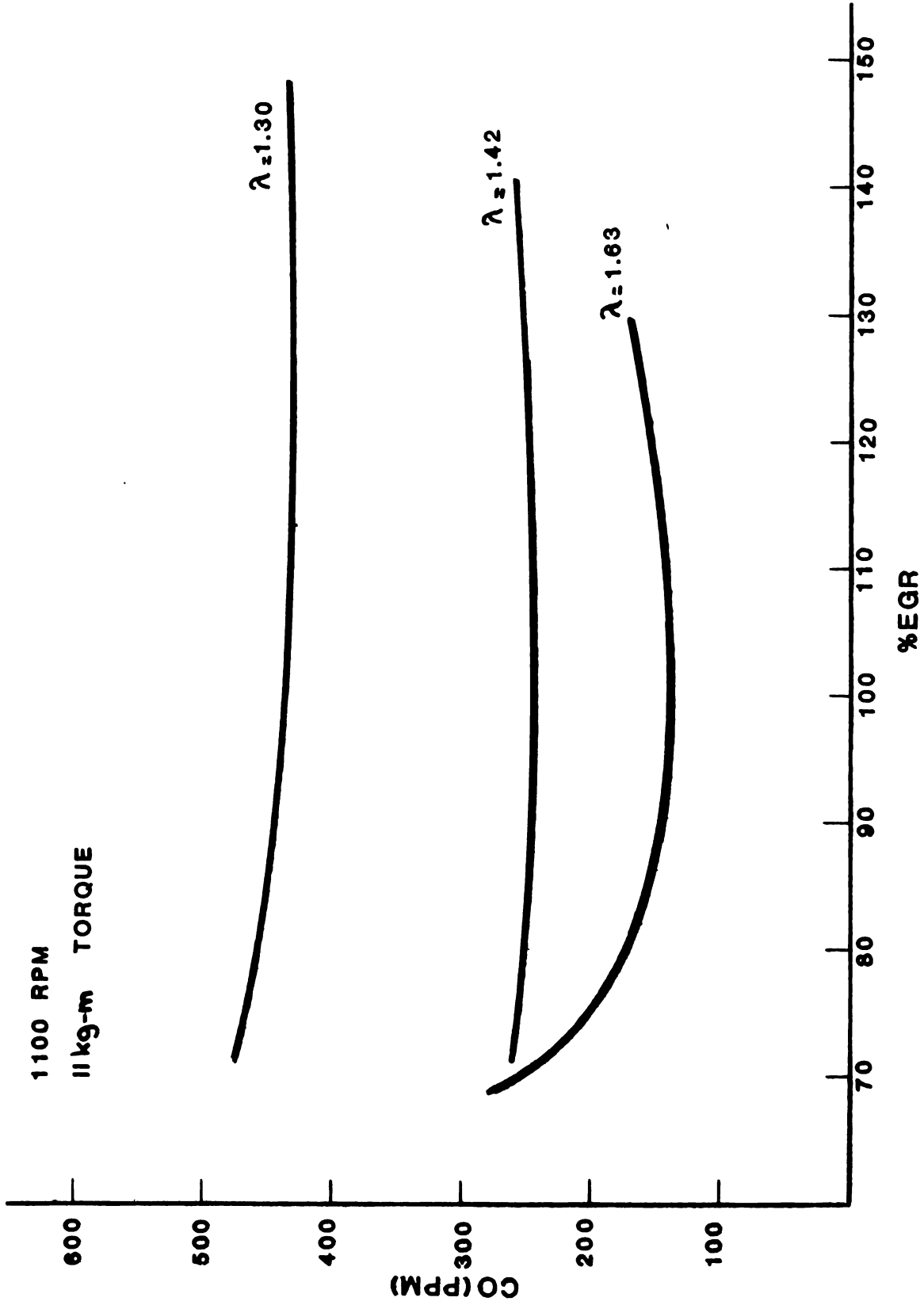
Figure 2.1-33   Vehicle Simulation Point #5

1100 RPM
11 kg-m TORQUE

$\lambda = 1.30$

$\lambda = 1.42$

$\lambda = 1.63$

%EGR

CO (PPM)
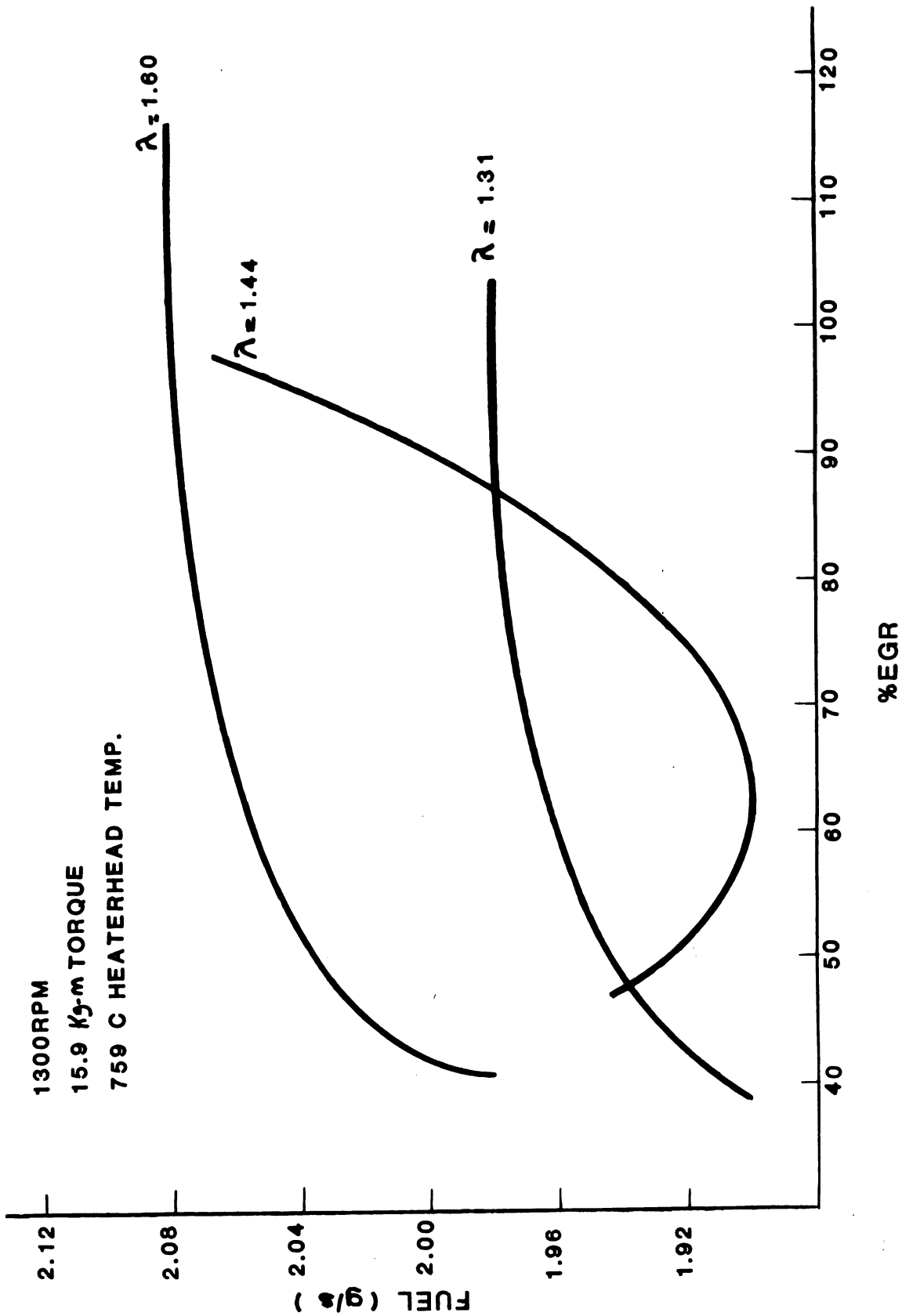
Figure 2.1-34   Vehicle Simulation Point #6 (1st run)

Chart labels:
- 1300RPM
- 15.9 Kg-m TORQUE
- 759 C HEATERHEAD TEMP.
- $\lambda = 1.60$
- $\lambda = 1.44$
- $\lambda = 1.31$
- %EGR (x-axis)
- FUEL (g/s) (y-axis)
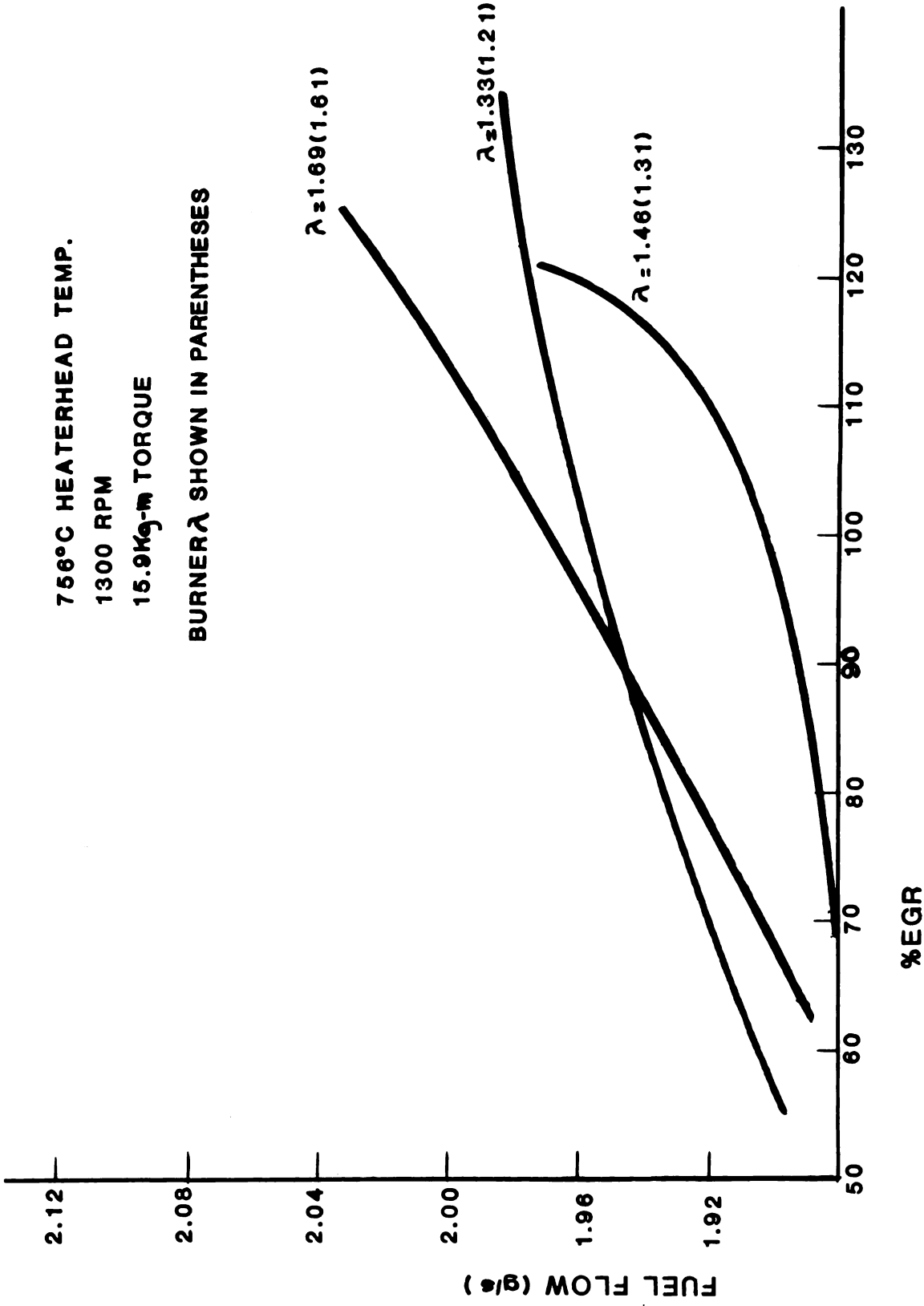
Figure 2.1-35   Vehicle Simulation Point #6 (2nd run)

47
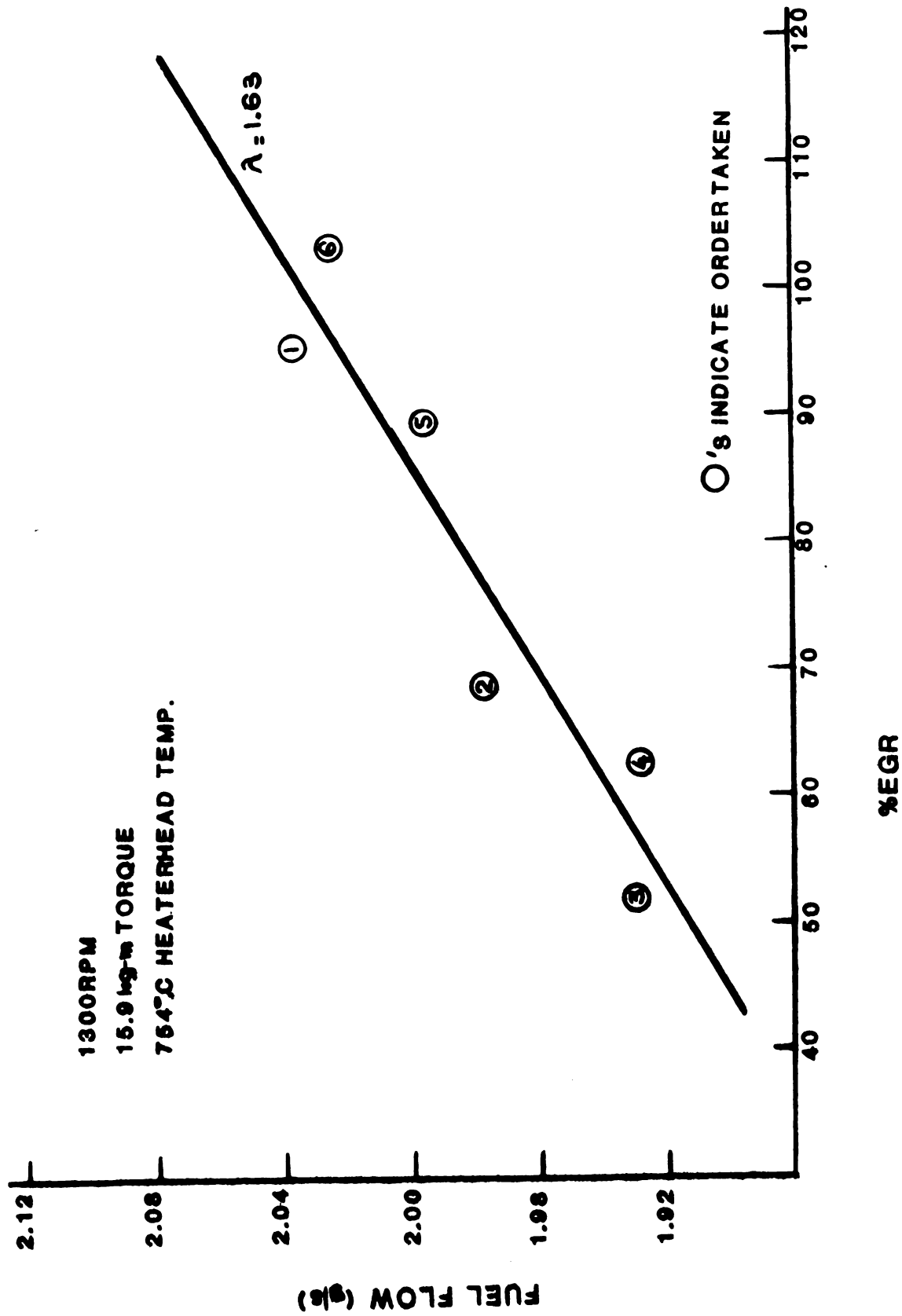
Figure 2.1-36   Vehicle Simulation Point #6 (3rd run)
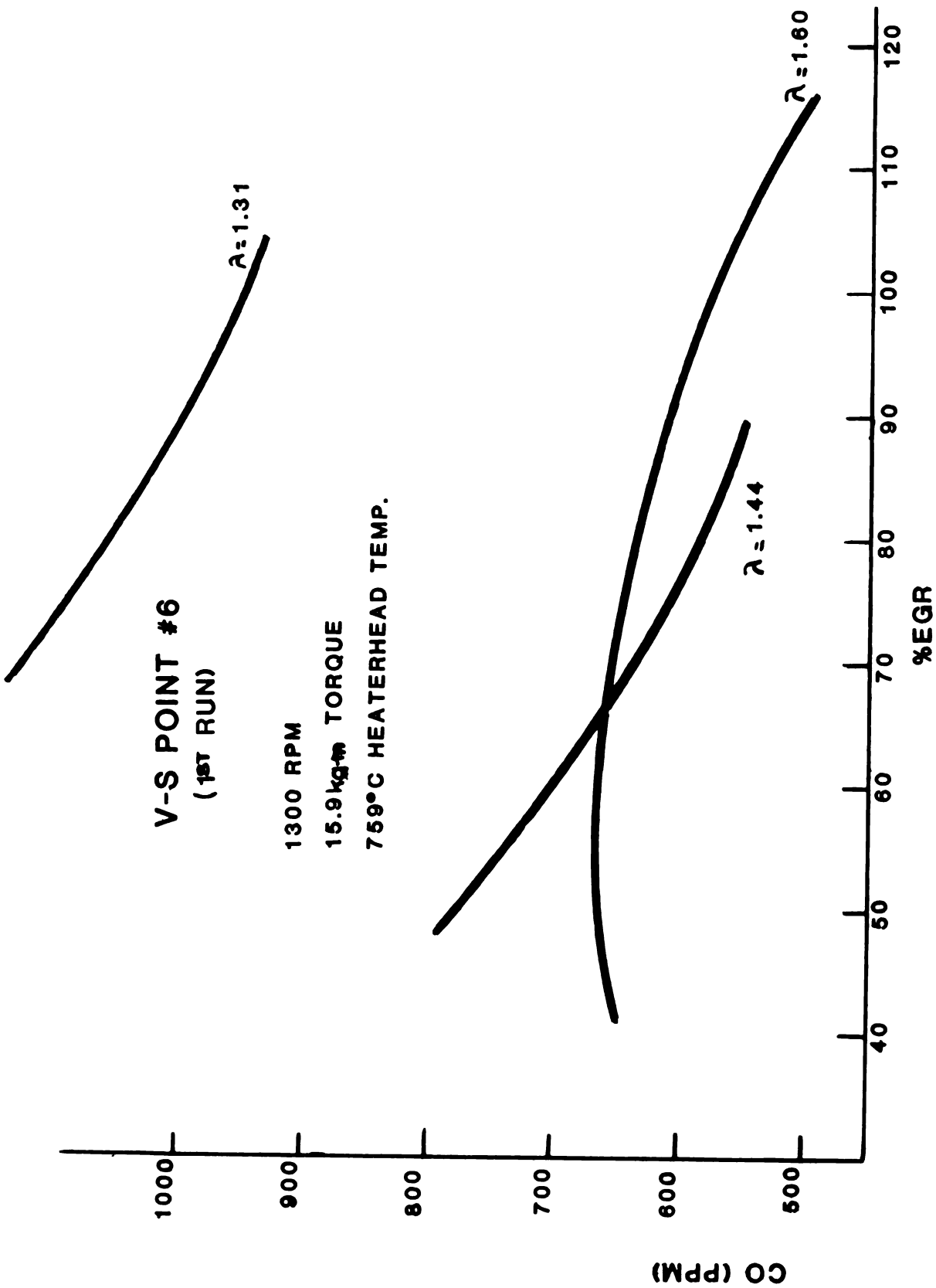
Figure 2.1-37   Vehicle Simulation Point #6 (1st run)

49

BURNER λ SHOWN IN PARENTHESES

1300 RPM

15.9 kg·m TORQUE

758°C HEATER HEAD TEMP.

$\lambda = 1.33$ (1.21)

$\lambda = 1.46$ (1.31)

$\lambda = 1.69$ (1.61)

%EGR

CO (PPM)
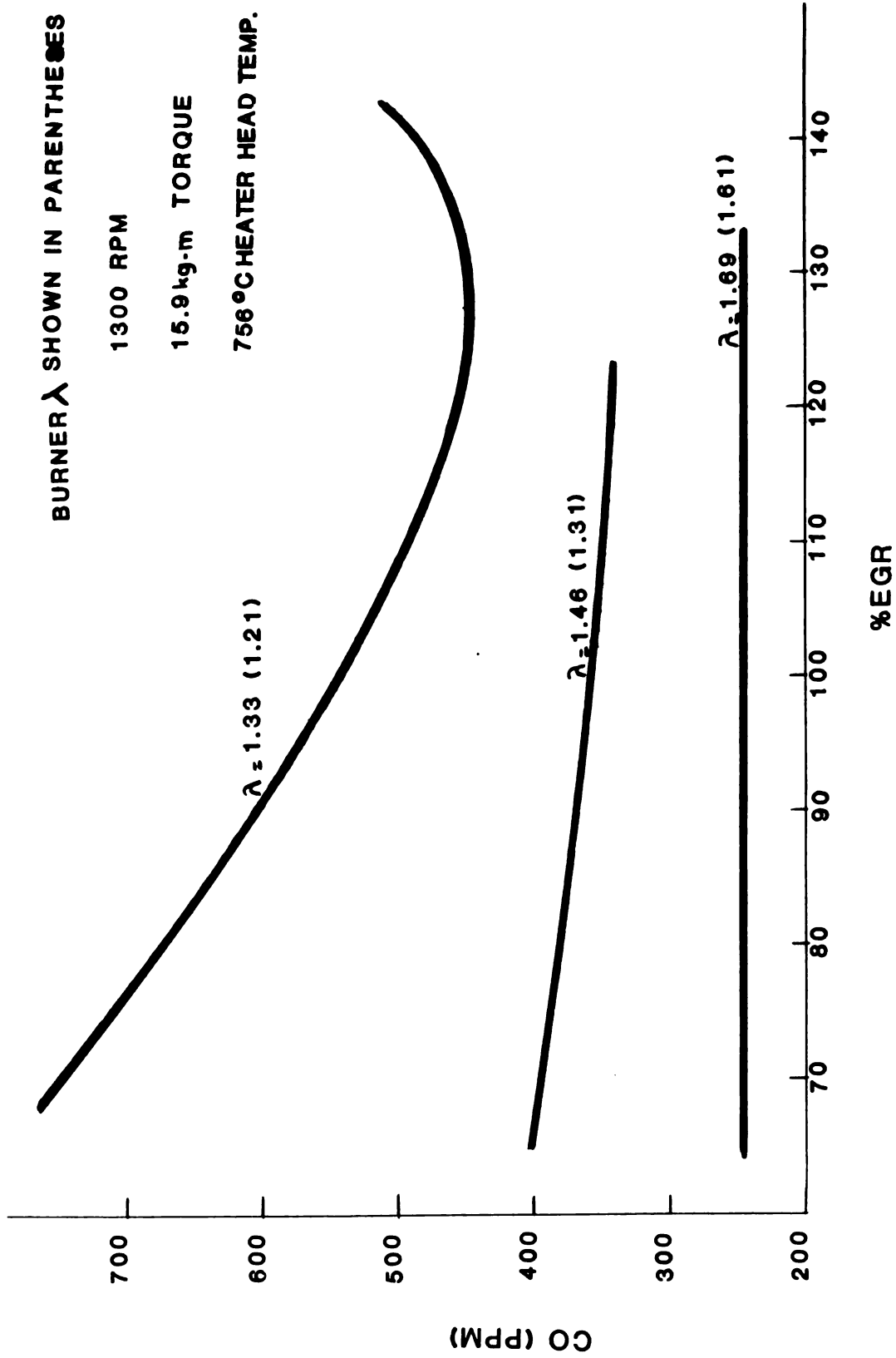
Figure 2.1-38 Vehicle Simulation Point #6 (2nd run)
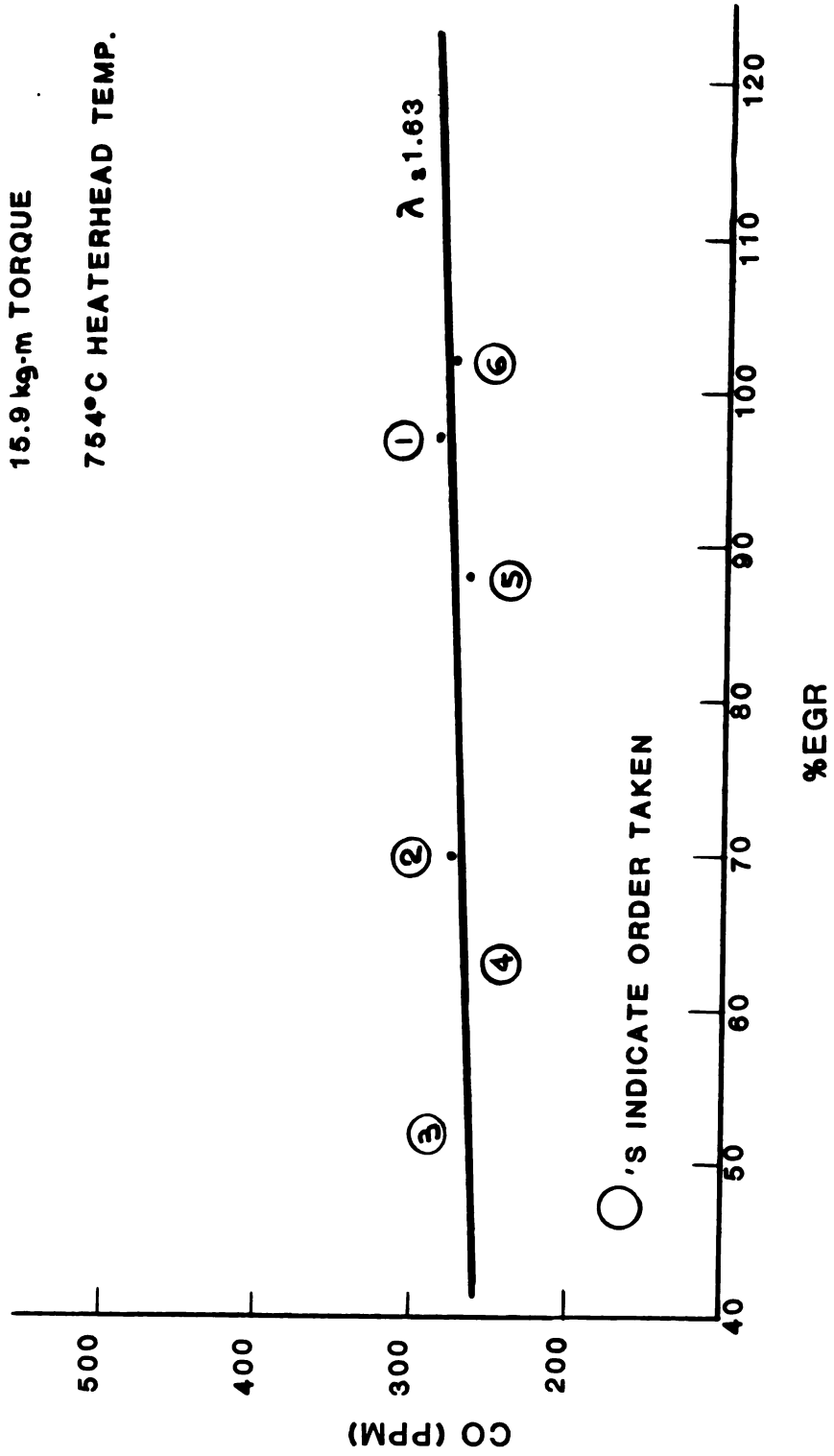
Figure 2.1-39   Vehicle Simulation Point #6 (3rd run)
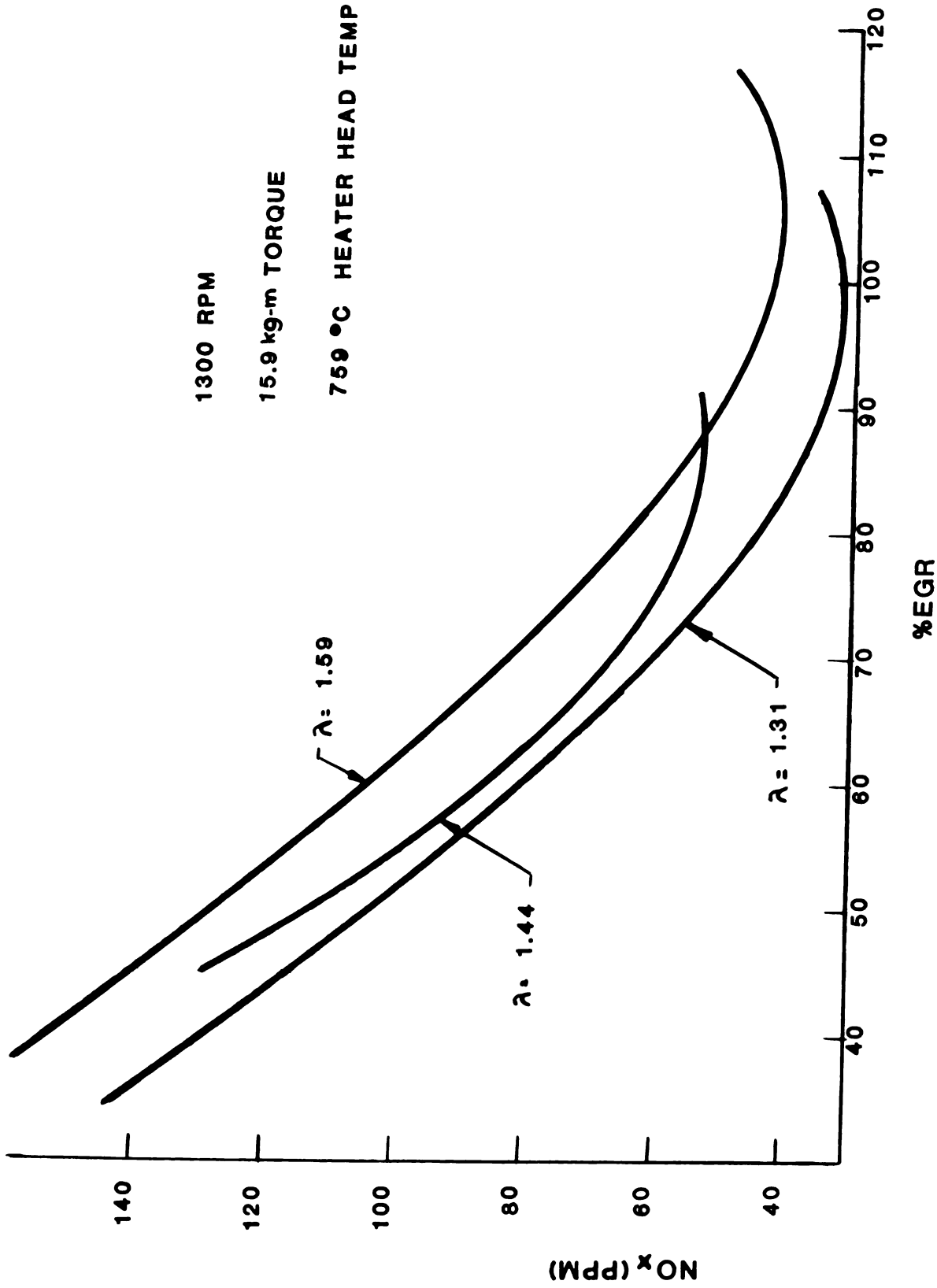
Figure 2.1-40   Vehicle Simulation Point #6 (1st run)

Chart details:
- 1300 RPM
- 15.9 kg-m TORQUE
- 759 °C HEATER HEAD TEMP
- Y-axis: NOₓ (PPM) — NO_x (PPM)
- X-axis: %EGR
- Curves labeled: $\lambda = 1.59$, $\lambda = 1.44$, $\lambda = 1.31$
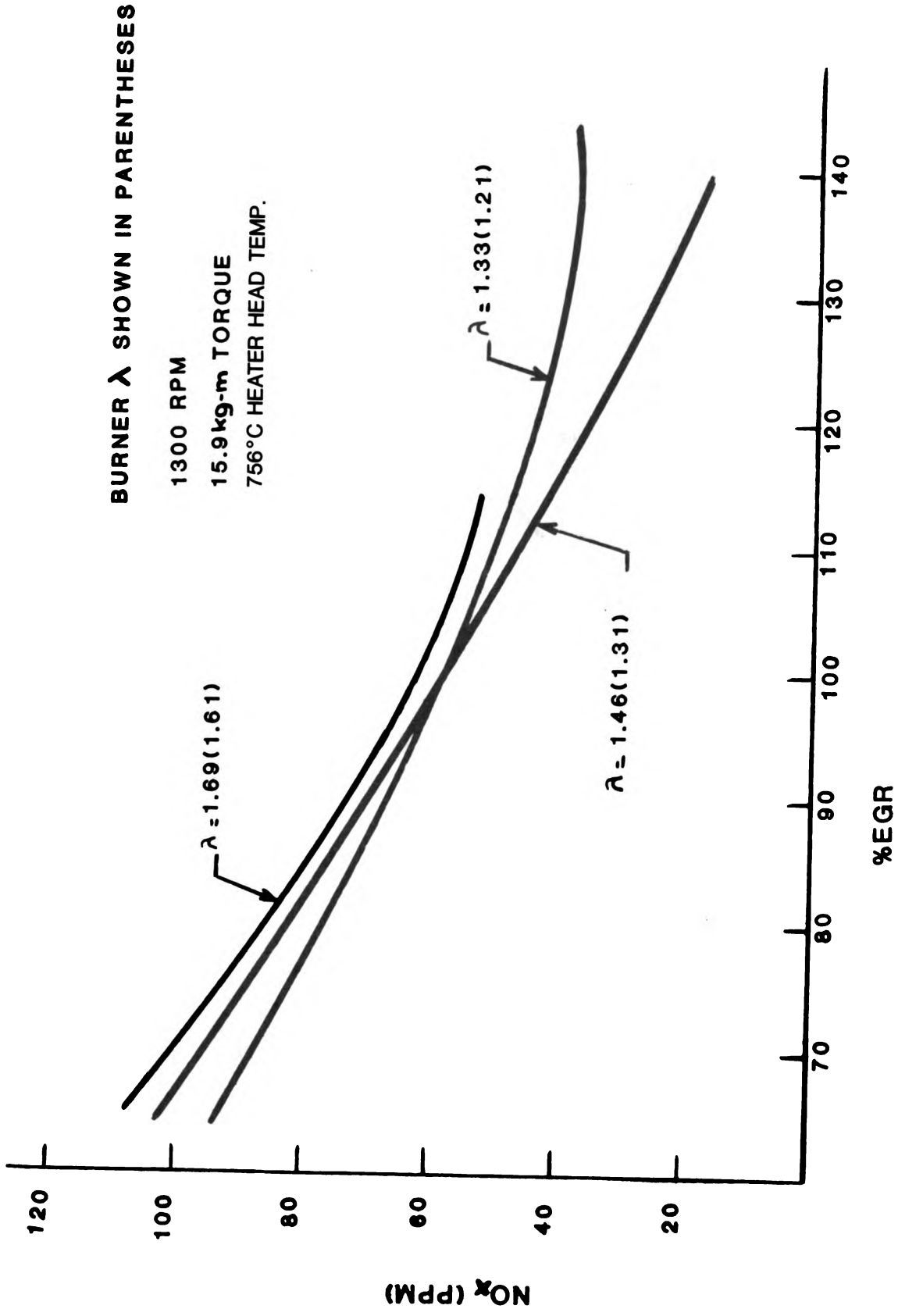
Figure 2.1-41   Vehicle Simulation Point #6 (2nd run)
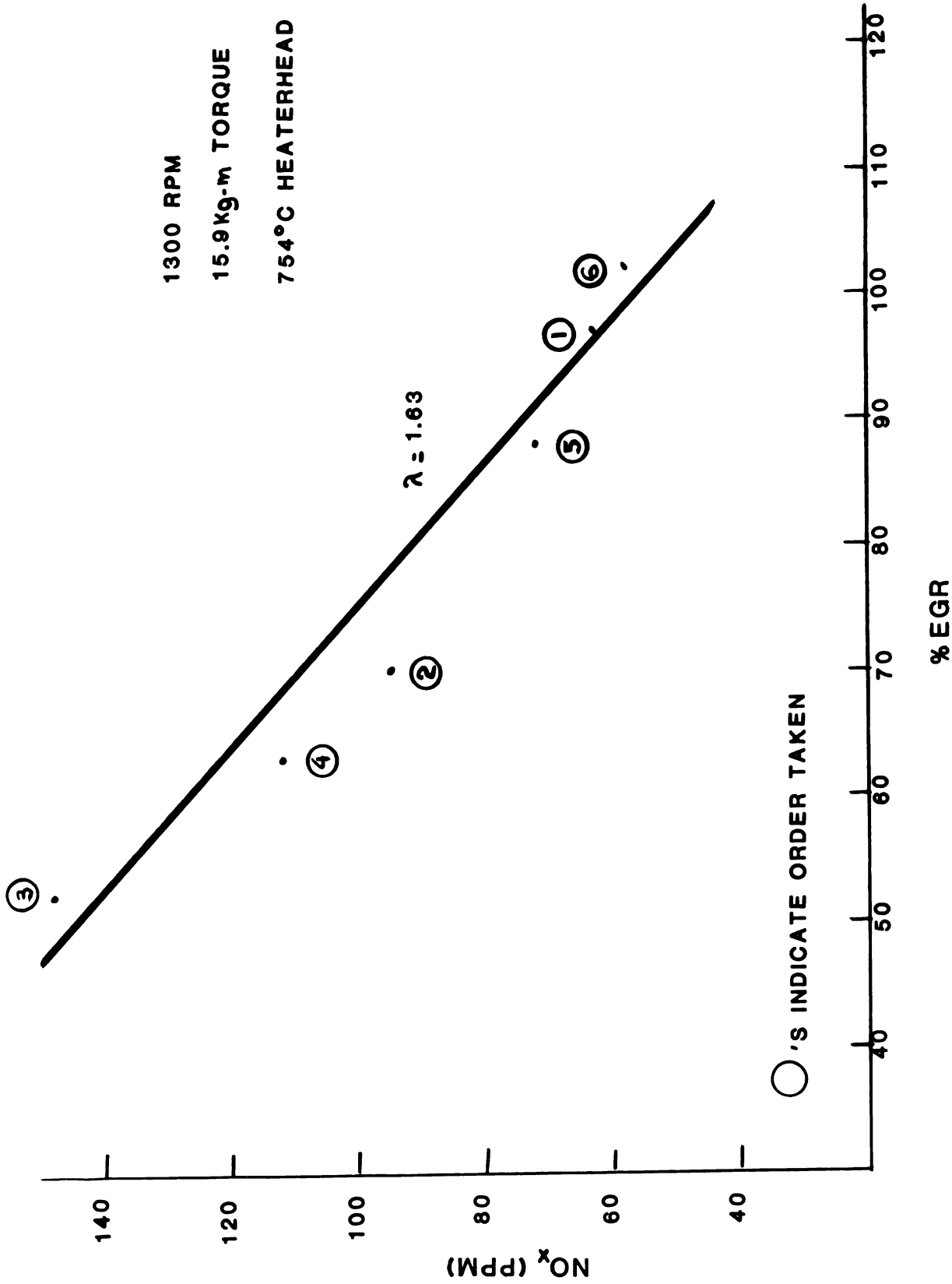
Figure 2.1-42   Vehicle Simulation Point #6 (3rd run)

54
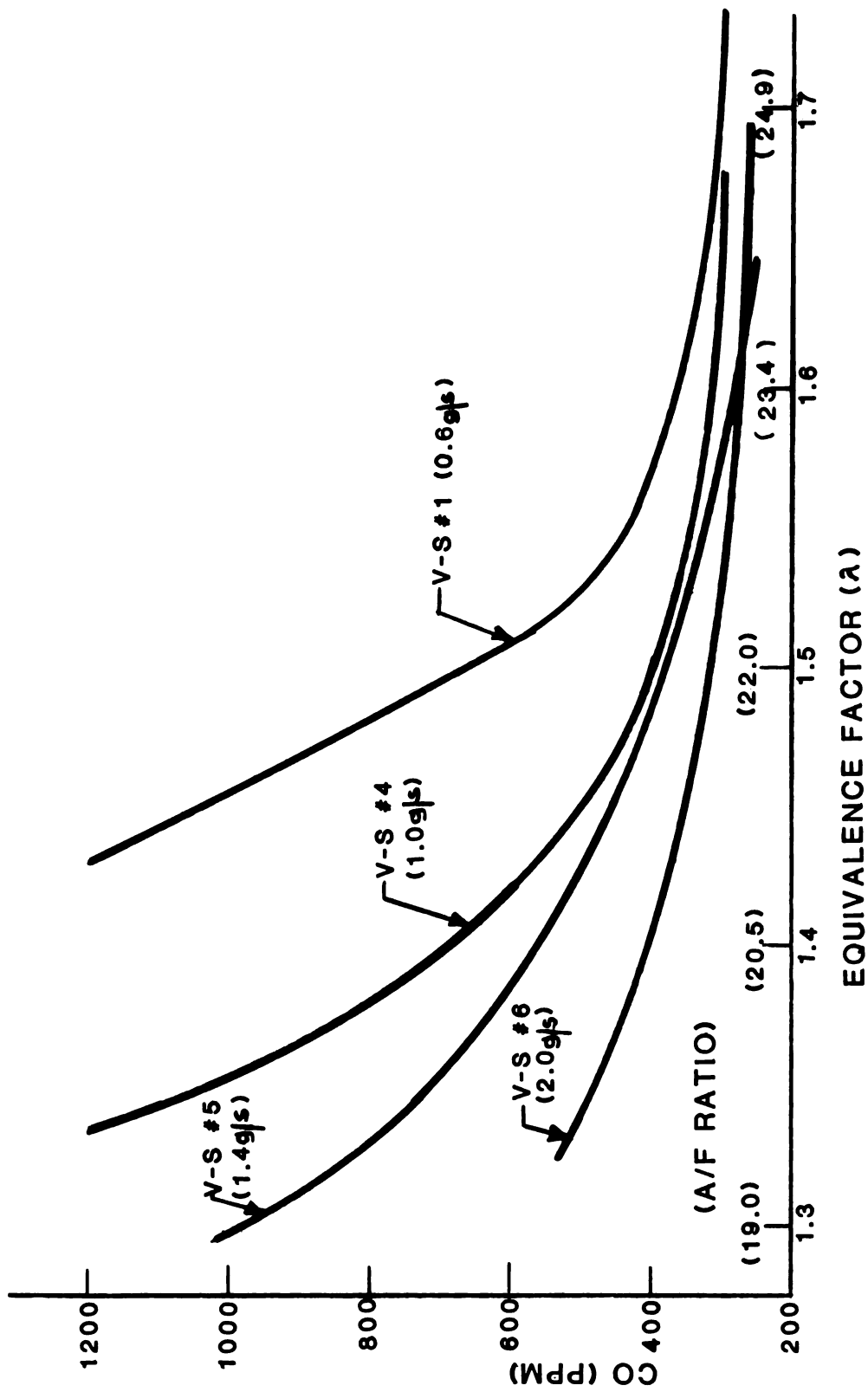
Figure 2.1-43   Exhaust CO vs. Air Equivalence (A/F Ratio)
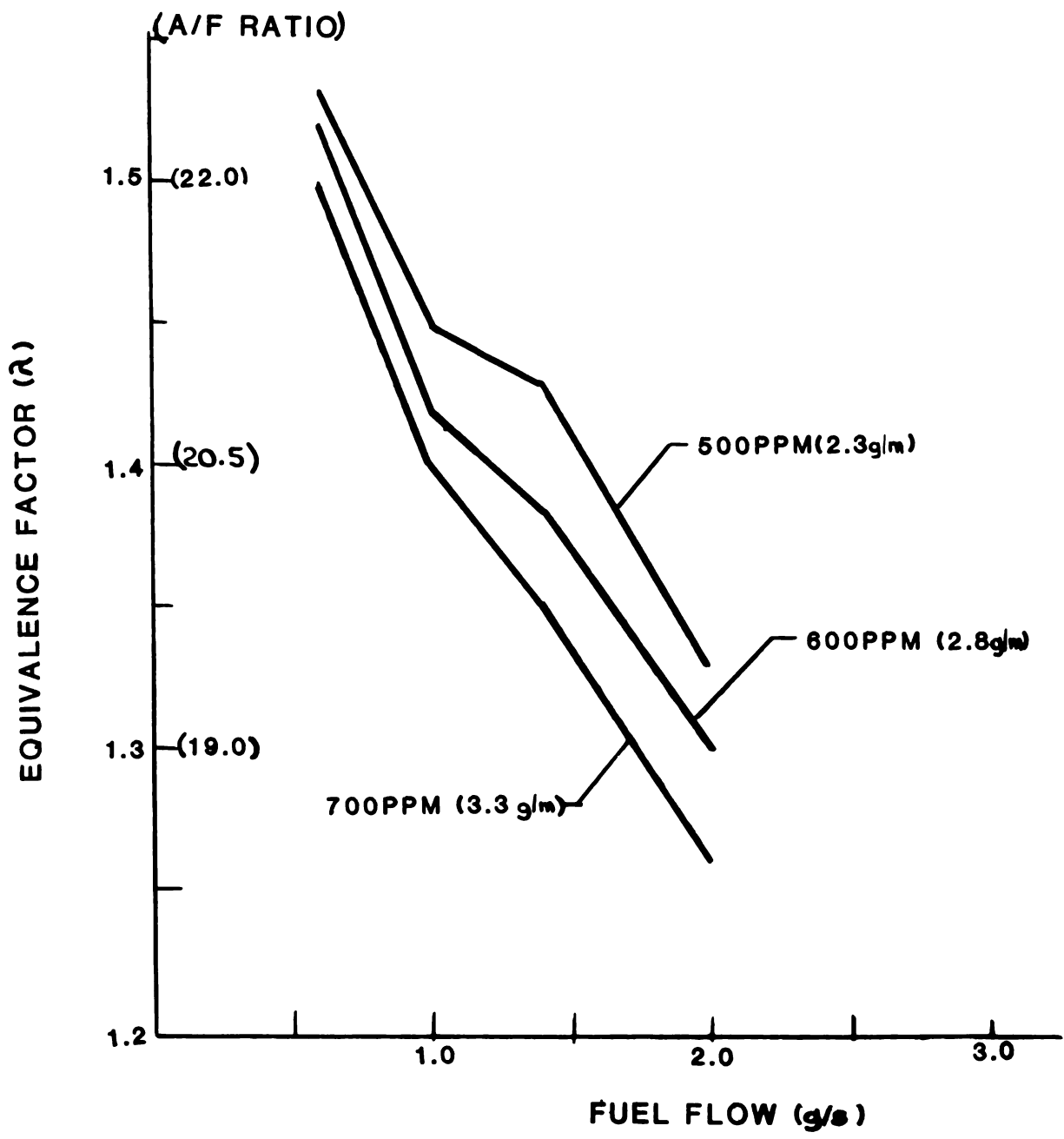
Figure 2.1-44   Air Equivalence (A/F Ratio) vs. Fuel Flow at Constant Exhaust CO

BURNER λ SHOWN IN PARENTHESES

λ = 1.40 (1.19)

λ = 1.49 (1.28)

λ = 1.61 (1.44)

λ = 1.64 (1.53)

5000
4000
3000
2000
1000

λ	%EGR
1.61	100
1.49	95
1.40	98
1.64	110
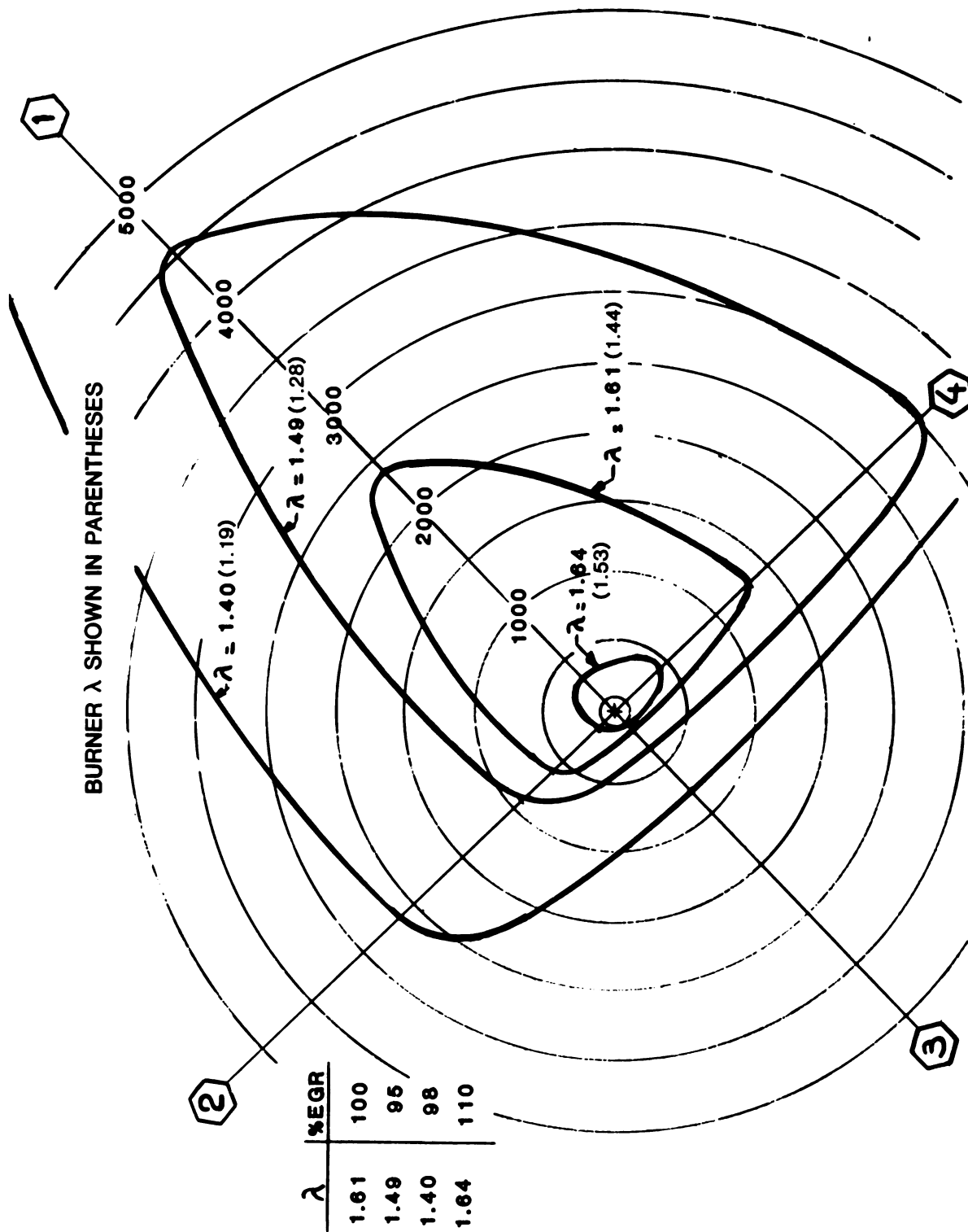
Figure 2.1-45   Burner CO (PPM) Vehicle Simulation Point #1

57
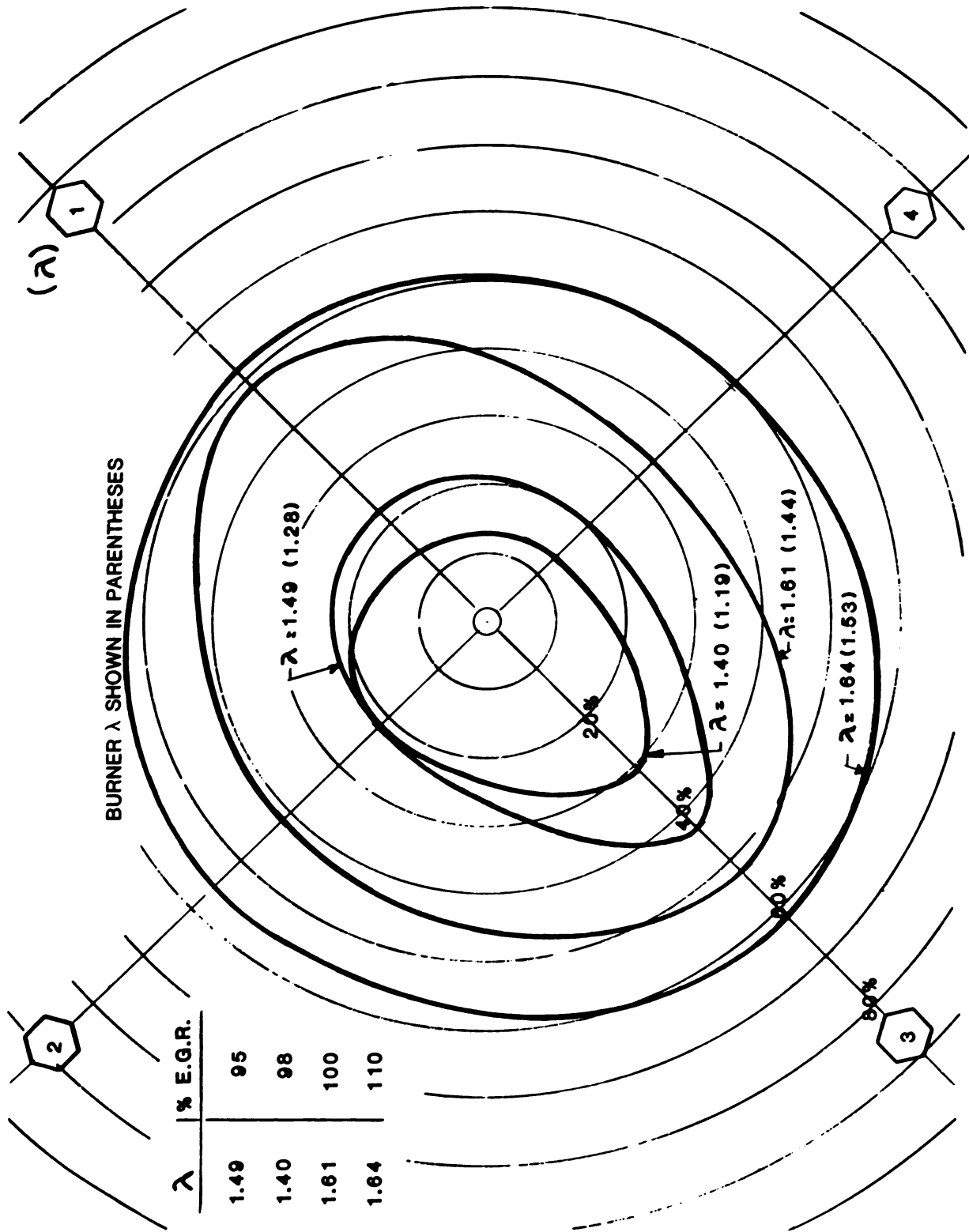
Figure 2.1-46   Burner Excess Air vs. Equivalence Ratio (λ) Vehicle Simulation Point #1

BURNER λ SHOWN IN PARENTHESES

$\lambda = 1.49$ (1.28)
$\lambda = 1.40$ (1.19)
$\lambda = 1.61$ (1.44)
$\lambda = 1.64$ (1.53)

20%
40%
60%
80%

λ	% E.G.R.
1.49	95
1.40	98
1.61	100
1.64	110

58
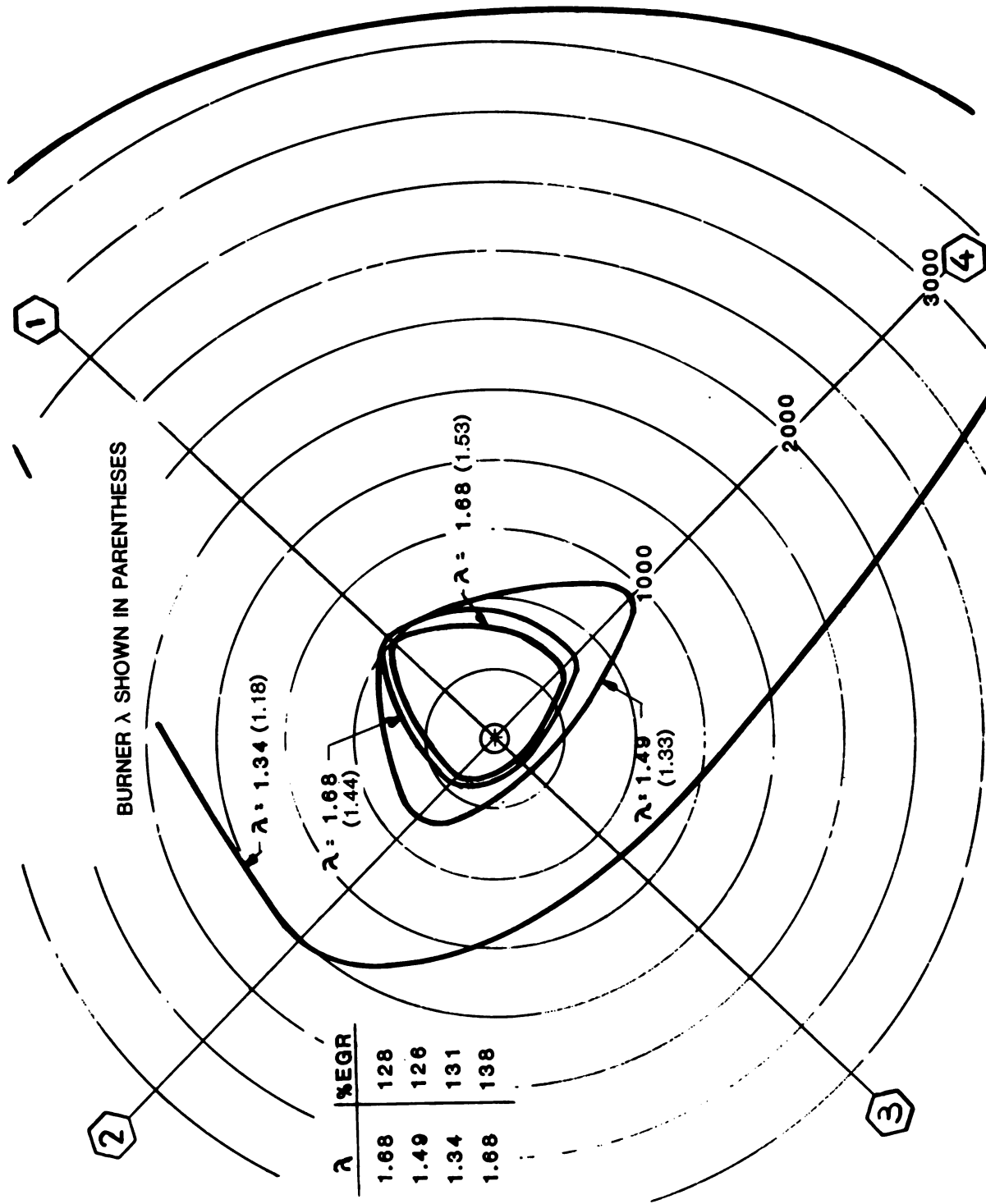
Figure 2.1-47   Burner CO (PPM) Vehicle Simulation Point #4

BURNER λ SHOWN IN PARENTHESES

λ = 1.68 (1.53)

λ = 1.34 (1.18)

λ = 1.68 (1.44)

λ = 1.49 (1.33)

λ	%EGR
1.68	128
1.49	126
1.34	131
1.68	138

59

V-S POINT #4

BURNER λ SHOWN IN PARENTHESES

λ = 1.68(1.53)

λ = 1.68(1.44)

λ = 1.49(1.33)

λ = 1.34(1.18)

20%

40%

60%

λ	%EGR
1.68	128
1.49	126
1.34	131
1.68	134
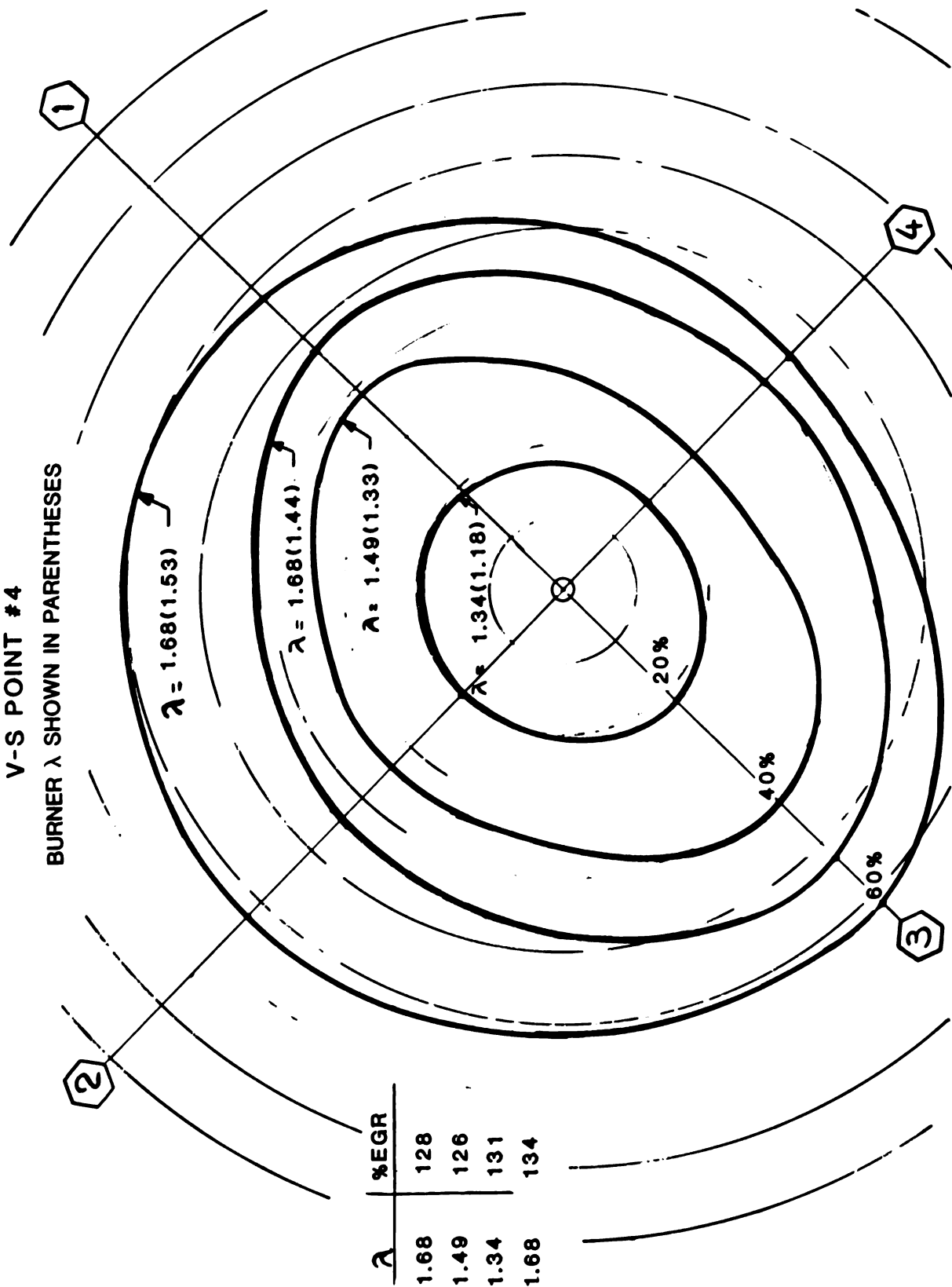
Figure 2.1-48   Burner Excess Air vs. Equivalence Ratio (λ)

BURNER λ SHOWN IN PARENTHESES

λ = 1.31(1.15)

λ =1.43(1.26)

λ =1.31(1.15)

8000

6000

4000

2000

λ	%EGR
1.31	92
1.43	107
1.60	103
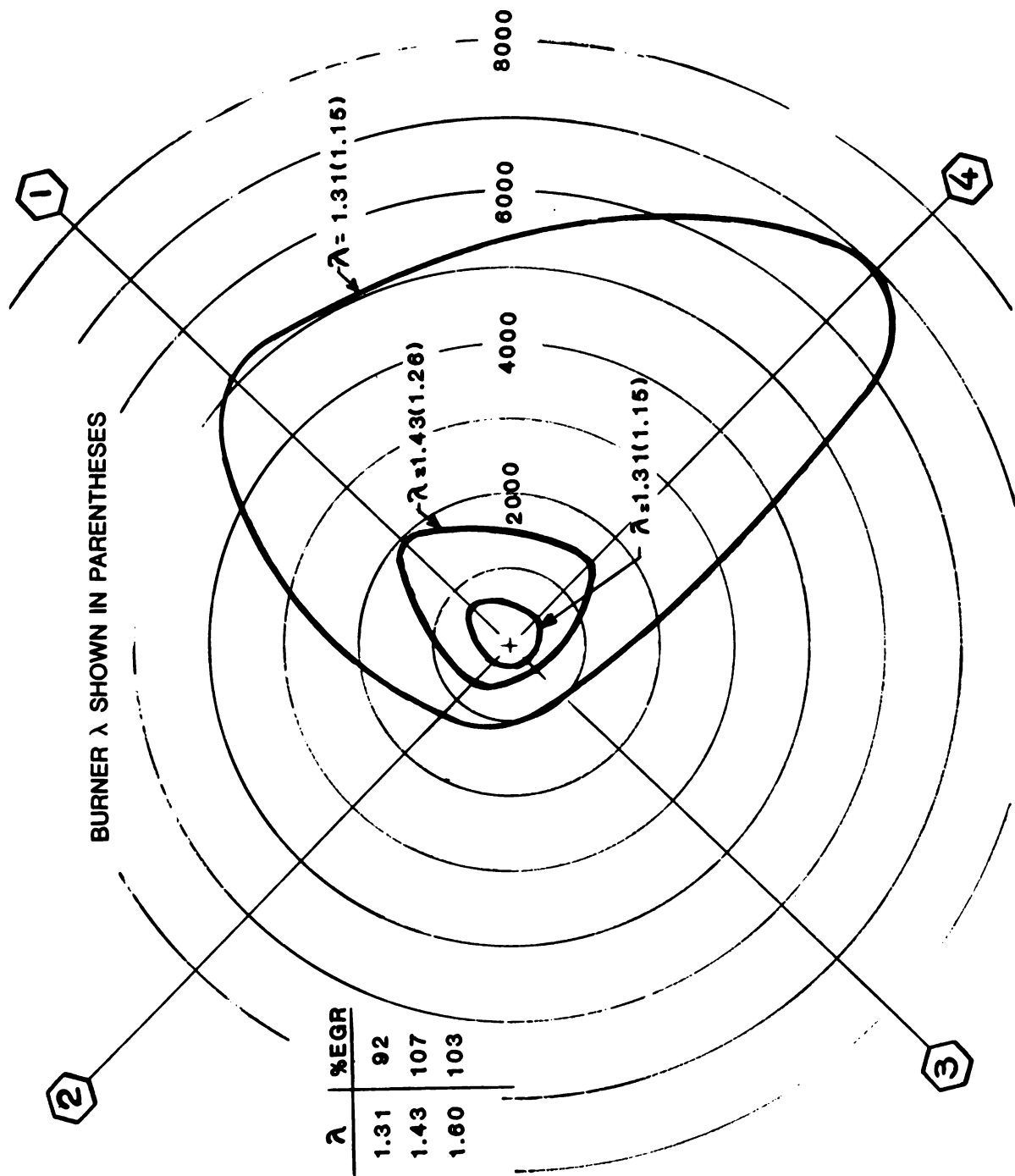
Figure 2.1-49   Burner CO (PPM) V-S Point #5 (2nd run)   (λ)

61
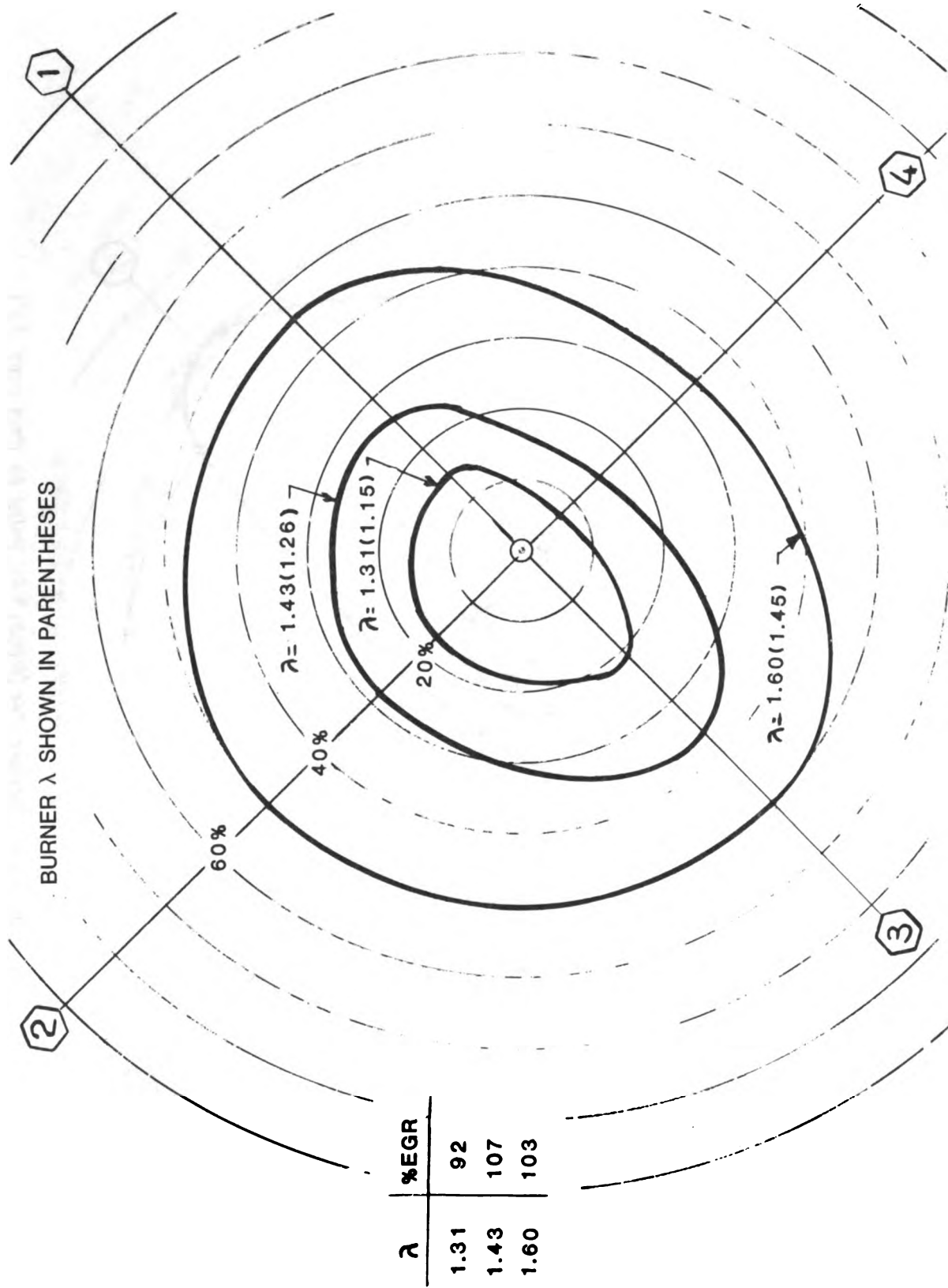
Figure 2.1-50   Burner Excess Air vs. Equivalence Ratio (λ) V-S Points #5 (2nd run)

λ	%EGR
1.31	92
1.43	107
1.60	103

BURNER λ SHOWN IN PARENTHESES

λ= 1.43(1.26)
λ= 1.31(1.15)
λ= 1.60(1.45)

20%
40%
60%

62

BURNER λ SHOWN IN PARENTHESES

λ= 1.32(1.19)

λ= 1.44(1.27)

λ= 1.61(1.36)

20%

40%

60%

λ	% EGR
1.61	116
1.44	105
1.32	90
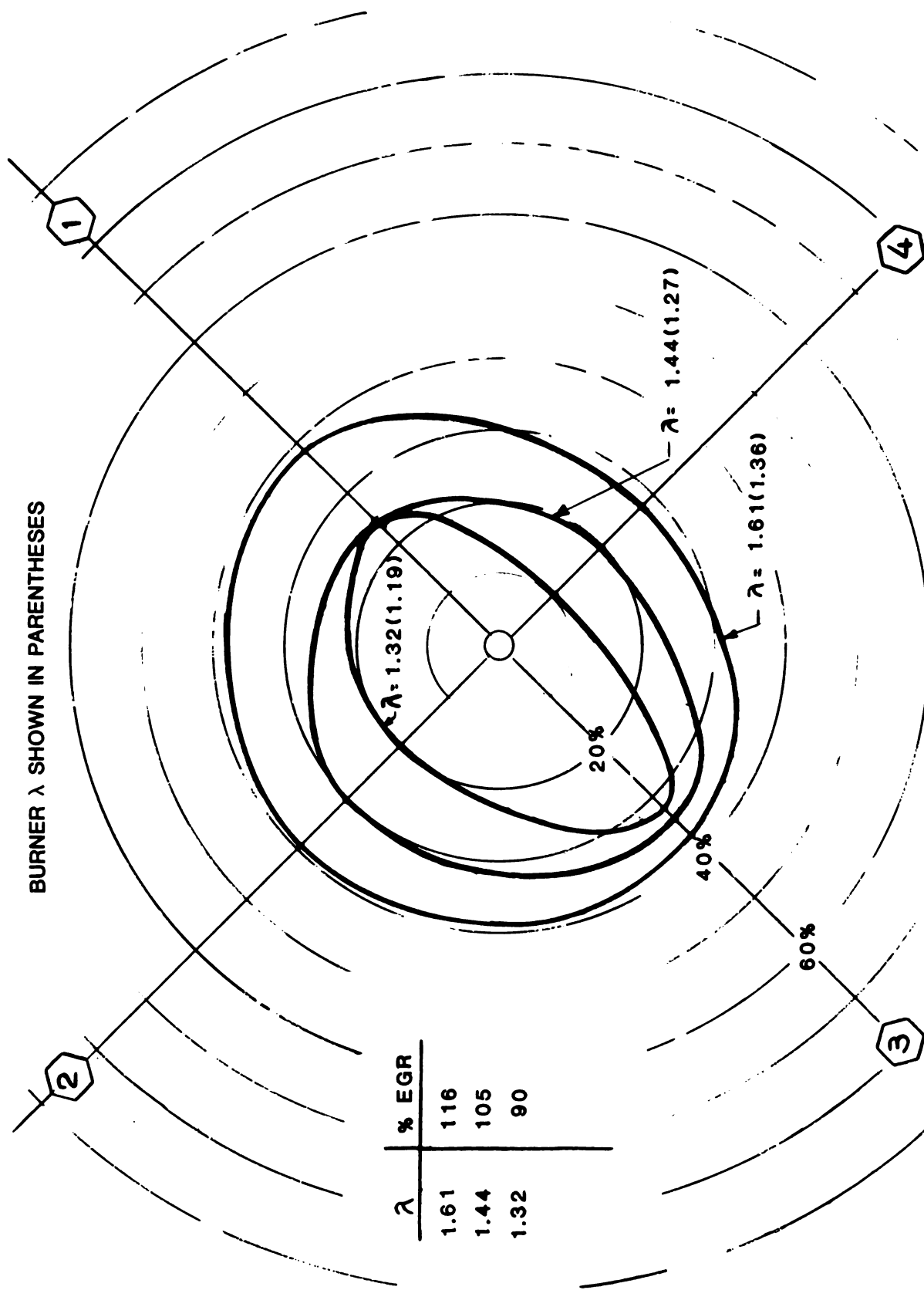
Figure 2.1-51   Burner Excess Air vs. Equivalence Ratio (λ) V-S Points #6 (1st run)

63
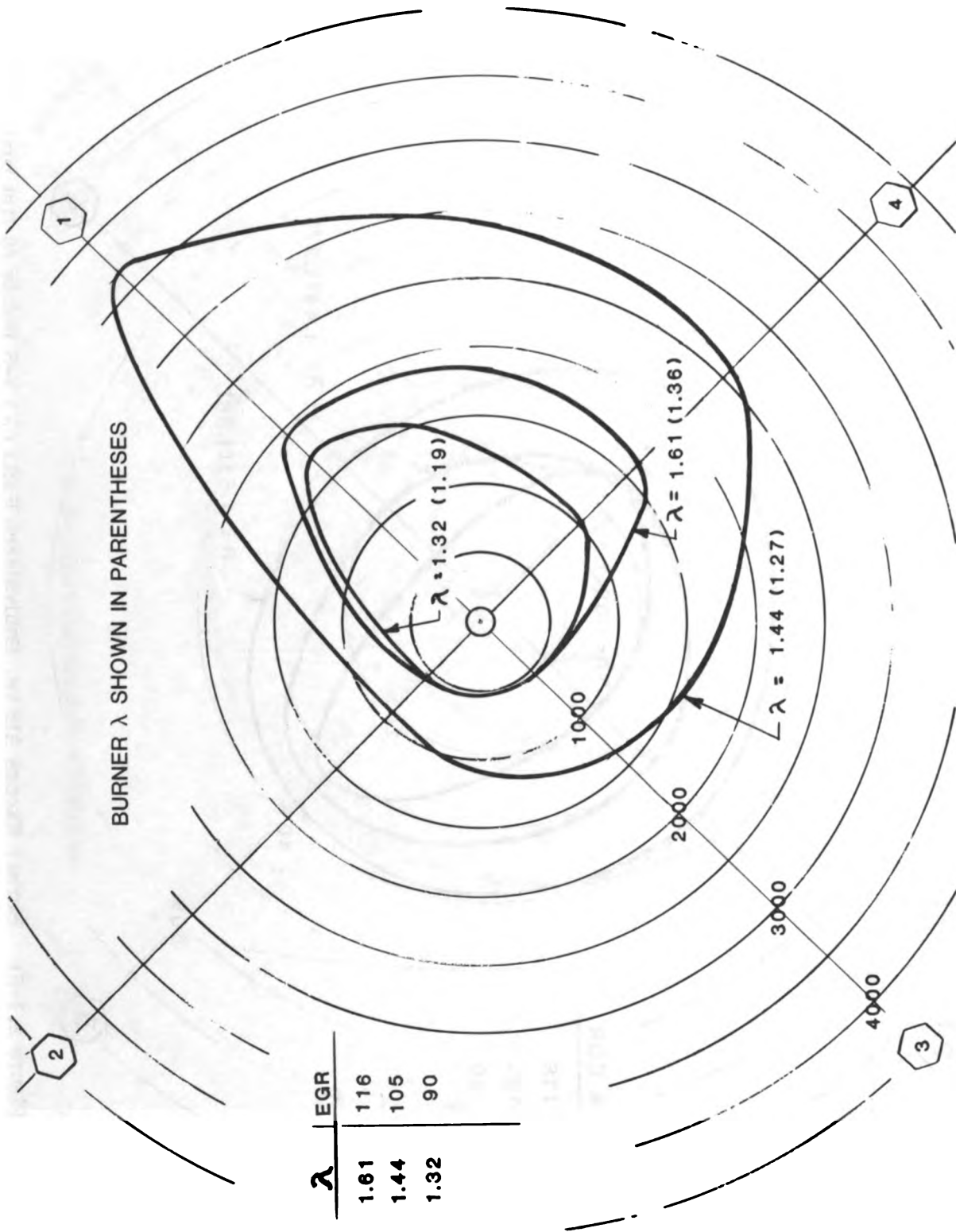
Figure 2.1-52   Burner CO (PPM) V-S Point #6 (1st run)

BURNER λ SHOWN IN PARENTHESES

λ = 1.32 (1.19)

λ = 1.61 (1.36)

λ = 1.44 (1.27)

1000

2000

3000

4000

λ	EGR
1.61	116
1.44	105
1.32	90
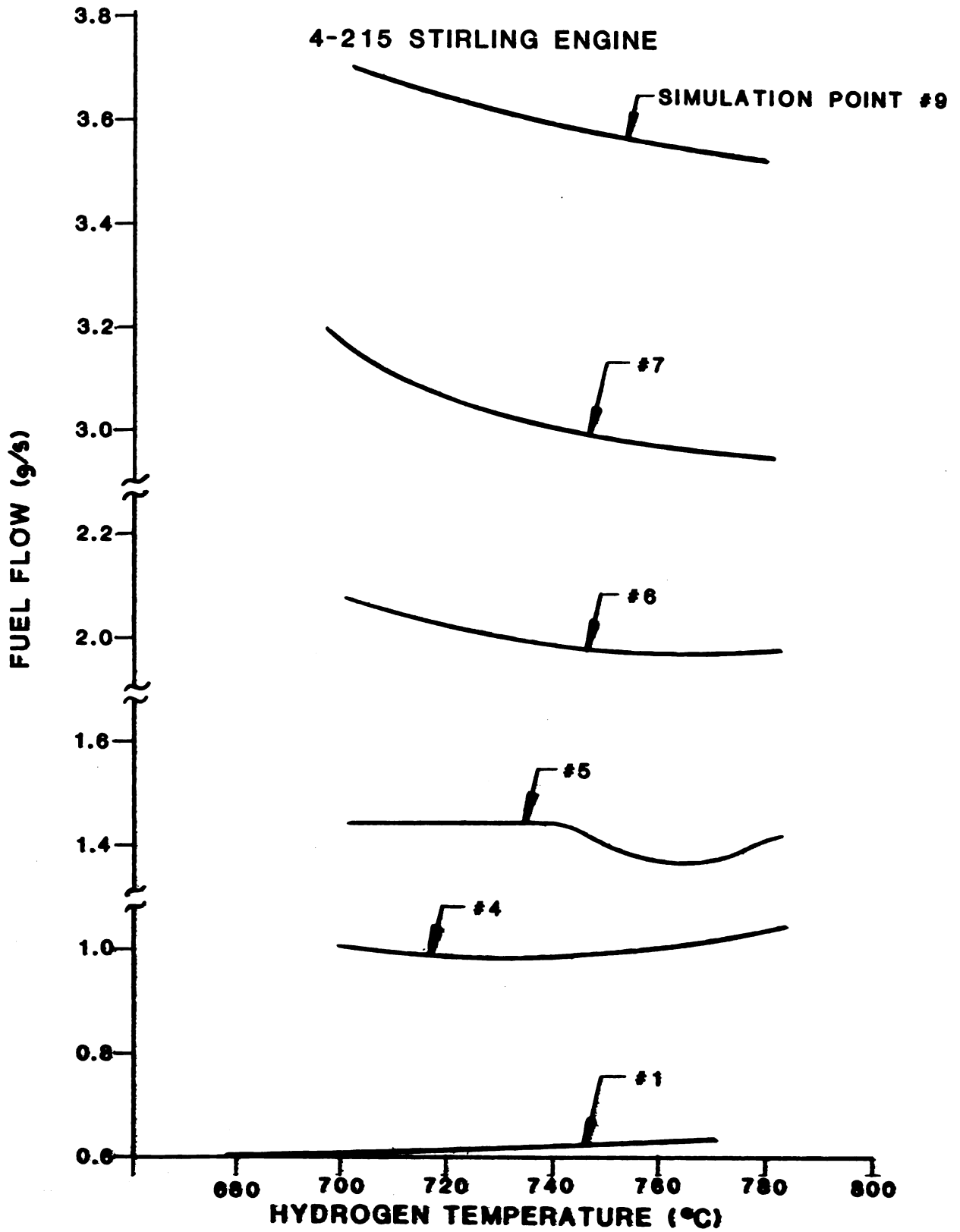
Figure 2.1-53   Fuel Flow vs. Hydrogen Temperature
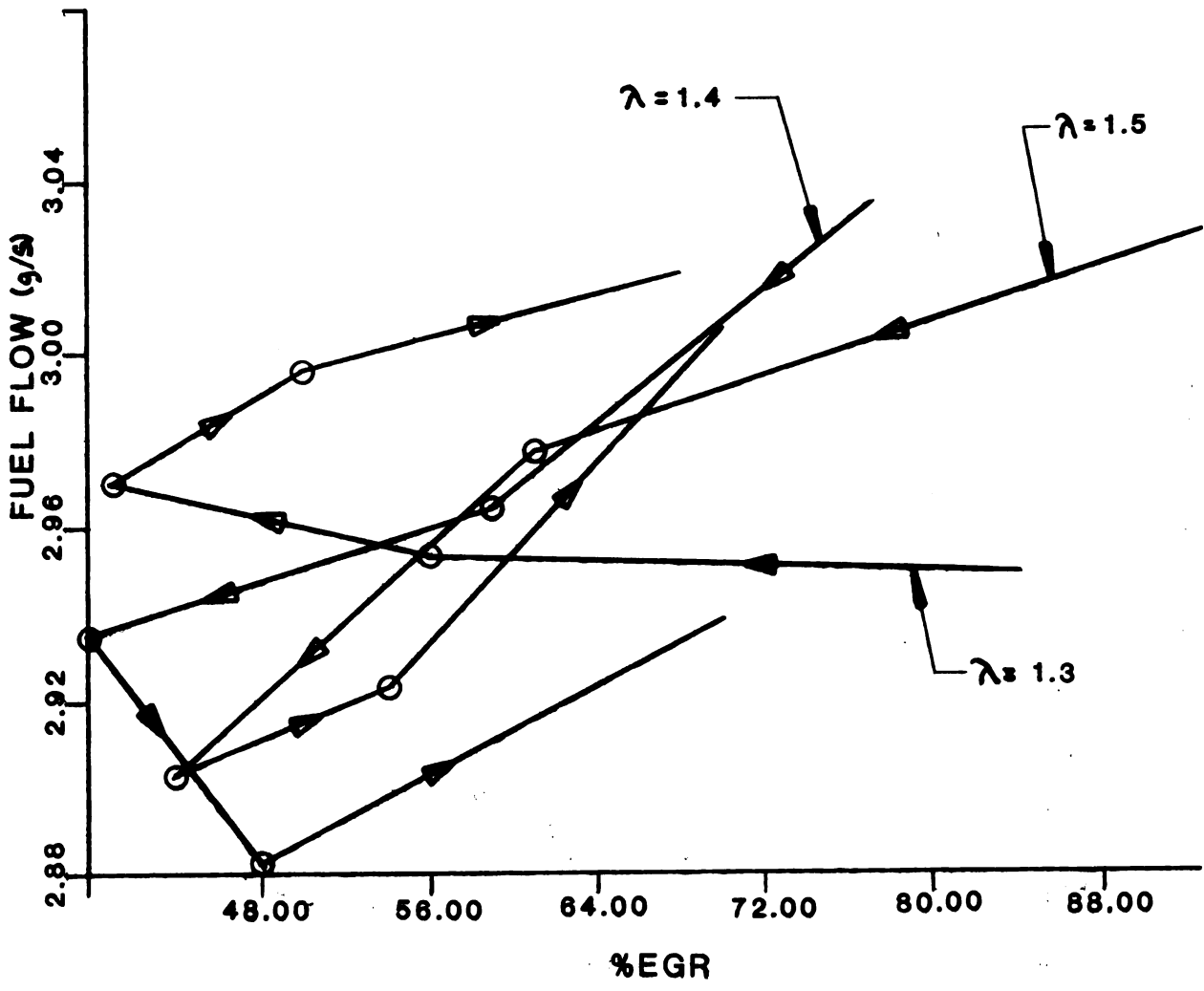
Figure 2.1-54   Vehicle Simulation Point #7
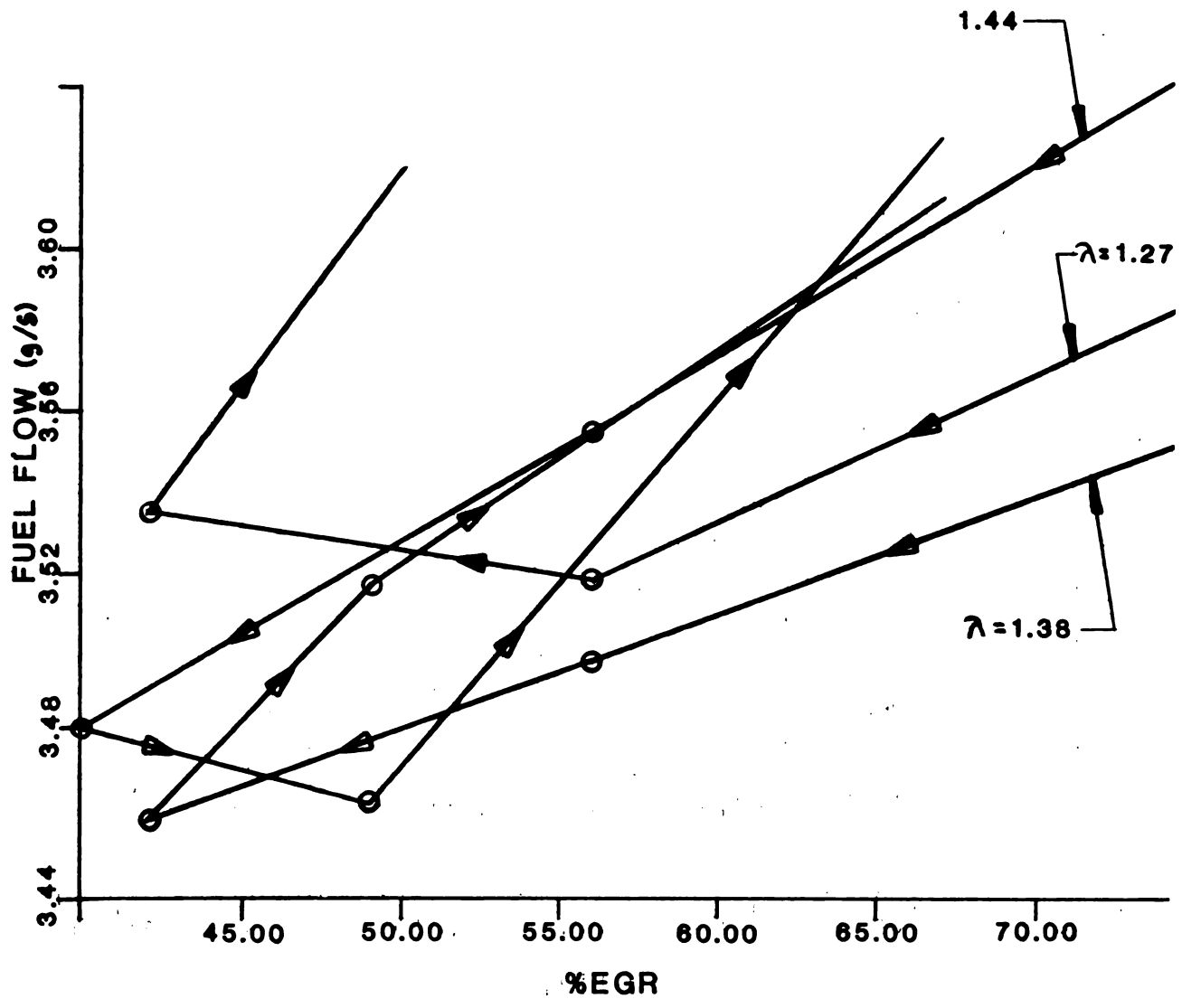
Figure 2.1-55   Vehicle Simulation Point #9
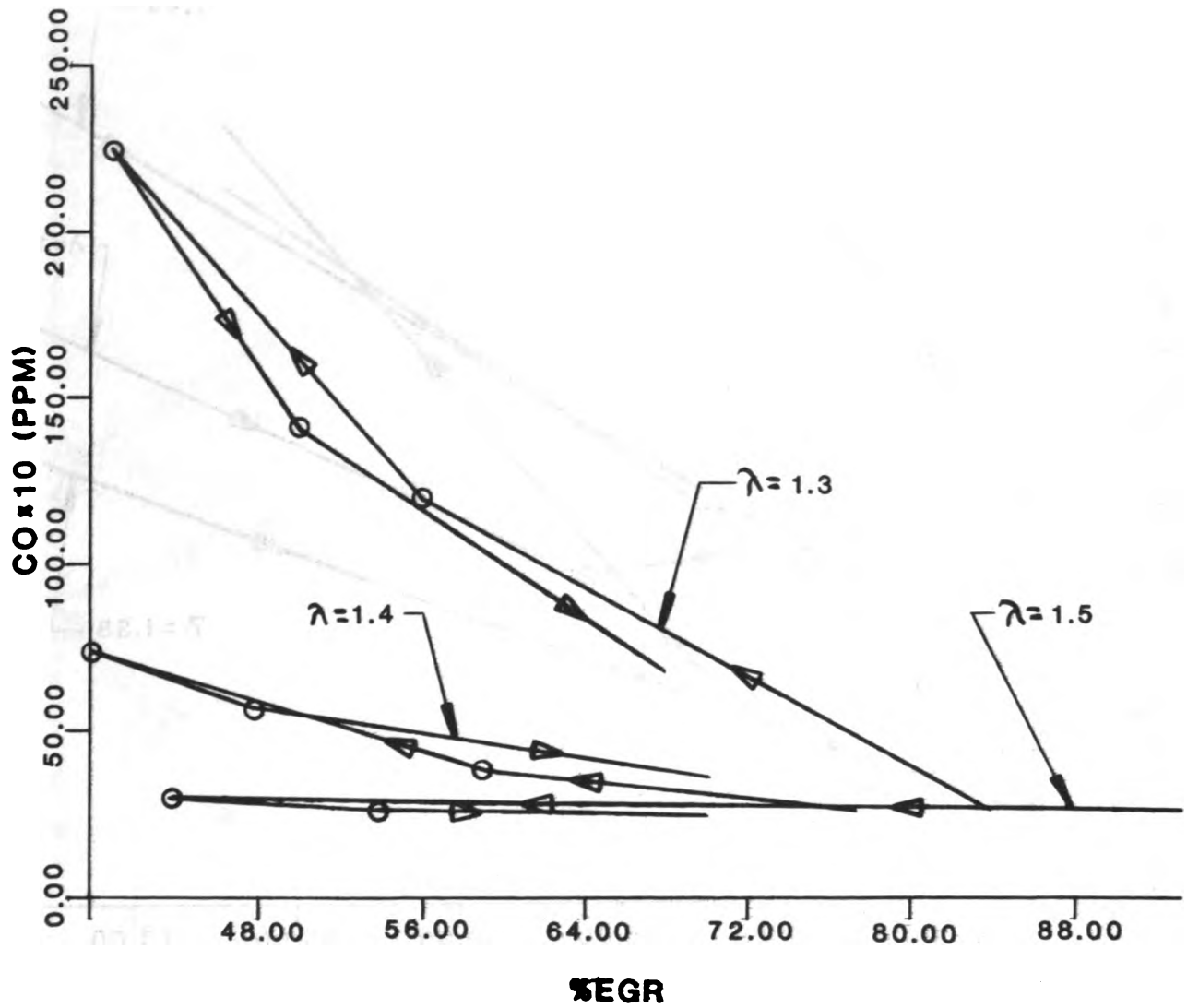
Figure 2.1-56   Vehicle Simulation Point #7
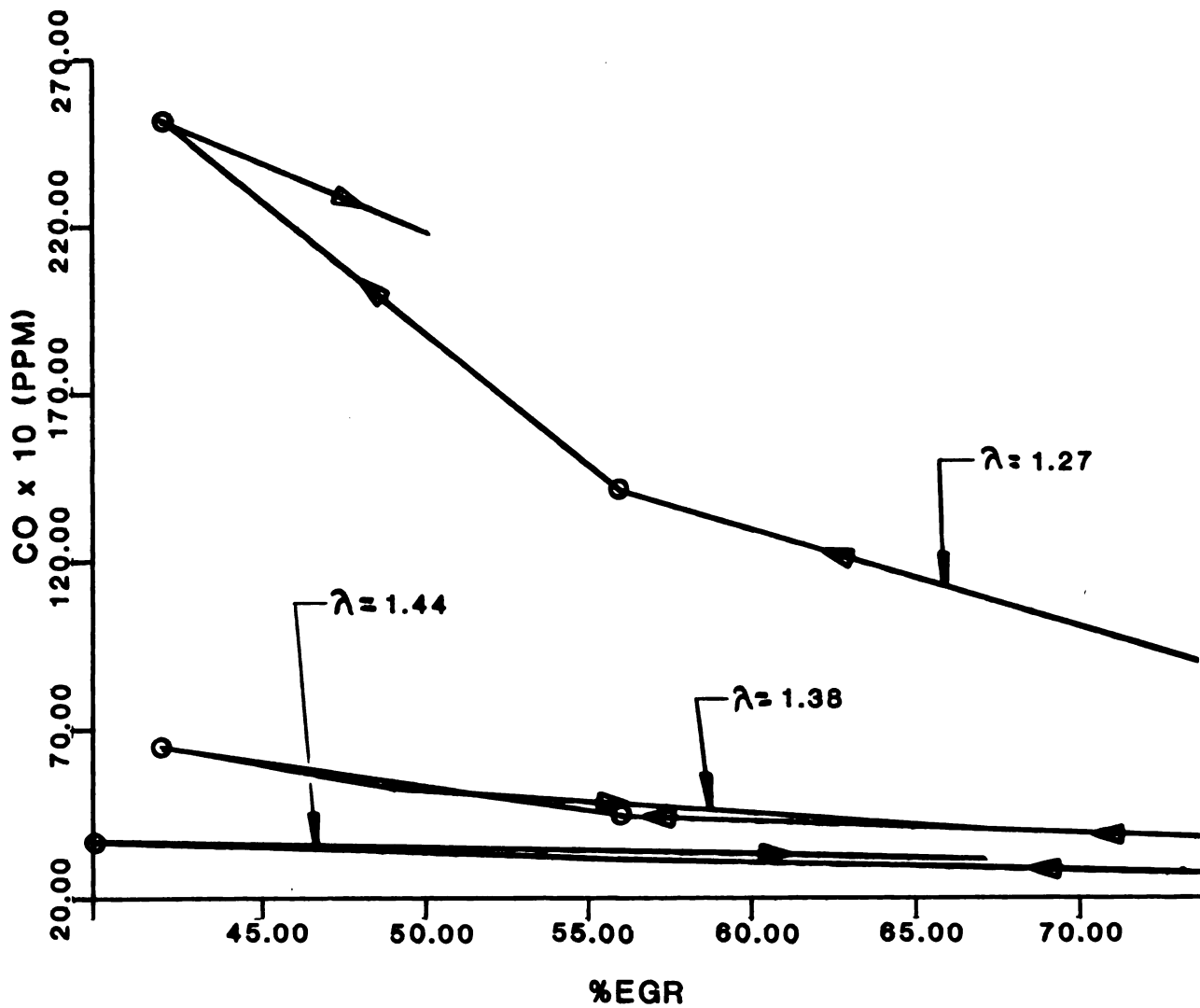
Figure 2.1-57   Vehicle Simulation Point #9
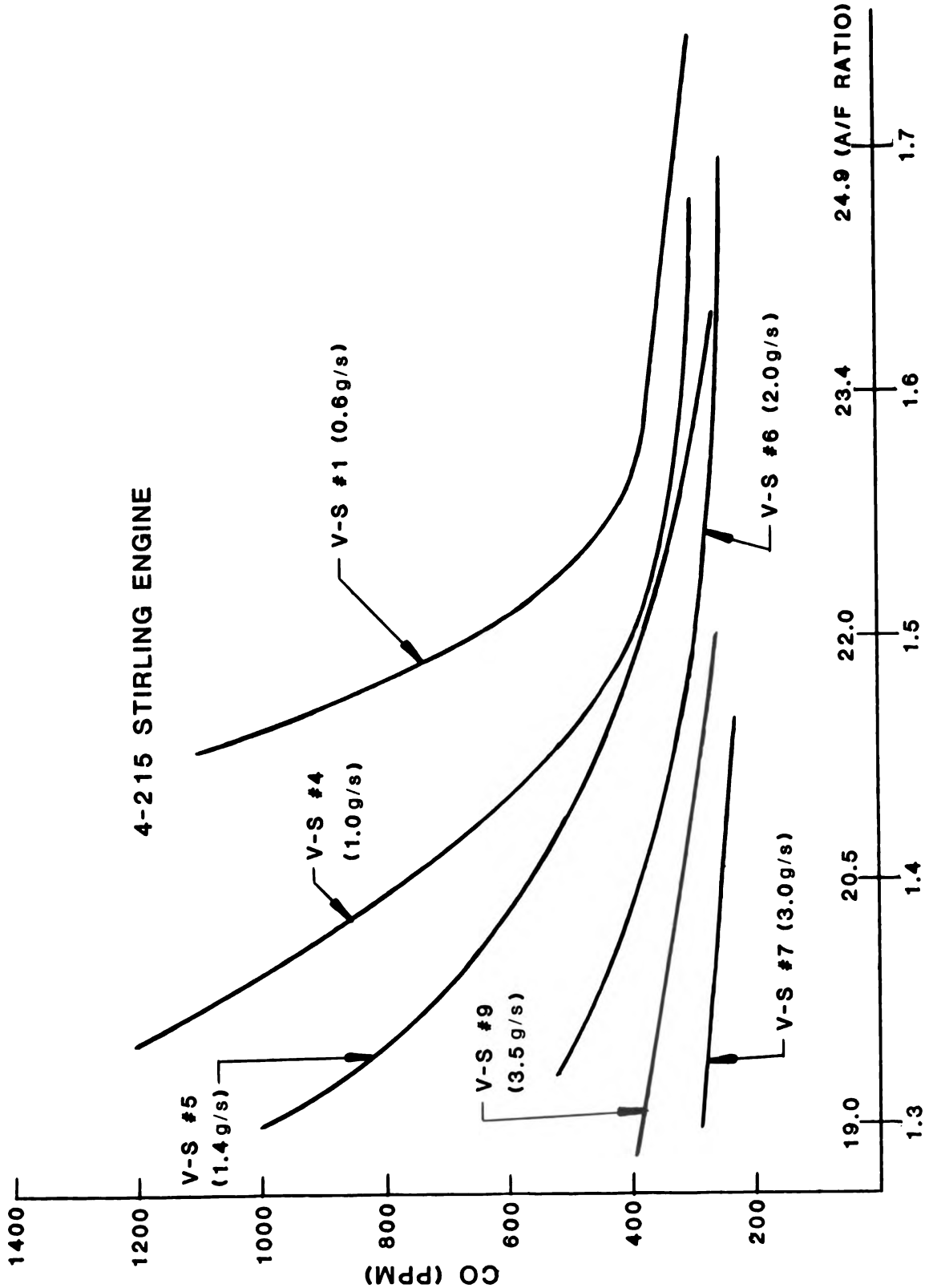
Figure 2.1-58   Exhaust CO vs. Equivalence Ratio (A/F Ratio)
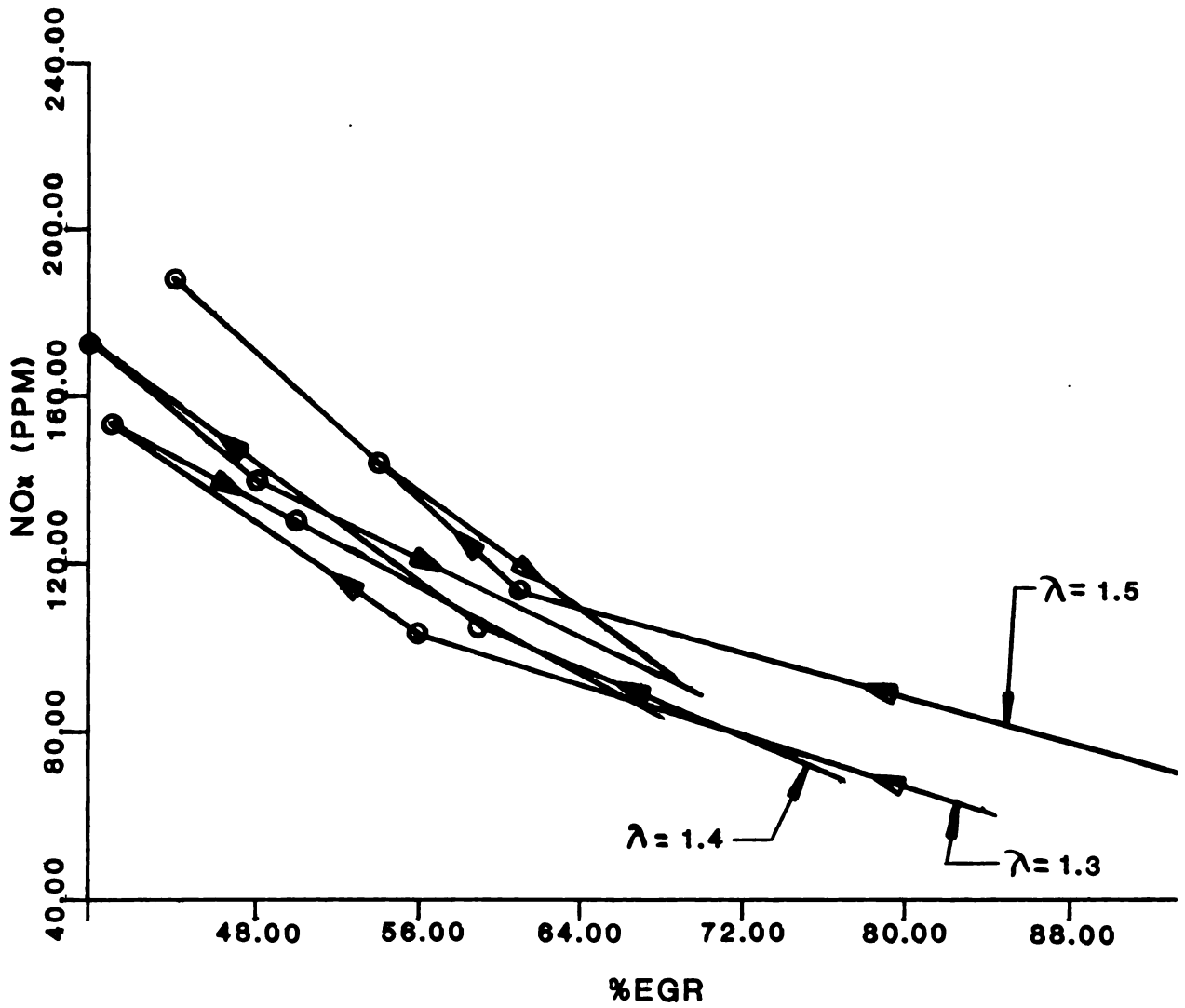
Figure 2.1-59   Vehicle Simulation Point #7
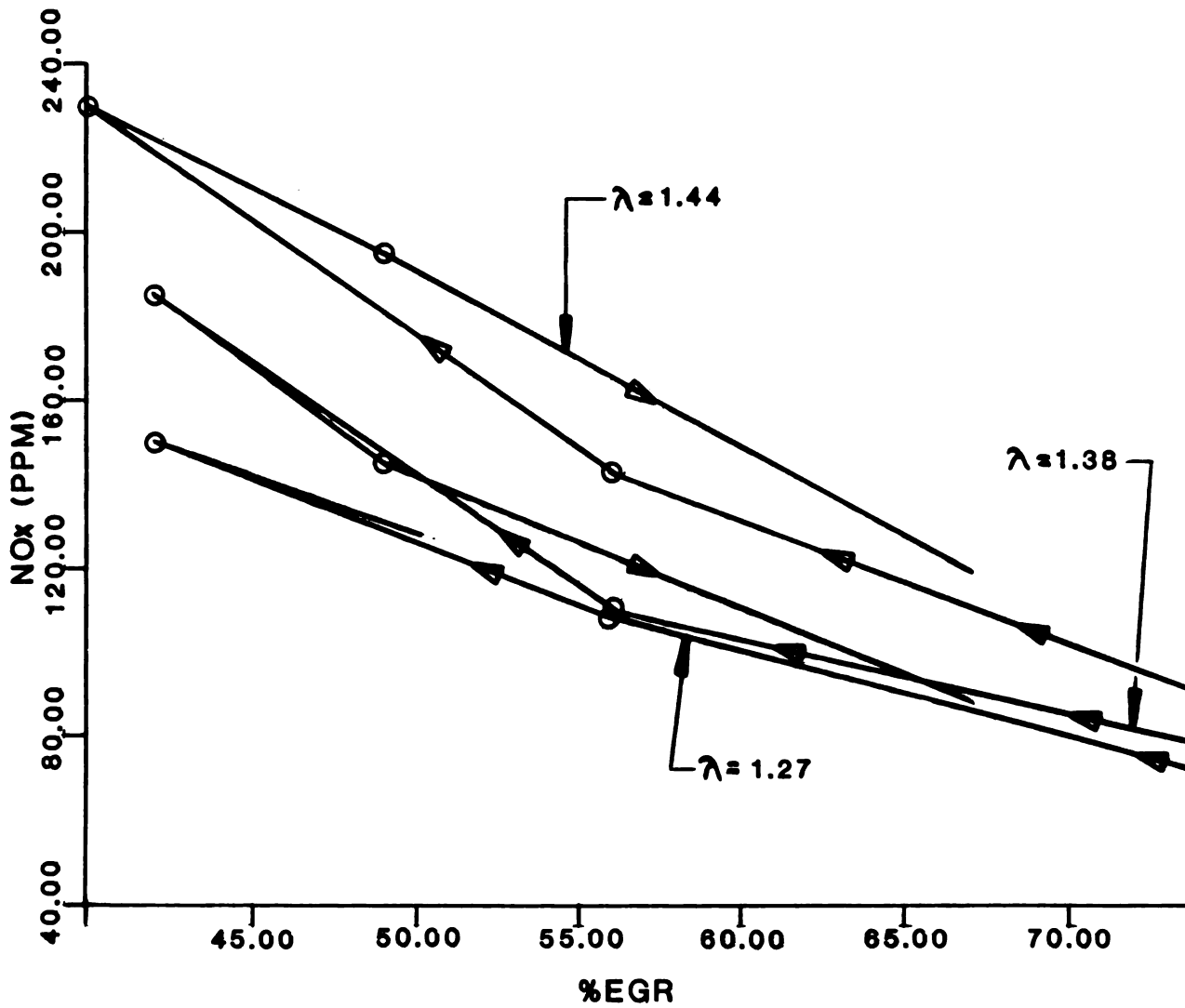
Figure 2.1-60   Vehicle Simulation Point #9

2.2 Burner System

Work in this area was undertaken in order to define what changes would have to be made in the current burner hardware so that reductions in burner system pressure drop and improvements in heater head temperature distribution could be realized. Reducing the total pressure drop through the combustion system was recognized to be an important factor in lowering blower power consumption and improving fuel economy. Likewise, it was judged that improving the heater head temperature distribution would contribute to a more stable and consistent control system operation, thereby improving engine performance while minimizing fuel flow fluctuations. For the 4-215 engine, it has been shown that the best fuel economy is obtained when the engine is operated with inside heater tube wall temperatures of 750°C, the original design value. Temperature excursions on either side of this value tend to reduce operating efficiency by either lowering the temperature difference between the hot and cold spaces of the engine, or by increasing thermal conduction losses.

Therefore, the objective of this section was to determine the fuel economy improvements associated with minimizing the combustion gas pressure drop through the burner and achieving a combustion gas flow pattern such that the heater head temperature variation is minimized. Accordingly, this section was divided into four (4) main areas of investigation, the results of which would lead to better fuel economy. The areas were the development and utilization of an engine simulator test rig, an atmospheric burner test rig, development of an impingement jet stabilized (IJS) burner, and testing and evaluation of several different fuel nozzles.

Additionally, this section was originally assessed a total fuel economy improvement opportunity of .15 MPG (gasoline) toward the overall fuel economy improvements outlined in the original contract objectives; the current assessment for this section is .02 MPG (gasoline). The reasons for the difference in assessed opportunities, as well as the current expected contribution, are covered further on in this section.

2.2.1 Engine Simulator Test Rig

2.2.1.1 Summary — This test rig was designed to duplicate actual engine operating conditions insofar as the external combustion system is concerned. The primary objective of using this rig was to provide quantitative information regarding such combustion system parameters as the heater head temperature distribution, complete emissions measurements, burner system evaluation, and the effect of EGR and excess air on combustion characteristics. A schematic diagram of this test rig is shown in Figure 2.2-1 and a picture of the actual cell installation is shown in Figure 2.2-2.

No emissions measurements or heater head temperature distribution measurements were made for the baseline (Philips) burner system. Data taken for the new impingement jet stabilized combustor (IJS) is considered too preliminary to report.

Due to delays in material, installation, and scheduling, the Engine Simulator Rig was not used to the extent which was originally planned at the start of the joint development program. In fact, testing was limited to preliminary checkout only, prior to the failure in the rig in late August, 1978. This failure occurred at the gasket which separates the cooling water jacket from the heater

73

tube cooling air supply (see Figure 2.2-1). Testing of the rig up to this time was primarily devoted to exercising the cooling air system for fuel flows from .5 to 3.5 g/s, and monitoring the operation thereof.

2.2.1.2 Results — Initial testing of the Engine Simulator Rig revealed that due to the manner in which the heater head thermocouples were attached to the tubes, the closed-loop temperature control system would not function as planned. Because each thermocouple was welded to the heater tube, the thermocouple junction was grounded. The electronics of the control system were designed around un-grounded thermocouple junctions, such as those existing within the heater tubes of an operating 4-215 engine. This problem necessitated manual control of the fuel and cooling air to maintain a desired tube wall temperature. Aside from this complication, no other major problems were encountered prior to the gasket failure.

During the initial checkout period, the baseline burner system was in use, utilizing the Philips fuel nozzle and standard preheater. See section 2.2.4 for a description of the fuel nozzle and section 2.3 for a description of the preheater.

As previously mentioned, a failure of the gasket separating the cooling water jacket from the cooling air supply occurred during testing of a modified version of the IJS combustor having a radial swirler and seven (7) impingement air holes. The decision to proceed with testing of this hardware combination was based on atmospheric rig test results (See section 2.2.2).

Because only two (2) complete data points were run on the simulator rig prior to the mentioned failure, we feel that the data derived from these tests is of insufficient quality to use as a comparison with engine test results or simulator rig projections. What can be reported, however, was that a temperature difference in excess of $100^{\circ}C$ existed around the circumference of the heater head, and that cooling air flow was somewhat less than calculated in order to maintain proper tube temperature.

Figure 2.2-3 shows the results of a calculation simulating operation of the rig at a fuel flow of 0.5 g/s, cooling air flow of 100 g/s, A/F ratio of 20:1 and 100% EGR. Temperatures are given in $^{\circ}C$ and heat flows in watts. The original Engine Simulator Rig analysis program has been added to the Ford-developed Stirling burner program to produce the results shown in this figure.

2.2.1.3 Recommendations — In order to increase test rig reliability and accuracy, the following work should be accomplished before resumption of testing:
a. Install "O" ring seals around each of the cylinder and regenerator bores at the interface between the heater head rear face and Simulator Rig mounting plate;
b. Remove the cooling water discharge nozzles nearest the heater tubes in each of the regenerator bores. This would prevent water from mixing with the discharging cooling air prior to measuring the air temperature;
c. Install thermocouples in each of the regenerator bores to measure cooling air discharge temperature. The thermocouples should be shielded or else placed in the heater tubes themselves to insure against contact with the cooling water;
d. Repair failed thermocouples welded to the outside of the heater tubes. Three

(3) have failed to date, out of a total of twenty-four (24).

2.2.2 Atmospheric Burner Rig

2.2.2.1 Summary — The primary use for this test rig was to provide visual observation of the burner system operation. The qualitative information obtained from testing alternative hardware combinations was used to determine which components would be further evaluated in the Engine Simulator Rig. A schematic diagram of this test rig is shown in Figure 2.2-4.

The baseline burner and several derivations of the IJS burner were evaluated on this rig. A video-tape recording system was used to make permanent records of the majority of tests run on this rig.

2.2.2.2 Results — The Atmospheric Burner Rig was used to evaluate those burner hardware combinations shown in Figure 2.2-5. For all of the runs summarized on this table, either the original Philips partition plate or a modified version thereof was used.

Figure 2.2-6 through 2.2-17 present the results of Atmospheric Rig Testing for those test series listed in Figure 2.2-5. The following table provides a description of the various qualitative terms used to describe the swirl, atomization and flame appearance of any test point.

Swirl	Strong:	Swirl is strong and well developed;
	Weak:	Swirl is not well developed;
	Varying:	Swirl varies or changes with time;
	Compact:	Swirl is well tucked up into combustor can.
Atomization	Considered good if there is no indication of fuel burning on inside surface of combustor or burning in obvious streaks emanating from combustor. In severe instances of poor atomization, raw fuel may also be observed on the sides of the combustor.	
Flame	Stable:	In general, combustion is steady with time;
	Pulsating:	Flame exhibits a tendency to shrink and grow in intensity with time;
	Burnout:	Flame extinction and re-light.

In addition, the following figure gives a description of the schematic sketch used in Figures 2.2-6 through 2.2-17 to describe the appearance of the flame when viewed from the end of the exhaust barrel.

2.2.2.2.1 Baseline Philips Combustor (Figure 2.2-6 and 2.2-7) — This combustor was tested with the Philips and Excello fuel nozzles. With the exception of test points 26 and 28, air assist pressure for the Philips nozzle was maintained at or near .66 atm. (20" Hg.), the value used during dynamometer testing. At test point 26, the assist pressure was set at 0.5 atm. and 1.34 atm. at point 28. The low assist pressure gave rise to poor atomization with the result that fuel was observed burning on the surface of the combustor. The higher assist pressure of run 28 resulted in a somewhat
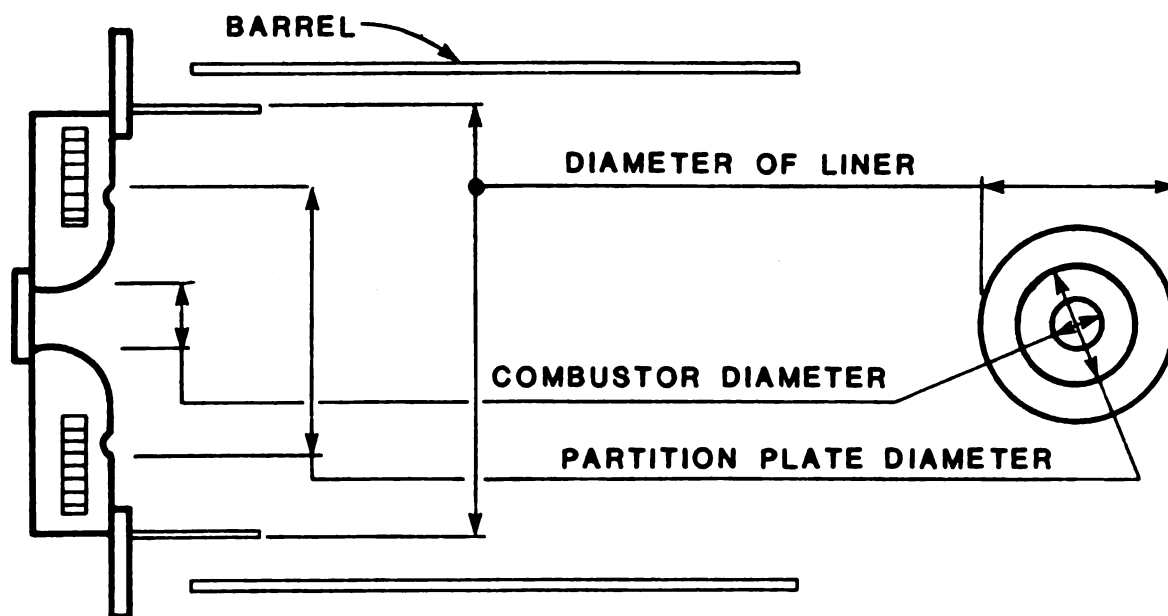
**SKETCH SHOWING RELATIONSHIP BETWEEN RIG COMPONENTS &
SCHEMATIC DIAGRAM USED TO DESCRIBE FLAME PROFILE**

more compact swirl than in run 27 (for the same fuel flow) and also contrib-
uted to a stabilization of the combustion. Frequent blowout was noted in run
27, but not in run 28. Run 32 is similar to 29 except that excess air was
increased.

When using the Excello nozzle with the other baseline hardware, the majority
of testing was done at an air assist pressure of about .5 atm. (15" Hg.) at
the nozzle. Although this air assist pressure is generally lower than the
pressures required for the Philips nozzle, the design of the Excello nozzle
permits substantially higher mass flows. Figure 2.2-18 shows the relation-
ship between upstream flow orifice pressure and pressure at nozzle discharge
for both the Philips and Excello nozzles. Test runs 14 and 18 were conducted
at essentially the same fuel flows and excess air ratios, but at quite different
values of air assist pressure/flow. Note the differences in swirl and atom-
izing quality between the two runs.

At .5-.66 atm. air assist nozzle pressure, substantial back pressuring of the
fuel takes place in the Philips nozzle while no noticeable back pressure is
present using the Excello nozzle. The Philips nozzle was operated at an air
assist pressure of .66 atm. because at this time this was the pressure used
in dynamometer testing to achieve satisfactory light-off and combustion. The
assist pressure and flow used during the Excello nozzle tests exceeded the

capability of the current electric atomizing pump used in vehicle testing. Refer to Figure 2.2-19 for descriptive curves relating flow and ΔP for the Excello nozzle and the Gast air atomizing pump. Also, note the location of test run 14 on Figure 2.2-19 and the test results in Figure 2.2-7 for the same run.

Operation of the Philips nozzle at fuel flows of .4 and .5 g/s was unstable at λ values of 1.3 to 1.5. Even at $\lambda = 1.9$ and 2.0 frequent blowout/re-light occurred. At corresponding conditions, using the Excello nozzle, no blowout occurred but pulsations in the flame were noted. The predominant flame color during most of the test runs was luminous yellow/yellow orange, indicating the oxidation of free carbon atoms.

For succeeding tests, operation simulating the use of EGR was included for each hardware combination. In general, those runs having a λ value (excess air value) greater than 2 represent a case when the effects of EGR was simulated by increasing the overall A/F ratio in an effort to approximate the combustor gas/fuel ratio during actual engine operation. Although this does result in greater air velocities, thus increasing turbulence and mixing, the technique has the drawback of contributing additional oxygen to the combustion process. This serves to lean-out the combustion and thus may somewhat distort the qualitative evaluation of the results. A permanent record of each test point was made using the video tape recording system. This system has several distinct advantages over the previous method of recording test results: It allows the recording of transient combustor operation and also provides for a frame-by-frame playback to aid in analysis.

2.2.2.2.2 Baseline LJS Combustor (Figures 2.2-8 and 2.2-9) — Testing of this combustor was carried out with the Philips and Excello fuel nozzles. Both hardware combinations exhibited less than acceptable swirl patterns at fuel flows of 2 g/s or less. Additionally, the desired recirculation, due in part to the impingement action of the downstream air holes, did not materialize. With this combustor, approximately 25% of the total flow area is represented by the primary air swirler, the remainder results from the film cooling slots and downstream impingement holes. To achieve good recirculation back into the area of the nozzle/ignitor, it was necessary to establish a pressure gradient within the combustor through the action of the primary air swirler. Evidently the velocity of the combustion air coming from the axial swirler was not sufficient to establish the required gradient. No quantitative measurements of this pressure gradient were made.

The atomizing performance of both nozzles was poor, with the Philips nozzle improving only when EGR was simulated. The swirl and atomizing problems resulted in luminous asymmetrical flames, and when the Excello nozzle was used, frequent flameout occurred. Because the atomizing characteristics of the Lucas and Excello nozzles were similar, the Lucas nozzle was not tested with the base LJS combustor.

2.2.2.2.3 Mod-1 LJS Combustor (Figures 2.2-10 and 2.2-11 — This combustor is the same as the baseline version except that the six (6) 25 mm diameter air holes have been replaced by seven (7) 16 mm diameter holes in an attempt to improve flow distribution around the combustor can and also increase the penetration of the impingement air jets. The combustor was tested with the Philips and Lucas nozzles.

Operation with the Philips nozzle resulted in good atomization at low fuel flows, but was accompanied by unstable combustion. Intermediate fuel flows with nominal air assist pressures resulted in poor atomization and yet stable combustion; at higher atomizing air flows improvements were noted.

Operation of the Lucas nozzle with fuel flows on the order of .5 g/s was not possible due to flameouts and atomizing problems. Operation at higher fuel flows was generally satisfactory in terms of the overall flame appearance and stability. However, the atomizing quality was poor.

No improvement in internal combustor recirculation was noted with this hardware as compared to baseline.

2.2.2.2.4 Mod-2 IJS Combustor (Figures 2.2-12 thru 2.2-14) — The impingement air hole pattern of this combustor was the same as the Mod-1 version, but the original axial swirler assembly was replaced by a radial swirler, as shown in Figure 2.2-20. Also, the ignitor was moved from near the nozzle to a point near the edge of the combustor can. This combustor concept was tested with all three available nozzles.

When the Philips nozzle was used in this combustor, swirl atomizing and flame appearance were all qualitatively acceptable, with the exception of the lowest fuel flow point simulating no EGR. Yellow combustion (high radiation) was predominant when no EGR was simulated, with the flame tending to become bluer and more contained in the combustor during EGR simulation.

Fairly good recirculation was also visible on some of the video tapes for this series of test points.

At fuel flows below 1 g/s, swirl and atomizing quality were acceptable when using the Excello nozzle and this combustor. At flows greater than 1 g/s, atomizing quality deteriorated. At fuel flows of 2 g/s and less, the combustion process was unstable, resulting in frequent blowout and pulsations. In addition, the flame had a tendency to extend quite far into the surrounding barrel, indicating little containment due to impingement jet action or internal recirculation.

Although a strong swirl and stable combustion was obtained over most of the Lucas nozzle operating range, atomizing quality continued to be poor. Also, the impingement air jets seemed to have little effect in containing the flame, resulting in excursions up to 18" into the barrel.

2.2.2.2.5 Mod-3 IJS Combustor (Figures 2.2-15 thru 2.2-17) — This modification of the baseline IJS combustor has the same combustor can shape and radial swirler as Mod-2, with the exception of having all impingement air holes plugged so that the total combustion air must go through the radial swirler.

With the Philips fuel nozzle, atomizing was acceptable above .5 g/s with and without EGR simulation, and swirl appearance was generally fair. During operation at intermediate fuel flows without EGR, the flame had a tendency to completely escape the combustor and follow the contour of the partition plate

out to the barrel. When simulating EGR, the flame became more symmetrical but still had a tendency to extend into the barrel indicating little or no containment due to recirculation induced by the radial swirler.

Operation with the Excello nozzle was generally the same as with the Philips nozzle, except that fuel atomization characteristics were not as good. In addition, operation at fuel flows less than .7 g/s was not possible due to combustion stability problems.

With the Lucas fuel nozzle, satisfactory atomization was obtained only at higher fuel flows during EGR simulation. In general, the swirl intensity with this hardware combination was satisfactory, as was the overall flame symmetry.

Because this series of test runs were made with all downstream air holes plugged, nearly 86% of the primary combustion air passed through the radial swirler. Because of this, the velocity near the nozzle was quite high resulting in several instances of good recirculation being visible; i.e., runs 92, 93, 100, 103 (at high air assist), 109, and 110.

2.2.2.3 Conclusions and Recommendations — In general, operation of the baseline hardware with both the Philips and Excello nozzles was qualitatively satisfactory at fuel flows > 1 g/s. At flows less than 1 g/s both systems exhibited problems in maintaining stable combustion and/or satisfactory atomization.

An examination of the test data indicated that the Mod-2 IJS combustor (using a radial instead of axial swirler), fitted with the Philips fuel nozzle, was the most promising hardware combination and was further evaluated on the Engine Simulator Test Rig. The qualitative test data also indicated that the atomizing air exit velocity for the Excello and Lucas fuel nozzles was too low to provide adequate atomization and fuel dispersion. Additionally, even though the Lucas nozzle as received from USS had an outer cone spray angle on the order of 110°, approximately 80% of the total fuel mass flow was contained within a 70° cone. This type of distribution may not be suitable for the IJS combustor.

Moving the ignitor from its original location (near the nozzle) to a position near the combustor periphery seemed to result in easier light-off. The ignitor, at this outward location, seemed to be more tolerant of start-up A/F ratio variances than when located near the nozzle. This was verified via additional testing.

Additional tests should be conducted on the fuel nozzles used in order to better define the minimum air assist flow requirements compatible with satisfactory burner operation.

The overall objective of the Atmospheric Burner Rig testing was to qualitatively evaluate burner hardware combinations in order to proceed quickly to testing on the Engine Simulator Rig. Based on atmospheric rig results, it was recommended that Engine Simulator Rig testing begin with the Mod-2 IJS combustor and Philips fuel nozzle. Testing was to continue with this combustor and the Excello fuel nozzle.

Further, it is recommended that the atomizing air flow passages in both the Excello and Lucas nozzles be reduced in cross-sectional area in order to increase

the exit velocity of the atomizing air. Increasing the relative velocity between the fuel and atomizing air should promote better atomization.

For the Mod-2 IJS burner, redesign of that portion of the combustor where the cylindrical body joins the dome should be accomplished in order to provide a somewhat rounded corner to eliminate dead space and promote internal combustor recirculation.

Additional work on designing properly configured radial and/or axial swirlers should also be undertaken; improvements over both existing designs can undoubtedly be made.

2.2.3 Impingement Jet Stabilized (IJS) Burner

2.2.3.1 Summary — The basic IJS burner is a cylindrical combustor having axial swirler vanes and downstream air impingement holes. Through the interaction between the swirler and air holes, it was hoped that an internal recirculation pattern would be established that would constantly re-introduce downstream combustion products to the primary burning zone. A schematic sketch of this burner is shown in Figure 2.2-21, and a picture of the baseline version is shown in Figure 2.2-22.

No substantive emissions or temperature distribution data were taken for any of the IJS combustors tested. Based on Atmospheric Rig tests, the IJS combustor with radial swirler offered the best potential for further development.

2.2.3.2 Results and Recommendations — Except for some preliminary testing in the Engine Simulator Rig, testing of all versions of the IJS combustors was limited to qualitative evaluation in the Atmospheric Burner Test Rig. Figures 2.2-6 through 2.2-17 provide a fairly complete description of how the combustion appeared. Note that these combustors have only been evaluated near atmospheric pressure and ambient inlet temperatures. Operation in the engine with preheated air may result in substantial differences when compared to the subjective results of the Atmospheric Burner Rig.

Although pressure drop measurements across each combustor were made at the time each version was tested, the differences between one IJS burner and another were, in general, quite small. The following table gives these pressure drop readings for several of the combustor concepts when burning 3 g/s fuel. At lower fuel flows, the differences are less. No measurements were taken on the baseline Philips combustor.

Test Series	P_{rig} "H_2O		
2-01	7.8		
2-02	9.2	Fuel	= 3 g/s
2-03	7.4	EGR	= 100%
2-04	12.3		

Test Series	P_{rig} "H_2O
4-04	8.6
6-02	8.4
6-03	7.9
6-04	11.6

Atmospheric Rig Pressure Drops For Several LJS Combustor

More accurate measurements should be made in the Engine Simulator Test Rig while maintaining actual engine conditions to establish more representative combustor pressure drop characteristics.

2.2.4 Fuel Nozzle Evaluation

2.2.4.1 Summary — During the course of this development program, it was planned to evaluate three (3) types of pressure atomized fuel nozzles — the original Philips pintle nozzle, the Excello nozzle, and a modified Lucas/USS nozzle. Those nozzles all had slightly different characteristics regarding atomizing air requirements, spray angle and distribution and operational fuel flow range. These nozzles are shown in Figure 2.2-23.

Other than qualitative performance data gathered as a result of Atmospheric Rig testing, no other data was accumulated by which to evaluate the available nozzles. The Philips pintle-type nozzle appeared to be compatible with the LJS combustors.

2.2.4.2 Results — Figure 2.2-24 is a schematic representation of the three fuel nozzles used during the joint development program, along with notable features. By referring again to Figures 2.2-6 through 2.2-17, nozzle performance characteristics for each combustor tested can be found.

In general, the following observations can be made regarding the operation of the fuel nozzles:

Philips Nozzle — This nozzle appeared to give more stable operation over the .5 to 3.0 g/s fuel flow range when compared to the other nozzles tested. For equivalent atomizing air mass flows, the nozzle Δ P is much higher for the Philips nozzle, indicating higher air velocities, leading to better atomization.

Excello nozzle — This type appeared to have more low and mid-range stability problems than the Philips nozzle. When operated with the Mod-3 LJS combustor (test series 4-04) operation at .5 g/s was not possible.

Lucas nozzle — Although the outer cone angle for this nozzle was 110°, 80% of the fuel was contained within an included angle of 70°. The resultant flame has a tendency to extend quite a distance out from the end of the various combustors. Operation of this nozzle at fuel flows less than .6 - .7 g/s was difficult due to combustion stability problems.

A more complete evaluation of the operation of individual nozzles would require that different combustor/nozzle hardware combinations be tested in either the Engine Simulator Rig or the engine. It should also be noted that nozzle and combustor development must proceed together due to the effect each component has on the operation of the other.

2.2.5 Fuel Economy Assessment — As mentioned previously, the original fuel economy improvement assessment for this section was .15 MPG, .02 of which represents the contribution of a low pressure drop burner, and .13 MPG attributed to improving the heater head temperature distribution through burner improvements. However, based on studies performed this past year and previously reported on, it was extremely difficult to predict the fuel economy implications of an uneven burner temperature distribution. For that reason, the fuel economy improvement opportunity of the theoretical analysis supporting the original estimate on the Fuel Economy Assessment Chart (see section 2.11) has been changed to zero. All that remains is the contribution due to a low pressure drop burner, which can only be determined by more exhaustive testing either on the Engine Simulator Rig or on the engine.

2.2.6 Conclusions — The following general conclusions can be made regarding the results of work on the burner system:

- The Engine Simulator Rig has shown the potential of becoming a powerful tool to use in the design and development of the Stirling engine. Because it will provide the opportunity for combustion system testing without the attendant problems of dynamometer or vehicle engine testing, its use should be continued and expanded;

- The Atmospheric Burner Rig used in conjunction with the video tape recording system has proved to be an excellent aid in evaluating the burner on a qualitative basis. Having the capability to continuously record the test results of a given hardware combination operated under certain conditions and then comparing those results with tests conducted previously is a definite advantage, especially when studying transient operation. The results of rig testing indicated that the IJS combustor having a radial swirler and fitted with the Philips fuel nozzle was the most satisfactory hardware combination evaluated. Upon completion of rig testing, this set of hardware was installed on the Engine Simulator Rig for further evaluation;

- Based on a qualitative evaluation as a result of Atmospheric Rig testing, the baseline Philips pintle-type fuel nozzle appeared to give the best results when operated over the 0.5 to 3.0 g/s fuel flow range. Further evaluation of the three nozzles tested is recommended, either in the Engine Simulator Rig, or the engine itself;

- The contribution made to overall fuel economy by the burner system alone was not determined during the period of testing.

Figure 2.2-1   Engine Simulator Test Rig

83

Figure 2.2-2   Engine Simulator Test Rig

```
••••••••••••••••••••••••••••••••••••••••••••••••••••••••••••••••••••••••
•           SIMULATOR RIG ANALYSIS PROGRAM                 •
•           FUEL=1.500 G/S    AIR=100.0 G/S                •
••••••••••••••••••••••••••••••••••••••••••••••••••••••••••••••••••••••••••
```

```
                -----------------------------------
               /    CROSSOVER PORTION ADIABATIC    \
              /                                     \
             /       DP= 0.419  DM=0.0058  EL= 7     \
            /            -----------------            \
           /            /                 \            \
          I+++++++++++I /                   \ I+++++++++++I
          I TB= 650.1 I                       I TB= 650.1 I
BOUNDARY 8 I PB=18.270 I                       I PB=18.689 I BOUNDARY 7
          I MB=0.2599 I                       I MB=0.2541 I
<-----<-----I  -  -  -  I----<-----<-----I  -  -  - I-----<-----<
STREAM 5   I TE= 700.0 I                   I TE= 603.1 I  STREAM 5
DT= 728.7  I TU=1290.5 I   DT= 660.6       I TU=1464.4 I
TG=1282.3  I DQ=22409. I   TG=2011.1       I DQ=20811. I  TG=2671.7
QG=28362.  I DP= 0.478 I   QG=50780.       I DP= 0.323 I  QG=71584.
DQ=22418.  I DM=0.0189 I   DQ=20804.       I DM=0.0153 I
TW=1300.8  I   EL= 8   I                   I   EL= 6   I  TW=1479.5
<-----<-----I  -  -  -  I----<-----<-----I  -  -  - I-----<-----<
          I TB= 751.1 I                       I TB= 554.3 I
BOUNDARY 9 I PB=17.792 I                       I PB=19.012 I BOUNDARY 6
          I MB=0.2787 I                       I MB=0.2387 I
<-----<-----I  -  -  -  I----<-----<-----I  -  -  - I-----<-----<
STREAM 4   I TE= 796.3 I                   I TE= 504.1 I  STREAM 4
DT= 663.6  I TU=1328.3 I   DT= 686.7       I TU=1410.9 I
TG=1320.0  I DQ=20416. I   TG=1983.6       I DQ=21626. I  TG=2670.3
QG=29503.  I DP= 0.498 I   QG=49926.       I DP= 0.307 I  QG=71547.
DQ=20423.  I DM=0.0185 I   DQ=21610.       I DM=0.0160 I
TW=1337.7  I   EL= 9   I                   I   EL= 5   I  TW=1426.6
<-----<-----I  -  -  -  I----<-----<-----I  -  -  - I-----<-----<
          I TB= 841.3 I                       I TB= 451.9 I
BOUNDARY 10 I PB=17.294 I                      I PB=19.319 I BOUNDARY 5
          I MB=0.2973 I                       I MB=0.2227 I
<-----<-----I  -  -  -  I----<-----<-----I  -  -  - I-----<-----<
STREAM 3   I TE= 881.1 I                   I TE= 396.4 I  STREAM 3
DT= 602.3  I TU=1359.7 I   DT= 714.3       I TU=1353.8 I
TG=1352.2  I DQ=18539. I   TG=1954.5       I DQ=22487. I  TG=2668.8
QG=30479.  I DP= 0.532 I   QG=49025.       I DP= 0.294 I  QG=71504.
DQ=18546.  I DM=0.0188 I   DQ=22479.       I DM=0.0171 I
TW=1368.2  I   EL=10   I                   I   EL= 4   I  TW=1370.2
<-----<-----I  -  -  -  I----<-----<-----I  -  -  - I-----<-----<
          I TB= 922.2 I                       I TB= 341.1 I
BOUNDARY 11 I PB=16.762 I                      I PB=19.613 I BOUNDARY 4
          I MB=0.3161 I                       I MB=0.2056 I
<-----<-----I  -  -  -  I----<-----<-----I  -  -  - I-----<-----<
STREAM 2   I TE= 958.1 I                   I TE= 281.6 I  STREAM 2
DT= 544.2  I TU=1387.4 I   DT= 742.9       I TU=1294.4 I
TG=1380.3  I DQ=16763. I   TG=1924.5       I DQ=23376. I  TG=2667.4
QG=31338.  I DP= 0.569 I   QG=48097.       I DP= 0.283 I  QG=71465.
DQ=16759.  I DM=0.0195 I   DQ=23360.       I DM=0.0188 I
TW=1395.1  I   EL=11   I                   I   EL= 3   I  TW=1311.4
<-----<-----I  -  -  -  I----<-----<-----I  -  -  - I-----<-----<
          I TB= 994.5 I                       I TB= 220.6 I
BOUNDARY 12 I PB=16.194 I                      I PB=19.896 I BOUNDARY 3
          I MB=0.3356 I                       I MB=0.1869 I
<-----<-----I  -  -  -  I----<-----<-----I  -  -  - I-----<-----<
STREAM 1   I TE=1027.0 I                   I TE= 155.6 I  STREAM 1
DT= 489.9  I TU=1410.9 I   DT= 772.6       I TU=1230.6 I
TG=1403.5  I DQ=15087. I   TG=1893.3       I DQ=24302. I  TG=2665.9
QG=32046.  I DP= 0.611 I   QG=47128.       I DP= 0.272 I  QG=71426.
DQ=15082.  I DM=0.0208 I   DQ=24298.       I DM=0.0211 I
TW=1417.8  I   EL=12   I                   I   EL= 2   I  TW=1248.3
<-----<-----I  -  -  -  I----<-----<-----I  -  -  - I-----<-----<
          I TB=1056.8 I                       I TB=  90.0 I
BOUNDARY 13 I PB=15.582 I                      I PB=20.168 I BOUNDARY 2
          I MB=0.3564 I                       I MB=0.1657 I
          I+++++++++++I                       I+++++++++++I
         /            I                       I            \
        / REGENERATOR I                       I  CYLINDER   \
<-----<--/ CONNECTION /                         \ CONNECTION \--<-----<
TX=1056.8   ADIABATIC /                          \ ADIABATIC  TN=  90.0
PX=14.690            /                             \          PN=20.996
MX=0.3781          /                                \         MN=0.1592
DM=0.0216        /                                   \
<-----<-----<----/                                    \-----<-----<----<
```

LEGEND:

Temperatures (^{o}C):

T_n : Cooling air entrance

T_b : Element Boundary

T_w : Inner/outer wall

T_g : Upstream/downstream Flue gas

T_e : Average interior element

DT : Flue gas change

T_x : Cooling air exit

Heat Flows (Watts):

QG : Upstream/downstream flue gas

DQ : Inner/outer net change

Pressure (PSI):

P_n : Entrance

P_b : Boundary

DP : Element change

P_x : Exit

Mach Number:

M_n : Entrance

M_b : Boundary

DM : Element change

M_x : Exit

Typical gas flow stream

Heater tube

Figure 2.2-3   Results of a Calculation Simulating Operation
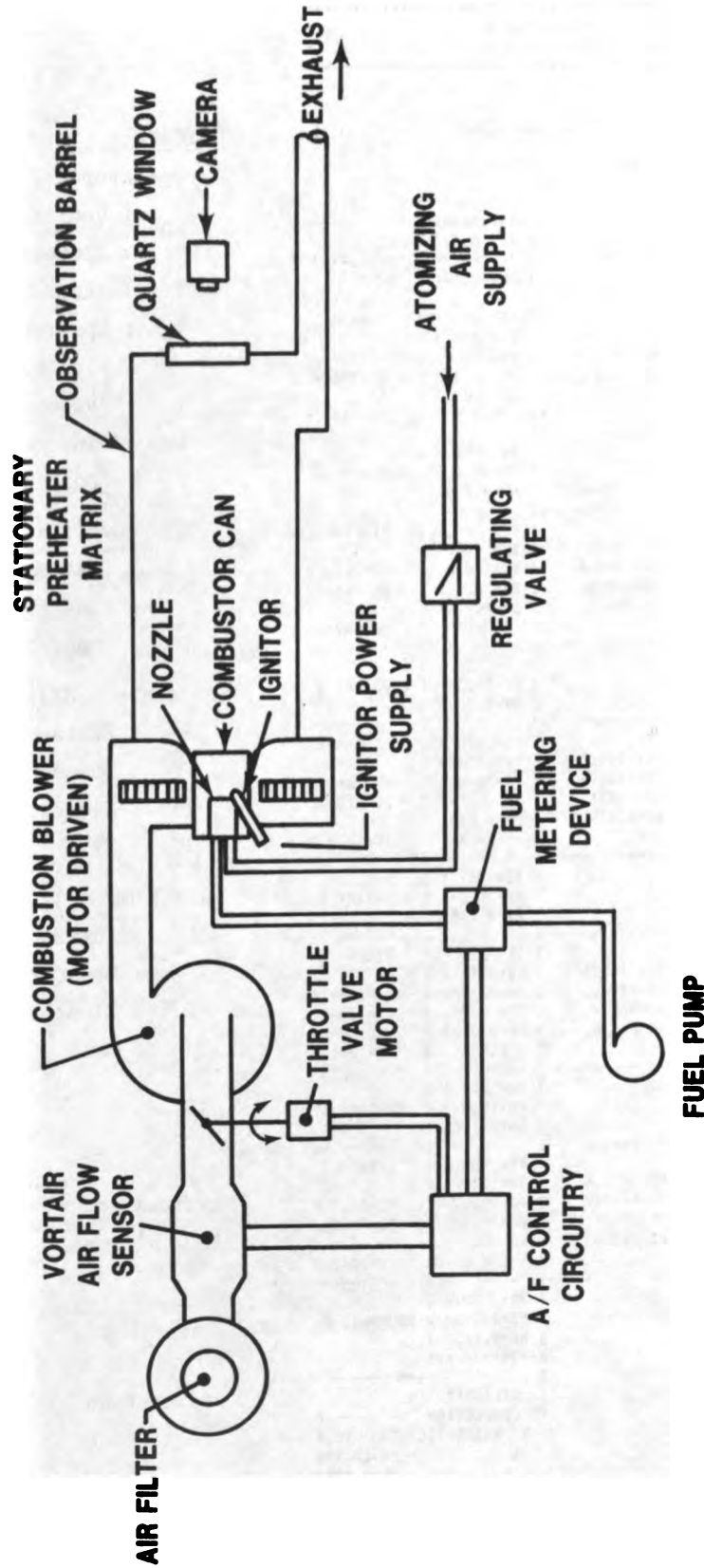
Figure 2.2-4   Schematic of Atmospheric Burner Test Rig

Test Series	Philips Combustor Can	Base IJS Combustor	MOD-1 IJS Combustor	MOD-2 IJS Combustor	MOD-3 IJS Combustor	Philips Nozzle	Excello Nozzle	Lucas Nozzle	Note
			Note 3						
1-01	X					X			
2-01		X				X			
3-01	X						X		
4-01		X					X		
5-01	X							X	1
6-01		X						X	1
1-02	?					X			2
2-02			X			X			
3-02	?						X		2
4-02			X				X		1
5-02	?							X	2
6-02			X					X	
1-03	?					X			2
2-03				X		X			
3-03	?						X		2
4-03				X			X		
5-03	?							X	2
6-03				X				X	
1-04	?					X			2
2-04					X	X			
3-04	?						X		2
4-04					X		X		
5-04	?							X	2
6-04					X			X	

NOTES:

(1)   Tests not run.

(2)   Tests involving some modification of the Philips combustor, to be determined.

(3)   Base IJS: As described in text.
MOD-1 IJS: Seven (7) 16 mm secondary air holes instead of six (6) 25 mm.
MOD-2 IJS: Same as MOD-1 with addition of radial swirler.
MOD-3 IJS: Same as MOD-2 but with secondary air holes plugged.

Figure 2.2-5   Atmospheric Burner Rig Testing

Baseline Hardware & Philips Fuel Nozzle

Figure 2.2-6
ATMOSPHERIC BURNER TEST RIG RESULTS

Test Series: 1-01

Run No.	Fuel Flow (g/s)	Air Assist Pressure (Atm.)	Air Assist Flow (g/s)	Swirl Quality	Atomizing Quality	λ Vortair	λ Burner	Flame Color	Flame Profile	Additional Comments
26	0.42	0.50	0.65	Strong, but not compact	Instances of fuel burning on combustor surface	1.92	2.03	Frequent blowout / Yellow-orange		Difficult to maintain stable combustion at values near 1.3-1.5
27	1.01	0.67	0.74	Strong, but not compact	Good	1.40	1.45	Frequent blowout / Yellow-orange		Very unstable flame
28	1.01	1.34	1.17	Strong, more compact than #27	Good	1.40	1.48	Stable flow / Yellow-orange		Flame appears stronger than in run #27
29	2.04	0.69	0.7	Weak	Good	1.45	1.48	Stable flow / Yellow-orange		
30	3.03	0.72	0.69	Weak	Good	1.35	1.37	Stable flow / Yellow-white		Flame extends well into barrel
32	2.02	0.66	0.66	Strong, but not compact	Good	2.00	2.02	Stable / Yellow-hint of blue		Compare to run #29

Figure 2.2-6   Atmospheric Burner Test Rig Results
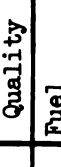
Baseline hardware & Excello nozzle

Figure 2.2-7

ATMOSPHERIC BURNER TEST RIG RESULTS

Test Series: 3-01

Run Number	Fuel Flow (g/s)	Air Assist Pressure (Atm)	Air Assist Flow (g/s)	Swirl Quality	Atomizing Quality	Vortair / Burner	Flame Quality — Flame Color	Flame Profile	Additional Comments
14	0.50	0.13	0.62	Weak, varying	Fuel burning on combustor surface	1.75	Stable flow		Swirl is definitely unstable - varying
						1.83	Yellow-orange		
18	0.45	0.51	1.53	Strong, compact	Good	1.78	Pulsating		
						2.01	Blue-yellow		
19	1.05	0.52	1.54	Strong	Good	1.41	Pulsating		
						1.52	Yellow		
20	1.99	0.52	1.52	Weak	Good	1.52	Stable flow		
						1.57	Yellow		
21	3.04	0.51	1.53	Weak	Good	1.39	Stable flow		Flame extends far into barrel
						1.43	Yellow		
25	3.25	0.52	1.54	Strong, but not compact	Good	1.88	Stable flow		
						1.92	Yellow		

Figure 2.2-7   Atmospheric Burner Test Rig Results

BASELINE IJS COMBUSTOR
AND PHILIPS FUEL NOZZLE

Figure 2.2-8

Test Series: 2-01

ATMOSPHERIC BURNER TEST RIG RESULTS

Run Number / Fuel Flow (g/s)	Air Assist Pressure (Atm.)	Air Assist Flow (g/s)	Swirl Quality	Atomizing Quality	λ Vortair / λ Burner	Flame Quality / Flame Color	Flame Profile	Additional Comments
48	.11	.25	Weak Not Compact	Raw Fuel Sprayed Into Barrel	1.54	Pulsating With Blowout		Flame out at .17 ATM atomizing air pressure
.57					1.56	Yellow-Orange		See #54
49	.34	.49	Strong, Not Compact	Raw Fuel Visible	1.50	Stable Flow		No flame-out through 2.37 ATM atomizing air pressure
2.02					1.52	Luminous Yellow		See #52
50	.37	.45	Fair Strength, Not Compact	Fuel Burning in Streaks From Combustor	1.35	Stable Flow		Flame turns blue at 1.7 ATM atomizing air pressure
3.0					1.37	Yellow with Orange tips		See #51
51	.35	.43	Compact, Well Defined	Same as #50	2.66	Stable Flow		Simulating 100% EGR at .85 ATM atomizing pressure atomizing quality is O.K.
3.04					2.67	Yellow, Some Blue		
52	.31	.44	Fair, Compact	Good	2.87	Stable Flow		Simulating 100% EGR blue combustion increase near .68 ATM atomizing air pressure
2.02					2.88	Yellow-Orange, Some blue		
54	.33	.53	Compact, Well-Defined	Good	2.59	Stable Flow		Simulating 100% EGR blowout & relight at .44 ATM atomizing air pressure
.52					2.66	Luminous Yellow		

Figure 2.2-8   Atmospheric Burner Test Rig Results
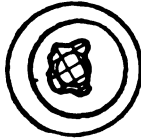
BASELINE IJS COMBUSTOR AND EXCELLO FUEL NOZZLE

Figure 2.2-9

ATMOSPHERIC BURNER TEST RIG RESULTS

Test Series: 4-01

Run Number / Fuel Flow (g/s)	Air Assist Pressure (Atm.)	Air Assist Flow (g/s)	Swirl Quality	Atomizing Quality	λ Vortair / λ Burner	Flame Quality / Flame Color	Flame Profile	Additional Comments
38 / .50	.07	.48	Weak, Not Developed	Instances of Fuel Burning on Combustor Surface	1.62	Pulsating		Flame-out at .21 ATM atomizing air pressure
					1.68	Yellow, Yellow-Orange		See #42
39 / 2.07	.07	.47	Strong, Not Developed	Burning Fuel Particles out of Combustor	1.40	Stable Flow		Flame-put at .68 ATM atomizing air pressure
					1.41	Yellow-White		See #43
40 / 3.02	.07	.47	Strong, Not Compact	Burning Fuel Particles out of Combustor	1.34	Stable Flow		
					1.35	Yellow-White		See #44
42 / .52	.07	.48	Strong, Compact	Burning Fuel on Combustor Surface & Out Of Combustor	3.11	Frequent Blowout		Simulating 100% EGR flame-out at .17 ATM atomizing air pressure
					3.17	Luminous Yellow		
43 / 2.19	.08	.48	Fair, Compact	Same as #42, above	2.61	Stable Flow		Simulating 100% EGR flame-out prior to reaching 2 g/s fuel flow.
					2.63	Luminous Yellow, some Blue		
44 / 3.01	.07	.47	Strong, Compact	Burning Fuel Particles Out Of Combustor	2.68	Stable Flow		Simulating 100% EGR flame-out at .09 ATM atomizing air pressor
					2.70	Yellow, Blue Near IJS Holes		

Figure 2.2-9   Atmospheric Burner Test Rig Results
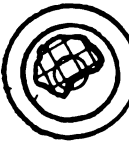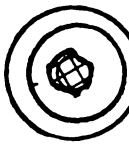
MODIFIED IJS COMBUSTOR (7 HOLE)
AND PHILIPS FUEL NOZZLE

Figure 2.2-10

ATMOSPHERIC BURNER TEST RIG RESULTS

Test Series: 2-02

Run Number / Fuel Flow (g/s)	Air Assist Pressure (Atm.)	Air Assist Flow (g/s)	Swirl Quality	Atomizing Quality	λ Vortair / λ Burner	Flame Quality / Flame Color	Flame Profile	Additional Comments
56	.14	.31	Weak, Not Compact	Good	1.68	Frequent Blowout		Unstable operation at air assist pressure .34 ATM.
.52					1.72	Yellow with Orange Core		See #62
57	.38	.53	Not Developed, Not Compact	Fuel Burning On Combustor Surface	1.33	Stable Flow		Flame extends well into barrel
2.02					1.35	Luminous Yellow		See #60
58	.43	.53	Weak, Not Compact	Fuel Burning in Streaks From Combustor	1.34	Stable Flow		Symmetrical, blue combustion at air assist pressure of 1.36 ATM
3.02					1.35	Luminous Yellow, White		See #59
59	.34	.43	Weak, Not Compact	Same as #58	2.67	Stable Flow		At air assist of .68 ATM flame becomes blue and more symmetrical
3.02					2.69	Yellow, Blue		
60	.31	.48	Fair, Loose	Same as #58	2.86	Stable Flow		Flame extends 12" into barrel. At air assist of .68 ATM Flame becomes blue and more symmetrical
2.0					2.88	Yellow, Blue		
62	.15	.31	Good	Good	3.37	Pulsating With Blowout		Good Symmetry and blue combustion at higher air assist pressures
.50					3.41	Yellow, Some Blue		

Figure 2.2-10   Atmospheric Burner Test Rig Results

MODIFIED IJS COMBUSTOR (7 HOLE) AND LUCAS FUEL NOZZLE

Figure 2.2-11

ATMOSPHERIC BURNER TEST RIG RESULTS

Test Series: 6-02

Run Number / Fuel Flow (g/s)	Air Assist Pressure (Atm.)	Air Assist Flow (g/s)	Swirl Quality	Atomizing Quality	λ Vortair / λ Burner	Flame Quality / Flame Color	Flame Profile	Additional Comments
63	.04	.45	Weak, Loose	Good	1.32	Stable Flow		Increasing atomizing air pressure does not improve combustion
1.02					1.35	Yellow-Orange		See #68
64	.04	.46	Weak, Not Compact	Fuel Burning in Streaks From Combustor	1.35	Stable Flow		No significant flame recirculation
2.0					1.36	Luminous Yellow-Orange		See #67
65	.05	.48	Weak, Not Compact	Same as #64	1.34	Stable		At air assist of .17 ATM noticeable improvement in atomizing quality
3.02					1.35	Luminous Yellow		See #66
66	.04	.42	Good, Compact	Good	2.68	Stable		Increasing air assist flow tends to make flame bluer.
3.01					2.69	Yellow, Some Blue		
67	.04	.42	Weak, Compact	Same as #64	2.64	Stable Flow		Good containment of combustion process; poor recirculation
2.04					2.65	Yellow, Some Blue		
68	.04	.44	Weak, not well Defined	Burning Fuel Streaks Plus Raw Fuel Visible	2.35	Pulsating with Burnout		No significant flame containment; extends 8" into barrel
1.29					2.37	Yellow-Orange		

Figure 2.2-11   Atmospheric Burner Test Rig Results
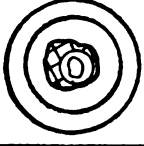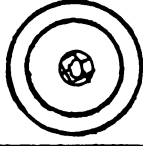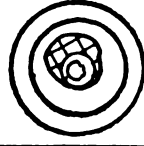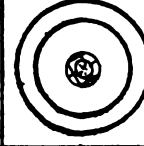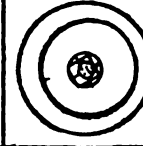
MODIFIED IJS COMBUSTOR WITH RADIAL SWIRLER AND PHILLIPS FUEL NOZZLE

Figure 2.2-12

ATMOSPHERIC BURNER TEST RIG RESULTS

Test Series: 2-03

Run Number / Fuel Flow (g/s)	Air Assist Pressure (Atm.)	Air Assist Flow (g/s)	Swirl Quality	Atomizing Quality	λ Vortair / λ Burner	Flame Quality / Flame Color	Flame Profile	Additional Comments
75	.17	.34	Weak	Good	1.75	Pulsating With Burnout		At .68 ATM (.77 g/s) air assist flow, combustion mostly blue with good stability & atomization. See #82
.50					1.80	Luminous Yellow		
77	.34	.42	Strong	Good	1.35	Stable		At 1 ATM (.94 g/s) air assist, combustion is partly blue; still very stable and symmetrical. See #80
2.0					1.36	Yellow with Transparent Core		
78	.34	.43	Strong	Good	1.35	Stable		No significant change up to 1.0 ATM air assist pressure. See #79
3.0					1.36	Yellow with Transparent Core		
79	.34	.39	Strong	Good	2.70	Stable		No significant change up to 1.0 ATM air assist pressure
3.0					2.71	Yellow with Blue Core		Simulating EGR
80	.68	.78	Strong	Good	2.70	Stable		No significant change up to 1.0 ATM. Air assist pressure
2.0					2.71	Yellow with Blue Core		Simulating EGR
82	.34	.50	Strong, varying	Good	2.70	Stable		More blue and better swirl at .7 ATM air assist pressure
.50					2.76	Yellow with Blue Core		Simulating EGR

Figure 2.2-12   Atmospheric Burner Test Rig Results
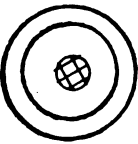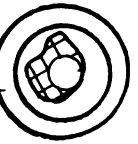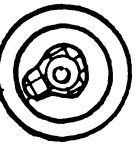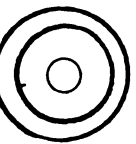
MODIFIED IJS COMBUSTOR WITH
RADIAL SWIRLER AND EXCELLO
FUEL NOZZLE

Figure 2.2-13
ATMOSPHERIC BURNER TEST RIG RESULTS

Test Series: 4-03

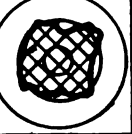| Run Number / Fuel Flow (g/s)	Air Assist Pressure (Atm.)	Air Assist Flow (g/s)	Swirl Quality	Atomizing Quality	λ Vortair / λ Burner	Flame Quality (Flame Color)	Flame Profile	Additional Comments
83 / .52	.17	.81	Weak	Good	1.42	Pulsating		No improvement at higher air assist pressures; flameout at .34 ATM flame extends 9-10" into barrel
					1.53	Luminous Yellow		
84 / 1.0	.14	.70	Weak	Good	1.35	Pulsating with Blowout		Little change at air assist pressure up to ATM. Flame extends about 18" into barrel
					1.39	Luminous Yellow, Orange		
85 / 2.03	.10	.58	Fair	Fuel Burning in Streaks From Combustor	1.33	Pulsating		Combustion process very unsteady. Flame extends about 8" into barrel
					1.35	Luminous Yellow		
86 / 3.02	.17	.78	Fair	Same as #85	1.33	Stable		At higher air assist pressures, combustion becomes more symmetrical extends 18" into barrel (using brass spacer)
					1.36	Luminous Yellow		
87 / 3.02	.17	.78	Strong	Same as #85	1.34	Stable		Transparent core stable up to .68 ATM air assist pressure (using brass spacer)
					1.36	Luminous Yellow		

Figure 2.2-13   Atmospheric Burner Test Rig Results

MODIFIED IJS COMBUSTOR WITH
RADIAL SWIRLER AND LUCAS
FUEL NOZZLE

Figure 2.2-14
ATMOSPHERIC BURNER TEST RIG RESULTS

Test Series: 6-03

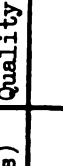| Run Number / Fuel Flow (g/s)	Air Assist Pressure (Atm.)	Air Assist Flow (g/s)	Swirl Quality	Atomizing Quality	λ Vortair / λ Burner	Flame Quality / Flame Color	Flame Profile	Additional Comments
69 / .82	.102	.68	Weak	Good	1.23	Pulsating Flow		Extends about 12" into barrel. Unsteady above .102 ATM air assist pressure.
					1.29	Luminous Yellow		
70 / 1.0	.068	.58	Weak, Varying	Fuel Burning in Streaks From Combustor	1.35	Pulsating Flow		Atomizing much better at .9 g/s air assist flow; flame has
					1.39	Yellow, some Blue		
71 / 2.0	.10	.71	Strong	Same as #70 plus Raw Fuel Visible	1.35	Stable		Transparent flame core good atomization ATM .34 air assist pressure (1.42 g/s) See #73
					1.37	Luminous Yellow		
72 / 3.0	.17	.94	Strong	Same as #70	1.35	Stable Flow		At .5 ATM (1.7 g/s) air assist, flame extends 18" into barrel See #73
					1.37	Yellow-Blue Core		
73 / 3.0	.17	.93	Strong	Good	2.70	Stable		Flameout at .27 ATM (1.3 g/s) air assist. Simulating EGR
					2.71	Blue		
74 / 2.04	.09	.66	Strong	Fuel Burning in Streaks From Combustor	2.70	Stable		Pronounced rumble and improved atomization at .34 ATM (1.36 g/s) air assist Simulating EGR
					2.72	Blue with Yellow tips		

Figure 2.2-14   Atmospheric Burner Test Rig Results
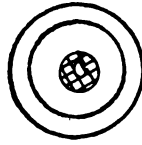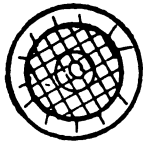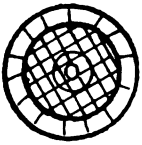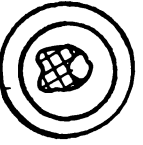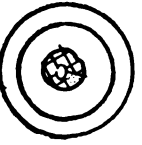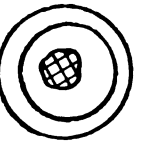
RADIAL SWIRLER IJS COMBUSTOR WITH PLUGGED SECONDARY AIR HOLES AND PHILLIPS FUEL NOZZLE
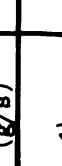
Figure 2.2-15

ATMOSPHERIC BURNER TEST RIG RESULTS

Test Series: 2-04

Run Number / Fuel Flow (g/s)	Air Assist Pressure (Atm.)	Air Assist Flow (g/s)	Swirl Quality	Atomizing Quality	λ Vortair	λ Burner	Flame Color	Flame Profile	Additional Comments
88 / .50	.29	.42	Weak.	Fuel Burning on Combustor Surface	1.62	1.67	Pulsating / Yellow, some blue		Sight blue color around edges. See #95
90 / 2.0	.34	.40	Weak	Good	1.35	1.36	Stable / Yellow, Orange		Transparent core. No containment; flame follow contour of partition plate out to barrel line. See #93
91 / 3.0	.34	.38	Fair	Good	1.35	1.36	Stable / Luminous Yellow		Same as #90. No significant change up to 1.0 ATM atomizing air pressure. See #92
92 / 3.0	.34	.39	Good	Good	2.70	2.71	Stable / Yellow, Some Blue		Becomes bluer with better containment 1. ATM. atomizing air pressure. Simulating EGR
93 / 2.0	.34	.42	Strong	Good	2.70	2.71	Stable Flow / Yellow, Blue		Becomes bluer and somewhat transparent with higher air assist pressure extends 10" into barrel. Simulating EGR
95 / .50	.34	.45	Weak	Same as #88	2.70	2.75	Stable / Yellow		Extends about 2" into barrel. Simulating EGR

Figure 2.2-15   Atmospheric Burner Test Rig Results

RADIAL SWIRLER IJS COMBUSTOR WITH PLUGGED SECONDARY AIR HOLES AND EXCELLO FUEL NOZZLE

Figure 2.2-16

ATMOSPHERIC BURNER TEST RIG RESULTS

Test Series: 4-04

Run Number / Fuel Flow (g/s)	Air Assist Pressure (Atm.)	Air Assist Flow (g/s)	Swirl Quality	Atomizing Quality	λ Vortair / λ Burner	Flame Quality / Flame Color	Flame Profile	Additional Comments
96 / .70	.10	.40	Strong	Fuel Burning in Streaks From Combustor	1.44 / 1.48	Pulsating with Burnout / Yellow		No improvement up thru .41 ATM (.83 g/s) air assist. could not get .5 g/s fuel flow
97 / 1.0	.10	.41	Good	Good	1.35 / 1.37	Stable Flow / Luminous Yellow		At higher air assist flows, atomizing quality deteriorates; flame extends 8-10" into barrel
98 / 2.0	.10	.40	Strong	Same as #96	1.35 / 1.36	Stable / Luminous Yellow		Flame follows partition plate contour. Atomising improves at higher air assist. Some blue visible See #101
99 / 3.0	.10	.41	Weak, Not Compact	Same as #96 plus Raw Fuel	1.35 / 1.36	Pulsating Flow / Luminous Yellow		Flame jumps from interior to edge. At air assist, color change between yellow & blue See #100
100 / 3.0	.10	.41	Weak, Not Compact	Fuel Burning in Streaks From Combustor	2.24 / 2.25	Pulsating with Burnout / Yellow, Some Blue		Not able to simulate 100% at higher air assist flows combustion becomes and more stable Simulating EGR (70%)
101 / 2.07	.11	.43	Good	Same as #100	2.60 / 2.62	Stable, Some Pulsating / Yellow, Blue		Consistent flame out at higher air assist pressure/flows. Simulating EGR (100%)

Figure 2.2-16   Atmospheric Burner Test Rig Results
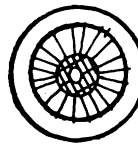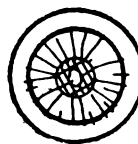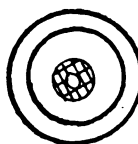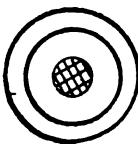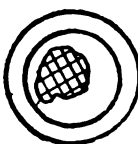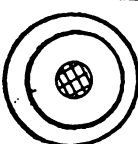
RADIAL SWIRLER IJS COMBUSTOR
WITH PLUGGED SECONDARY AIR
HOLES AND LUCAS FUEL NOZZLE

Figure 2.2-17
ATMOSPHERIC BURNER TEST RIG RESULTS

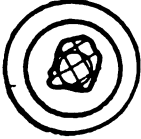Test Series: 6-04

Run Number	Fuel Flow (g/s)	Air Assist Pressure (Atm.)	Air Assist Flow (g/s)	Swirl Quality	Atomizing Quality	λ Vortair	λ Burner	Flame Quality Flame Color	Flame Profile	Additional Comments
103		.10	.42	Good	Fuel Burning In Streaks From Combustor		1.39	Stable Flow		Flame follows partition plate contour; no containment. At higher air assist, flame becomes blue with good recirculation. See #110
	3.0				Same as #103		1.40	Luminous Yellow		
104		.10	.43	Strong, Not Compact			1.35	Pulsating Flow		Some recirculation visible—flame follows partition plate contour. No significant change at higher air assist flow See #109
	2.0						1.36	Luminous Yellow		
106		.17	.55	Weak, Compact	Fuel Burning On Combustor Surface		1.35	Pulsating with Burnout		Not much better at higher air assist flow
	.50						1.42	Yellow with Orange Tips		See #107
107		.07	.35	Strong, Not Compact	Fuel Burning On Combustor Surface & In Streaks From Combustor		2.54	Pulsating with Burnout		No significant change at higher air assist flows.
	.53						2.58	Luminous Yellow		
109		.10	.46	Strong, Compact	Good		2.70	Pulsating Flow		Simulating EGR Good recirculation increased blue combustion and tendency to flame out at higher air assist simulating EGR.
	2.0						2.71	Yellow		
110		.10	.45	Strong	Good		2.74	Stable		Good containment. Some blue at higher air assist Very symmetric
	3.0						2.75	Yellow		Simulating EGR

Figure 2.2-17   Atmospheric Burner Test Rig Results
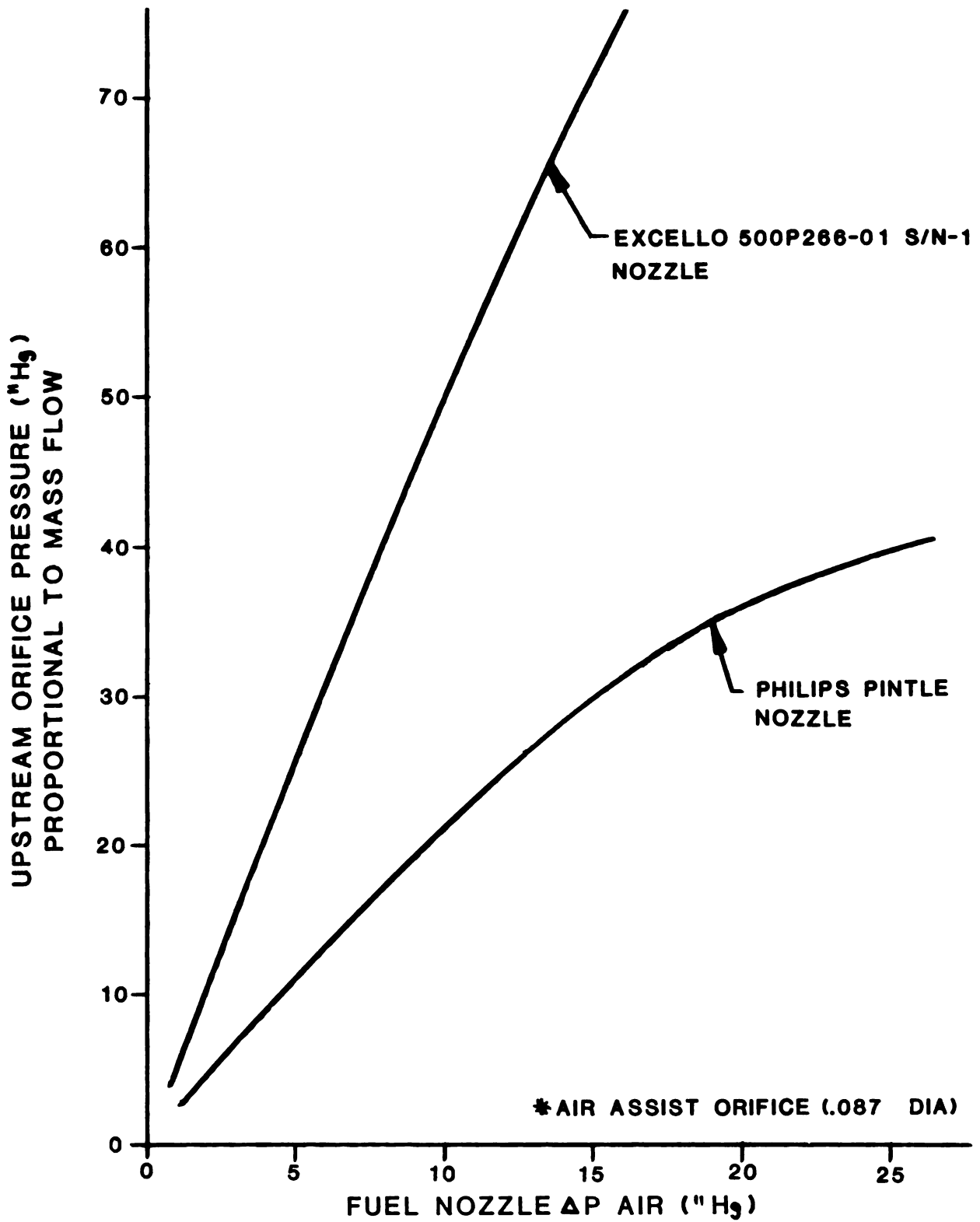
Figure 2.2-18   Upstream Orifice Pressure* vs. Pressure at Fuel Nozzle for
N. V. Philips and Excello Nozzle
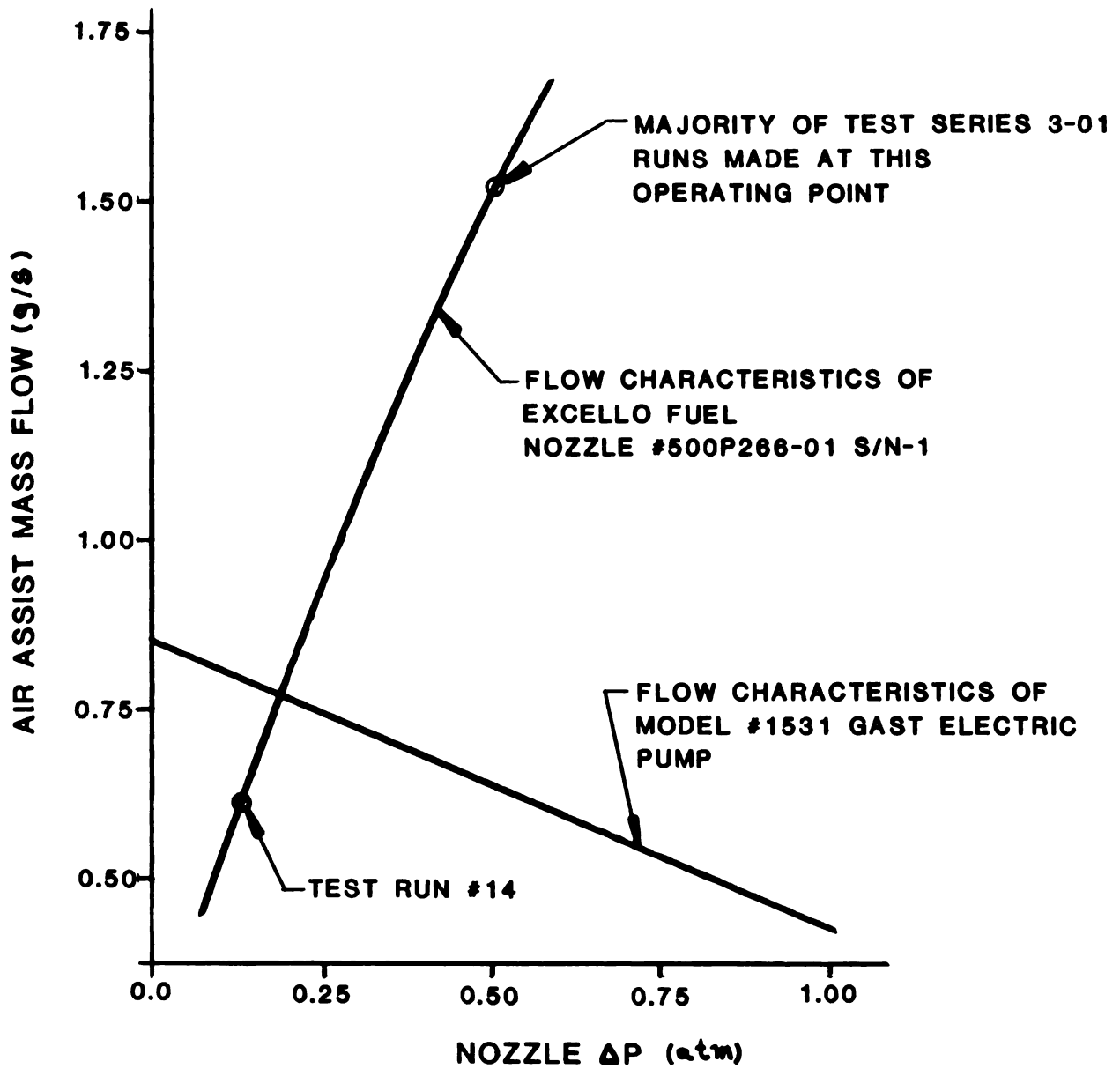
Figure 2.2-19   Air Flow vs. Nozzle Δ P for Excello Fuel Nozzle and Gast Pump
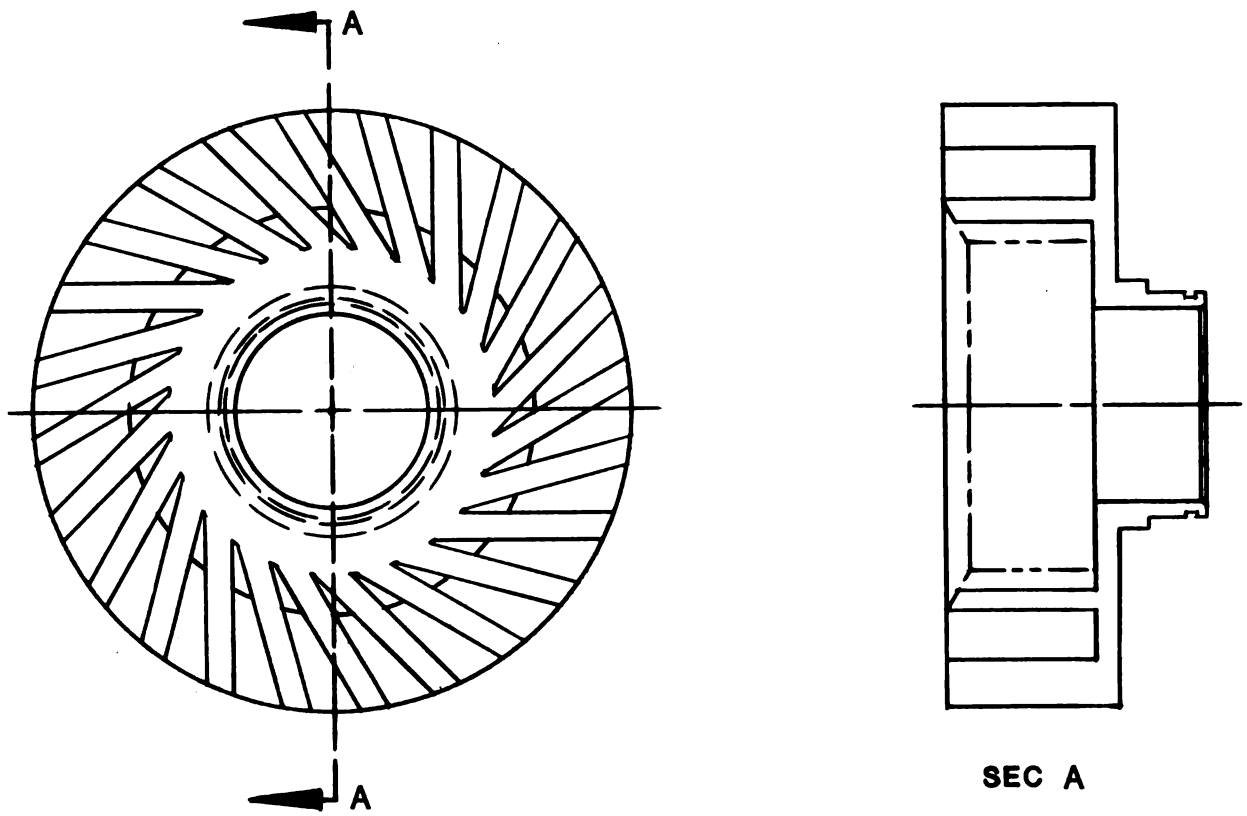
Figure 2.2-20   Radial Swirler

SEC A

IMPINGEMENT JET STABILIZED BURNER

REWORKED BURNER-PARTITION PLATE

IGNITION HOUSING
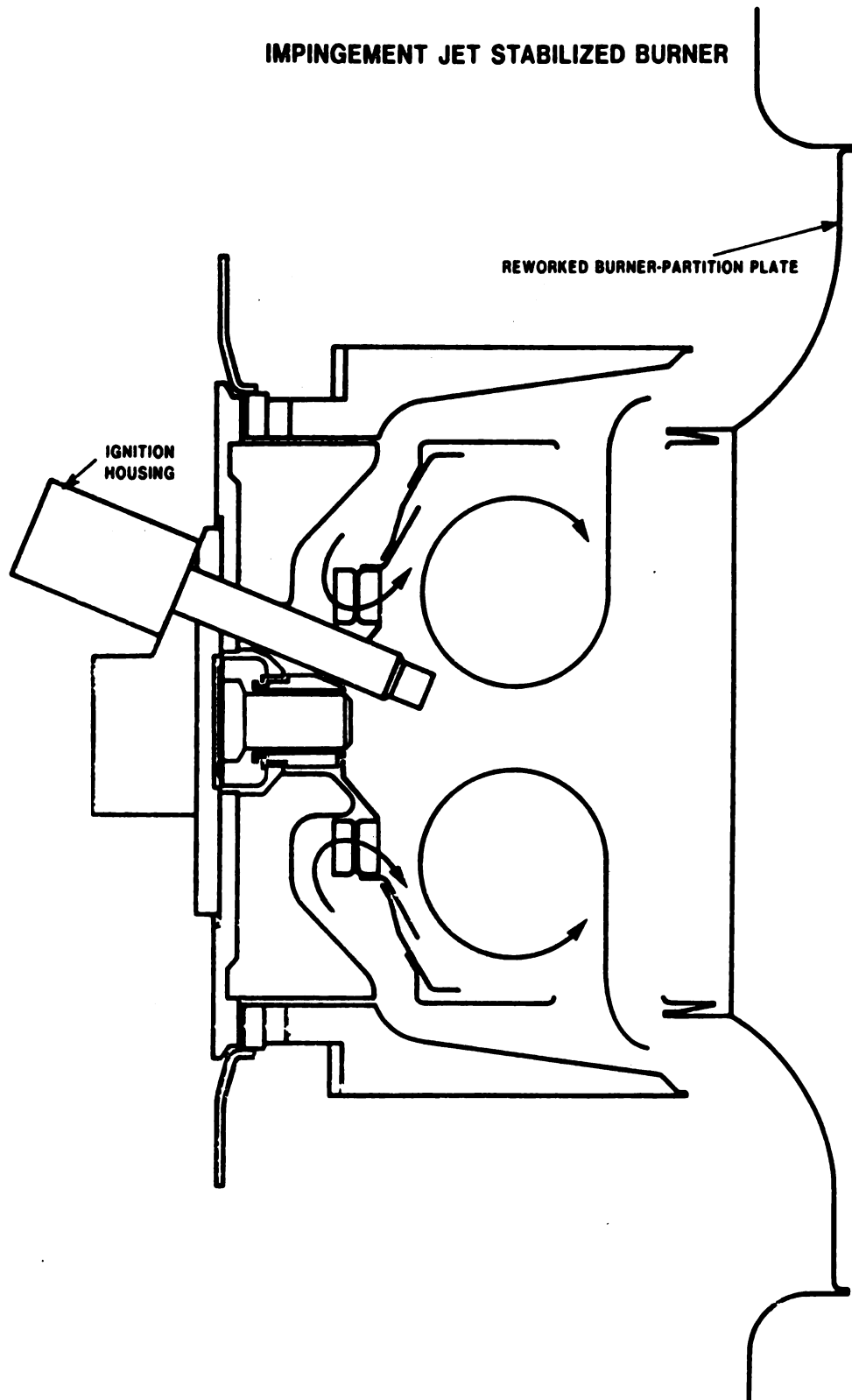
Figure 2.2-21   Impingement Jet Stabilized Burner
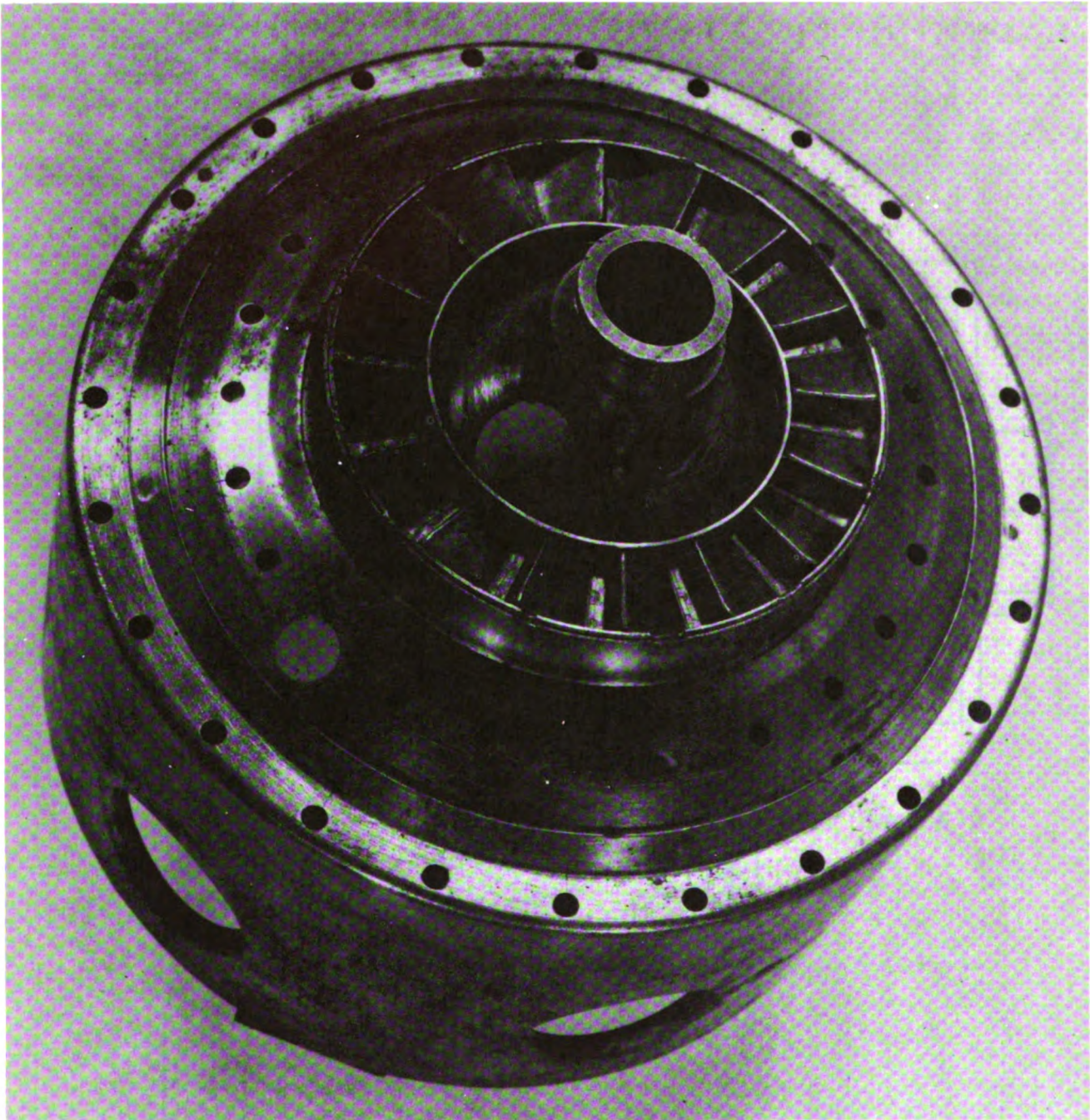
Figure 2.2-22   Baseline Version of Stabilized Burner

PHILIPS PINTLE NOZZLE

EXCELLO NOZZLE

LUCAS/USS NOZZLE
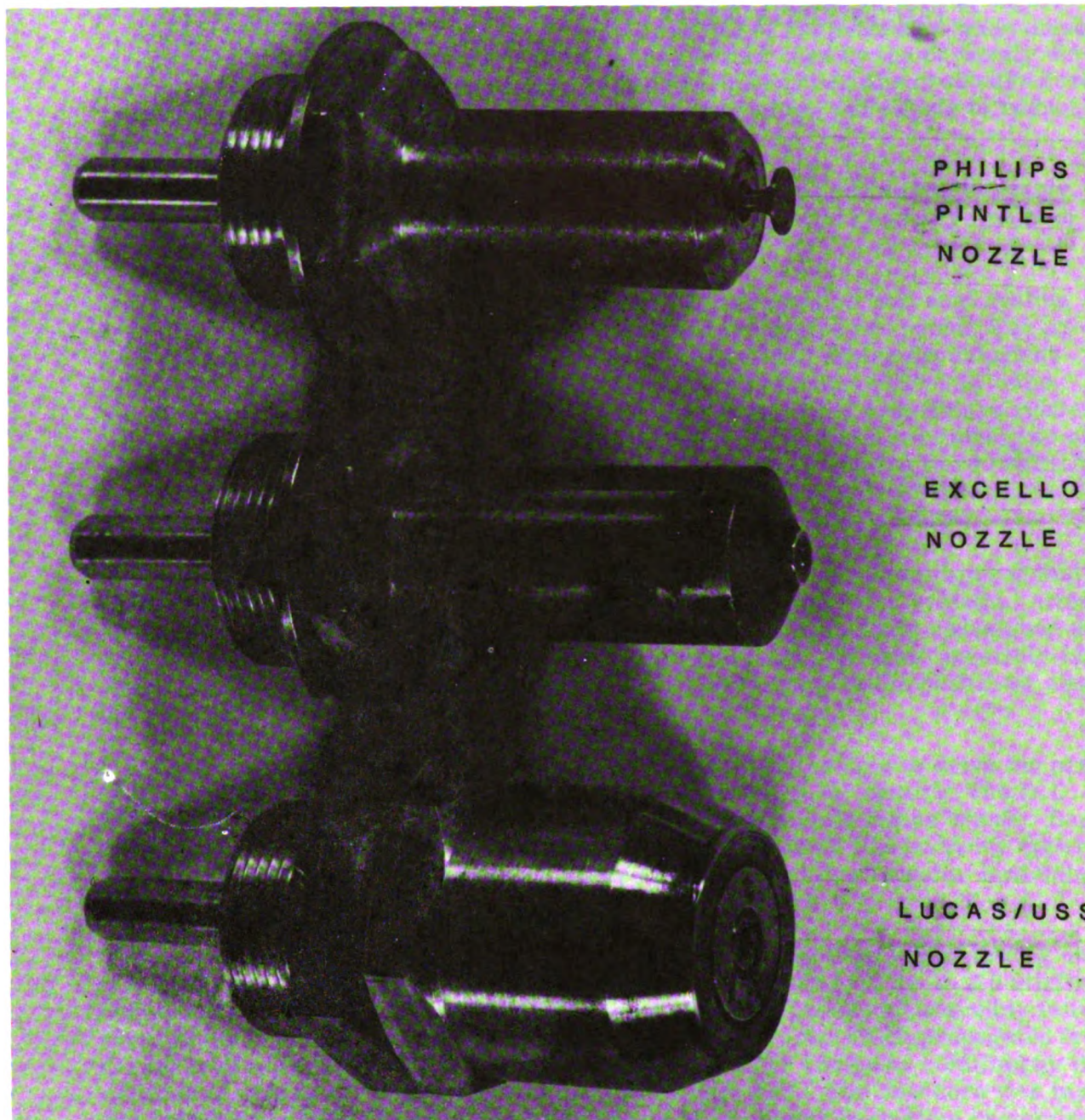
Figure 2.2-23   Pressure Atomized Fuel Nozzles

Digitized by Google

PHILIPS PINTLE NOZZLE
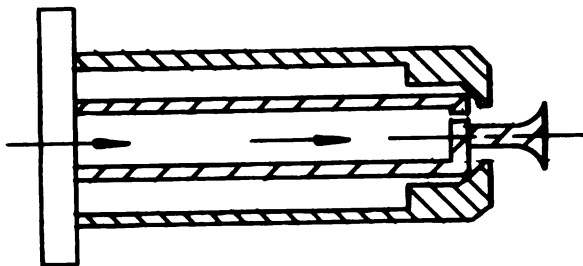
* Internal Mixing

* Fuel Backpressured by Air Assist

* Variable Cone Angle
  (90° - 160°)

EXCELLO NOZZLE
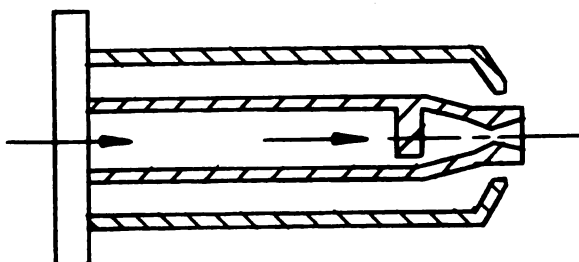
* Designed by Excello to Ford Specs.

* External Mixing

* Constant Cone Angle (120°)

LUCAS/USS NOZZLE
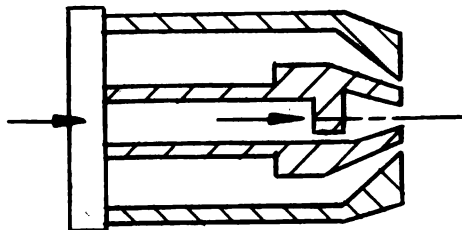
* Higher Air Assist Flow for Same   p

* External Mixing

* Constant Cone Angle (110°)

Figure 2.2-24   Fuel Nozzles

106

2.3 Preheater Development

2.3.1 Summary — The objective of this effort was to determine the fuel economy improvement opportunity resulting from a redesign of the 4-215 Stirling engine preheater. An evaluation of the functional capability of the preheater when driven directly from the engine accessory power shaft, rather than by the currently employed electric motor drive, was also scheduled. In addition, the preheater core was to be modified to include the latest ceramic technology and efforts to reduce seal leakage and friction were to be undertaken.

A Preheater Test Rig was to be built to test the redesigned preheater assembly. After functional characteristics were achieved the preheater assembly was then to be installed on the 4-215 Stirling engine for testing.

Much of the technology employed in the design of the preheater and seal system was obtained from Ford Motor Company's gas turbine engine program. The present preheater disk matrix configuration used in the 4-215 engine development program is the same as that used in the model 707 gas turbine (T20-38). The preheater disk is presently bonded to a large ring gear with a proprietary rubber compound. The gear with the bonded core is supported at three positions; two of the positions are rollers, one fixed and one spring loaded, and the third position is a pinion gear driven through a gearbox. The core is supported between two rubbing seals that are held against the core face by diaphragm springs.

Based upon 4-215 engine tests at both N.V. Philips and Ford, it was agreed that changes and improvements should be made to the 4-215 preheater system. After discussions with personnel from Philips in September of 1977 Ford redesigned the preheater system. A cross section of the original design preheater assembly is shown in the following figure. Figure 2.3-1 is a photograph of the preheater assembly showing the "hot" side of the core and the hot side seals.

2.3.2 Summary of Tests — Rig tests indicated that it is feasible to drive the preheater with the engine via an over-running clutch on the D.C. motor. The D.C. motor would drive the preheater in the interim of ignition and engine crank. Based upon torque measurements from these rig tests, a maximum fuel economy opportunity increase of 0.16 MPG could be expected by reducing the alternator load using the engine drive concept.

The redesigned preheater accumulated a total of 60 hours of durability testing on the Preheater Test Rig and an additional 9.8 hours of testing on the 4-215 Stirling engine. The original preheater core for the redesigned preheater assembly failed after 20 hours of testing. The failure was caused by cracks which propagated from the inner diameter (see Figure 2.3-2). A new preheater core was modified by the addition of stress relief slots in the inner core diameter. The new core was installed in the preheater assembly and experienced no problems during the remaining 49.8 hours of testing.

Testing revealed that no increase in fuel economy could be expected from the new preheater assembly. Due to the relatively short test time of the redesigned preheater system on the 4-215 engine, any improvements to exhaust emissions are inconclusive; however, the CO measurements and maximum temperature distribution at the lower vehicle simulation point loads appear to be lower than those of the

basic (original) preheater system.

4-215 STIRLING ENGINE
BURNER-PREHEATER CROSS SECTION
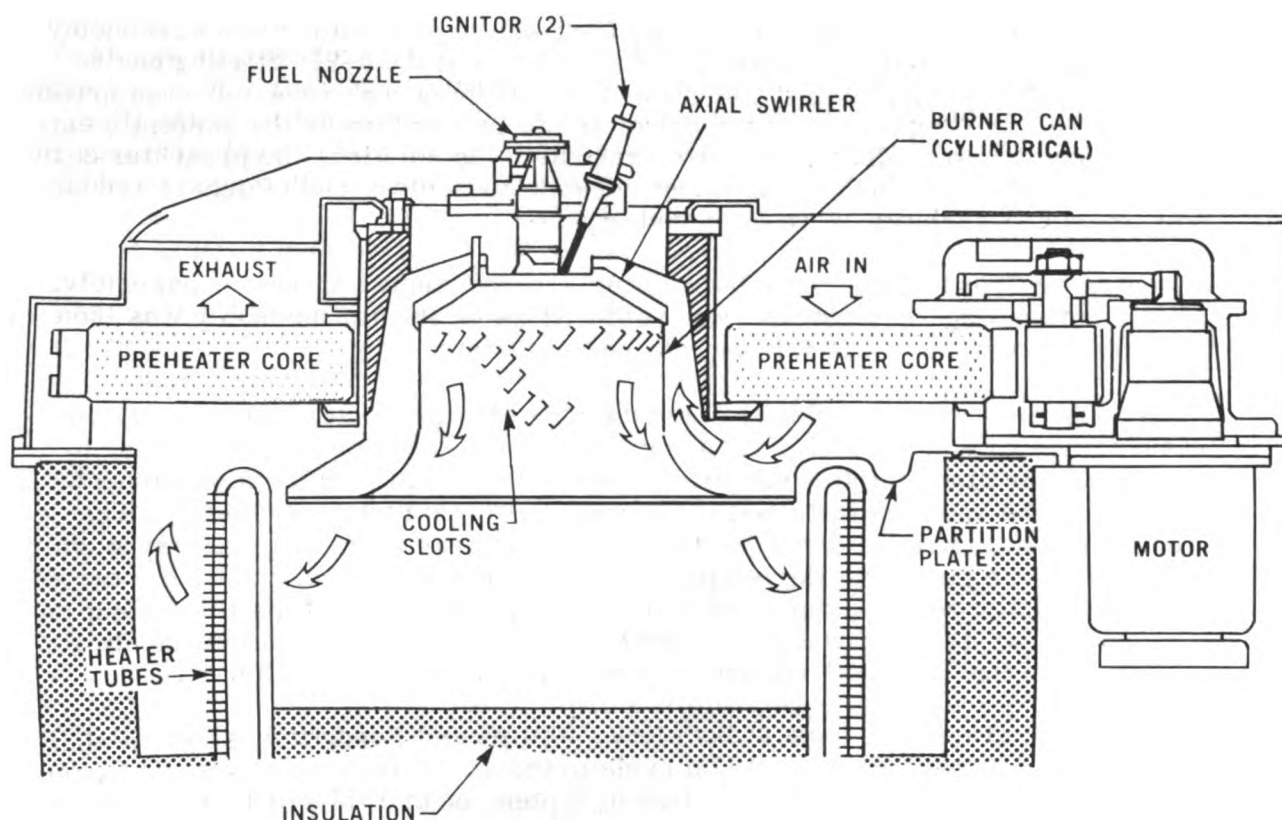
Diagram labels: IGNITOR (2), FUEL NOZZLE, AXIAL SWIRLER, BURNER CAN (CYLINDRICAL), EXHAUST, AIR IN, PREHEATER CORE, PREHEATER CORE, COOLING SLOTS, PARTITION PLATE, MOTOR, HEATER TUBES, INSULATION

The thinwall preheater core was tested on the 4-215 engine for 2.5 hours in the basic preheater assembly design. Test results based on one test series indicated that the new preheater core yielded a 0.44 MPG fuel economy improvement.

2.3.3 Results of Tests — The testing of the preheater concentrated on three areas of the preheater: The basic preheater system, redesigned preheater system, and the engine driven preheater.

2.3.3.1 Basic Preheater System — In order to identify the problems associated with the preheater system without interrupting engine testing, a Preheater Test Rig was designed and built in a dynamometer cell. The rig was equipped to measure pressure and temperature of inlet air and the exhaust gas before and after the ceramic core. A sketch of the rig is shown in Figure 2.3-3.

The functional rig is shown in Figure 2.3-4. The preheater is driven by a one horsepower electric motor through a Lebow torque sensor as shown in Figure 2.3-5.

The burner assembly is similar to the one used on the 4-215 Stirling engine except that the Champion ignitor and an Excello low flow nozzle were used with a

108

swirler that was restricted by a 25.4 mm wide band because of the lower fuel requirement.

The objective of the preheater rig tests was to run the preheater assembly at engine operating conditions of pressure, temperature, and air flow to determine the torque required to drive the core and evaluate the durability of the core, seals, and diaphragms. The tests revealed that with proper seal clearance the torque required to drive the core at the preheater input shaft ranged from .32 to .38 Nm (45-54 in. oz.). The seal clearance was critical because of possible binding of the core and a resultant rapid increase in the drive torque.

The basic preheater core, seals, and diaphragms performed well under both rig and engine tests. Several hundred hours of testing were accumulated on several sets of preheater hardware with the most serious problem being distortion of the burner can and partition plate.

2.3.3.2 Redesigned Preheater System — The redesigned preheater was tested on the same rig used for testing the basic preheater system.

REDESIGNED PREHEATER
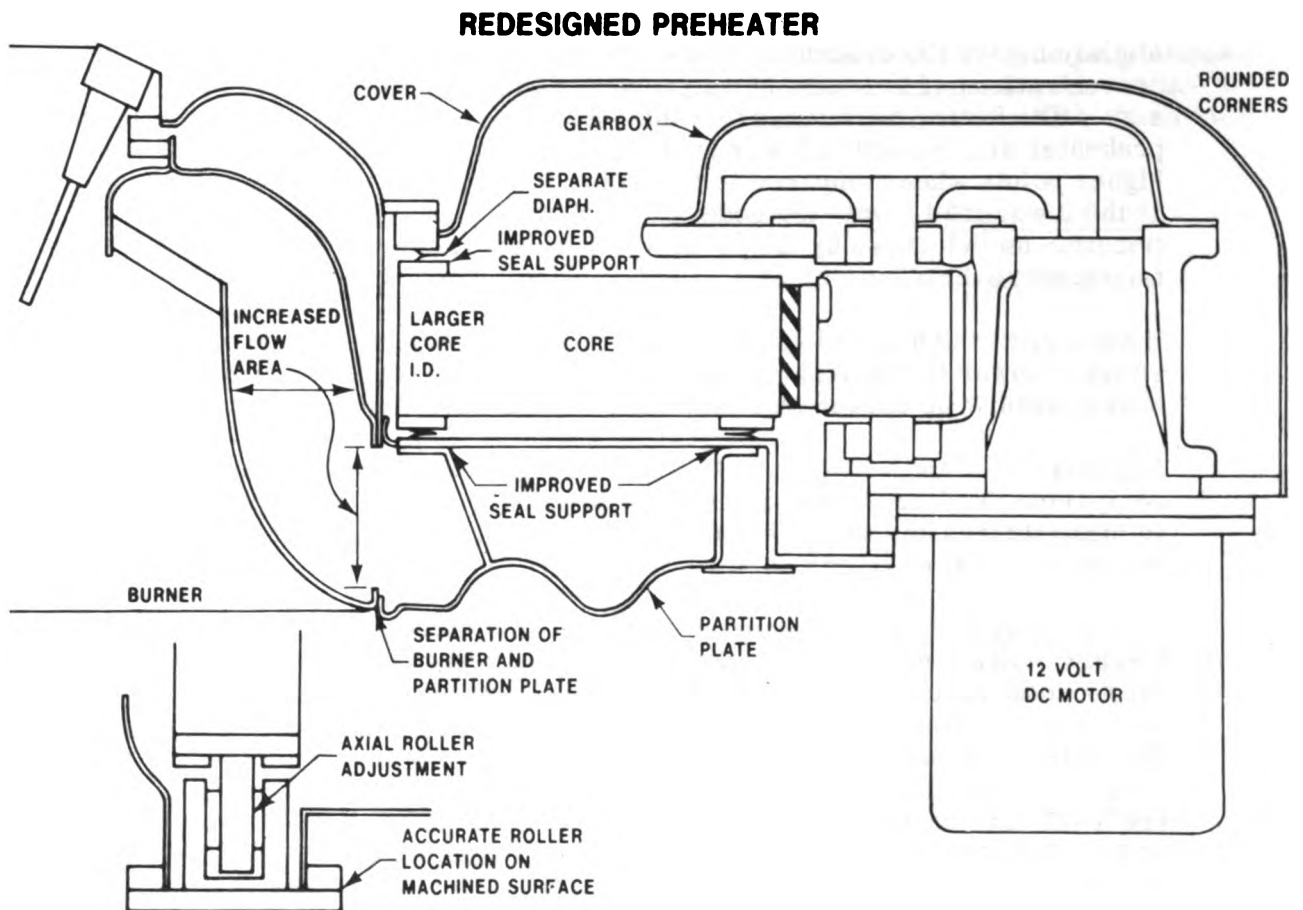
The objective of the tests on the rig was to run the redesigned preheater assembly at engine operating conditions of pressure, temperature, and air flow to determine the torque required to drive the core and evaluate the durability of the core seals and diaphragms. The preceding figure shows the redesigned preheater.

The tests indicated that the torque required to drive the core at the motor input shaft ranged between 0.17 to 0.52 Nm (24 to 73 in. oz.) and was equivalent to the torque required for the basic preheater. Although there was a core failure after the first 20 hours of testing (see Figure 2.2-2), a second core with stress relief slots on the inner diameter accumulated 40 additional test hours on the rig with no problems. The seals and diaphragms performed well, although the test time was not long enough to evaluate the durability. The redesigned preheater system accumulated 9.8 hours of testing on the 4-215 engine.

Figure 2.3-6 compares the engine exhaust emissions, preheater leakage, and maximum heater head temperature distribution for both preheater system designs on the 4-215 engine. Figures 2.3-7 and 2.3-8 show the projected fuel economies based upon engine test data using the 10 vehicle simulation points.

The most noticeable effect on the emission comparison is that the redesigned preheater has lower CO concentrations at the lower simulation points and slightly higher CO concentrations at the higher simulation load points. The NOx concentrations of the redesigned preheater are higher than those of the basic design. The heater head maximum temperature distributions of the redesigned preheater are somewhat lower at the load points and slightly higher at the higher points when compared to the basic design. The test results indicate that at the lower load points the redesign improved the air-fuel mixing and distribution as evidenced by the lower CO concentrations and the heater head temperature distribution.

However, at the higher load points, another mechanism is overpowering this effect of lower CO emissions and heater head temperature distribution which could possibly be caused by a difference in the swirlers or fuel nozzles.

Figures 2.3-7 and 2.3-8 show that there is no change in fuel economy when comparing the original and redesigned preheater. Both of the projections given in these figures and the comparison in Figure 2.3-6 are on the 4-215 engine without internal hydrogen compressors.

2.3.3.3 Engine Driven Preheater — The engine driven preheater hardware, which consisted of a D. C. preheater drive motor with an extended shaft and overrunning clutch, was tested on the Preheater Rig for 20 hours.

The preheater motor was run 2 minutes before and 3 minutes after ignition, then it was shut off and the core was driven by the auxiliary motor at 1750 RPM (10 RPM core speed). The current draw of the preheater motor was 8 amps. at 12 volts, and the torque requirement motor was approximately .353 Nm (50 in./oz.). At each hour for 20 hours, the preheater motor was run for 5 minutes without the auxiliary motor. The core speed was changed from 10 RPM to 5.8 and 17.5 RPM to simulate the idle and maximum speed of the driving cycle. A diode was added to the electrical circuit to prevent the preheater motor from

acting as a generator and overheating.

The preheater motor with the overrunning clutch performed well; however, this concept was not tested on the 4-215 engine to verify the fuel economy improvement of 0.16 MPG (M-H).

2.3.3.4 Thinwall Preheater Core — Due to the limited availability of the test cell and technician time in the dynamometer cell, which was being shared with the two burner test rigs, the thinwall preheater core was not checked out on the preheater rig prior to testing in the engine. The thinwall preheater core was installed on engine 1X20 in another dynamometer cell (#10) and accumulated 2.5 hours of operation in the basic preheater design.

Figure 2.3-9 compares the significant characteristics of the matrix configurations of the two cores at the vehicle simulation points (1 thru 10). It can be seen that the exhaust temperature and fuel flows of the thinwall matrix are somewhat lower than those of the standard core matrix. These effects verify the theoretical projection of improved effectiveness for the thinwall core. A comparison of the required blower pressure head shows very little difference between the two.

Figure 2.3-10 is the fuel economy projection for the thinwall preheater core which can be compared to Figure 2.3-8 for the standard core. The projections are for the CVS-H and highway portion of the M-H test only, and does not include the effects of cold start. The following calculations account for the cold start and the complete M-H projection.

	Standard Core	Thinwall Core
CVS-H FUEL, g	1365.7	1334.5
COLD START PENALTY, g	148.9	142.0
CVS-CH FUEL, g	1514.6	1476.5
CVS-CH, MPG	13.88	14.24
HIGHWAY, MPG	20.48	21.07
M-H, MPG	16.23	16.67

The fuel economy projection for the thinwall core over the standard core in the 4-215 engine was 0.44 MPG, including the slight difference in the cold-start penalty. This projection compares to a theoretical projection 0.26 MPG (M-H).

2.3.4 Open Issues — With the very limited engine time on both the redesigned preheater hardware and the thinwall core material, long-range durability problems, even for prototype engine running, cannot be assessed.
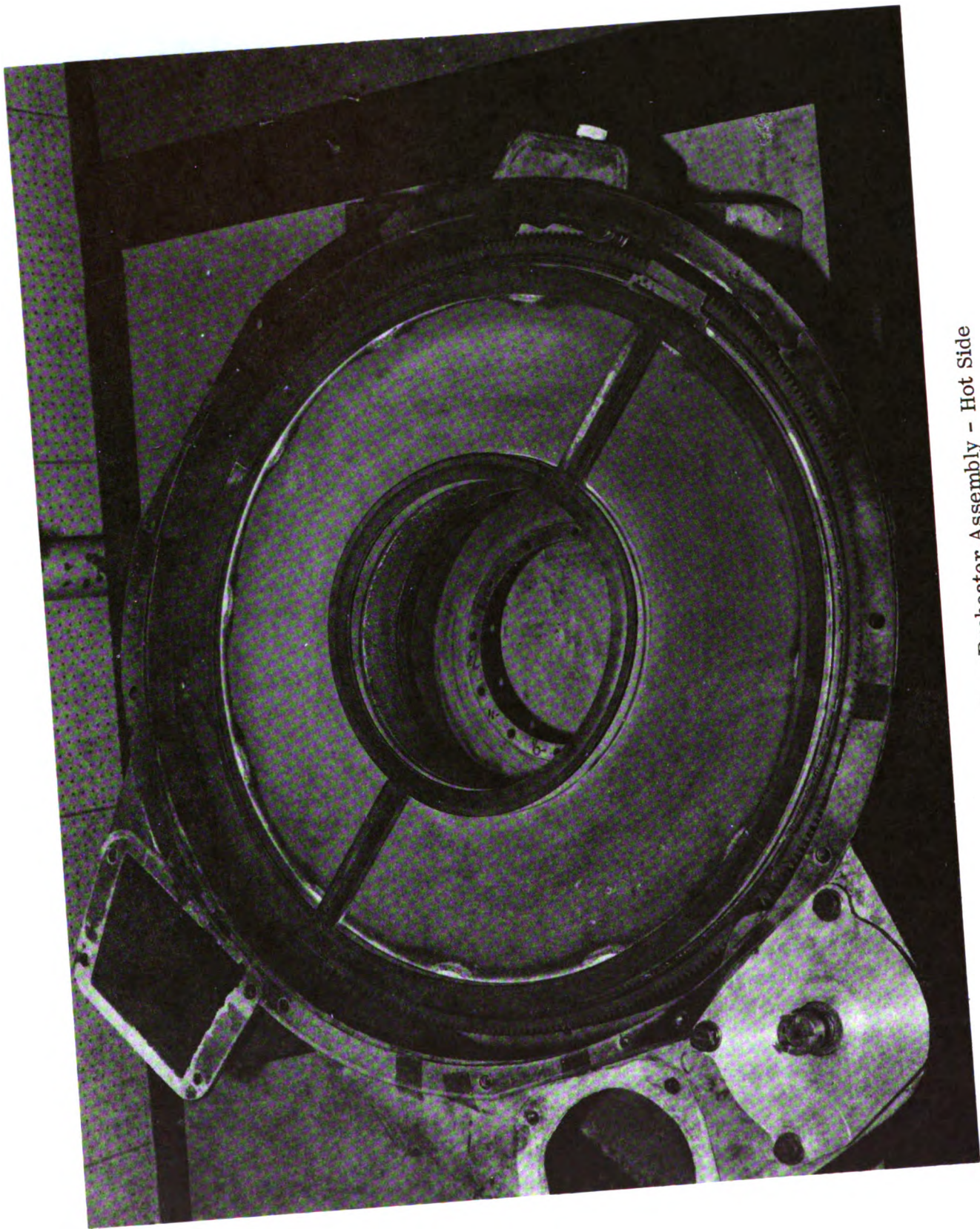
Figure 2.3-1   Preheater Assembly – Hot Side
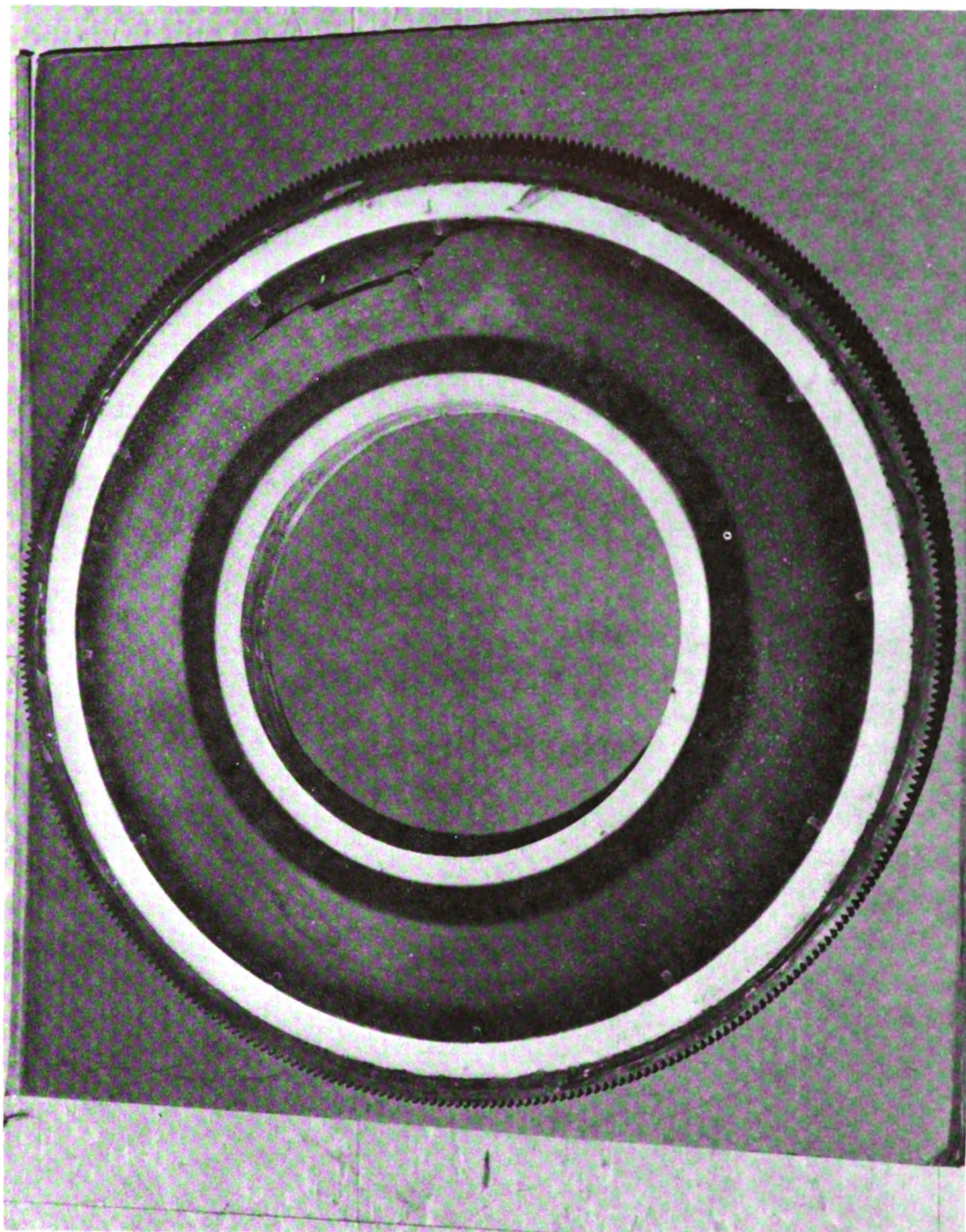
Figure 2.3-2 Preheater Failure

SUB-TASK 03 — PREHEATER DEVELOPMENT
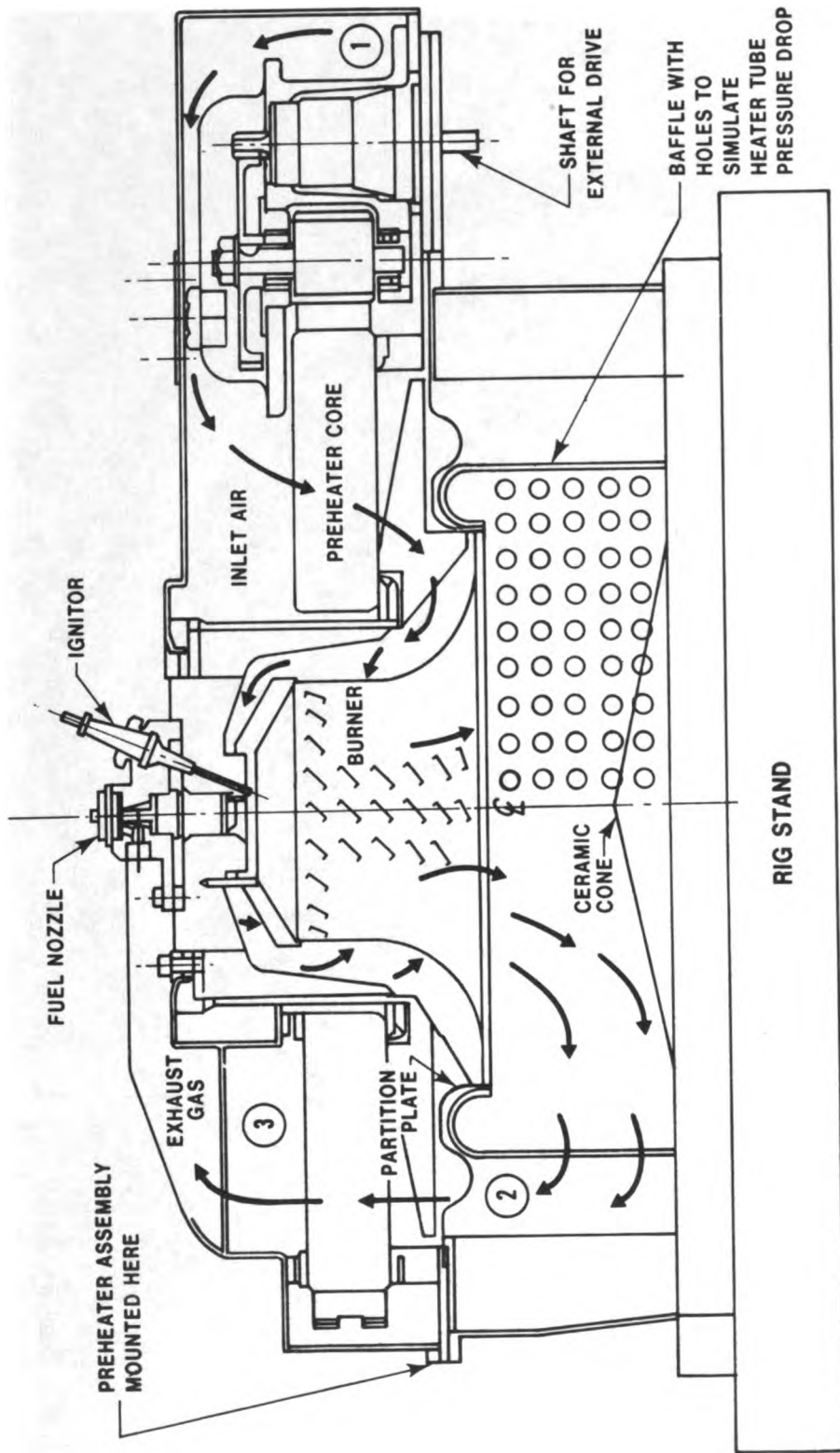
INSTRUMENTATION

1. AIR FLOW, TEMPERATURE, AND PRESSURE AT INLET TO RIG

2. TEMPERATURE INLET TO PEHEATER ON EXHAUST SIDE

3. TEMPERATURE AND PRESSURE ON EXHAUST FROM RIG

4. PREHEATER DRIVE TORQUE AND SPEED

Figure 2.3–3   Preheater Rig Cross Section
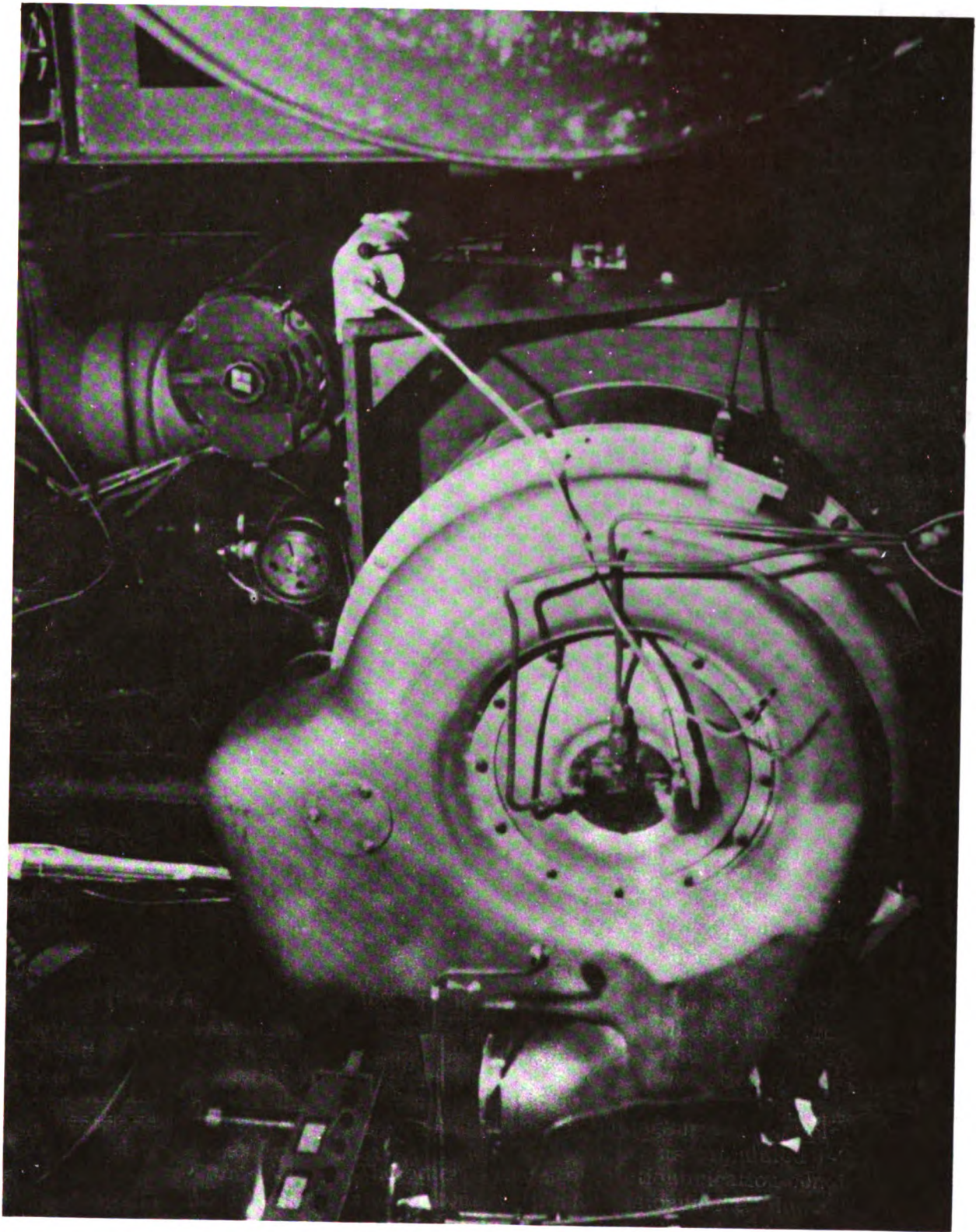
Figure 2.3-4 Preheater Rig
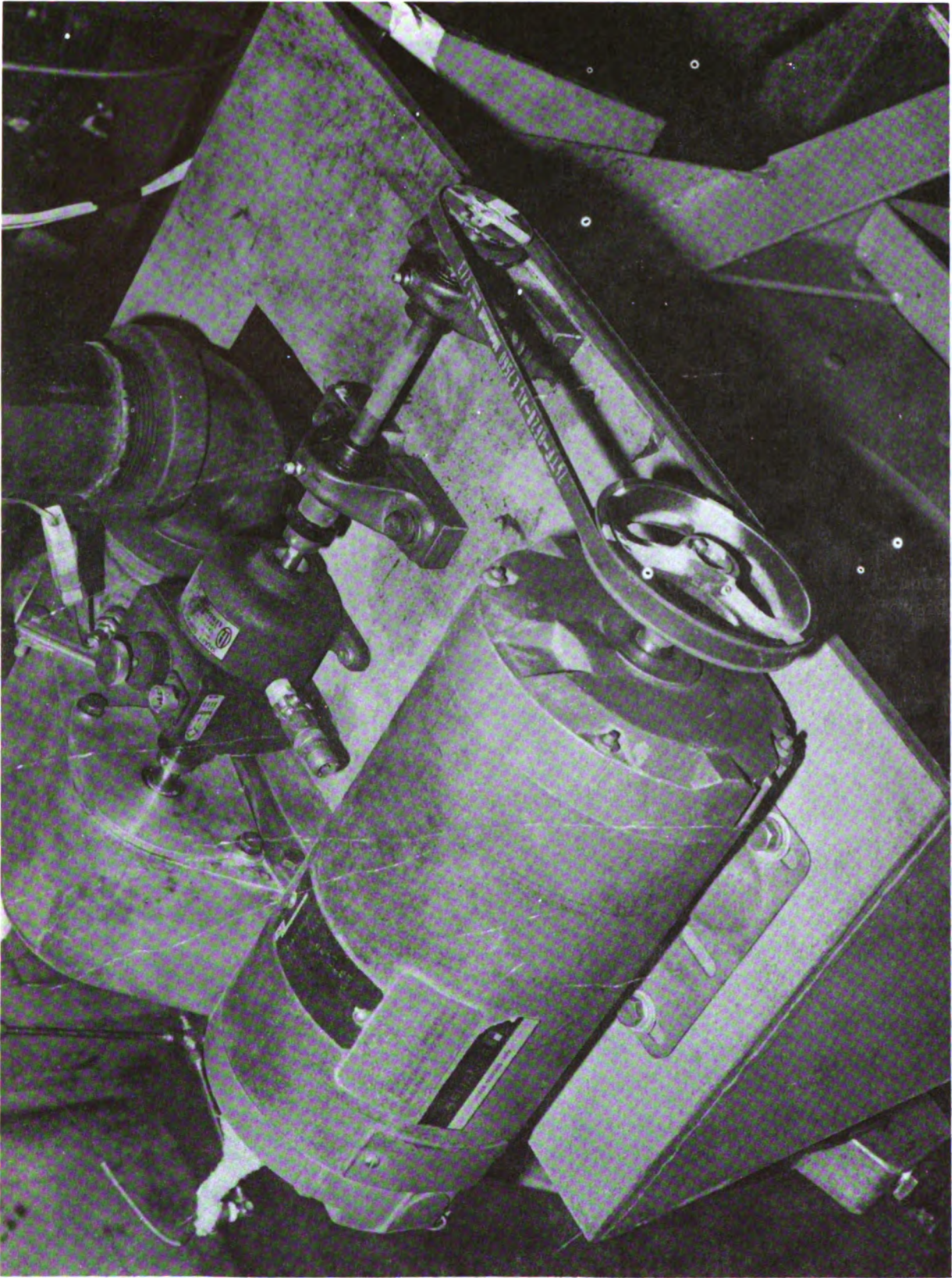
Figure 2.3-5   Preheater Rig Drive System

Vehicle Simulation Point	Redesigned Preheater (T20-38)					Basic Preheater (T20-38)				
	Exhaust Emissions			Preheater Leakage %	H.H. Max °C T	Exhaust Emissions			Preheater Leakage %	H.H. Max °C T
	HC PPM	CO PPM	NOx PPM			HC PPM	CO PPM	NOx PPM		
1	16	106	60	20.3	87	2	397	30	19.6	122
2	27	151	25	31.9	65	4	379	30	27.0	107
3	14	106	93	23.7	117	5	54	30	13.3	120
4	7	191	63	17.7	70	2	379	30	21.2	101
5	7	209	70	21.9	85	2	361	34	16.6	94
6	16	477.	105	17.4	104	2	522	52	17.7	91
7	6	766	113	18.0	135	3	595	72	19.5	95
8	6	863	90	17.1	111	4	499	25	18.0	82
9	6	766	138	11.7	145	4	545	49	22.5	104
10	8	676	92	18.8	123	5	545	71	20.2	72

Figure 2.3-6   Preheater Design Comparison

STIRLING ENGINE DYNAMOMETER EMISSION & FUEL ECONOMY

T20-38 REDESIGNED PREHEATER CONFIGURATION

| | | ENGINE BUILD---- | | | | | | | | | | | | ENGINE TEST---- | | | |
RUN NO	TIME s	FUEL FL. g/s	FUEL TOT. g	A/F	HC ppm	HC EI g/kg	HC g	CO ppm	CO EI g/kg	CO g	NOX ppm	NOX EI g/kg	NOX g	TIME s	FUEL FL. g/s	FUEL TOT. g	EGR %
1	663. 362.	0.56	202.9	20.6	6.0	0.166	0.034	106.	2.218	0.450	60.	2.063	0.419	10.	0.56	5.8	112.
2	662. 272.	0.60	163.3	20.0	7.0	0.272	0.044	151.	3.072	0.502	25.	0.836	0.136	5.	0.60	3.1	244.
3	661. 74.	0.35	25.9	21.0	4.0	0.148	0.004	106.	2.259	0.059	93.	3.257	0.084	52.	0.35	18.2	158.
4	660. 167.	0.81	135.4	20.3	7.0	0.072	0.010	191.	3.942	0.534	63.	2.136	0.289	29.	0.81	23.6	105.
5	659. 186.	1.15	213.6	21.0	7.0	0.074	0.016	209.	4.455	0.951	70.	2.451	0.523	33.	1.15	37.7	105.
6	658. 147.	1.70	250.2	20.9	6.0	0.168	0.042	477.	10.121	2.533	105.	3.660	0.916	46.	1.70	78.0	74.
7	657. 58.	2.53	147.5	20.6	6.0	0.062	0.009	766.	16.030	2.364	113.	3.885	0.573	73.	2.53	183.9	70.
8	656. 58.	1.72	98.9	20.7	6.0	0.062	0.006	863.	18.144	1.794.	90.	3.109	0.307	331.	1.72	570.0	70.
9	655. 36.	3.11	112.3	20.4	6.0	0.062	0.007	766.	15.882	1.783	138.	4.701	0.528	77.	3.11	238.8	60.
10	654. 12.	2.26	26.0	20.7	8.0	0.083	0.002	676.	14.212	0.369	92.	3.178	0.083	108.	2.26	243.6	79.

CYS-H= 1375.9   HC TOTAL= 0.174   CO TOTAL= 11.34   NOX TOTAL= 3.859   HUY= 1402.8

HC= 0.023g/mile   CO=1.51g/mile   NOX= 0.514g/mile

CVS-H=15.25mpg

HUY=20.43mpg

Figure 2.3-7   Stirling Engine Dynamometer Emission and Fuel Economy – T20-38 Redesigned Preheater Configuration

STIRLING ENGINE DYNAMOMETER EMISSION & FUEL ECONOMY

T20-38 BASIC PREHEATER CORE DESIGN CONFIGURATION
ENGINE TEST

ENGINE BUILD 120

RUN NO	TIME s	FUEL FL. g/s	FUEL TOT. g	A/F	HC ppm	HC EI g/kg	HC g	CO ppm	CO EI g/kg	CO g	NOX ppm	NOX EI g/kg	NOX g	TIME s	FUEL FL. g/s	FUEL TOT. g	EGR %
653.	362.	0.53	192.0	20.1	2.0	0.020	0.004	397.	8.116	1.558	30.	1.008	0.193	10.	0.53	5.5	91.
652.	272.	0.58	157.8	21.4	4.0	0.043	0.007	379.	8.225	1.298	30.	1.070	0.169	5.	0.58	3.0	119.
651.	74.	0.31	22.9	24.0	5.0	0.060	0.001	54.	1.308	0.030	30.	1.194	0.027	52.	0.31	16.1	145.
650.	167.	0.84	140.4	20.2	2.0	0.020	0.003	379.	7.785	1.093	30.	1.012	0.142	29.	0.84	24.4	124.
649.	186.	1.17	217.3	20.3	2.0	0.020	0.004	361.	7.450	1.619	34.	1.153	0.250	33.	1.17	38.4	105.
648.	147.	1.71	251.7	20.1	2.0	0.020	0.005	522.	10.671	2.686	52.	1.746	0.440	46.	1.71	78.5	79.
647.	58.	2.56	149.2	20.1	3.0	0.030	0.005	595.	12.164	1.815	72.	2.418	0.361	73.	2.56	186.1	67.
646.	58.	1.75	100.6	20.1	4.0	0.041	0.004	499.	10.201	1.026	63.	2.099	0.211	331.	1.75	580.0	71.
645.	36.	3.00	108.3	20.1	4.0	0.041	0.004	545.	11.141	1.207	123.	4.114	0.446	77.	3.00	230.4	50.
643.	12.	2.20	25.3	20.4	5.0	0.051	0.001	545.	11.300	0.286	71.	2.418	0.061	108.	2.20	237.2	74.

CVS-H= 1365.7   HC TOTAL= 0.039   CO TOTAL= 12.62   NOX TOTAL= 2.301   HWY= 1399.5

HC= 0.005g/mile   CO=1.68g/mile   NOX= 0.307g/mile

CVS-H=15.37mpg

HWY=20.48mpg

Figure 2.3-8   Stirling Engine Dynamometer Emission and Fuel Economy - T20-38 Basic Preheater Core Design Configuration

Vehicle Simulation Point	Thin Wall Preheater (T14-20)				Standard Preheater (T20-38)			
	Fuel Flow g/s	Preheater Leakage %	Exhaust Temp. °F	Blower P In. H_2O	Fuel Flow g/s	Preheater Leakage %	Exhaust Temp. °F	Blower P In. H_2O
1	.527	13.4	287	4.2	.53	19.6	311	4.4
2	.561	11.2	288	7.5	.58	27.0	314	7.6
3	.314	4.0	279	10.1	.31	13.3	302	9.0
4	.855	13.2	277	12.4	.84	21.2	327	11.6
5	1.12	18.2	327	14.7	1.17	16.6	346	14.1
6	1.65	18.5	364	20.4	1.71	17.7	369	19.4
7	2.49	18.6	419	28.4	2.56	19.5	418	27.5
8	1.66	20.0	371	32.9	1.75	18.0	395	31.1
9	2.99	20.9	440	36.0	3.00	22.5	422	35.8
10	2.2	17.1	397	42.8	2.20	20.2	413	41.7

Figure 2.3-9   Preheater Matrix Comparison

120

STIRLING ENGINE DYNAMOMETER EMISSION & FUEL ECONOMY

T14-20 THIN WALL PREHEATER CORE

ENGINE BUILD 1X20   ENGINE TEST _____

RUN NO	TIME s	FUEL FL. g/s	FUEL TOT. g	A/F	HC ppm	HC EI g/kg	HC g	CO ppm	CO EI g/kg	CO g	NOX ppm	NOX EI g/kg	NOX g	TIME s	FUEL FL. g/s	FUEL TOT. g	EGR %
673.	362.	0.53	190.9	20.8	1.0	0.115	0.022	327.	6.907	1.319	28.	0.972	0.186	10.	0.53	5.4	136.
672.	272.	0.56	152.6	20.7	6.0	0.167	0.025	277.	5.824	0.889	30.	1.036	0.158	5.	0.56	2.9	146.
671.	74.	0.31	23.2	24.1	2.0	0.024	0.001	151.	3.672	0.085	51.	2.038	0.047	52.	0.31	16.3	86.
670.	167.	0.86	143.0	20.1	9.0	0.192	0.028	1322.	27.026	3.863	39.	1.310	0.187	29.	0.86	24.9	86.
669.	186.	1.12	208.0	20.9	4.0	0.042	0.009	327.	6.938	1.443	48.	1.873	0.348	33.	1.12	36.7	105.
668.	147.	1.65	242.9	20.6	2.0	0.021	0.005	456.	9.543	2.318	75.	2.579	0.626	46.	1.65	75.7	76.
667.	58.	2.49	145.2	20.4	3.0	0.031	0.004	569.	11.797	1.713	85.	2.895	0.420	73.	2.49	181.0	72.
666.	58.	1.66	95.4	20.4	4.0	0.041	0.004	569.	11.797	1.126	89.	3.032	0.289	331.	1.66	550.1	69.
665.	36.	2.99	107.9	20.4	4.0	0.041	0.004	522.	10.823	1.168	118.	4.019	0.434	77.	2.99	229.6	60.
664.	12.	2.20	25.3	20.3	7.0	0.072	0.002	797.	16.447	0.416	88.	2.983	0.075	108.	2.20	237.2	71.

CYS-H = 1334.5   HC TOTAL = 0.104   CO TOTAL = 14.34   NOX TOTAL = 2.772

HWY = 1360.0   HC = 0.014g/mile   CO = 1.91g/mile   NOX = 0.370g/mile

CVS-H = 15.73mpg

HWY = 21.07mpg

Figure 2.3-10   **Stirling Engine Dynamometer Emission and Fuel Economy - T14-20 Thin Wall Preheater Core**

2.4 Engine Drive System

The objective of this section was to identify and quantify fuel economy improvements in the engine drive system. By definition, the engine drive system sub-task included: 1) the mechanism for converting reciprocating piston motion into rotary shaft motion, 2) accessory drive system, 3) engine fuel and air atomizer pump, and 4) reduction of friction in the piston rings.

2.4.1 Crankshaft Vs. Swashplate Drive System

2.4.1.1 Summary — This portion of section 2.4 was dedicated to determining the fuel economy improvements possible in the engine drive system by providing the designs and analyses necessary to compare the mechanical efficiency of the swashplate drive system with one or more crankshaft and connecting rod types of drive systems. For each of the drive systems which were evaluated, a concept engine assembly drawing was prepared as part of Reference Engine, Section 3.2, and the feasibility of packaging this concept in an automotive engine compartment was assessed.

At the start of the Ford-Philips Stirling Engine Program, a number of engine configurations were considered for installation in the Torino vehicle. Among these configurations were the swashplate mechanism, the rhombic drive, and the familiar crankshaft drive. From these alternatives, the swashplate engine was chosen for the vehicle for a number of reasons. First, the swashplate engine was the most compact and had the lowest profile of the three configurations considered. It therefore presented the least difficulty in packaging. Secondly, the swashplate engine could be completely balanced with the addition of counterweights on the mainshaft.

However, part way through the program the dual crankshaft drive pictured schematically with the swashplate drive in Figure 2.4-1, came under consideration. This engine appeared to have some advantages over the swashplate engine and therefore analytical studies of the drive were performed.

The results of the engine drive evaluation show that the swashplate and crankshaft engines could be designed to have approximately the same friction, packaging either the dual or single crankshaft engine would present problems, and the cost of the swashplate drive system is substantially higher than that of the crankshaft drive.

2.4.1.2 Analysis of Drive Systems — To have a basis for comparison of the swashplate and crankshaft drive Stirling engines, a computer program was written which calculates the bearing loads in the crank engine as a function of crank angle. This program allows for the differential gas pressure acting on the engine pistons, reciprocating mass inertia, and the rotating inertia of the crank and connecting rods to calculate the resultant forces on the wrist pin, crank pin, and main bearings. The program was later expanded to calculate the required size of these bearings and also the frictional losses occurring in them. These calculations are based on polynomial equations fit to data published by the Cast Bronze Bearing Institute relating such parameters as length/diameter ratio, eccentricity ratio, lubricant viscosity, bearing clearance, characteristic number and load. With the proper input, the program sizes the bearings such

123

that stable hydrodynamic lubrication exists. Figures 2.4-2 and 2.4-3 are typical polar plots of the front main bearing and crank pin forces in the crankshaft drive Stirling engine at one operating condition.

Once the optimum bearing parameters have been established, the frictional power losses are calculated using the equation below, which was taken from the Cast Bronze Bearing Design Manual.

$$P_f = m \ (K_f) \quad DNW \times 10^{-6} \qquad\qquad Eq \ 2.4-1$$

Where: P_f = frictional power loss, H. P.

K_f = frictional power factor based upon characteristic number

D = journal diameter, in.

N = rotational speed, RPM

W = bearing load, lbs.

m = clearance factor = 1000 (2C)/10

The journal bearing friction losses for a dual crankshaft drive Stirling engine with the same power output as the 4-215 were calculated using this program. These bearings included the main bearings and both connecting rod bearings. The equivalent friction losses were calculated for the swashplate engine using the Philips computer programs. The table below contains a comparison of this data for each of the speed-load points of a typical metro highway driving cycle.

SWASHPLATE BEARING FRICTION VS. DUAL CRANKSHAFT DRIVE BEARING FRICTION*

M-H Point No.	Speed RPM	Mean Pressure ATM	Friction Losses 4-215 (HP)	Friction Losses Dual-Crank (HP)
1	600	32.5	0.31	0.81
2	800	27.6	0.44	0.78
3	900	12.1	0.44	0.53
4	1000	36.5	0.67	1.09
5	1100	50.5	0.87	1.59
6	1300	68.3	1.26	2.37
7	1600	88.47	1.89	3.30
8	1700	53.6	1.65	2.37
9	1800	96.3	2.32	3.98
10	2000	62.7	2.19	3.90

* Excluding piston and crosshead friction.

For both cases in the preceeding table, the friction losses of the piston and crossheads were excluded. In the case of the pistons, this exclusion was justified because the pressure history (and therefore piston loading) and piston

124

dimensions in the engine were nearly identical. Because of this the friction losses were the same. In the case of the crankshaft drive, time did not permit an accurate calculation of friction losses.

An investigation of two types of Stirling engines was undertaken to establish the friction losses which could be expected in each engine when compared over an equivalent operating cycle. The engines which were analyzed differed in the type of mechanical drive system which was employed, the first using a swashplate mechanism as in the Philips 4-215 engine, the second having a dual crankshaft drive.

Two approaches can be taken in the determination of friction losses in the swashplate engine depending upon the lubrication conditions which are assumed to exist. If, as in the Philips analytical program, stable full film (hydrodynamic) lubrication exists between all bearing surfaces then losses are mainly the result of viscous friction and are calculated based upon lubricant viscosity, film thickness and relative velocity of the bearing surfaces.

However, from examination of crossheads which have undergone testing in an engine it is apparent that for a portion of each swashplate revolution the oil film between the crossheads and their bores breaks down and metal to metal contact occurs. When this happens, the coefficient of friction between the surfaces increases greatly and friction losses increase accordingly. In order to estimate the extent of losses of this type it was necessary to determine the deflection characteristics of the crossheads under the action of an axial (tensile) load while unconstrained by the cylinder bores. The crossheads were assumed to be rigid except for the bridge section which bends because of the moment applied to it. Figures 2.4-4 and 2.4-5 are schematic diagrams of a crosshead in its undeformed and deformed conditions (Figure 2.4-4b is highly exaggerated).

The equation of the elastic curve of the bridge section was determined by integrating the equation:

$$\frac{d^2y}{dx^2} = \frac{M}{EI} \qquad \text{Eq 2.4-2}$$

By assuming the symmetry about the midpoint of the bridge and using the boundary conditions of zero slope and deflection of the center of the bridge this equation was found to be:

$$Y_b = \frac{M}{2EI} (x^2 - 2L_b x + L_b^2) \qquad \text{Eq 2.4-3}$$

Where:
Y_b = deflection of bridge end

x = coordinate parallel to bridge axis

L_b = bridge length/2

M = applied moment at bridge end

E = modulus of elasticity

125

$$\text{I} = \text{cross sectional moment of inertia}$$

Then the total deflection at the ends of the crosshead was calculated knowing the deflection at the ends of the bridge and the slope of the bridge at these points.

This total deflection was equal to:

$$Y_t = \frac{ML_b}{EI} \frac{(L_b + L_c)}{2} \qquad \text{Eq 2.4-4}$$

Where: L_c = length of cylindrical section

However, when in the engine, the crossheads could deflect no more than that allowed by the radial clearance between the crossheads and cylinders. Therefore, the difference between this deflection and that in the unrestrained case was thought to be caused by moments applied to the crosshead ends by the normal forces between the crossheads and bores. These forces act at the ends of the crosshead on the outside (furthest from the engine centerline) and at the point at which the crossheads contact the bore at the inner side. These points are indicated in Figure 2.4-5. Because the amount the crossheads protruded from the bores at the inner side changed throughout the revolution of the swashplate, the distance between the normal forces changed. Therefore, the magnitude of the forces changed to provide the required moment.

It was assumed when calculating power losses that when crosshead deflection occurred, metal-to-metal contact existed between the crosshead and bores.

Therefore, these friction losses represented the maximum that could be expected due to crosshead deflection. However, it was probable that even though deflection had occurred, an oil film was maintained between the moving parts as long as the relative velocity between them remained above a certain magnitude. This was probably the case when the crossheads were near the center of their stroke when velocities were highest.

It was assumed that mixed film lubrication existed when metal-to-metal contact occurred. A coefficient of friction of 0.05 was assumed for these conditions and the frictional forces were calculated accordingly.

These forces were calculated at 20 degree increments of swashplate rotation. To arrive at the power loss the increments of energy dissipated during each interval were summed up and divided by the time per revolution.

In calculating the friction losses in the dual crankshaft engine, two types of bearings were considered. Most of the bearings in this engine were of the journal type and were assumed to operate with full film lubrication at all times. The losses in these bearings were calculated as indicated previously.

The other sources of friction in this engine were the crossheads and pistons (the pistons were not considered here because the losses attributable to them were assumed to be the same for either the swashplate or dual crank engine). The crossheads were assumed to operate with full film lubrication at all times for

a number of reasons. First, when the speed of the crossheads was low (at the extremes of the stroke) and metal-to-metal contact could occur, there were practically no side loads on the crossheads. Second, experimental observations of similar mechanical arrangements using transparent cylinder walls verified the existence of an oil film. Third, in these experiments, the addition of lubricants which were known to reduce the coefficient of friction greatly when boundary lubrication existed had little or no effect on friction losses. Therefore, the friction losses were calculated based on lubricant viscosity, crosshead speed, etc.

A summary of the frictional power losses of the three engines at each of the speed-load points in a typical metro-highway driving cycle is shown in the following table. The increased fuel flow required to produce this power was calculated based upon the indicated efficiency of the engine at each of the points. These flow rates were used to adjust the quantity of fuel consumed over the driving cycle. Using the fuel economy of the theoretical Stirling engine (i.e., as determined using the Philips program) as the baseline, the additional fuel consumed by the dual crankshaft reduced this projection by 0.3 MPG. The fuel economy of the swashplate engine, when increased crosshead friction was considered, was reduced by 1.8 MPG.

SWASHPLATE BEARING FRICTION VS. DUAL CRANKSHAFT DRIVE BEARING FRICTION [1]

M-H Point No.	Speed RPM	Mean Pressure ATM	Friction Loss 4-215 HP[2]	Friction Loss Dual Crank HP	Friction Loss 4-215 HP[3]
1	600	32.5	0.357	0.85	2.39
2	800	27.6	0.534	0.85	2.92
3	900	12.1	0.542	0.62	2.50
4	1000	36.5	0.82	1.20	3.90
5	1100	50.5	1.055	1.73	5.08
6	1300	68.3	1.509	2.56	6.98
7	1600	88.5	2.265	3.58	9.45
8	1700	53.6	2.075	2.69	7.05
9	1800	96.3	2.803	4.35	11.50
10	2000	62.7	2.771	3.35	7.90

[1] — Excluding piston friction.
[2] — From Philips analytical model
[3] — With adjusted crosshead friction.

Since the increased friction losses discussed above manifest themselves in increased heat rejection, an attempt was made to correlate the calculated losses with the results of available test data. Figure 2.4-6 is a plot of various heat rejection curves at each of the speed-load points in a typical M-H driving cycle.

Curve A is a plot of heat rejection (friction losses) of the 4-215 Stirling engine as calculated using the analytical model. These losses are based upon ideal lubrication conditions and perfectly rigid crossheads and, therefore, are relatively low. Curve B is based upon test data accumulated at Ford during dynamometer testing of the 4-215 Stirling engine. The data was obtained by

measuring the flow rate and temperature rise of the engine lubricant. It was apparent from this curve that there was heat generation (friction) in the drive system of the engine that was not considered in the Philips analytical model. Curve C was also based upon Ford test data with corrections applied to account for heat losses through conduction, convection, and radiation which were not apparent in lubricant temperature rise. Curve D was based upon the theoretical calculations. However, in this case the additional friction caused by crosshead deflection and "binding" was included. It should be noted that Curve D represents a "worst case" situation in that it assumed that any time the crossheads have deflected an amount equal to the clearance in the bores, the lubrication film broke down and boundary lubrication existed with a marked increase in the coefficient of friction. This was probably not true but it was not possible to determine the exact point of transition from full film to boundary lubrication.

The data from curves C and D was used to quantify the fuel economy degradation which was expected over the M-H driving cycle. The baseline fuel economy was that of a 4500 lb. vehicle equipped with the 4-215 Stirling engine which performed according to the calculations of the analytical model. Using the data from Ford tests, with additional heat losses (curve C), the fuel economy decreased by about 1.1 MPG. When additional crosshead friction was considered (curve D) the 1.1 MPG loss in fuel economy figure increased to 1.8 MPG.

Dynamometer tests of the 4-215 engine have yet to substantiate the projected fuel economy of 15.7 MPG. The best measurement was approximately 14.4 MPG. Considering the fuel economy penalties imposed by increased engine friction, it was possible that incorrect estimates of friction offered a partial explanation of this.

As discussed above, the increased friction losses in the 4-215 engine were attributed to distortion of the crossheads during the portion of each engine revolution when they are subjected to tensile loads. This condition could be remedied by increasing the section modulus of the crosshead bridge so that the crossheads would become effectively rigid. (It was assumed that distortion occurred only in the bridge). However, the present design of the crankcase did not permit this type of modification because of dimensional constraints. As an alternate solution, it was decided to stiffen the crosshead bridges as much as possible and then modify the lands of the crossheads so that whatever distortion still existed could not result in contact with the cylinder bores.

The deflection and slope of the end of the bridge are given by:

$$y \quad = \frac{ML^2}{2EI} \qquad\qquad \text{Eq 2.4-5}$$

$$\text{and } \frac{dy}{dx} \quad = \frac{ML}{EI} \qquad\qquad \text{Eq 2.4-6}$$

Where: y = deflection

$\frac{dy}{dx}$ = slope

$$M \quad = \text{ applied moment}$$

$$L \quad = \text{ bridge length}$$

$$E \quad = \text{ modulus of elasticity}$$

$$I \quad = \text{ moment of inertia}$$

From equation 2.4-5 it was apparent that the deflection was proportional to the square of the bridge length. Therefore, it was advantageous to reduce this length as much as possible. This was done by reducing the thickness of the swashplate. The thickness of the swashplate was based upon stress considerations rather than the requirement of containing tungsten balance weights as was the case with the current 4-215 swashplate. For a disk supporting a single concentrated load at its outer edge, the maximum radial stress is given by:

$$\sigma_r \quad = \frac{BW}{t^2} \qquad\qquad \text{Eq 2.4-7}$$

Where: $W \quad = \text{load}$

$t \quad = \text{thickness}$

and B may be found from the following table:

a/b	1.25	1.5	2.0	3.0	4.0	5.0
B	3.7	4.25	5.2	6.7	7.9	8.8

Where a and b are the outer and inner radii respectively.

Assuming a fatigue strength of 40,000 psi for nodular iron, equation 2.4-7 yields a minimum required thickness of 1.16 in. (2.95 cm) or a reduction of 0.9 in. (2.29 cm). Therefore, the crosshead bridge can be shortened by 0.45 in. at either end.

Equation 2.4-6 could then be used to calculate the maximum slope in the bridge and therefore the amount of rotation of the crosshead land sections that would have to be allowed for. As shown in Figure 2.4-7 the interference that would exist between the crosshead and bore could be eliminated by providing "barrel shaped" or arced surfaces at either end of the crossheads. With this arrangement, the lateral alignment of the crossheads could be maintained. The chord length of these arcs is important since it determines, in part, the lateral load carrying capacity of the crossheads if a full oil film separating the crossheads and bores is to exist. The required chord length could be estimated by assuming that when the crossheads are at the extremes of their stroke, with minimum velocity, the bearing surfaces act as journal bearings with zero relative velocity. Figure 2.4-8 shows an enlarged view of one of the crosshead bearing surfaces and its relationship to the cylinder bore. For this type of bearing, the time required for the oil film thickness to be reduced to a specified value is given by:

$$\Delta t = \frac{24\,\mu\,br}{Wm^2} \left[\tan^{-1}\left\{ \left(\frac{1+E}{1+E}\right)^{1/2}\right\} \frac{E}{(1-E^2)^{1/2}} \right]_{E_1}^{E_2} \qquad \text{Eq. 2.4-8}$$

<div align="center">Eq 2.4-8</div>

Where: Δt = time increment

μ = viscosity

b = bearing length

r = bearing radius

W = load

m = clearance ratio

E_1 = original journal eccentricity

E_2 = final journal eccentricity

The allowable time (Δt) could be calculated with the known engine speed and duration of maximum load throughout a revolution of the engine.

Rearranging equation 2.4-8 the bearing length, b, was determined to be about 0.46 inches (1.17 cm). It was assumed that squeeze film lubrication was maintained during periods of zero relative velocity, lubrication conditions would change to hydrodynamic as relative velocity increased and loads diminished.

With the crossheads modified as described above, a substantial moment would be applied to the piston rods during the portion of the swashplate revolution when tensile loads existed in the rods. To prevent this, the original press fit connections between the rods and crossheads had been replaced by pin joints similar to the wrist pins in a conventional IC engine. This would substantially reduce lateral loads on the sliding seals, guide bushings, etc. The required size of the pins was determined using equation 2.4-8. It was estimated that a pin of 1.0 in. (2.54 cm) diameter would provide adequate service.

Figure 2.4-9 compares the proposed new drive design with the present 4-215 engine drive. Although this proposal does not represent the shortest possible arrangement, it allows use of the existing block castings. The main advantages of this design are:

1) Reduced drive friction.

2) Improved rod sealing potential.

3) Improved mainshaft bearing installation.

4) Reduced weight.

5) Reduced cost.

<u>2.4.1.3 Engine Drive Cost Study</u> — A comparative cost study was performed for the dual crank and swashplate engines. The comparison covered only the major drive components (i.e., swashplate, crankshaft, crossheads). The results of the comparison indicated that the swashplate engine would cost approximately $67,00 more than the crankshaft engine based on a production rate of 500,000 units per year. However, most of this additional cost was due to the accessory drive system required by the swashplate engine (i.e., the drive shaft, chain drive and the casting which houses and supports the driveshaft).

The dual crankshaft engine utilized a conventional accessory drive system whereby power was transmitted from a main crankshaft pulley to the various accessories by means of flexible belts. In contrast, the swashplate engine required an additional drive shaft which was driven by a chain and sprocket system located at the rear of the engine. The accessory drive shaft was supported in a casting above the engine and is parallel to the engine centerline. Power was then transmitted from the driveshaft to the various accessories via conventional V-belts and pulleys.

The additional power consumed by the accessory driveshaft bearings and the chaindrive system was found to be responsible for about 0.05 MPG penalty over the M-H driving cycle.

<u>2.4.1.4 Conclusion</u> — Neither the crankshaft nor the swashplate drive system offers a significant advantage in friction reduction. However, the swashplate drive must be redesigned before meeting the lower friction levels calculated by the analytical model. Also, the present swashplate engine accessory arrangement results in a prohibitive cost penalty over the crankshaft engine.

<u>2.4.2 Reduction of Losses in the Accessory Drive System</u>

<u>2.4.2.1 Summary</u> — This portion of the effort was dedicated to quantifying the fuel economy improvement which could be realized by reducing the excess capacity of the accessories by utilizing a variable drive ratio.

The accessory drive system for automotive engines has been considered inefficient since accessory power become a significant portion of indicated engine power. This is because accessory drive ratios are determined by requirements at engine idle, which results in excess capacity at higher speeds. Variable or 2-speed accessory drives which reduce accessory power at higher engine speeds have long been available. Due to government mandated fuel economy requirements, these accessory drives are now being considered despite a cost penalty. Because the 4-215 Stirling engine requires a combustion air blower and a large electrical power generation capacity, gains in efficiency of the accessory drive system would benefit the Stirling engine more than its I.C. counterpart. The potential fuel economy improvement resulting from this item was 0.35 MPG.

<u>2.4.2.2 Summary of Analysis</u> — The analysis used, as its baseline, a 4-245 Stirling engine (See Section 2.8-8) and 4500 lb. IWC 1977 LTD II. However, the accessory loads in the engine map were changed in order to allow evaluation of the effects of the 2-speed accessory drive.

The engine accessories included in this study are the blower, alternator, water pump, cooling fan, power steering pump, and oil pump. The blower is the only accessory not normally included on an I.C. engine.

For the 2-speed accessory drive used on the 4-245 Stirling engine, it was found that at engine speeds below 2000 RPM the optimum blower drive ratio was 5:1 and at engine speeds above 2000 RPM the optimum blower ratio was 3.5:1. Accordingly, it was assumed that the 2-speed accessory drive changed its drive ratio at an engine speed of 2000 RPM and that the accessory speeds were reduced by a factor of 0.70 (3.5/5.0).

It should be noted that analysis revealed that for the water pump the highest power requirements for this accessory existed at high engine power/speed conditions. Accordingly, reducing the speed of the water pump as engine speed increased was not advantageous for the Stirling engine. Therefore, if the water pump was to be included on the 2-speed accessory drive shaft, it would be necessary to operate this component at excessive speed for engine speeds below 2000 RPM. This in turn would result in a decrease in fuel economy and performance benefit of the 2-speed accessory drive.

Accordingly, the benefits of the 2-speed accessory drive were compared on the assumption that the water pump was on the 2-speed accessory drive shaft as well as on the assumption that the water pump was not included on this shaft.

The TOFEP computer program (See section 5.3 for a description of all computer programs) was used to assess the fuel economy benefit of a 2-speed accessory drive for the 4-245 Stirling engine.

Figure 2.4-10 contains the accessory torque losses as a function of engine speed for the case where a 2-speed accessory drive was not used as well as for the case where the 2-speed accessory drive was used.

Figure 2.4-11 shows the accessories presently proposed to be powered by the accessory drive shaft for the fourth generation Stirling engine. In addition to the components studied in this report, Figure 2.4-11 shows that the air atomizing pump, engine preheater, fuel pump, and air conditioning compressor were also supplied with power from the accessory drive shaft. These four components were compatible with a 2-speed accessory drive, although the fuel economy savings associated with placing these four components on a 2-speed accessory drive shaft was small. For instance, the torque required for these four components at an engine speed of 4500 RPM was estimated to be less than 0.5 ft.-lbs. which was less than 2% of the accessory torque required at this engine speed. (Note: The air conditioner compressor was operating with only drive losses during chassis roll dynamometer M-H fuel economy testing).

To provide a basis for comparison, a TOFEP computer run was made in which the power required to drive the alternator, fan, power steering pump, water pump, oil pump, and blower was reduced to zero.

Fuel economy benefits which may be attributed to a 2-speed accessory drive may be achieved in two ways. The first is a direct fuel economy benefit achieved by the fact that the accessory power draw is reduced at engine speeds above 2000

132

RPM. The second is that, due to the reduced accessory power draw, faster 0-60 MPH acceleration times are obtained. This in turn allows the use of a smaller engine in order to obtain a specified 0-60 MPH acceleration objective. In this report, improvements in M-H fuel economy resulting from both of these benefits have been credited.

2.4.2.3 Results — The results obtained from this study are shown in Figures 2.4-12 and 13.

Figure 2.4-12 shows that using a 2-speed accessory drive with the water pump included on the drive shaft caused a decrease in M-H fuel economy of 0.21 MPG. However, it is further seen that the 0-60 MPH acceleration time was decreased by 0.5 seconds. Figure 2.4-13 shows that, if the engine is scaled down to provide equivalent performance, only a 0.02 MPG decrease in M-H fuel economy will result. This analysis shows no advantage will be gained by the use of a 2-speed accessory drive if the water pump is included on the accessory drive shaft.

Figure 2.4-12 shows that using a 2-speed accessory drive with the water pump not included on the drive shaft caused an increase in M-H fuel economy of 0.17 MPG with a decrease in the 0-60 MPH acceleration time of 0.5 seconds. Figure 2.4-13 shows that an additional 0.19 MPG incremental fuel economy gain is achieved by scaling down the 4-245 Stirling engine to provide equivalent performance. This provides an overall fuel economy improvement of 0.35 MPG.

2.4.3 Engine Drive for Fuel and Air Atomizer Pumps

2.4.3.1 Summary — This portion of the effort was devoted to quantifying the fuel economy improvements that would result from replacing the electric fuel and air atomizing pumps with mechanical pumps driven by the engine.

An analysis was performed of the power requirements for a typical mechanically driven fuel pump and a pump (Gast Model 0440-P103) to provide atomizing air for the 4-215 engine. These requirements were compared to those of the existing electrically driven pumps. (See Figure 2.4-14 for schematics of the drive systems). The mechanical drive for these auxiliaries resulted in a power saving which would produce an improvement of about 0.24 MPG over the M-H cycle.

2.4.3.2 Analysis

The following procedure was used to assess the fuel economy gains of a mechanical belt drive system over the currently used electrical drive system.

    a. The total engine shaft power related to the electrical drive for the fuel and air atomizer pumps was calculated.

    b. The maximum flow and mechanical power requirements for the fuel pump and air atomizer pumps were defined.

    c. The ECONCALC computer program was used to calculate the M-H fuel economy using the electrical components.

    d. The adjusted accessory power requirements were used to adjust the M-H fuel economy.

133

The following assumptions were used in the calculations.

   a. Efficiencies - Belt 95%, Chain 97%.

   b. Fuel pressure remained constant at 40 psi.

   c. Fuel pump efficiency was estimated based upon state of the art.

   d. The air flow requirement was the same as that used in dyno testing.

   e. The alternator was continuously charging at 14.5V.

   f. The air atomizer power is as shown on Figure 2.4-15.

Results of Analysis — The results of the calculations indicated that the improvement in fuel economy using the new air pump was about 0.24 MPG over the M-H cycle.

Package studies were performed which indicated that belt driven air atomizer and fuel pumps were packageable in the baseline vehicle and could be driven by either the blower motor during start-up, or the engine during normal running. One of the possible package layouts is shown in Figure 2.4-16.

Upon mutual agreement by Ford and NASA, testing of the belt driven fuel pump was deleted from the Task I plan due to the non-availability of a pump meeting our requirements.

2.4.4 Piston Ring Friction

2.4.4.1 Summary — The 4-215 Double Acting (D.A.) Stirling engine uses two rings per piston to seal gas in the expansion space from gas in the compression space. Ring friction and gas leakage past the rings substantially reduce the fuel economy of the engine. This represents a loss in net work output from the engine and results in a reduction in cycle efficiency.

The initial intent of the piston ring task was to reduce the ring friction by pressure balancing the rings and by using Rulon J in place of Rulon LD as the ring material because of its lower published coefficient of friction. Pressure balancing a ring decreases the unit loading on the ring face and consequently reduces wear. If the axial width of the ring is not increased, pressure balancing also reduces the seal friction. However, leakage will probably increase since both the unit loading and the length of the effective leakage path are reduced. The purpose of testing pressure balanced rings was to evaluate the trade-off between friction and leakage.

2.4.4.2 Analysis — Cross sections of the current ring and of a pressure balanced ring are shown below. A face pressure balanced ring uses axial bleeder slots and a circumferential groove to introduce high pressure across a portion of the ring face as shown in figure (b). The pressure on the ring face opposes the high pressure on the opposite side of the ring so that the unit loading on the ring face is reduced.

134

CURRENT RING
(a)

PRESSURE BALANCED RING
(b)
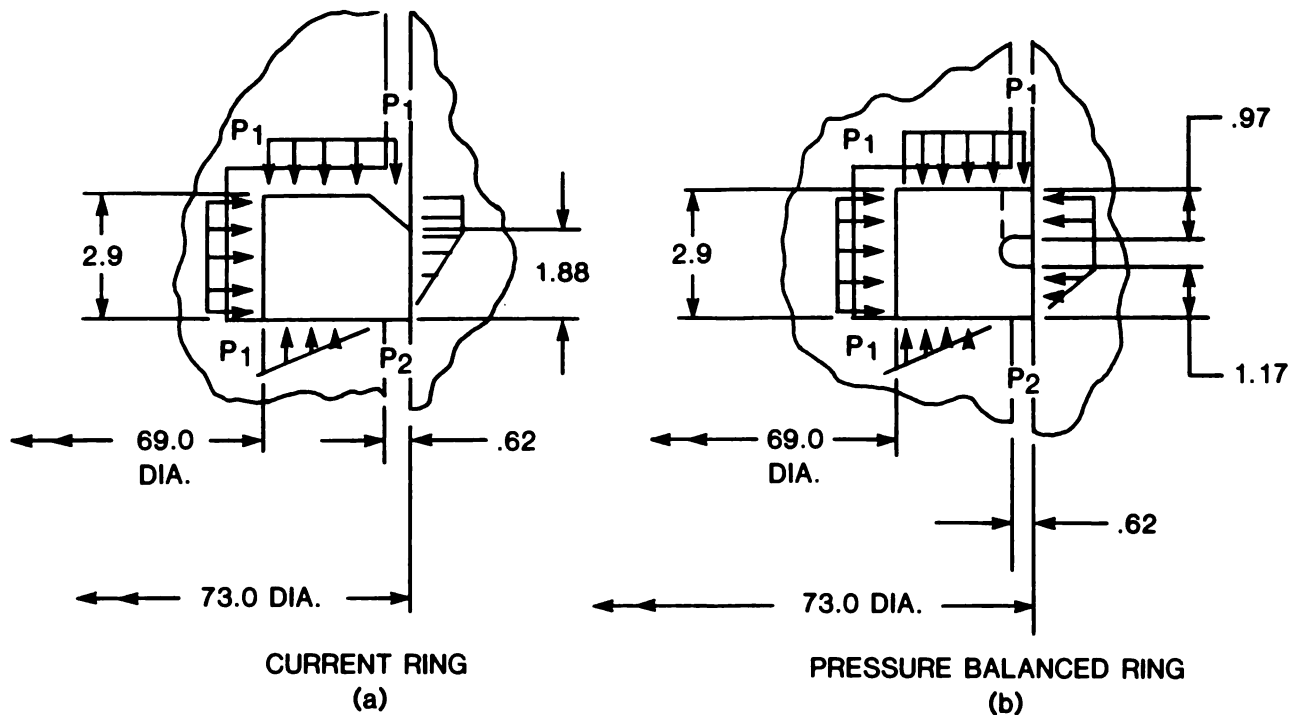
Referring to figure (b) the cantilevered section of the ring is subject to a bending moment resulting from the pressure difference across the ring. To insure that the strength of the ring is adequate, the minimum height of the unsupported section of the ring required at a mean pressure of 200 atm. was estimated to be 1.13 mm. This was estimated by allowing a safety factor of 1.2 and assuming the tensile strength of the Rulon to be 1900 psi.

The dimensions of the pressure balanced ring as tested are shown in figure (b).

The expected reduction in friction due to pressure balancing was calculated by comparing the forces acting on the current and the pressure balanced ring cross sections. The friction force is equal to the contact force between the ring and the cylinder multiplied by the coefficient of friction. When the outward force of the inner metal backup ring was neglected, the contact force was equal to the net radial pressure force. To simplify the analysis, it was assumed that pressure drop across the sealing surface was linear. The net radial pressure force was calculated for the current and the pressure balanced rings and a 36% reduction in friction was predicted.

Calculation of the forces acting on the ring cross-section was also required to insure that the ring was seating axially and radially. For the ring to seat axially, the axial pressure force had to be greater than the axial drag force on the cylinder wall. For the seal to seat radially, the radial pressure forces had to be greater than the radial forces showed that the ring would seat axially and radially.

The rate of wear for Rulon is mainly a function of the PV (pressure velocity) number at which the material is run. PV numbers for the pressure balanced

ring were lower than those of the current ring because the unit loading on the seal face was reduced.

Comparison of PV numbers using equations 2.4-9 and 10 showed that the pressure balanced ring operated at PV numbers about 45% lower than the current ring.

$$PV = \frac{load \ (lb.f)}{bearing \ area \ (in.^2)} \quad \cdot \quad velocity \ (ft/min.) \qquad Eq \ 2.4\text{-}9$$

$$PV = \frac{net \ radial \ pressure \ force \ (lb.f)}{ring \ contact \ area \ (in.^2)} \quad \cdot \ velocity \ (ft./min.) \qquad Eq \ 2.4\text{-}10$$

PV numbers at a typical M-H point of operation were calculated as follows:

Engine Speed   =   1500 PRM

Mean Pressure =   65 atm

Average ring velocity = 2 · stroke · RPM = 512 ft./min.

Average Δ P across rings = 1/2 ($P_{max.}$ -$P_{min.}$) = 19.5 atm = 287 psi.

Using these values, the PV number for the current ring was 73,500 and for the pressure balanced ring the PV number was 41,000.

The numbers were high for continuous operation and would have resulted in relatively rapid wear of the rings. The values of PV could be decreased by increasing the axial width and pressure balancing a larger portion of the ring. Alternatively, a number of rings could be used in series so that the pressure drop across each ring would be reduced.

2.4.4.3 Testing — A Piston Ring Test Rig (See Figure 2.4-17) was utilized which consisted of a small single cylinder engine coupled to a variable speed electric motor to drive an hour-glass shaped piston. The rings were carried at the top and bottom of the piston and pressure was introduced in the midsection. In the fixture the rings were exposed to a constant pressure difference whereas in the engine the pressure difference across the rings would vary cyclically between zero and Pmax.-Pmin. Thus, tests performed in the Piston Ring Test Rig would not simulate piston ring operation in the engine. However, the tests did determine relative values for friction, leakage, and wear between various ring designs.

The cylinder in which the pistons ran is isolated from the mechanical drive by four force transducer columns. The friction force of the rings on the cylinder caused deflection of the transducers. Output from the transducers was amplified and then displayed on the oscilloscope. The display of force on the oscilloscope was calibrated by dead weighting the cylinder.

A typical oscilloscope display is shown in Figure 2.4-18a. The high frequency oscillations of the trace were due to vibration of the cylinder spring-mass sys-

tem. To decrease the possibility of data interpretation error, a 150 Hz filter was installed. The oscilloscope display with this filter is shown in Figure 2.4-18b.

By testing at various speeds and pressures, the dynamic coefficient of friction as a function of velocity and pressure was determined. The relative leakage rate was measured by closing the solenoid valve in the inlet pressure line and measuring the time required for the pressure to decrease to a specified value. Relative piston ring life was measured by weighing the rings after break-in and again after they have been run for specific intervals.

A cross-section of the original test piston is shown in Figure 2.4-19a. Rulon tape was bonded to the piston to function as guide bushings. During initial testing, excessive friction resulted because of interference between the bushings and the cylinder. This was due to inadequate clearance at operating temperatures between the aluminum piston and the steel cylinder. After the piston was modified for proper clearance, excessive friction occurred as a result of failure of a guide bushing bond. Gas pressure between the bushing and seal due to leakage past the seal then forced the bushing against the cylinder wall, resulting in increased friction. Guide bushings of thicker cross-section were fabricated and provision was made to mechanically clamp the bushings to the cylinder.

With further testing, friction measurements were inconsistent. Since gas pressure between the bushing and the seal increased as the seal leakage increased, a varying leakage caused a varying pressure drop across the seal resulting in inconsistent friction measurements. As shown in Figure 2.4-19a, the pressure drop across the piston rings was equal to $P_2 - P_1$ only if $P_s - P_1$ was negligible. To accomplish this, pressure bleed holes were drilled in the test piston. The current test piston is shown in Figure 2.4-19b.

Subsequent test results indicated that the reduction in friction due to pressure balancing reasonably correlated with the calculated value. However, increased leakage results in a net fuel economy loss with the pressure balanced rings. The test results also indicated that the coefficient of friction of Rulon J was less than that of Rulon LD.

Leakage was high and inconsistent throughout the testing. The excessive leakage was thought to occur via the ring scarf joint which is shown below.

DIAGONAL SCARF JOINT
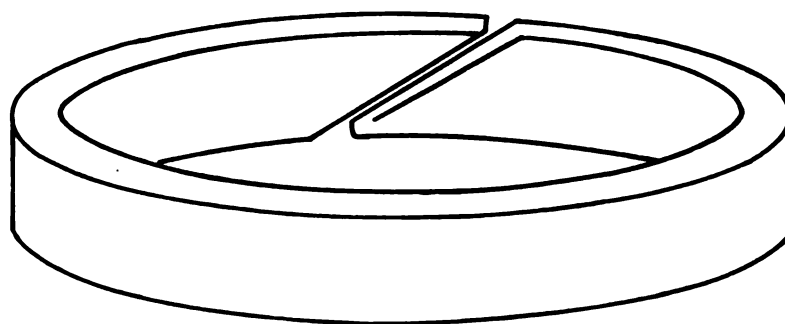
Inconsistent leakage with the scarf joint was due to the fact that the joint increases with ring wear and varies with temperature because the coefficient of thermal expansion of Rulon is very high. Optimum ring contact is shown in Figure 2.4-20a. Ring wear, or operation at low temperature, results in a joint gap as shown in Figure 2.4-20c. Sustained operation at high speed and load resulted in an increase in seal temperature and caused distortion of the ring as shown in Figure 2.4-20b. Ring wear or deformation as shown in Figure 2.4-21b provided evidence that this condition occurred during some of the testing. Increased leakage with ring wear was shown by leak testing a set of Rulon LD scarf joint rings after a 2 hour break-in at 500 RPM and 500 psi and retesting after 8 additional hours of operation. The time required to leak down from 1000 psi to 150 psi over the speed range of 300-900 RPM decreased by approximately a factor of four.

Test fixture operation at 500 psi and 500 RPM resulted in ring operation at a PV of 39,500. This value of PV corresponded to engine conditions.of, for example, a mean pressure of about 50 atm. and an engine speed of 1000 RPM. This limited data indicated that the ring leakage increased rapidly with operation at typical engine running conditions.

A step joint is an alternative to the scarf joint which maintained a sealing surface at the joint as the ring wore or as the temperature of the ring varied. The step joint is shown in Figure 2.4-22. A backup ring of Rulon or other material of relatively low modulus which would conform to the piston ring would be required to seal the joint gap on the low pressure side of the ring. The rings should be pinned in the grooves to prevent alignment of the ring joints. The step joint would be more difficult to fabricate than the scarf joint, but testing of the step joint is warranted on the basis of the theoretical reduction in joint leakage.

2.4.4.4 Conclusions

a. Decreasing the leakage of the current ring had a greater effect on fuel economy than a reduction of ring friction.

b. The current piston ring resulted in excessive and inconsistent leakage at the ring scarf joint. The leakage increased rapidly as the ring wore.

c. The pressure balanced ring, as designed, resulted in a net fuel economy loss due to increased leakage. The reduction in friction due to pressure balancing was in reasonable agreement with the calculated value.

d. The current piston ring operates at relatively high values of PV (pressure velocity) and will thus probably wear at a high rate.

e. Rulon J had a frictional advantage over Rulon LD.

2.4.4.5 Recommendations

a. The step joint piston ring should be tested since theoretically leakage past the ring joint will be greatly reduced and should not increase as the ring wears.

b.   The values of PV at which the ring operates could be decreased and the ring durability improved by pressure balancing. The axial width should be increased so that the length of the effective leakage path past the ring face is not reduced.

c.   The wear life of Rulon J compared to Rulon LD should be investigated.

2.4.5 Conclusions — The engine drive study resulted in a fuel economy improvement projection of up to 1.94 MPG. Most of this would be achieved from a redesign of the crossheads to reduce friction.

Comparisons between crankshaft and swashplate drives show essentially equal efficiencies, and the crankshaft drive having a substantial cost advantage due to the simplified accessory drive.

The improvement in fuel economy resulting from the variable speed accessory drive and the mechanical drive for the fuel and air atomizer pumps may be outweighed by increased cost and complexity.

During the piston ring friction study, it became apparent that a substantial improvement is required in the 4-215 engine piston rings. The basic ring becomes severely distorted in operation causing high leakage and loss of engine efficiency.

SWASHPLATE

SWASHPLATE

MAIN BEARING

SLIDER BEARING

PISTON-CROSSHEAD

DUAL CRANKSHAFT

PISTON

CROSSHEAD

ROD BEARING

WRIST PIN BEARING

LEFT CRANK

SYNCHRONIZING GEARS

RIGHT CRANK#

LEFT CRANK
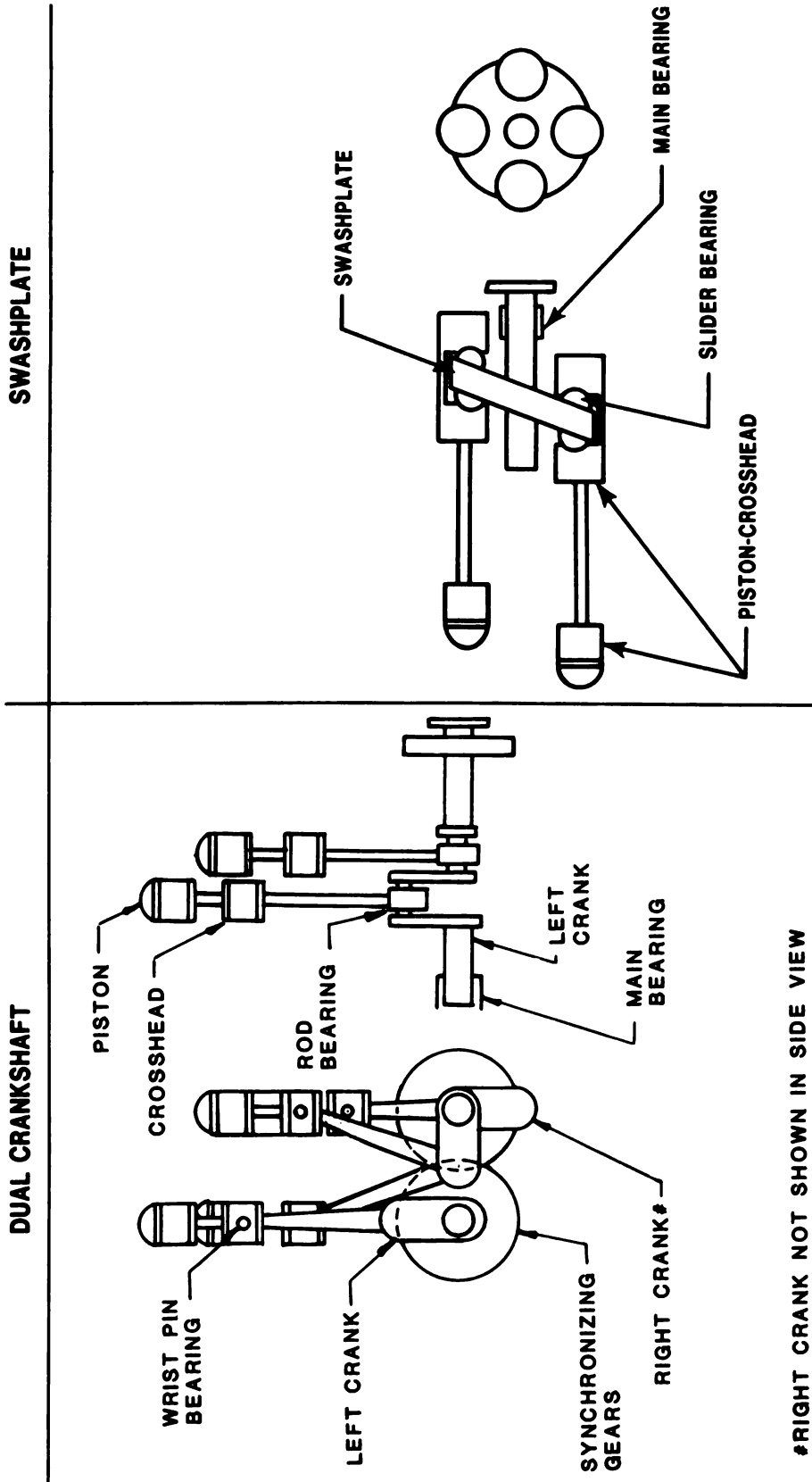
MAIN BEARING

#RIGHT CRANK NOT SHOWN IN SIDE VIEW

Figure 2.4-1   Stirling Engine Drive Configurations

140

DUAL CRANKSHAFT STIRLING ENGINE

FRONT MAIN BEARING FORCE VS CRANK ANGLE
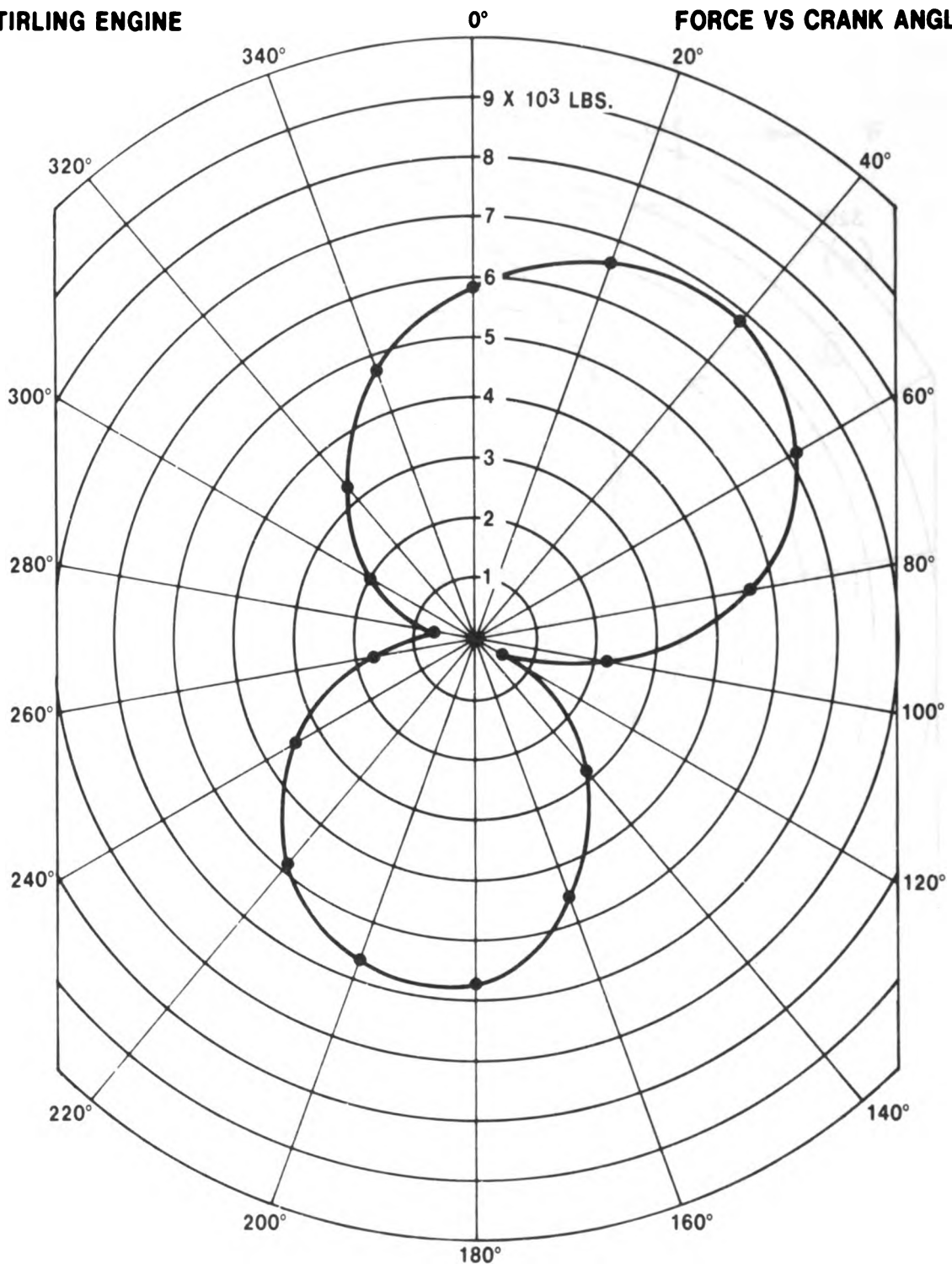
ENGINE SPEED = 2000 RPM
MEAN PRESSURE = 200 ATM

Figure 2.4-2   Front Main Bearing Force vs. Crank Angle

DUAL CRANKSHAFT STIRLING ENGINE

CRANKPIN BEARING FORCE VS CRANK ANGLE
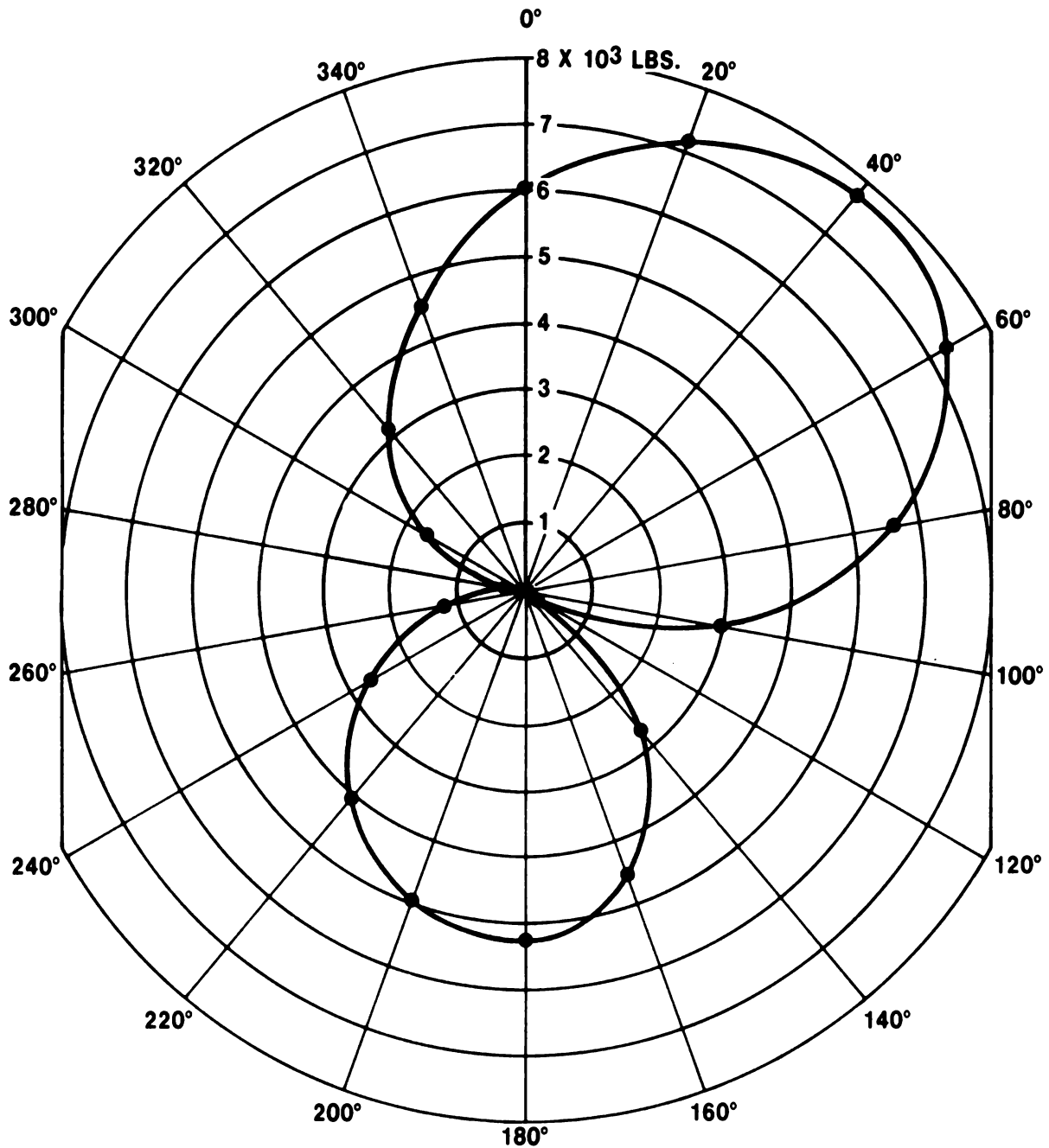
ENGINE SPEED = 2000 RPM
MEAN PRESSURE = 200 ATM

Figure 2.4-3   Crankpin Bearing Force vs. Crank Angle

$$\theta = \tan^{-1} \frac{dy}{dx}$$
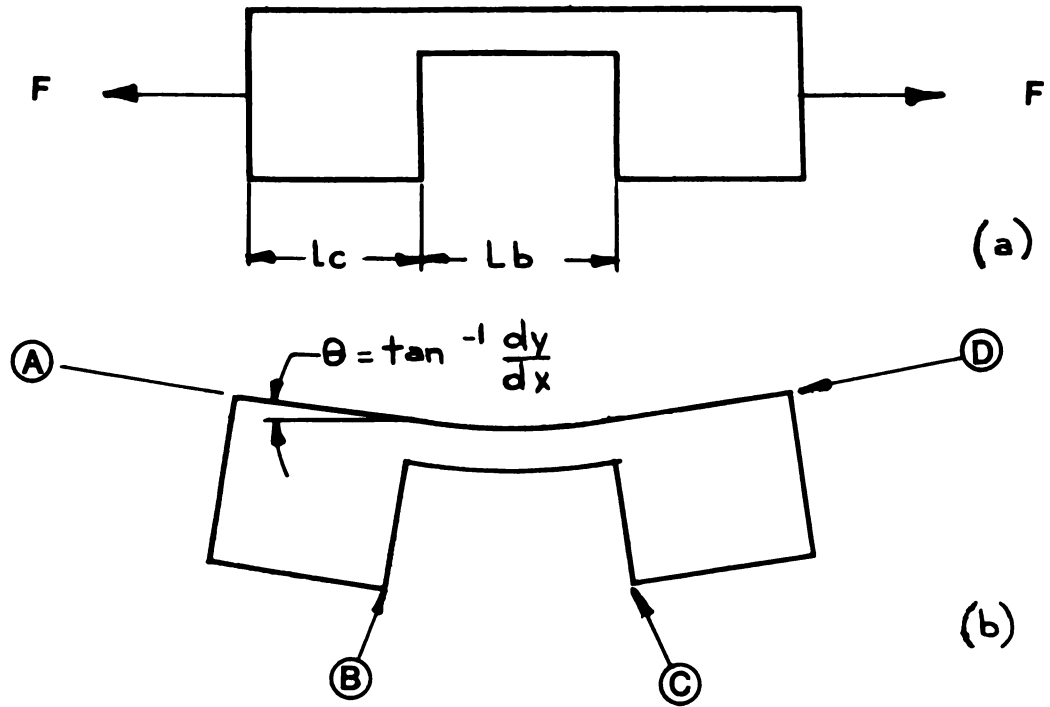
Figure 2.4-4   Crosshead Deflection Mode
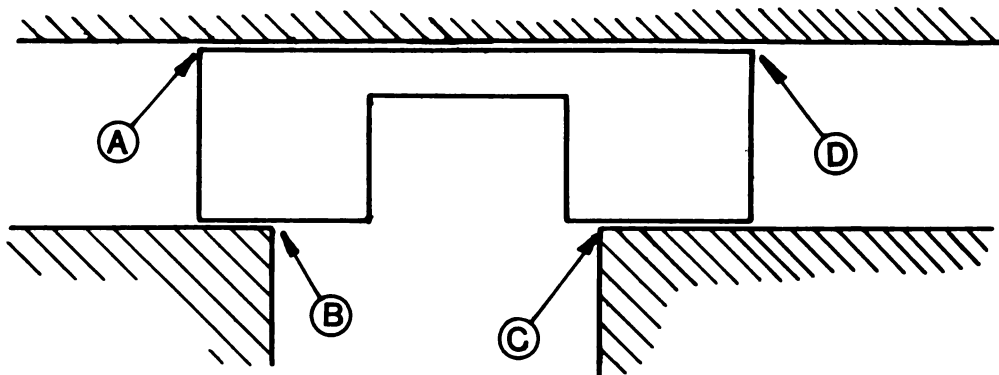
Figure 2.4-5   Relationship of Crosshead to Bore

143
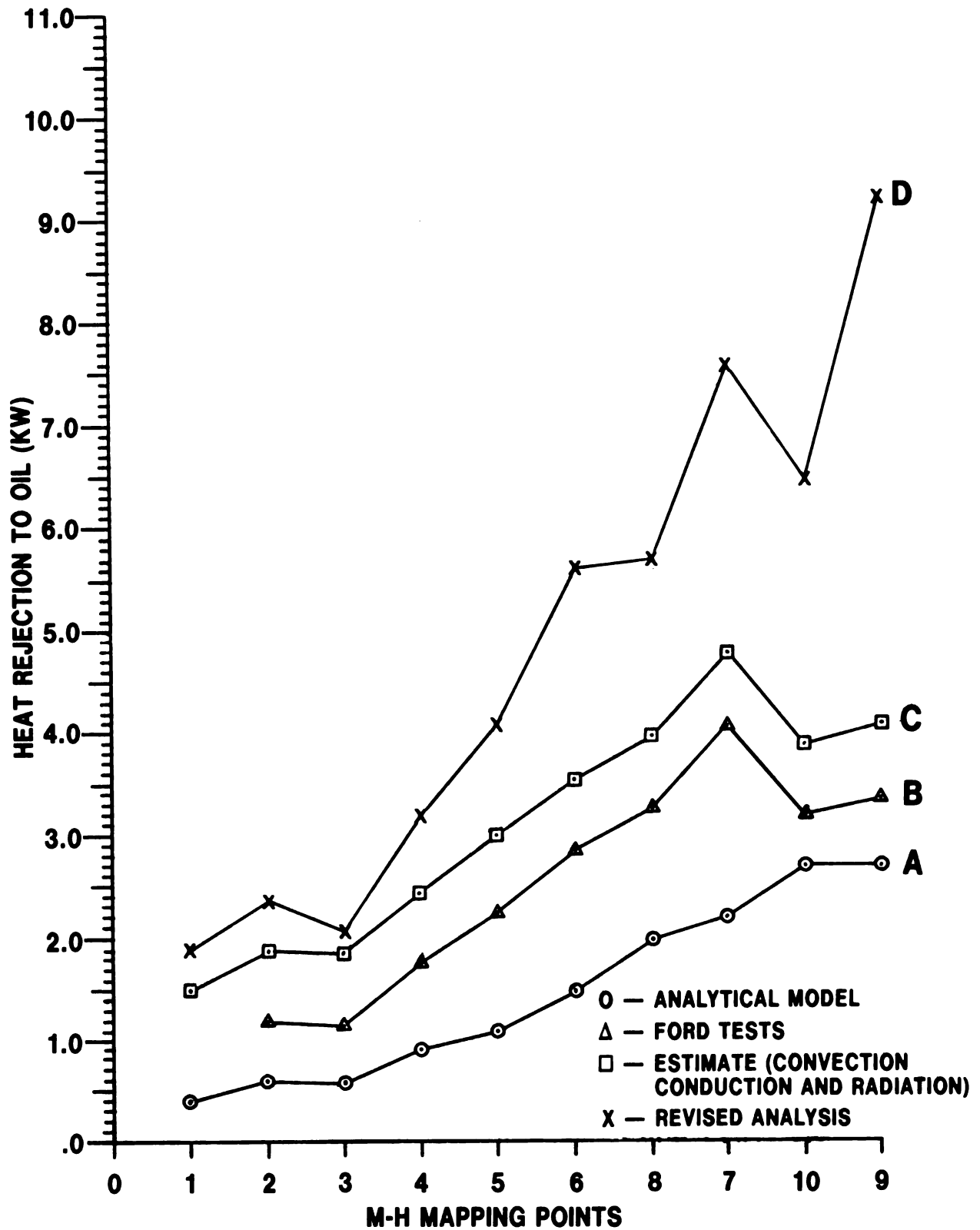
Figure 2.4-6   Friction Heat Rejection – Stirling Engine
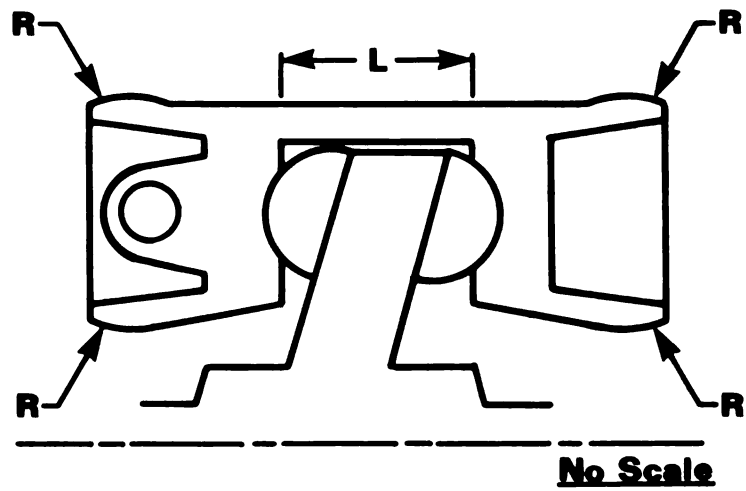
Figure 2.4-7   New Crosshead Design
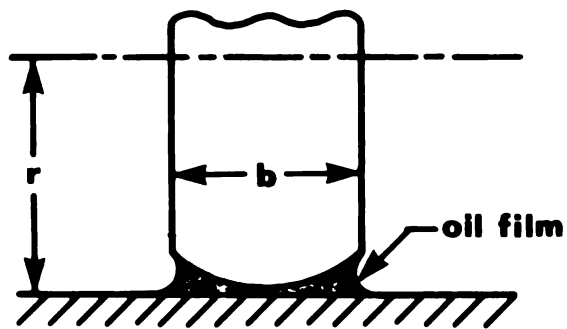
Figure 2.4-8   One Crosshead Bearing Surface
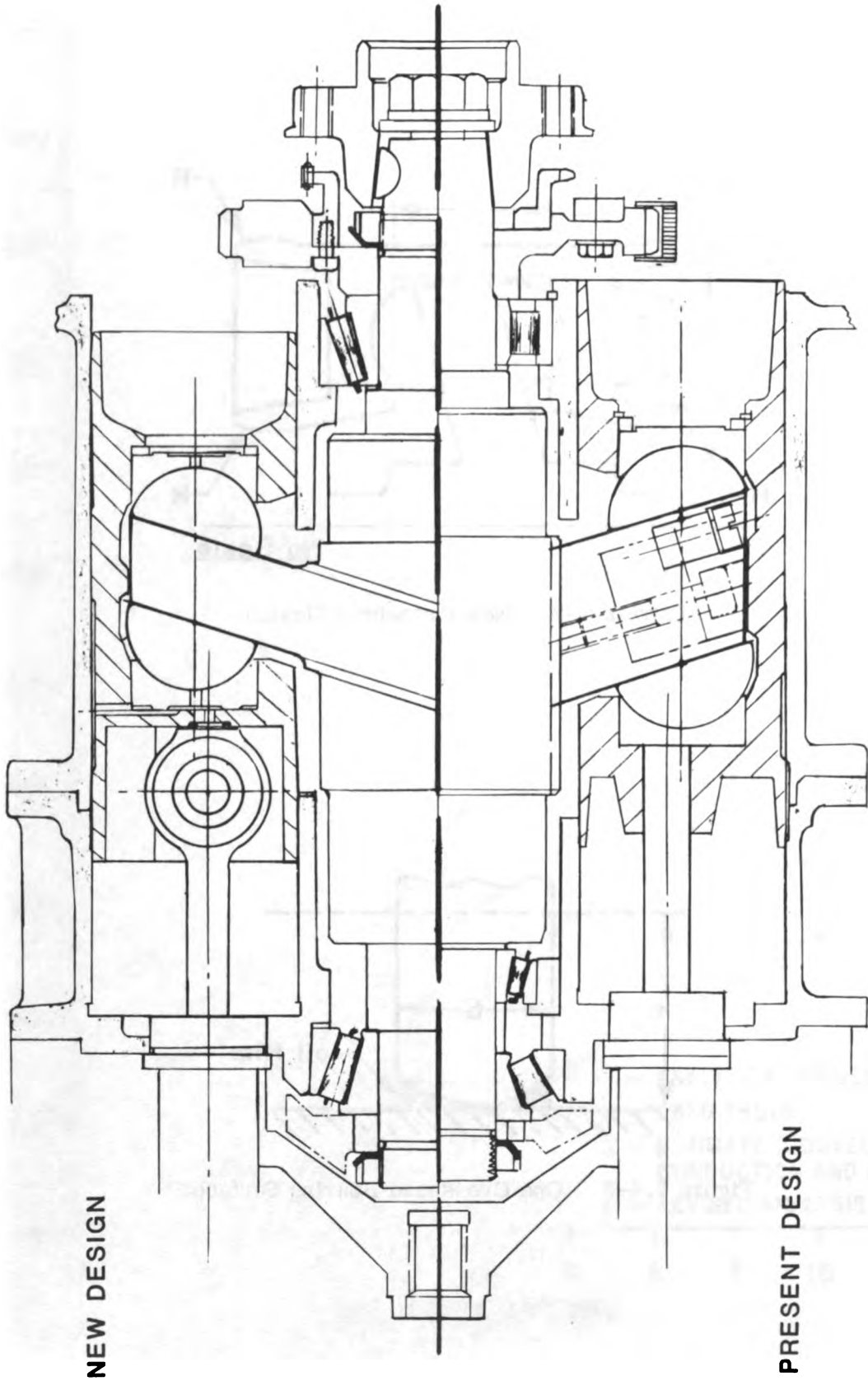
Figure 2.4-9   Engine Drive Comparison

NEW DESIGN

PRESENT DESIGN
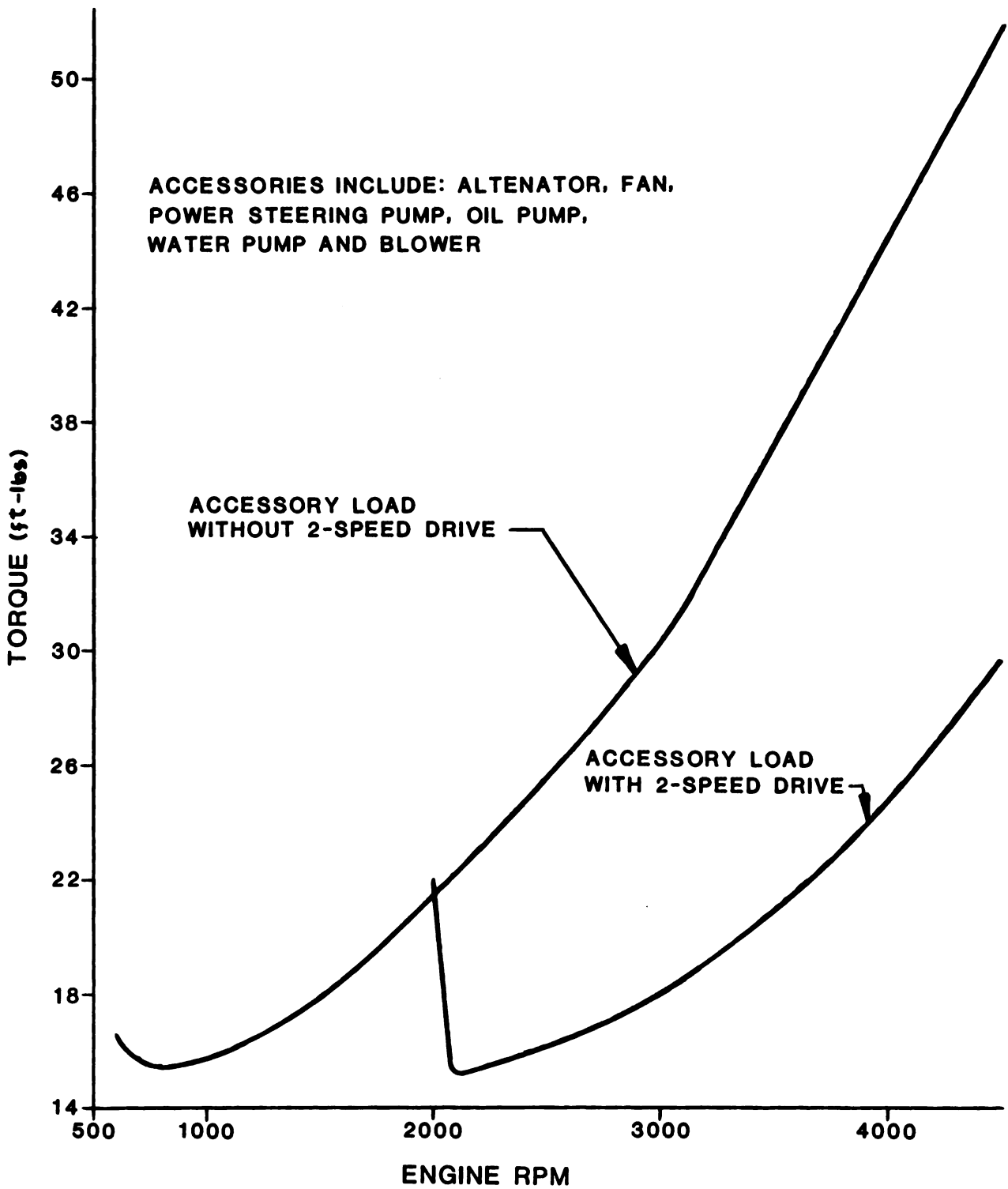
Figure 2.4-10   Total Accessory Torque vs. Engine RPM (4-245 Stirling Engine)
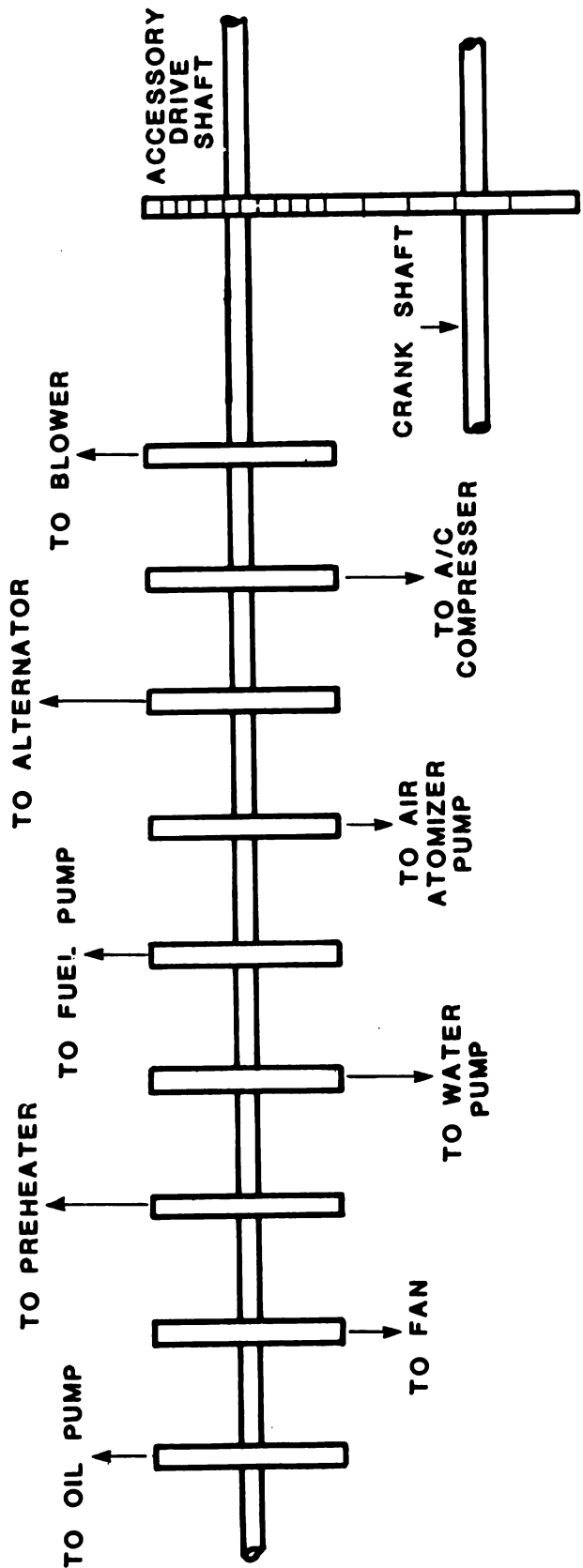
Figure 2.4-11   4th Generation Stirling Engine Accessory Drive Shaft

	M-H Fuel Economy (MPG)	0-60 MPH Time (Sec)
4-245 without 2-speed accessory drive	22.14	12.4*
4-245 with 2-speed accessory drive - water pump not included	22.31	11.9
4-245 with 2-speed accessory drive - water pump included	21.93	11.9
4-245 without accessories	24.59	11.5

* A TOFEP projected 0-60 MPH acceleration time of 12.4 seconds is considered to correspond to a test track value of 13.3 seconds for 0-60 MPH acceleration time.

Figure 2.4-12   Projected Performance and M-H Economy for 2-Speed Accessory Drive

	M-H Fuel Economy (MPG)
4-245 Without 2-Speed accessory drive	22.14
4-245 With 2-Speed Accessory Drive - Water Pump Not Included	22.50
4-245 With 2-Speed Accessory Drive - Water Pump Included	22.12
4-245 Without Accessories	24.99

Figure 2.4-13   Projected M-H Economies for 2-Speed Accessory Drive at Constant Performance Level

PROPOSED SYSTEM
BELT DRIVE

ACCESSORY DRIVE-
MAIN SHAFT

CHAIN DRIVE
(.97 EFFICIENCY)

ENGINE DRIVEN BELT (.95 EFFICIENCY)
TO POWER BLOWER & AIR ATOMIZER PUMP

ALTERNATOR
(.50 EFFICIENCY)

ENGINE MAIN SHAFT

INTEGRAL
FUEL-AIR ATOMIZER
BELT DRIVEN
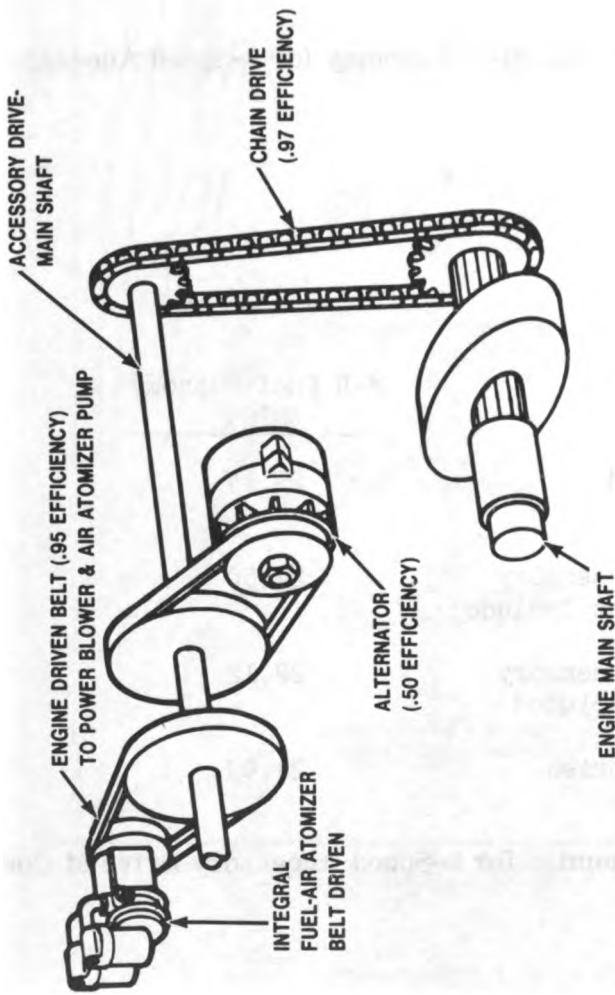
CURRENT SYSTEM
ELECTRICALLY POWERED

ALTERNATOR DRIVE BELT (.95 EFFICIENCY)

ACCESSORY DRIVE — MAIN SHAFT

CHAIN DRIVE
(.97 EFFICIENCY)

ENGINE MAIN SHAFT

ALTERNATOR
(.50 EFFICIENCY)

14.5V 4.7 AMPS

FUEL PUMP

14.5V 7.3 AMPS
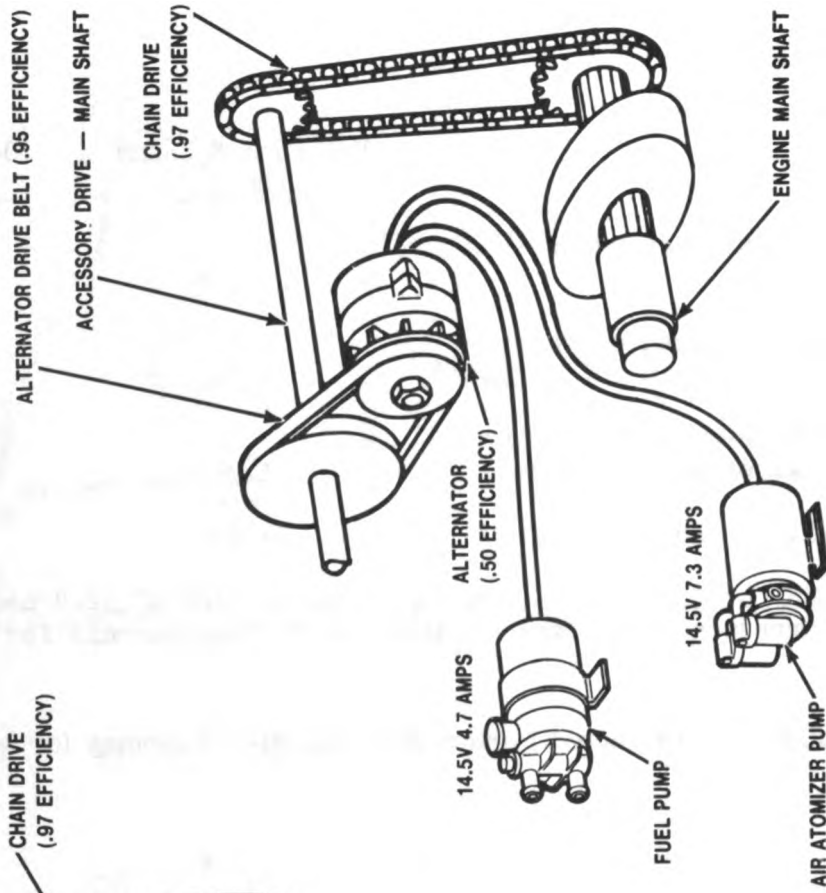
AIR ATOMIZER PUMP

Figure 2.4-14   Drive System – Fuel and Air Atomizer Pumps
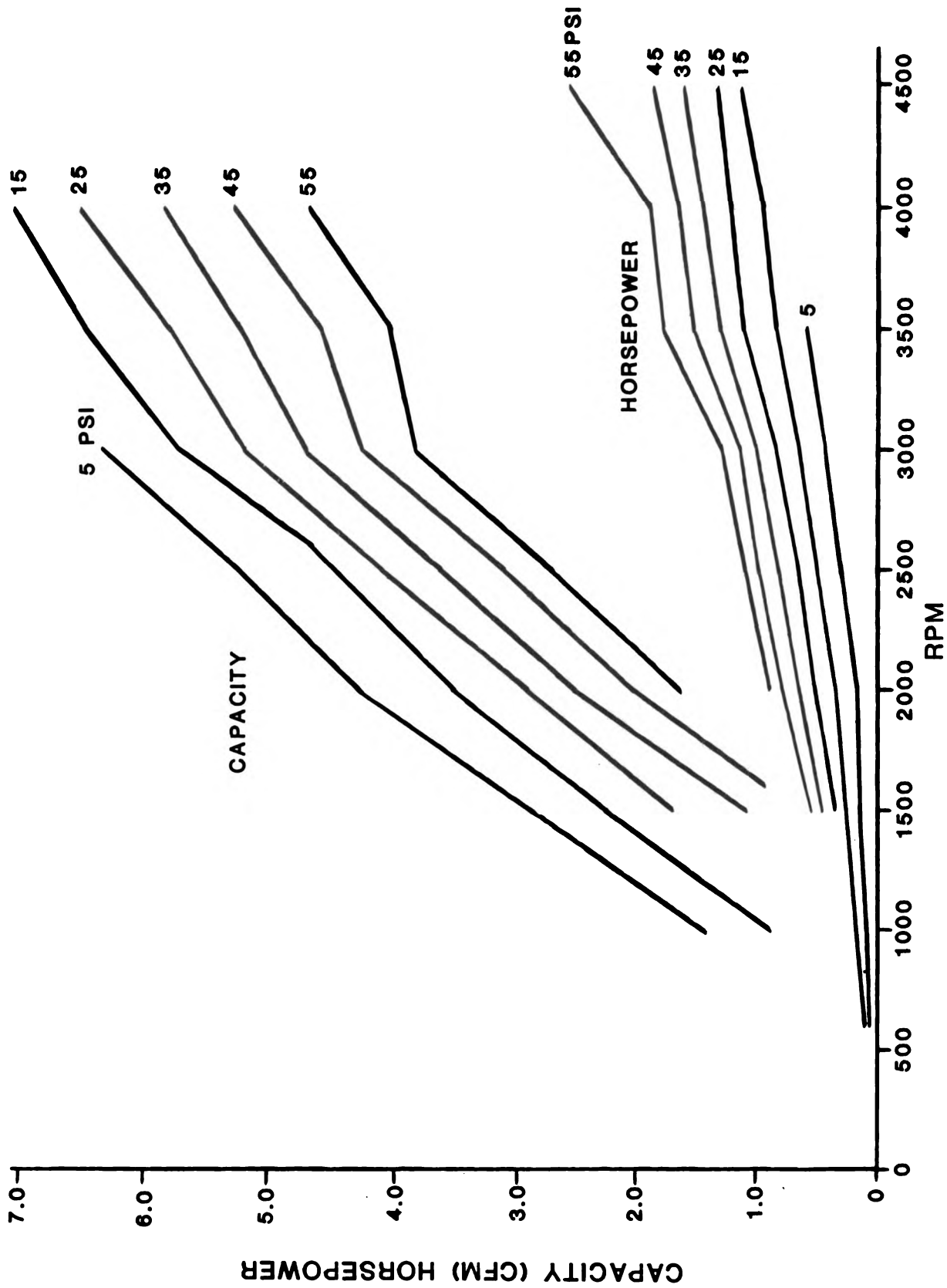
Figure 2.4-15   Capacity and Horsepower vs. RPM Gast Model #0440-P103 Compressor

151
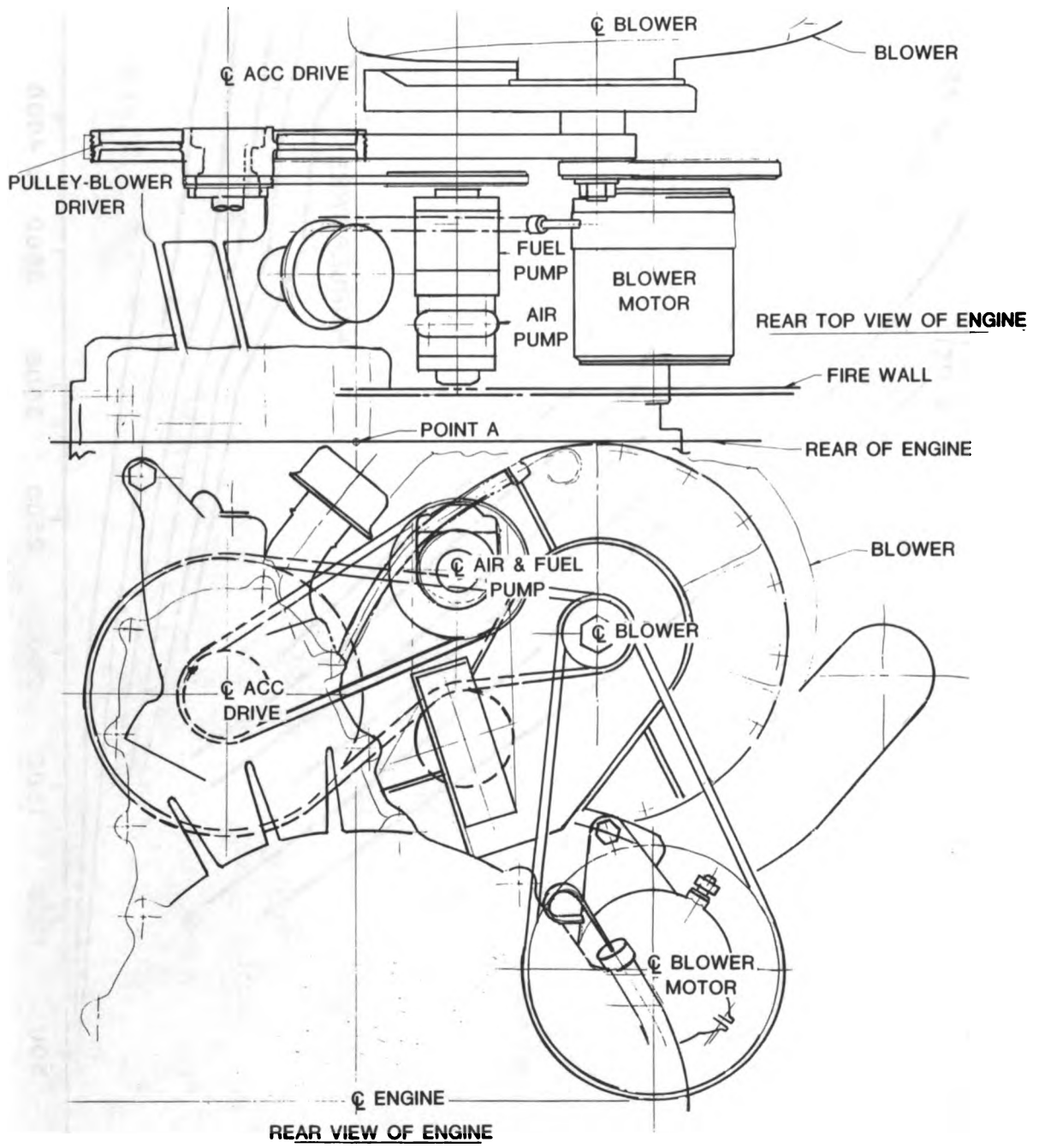
Figure 2.4-16   Possible Package Layout – Belt Driven Air Atomizer and Fuel Pumps
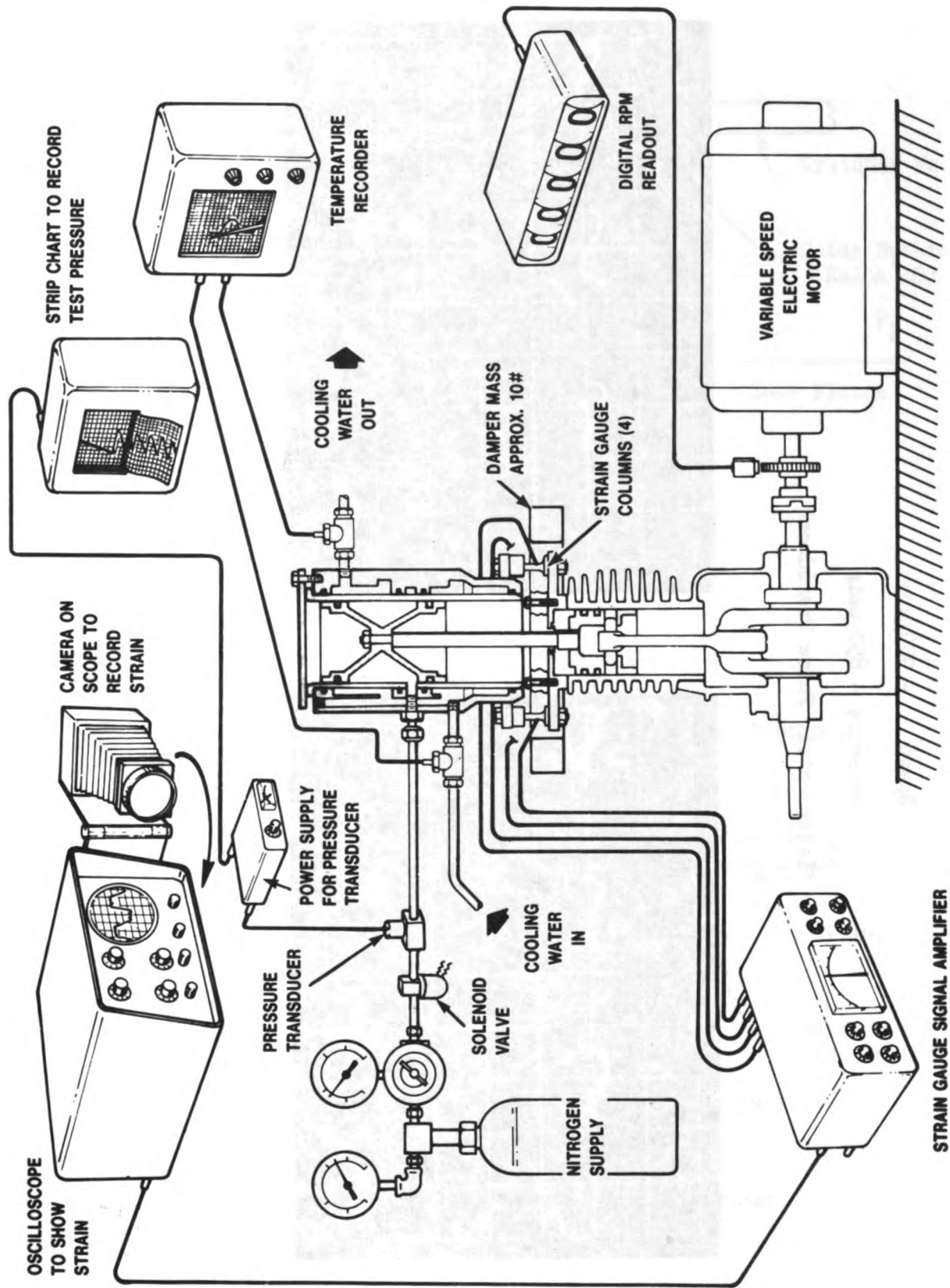
Figure 2.4-17 Piston Ring Friction – Test Rig Schematic

153

Speed — 900 cps

Pressure — 850 psig

Piezoelectric Force Transducer

Filtered Transducer Output (150 Hz)

(b)

Oscilloscope Display of Transducer Output

(a)

Figure 2.4-18   Filter Effect on Friction Measurement

154

(a)

Piston Ring

P_s

Cylinder Wall

Guide Bushing
(Rulon LD)

Test Piston
(Aluminum)

P_2

P_1

Test Piston
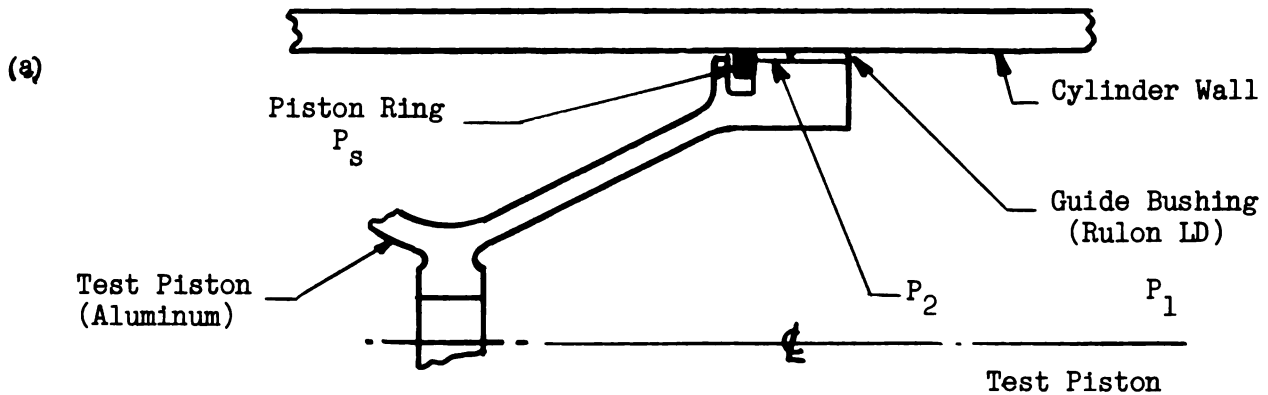
$$P_{ring} = (P_s - P_1) - (P_2 - P_1)$$

If: $P_s - P_1$ is negligible

Then: $$P_{ring} = (P_s - P_1)$$

Where:

P = Pressure across the ring
P_s = Supply pressure
P_1 = Atmospheric pressure
P_2 = Pressure between ring and bushing, caused by leakage

(b)

P_2

Piston Ring

Cylinder Wall

P_s

Test Piston
(Aluminum)

Guide Bushing
(Rulon LD)

P_1

Test Piston

Bleed Hole
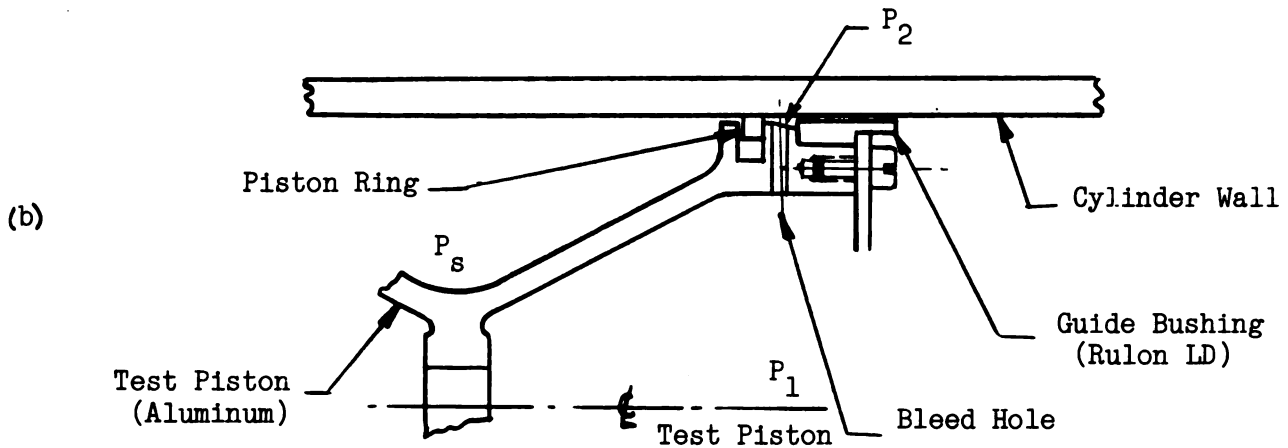
Figure 2.4-19   Piston Ring Installation in Test Rig

155

Digitized by Google

a
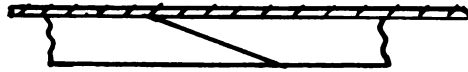
Ring in contact with itself and the ring
groove wall

b

Distorted portion of ring that allows
leakage

c

Ring joint gap that allows leakage

Figure 2.4-20   Diagonal Scarf Joint – Ring Groove Wall and Contact Surface
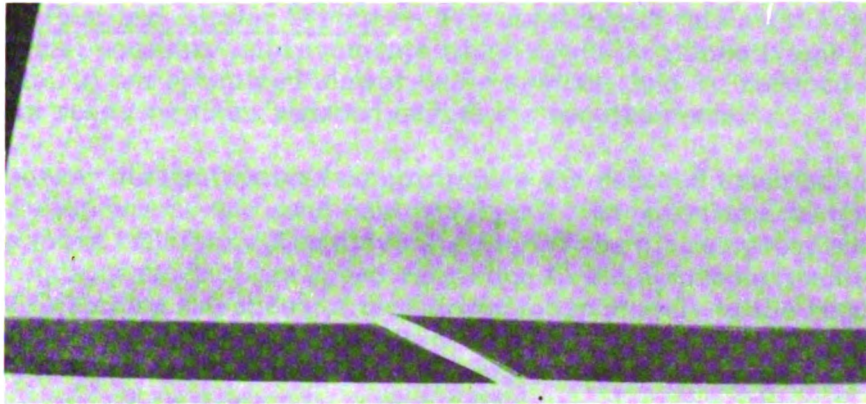
(A)

NEW RING - DIAGONAL SCARF JOINT
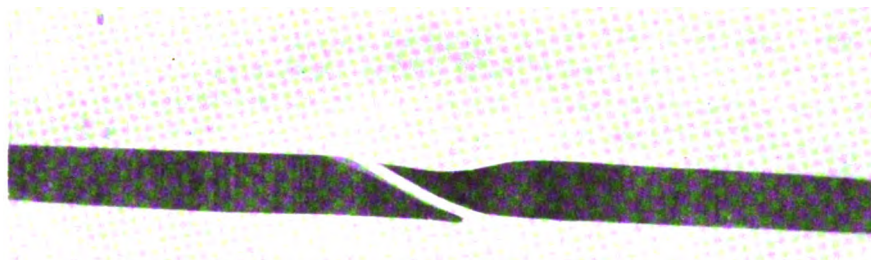
(B)

WORN RING - UNUSUAL CONDITION AT JOINT

Figure 2.4-21   Piston Ring Comparison – Standard Piston Ring – Rulon LD
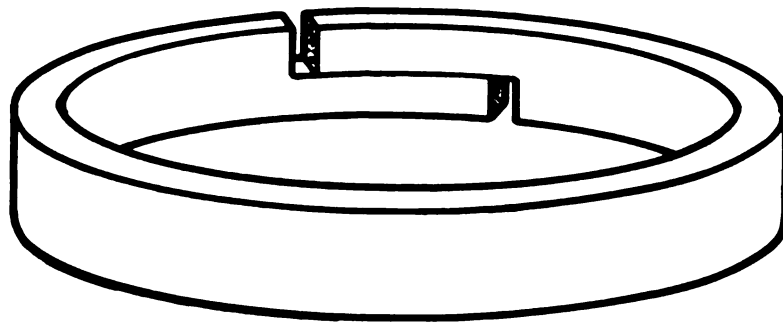
Figure 2.4-22   Step Joint Piston Ring

2.5 External Heat and Blower System — The objective of this section was to identify and quantify fuel economy improvements which could be gained from: 1) an improved blower design, 2) an optimized blower drive system, and 3) reduced blower power requirements resulting from reduced engine air requirements.

The 4-215 blower design involved compromises for reduced manufacturing cost (i.e. straight impeller vanes, and sand cast housings). An optimized design would be expected to be more efficient. The drive system for the blower provides excess blower capacity throughout most of the speed range due to the disproportionate requirements at low speeds. Matching the speed of the blower more closely to the requirements would result in a power saving. Also, the air flow requirements of a 30% more efficient engine (program objective) would be 30% less and therefore the power saving would be substantial.

Following is a detailed description of the work done under this section.

2.5.1 Improved Blower Design

2.5.1.1 Summary — The objective of this section was to design a combustion air blower to provide the reduced engine air requirements of the Fourth Generation Engine and quantify the resulting fuel economy improvement.

The increased efficiency and therefore reduced air flow requirements of the Fourth Generation Stirling engine presented the opportunity for designing a blower better suited to the engine requirements. A new blower offered the advantages of higher efficiencies at most operating points, reduced size, and wider operating range.

The 4-247 Stirling engine was the proposed Fourth Generation engine at the time this study was initiated.

The air flow requirements as determined from the burner computer program for the significant operating points are listed in Figure 2.5-1. The points were chosen by selecting the minimum power, maximum power and maximum flow conditions at each of the speeds in the engine map. It is important to note that at speeds below 2000 RPM the maximum power is limited by the torque converter stall torque curve. In a vehicle installation the engine will not develop more torque than torque converter stall without accelerating, therefore, it was decided that providing blower capacity for high torque low speed operation was unnecessary.

Along with the data in Figure 2.5-1, the following design restrictions were imposed:

a. The new blower must be no larger than the current blower.

b. Flow control will be effected by throttling of the inlet.

c. The blower will have a constant ratio drive and will run at 6.25 times engine speed or less.

The aerodynamic design results are outlined in Figure 2.5-2 and Figure 2.5-3. The blower has a "two-dimensional" rotor with backward curved vanes. "Two dimensional" means that the vanes are in the radial direction only, they do not turn into the inlet. The housing consists of a vaneless diffuser and a collector scroll. Figure 2.5-4 shows the characteristics of such a blower with the 4-247 operating points superimposed. Figure 2.5-5 contains a summary of the important information for each of the operating points in Figure 2.5-1. The input power is the power that must be supplied to the impeller. It does not include bearing losses or drive losses. The power factor is the ratio of the required input power to that needed if the blower was operating at 80% efficiency. This is an indication of the losses involved in throttling the blower to the desired flow.

2.5.1.2 Analysis — In the mechanical design of the blower it was decided that a reduction in overall diameter from the current blower would be highly desirable. A reduction in the diameter of the housing was accomplished by locating the collector scroll on the face of the housing, rather than on the periphery. To make a significant change it was necessary to turn the end of the last third of the vaneless diffuser approximately 40° towards the axis of the rotor. This is expected to have a small effect on performance and is justified by the 23% reduction in diameter. The new blower is compared to the current blower in Figure 2.5-6. In the new blower the drive pulley is supported between the shaft bearings. This permits use of ball bearings with a 6.25:1 blower drive ratio rather than needle bearings as required in the 4-215 blower, and will insure quieter operation of the blower and extend the range of possible drive ratios to 8:1.

To make an estimate of the fuel economy improvement resulting from a new blower design, it was first necessary to calculate the power input to the impeller. This was obtained via the following calculations:

Blower speed (N_B) = N_E x (Blower drive ratio)

Head coefficient $(Q) = H/u^2/g$

Where: H = adiabatic head

$$H = \frac{K}{K-1} (R\ T_{IN}) \left[\left(\frac{P_2}{P_1} \right)^{\left(\frac{K-1}{K} \right)} -1 \right]$$

u = impeller tip speed

g = gravitational constant

K = ratio of specific heats

R = gas constant

N_E = engine speed (RPM)

Flow coefficient $(\emptyset)$ = $\dfrac{\text{Axial Inlet velocity (C)}}{u}$

160

$$\text{Compression Work} \;\; (W_C) \;\; = \frac{KP_1}{K-1} \;\; V_1 \left[\frac{P_2}{P_1}^{\left(\frac{K-1}{K}\right)} -1 \right]$$

$$\text{Impeller input power} \;\; = \frac{W_C}{\eta_B} \;\; x \;\; \frac{Q_B}{Q_A}$$

Where: η_B = Blower efficiency

Q_A = Maximum head capacity

Q_B = Operating point head capacity

An example of this method is shown below.
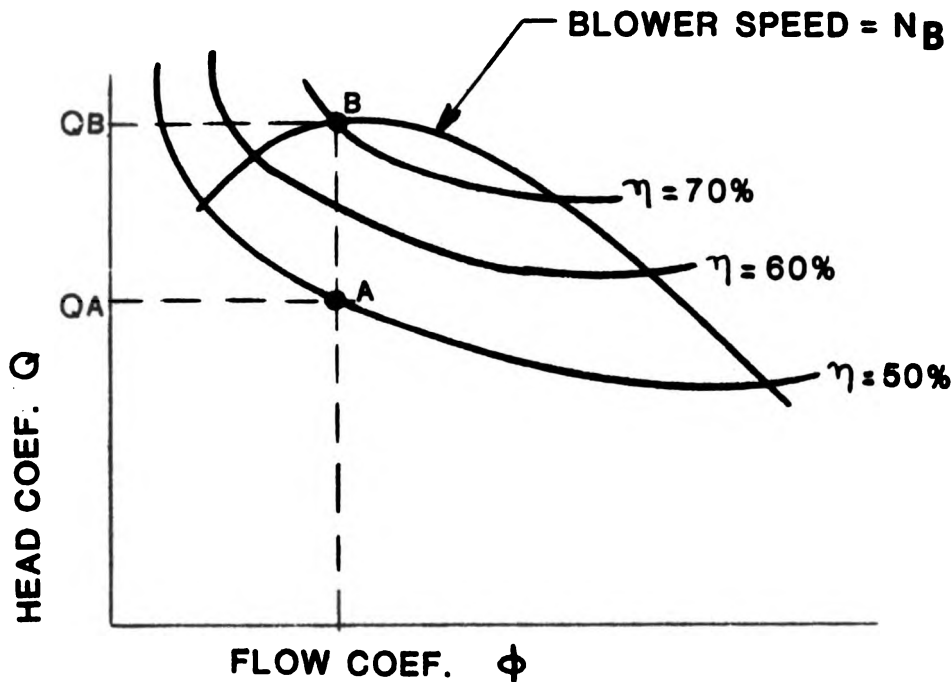
The bearing losses and drive efficiencies must be added to the impeller input power. It was calculated that the blower bearings and drive belt consume an additional amount of power equal to 3% of the impeller input power, but never less than .079 kW. This yields the blower input power at the accessory drive shaft.

The chain drive between the accessory drive shaft and the engine output shaft is assumed to be 97% efficient. So the power consumption of the blower as measured at the engine output shaft can now be calculated. To compare the power consumption and the fuel economy effect of the new blower with that of

the current blower, it was necessary to select a lower drive ratio for the current blower so that both blowers have approximately the same capacity. The ratio chosen was 4.75:1.

2.5.1.3 Results — The power consumption of the two blowers is compared in Figure 2.5-7. For the most of the ten VSIM test points the new blower consumed less power than the current blower. The difference yields a M-H fuel economy increase of 0.11 MPG (gasoline).

2.5.2 Improved Blower Drive — The current blower drive consists of a belt drive off of the engine accessory drive shaft and a viscous clutch to limit the maximum blower speed. Since the engine air flow requirements at high engine speeds are substantially less than the blower capacity at corresponding blower speeds, limiting the blower speed with a viscous clutch would reduce the blower excess capacity. The viscous clutch acts as a variable ratio as the engine speed increases. This saves blower power by reducing the amount of throttling; however, the viscous clutch consumes a substantial portion of the power saved making the net savings small. A more efficient variable or multiple speed blower drive would produce significant reductions in blower power consumption and therefore increase fuel economy. Under Section 2.4, Engine Drive Study, work was initiated on a two-ratio accessory drive as a means of reducing accessory power which included the blower. Results of the study are presented in Section 2.4.

2.5.3 Reduced Air Flow Requirements

2.5.3.1 Summary — The higher efficiency of the Fourth Generation Stirling engine results in reduced air flow requirements, and therefore a reduction in blower power consumption. The engine fuel control system automatically adjusts the blower inlet throttle to produce the required air mass flow. If the blower speed is reduced, air mass flow is reduced with less throttling, resulting in a power savings. An analysis was performed to quantify the fuel economy improvement possible with the current blower.

2.5.3.2 Analysis — Figure 2.5-8 shows the head-capacity curves for the current combustion air blower. The curves for different inlet Mach numbers are directly related to impeller speed. The characteristics are not arranged in order of increasing Mach number due to experimental error and the extremely low pressures measured at the low speeds.

For a given engine operating condition, the required air flow, temperature, and blower pressure ratio can be determined from the burner computer program. If a blower speed is assumed, the head and flow coefficients can be determined. The operating point can then be compared with the blower capacity (see Figure 2.5-8). Point A is beyond the capacity of the blower. If the blower speed is increased, point A moves to A'. Now the blower has more capacity than the operating point requires, so the blower must be throttled. Throttling is represented on the head capacity curve as a change in head coefficient so that the blower is capable of operating at B although it is throttled to A'. The ratio of the head coefficient the blower can produce in relation to the head coefficient that it is throttled to is an indication of the power consumed by throttling. Therefore, it is desirable to adjust the blower speed so that a minimum of throttling is required.

At the time of this analysis the Fourth Generation engine was the 4-245. Its air flow requirements are approximately the same as the 4-247. Figure 2.5-9 shows the maximum air-flow engine operating points for each of the engine speeds used on the engine map DKEM245. The head and flow coefficients were calculated using the current 4-215 blower drive with a 6.24:1 belt drive and a viscous clutch to limit the maximum blower speed. There is a substantial amount of throttling, especially at the lower engine speeds where all of the fuel economy testing occurs. Therefore, a reduction in blower speed will reduce the amount of throttling and, consequently, the power consumption.

Figure 2.5-10 shows the 4-245 air flow requirements with a constant ratio blower drive. The drive ratio has been reduced to 4.75:1. This was chosen as the minimum drive ratio because the flow requirement at 1600 RPM exceeds the blower capacity. Since this occurs over a relatively narrow speed band and only at maximum torque, it is not expected to restrict engine operation. Figure 2.5-11 also shows that above 1600 RPM a large amount of throttling is needed.

By using a viscous clutch similar to the one on the current 4-215 engine, the blower drive ratio is reduced at high engine speeds. While the viscous clutch consumes power when it is slipping, there is a net reduction in total blower power consumption. Figure 2.5-11 shows the 4-245 maximum flow require-ments using a 4.75:1 belt drive in combination with a viscous clutch. The clutch curve was designed to provide adequate blower capacity at 4500 RPM and essentially no slip at less than 1600 RPM.

Two maps were then created for the 4-245 engine using the MAPALT computer program. One map used the 6.24:1 drive with the original viscous clutch curve, and one used a 4.75:1 drive ratio with the newer viscous clutch curve. The two maps were then used in the ECONCALC computer program to predict the dif-ference in M-H fuel economy due to the reduced blower drive allowed by the re-duced engine air flow requirements. Figure 2.5-12 summarizes the difference between the two. The reduced drive ratio gives a power savings of up to .73 kW on the VSIM test points and yields a M-H fuel economy increase of .24 MPG (gasoline).

2.5.4 Fuel Economy Assessment — The projected fuel economy improvement of section 2.5, External Heat and Blower System, is 0.35 MPG (gasoline). The im-provement for the separate sub-sections are as follows:

- Improved blower design   0.11 MPG

- *Improved blower drive   0.0

- Reduced air flow requirements 0.24 MPG

        Total: 0.35 MPG (gasoline)

* Transferred to section 2.4.

The work on engine air flow requirements was based on steady-state conditions. At low speeds it was assumed that engine torque was limited by the torque con-verter stall torque. These conditions lead to relatively low air-flow requirements

at low steady-state engine speeds. However, transient operation may raise the air-flow requirements. When the load on the engine is rapidly increased, the power control adds hydrogen to the engine increasing the mean pressure. The new gas is cool and must be raised to the heater tube temperature when moved to the hot side. It may be necessary to increase the blower drive ratio to provide the reserve capacity for transient operation. As yet, there are no projections of transient engine air-flow requirements or the effect of transient air-flow requirements on fuel economy.

Engine Speed	$\dot{m}$ (g/s)	T_{in} ($^\circ$C)	V_{in} (m^3/s)	P_{out}/P_{in}
600 RPM				
Min Power	15.88	69.37	.01529	1.00625
Max Power	19.51	66.59	.01862	1.00726
1000 RPM				
Min Power	29.75	93.60	.03056	1.00987
Max Power	50.71	132.46	.05088	1.01729
1500 RPM				
Min Power	36.49	102.50	.03831	1.01212
Max Power	105	87.99	.10258	1.04555
1725 RPM	97.02	31.43	.07993	1.04577
1800 RPM				
Min Power	91.21	20	.07249	1.04338
Max Power	104.72	91.63	.10335	1.04554
2000 RPM				
Min Power	42.27	114.36	.04557	1.01426
Max Power	97.36	20	.0708	1.0475
Max Flow	132.75	103.44	.1328	1.06481
2500 RPM				
Min Power	47.04	119.18	.05137	1.0161
Max Power	121.08	20	.09428	1.06507
Max Flow	127.08	92.46	.12377	1.06182
3000 RPM				
Min Power	51.24	119.82	.05595	1.01793
Max Power	129.85	20	.10042	1.07253
3500 RPM				
Min Power	54.91	117.37	.05949	1.01949
Max Power	109.06	20	.12633	1.10985
4000 RPM				
Min Power	58.12	113.55	.06227	1.02089
Max Power	192.94	20	.14074	1.13691
4500 RPM				
Min Power	60.94	110.21	.06465	1.02215
Max Power	216.58	20	.15393	1.16686

Figure 2.5-1   4-247 Air Flow Requirements
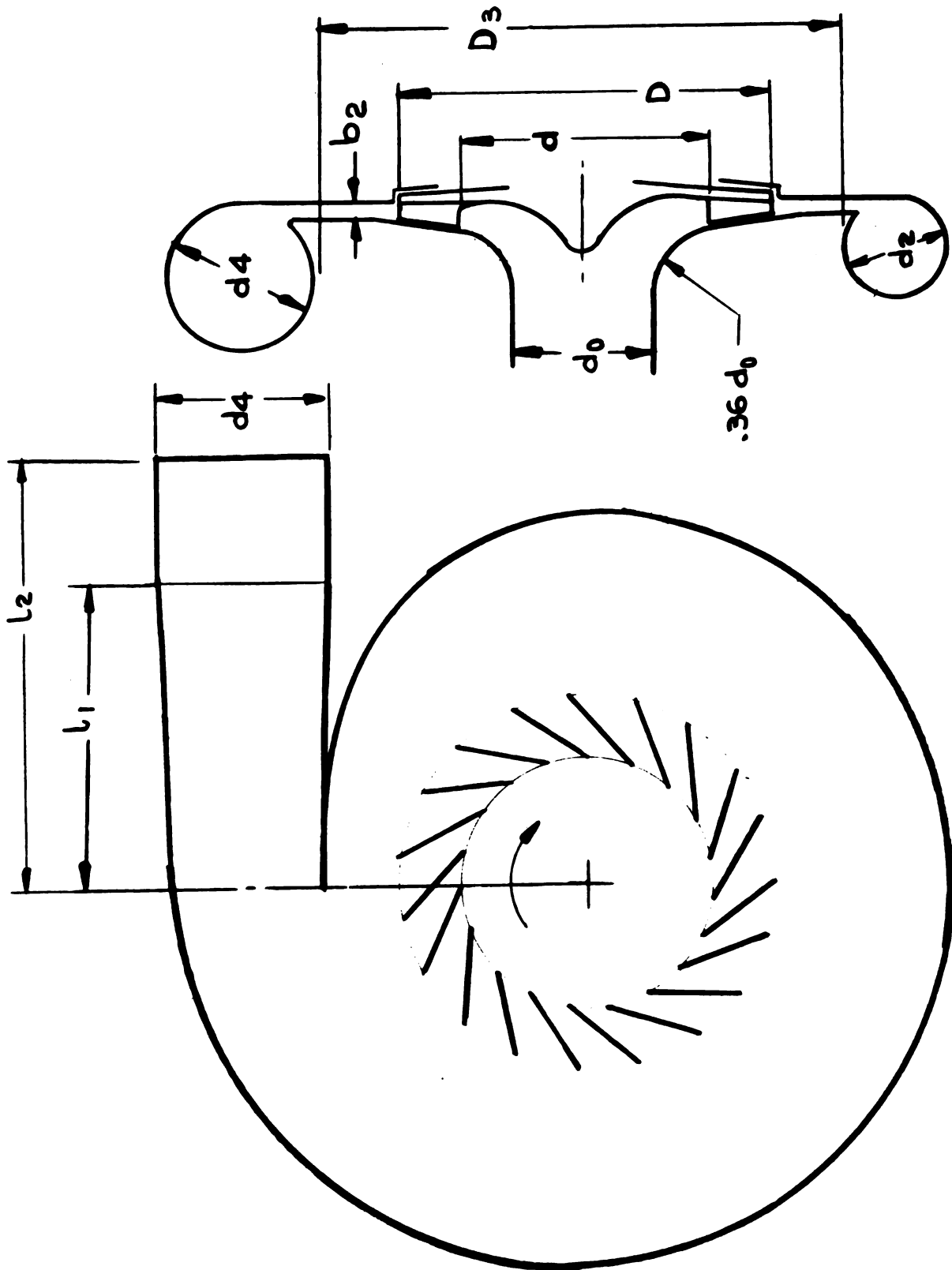
Figure 2.5-2   Proposed Blower Design

d_o	=	73	mm	Rotor blade inlet angle:	$26.3°$
d	=	125.67	mm	Rotor blade exit angle:	$50°$
D	=	188.5	mm	Blade thickness (constant):	.5 mm
D_3	=	262	mm	Rotor blade number:	19
b_2	=	7.8	mm	Shape of rotor blade camber line:	circular arc
d_2	=	46	mm	Blade height at rotor inlet:	10.6 mm
d_4	=	67	mm	Face clearance:	.55 mm
l_1	=	0	mm		
l_2	=	130	mm		

Figure 2.5-3   Blower Dimensions

U_2 — IMPELLER TIP SPEED

η — BLOWER EFFICIENCY

k — RATIO OF SPECIFIC HEATS

R — GAS CONSTANT

g — GRAVITATIONAL ACCELERATION

$$Ma^* = \frac{U_2}{\sqrt{\frac{2k}{k+1} RgT_1}}$$

□ MIN. POWER
● MAX. POWER
+ MAX. FLOW
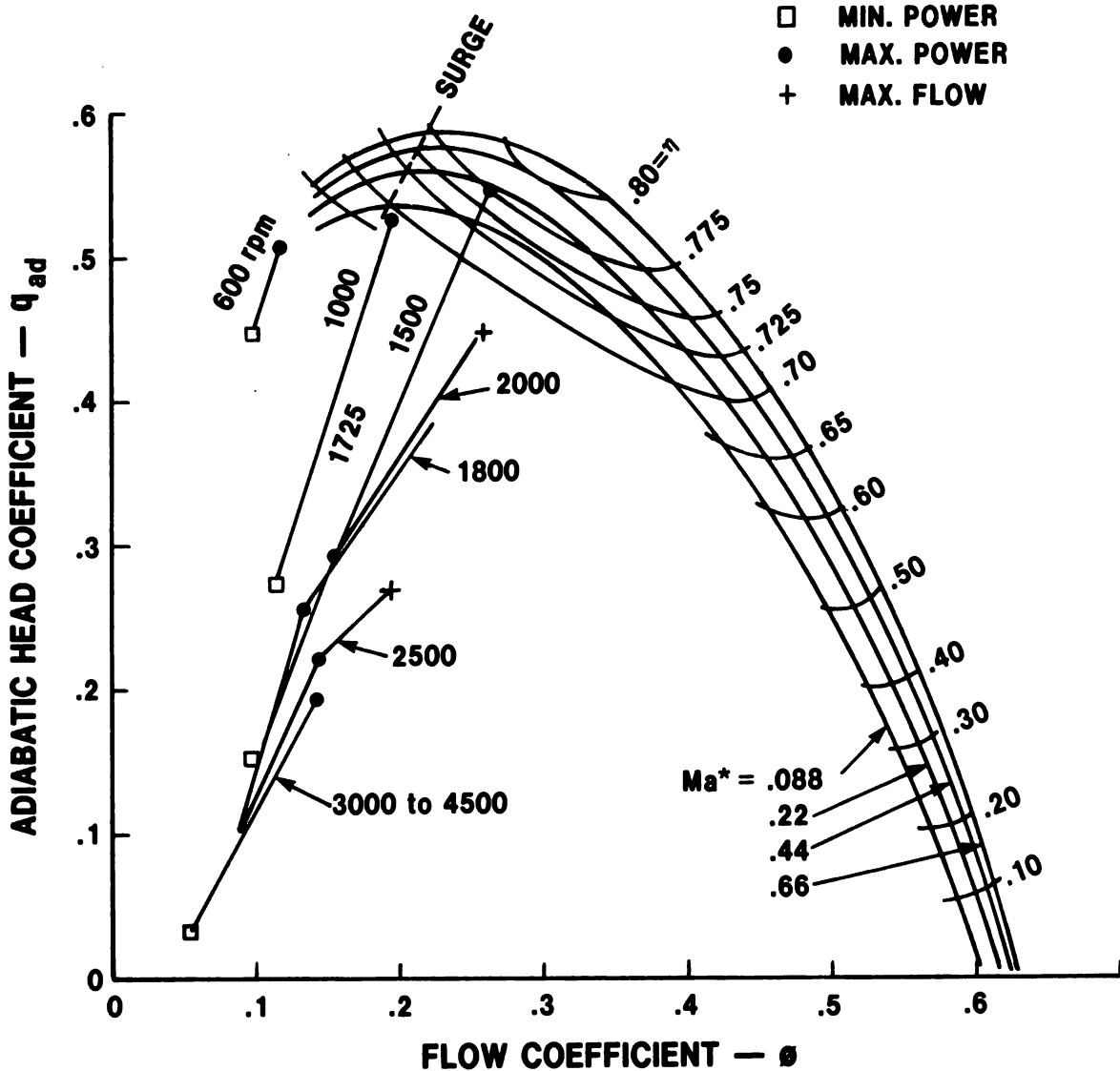
Figure 2.5-4   Operating Points in Blower Characteristic

Engine Speed	n	Desired		Blower Capability			Power Factor	Input Power (kW)
		ϕ	q_{ad}	ϕ	q_{ad}	η		
600 RPM								
Min Power	6.25	.0985	.4473	.19	.53	.69	1.3738	.01671
Max Power	6.25	.12	.515	.19	.53	.69	1.19	.02047
1000 RPM								
Min Power	6.25	.1181	.272	.2	.545	.71	2.2577	.08683
Max Power	6.25	.1967	.5255	.2	.545	.71	1.168	.14796
1500 RPM								
Min Power	6.25	.0987	.1519	.21	.56	.725	4.06	.2407
Max Power	6.25	.2644	.5425	.2644	.5425	.725	1.103	.672
1725 RPM	6.25	.1791	.3476	.213	.563	.727	1.78	.849
	6.25							
1800 RPM								
Min Power	6.25	.1557	.2941	.215	.565	.73	2.1	.86
Max Power	6.25	.222	.3804	.222	.564	.75	1.58	.97
2000 RPM								
Min Power	6.25	.0881	.1036	.216	.568	.74	5.92	.493
Max Power	6.25	.1369	.2581	.216	.568	.74	2.379	1.137
Max Flow	6.25	.2567	.4498	.2567	.558	.785	1.264	1.435
2500 RPM								
Min Power	6.25	.0794	.0758	.218	.572	.74	8.158	.864
Max Power	6.25	.1458	.2249	.218	.572	.74	2.75	2.225
Max Flow	6.25	.1914	.2668	.218	.572	.74	2.318	2.335
3000 RPM								
Min Power	6.25	.0721	.0587	.22	.575	.75	10.449	1.337
Max Power	6.25	.1294	.1737	.22	.575	.75	3.53	3.4
3500 RPM								
Min Power	6.25	.0657	.0465	.222	.578	.76	13.084	1.946
Max Power	6.25	.1395	.1908	.222	.578	.76	3.189	3.86
4000 RPM								
Min Power	6.25	.0602	.0378	.224	.582	.77	16	2.67
Max Power	6.25	.136	.1805	.224	.582	.77	3.35	8.87
4500 RPM								
Min Power	6.25	.0555	.0314	.225	.585	.775	19.232	3.53
Max Power	6.25	.132	.1722	.225	.585	.775	3.507	12.59

Figure 2.5-5   Operating Conditions

IMPELLER

DRIVE SHAFT

AIR INTAKE →

HOUSING

**ORIGINAL
4-215 BLOWER**

IMPELLER

DRIVE SHAFT

AIR INTAKE →

HOUSING ←
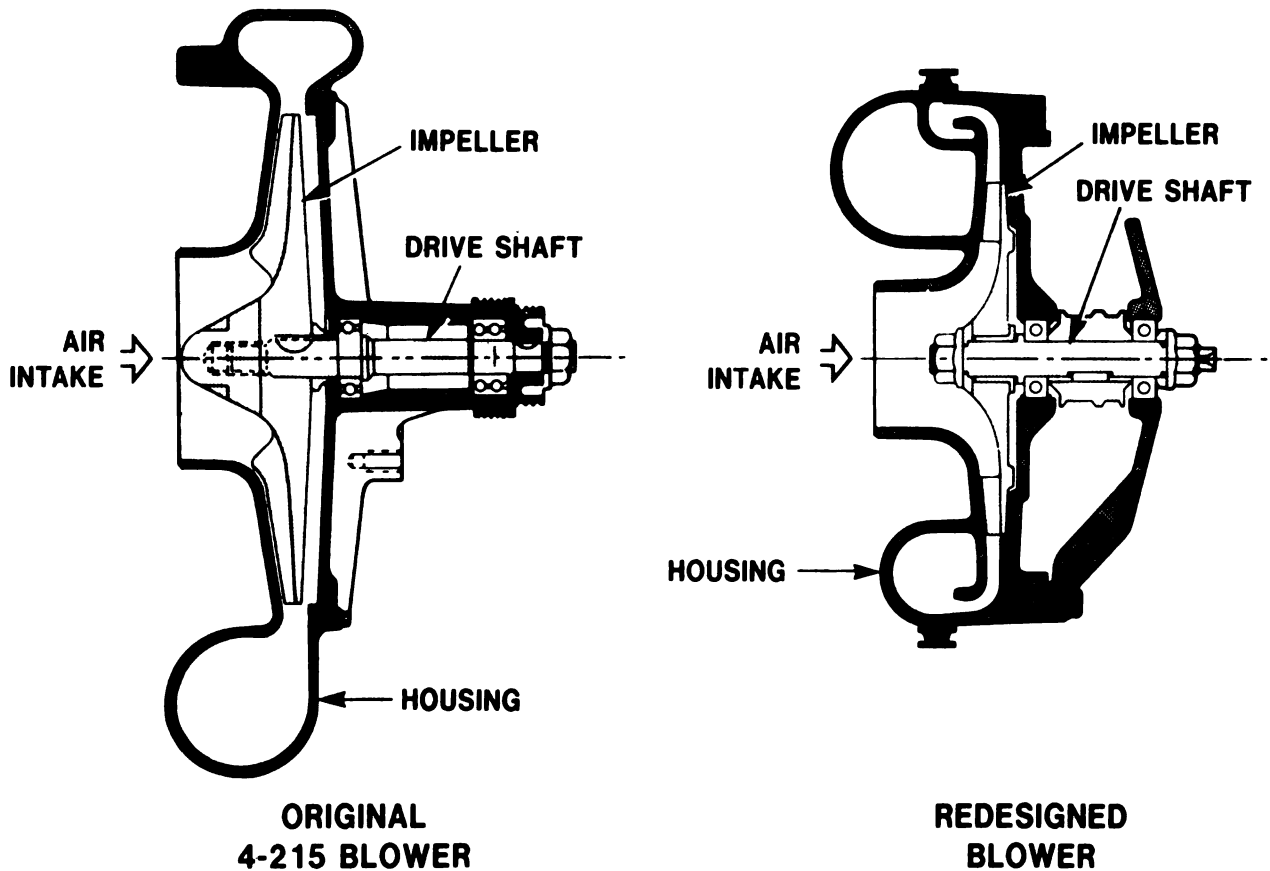
**REDESIGNED
BLOWER**

	ORIGINAL BLOWER	REDESIGNED BLOWER
Impeller Diameter	254 mm	188.5 mm
Overall Diameter	397 mm	305 mm
Available Drive Ratio (Max.)	5.0:1	8.3:1
Engine Requirements (Max.) Flow/Pr. Ratio	$.282m^3/s$ 1.34	$.154m^3/s$ 1.17

Fuel Economy Assessment:

The redesigned blower gives a 0.11 MPG improvement on the
Fourth Generation engine.

Figure 2.5-6   Blower Comparison

BLOWER POWER COMPARISON

ENGINE MAP: TDEM247C

DRIVE SYSTEM: Current Blower –
4.75:1 Ratio + Viscous Clutch

New Blower –
6.25:1 Ratio + Viscous Clutch

*VSIM Test Point	Current Blower	New Blower
1	.07 kW	.11kW
2	.14	.15
3	0	0
4	.23	.21
5	.35	.29
6	.57	.44
7	1.07	.77
8	1.00	.71
9	1.60	1.08
10	1.53	1.06
Fuel Economy M-H (Gasoline)	18.78 MPG	18.89 MPG

*M-H Data File: MH215.45

Figure 2.5-7   New vs. Current Blower
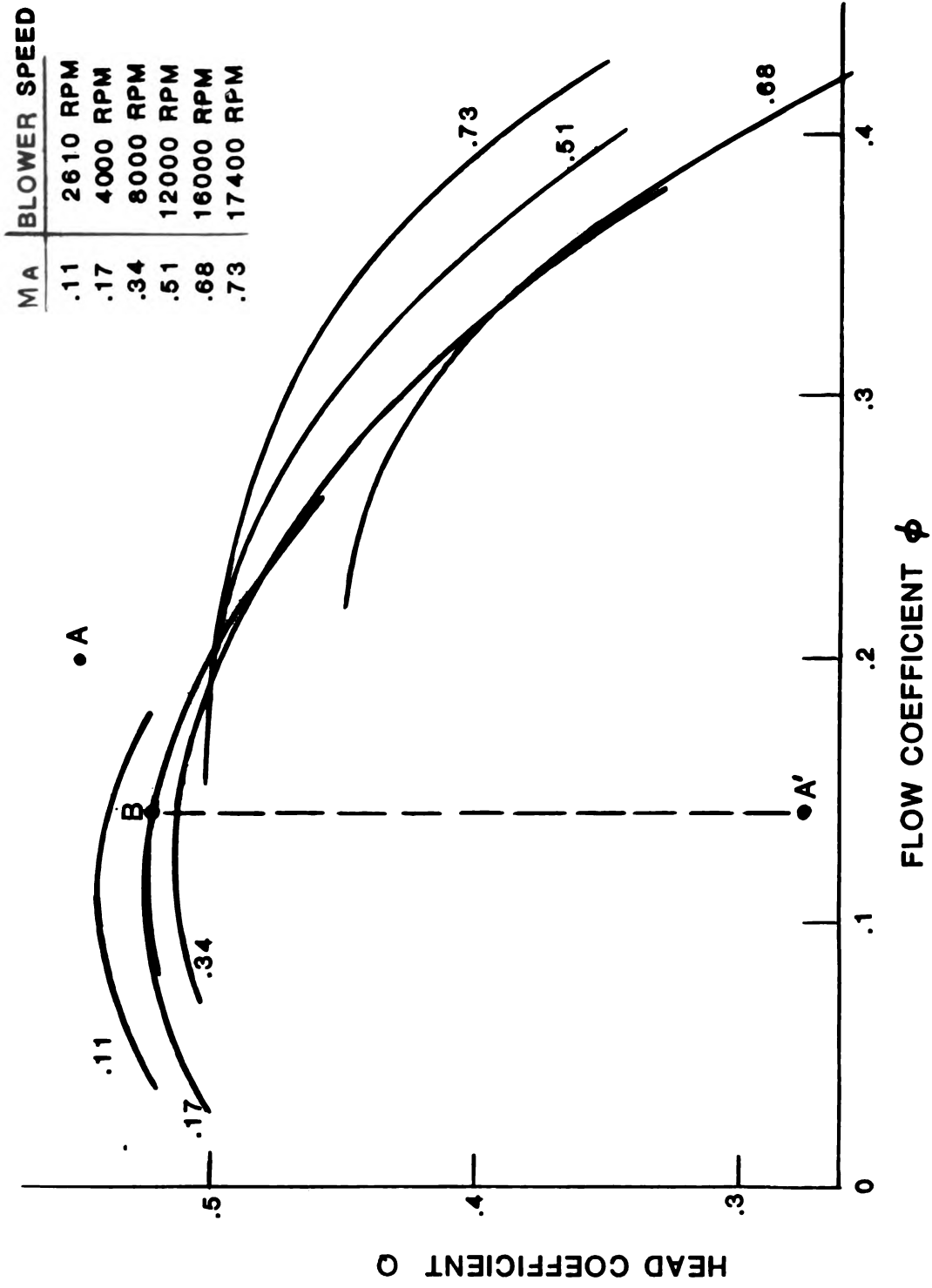
Figure 2.5-8   Combustion Air Blower
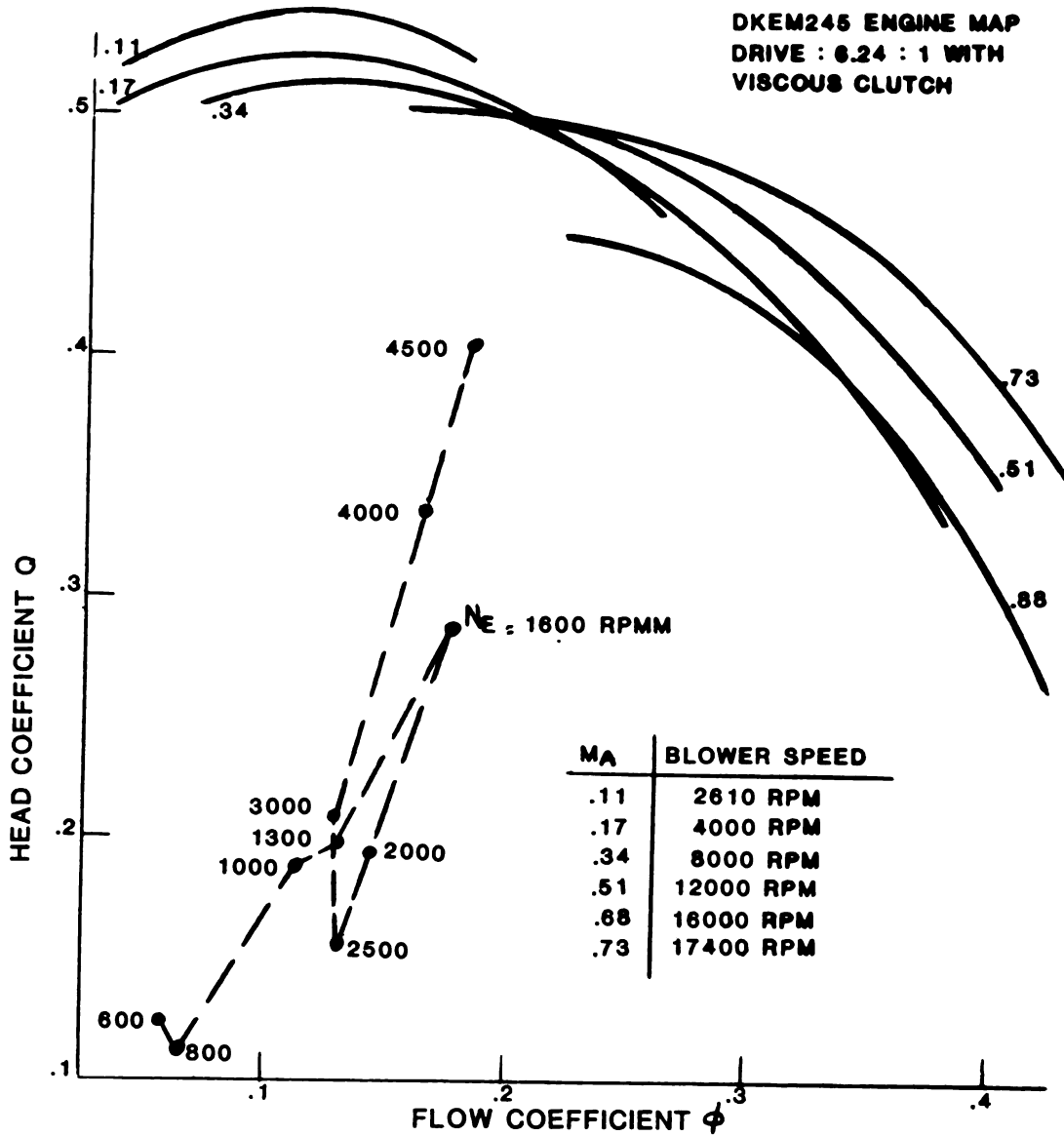
Figure 2.5-9   Combustion Air Blower

24 VANE ROTOR

MAXIMUM AIRFLOW
REQUIREMENTS

DKEM245 ENGINE MAP
DRIVE : 4.75 : 1

M_A	BLOWER SPEED
.11	2610 RPM
.17	4000 RPM
.34	8000 RPM
.51	12000 RPM
.68	16000 RPM
.73	17400 RPM

HEAD COEFFICIENT Q

FLOW COEFFICIENT ϕ

$N_E = 2000$ RPM
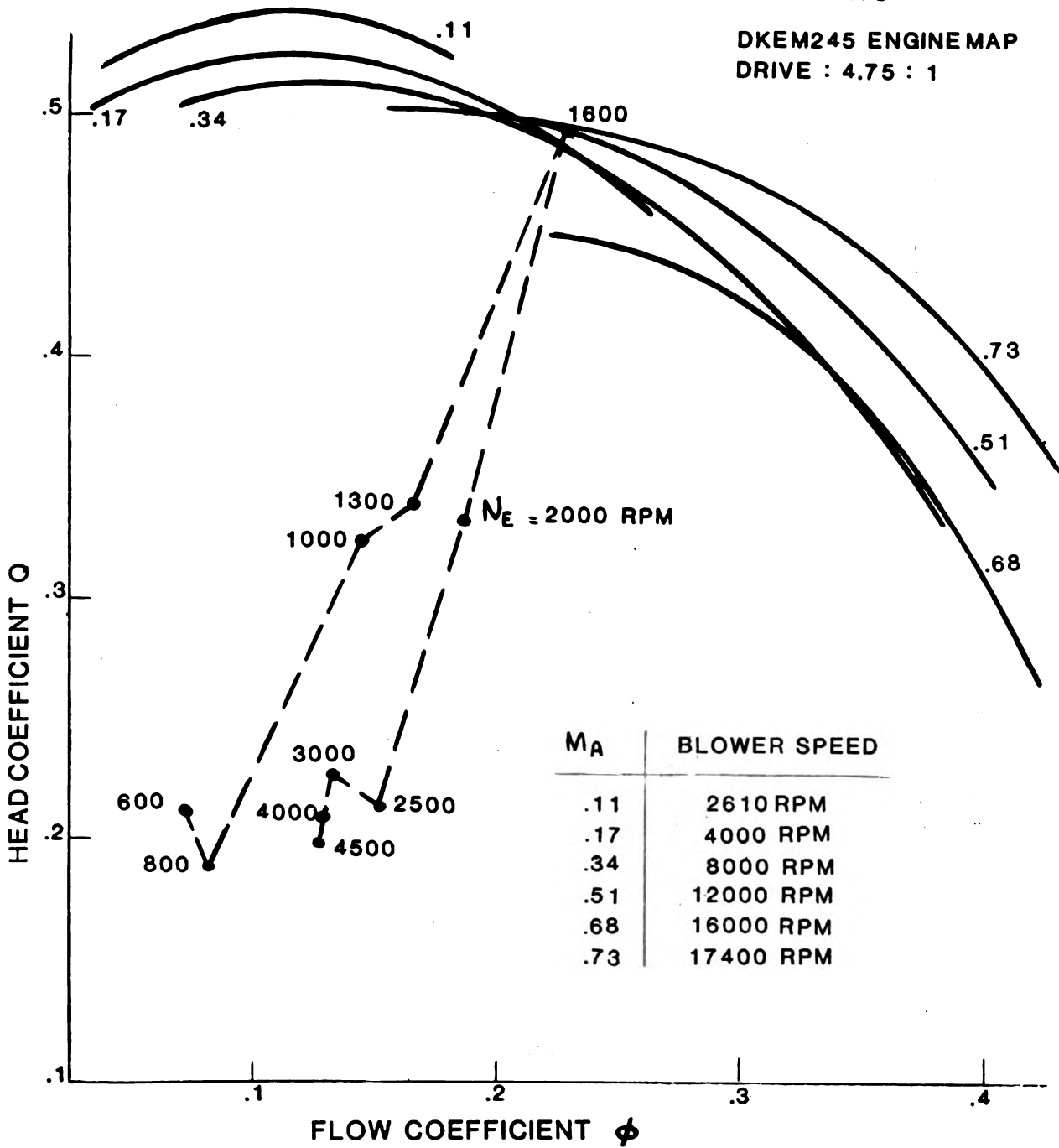
Figure 2.5-10   Combustion Air Blower

24 VANE ROTOR

MAXIMUM AIRFLOW
REQUIREMENTS

DKEM245 ENGINE MAP
DRIVE: 4.75 : 1 WITH
VISCOUS CLUTCH

M_A	BLOWER SPEED
.11	2610 RPM
.17	4000 RPM
.34	8000 RPM
.51	12000 RPM
.68	16000 RPM
.73	17400 RPM
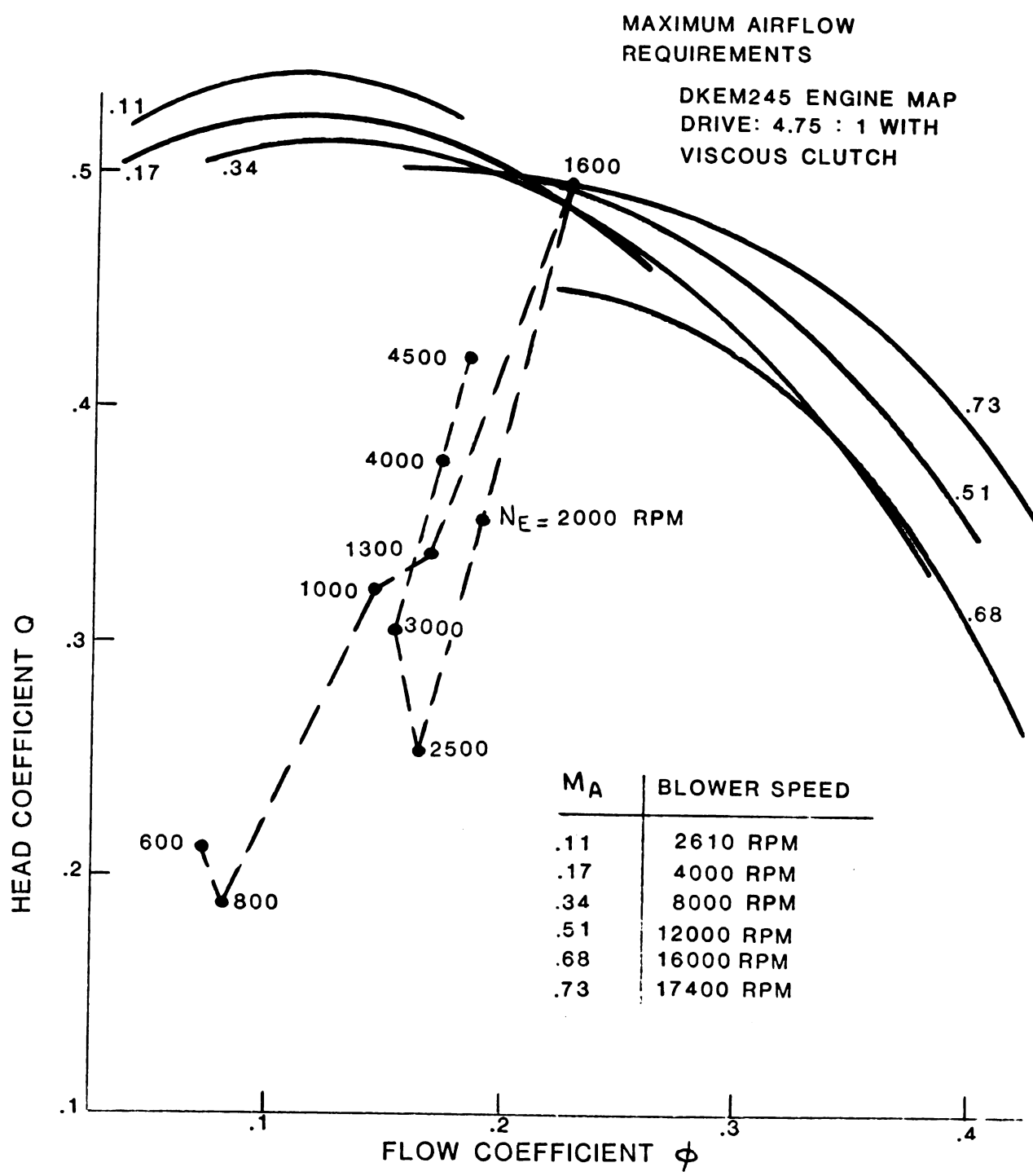
Figure 2.5-11   Combustion Air Blower

ENGINE MAP: DKEM245C

DRIVE SYSTEM: Belt Drive & Viscous Clutch

*VSIM Test Point	6.24:1 Ratio	4.75:1 Ratio
1	.09 kW	.07 kW
2	.17	.13
3	0	0
4	.36	.28
5	.52	.39
6	.85	.62
7	1.69	1.17
8	1.64	1.13
9	2.36	1.77
10	2.49	1.76
Fuel Economy M-H (Gasoline)	21.52 MPG	21.76 MPG

*M-H Data File: MH2.5-10

Figure 2.5-12   Blower Power Comparison

2.6 Power Control

2.6.1 Summary

2.6.1 Summary — The objective of this section was to determine the fuel economy improvements that could be achieved by modifying the power control method, the hydrogen compressor system components, and other power control components.

The results of the sub-task indicate a total fuel economy improvement of 2.9 MPG, M-H. This improvement results primarily from the use of an internal compressor, short circuited when not needed (2.2 MPG improvement) and the use of dead volume control in addition to mean pressure (0.7 MPG improvement). Additionally, a new easily maintained power control valve has been shown to be suitable for engine use.

The primary power control method used on the 4-215 engine is mean pressure wherein hydrogen is added to the engine to increase the torque level and the hydrogen is removed to reduce the torque level. This control method is compact, free of basic operational problems and gives very good part load fuel economy. The hydrogen transfer to and from the engine requires the hydrogen to go through the compressor. The compressor was constructed by attaching two small (11 mm dia.) plungers to the bottom of the main engine piston. The advantage of this construction is that no additional compressor drive mechanism is necessary while the disadvantage is that compressor piston ring leakage changes the engine's working gas quantity.

The power control valve directing the hydrogen flow consisted of an assembly of five individual valves, each valve opened by a valve on one rotating camshaft and closed by a spring. In general this valve performed its function well except that hydrogen contaminants often prevented the valve from functioning properly and subsequent valve maintenance was very time consuming.

The work performed under Section 2.6 is arranged in the following categories:

2.6.2 Alternate Power Control

2.6.3 Power Control Valve

2.6.4 Analytic Compressor Loss Study

2.6.5 Compressor Test Rig

2.6.6 Dyno Testing of Compressorless Engine

2.6.2 Alternate Power Control

2.6.2.1 Summary — Analytical and design studies have indicated that a combination of dead volume and mean pressure control methods could increase the M-H fuel economy by 0.74 MPG over a mean pressure control only and that the necessary dead volume could be packaged into the existing 4-215 engine. In this concept, most driving conditions could be met with the control dead volumes active, the control dead volume would be closed (deactivated) only during peak torque requirements.

2.6.2.2 Work Performed — Cycle analysis with additional dead volume was done with both the USS and Philips computer program to evaluate the effects on engine fuel economy. Vehicle M-H fuel consumption was then calculated and presented against control dead volume.

An optimum value of control dead volume was determined that gave most of the fuel consumption improvement. The new compressor capacity was then determined, the control volume valve size determined and a design completed.

2.6.2.3 Results — The underlying hypothesis of this investigation was that increased amounts of dead volume in the cold compression space were reflected as decreased torque output and, to a point, increased indicated engine efficiency. Initial engine simulations with the USS computer program of a 4-215 type engine indicated the trends as illustrated in Figure 2.6-1.

Indicated engine efficiency increased by 2% units when additional control dead volume was increased from zero to three times swept engine volume. Further increases in control volume resulted in an efficiency decrease to the baseline level at approximately eight times swept volume. At the same time, indicated power decreased by about 80%.

The engine efficiency improvements were reported as increased miles-per-gallon throughout the M-H driving cycle. A Ford Motor Company computer program, "ECONCALC," existed for this specific purpose. The required input was a speed/torque/fuel flow engine map as prepared by the Philips computer program. All future computer calculations were via the Philips programs.

The Philips and USS computer predictions differed in absolute values of efficiency since the Philips program account for more losses, but the trends remained similar. The Philips program showed an increase of 3 1/2 vs. the USS program which showed an increase of 2% over a dead volume range of zero to eight times swept engine volume.

In modeling the control dead volume elements in the Philips program, the additional volume was added entirely in the adiabatic dead space on the compression side. Adiabatic dead space was entered as a percentage of swept engine volume.

An efficiency comparison of dead volume and mean pressure control systems was completed. The dead volume control gave generally higher predicted efficiency than the predicted mean pressure control system. However, the pure dead volume system required large amounts (4000%) of additional volume to reach idle. Disregarding engine short-circuiting as an idle control, a hybrid dead volume/mean pressure control was devised which although more compact, is more complex. Mean cycle pressure would continue to be the controlling parameter at most driving points. The dead volume would be closed to the cycle only during peak power situations. All three systems are compared for efficiency in Figure 2.6-2.

In order to evaluate the projected fuel economy improvements using a hybrid dead volume/mean pressure power control system, a series of engine maps and corresponding M-H fuel economy estimates were generated. A 4-215 D.A.

178

engine was modeled with varying amounts of adiabatic dead space and the assumption that the additional control dead volume would be open to the engine throughout the drive cycle as modeled by the steady state vehicle simulation points, (refer to Section 2.9). A graph of M-H fuel economy vs. amount of control dead volume was constructed in Figure 2.6-3. Fuel economy generally followed the trends of indicated efficiency shown previously and a maximum calculated improvement of .94 MPG was reached at about 300% control volume. Figure 2.6-3 also indicates that a large portion of the fuel economy improvement is attainable with much smaller control dead volume. An improvement of .74 MPG is indicated with a control volume of 142%.

The effects of this additional control dead volume element on other engine parameters was also investigated. Figure 2.6-4 shows torque vs control dead volume at various levels of constant mean pressure. Figure 2.6-5 shows the effects of the additional dead volume on cycle P-V diagrams. Figures 2.6-6 and 7 show that the average gas temperatures in both the cooler and heater approach the respective wall temperatures as the dead volume is increased, thus increasing the engine efficiency nearer to the Carnot efficiency defined by the heater and cooler wall temperatures.

Increased compressor capability was needed to maintain pump down rates as the engine cycle contained more hydrogen gas. Figure 2.6-8 shows the relationship between torque and hydrogen quantity for two values of control dead volume, i.e., $X_c = 0$ and $X_c = 1.42$. For the $X_c = 1.42$ case, the relationship is shown for the case with the control dead volume inactivated ($X_{ca} = 0$, $X_{cl} = 1.42$) and for the control dead volume activated ($X_{ca} = 1.42$, $X_{cl} = 0$). The relationship of compressor size and control dead volume is presented graphically in Figure 2.6-9. Although the 4-215 uses a hollow piston dome configuration, both sealed and hollow dome data is given as future engines assume sealed pistons.

The effects of flow restriction on indicated engine torque as predicted by "FCDVAREA" is shown in Figure 2.6-10. This computer program, "FCDVAREA," was written at Ford Motor Company to investigate flow restrictions between the control dead volume and the cycle. At large flow areas, the engine torque level was no longer influenced by the flow area but the additional dead volume. If the valve was completely closed, the engine cycle variations were not open to the dead volume. At certain intermediate points, however, the indicated torque will dip below the torque levels associated with large flow areas. The torque dip will extend into the negative torque region for large control dead volume and small flow area.

This characteristic was caused by the varying phase difference between the control volume pressure and the engine cycle pressure. Figure 2.6-11 shows this effect by the change in engine pressure-volume diagrams for several valve openings. It should be noted that Figure 2.6-11 is a far larger control dead volume, $X_c = 7000\%$ than the $X_c = 1.42$ control dead volume used in Figure 2.6-10. This was done to emphasize the effects on the pressure-volume diagrams.

From Figure 2.6-10 a minimum equivalent flow area of 100 mm^2 between the control dead volume and the cycle must be maintained in a 4-215 engine with

a control dead volume of 142% (308 cm^3).

Results of design studies of a control dead volume module with a volume of 308 cm^3 is shown in Figure 2.6-12. This module could be installed on the 4-215 engine with only minor engine modifications, however, this design with the control dead volume connects only to one of the two cold connecting ducts in each cycle and requires additional studies as the flows through the two intercoolers may be unbalanced.

The incorporation of the control dead volume into the power control system is shown in Figure 2.6-13, depicting a two level dead volume system. Other differences between the proposed hybrid power control and the existing 4-215 power control is that the compressor is short circuited when not pumping and the reservoir is large enough to require the compressor to operate only during torque reductions.

2.6.2.4 Conclusions — The combination of mean pressure and dead volume power control method produced better fuel economy than either method by itself. The analysis indicates that most of the fuel economy improvement can be attained with only a small control dead volume. (0.74 MPG M-H improvement with X_c = 142%). The maximum improvement was 0.94 MPG M-H with X_c = 300%.

Design studies have indicated that the proposed control dead volume could be packaged in the 4-215 engine after some minor modifications to the accessory drive. However, because the proposed control dead volume occupies the same space as the existing engine mounts, new engine mount locations will have to be designed. A hybrid power control scheme has been devised that is capable of giving most of the potential fuel economy with a minimum of additional complexity.

2.6.2.5 Recommendations — Recommendations for future work in this area concentrate on confirmation of the collected analytical data by engine modification and test. Following the scheme of Figure 2.6-12, a control dead volume could be fitted to the 4-215 engine at an early date. The valve connecting dead volume to cycle could be designed, built, and tested as a separate component prior to engine running.

The effects of heat transfer from the control dead volume must be evaluated. Heat will be rejected from the engine to the atmosphere through the dead volume walls. Also, heat transfer will occur between the cycle gas and the dead volume walls as the gas temperature oscillates about the mean temperature of the walls.

2.6.3 Power Control Valve

2.6.3.1 Summary — An easily maintained, hydraulically operated power control valve having positive opening and closing characteristics was designed, built, and tested. A commercial servo valve was used to control the hydraulics. The valve design featured rectangular cross sectional seal rings backed up with "O" rings fitted into grooves in the stationary valve body. This arrangement unseats the seal ring from the spool ports when the ports slide pass

180

the seals.

Test results indicated good repeatable opening characteristics, adequate response without requiring excessive hydraulic power, and to the extent tested, good seal life.

2.6.3.2 Work Performed — Early 4-215 engine operating experience indicated a need for a simpler, more durable power control; hence, a linear power control was designed and built. Figure 2.6-14 illustrates in schematic form its operating principle and its function in the engine power control circuit.

Using a MOOG P/N 3-/1.5/0500/I/0200 as a servo, the unit was plumbed and instrumented per Figure 2.6-15 and subjected to a series of bench tests. A sample of a portion of the recorded data collected from one of the tests performed is included as Figure 2.6-16.

On first assembly, leaks through the switch-over valve seals could not be reduced to an acceptable level; consequently, a plug was fitted in place of the switch-over spool to permit continuation of tests on the main control. No further work on the switch-over valve or its seals was done to correct the problem encountered.

An initial series of tests was conducted on the original power control configuration (except as noted above) to establish the flow rates through the several valves, determine suitable hydraulic actuation pressure and flow requirements, and evaluate the radial Teflon type spool seals.

Subsequent to the initial test series, the control valve spool was modified to provide additional flow area through three of the four flow passages. This was done to decrease the dead zone between supply and pump-off, decrease the slope of the supply and pump-off flow curves, and provide some overlap of the pump-off and short circuit modes. Calculated flow areas for the original and revised spools are plotted in Figure 2.6-17. Because flow restriction in the nitrogen tank to power control line was noted during the first test series, all external nitrogen flow lines were replaced by 3/8 inch lines before any tests were conducted on the revised spool.

The second test series was conducted to check flow rates through the revised spool, verify valve response times for the hydraulic actuation pressure and flow selected from the first test series, and check out an electronic circuit package developed by the electronics section to replace the lab breadboard circuitry used to this point. In addition, seal performance was evaluated.

2.6.3.3 Results — Test Series I and II were as follows:

a.   Test Series I — test runs on the original spool configuration using lab breadboard electronic circuitry produced the full supply mode travel response time data shown in Figure 2.6-18. Four hydraulic flow rates at each of three hydraulic actuation pressure levels were checked. Hydraulic oil flow rates were set with flow limits. Actuation times of from over a second to as little as 0.2 sec. were recorded.

More than 10,000 operating cycles were accumulated on all but one seal. The replaced seal leaked excessively after 3600 cycles. At test conclusion, leakage rates measured with 6895 kPa (1000 psi) nitrogen pressure across each seal system ranged from 100 cc/min to 600 cc/min.

b. Test Series II — Full supply mode spool travel time data from Test Series I indicated that a hydraulic actuation pressure of 827 kPa at a flow rate of .49 l/min was adequate for engine operation. Hence, all second series tests were conducted using these hydraulic supply conditions.

From second series test data plotted in Figure 2.6-19 nitrogen flow rates through all four valves exceeded 60 gms/sec with 6895 kPa inlet pressure (in terms of hydrogen flow under the same conditions, more than 225 gms/sec could be expected). In all four valve flow tests, limiting flows occurred at about three millimeter spool travel which is somewhat short of the travel required to produce "wide open" flow areas. At a spool position of three millimeters, each valve has a calculated flow area of about 30 mm^2, which is also approximately equal to the 34mm^2 minimum area of the 3/8 inch tube fittings used for the nitrogen system external plumbing. Hence, the external plumbing limited the flows measured.

With the developed vehicle electronic circuitry used for Test Series II, it was possible to program any desired spool travel length of from 0.5 to 6.6 mm and to record the time required to achieve the travel programmed. Results of five test runs conducted are plotted in Figure 2.6-20. Ninety percent of full supply mode demand was realized in 250 ms and the 22 mm^2 flow area (which occurred at about one-third of maximum travel) was crossed at about 100 ms.

A total of 10,400 full stroke cycles were put on the control spool during the second test series. Leakage rates (again measured with 6859 kPa nitrogen across each seal system) were as follows:

P_{vess} to P_{dist}	700 cc/min
P_{vess} to P_{max}	zero
P_{max} to P_{suc}	1100 cc/min
P_{max} to P_{min}	4000 cc/min

Leakage from the end seals to the atmospheric vents was not measured.

After Test Series II was completed, the control was disassembled to determine the cause for the leakage noted. An axial scratch on the spool surface about 0.3 mm deep and 10 mm long was found emanating from a third row supply port and a 0.3 mm raised area was found at the edge of a second row short circuit port. Both of these discrepancies could be the cause for the leakage recorded. The Pmax to compressor section areas are isolated by two seals; hence, the leakage found could be from both or either seal. The condition of these seals at the end of the test exhibited no apparent cause for the leak found.

At present, the seals cannot be removed without damaging them locally and the Pmax to compressor suction seals cannot be leak-checked individually. Further, the several dozen seals used for the tests were selected from more than 150 purchased. Most of the seals not used were rejected because of rough surfaces.

In general, the linear control with its associated electronics operated smoothly during all tests conducted and spool positions were repeatable to less than 0.1 mm.

2.6.3.4 Conclusion — This "state of the art" linear power control is suitable for dynamometer engine installation.

2.6.3.5 Recommendations — The following recommendations can be made on the power control valve.

a. Test in-house designed and fabricated seals in all areas of the control including the switch-over valve.

b. Devise a fixture to individually check each of the Pmax-to-compressor suction seals.

c. Install the linear power control on a dynamometer engine for further tests.

d. Investigate power control valve actuators that are less expensive and valve configurations that do not require dynamic sealing to the atmosphere.

2.6.4 Analytical Compressor Loss Study

2.6.4.1 Summary — The effect of compressor mechanical function on metro-highway fuel economy was evaluated. This was done to determine if external or internal compressors produced the least friction work over the driving cycle and to determine the most efficient method of unloading the compressor. This study was deemed necessary as the friction power consumption of an external compressor could eliminate it from further serious consideration as an alternate compressor design, in addition to determining fuel consumption penalty of the internal compressor.

An external compressor was designed and its friction characteristics was determined, which were then used to generate an engine fuel consumption map. Other engine fuel consumption maps were generated for the internal compressor with several methods of compressor unloading. These fuel consumption maps were then used to generate metro-highway driving cycle fuel consumption.

Complete removal of the compressor would improve fuel economy by 0.63 MPG, short circuiting the internal compressors would give almost as much, 0.62 MPG, and the external compressor would improve the fuel consumption by 0.56 MPG over the base internal compressors with suction shut off.

2.6.4.2 Work Performed — The mechanical friction losses of the internal

compressor in the 4-215 engine were calculated and compared to the calculated friction losses of the proposed external compressor. The friction effects are presented according to their impact on M-H fuel economy.

The internal compressor pistons in the 4-215 engine were mounted directly on the engine piston which resulted in one side of the compressor pistons exposed to instantaneous engine pressure and the other side to compressor pressure. Figure 2.6-21 depicts the pressure variation on both sides of the compressor piston for two conditions; suction shut-off and short circuit at engine mean pressure.

This pressure - crank angle relationship indicated that there is always a pressure difference across the compressor piston ring belt. Short circuiting the internal compressor at mean engine pressure reduced the pressure difference but did not eliminate it. As a consequence, the piston ring friction could not be eliminated during the periods when the compressor operation was not needed.

The internal compressor studies were conducted with the N.V. Philips engine computer program to generate engine torque, speed, and efficiency maps for the suction shut-off (normal), the short circuited compressor at mean engine cycle pressure, and the compressorless engine conditions. These maps were then used with the ECONCALC computer program to calculate the vehicle fuel economy numbers. The N.V. Philips program calculated the compressor piston ring friction work by first calculating the pressure difference across the compressor piston rings, using the inputed friction coefficient to calculate the friction work for an incremental step. The total friction work then became the summation for one revolution of the incrementally calculated work. The program did not consider any other compressor losses.

Figure 2.6-22 shows the external compressor that was designed for the 4-215 engine and it is the compressor used to evaluate the friction of an external compressor. This design accommodated either rollsock or sliding rod seals. The displacement was increased from the 40 cc/engine revolution in the 4-215 engine to 53 cc/engine revolution to accommodate the increased hydrogen quantities in the hybrid power control.

Figure 2.6-23 shows all of the friction producing components in the external compressor. For this study, compressor piston ring friction was assumed to be zero as short circuiting would eliminate the piston rings pressure difference.

The external compressor losses were evaluated with a Ford computer program "COMPCRNK". The external compressor losses were than incorporated in the N.V. Philips engine computer program to generate new engine maps and in turn the engine maps were used in the ECONCALC program to calculate the vehicle fuel economy.

The base for this study was the normal 4-215 engine operating method wherein the suction was shut-off and the discharge was at storage vessel pressure (Pn) whenever the compressor was inoperative.

2.6.4.3 Results — Figure 2.6-24 shows the fuel economy changes due to the

two compressors under several operating conditions. The biggest fuel economy improvement occurred when the internal compressor was completely removed. Although this situation is unrealistic, it represents the maximum fuel economy improvement potential possible from the elimination of compressor friction. The study showed that removing the compressor plunger resulted in a fuel economy improvement of 0.63 MPG M-H. This improvement is due to a 0.74 MPG improvement resulting from piston ring friction elimination and a 0.11 MPG penalty resulting from increased engine cold swept volume and decreased cold adiabatic dead space that reduce the engine's indicated efficiency.

The second best fuel economy figure occurred with a short circuited internal compressor, the 0.62 MPG M-H improvement completely due to the reduction in the piston ring friction. Figure 2.6-21 depicts the way compressor piston pressure varies throughout the cycle.

The external compressors are next, showing improvements of 0.56 and 0.47 MPG M-H depending on the type of piston rod seal.

2.6.4.4 Conclusion — While this study indicated that the short circuited internal compressor had the best fuel economy improvement potential, compressor piston ring leakage losses not considered in the analytical model would make the external compressor the best candidate to attain the indicated fuel economy improvement.

Dynamometer tests at N.V. Philips have shown only a 0.3 MPG improvement with a short circuited compressor; the tests revealed the short circuiting improved fuel economy at low engine torques but decreased the fuel economy at higher engine torques. Analytical results indicated an improved fuel economy at all torques.

Results from the Compressor Test Rig, Figure 2.6-26, suggest that the dynamometer-computer simulation differences were caused by internal compressor flow losses; losses not considered in the analytical model. Figure 2.6-25 depicts the internal compressor flow passages in the 4-215 engine and in the Compressor Test Rig together with the measured input torque to the rig.

2.6.5 Compressor Test Rig

2.6.5.1 Summary — The purpose of constructing and testing the compressor test rig was to obtain experimental data on Rulon piston ring friction and leakage and to measure the power consumption of unloaded compressors. The friction data was to confirm the friction values used in the engine computer program. The ring leakage data was used to confirm by direct measurements independent of the engine the severity of the leakage.

The test rig was constructed by placing two plungers similiar to the 4-215 plungers on top of a single cylinder engine's piston and building a cylinder block and valve holder on top of the engine's cylinder block. The test rig was driven by a variable speed drive with a torque transducer in between.

Results indicate that piston ring friction was in agreement with published data, ring leakage was excessive and the Rulon rings had very short operating life.

185

The most efficient method of unloading the compressor was to short circuit the inlet and discharge ports with a low flow resistance path.

2.6.5.2 Work Performed — The Compressor Test Rig is shown in Figure 2.6-26. This rig consists of two compressor plungers of the same diameter as the compressor plungers in the 4-215 engine which are mounted on top of a single cylinder engine piston. The plungers operate in the water cooled cylinder, which can accommodate either the test head or the standard head. The test head has very low flow restrictions but cannot accommodate the check valves while the standard head can be installed with or without the check valves. The stroke of the single cylinder engine block is 62 mm, 10 mm longer than the stroke of the 4-215 engine. Each of the compressor bore diameters is 11 mm. Piston rings and check valves from the 4-215 engine were used for these tests. The piston rings were of Rulon LD with scarfed end joints (refer to Section 2.4).

The Compressor Test Rig was driven by a variable speed drive through a strain gage torque meter; the test configurations for these tests are shown in Figure 2.6-27. A description of the configuration is as follows:

a. Configuration A — Test Rig Friction - Test head used to pressurize the top of the plungers with no piston rings. Tests were run from 6000 to 2000 RPM at pressures up to 2760 kPa (400 psi).

b. Configuration B — Piston Ring Friction — Piston rings installed and the test head was used. Tests run at 1000 and 1500 RPM and the gas pressure ranged from 0 to 9800 kPa (1420 psi) with hydrogen and nitrogen gas.

c. Configuration C — Short Circuit — Standard head without check valves, suction and discharge ports connected together. Tests were run at 1000 and 1500 RPM and the gas pressures ranged from 0 to 9800 kPa (1420 psi) with hydrogen.

d. Configuration D — Short Circuit — Standard head was used with check valves, suction and discharge ports connected together. Tests were run at 1000 and 1500 RPM and the gas pressures ranged from 0 to 9800 kPa (1420 psi) with hydrogen.

e. Configuration E — Suction Shut-off — Compressor suction was shut-off and the pressure regulator prevented the discharge pressure from exceeding 22,080 kPa (3200 psi). Tests were run at 1000 and 1500 RPM, and the suction pressure ranged from 0 to 1311 kPa (190 psi) with hydrogen.

Not shown is the piston ring leakage test configuration which consisted of a 1900 cc (total) volume connected to the compressor. The test was conducted by pressurizing the 1900 cc gas volume after stopping the test rig and recording the pressure vs. time relationship.

The water-out temperature was not maintained constant for test points because of the high thermal mass and large heat transfer area of the test block. Water temperatures were between 20°C (68°F) and 60°C (140°F), lower than the 71°C (160°F) projected for the 4-215 engine.

2.6.5.3 <u>Results — Compressor Test Rig Friction</u> — The results of the Compressor Test Rig friction tests are shown in figure 2.6-28. The test rig friction torque is independent of gas pressure and is proportional to the square root of the speed. Excessive leakage past the ringless compressor plungers prevented the gas pressures to build up higher than 2760 kPa (400 psi).

<u>Piston Ring Friction</u> — Figure 2.6-29 shows the torque consumption vs. constant cylinder pressure at 1000 and 1500 RPM with both hydrogen and nitrogen. The slopes of the torque vs. pressure lines indicate that there was very little flow loss with hydrogen but the losses became significant with nitrogen, especially at 1500 RPM.

Using the relationship derived below to reduce the data, the average value of μ is .085 for hydrogen at 1000 and 1500 RPM. This is lower than the published values of 0.15 to 0.25 for Rulon LD running against dry steel; the difference is attributed to a thin film of oil on the test rig cylinder walls. Other tests have indicated $\mu = 0.10$ for 1000 and 1500 RPM with H_2 and 1000 RPM with N_2.

$$\mu = 734.3 \frac{T}{P}$$

Where: μ = friction coefficient

P = pressure change, kPa

T = torque change due to above pressure change, Nm

Piston ring friction was calculated as follows:

Piston ring friction work per revolution is

$$2 \pi T_f = 2 s F_f \quad \text{and piston ring friction is}$$

$$F_f = \pi d_1 h \frac{P_h}{2} \text{ per piston resulting in the coefficient of friction}$$

$$\mu = \frac{T_f}{s d_1 h P_h} \quad \text{for} \quad s = 61.9 \text{ mm}$$

$$d_1 = 11 \text{ mm}$$

$$= 734.3 \left(\frac{T_f}{P_h} \right) \quad h = 2 \text{ mm}$$

$$P_h \text{ is kPa}$$

$$T_f \text{ is Nm}$$

Where: T_f = input torque to overcome piston ring friction

F_f = piston ring friction

P_h = pressure difference across ring belt

s = stroke

d_1 = plunger diameter

h = piston ring height

The observed torque (T_o) for test configuration (B) included the test rig friction torque (T_r) in addition to the piston ring friction, i.e.,

$$T_o = T_f + T_r \quad , \quad T_f = T_o - T_r$$

Friction tests of the test rig have shown that rig friction varied with rig speed only, and was independent of pressure loading, i.e., T_r = constant for a constant speed.

From $\mu = 734.3 \dfrac{T_{f1}}{P_{h1}} = 734.3 \dfrac{T_{f2}}{P_{h2}}$

$$\frac{T_{o1} - T_r}{P_{h1}} = \frac{T_{o2} - T_r}{P_{h2}} \quad , \quad T_r = \frac{T_{o2}\,P_{h1} - T_{o1}\,P_{h2}}{P_{h1} - P_{h2}}$$

Substituting

$$\mu = 735.3 \left(\frac{T_{o1} - T_r}{P_{h1}} \right) = 734.3 \left[\frac{T_{o1}}{P_{h1}} - \left(\frac{T_{o2}\,P_{h1} - T_{o1}\,P_{h2}}{P_{h1} - P_{h2}} \right) \frac{1}{P_{h1}} \right]$$

$$\mu = 734.3 \frac{T_{o1} - T_{o2}}{P_{h1} - P_{h2}}$$

This expression indicates that the friction coefficient is proportional to the observed torque vs. gas pressure slope.

Piston Ring Leakage — After each series of tests, the Compressor Test Rig was stopped, pressurized with hydrogen, and the pressure-time relationship recorded. This pressure-time relationship was solely due to compressor piston ring leakage as all other potential leaks were static, and checked to ensure no leakage. Figure 2.6-30 depicts the pressure-time relationship after several hours of operation. This data is presented on semilog paper as the slope (k_1) is directly proportional to the leakage rate:

$$W_1 = \frac{VP}{RT} \times \frac{\ln P_1 - \ln P_2}{t_1 - t_2} = \frac{VP}{RT} \times k_1$$

Where: W_1 = leakage mass flow rate

V = system volume (1900 cc)

P = system pressure

R = gas constant

T = gas temperature

t = time

The following tabulated leakage values calculated with the above relationship show that leakage was at a minimum after 2.5 and 4.3 hours of operation and increased rapidly with continued operation. The tests were stopped before a stabilized leakage rate was established.

Operating Hours	Leakage Rate, grams/sec. at 6900 kPa
2	.24
2.5	.078
3.4	.058
4.3	.062
5.3	.108
5.8	.164

This data is used only to indicate where the rings were seated and some measure of leakage vs. operating time; no attempt was made to estimate leakage in an operating compressor.

Compressor Unloading — Figure 2.6-31 shows the torque for the short circuited and suction shut-off compressors. The short circuited compressor was run with three levels of internal losses. The least restrictive were the piston ring friction tests, then the standard head without check valves, and the most restrictive with the standard head and check valves.

The figures indicate that for a given compressor suction pressure, the suction shut-off unloading mode consumed more power than compressor short circuiting. Additionally, the figure indicates that internal compressor flow losses in the test rig were the predominant loss when the compressor was short circuited.

Pumping Capacity — Pumping tests could not be run due to the excessive external leakage past the compressor piston rings. This series of tests prohibited the introduction of make up gas during testing since it would affect the capacity

determination.

2.6.5.4 Conclusions — The results of the series of Compressor Test Rig Tests should be considered exploratory, indicating general relationships and helping determine new test objectives. The major effects that prevented conducting the tests as planned were the high piston ring leakage, difficulty to control the water temperature, and high internal flow losses. Piston ring friction tests indicated that the analytical treatment of piston ring friction in the engine computer program was accurate, both in the modeling and the value used for the friction coefficient. If the short circuit mode is chosen to unload the compressor, the internal flow losses should be kept to a minimum.

The Rulon LD piston rings have a very short life before leakage becomes excessive.

2.6.5.5 Recommendations — A serious effort be made either to find better compressor piston rings or design compressors that do not stress the piston rings as much as the 4-215 design. The current designs have too short a life and excessive leakage.

2.6.6 Engine Operation Without Internal Compressors

2.6.6.1 Summary — The internal compressors were removed from the 4-215 engine to determine experimentally the maximum effect the compressors have on fuel economy. Fuel economy improved 2.7 MPG CVS-H with the removal of the compressors; 1.9 MPG of the 2.7 MPG improvement is attributed to piston ring leakage effects.

2.6.6.2 Work Performed — The compressor plungers were removed and the compressor bores were plugged in the 4-215 engine. The engine was run at the same vehicle simulation points as for all other tests. Engine power was manually controlled by supplying hydrogen from an external gas cylinder or dumping engine hydrogen into the dynamometer cell pit.

The removal of the compressor plungers and plugging the bores was simulated on the engine computer program and the resultant vehicle fuel economy determined. The engine computer program did not include compressor piston ring leakage effects, only the effects of piston ring frictions and changed engine geometry were included.

2.6.6.3 Results — Figure 2.6-32 and 2.6-33 summarize the fuel economy and emissions for the CVS-H and Highway driving cycles of the 4-215 engine with and without the internal compressor plungers.

The resultant CVS-H — Highway composite fuel economies were:

Without compressor	-	17.31 MPG
With compressor	-	14.60 MPG
Difference		2.71 MPG

Correcting results of both test with a 148.9 gram fuel penalty (cold-start penalty), the fuel economies became:

Without compressor   -   16.22 MPG

With compressor   -   13.82 MPG

Difference   2.40 MPG

Figure 2.6-34 shows the fuel flow for each of the ten vehicle simulation points with and without the internal compressor as determined from computer analysis and dynamometer tests. The dynamometer comparison showed that the fuel flow for the engine without the compressor plungers was 80 to 90% of the fuel flow with the compressor plungers for all of the vehicle simulation points. The only exception was the number 3 point, which showed this fuel flow ratio to be 60%.

This figure also indicated that the unaccounted piston ring leakage in the analytic model could be the main reason for the difference between the analytic and measured fuel consumption.

2.6.6.4 Conclusion — The dynamometer tests revealed that the total fuel economy penalty arising from the use of the internal compressor in the 4-215 engine is substantial and greater than previously estimated. The previous estimates were based on compressor piston ring friction, leakage pumping work, and the small changes in the engine's cold swept and adiabatic dead volume. The dynamometer tests indicated that other causes were important. The current candidate to rationalize the difference was the detrimental effects of direct hydrogen leakage from the engine to the compressor through the compressor piston rings.

2.6.6.5 Recommendations — A double acting external compressor is recommended as the preferred compressor configuration. The fuel economy would be improved because of the following:

a.   The compressor piston ring leakage would be contained within the compressor.

b.   The configuration would provide better opportunity to design low flow loss passages with the small clearance volume. This would allow effective compressor unloading by short circuiting.

c.   The friction of the external compressor mechanism would be less than the piston ring friction of the internal compressor.

The fuel economy improvement, corrected for cold start, of the external compressor was estimated to be 2.24 MPG M-H. This represents a 2.4 MPG improvement resulting from the total effects of removing the internal compressor and a 0.16 MPG penalty for the frictional losses from the sliding seal external compressor.

DEAD VOLUME POWER CONTROL
4-215 D.A. ENGINE
200ATM - 1500RPM

$$X_c = \frac{DEAD\ VOLUME}{EXP.\ SWEPT\ VOLUME}$$
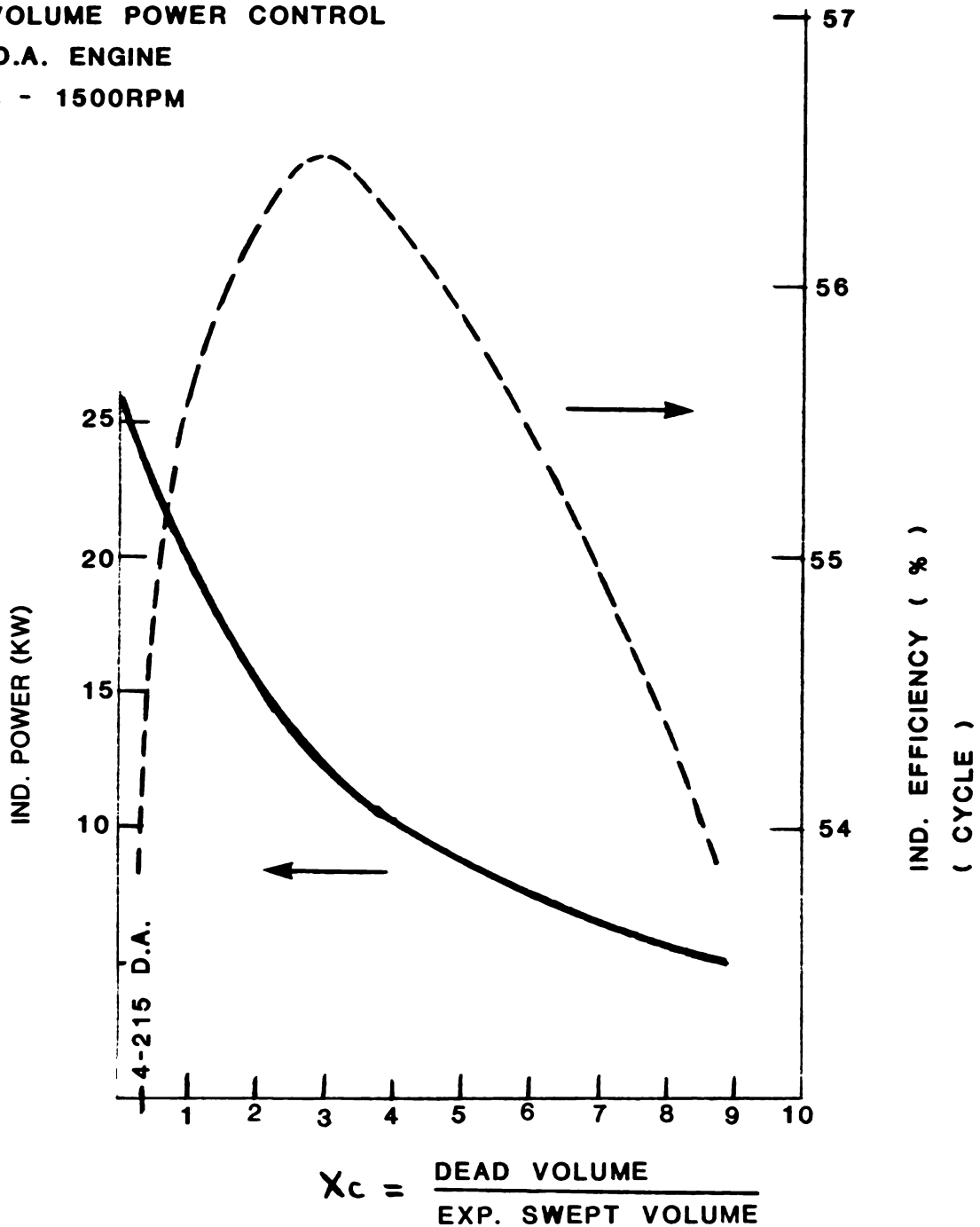
Figure 2.6-1   Indicated Power and Efficiency vs. X_c
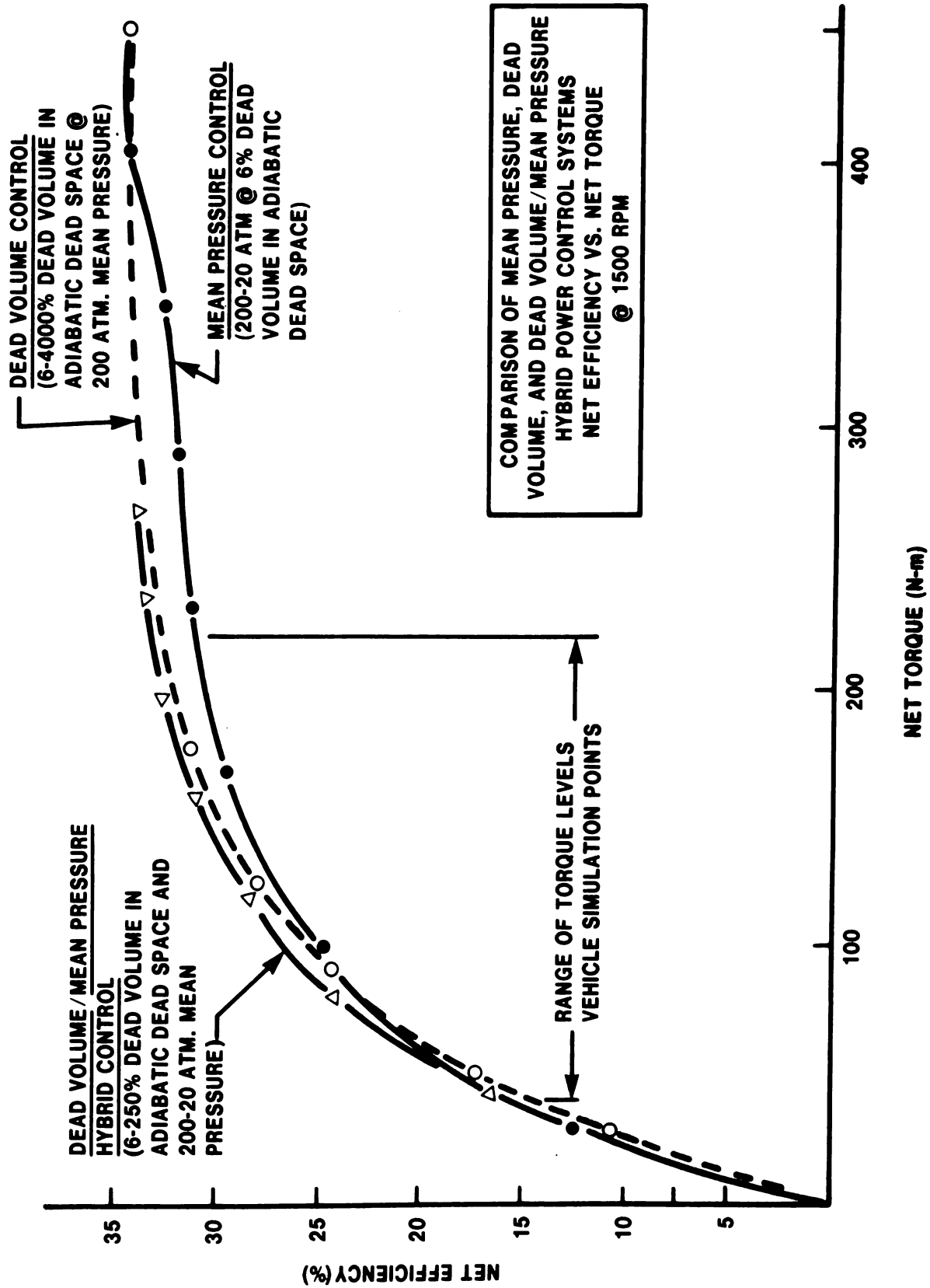
Figure 2.6-2   Comparison of Pressure Control Systems
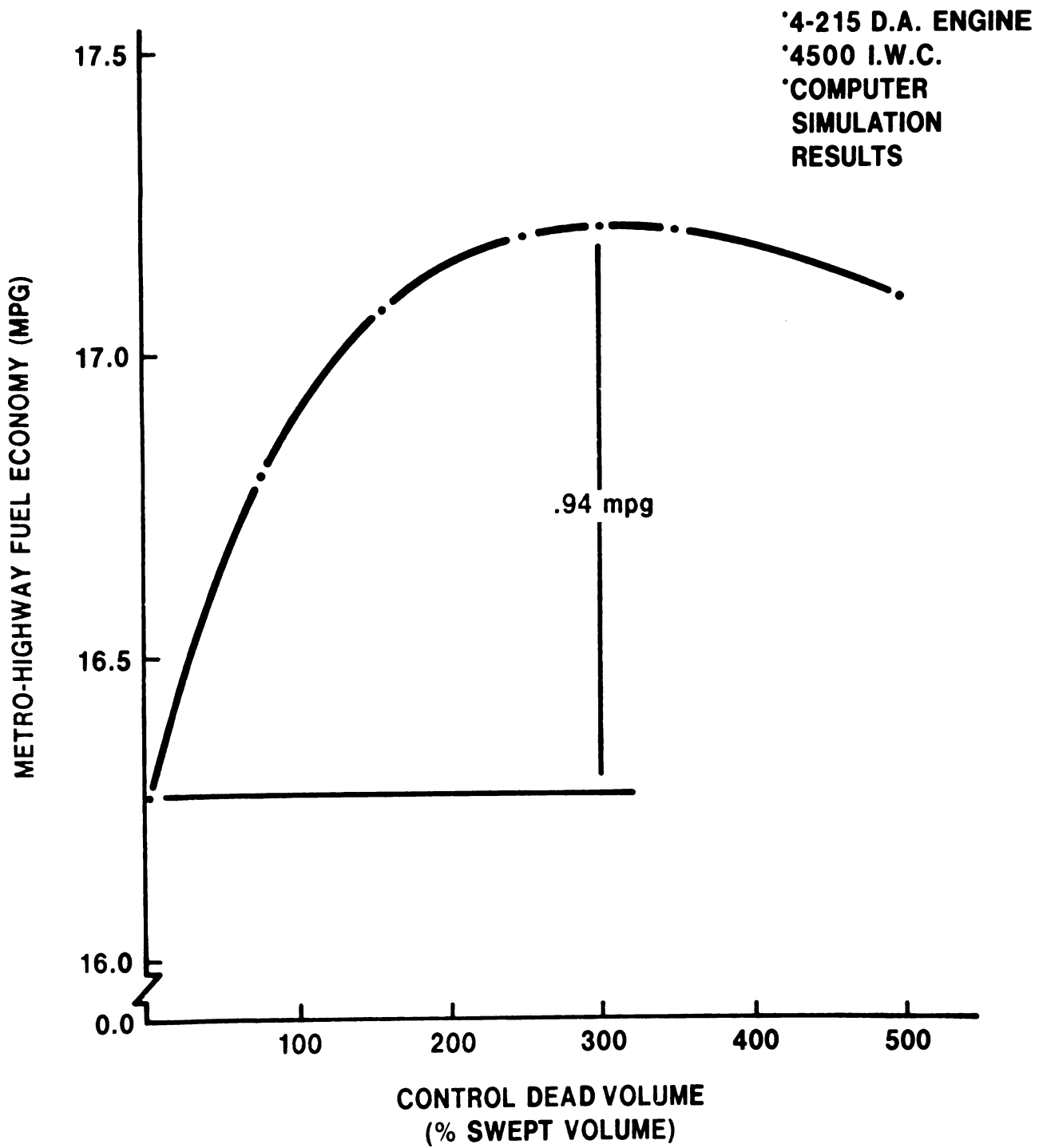
Figure 2.6-3   Metro–Highway Fuel Economy vs. Control Dead Volume
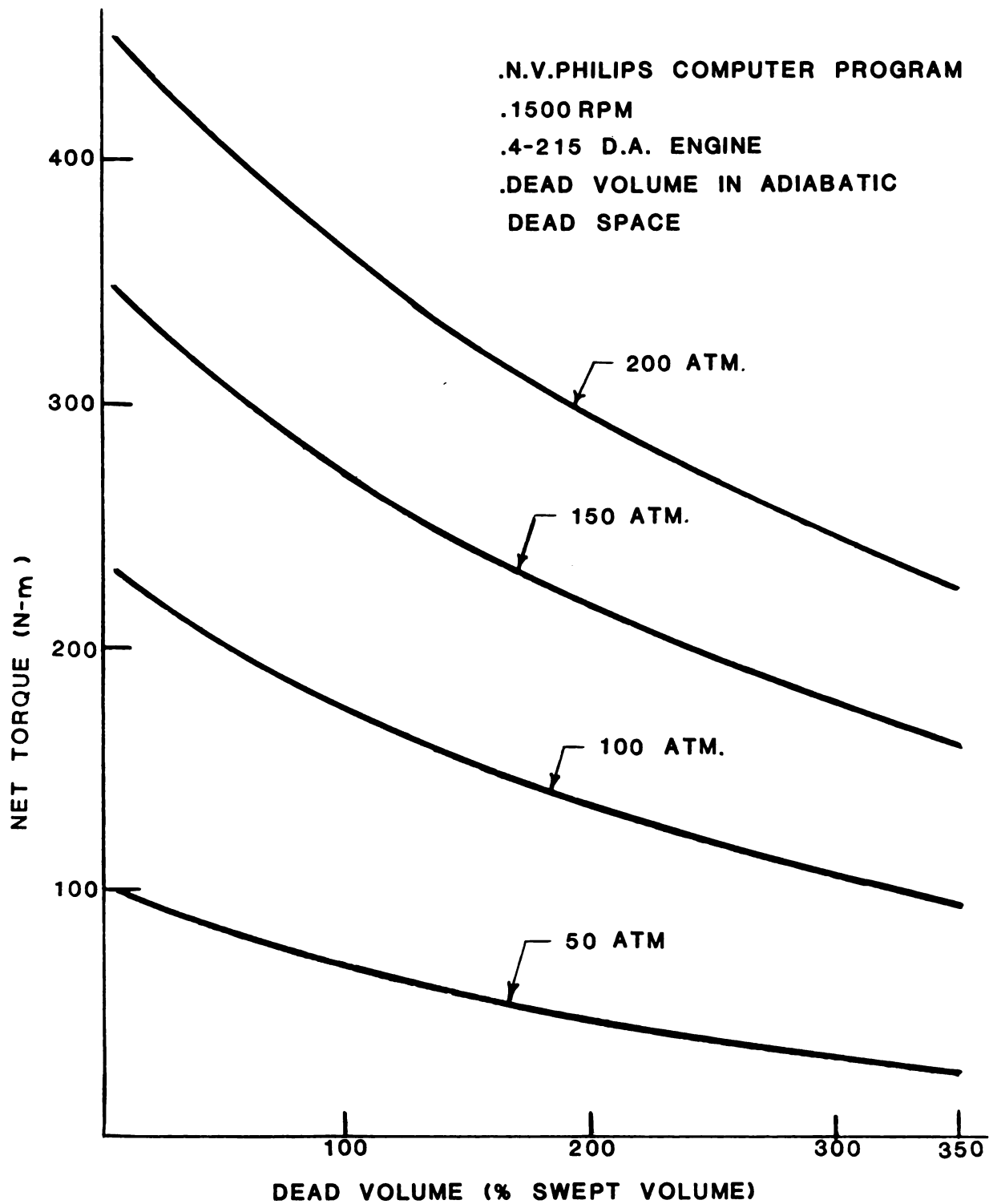
Figure 2.6-4   Net Torque vs. Dead Volume at Constant Mean Pressure

Figure 2.6-5   Pressure – Volume Diagrams at Various Amounts of Control Dead Volume

.4-215 D.A. ENGINE
.COMPUTER PROJECTION
V.A. U.S.S. SIMULATION ROUTINE

$X_c = \dfrac{\text{DEAD VOLUME}}{\text{EXP. SWEPT VOLUME}}$

.1500 ENGINE RPM

$X_c = .36$

$X_c = 3.4$

TOTAL VOLUME (cm³)

TOTAL VOLUME PRESSURE (BARS)

300   250   200   150   100   50

400   500   600   700   800   900   1000   1100   1200   1300   1400   1500

196
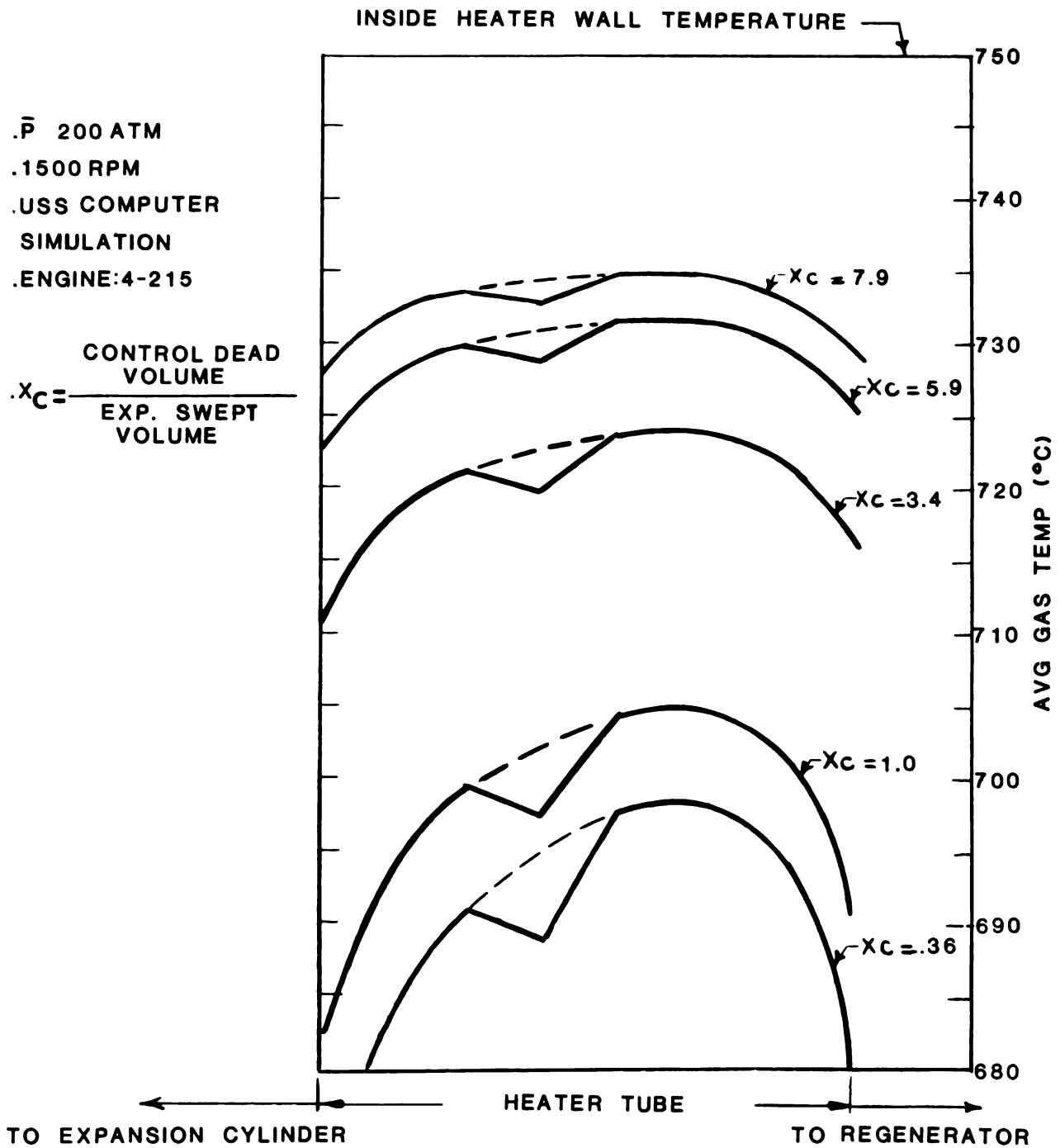
Figure 2.6-6   Average Gas Temperature Profile Along Heater Tube for Several Dead
Volume Ratios
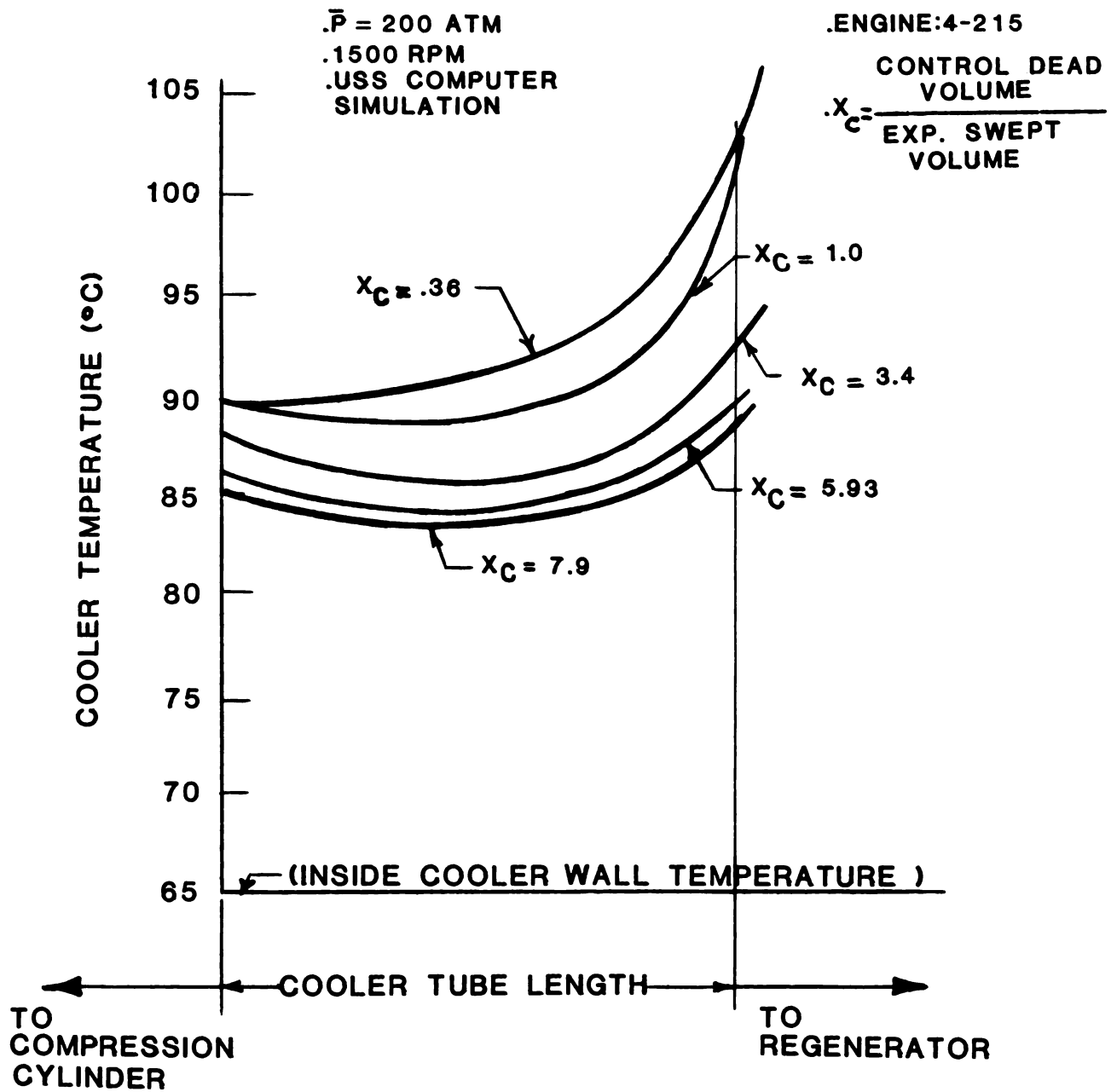
Figure 2.6-7   Cooler Temperature Profile Along Cooler Tube for Several Dead Volume
Ratios
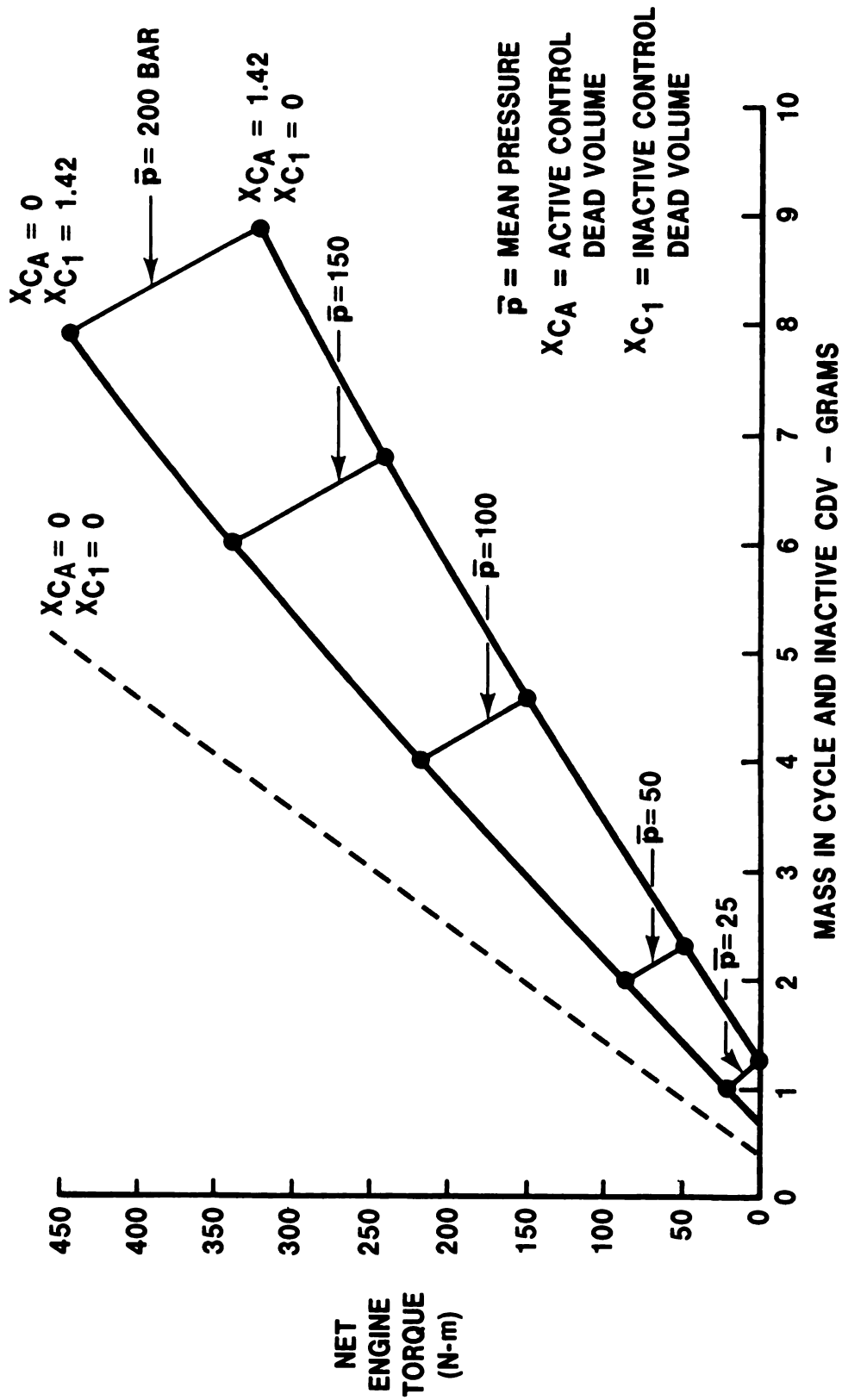
Figure 2.6-8   Higher Power Control Torque vs. Gas Charge – 4-215 Engine with Sealed Pistons
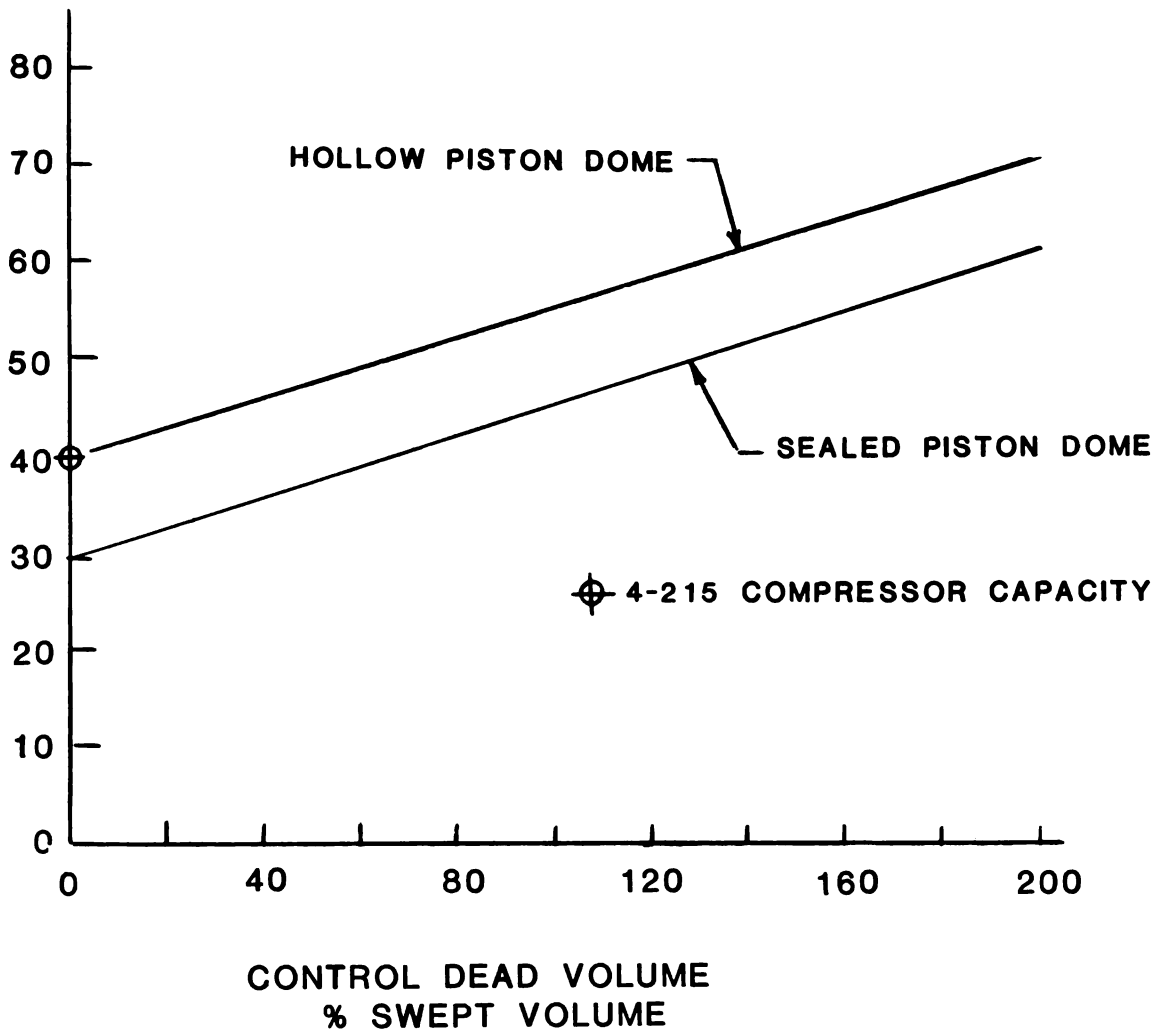
Figure 2.6-9   Compressor Capacity vs. Control Dead Volume

TORQUE VS. EQUIVALENT VALVE AREA

- SWEPT VOLUME = 217 CM³
- CONTROL DEAD VOLUME = 142% SWEPT VOLUME
- INITIAL MEAN PRESSURE = 19620 KPA
- REFERENCE: FORD COMPUTER PROGRAM "FCDVAREA"

600 RPM

2400 RPM

INDICATED TORQUE PER CYCLE (N—m)

EQUIVALENT VALVE AREA (MM²)
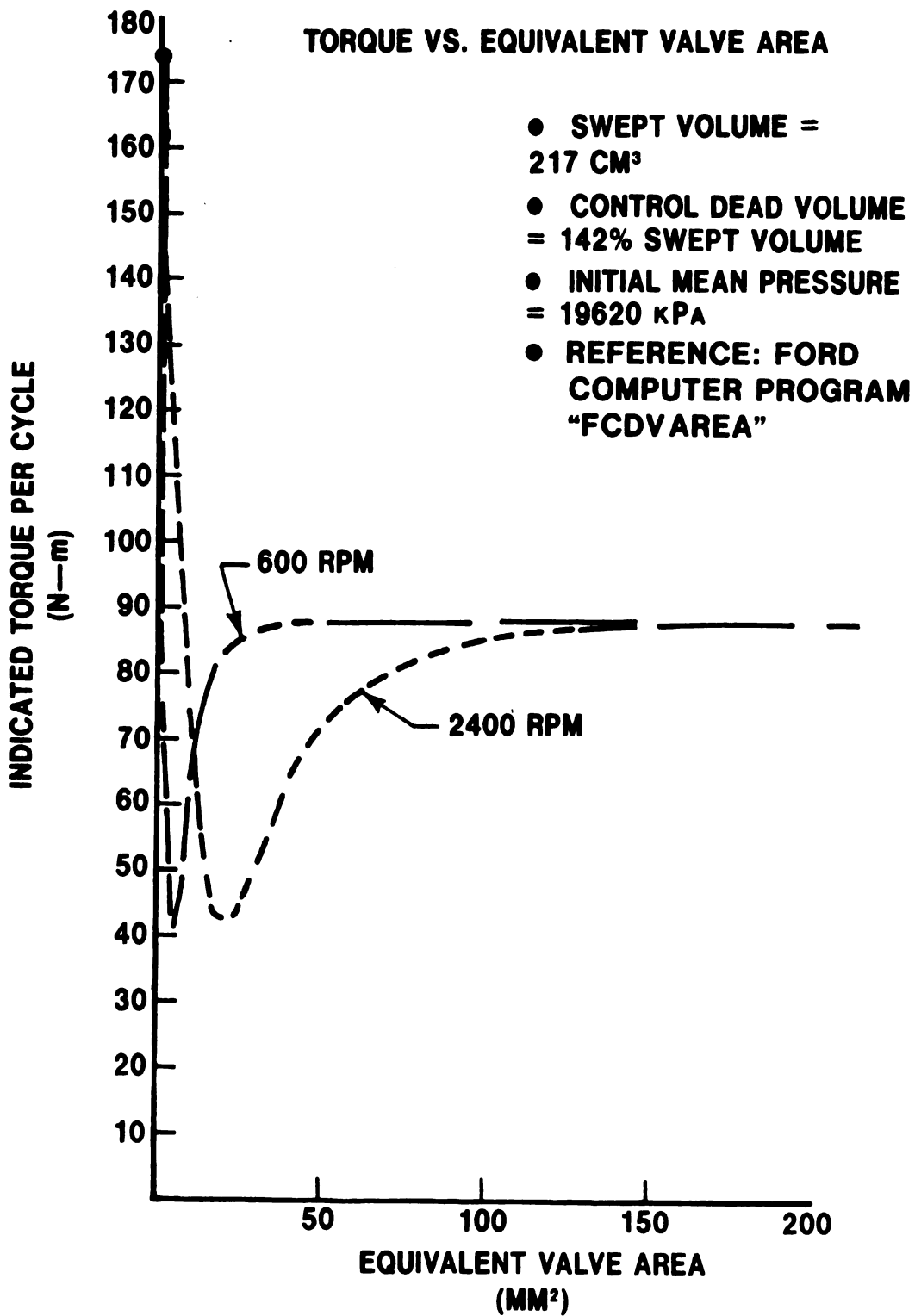
Figure 2.6-10   Dead Volume Mean Pressure Hybrid Power Control
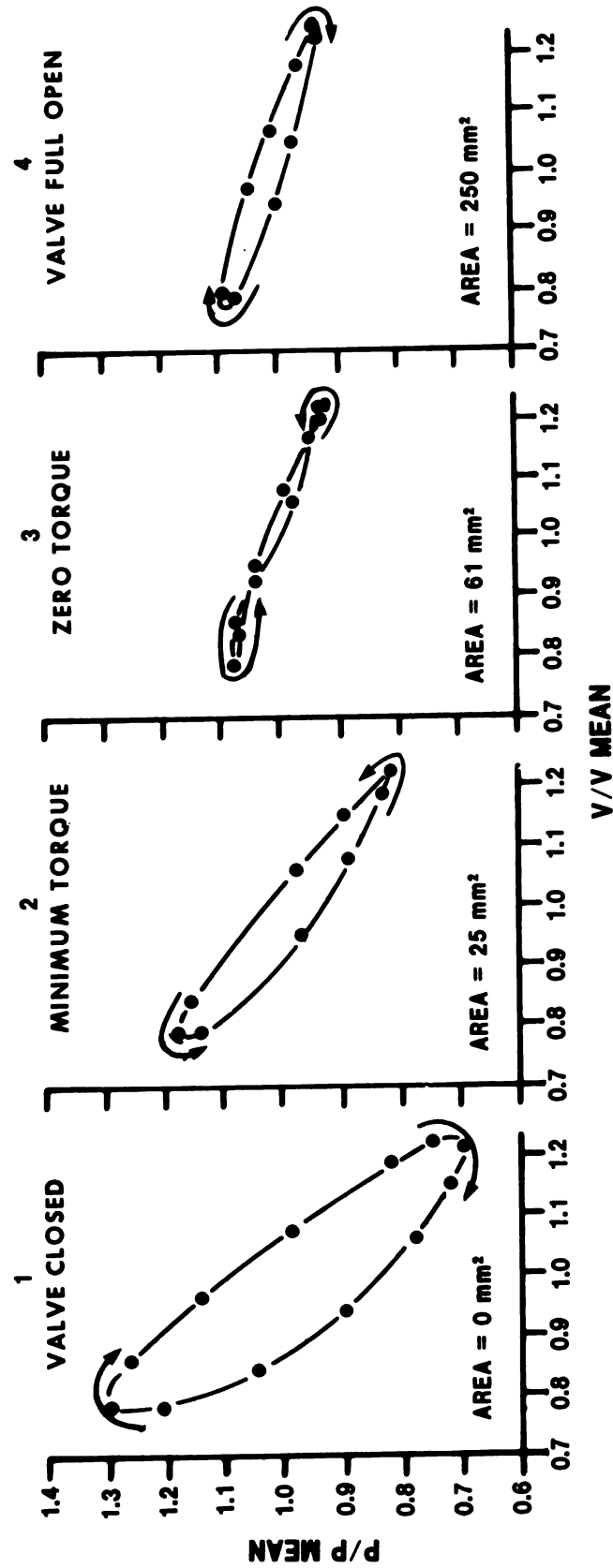
Figure 2.6-11 Pressure Volume Plots at Various Equivalent Flow Areas
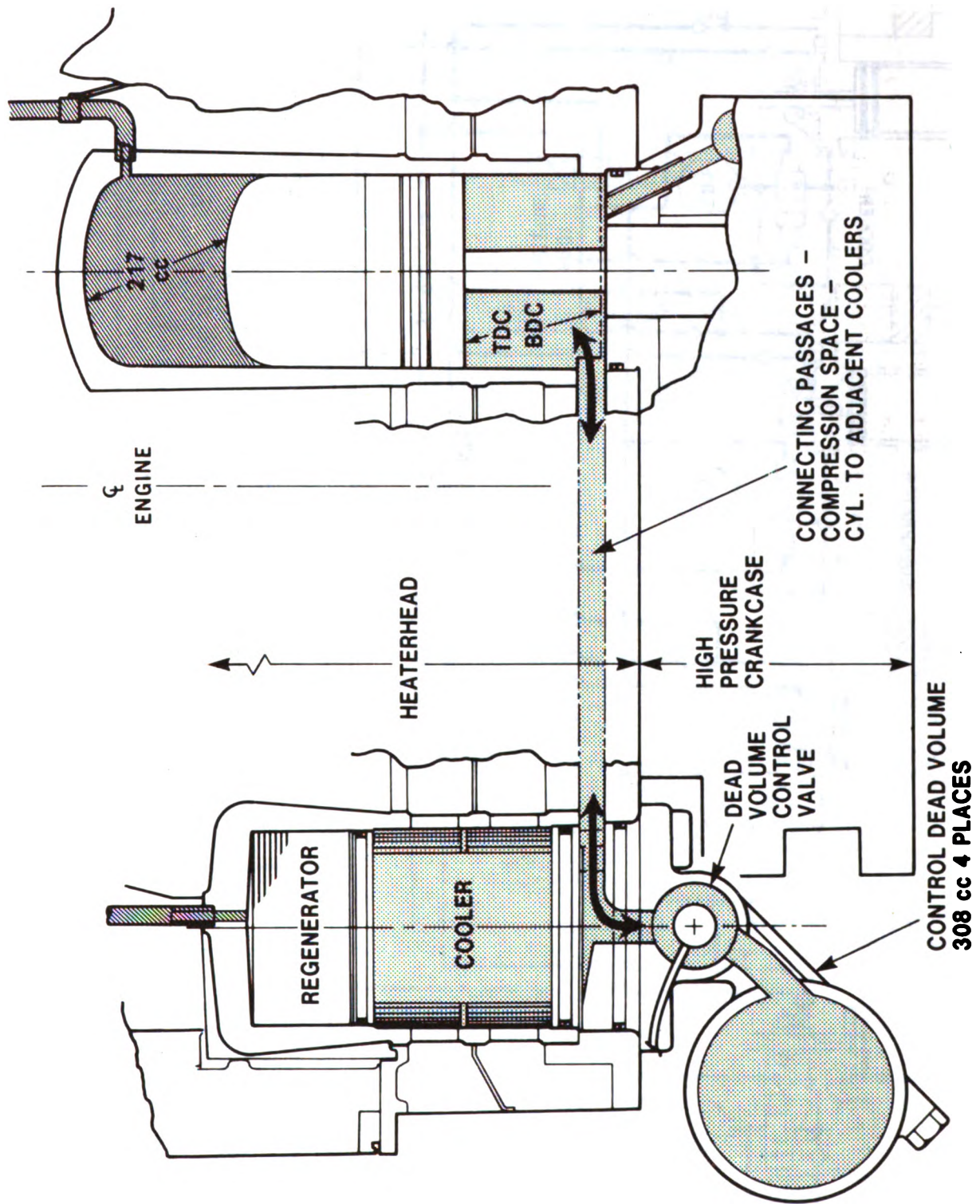
Figure 2.6-12   Control Dead Volume for Hybrid Power Control
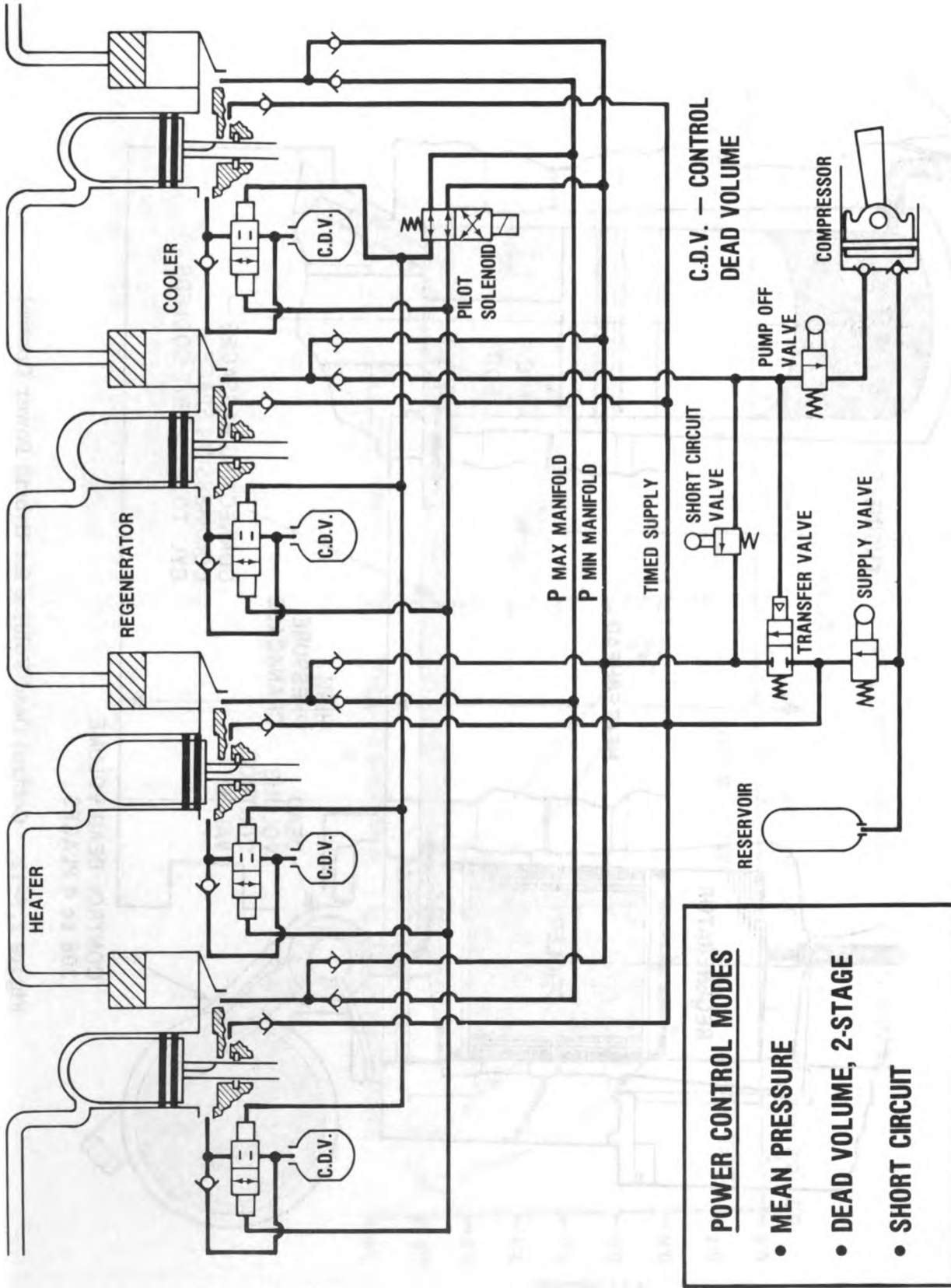
Figure 2.6-13   Proposed Hybrid Power Control

4-215 ENGINE LINEAR POWER CONTROL

SPOOL IS POSITIONED IN NEUTRAL
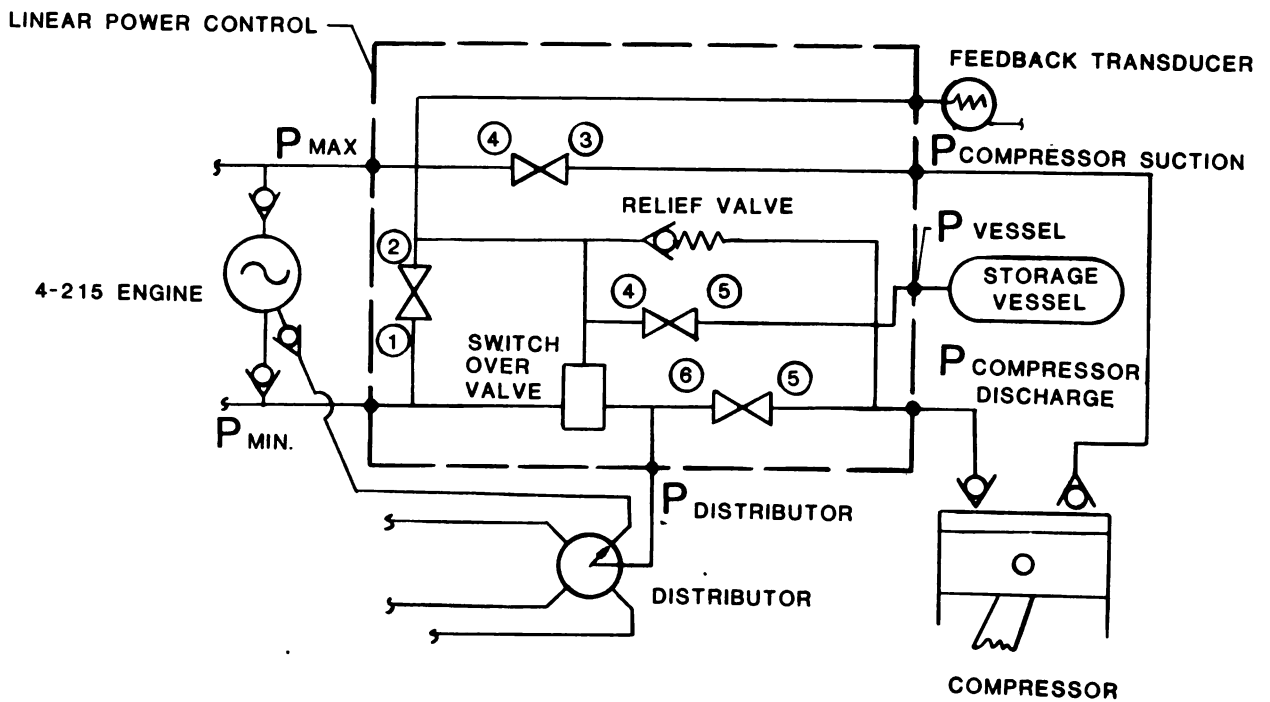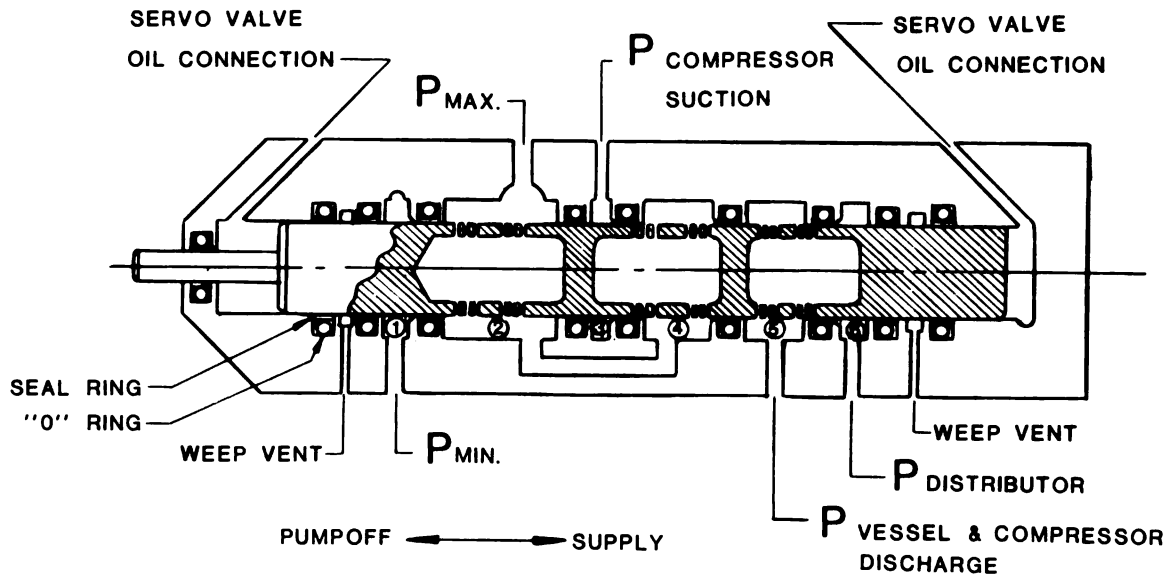
Figure 2.6-14   System Schematic
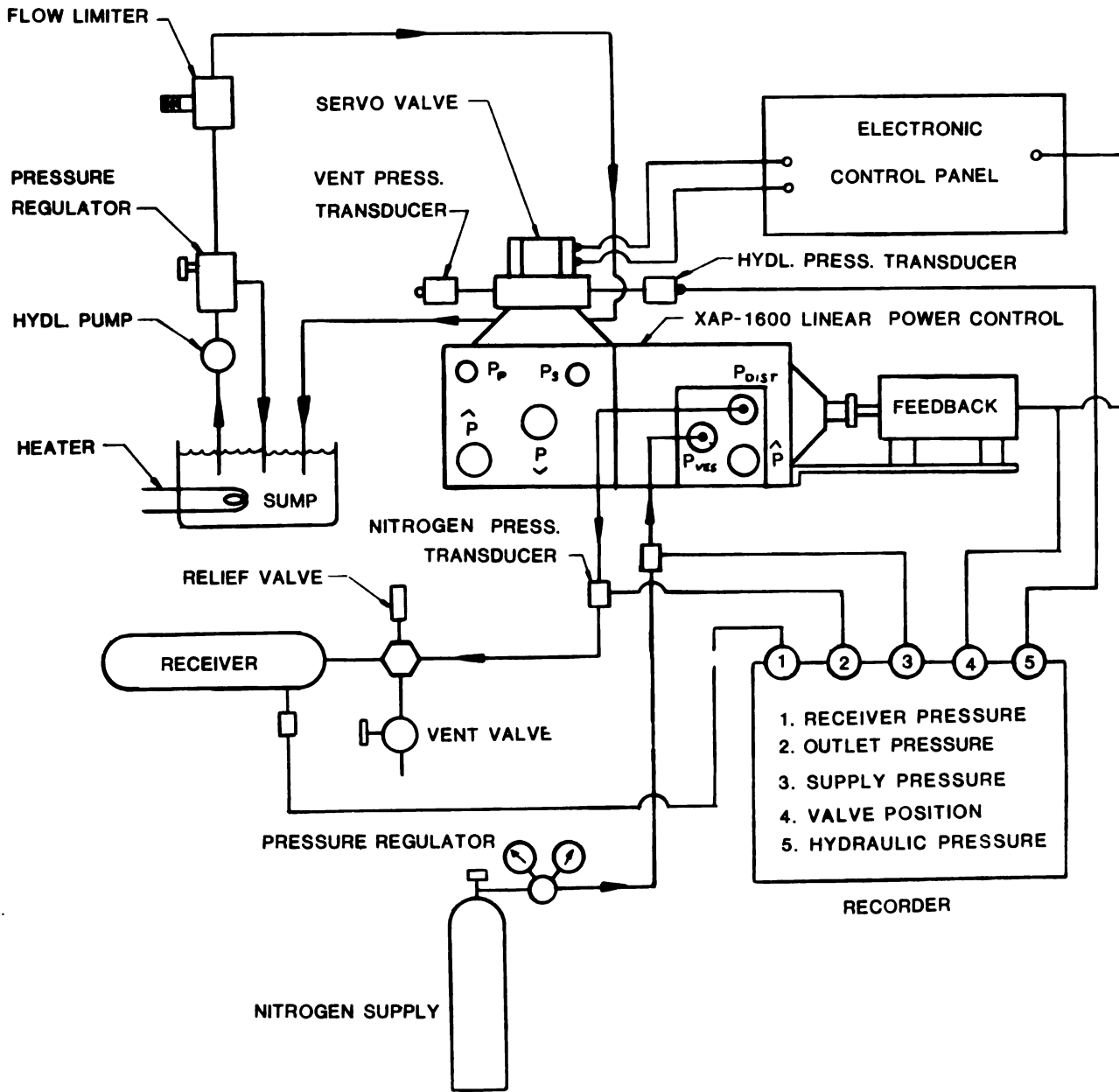
Figure 2.6-15   Linear Power Control Valve Test

SAMPLE RECORDER CHART SHOWING
SIGNAL INPUT ,POSITION &
HYDRAULIC PRESSURE VS. TIME
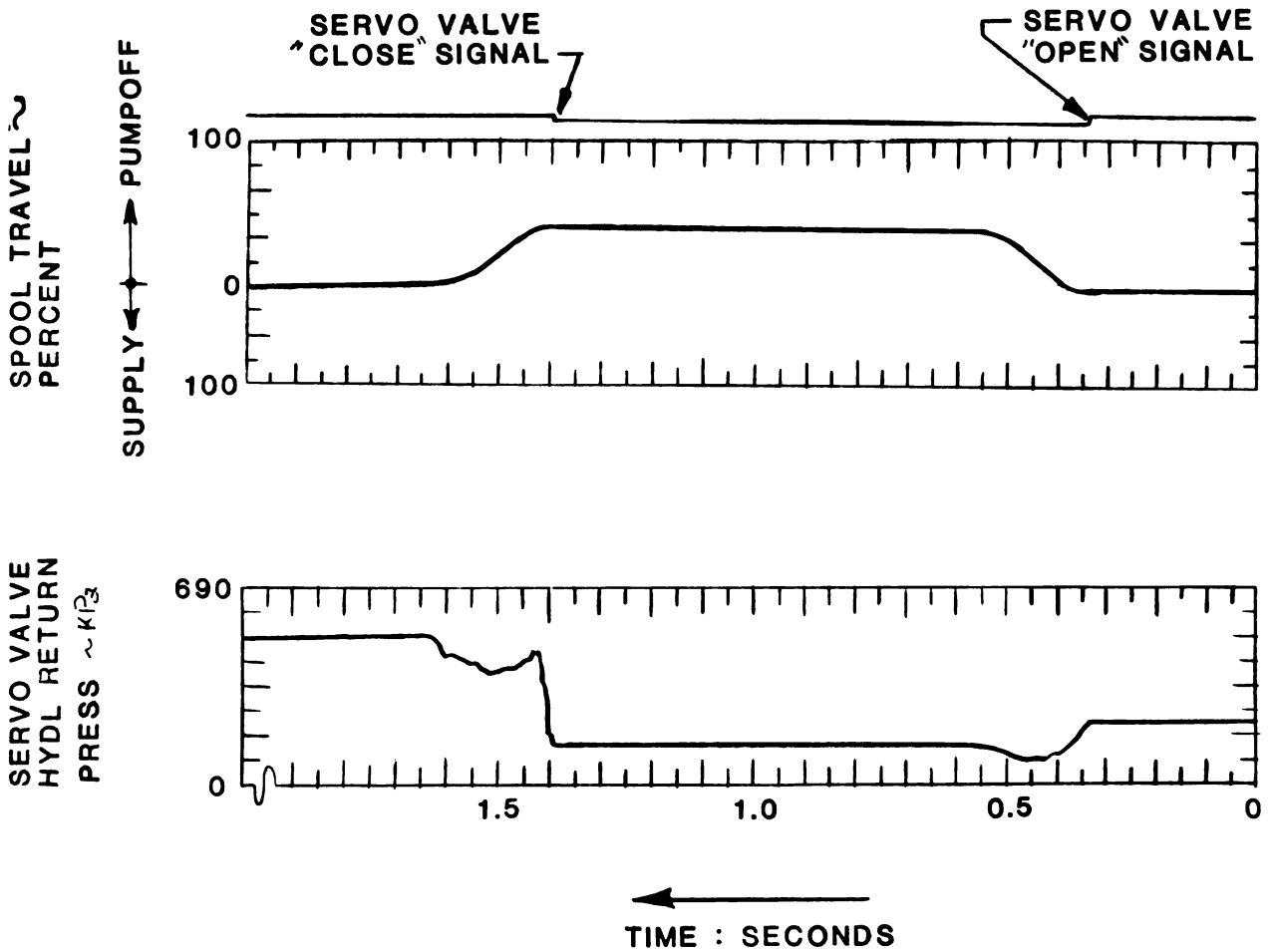
Figure 2.6-16   4-215 Linear Power Control Performance
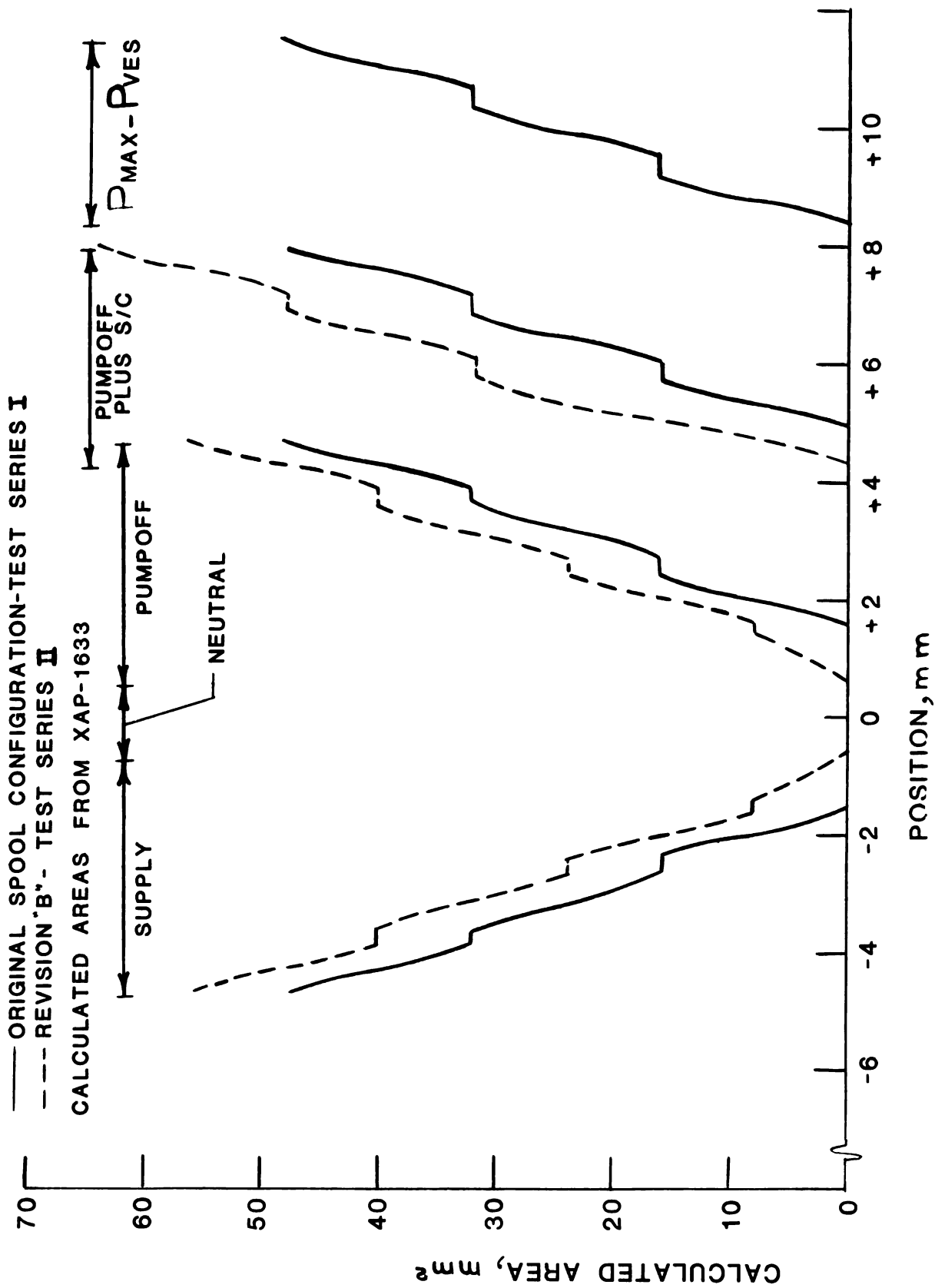
Figure 2.6-17   4-215 Linear Power Control Spool Position vs. Gas Flow Area

208
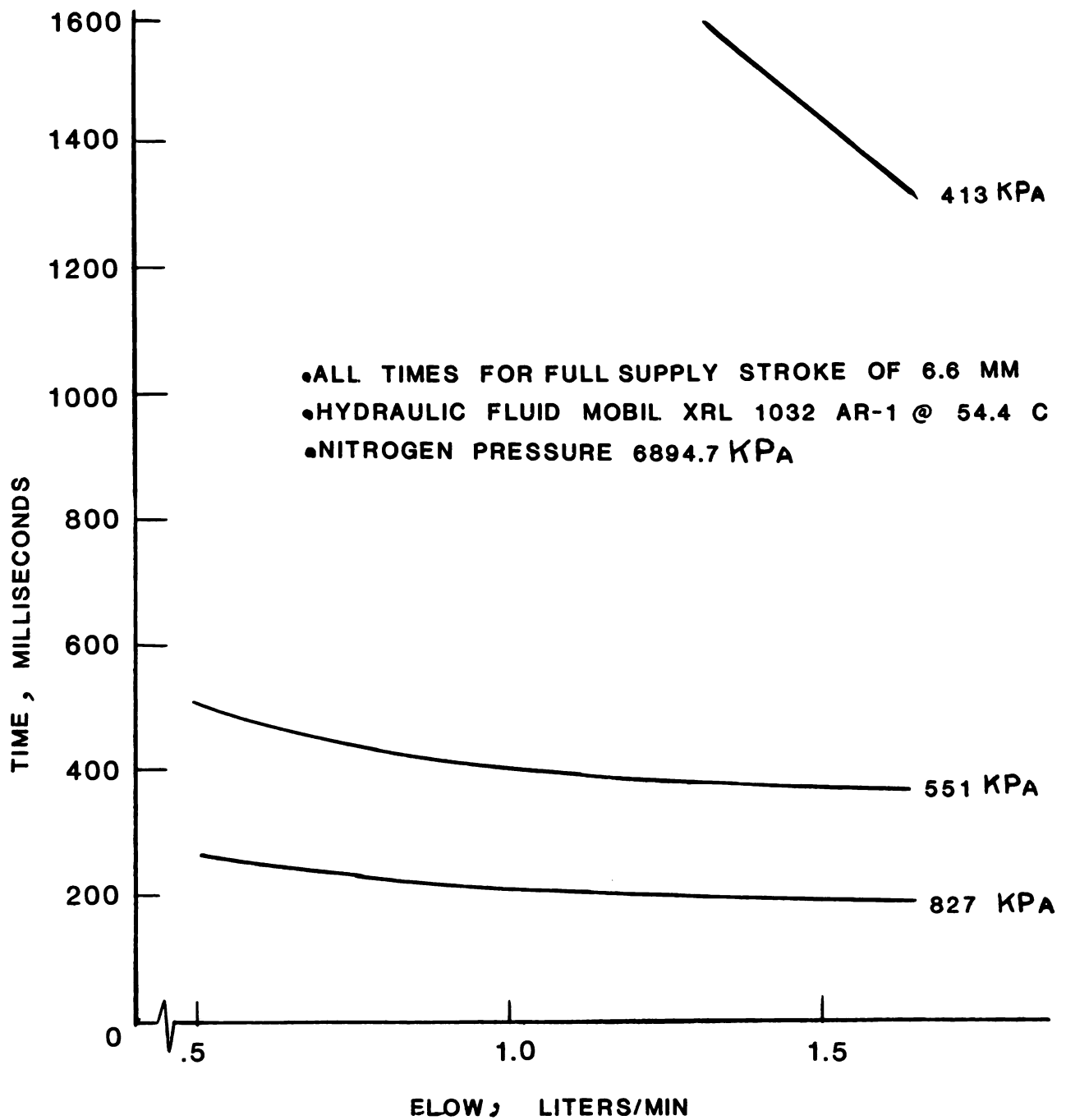
Figure 2.6-18   4-215 Linear Power Control Supply Actuation Time vs. Hydraulic
Flow – Test Series II

209
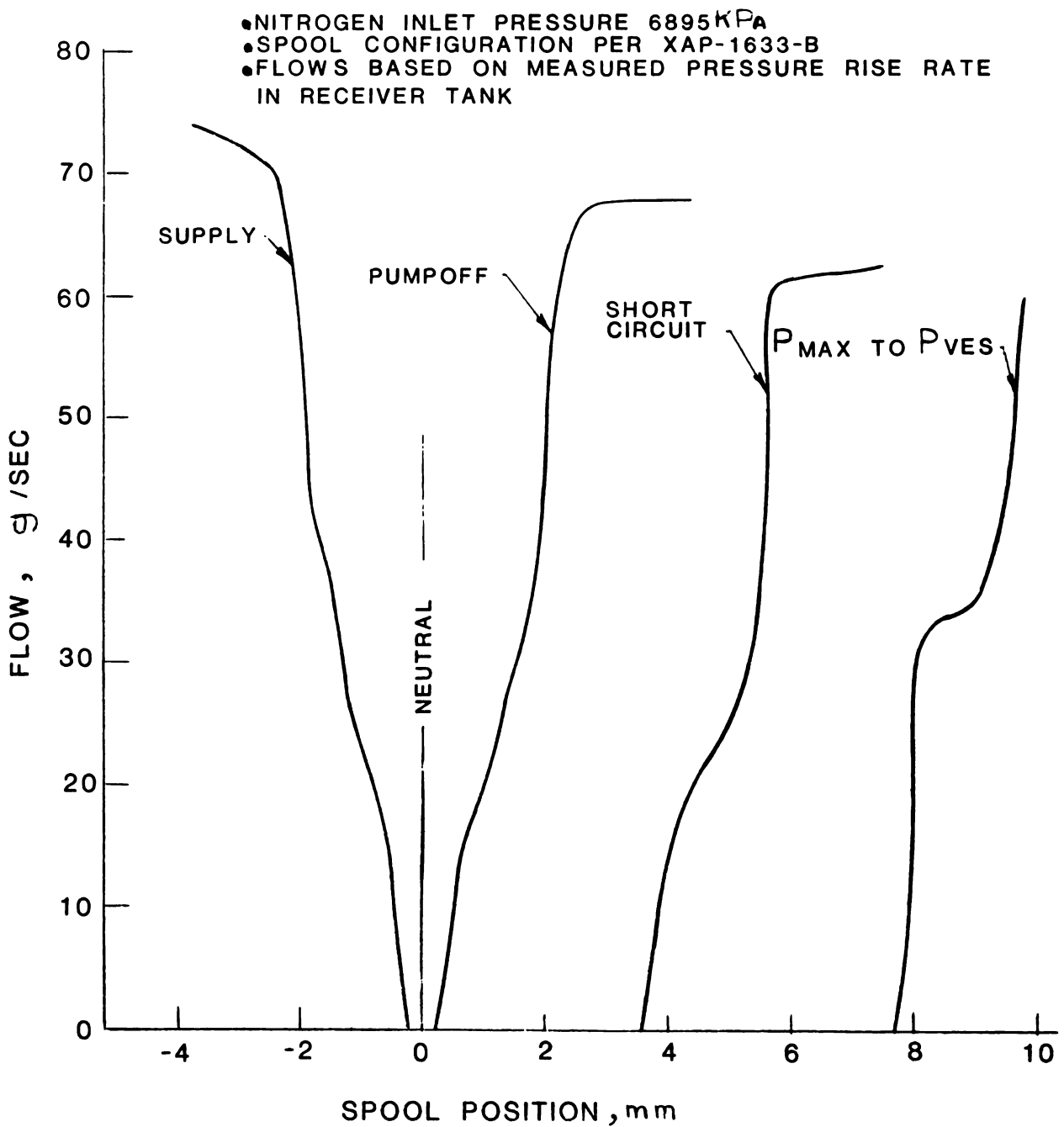
Figure 2.6-19   4-215 Linear Power Control Spool Position vs.
Gas Flow – Test Series II

●4-215 LINEAR POWER CONTROL XAP-1600
●HYDL FLUID   -XRL 1032 AR-1 @ 54.4° C
              -PRESSURE 827 kPa (120 PSI)
              -FLOW .49 l/min
●NITROGEN PRESSURE   6895 kPa (1000 PSI)
●MOOG SERVO 30/1.5/0500 /I /0200 /4CA/R/VIT
●BOURNS MODEL 157 POSITION TRANSDUCER WITH
 DEVELOPED VEHICLE ELECTRONIC CIRCUITRY
●TIME FROM NEUTRAL IN SUPPLY DIRECTION

$\frac{L}{L_o}$ = RATIO OF ACHIEVED TO PROGRAMMED STROKE

$\frac{L}{L_o}$ = .9

$\frac{L}{L_o}$ = .5

TIME, MILLISECONDS

PROGRAMMED SPOOL STROKE ,mm
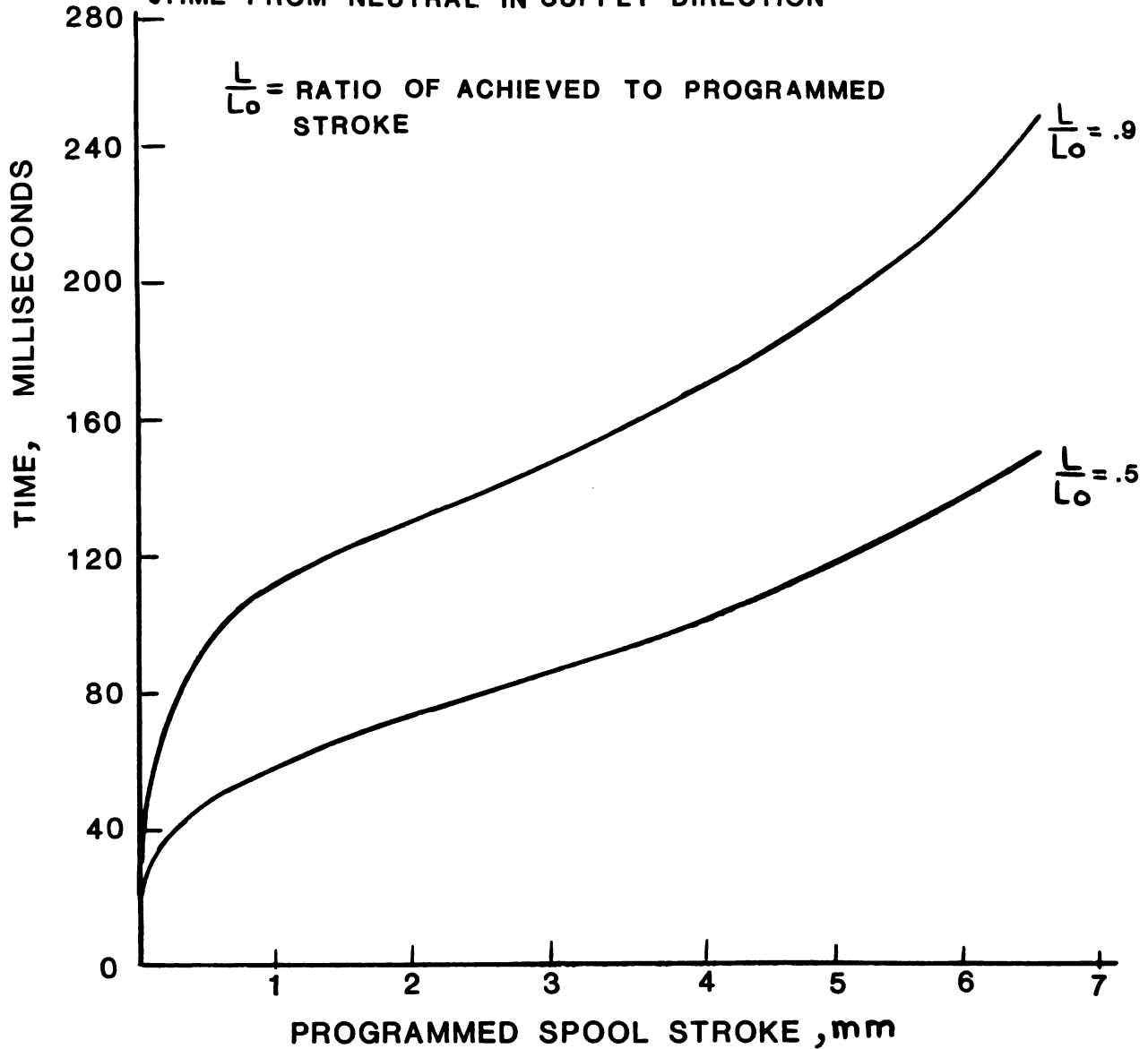
Figure 2.6-20   Programmed Spool Supply Stroke vs. Time – Test Series II
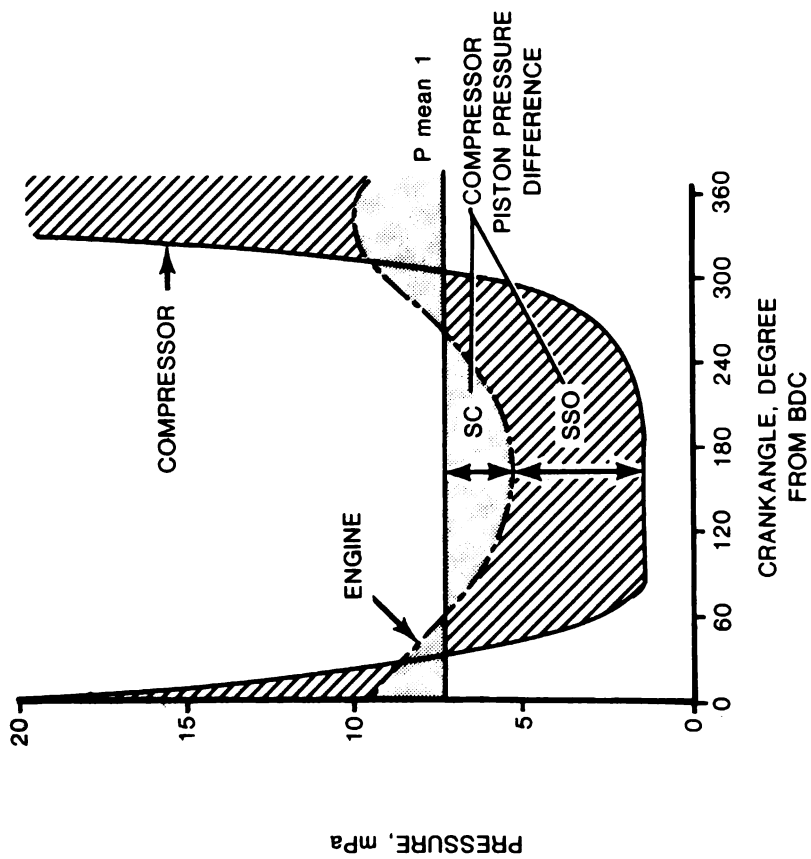
(A) COMPRESSOR PISTON PRESSURES, ENGINE PRESSURES FOR Pmean = 7.5 mPa
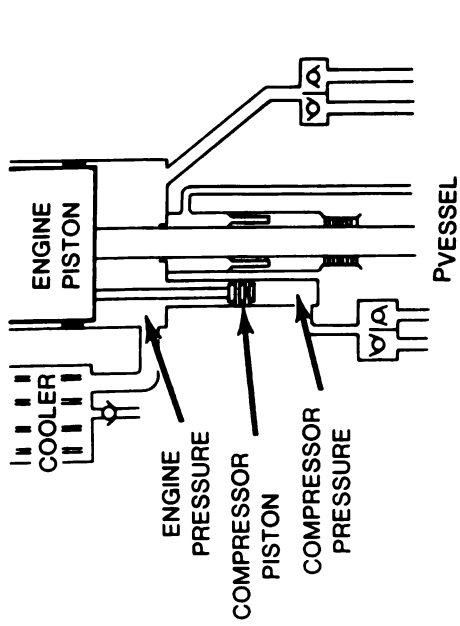
(B) SUCTION SHUT OFF (SSO) NORMAL 4-2N METHOD
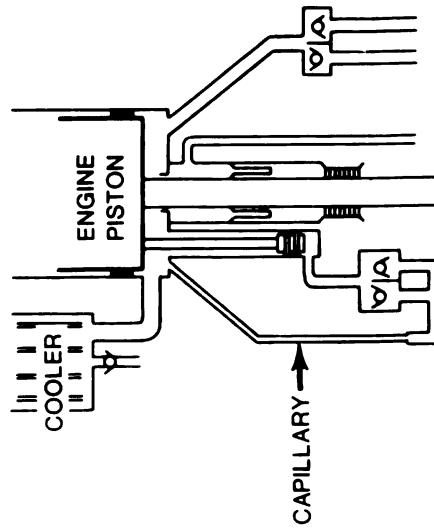
(C) SHORT CIRCUITED, (S-C)

Figure 2.6-21   Internal Compressor, Compressor Piston Pressures and Unloading Methods

SUCTION

DISCHARGE

OPTIONAL
CONSTRUCTION
SUCTION CHECK VALVES

SUCTION

SLIDING SEAL

WATER COOL

DISCHARGE

CROSS HEAD

ACCESSORY
DRIVE SHAFT

STROKE: 12.7mm (.50")
BORE DIA: 42.2 mm (1.66")

PISTON RING SUCTION VALVE
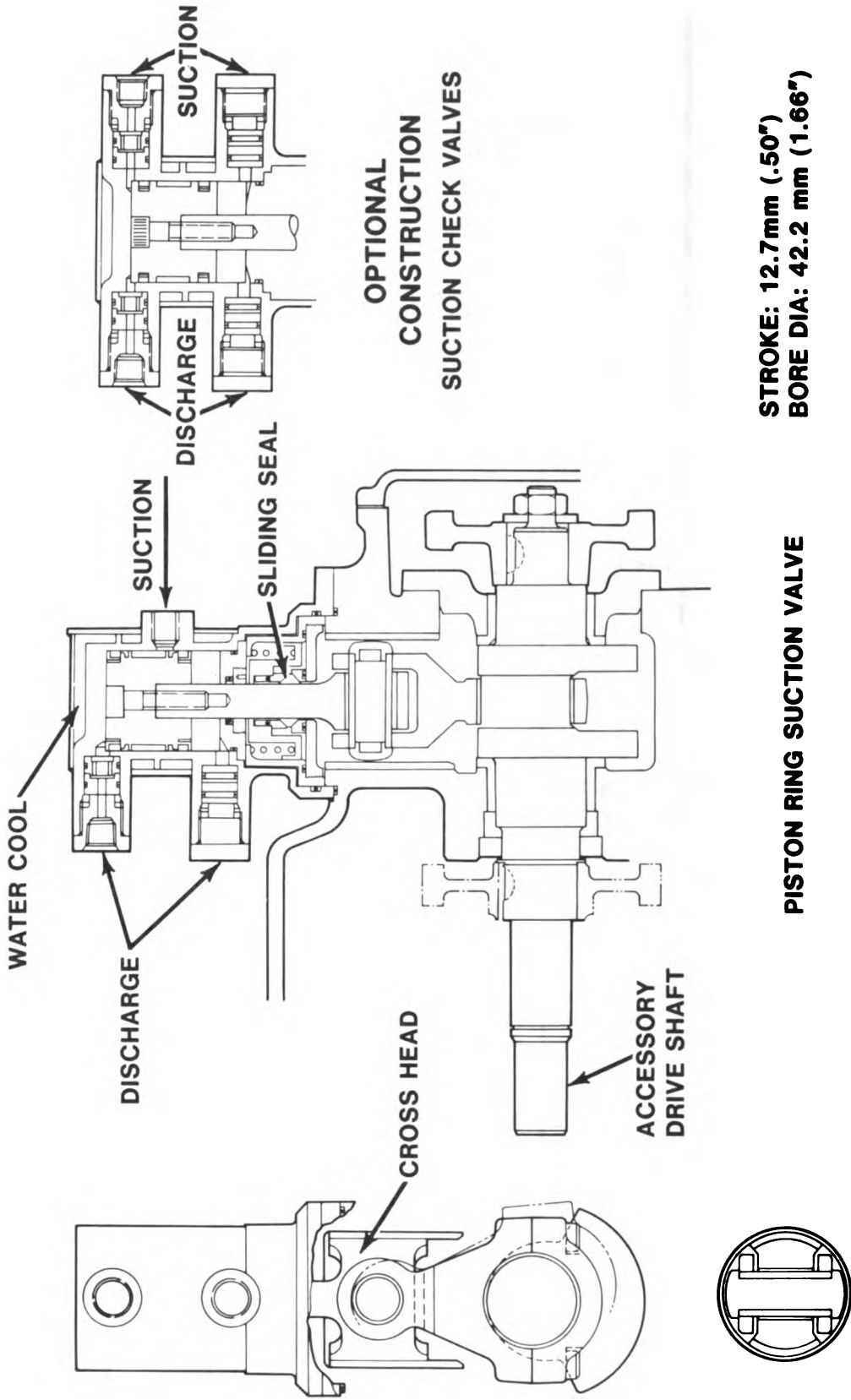
Figure 2.6-22   External Compressor

PISTON RING
FRICTION

CAP SEAL
FRICTION

OIL SCRAPER
FRICTION

SLIDING SEAL
FRICTION

WRIST PIN BEARING
FRICTION

CROSSHEAD
FRICTION

CRANK PIN
BEARING FRICTION

MAIN BEARING
FRICTION (2)
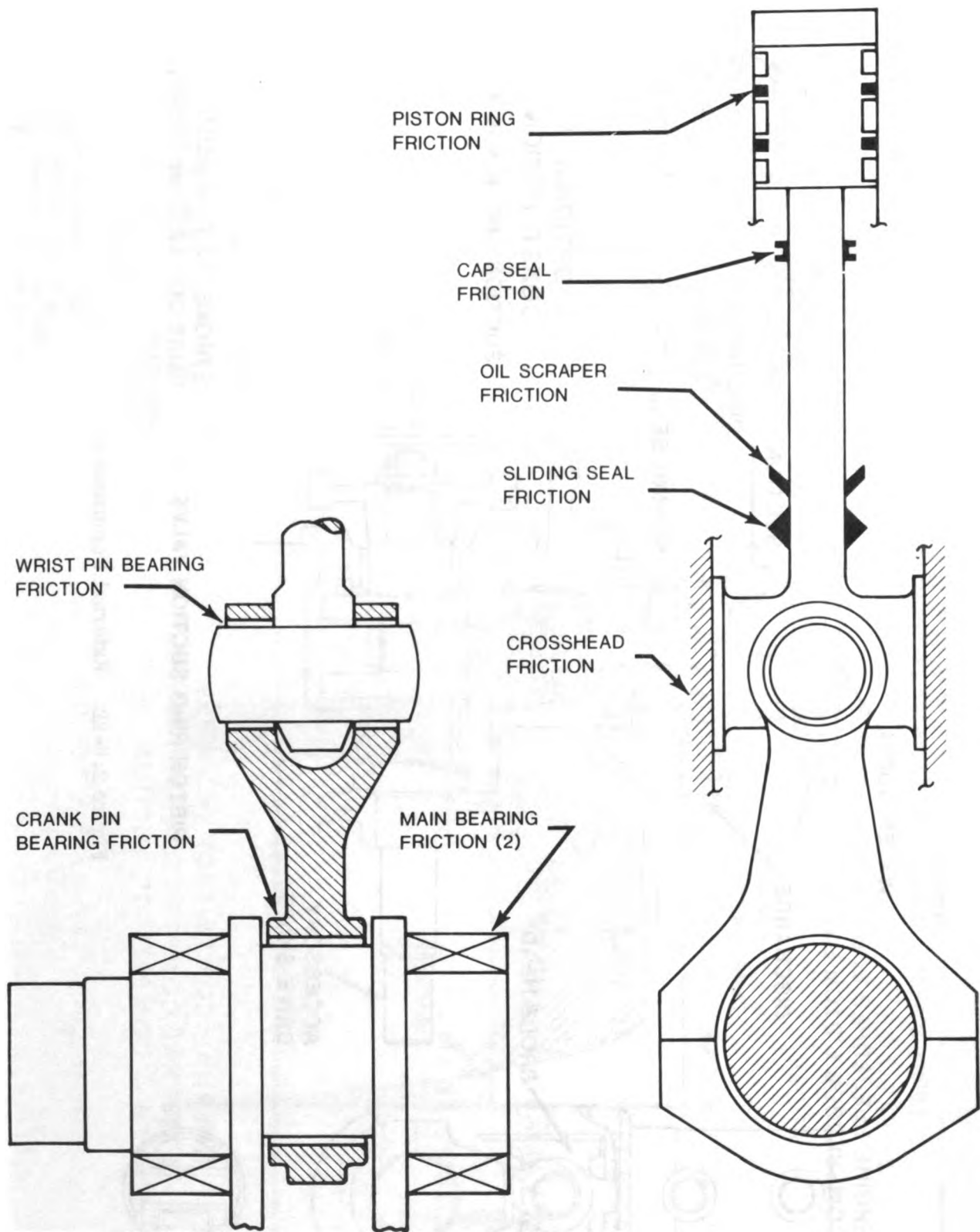
Figure 2.6-23   Compressor Friction Components

Figure 2.6-24   Fuel Economy Effects of Power Control Compressors and Compressor
Operating Conditions (Computer Simulations)
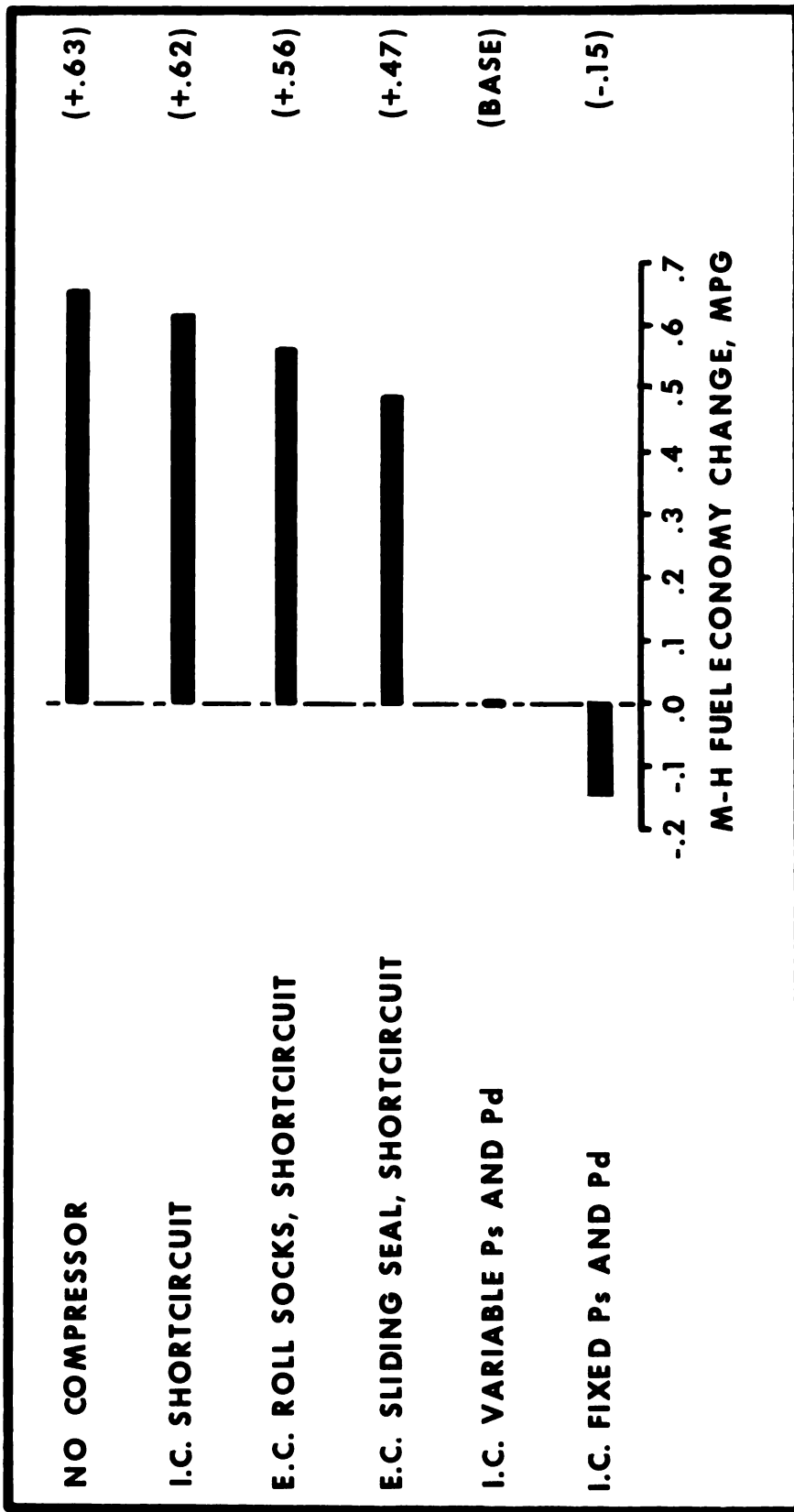
I.C. — INTERNAL COMPRESSOR (40cc/REV)
E.C. — EXTERNAL COMPRESSOR (53cc/REV)
Ps AND Pd — COMPRESSOR SUCTION AND DISCHARGE PRESSURES

POWER CONSUMPTION
SHORT CIRCUITED COMPRESSOR
COMPRESSOR TEST RIG XAP-1776-AA
HYDROGEN GAS, 1500 RPM

RESTRICTION
AS SHOWN IN(C) +
4-215 CHECK VALVES

INTERNAL
FLOW LOSS

MECH. FRICTION ONLY

TORQUE INPUT ON (N-m)

PRESSURE (mPa)
(A)

● ALL DIMENSIONS IN mm

90°

8

2φ

6.5

17R

1

3

3

3 x 1

4-215 ENGINE
(B)

5

4

2φ

5

2φ

CHECK VALVE

PISTON BORE

30

2φ

2φ

PISTON BORE
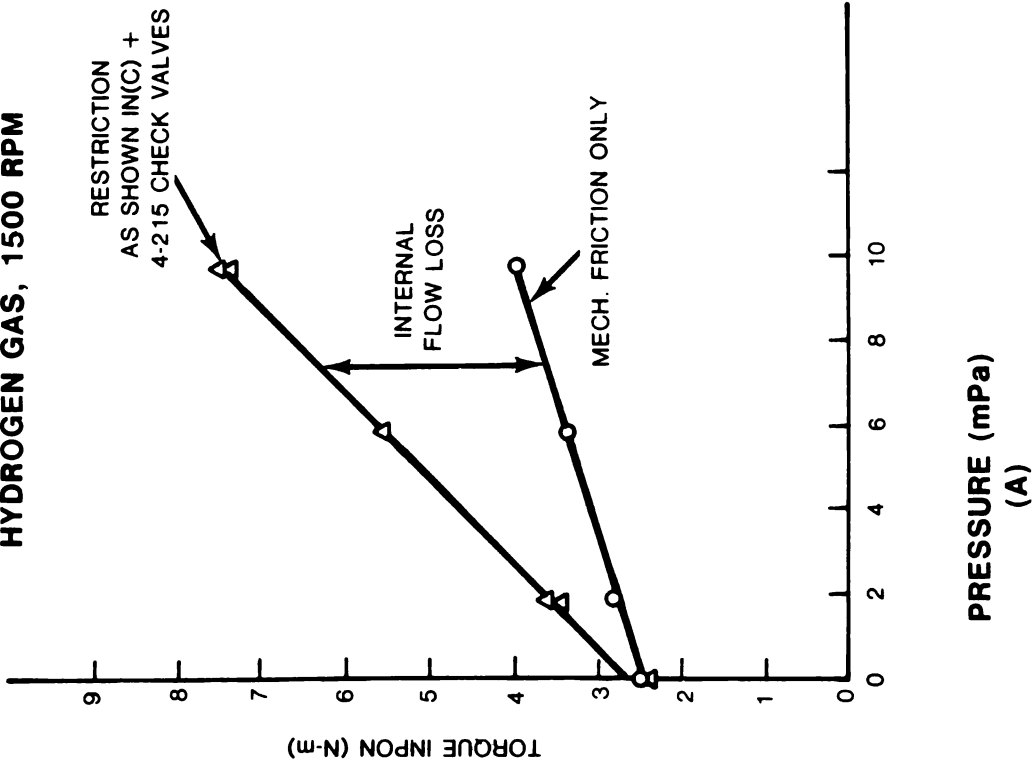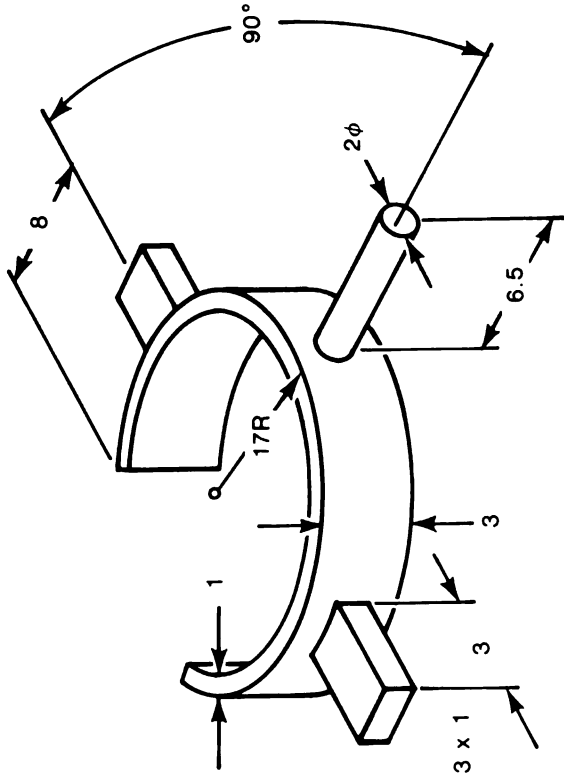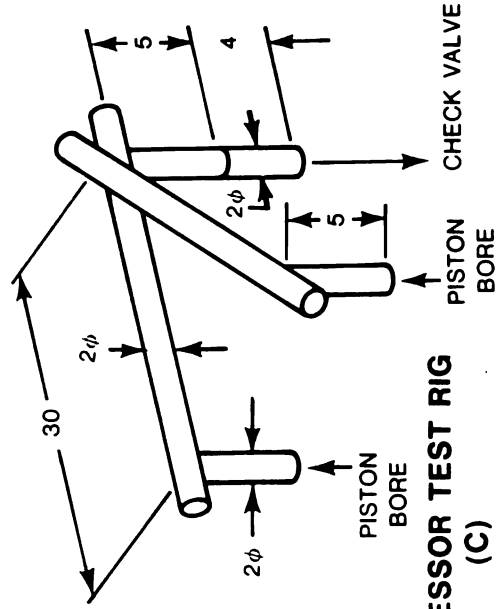
COMPRESSOR TEST RIG
(C)

Figure 2.6-25   Internal Compressor Passages
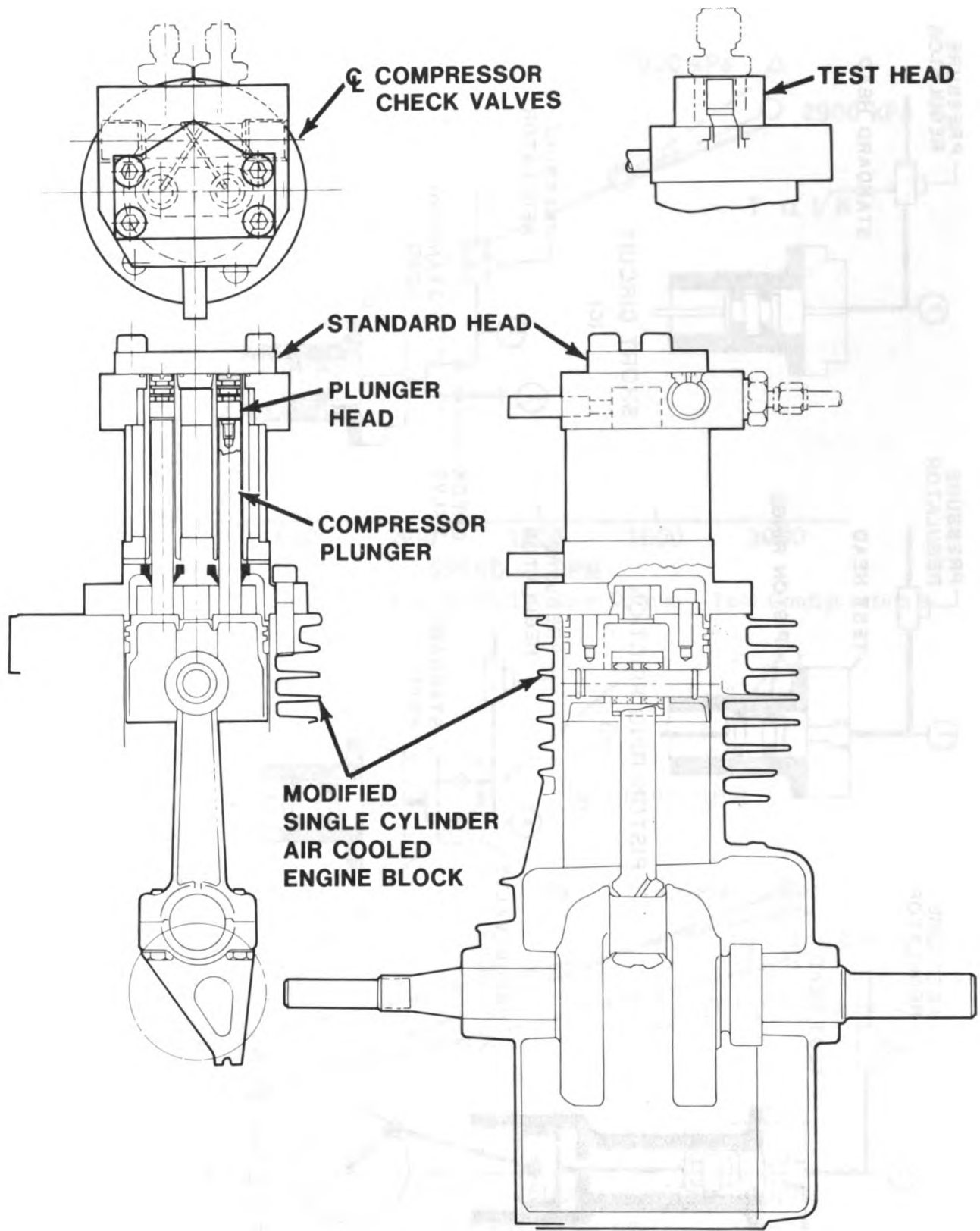
Figure 2.6-26   Compressor Plunger Seal Test Fixture
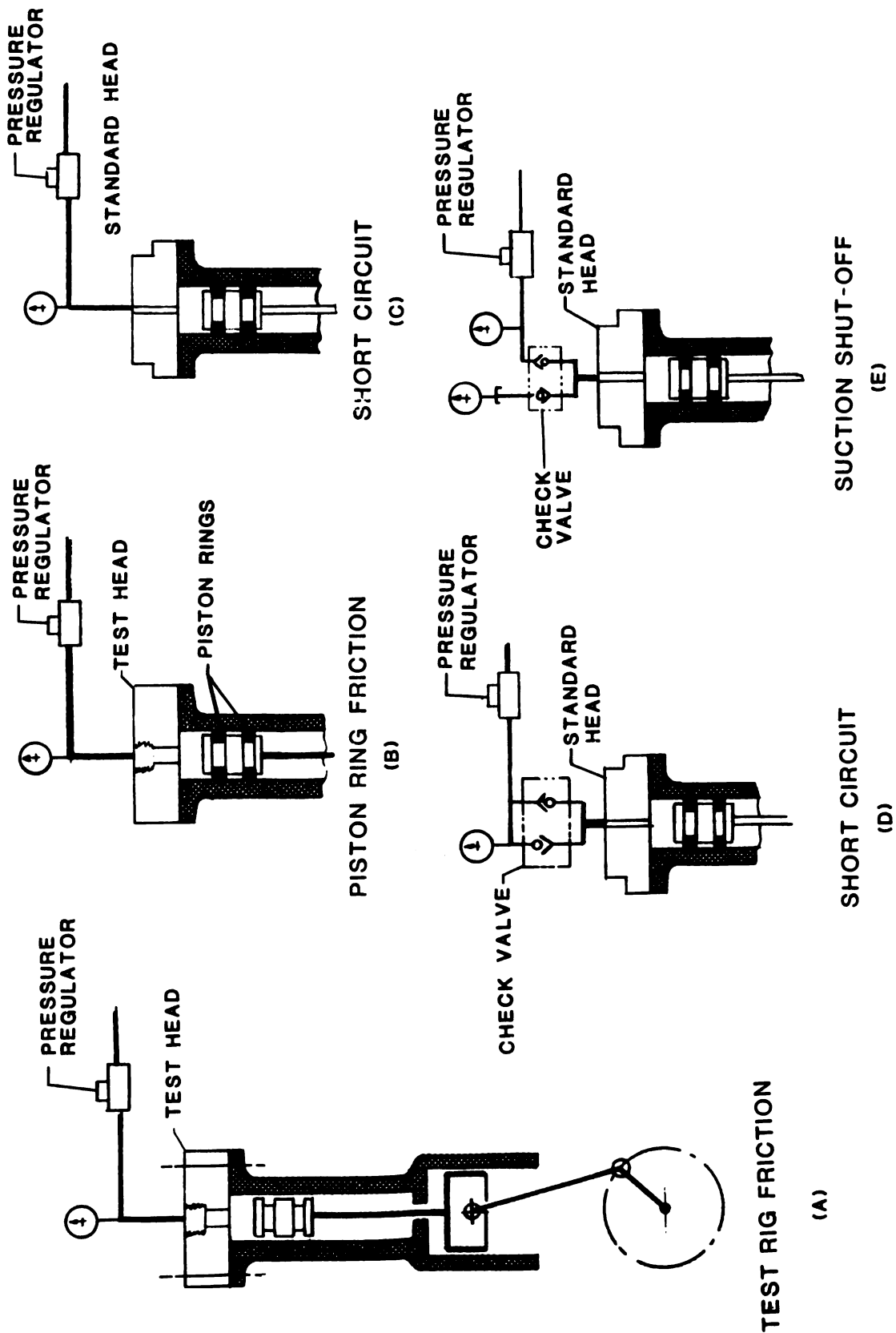
Figure 2.6-27 Compressor Test Configurations
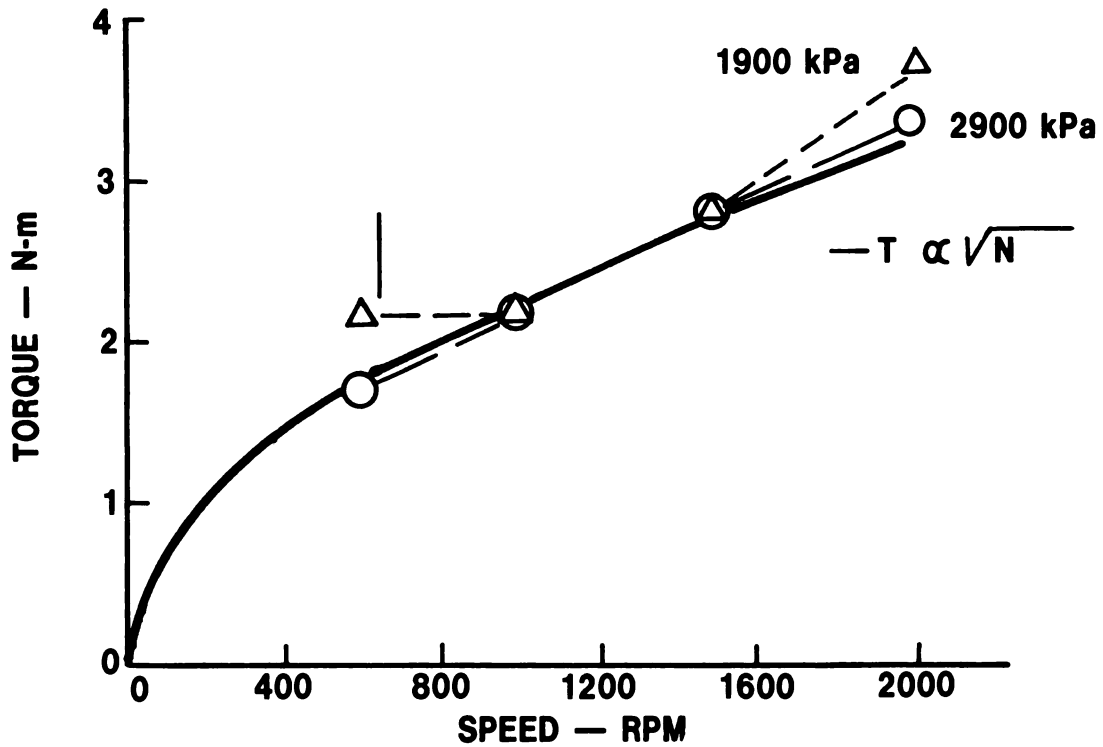
Figure 2.6-28   Compressor Test Rig Friction Torque – Test Configuration A
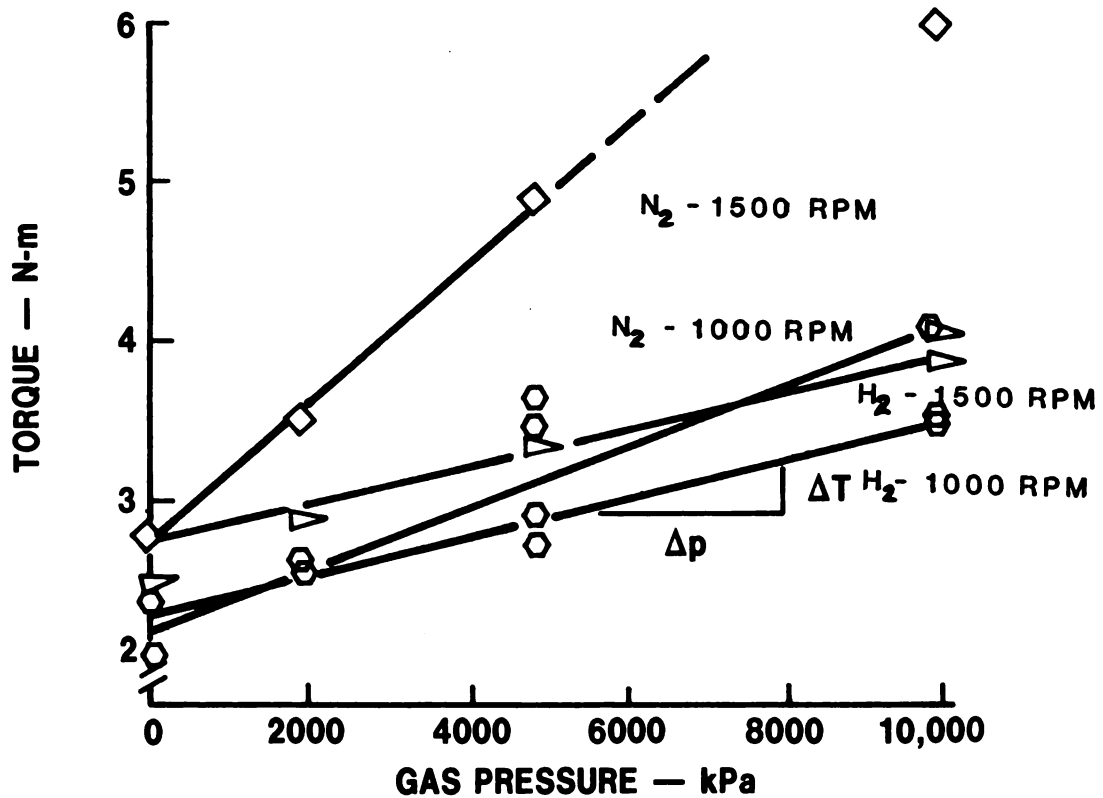
Figure 2.6-29   Piston Ring Friction – Test Configuration B

TOTAL GAS VOLUME — 1900cc
GAS TEMPERATURE — 20°C
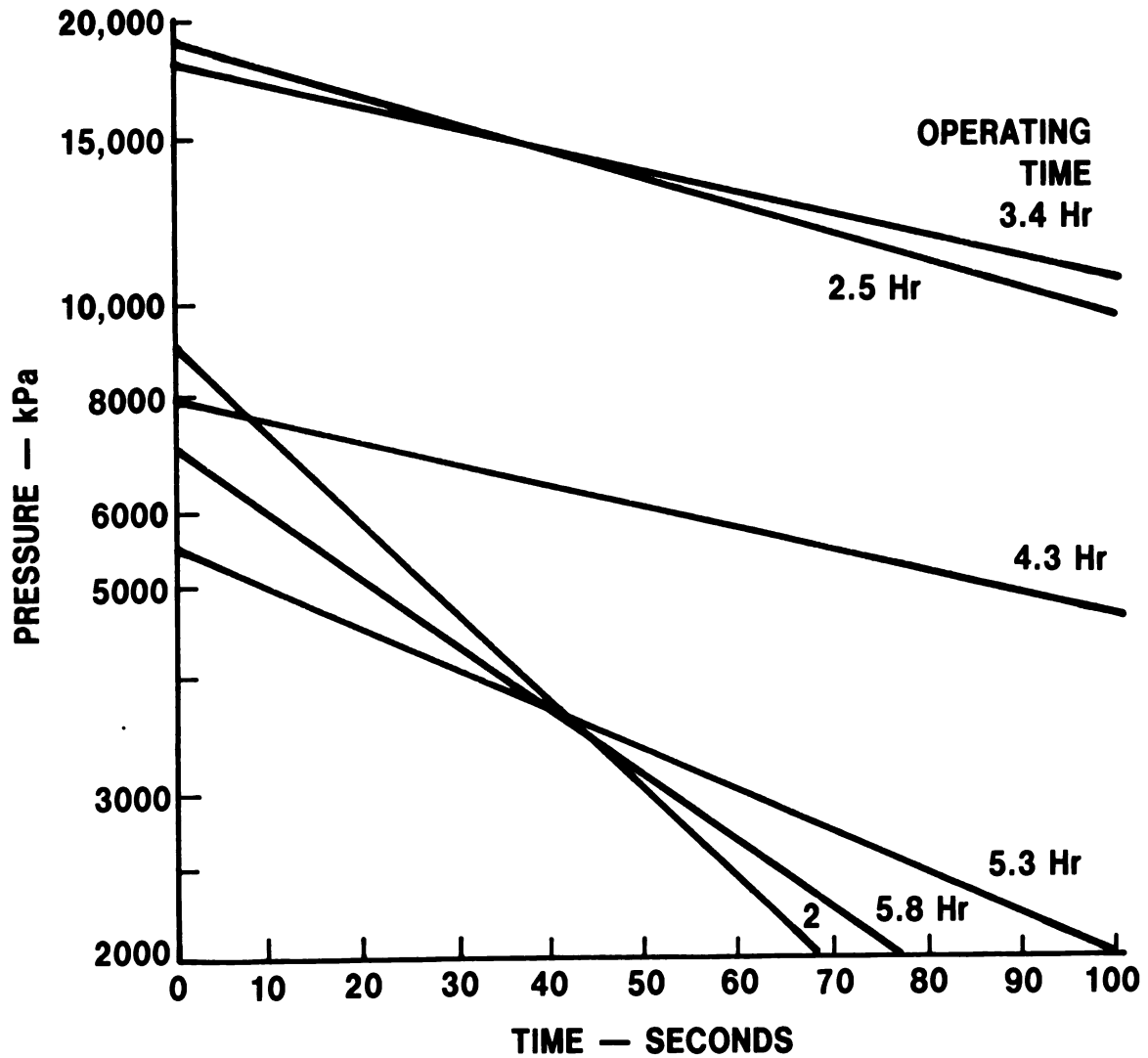
Figure 2.6-30   Pressure Decay Rate Compressor Test Rig Piston Ring Leakage Tests

COMPRESSOR SHORT CIRCUITED EXCEPT FOR SUCTION SHUT-OFF MODE

1500 RPM

COMPRESSOR
SUCTION
SHUT-OFF

VALVE LOSSES

INTERNAL FLOW LOSSES

PISTON RING FRICTION

TORQUE N-m

SUCTION PRESSURE — kPa

1000 RPM

COMPRESSOR
SUCTION
SHUT-OFF

VALVE LOSSES

INTERNAL FLOW LOSSES

PISTON RING FRICTION

TORQUE N-m

SUCTION PRESSURE — kPa
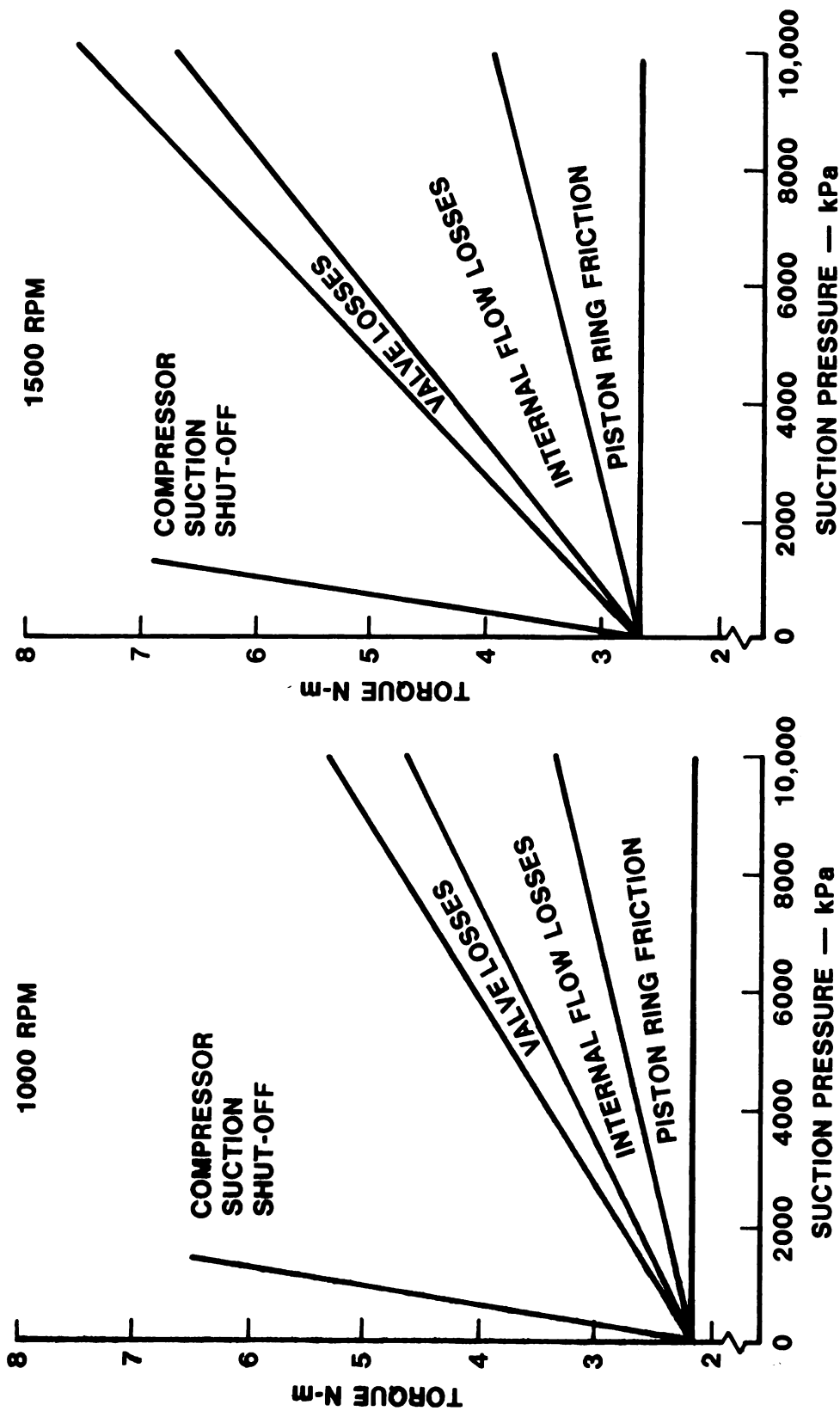
Figure 2.6-31   Compressor Torque Reqmts. for Suction Shut–Off and Short Circuiting,
Compressor Test Rig Hydrogen Gas

221

STIRLING ENGINE DYNAMOMETER EMISSION & FUEL ECONOMY

ENGINE BUILD---- 3X-17 ENGINE TEST---- 1

WITH INTERNAL HYDROGEN COMPRESSORS

RUN NO	TIME s	FUEL FL. g/s	FUEL TOT. g	A/F	HC ppm	HC EI g/kg	HC g	CO ppm	CO EI g/kg	CO g	NOX ppm	NOX EI g/kg	NOX g	TIME s	FUEL FL. g/s	FUEL TOT. g	EGR %
1	398. 362.	0.60	217.4	20.8	4.8	0.050	0.011	648.	13.686	2.975	47.	1.631	0.355	10.	0.60	6.2	93.
2	397. 272.	0.70	190.5	21.1	4.2	0.045	0.008	648.	13.875	2.643	40.	1.407	0.268	5.	0.70	3.6	105.
3	396. 74.	0.52	38.5	20.5	2.0	0.124	0.005	277.	5.770	0.222	35.	1.198	0.046	52.	0.52	27.0	126.
4	395. 167.	1.03	172.2	20.3	3.3	0.034	0.006	455.	9.390	1.617	29.	0.983	0.169	29.	1.03	30.0	130.
5	394. 188.	1.40	262.5	20.3	3.6	0.037	0.010	435.	8.977	2.356	38.	1.288	0.338	33.	1.40	45.9	112.
6	393. 147.	2.00	294.4	20.9	4.2	0.044	0.013	931.	19.754	5.816	61.	2.126	0.626	46.	2.00	91.8	83.
7	391. 58.	2.84	165.6	20.7	3.2	0.137	0.023	1117.	23.484	3.888	105.	3.627	0.600	73.	2.84	206.5	66.
8	390. 58.	2.10	120.8	21.0	1.6	0.228	0.028	594.	12.661	1.529	73.	2.556	0.309	331.	2.10	695.9	84.
9	389. 36.	3.57	128.9	20.8	3.0	0.345	0.044	931.	19.664	2.534	125.	4.337	0.559	77.	3.57	274.2	56.
10	388. 12.	2.57	29.6	20.8	9.6	0.100	0.003	896.	18.925	0.559	82.	2.845	0.084	108.	2.57	277.0	80.

CVS-H= 1620.2   HC TOTAL= 0.150   CO TOTAL= 24.14   NOX TOTAL= 3.354   HWY= 1658.2

HC= 0.020g/mile   CO=3.22g/mile   NOX= 0.447g/mile

CVS-H=12.95mpg   COMPOSITE = 14.6 MPG

HWY=17.28mpg

Figure 2.6-32   Stirling Engine Dynamometer Emission and Fuel Economy

STIRLING ENGINE DYNAMOMETER EMISSION & FUEL ECONOMY

ENGINE BUILD/محب   ENGINE TEST------   WITHOUT INTERNAL HYDROGEN COMPRESSORS

RUN NO	TIME s	FUEL FL. g/s	FUEL TOT. g	A/F	HC ppm	HC EI g/kg	HC g	CO ppm	CO EI g/kg	CO g	NOX ppm	NOX EI g/kg	NOX g	NOX TIME s	FUEL FL. g/s	FUEL TOT. g	EGR %
1	653. 362.	0.53	192.0	20.1	2.0	0.020	0.004	397.	8.116	1.558	30.	1.008	0.193	10.	0.53	5.5	91.
2	652. 272.	0.58	157.8	21.4	4.0	0.043	0.007	379.	8.225	1.298	30.	1.070	0.169	5.	0.58	3.0	119.
3	651. 74.	0.31	22.9	24.0	5.0	0.060	0.001	54.	1.308	0.030	30.	1.194	0.027	52.	0.31	16.1	145.
4	650. 167.	0.84	140.4	20.2	2.0	0.020	0.003	379.	7.785	1.093	30.	1.012	0.142	29.	0.84	24.4	124.
5	649. 186.	1.17	217.3	20.3	2.0	0.020	0.004	361.	7.450	1.619	34.	1.153	0.250	33.	1.17	38.4	105.
6	648. 147.	1.71	251.7	20.1	2.0	0.020	0.005	522.	10.671	2.686	52.	1.746	0.440	46.	1.71	78.5	79.
7	647. 58.	2.56	149.2	20.1	3.0	0.030	0.005	595.	12.164	1.815	72.	2.418	0.361	73.	2.56	186.1	67.
8	646. 58.	1.75	100.6	20.1	4.0	0.041	0.004	499.	10.201	1.026	63.	2.099	0.211	331.	1.75	580.0	71.
9	645. 36.	3.00	108.3	20.1	4.0	0.041	0.004	545.	11.141	1.207	123.	4.114	0.446	77.	3.00	230.4	50.
10	643. 12.	2.20	25.3	20.4	5.0	0.051	0.001	545.	11.300	0.286	71.	2.418	0.061	108.	2.20	237.2	74.

CVS-H= 1365.7   HC TOTAL= 0.039   CO TOTAL= 12.62   NOX TOTAL= 2.301   HWY= 1399.5

HC= 0.005g/mile   CO=1.68g/mile   NOX= 0.307g/mile

CVS-H=15.37mpg   COMPOSITE = 17.31 MPG

HWY=20.48mpg

Figure 2.6-33   Stirling Engine Dynamometer Emission and Fuel Economy
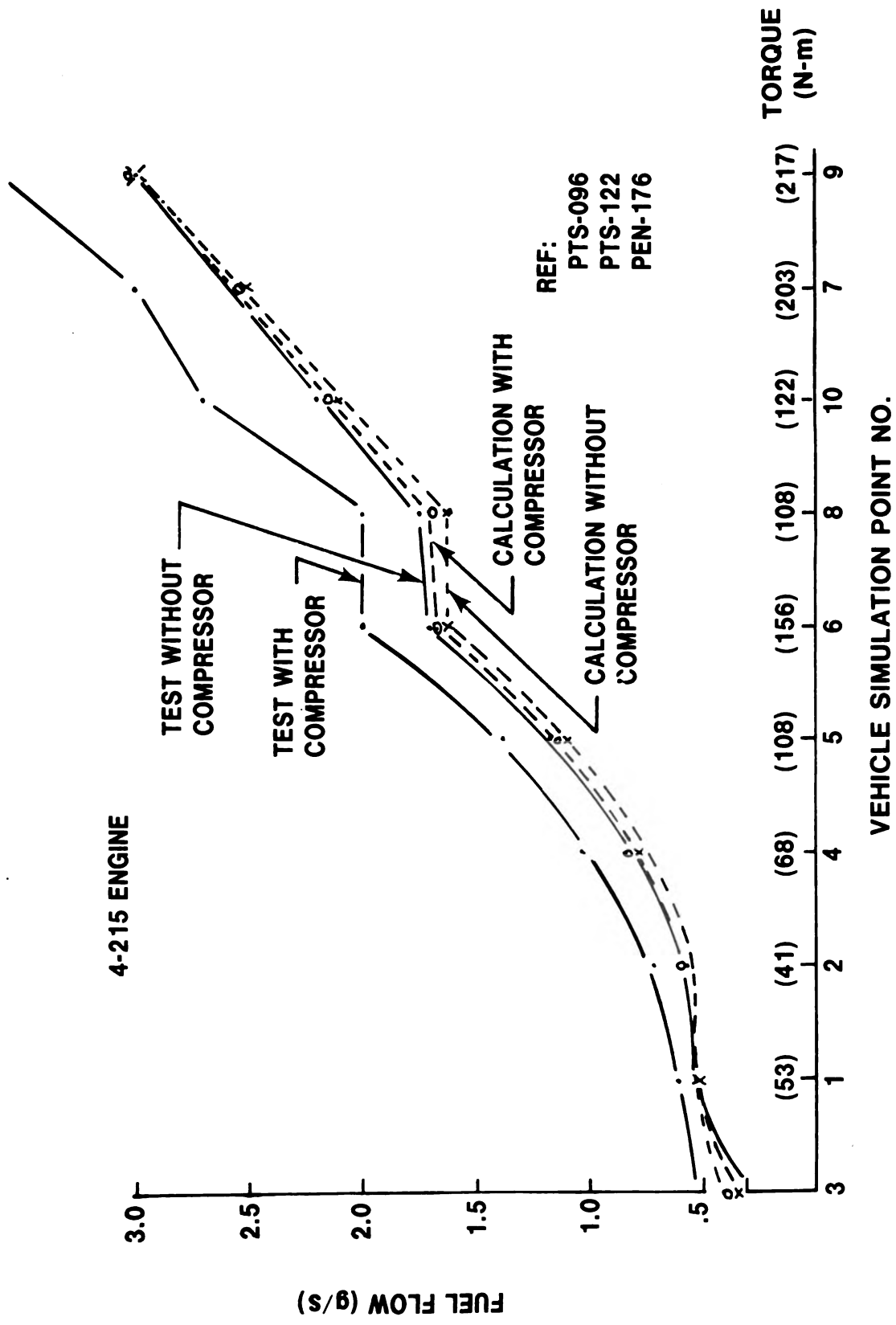
Figure 2.6-34 Internal Compressor Influence on Fuel Flow – Analytical and Experimental

2.7 Air/Fuel Control

2.7.1 Summary — The objective of this section was to develop an air/fuel control system which provided the following features:

a. Reduced pressure losses of the first generation air measuring device.

b. Permits a repeatable control of air/fuel ratio within a band of $\pm$ 1 air/fuel ratio number.

c. Permits a controlled program of exhaust gas recirculation (EGR).

d. Allows manual manipulation on the dynamometer during mapping exercises.

The Stirling engine derives power from its continuous external combustion process. All the heat supplied from the combustion process has to be transferred through metal walls (heater tubes) to the hydrogen working fluid. The P-V and T-S diagrams of the ideal Stirling cycle are shown in Figure 2.7-1.

These diagrams illustrate that heat is transferred to the working fluid during the constant-volume process (2-3) and during the isothermal expansion process (3-4). Heat is rejected during the constant volume process (4-1) and during the isothermal compression process (1-2). During the isothermal expansion process (3-4), heat addition occurs at the same rate at which work is produced by the fluid expansion. Therefore, to maintain maximum possible power out of the engine, the temperature of the working fluid must be maintained at a constant level and as high as possible, taking into consideration the metallurgical heat limit of the materials. The 4-215 engine design has been optimized for an inside wall temperature of 750°C, resulting in a hydrogen temperature of approximately 710°C.

The requirement for a constant hydrogen temperature is only one of the parameters which determines the design of the air/fuel control system. The other parameters which must be controlled are:

a. Air/fuel ratio, with the capability to vary the ratio as a function of engine load.

b. EGR rate, to be varied as a function of fuel flow.

Maintaining the desired air/fuel ratio is necessary for control of exhaust emissions and has some effect on engine efficiency. Unburned hydrocarbons in the exhaust, due to rich fuel mixture, represent an energy loss. An excess air mixture results in less efficient heat transfer and, therefore, a less efficient heating system. EGR is required for dilution and reduces generation of NOx emissions.

The complete air/fuel control system requires the following:

a. Measurement of the hydrogen temperature in the heater head.

b. Control of the combustion air flow.

c. Measurement of the combustion air flow.

d. Control of the fuel flow.

e. Control of the EGR flow.

The heater head hydrogen temperature is measured with a thermocouple inserted into the heater tubes. This measurement signal, after amplification, can now be compared to a reference voltage, representing the desired hydrogen temperature, and the difference in voltage used to control either fuel or air flow.

In the control mode, fuel flow following air flow, the time response for fuel flow change is approximately 75 milliseconds which is the approximate time for an air flow change to reach the combustion chamber at about the same time. In the alternate control mode, air flow following fuel flow, the time response for fuel flow change remains the same while the time response for air flow is dependent on blower speed which in turn is dependent on engine speed. For a full throttle acceleration, since the engine response is approximately 600 milliseconds, the air flow response can be as great as 600 milliseconds and a fuel rich mixture would result. Therefore, air flow was chosen to be controlled and fuel flow is metered to follow in the desired air/fuel ratio.

The fuel consumption of the 4-215 engine ranges from 0.4 grams/sec. to 15 grams/ sec. This is a fuel control ratio range of 37.5 to 1. Conventional fuel metering devices are not available which will accurately operate over this wide control range. The initial fuel control used was a hydro-pneumatic unit designed by Philips, but was found unacceptable for use with an engine installed in a vehicle. In addition, the air flow sensing device, although providing accurate, dependable air flow information to the fuel metering control, had an unacceptably high pressure drop most evident at low air flows.

The desired air/fuel system had requirements best satisfied by an electronic control with air flow measurement having a range of 7.5 to 300 grams/sec, and fuel metering having a range of 0.4 to 15 grams/sec. The measurement and metering were the main elements of the system. Ford Motor Company has had under development for several years a precision engine air inlet measuring meter which detects a created disturbance in the air stream. Essentially, a vortex generating rod is placed in the inlet air stream and the vortices generated are sensed and counted downstream from the rod.

The vortices are generated alternately on each side of the rod and the downstream rod senses the cooling effect of the vortices on its two self-heated nickel-on-glass elements. The resistance variation created is sensed in a bridge circuit. The sinusoidal signal is amplified and passed through a square wave generating circuit. The output of the air flow meter produces a square wave pulse the frequency of which is proportional to mass air flow, after ambient temperature and pressure sensor signals are used for correction. Vortex air flow motor tests have indicated the ability to follow air flow changes of up to 5500 grams/sec/sec with no pulse signal dropouts. The maximum rate of change of air flow for the 4-215 engine is approximately 5000 grams/sec/sec.

The one problem encountered with using the air flow meter is its non-linear relationship at low air flows.

Figure 2.7-2, a plot of hertz/grams/sec versus grams/sec of air flow, graphically illustrates the non-linear region. This region was compensated for by a non-linear gain circuit following the output of the Vortair.

The initial investigation of a fuel metering system was directed toward a fuel by-passing and metering spool-valve device operated by a proportional solenoid which moved as a function of delivered current. This effort was stopped when flow bench tests showed excessive non-linear and hysteresis characteristics for an open loop metering system, a highly desirable control mode. A fuel metering scheme, which has been around for some time on IC engines, looked promising and the injector system was designed and built.

The Vortair-injector fuel control system is comprised of the Vortair air flow sensor, three electrically operated fuel injectors mounted in parallel with common inlet and outlet manifolds, an electronic control package, an electric fuel pump, and a pressure regulator to maintain a constant pressure drop across the injectors (refer to Figure 2.7-3). The injectors, which have combined metering and atomizing orifices, are used in this application to serve only as metering valves. One of the three has a smaller flow orifice and covers the flow range of 0.4 to 2 grams/sec. The other two, operating together but 180° out of phase with each other, cover the flow range of 2 to 15 grams/sec.

The injectors are controlled with a constant period, variable width pulse generated in the electronic package.

The pulse output signal of the air flow sensor is converted to a DC level signal by the frequency to voltage converter. The DC signal is shaped in the next stage by a non-linear gain amplifier to compensate for the non-linear output of the air flow sensor. In addition, overall gain is controlled to provide adjustment of the air/fuel ratio. The compensated signal is then applied to the pulse width modulator circuits, which also have a signal input from the clock oscillator to set the repetition rate. The output of a level detector, the input of which is the compensated signal, is fed to the switching logic along with the output of the pulse width modulators. The logic circuit determines which injectors are turned on. The driver amplifiers boost the low level output of the switching logic to a high level current pulse for operating the injectors. Refer to Figure 2.7-4.

The fuel economy improvement resulting from a low pressure drop air flow meter, an improved air/fuel control, and reduced power loss in the control was estimated at 0.16 MPG.

2.7.2 Work Performed — The initial air/fuel control system used on the 4-215 engine was a hydro-pneumatic device using a shaped valve with a spring loaded flapper as the air flow sensing element. This system was found deficient in being able to provide a consistent air/fuel ratio with a narrow band of ratio variations. In addition, the pressure drop experienced in the air flow measuring valve was high at the low air flows, requiring the air blower size and speed to be sized for the low air flows.

2.7.2.1 Air Flow Sensors — The Philips designed shaped-valve air flow sensor was replaced with a Ford-designed Vortair device, described earlier, which was known to have low pressure losses. The Ford Vortair is a thermal sensing unit.

In addition to the Ford Vortair, another vortex shedding unit provided by J-Tec, utilizing acoustic sensing, was examined along with a turbine air flow meter from Autotronics. Figure 2.7-5 shows the pressure drops across each of the air flow meters tested and compared them to the N. V. Philips shaped valve.

2.7.2.1.1 Ford Thermal Vortair — The tests performed with the unit here showed that the repeatability is +2.4%, -1.7% of a reading. The output frequency stability is +2.0% of reading at 4.0 grams/second air flow rate and better than +1.0% for all other flow rates. The interchangeability tests indicated the units are not interchangeable in the Stirling engine open loop application without recalibration of the shaping and gain circuits. The unit-to-unit variation in output frequency was as great as 19% at the minimum air flow rate and 6.5% at all other air flow rates. The thermal unit has a non-linearity of +5.6% at the low air flows. The shaping and gain circuit contains a linearization portion for compensation. Figure 2.7-2 is a plot of hertz/grams/sec versus grams/sec and illustrates the area and extent of the non-linearity.

2.7.2.1.2 J-Tec Acoustic Vortair — Five J-Tec acoustic units were evaluated for use with the Stirling engine air/fuel system. Repeatability was found from ten test runs and was +1.6%, -1.2%, of a reading. The frequency stability was +1.4% of a reading at 8.0 grams/second and less than +5.1% at 8 grams/second and a maximum of +2.3% at all other flows. As with the thermal Vortair unit, a linearization circuit is required for compensation. Figure 2.7-6 is a plot of hertz/grams/sec versus grams/second.

2.7.2.1.3 Autotronic Air Flow Transducer — A turbine air flow meter from Autotronics was evaluated for use with the Stirling engine and found unacceptable bacause of its excessive pressure drop. The unit exhibited very good repeatability, +0.3% of a reading, and linearity, +0.4% of a reading

A comparison chart of characteristics for the various air flow measurement devices is shown in Figure 2.7-7.

2.7.2.2 Fuel Metering Methods — The open loop fuel metering concept was very desirable but entirely dependent upon an accurate means to control fuel as a function of air flow. The fuel metering methods investigated were fuel injectors, proportional solenoid, and variable speed pump.

2.7.2.2.1 Fuel Injectors — Injectors obtained from Bosch were examined and used for fuel metering on the Stirling engine. Flow bench tests showed a linearity of +2.4% and a repeatability of +3%.

2.7.2.2.2 Ford Proportional Solenoid — Bench testing of the proportional solenoid revealed excessive non-linearity and hysteresis characteristics which made it unacceptable for use with the Stirling engine air/fuel system.

2.7.2.2.3 United Stirling of Sweden Dual Pump — The dual pump fuel metering system as supplied by United Stirling of Sweden was found not acceptable for use with the Stirling engine air/fuel system. Test results show that due to the varying torque requirements at low speeds, a constant fuel flow could not be obtained in the very low flow range with the supplied motor and speed

control. The fuel flow fluctuated excessively below 0.7 grams/seconds.

2.7.2.2.4 Autotronics Electrosonic 5 — The variable speed pump metering system as supplied by Autotronics Control Corporation was found not acceptable for use with the Stirling engine air/fuel system. The fuel flow at less than 0.65 grams/second was unstable due to fluctuating drive motor speeds. The system must be capable of stable operation down to at least 0.4 grams/second.

A comparison chart of metering device characteristics is shown in Figure 2.7-8.

The combination Vortair-injector air/fuel system was used successfully to control the engine through all of the dynamometer cell engine mapping and optimization tests. Figures 2.7-9 through 2.7-13 are plots of air/fuel ratio vs. fuel flow for several Vortair-injector systems as calibrated on the flow bench. Figure 2.7-14 is a plot of air/fuel ratio vs fuel flow comparing engine tests results with the flow bench calibrations.

2.7.2.3 EGR Control — The air flow and EGR rate was controlled by positioning the throttle plates in the air flow path and in the crossover pipe. The controlling signal for positioning the throttle plate was obtained from fuel flow and hydrogen temperature and had to be shaped in the differential drive circuit.

The air flow and EGR flow throttle plates were positioned by a differential drive circuit, Figure 2.7-15, and a small DC motor geared to the plate shaft.

2.7.3 Test Conducted — The following is a list of the tests conducted, conditions, procedure, equipment and instrumentation for air and fuel flow bench testing:

a. Calibration

    1. Vortair air flow meters (thermal)

    2. Fuel metering injectors

b. Repeatability

    1. Vortair air flow meters (thermal)

    2. Fuel metering injectors

c. Interchangeability

    1. Vortair air flow meters (thermal)

    2. Fuel metering injectors

d. Stability

    1. Vortair air flow meters (thermal)

2. Fuel metering injectors

e. Repeated tests 1, 2, 3, and 4 for an acoustic Vortair.

f. Repeated tests 1, 2, 3, and 4 for alternate air-fuel systems available and considered suitable for use on a 4-215 Stirling engine.

2.7.4 Procedure — The tests were conducted at room temperature and local barometric pressure. The fuel was heated to 80°F. Indolene Clear (ESE-M4C50-C) was used as test fuel.

The following is the procedure which was used for the testing:

a. Set up the flow bench, test rig, and instrumentation according to Figure 2.7-17.

b. Calibrate and check out the instrumentation.

c. Turn on the flow bench system. Before continuing, wait until the fuel temperature has stabilized at 80% F.

d. Vortair Calibration Test — Adjust the air flow by varying the blower speed and the butterfly value angle to 20 g/s as measured by the laminar flow element. Record the Vortair frequency output. Continue up to 110 g/s in steps of 10 g/s. Also record ambient temperature and pressure.

e. Injector Calibration Test — Meter fuel with just one injector into a graduated cylinder for a period of 30 seconds. Record the amount of fuel in the graduated cylinder. Repeat, varying the pulse widths that the injector stays open, by increments of 1 millisecond from 1.5 milliseconds to 17.5 milliseconds.

f. Repeatability Test (Air Fuel Set Point Test) — Set air/fuel potentiometer on the Electronic Control Box (ECB) to read a specific air/fuel ratio. Vary the fuel flow from 0.4 g/s to 5.0 g/s in steps 0.2 g/s. Record air flow as measured by the laminar flow element and Vortair. Calculate the air/fuel ratios and plot air/fuel ratios vs W_f (g/s).

g. Duration (or Stability) Test — Set the system to run at a specific air flow. Record air flow, fuel flow, ambient conditions, and settings of the ECB. Run the system for 6 hours. Record data every hour. Determine factors that caused changes, if any, in the air/fuel ratio during the test. Perform the test for low and high air flow rates.

2.7.5 Equipment and Instrumentation — The following equipment and instrumentation was used for these tests:

a. Air-Fuel Metering System for a 4-215 Stirling Engine (See Figure 2.7-3).

b. Flow Bench System (See Figure 2.7-17).

c. Electronic Counter

d.   Digital Voltmeter

e.   Oscilloscope

f.   Micromanometer

g.   Merian Laminar Flow Element

h.   Fuel Flowrotor

2.7.6 Definitions — The following are definitions of terms used in section 2.7.

Linearity — A straight line is drawn through the experimental points using the technique of linear regression by the method of least squares. The percent linearity is the deviation from this line.

Repeatability — The percent deviation from the average of ten test runs.

Stability — The maximum percent deviation from the original set point during a six hour test.

Frequency Stability — A percent deviation in output frequency while at a specific set point.

2.7.7 Conclusions — The estimated incremental improvement in M-H fuel economy is a possible 0.16 MPG. The following is a breakdown of this improvement:

a.   A low pressure drop air flow meter in conjunction with a redesigned blower yielded a 0.06 MPG increase.

b.   Air/fuel system capable of holding a desired A/F ratio throughout the operating range gave an estimated 0.1 MPG increase.

c.   A calculated increase of 0.09 MPG obtained by replacing the air throttle plate positioning torque motor with a small DC motor servo device was offset by the DC power requirement of the added Vortair-injector giving a net zero increase.

The objective of providing a repeatable, reliable, adjustable, low air pressure drop air/fuel control system was met.

2.7.8 Recommendations — The Vortair-injector air/fuel system has demonstrated a capability of holding an air/fuel ratio of +1 air/fuel number. This is the best accuracy obtainable with the available fuel injectors used in an open loop metering control. Future development effort on Stirling engine air/fuel controls should exclude:

a.   Investigate using an exhaust gas oxygen sensor which would give a direct air/fuel ratio measurement and allow a closed loop adjustment of fuel flow for tighter control of the A/F ratio.

b.   Using a digital microprocessor based control to improve the accuracy and

drift characteristics of the system.

c.   Continued investigation of alternate control devices such as:

     1.   Acoustic sensing Vortair air flow meter.

     2.   Turbine rotor air flow meter.

     3.   Ion detection air flow meter.

     4.   Variable speed pump fuel metering device.

     5.   Fuel injectors for metering.

d.   Engine and control characterization by measuring open and closed loop response of individual control loops while operating engine on dynamometer.

e.   Engine and control transient operation evaluation both on engine dynamometer and in vehicle.

2.7.9 Open Issues:

a.   The air/fuel control system was not evaluated and tested for transient operation.

b.   A drift problem was experienced with the fuel injectors switch over point. The problem is in the fuel metering circuit electronics but not isolated and eliminated.

c.   The investigation of shutting fuel off during a hydrogen over temperature set point condition which occurs during engine deceleration was not completed. The heat rejection analysis and effect on emissions during relights remain as open items.

d.   A satisfactory flame detection system was not developed and is required for investigation of flame out conditions during transient engine operation.
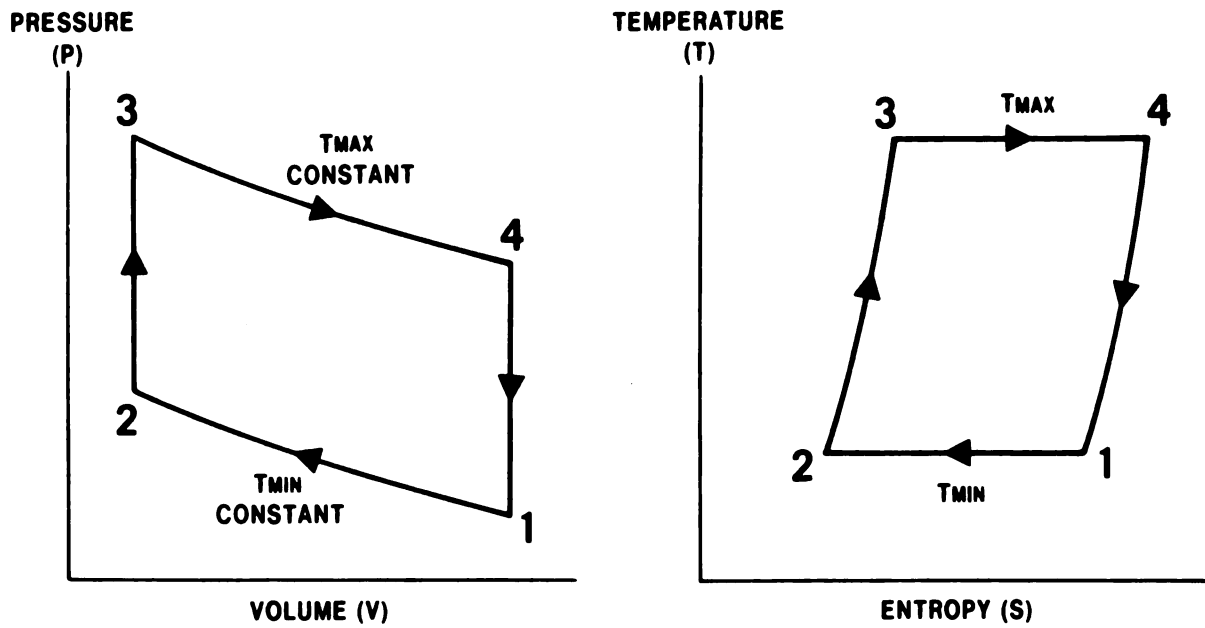
Figure 2.7-1   P-V and T-S Diagrams – Ideal Stirling Cycle

AIR FLOW RATE IN GRAMS/SEC

K-FACTOR IN HERTZS/GRAMS/SEC
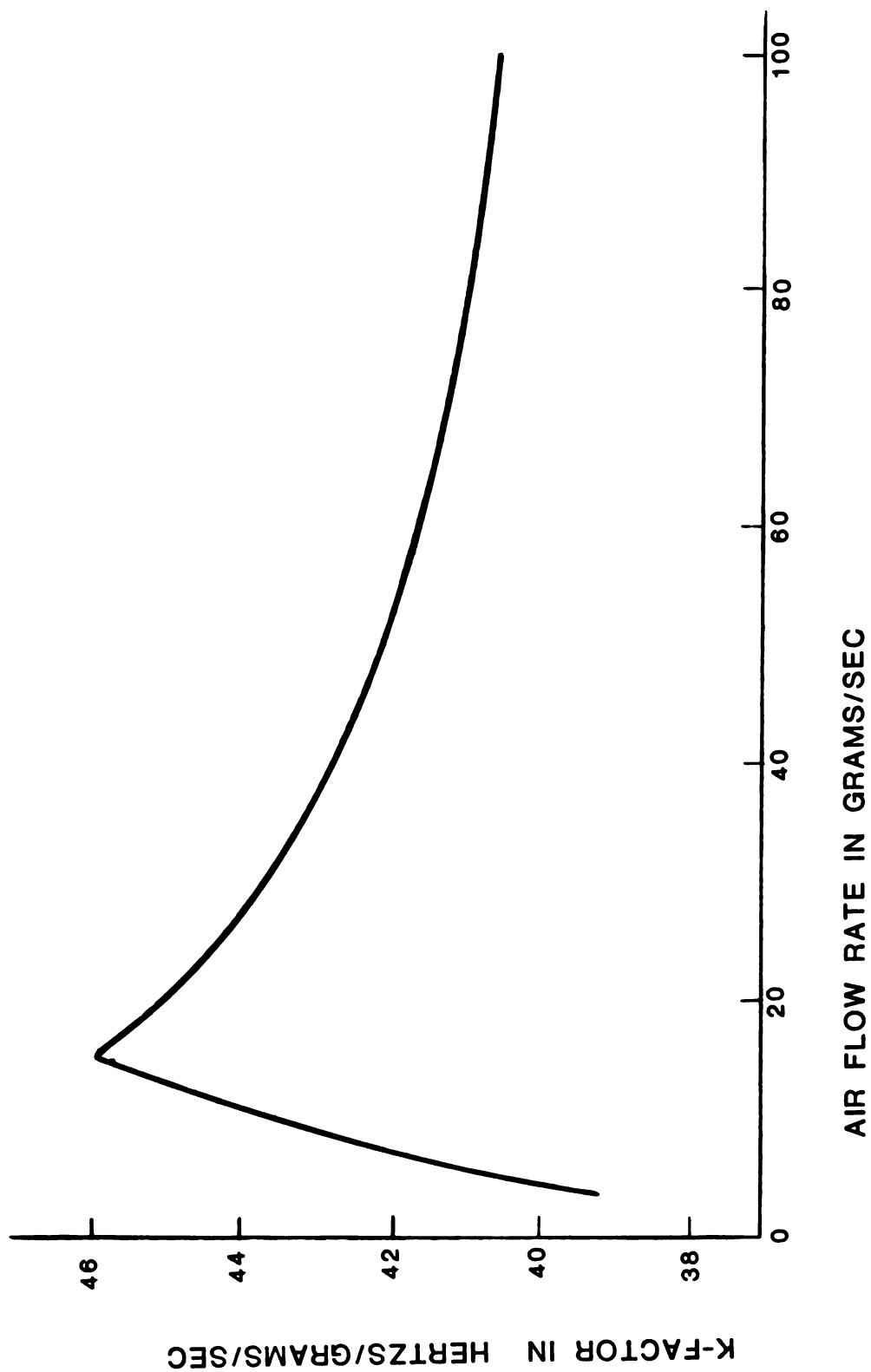
Figure 2.7-2   K-Factor vs. Air Flow for Ford Thermal Vortair

234
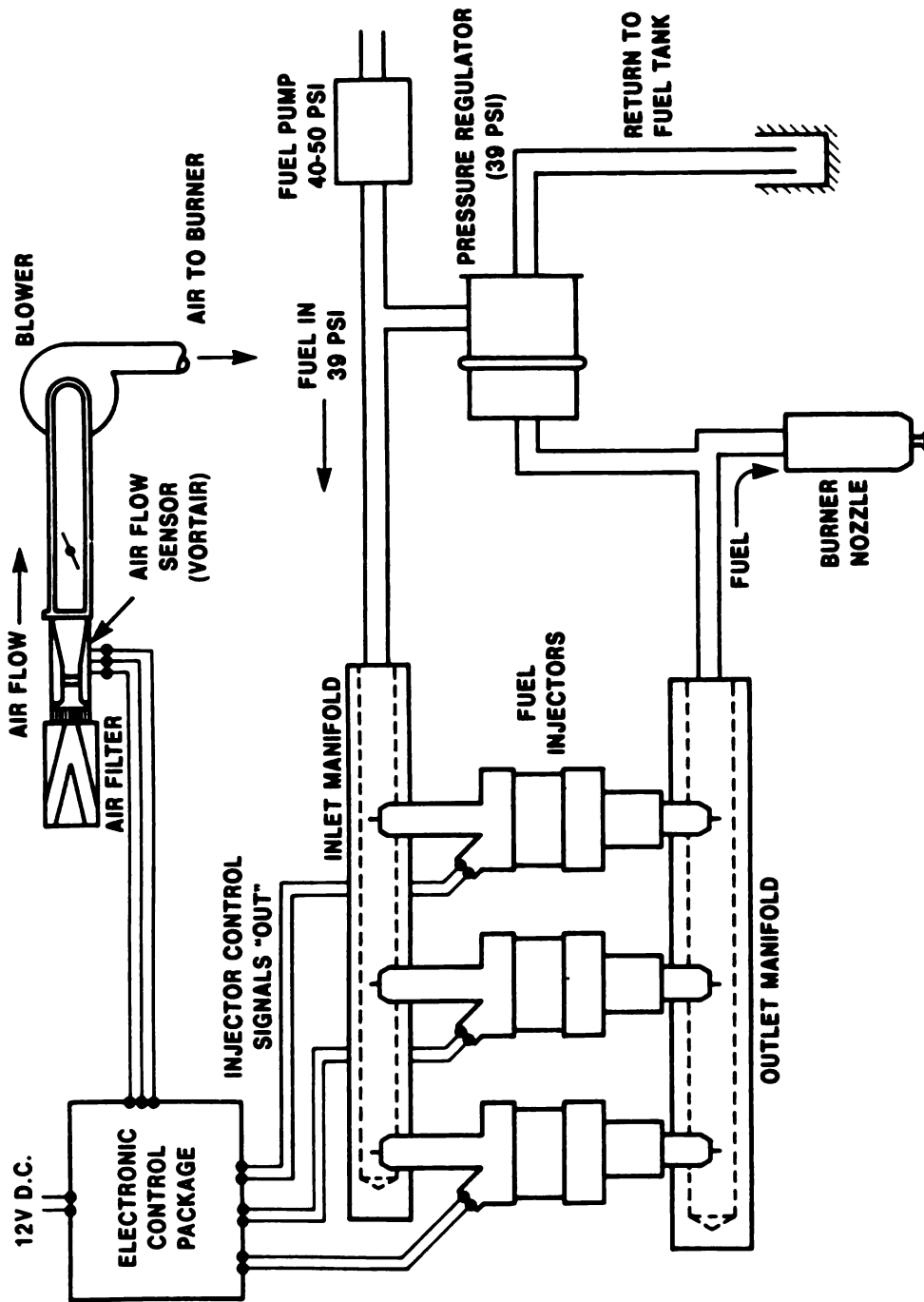
Figure 2.7-3 Air/Fuel Control System
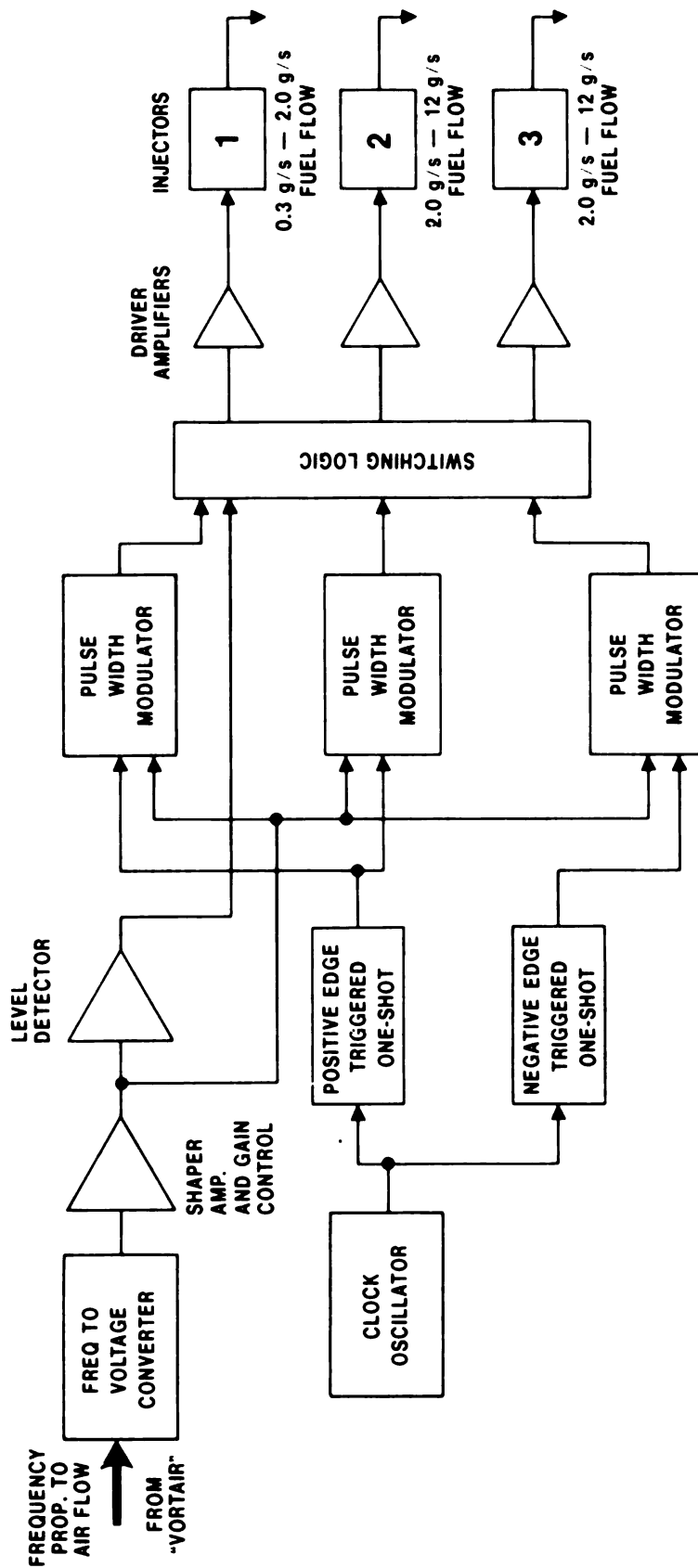
Figure 2.7-4   Block Diagram of Electronic Shaping Circuitry in Control Package
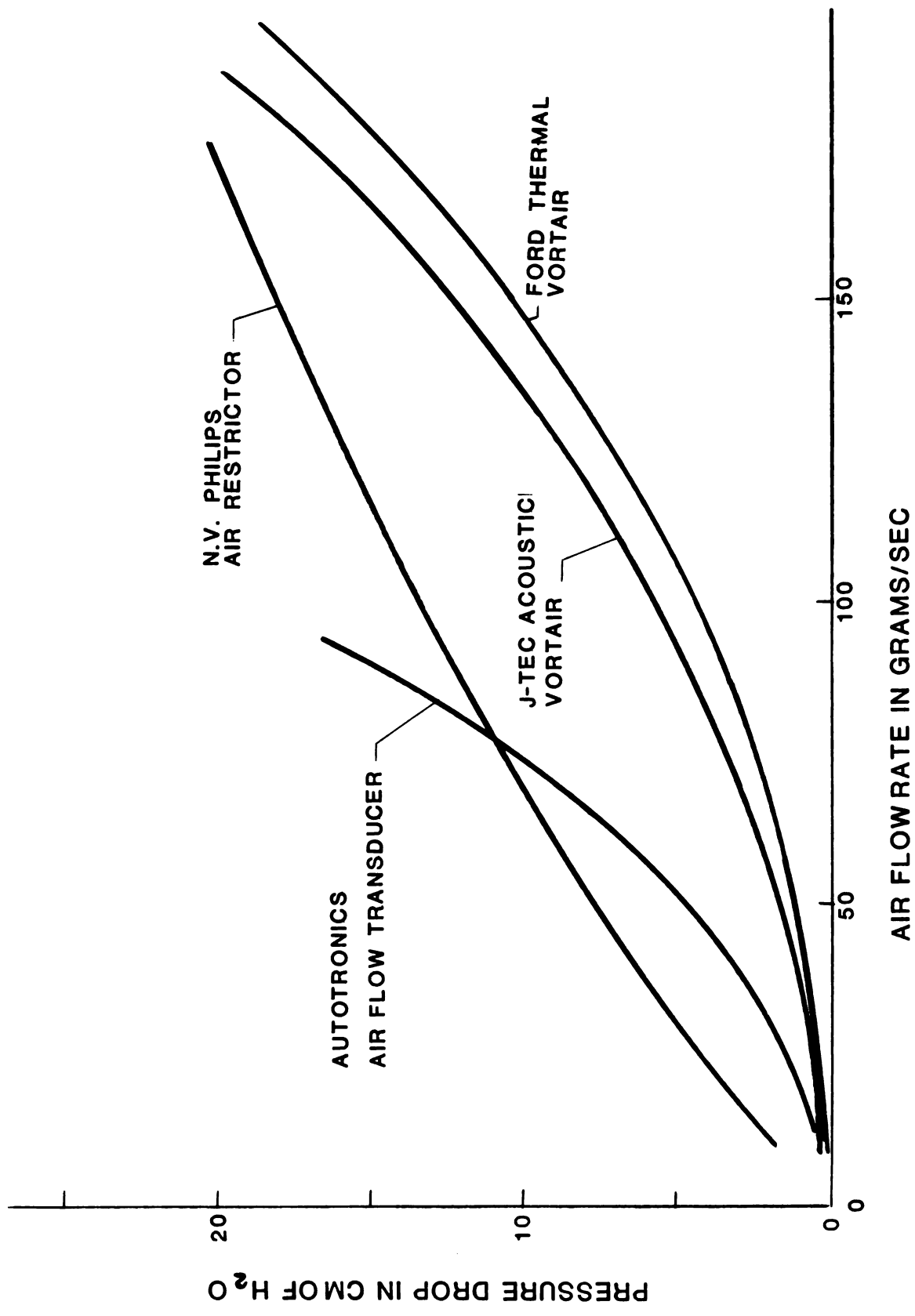
Figure 2.7-5   Insertion Pressure Drop for Air Flow Sensors

AIR FLOW RATE IN GRAMS/SEC

K-FACTOR IN HERTZS/GRAMS/SEC
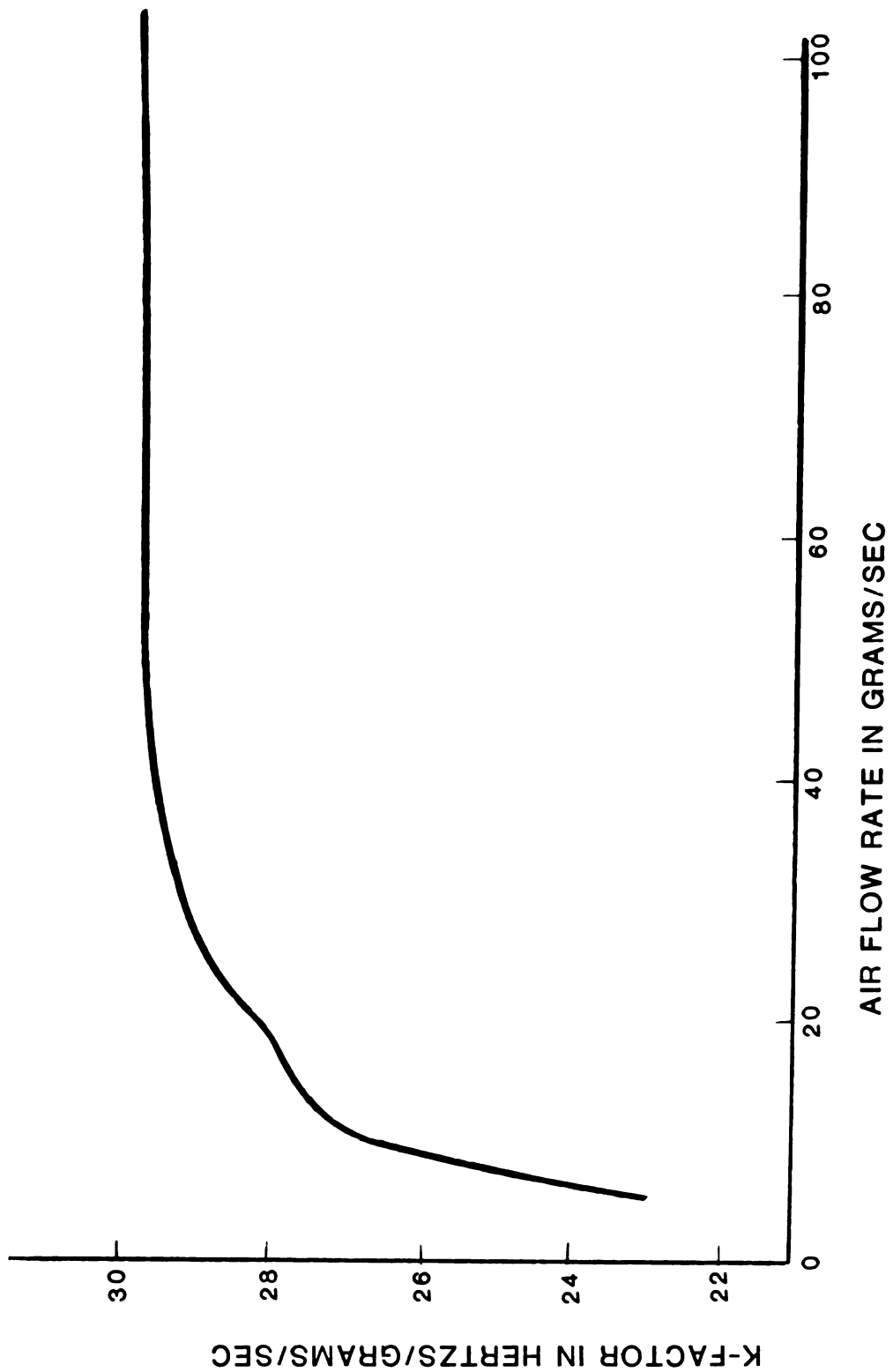
Figure 2.7-6   K-Factor vs. Air Flow for J-Tec Acoustic Vortair

238

DEVICE	NO TESTED	RANGE	LINEARITY	REPEAT ABILITY	STABILITY	FREQUENCY STABILITY
FORD THERMAL VORTAIR	5	64:1 3.9-249 G/S	5.6% a 8 GMS/SEC. ±3.2% OTHERWISE	+ 2.4% - 1.7%	.7%	± 2.0% a 4.0 G/S ± 1.0% OTHERWISE
J-TEC ACOUSTIC VORTAIR	5	67:1 3.3-221 G/S	5.1% a 4 G/S ±2.3% OTHERWISE	+ 1.6% - 1.2%	.3%	± 1.4% a 8 G/S ± .8% OTHERWISE
AUTOTRONICS AIR FLOW TRANSDUCER	2	60.5:1 3.3-200 G/S	± .4%	± .3%		

Figure 2.7-7   Air Flow Meter Characteristics

DEVICE	NO. TESTED	RANGE	LINEARITY	REPEAT ABILITY	HYSTERESIS
BOSCH FUEL INJECTORS	6 12	.2-2.4 GMS/SEC. .4-9.0 GMS/SEC.	± 2.4% ± 2.4%	± 3.0% ± 3.0%	
AUTOTRONICS ELECTROSONIC 5	1	20:1 .8-16.0GMS/SEC.	5.5%@.8GMS/SEC. ± 2.5% OTHERWISE	±1.3%@.8GMS/SEC. ±1.0% OTHERWISE	
FORD PROPORTIONAL SOLENOID VALVE	1	32.5:1 .4-13.0GMS/SEC.	89%@MIN.FLOW 20%@MAX.FLOW		10%
UNITED STIRLING OF SWEDEN DUAL PUMP	1	18.6:1 .7-13.0GMS/SEC.	3.8@4GMS/SEC.	± 2.4%	

Figure 2.7-8   Fuel Metering Devices
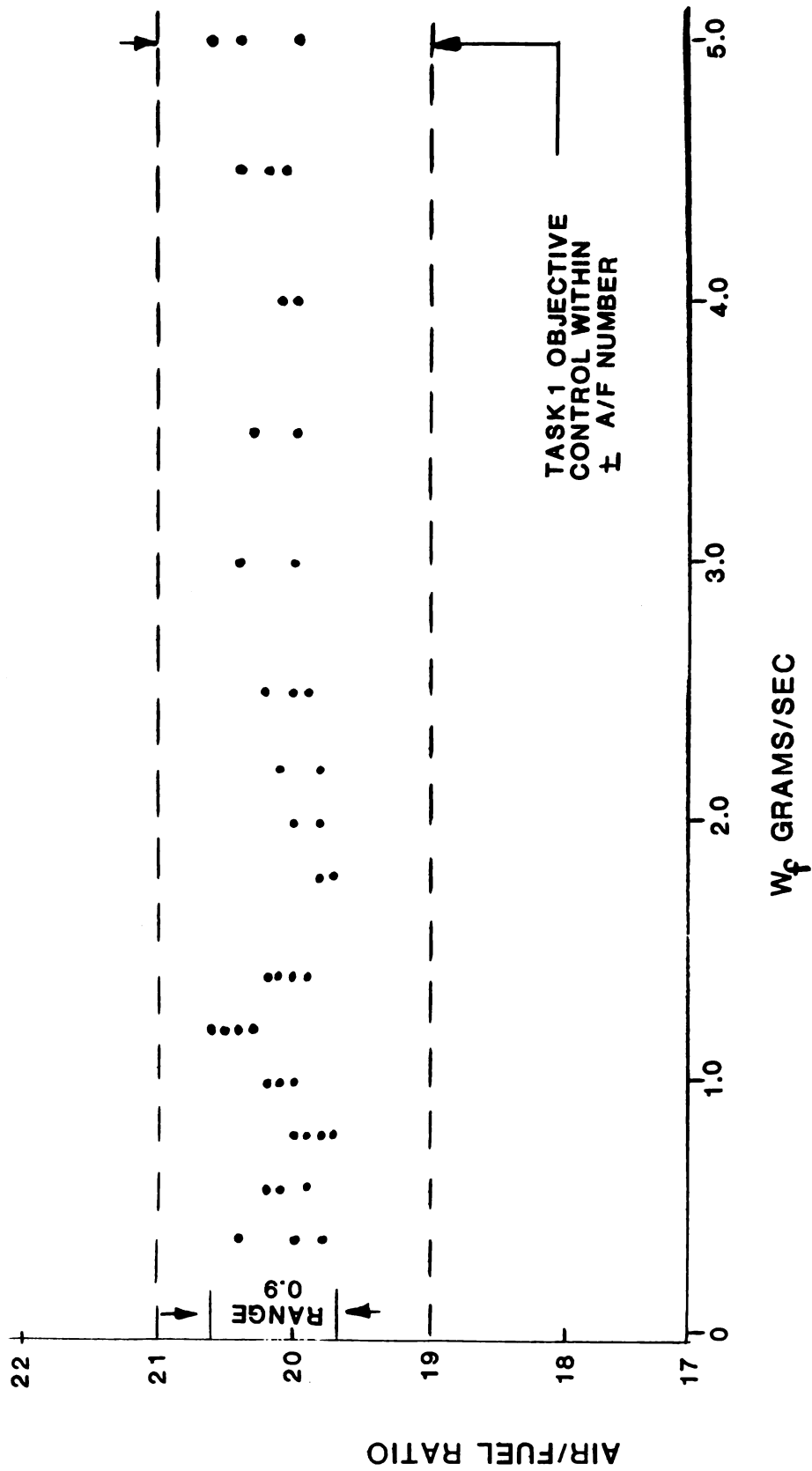
Figure 2.7-9   Air-Fuel Ratio vs. Fuel Flow (Vortair Unit 76-12-Z)

241
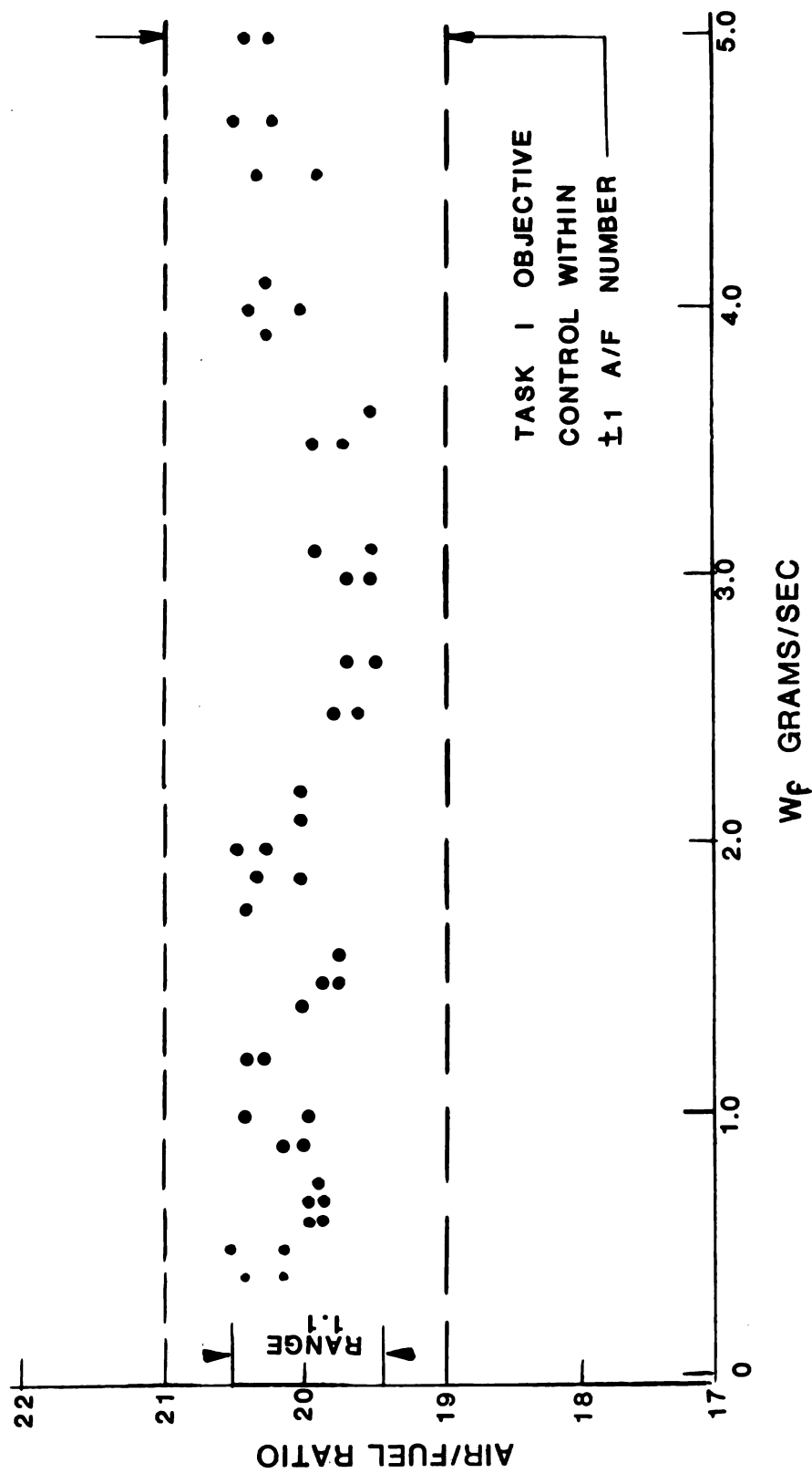
Figure 2.7-10   Air-Fuel Ratio vs. Fuel Flow (Vortair Unit 76-12)
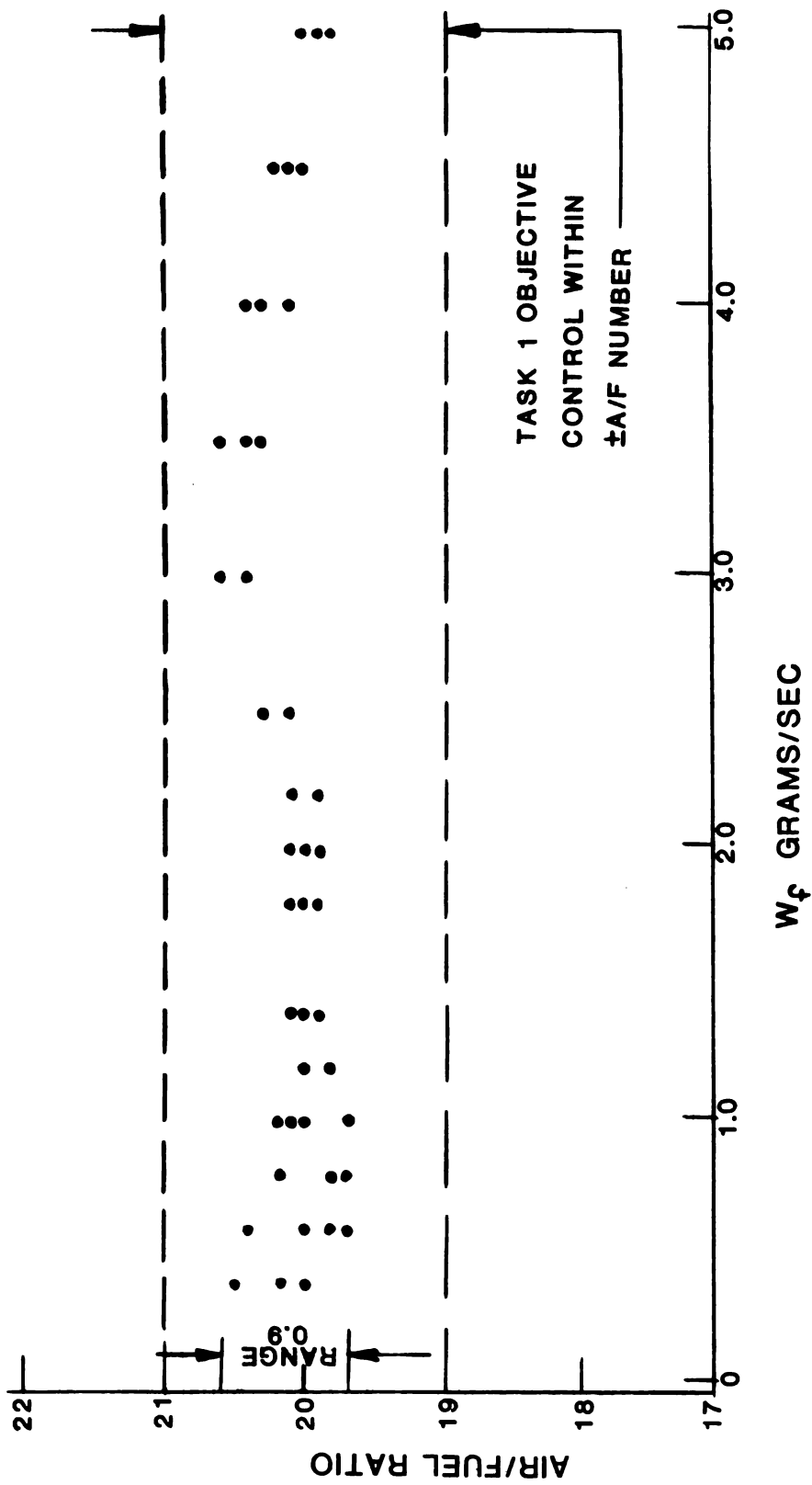
Figure 2.7-11   Air-Fuel Ratio vs. Fuel Flow (Vortair Unit 5)

243
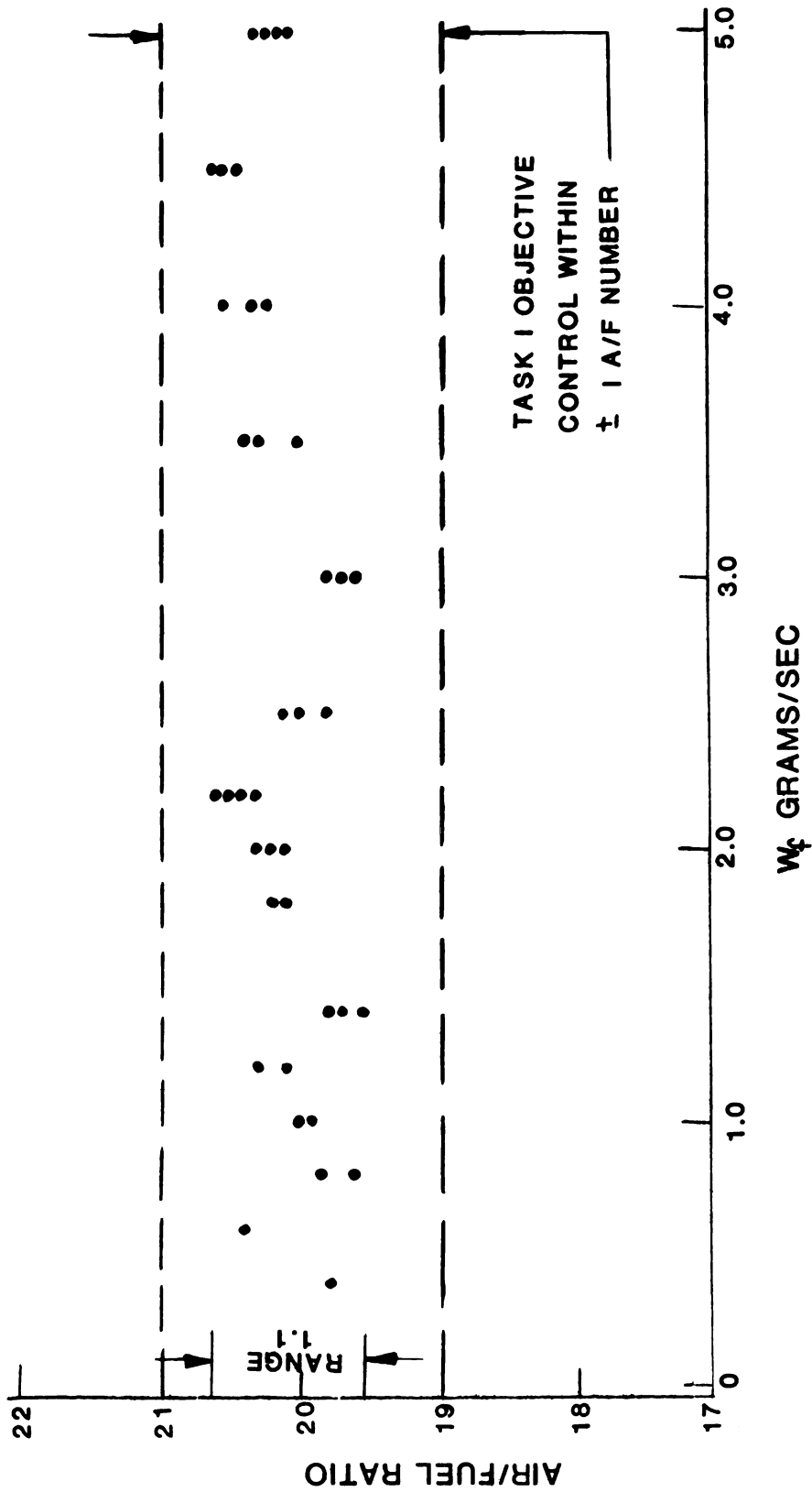
Figure 2.7-12   Air–Fuel Ratio vs. Fuel Flow (Vortair Unit 4)
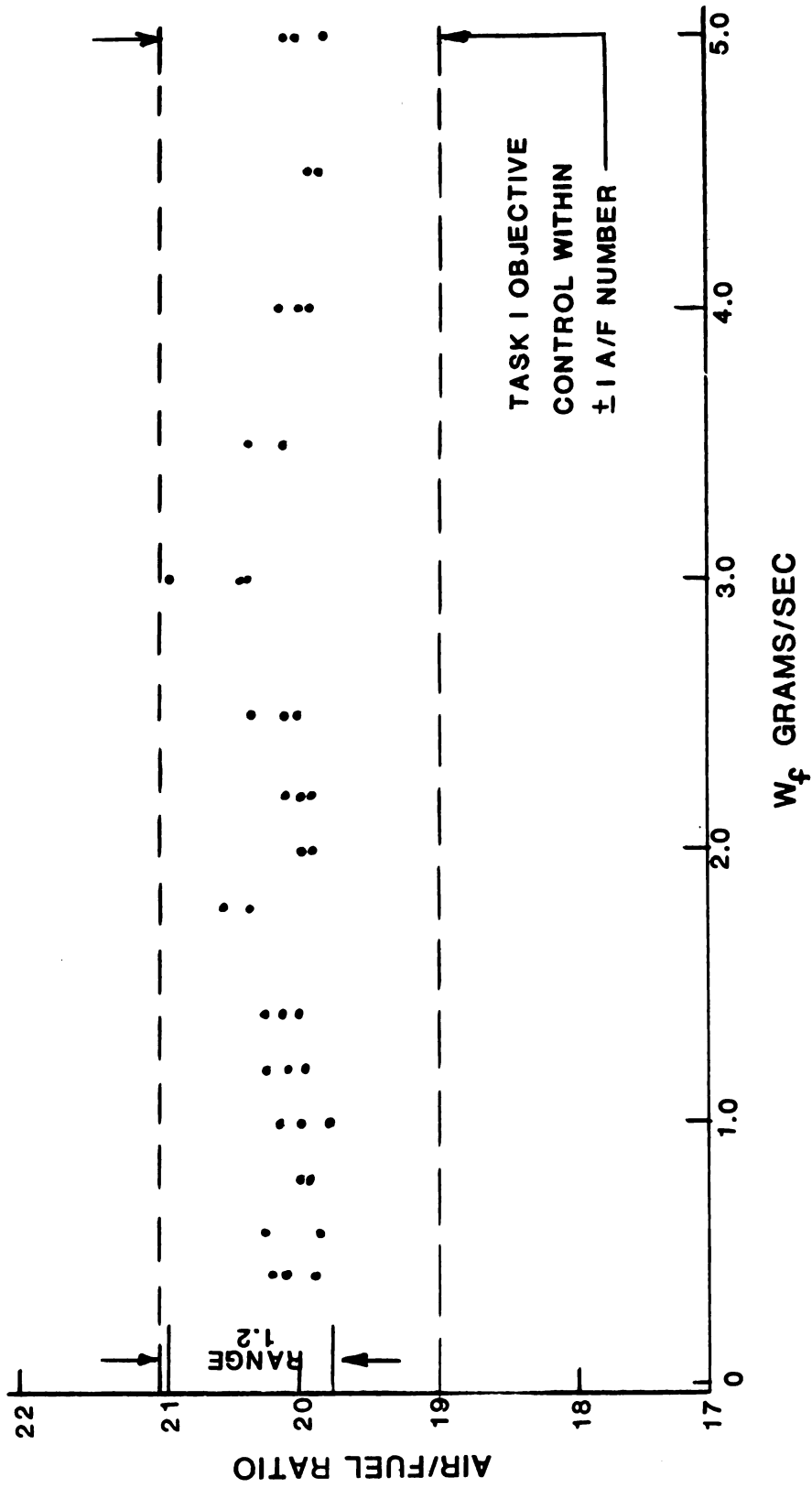
Figure 2. 7-13   Air-Fuel Ratio vs. Fuel Flow (Vortair Unit 19)
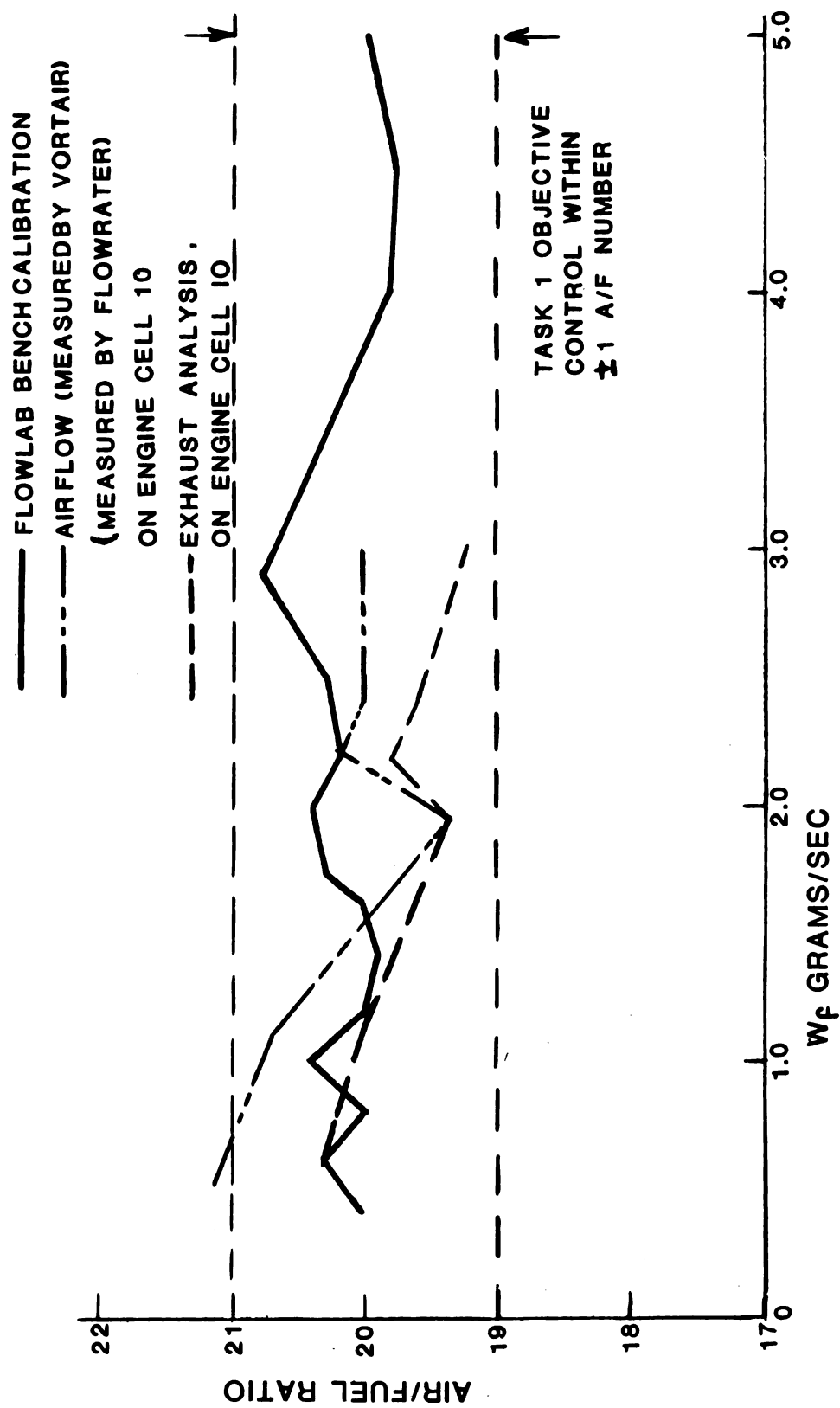
Figure 2.7-14   Air-Fuel Ratio vs. Fuel Flow (Vortair Unit 76-12-Z)

246
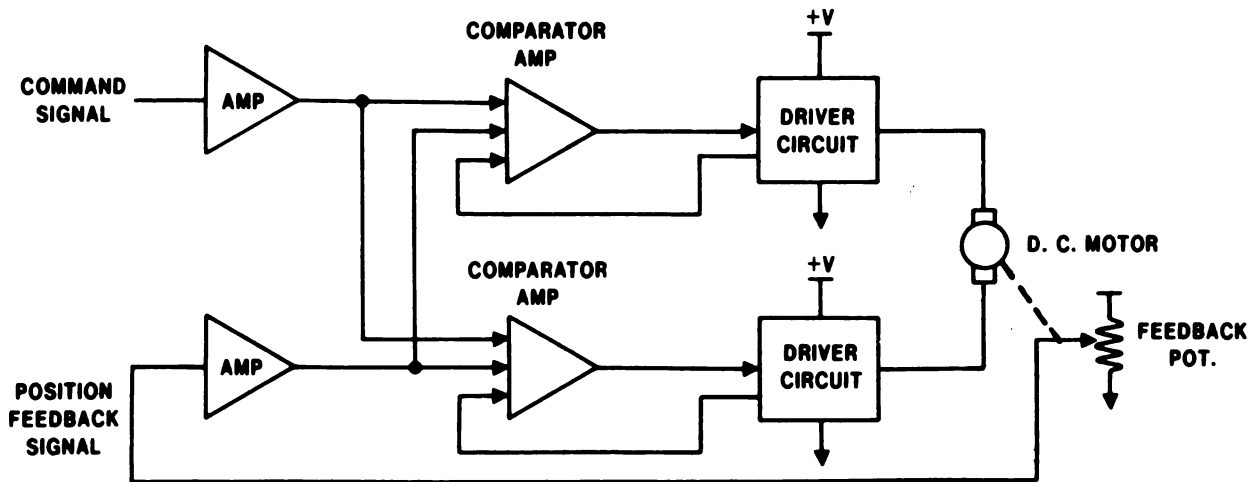
Figure 2.7-15   Differential Drive Positioning Circuit

A position potentionmeter, also geared to the motor, provides a signal to the position feedback loop. Figure 2.7-16 is a sketch of the positioning mechanism.
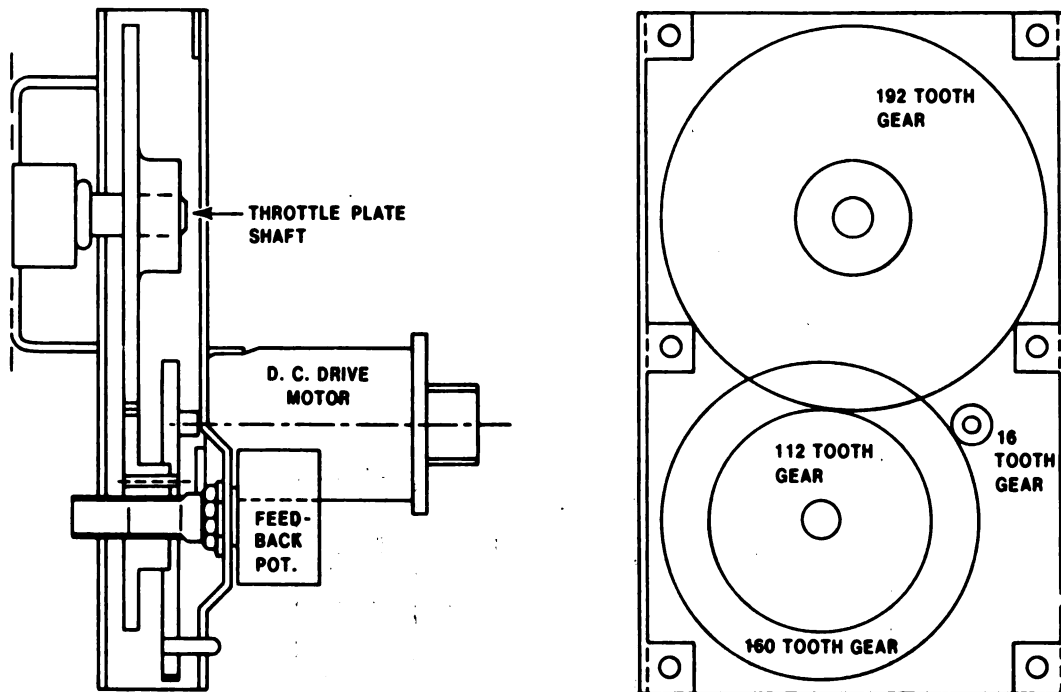
Figure 2.7-16   Air Intake and EGR Throttle Valve Positioner
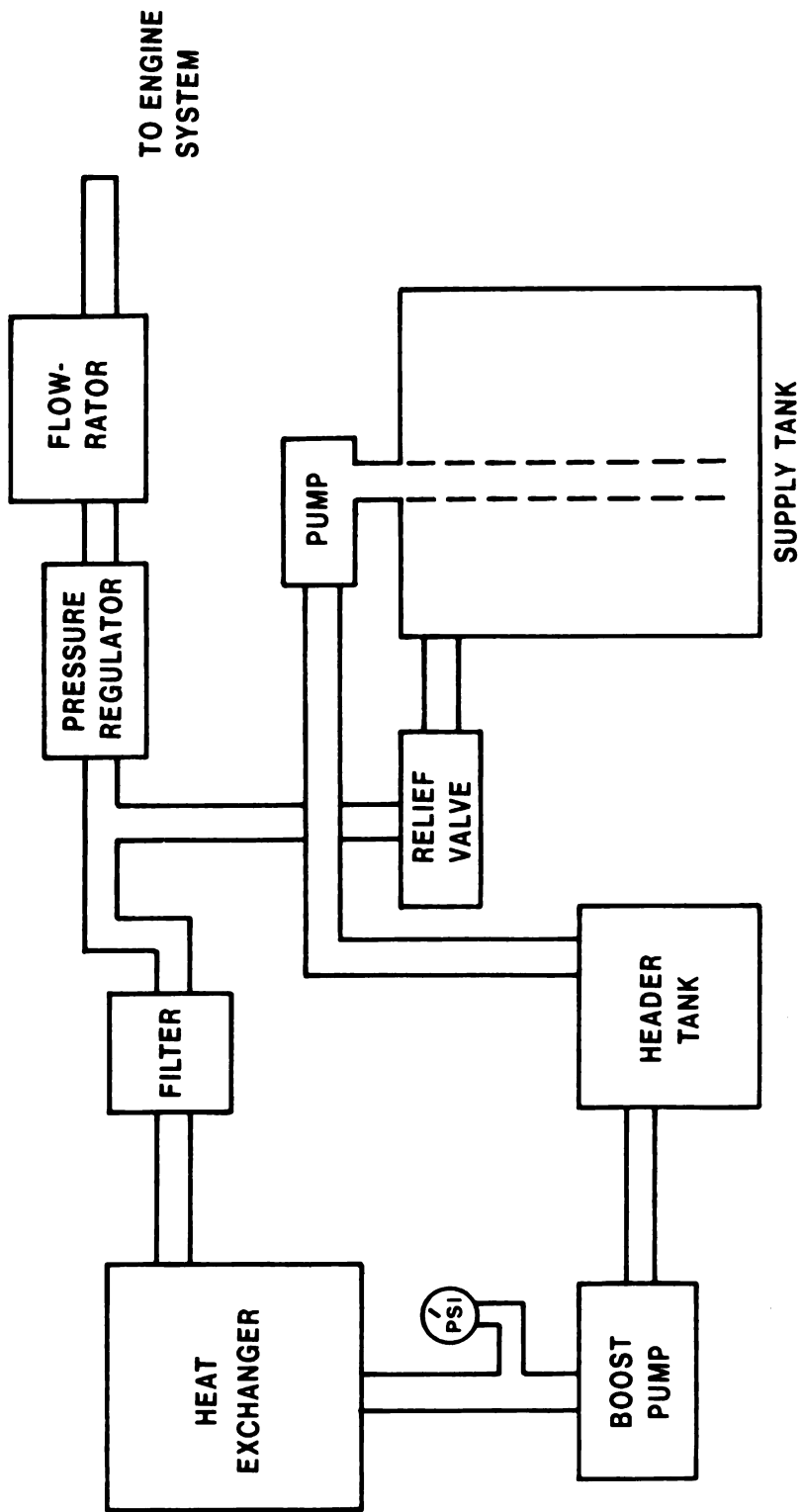
Figure 2.7-17   Flow Bench System

2.8 Cycle Analysis — The primary objective of this section was to determine potential fuel economy improvements which would result from changes to the basic Stirling cycle. Computer analysis was used as the method of demonstrating these improvements.

One of the major areas of investigation for improved fuel economy was in the Stirling cycle itself. Computer analyses were employed for this investigation in an effort to examine the following:

— Improve the indicated cycle efficiency of the engine through reoptimization for 0-60 MPH performance of 13.3 seconds at 4500 lbs. IWC, assuming a swashplate engine of the same physical size as the current 4-215 engine.

— Reoptimize the engine at representative part-load points other than maximum horsepower.

— Incorporate into the reoptimization those improvements with high confidence levels which include aluminum cooler tubes and reduced appendix gap effect.

— Effects of heater tube heat flux.

— Effects and possibilities of reduced thermal losses.

— Reduced amount of fuel required for engine warm-up.

The results of these analyses were used in conjunction with the package environment of the present 4-215 engine.

The majority of the cycle analyses were performed using a complex of computer programs which were written by N. V. Philips. A description of all programs used is provided in section 4.3. The most exercised option within this complex was the "optimization" program. Other program complex options include the analysis of single and multiple steady-state operating points of any engine, burner/preheater systems, engine drives, and accessories. Also, maps including the engine, preheater, drive, and accessories over the complete engine operating range can be generated.

The discrepancy between fuel consumption, computer predictions and measurements are considered to be largely caused by the computer program not considering compressor piston ring leakage. (See, for example, Figure 2.1-9). The compressorless engine study has indicated much better correlation between the predicted and measured fuel consumption for the case of the compressorless engine than for the case with internal compressors.

With the exception of the 4-215 Stirling engine, all other engines referred to in this section of the report exist only as computer models and not as hardware.

2.8.1 Reduced Power Optimization

2.8.1.1 Summary — Early in the cycle analysis study, a number of optimization runs were made which had a net power requirement of 145 HP at full load, as compared to the 170 HP for the baseline 4-215 engine. The lower power requirement was arrived at through performance studies, which indicated that

the original 4-215 engine/Torino vehicle package was overpowered when compared to the baseline vehicle. By allowing the reoptimized engine to be as large (total box volume) as the 4-215 engine, it was hoped that efficiency improvements associated with lower specific power engines could be realized.

2.8.1.2 Results — One of the reoptimizations resulted in the 4-270 engine, having a maximum design speed of 2500 RPM. This engine has become known as the "slow-speed" engine. Because of the much lower maximum engine speed, a new driveline description was necessary before a fuel economy projection could be made. Figure 2.8-1 is the calculation of the projected M-H fuel economy based upon a set of eight new simulation points. Figure 2.8-2 describes the driveline for the slow speed engine.

In another case, an optimization with maximum power at 4000 RPM was performed. This optimization resulted in the 4-204 engine, which gave approximately the same improvement in fuel economy as the 4-270 engine for the same full load power. The projection for the 4-204 engine is shown in Figure 2.8-3.

2.8.1.3 Recommendations and Conclusions — At about this time the partload optimization technique was being developed (See section 2.8.7). Because the initial results using this approach looked very attractive, and since it appeared that there was no significant advantage in relying on a slow-speed engine, further optimizations concerned exclusively with reduced power were abandoned in favor of the partload approach. The slow speed engines also had the disadvantage of requiring a larger and stronger drive mechanism to transmit the power.

2.8.2 Reduced Thermal Losses

2.8.2.1 Summary — In an automotive application, the majority of engine operation is at part-load conditions. Therefore, for maximum fuel economy, high efficiency at part-load was more important than full-load efficiency. A study focusing on regenerator heat conduction was undertaken to determine if increases in part-load efficiency with a minimal sacrifice of full-load efficiency could be achieved.

The heat loss in the regenerator housing wall is caused by the conduction of heat from the regenerator top to the cooling water. This loss is dependent on the temperature difference between the heater and cooling water and represents a greater percentage loss at low load than at full power.

The purpose of this study was to determine what gains, if any, could be made in fuel economy by forcing the optimization procedures to artificially reduce partload heat conduction while sacrificing full-load efficiency.

2.8.2.2 Analysis and Results — The 4-270 engine (see section 2.8.1) was chosen as a reference and the optimization program was run for two cases (4-223 and 4-256) holding the maximum power, engine length, and maximum pressure the same as the 4-270. In one case, the regenerator heat conduction was reduced by 50% (4-223), in the other it was increased 50% (4-256). The resulting 4-223 engine (reduced heat conduction) has a much lower indicated efficiency at full power than the 4-270 or the 4-256 (increased heat conduction).

250

A full map of each engine was made using the numerical program so that part-load efficiencies and M-H fuel economies could be compared. The M-H fuel economy was calculated for each engine based on the same simulation speed/load points and is listed in the following table:

Reduced Regenerator Heat Conduction Fuel Economy Comparison

Engine	Full Power Indicated Efficiency	M-H Fuel Economy, MPG
4-223 (50% reduction)	36.5	18.26
4-270	45.0	18.26
4-256 (50% increase)	44.1	17.31

The 4-223, 4-270, and 4-256 engines were very different in terms of design and constructional details, with all three satisfying the full power requirement. Because one would expect an engine with reduced heat conduction losses to be more fuel efficient, it was concluded that perhaps the full load optimization technique did not produce the "best" engine in terms of minimizing fuel consumption during low load operation. Emphasis was again placed on developing a reliable part-load optimization procedure, the use of which would result in an engine more fully suited to efficient operation at intermediate load points.

It should also be noted that the 4-223 engine had a much higher heater tube heat flux and higher preheater inlet temperatures than the other two engines. This probably would not be acceptable for an actual engine design.

2.8.3 Modified Appendix Gap

2.8.3.1 Summary — Among the parameters affecting the performance of the Stirling engine is the length of the appendix gap, i.e., the annulus separating the piston dome and cylinder wall. This gap is of interest since it has an influence on a phenomenon known as the "appendix effect" which affects the heat transfer from the hot pistons to the cooler cylinder walls through various means. Several computer programs were used to predict quantitatively the results of a change in this gap on the M-H fuel economy of a Stirling engine equipped vehicle.

The length of this gap can be defined by two dimensions (LDD1 and LDD2), both referenced to piston at mid position (see Figure 2.8-4). The total gap length is thus the sum of these two lengths.

The minimum limit of LDD2 was constrained so that the Rulon piston ring stayed within the constant temperature portion of the cylinder during the entire stroke. Therefore,

$$\text{LDD2} = \frac{\text{Stroke}}{2} \qquad \text{Eq. 2.8-1}$$

Both the 4-215 engine and the part-load optimized 4-247 engine were used in this study.

2.8.3.2 Results — Length LDD2 on the 4-215 engine, as tested, was 31.5 mm, while the stroke was 52.0 mm. Therefore, the top piston ring could be moved 5.5 mm, reducing gap length LDD2 to 26.0 mm.

Reducing the appendix gap length results in a theoretical reduction of heat transfer and pumping losses. An analysis of the 4-215 engine with the piston ring moved 5.5 mm, so that LDD2 = 26 mm, revealed a M-H fuel economy improvement of 0.12 MPG (gasoline).

For purposes of experimental validation, the effects of this reduced gap on the 4-215 engine could be realized by testing the engine with a Rulon tape around the piston, or by redesigning the piston with a relocated piston ring.

Additional appendix gap studies were carried out using the 4-247 engine. (See section 2.8.7 for 4-247 details). This engine had been optimized at part-load using the Philips optimization program in order to provide improved efficiency throughout the speed/load range encountered in the metro-highway driving cycle. The vehicle was assumed to be in the 4500 lb. inertia weight class (IWC).

The M-H fuel economy calculations were carried out for three engines that were identical with the exception of the appendix gap length LDD2. This length was increased in increments of 6.0 mm (0.236 in.) from 23.81 mm (0.937 in.) to 35.81 mm (1.41 in.).

As was indicated by the Philips program, which originally optimized the 4-215 engine with respect to efficiency holding the appendix gap length constant, the peak efficiency (and therefore fuel economy) was reached with a LDD1 gap length of 29.81 mm (1.17 in.). This is shown in Figure 2.8-5 where it is apparent that the fuel economy decreased at an increasing rate as the appendix gap length departed from the optimum value.

While the numbers in the figure apply to only a particular engine, the indicated trend is probably of a general nature, suggesting that including the appendix gap length as one of the variables in future optimization runs would be advisable.

2.8.4 Cooler Tube Material

2.8.4.1 Summary — Theoretically, the efficiency (and therefore fuel economy) of a given Stirling engine powered vehicle increases as the temperature of the working fluid (hydrogen) in the compression space of the engine is reduced. One of the ways of reducing this temperature for a given heat rejection rate is to increase the thermal conductivity of the cooler tube walls, assuming the cooling system operates at constant temperature. An analysis was performed to determine the effect of cooler tube material properties (i.e., thermal conductivity) on the M-H fuel economy of a Stirling engine powered vehicle using the part-load optimized 4-247 engine (Refer to section 2.8-7).

2.8.4.2 Results — Figure 2.8-6 is a schematic illustration showing the effect an increase in the thermal conductivity of the tube material has on the thermal gradient through the tube wall. Note that this assumes a constant coolant bulk temperature.

252

With a reduction in the inside tube wall temperature, the bulk hydrogen temperature (T_H) then decreases for constant heat flux thereby increasing engine efficiency. In the case of the 4-247 Stirling engine, however, the temperature drop across the tube wall is very small even with stainless steel tubes which have a relatively low thermal conductivity (k = 17 w/m-^{O}C). Therefore, changing the tubes to aluminum (k = 167 w/m ^{O}C) results in only a small drop in the bulk hydrogen temperature and very little increase in the engine efficiency for constant radiator top water temperature.

The metro-highway fuel economy figures were computed and found to be nearly the same (18.84 MPG and 18.85 MPG for conductivities of 17 and 167 c/m-^{O}C respectively).

2.8.4.3 Conclusions and Recommendations — Based on the results of the foregoing analysis, there is little justification for switching to aluminum cooler tubes on the basis of an increase in efficiency, and considering other factors such as strength and corrosion resistance, the stainless steel tubes may be the more suitable of the two.

2.8.5 Reduced Fuel During Warm-Up

2.8.5.1 Summary — The cold start fuel consumption is proportional to the amount of fuel required to raise the temperature of the hot section of the engine from ambient to steady state operating conditions. The method of calculating the cold start fuel consumption was added to the optimization routines, and those routines which generated net power engine maps. While the resulting numerical value is important when calculating fuel economy over a given driving cycle, use of this procedure in an effort to improve optimization results was inconclusive.

2.8.5.2 Analysis — Because the vehicle simulation computer programs calculate engine fuel requirements assuming a stabilized engine, a procedure was developed which added a certain quantity of fuel to the total consumed in the driving cycle. The chassis roll dynamometer cycle prescribes a test which is conducted in three parts:

ct = cold start transient (0-505 seconds)

s = cold start stabilized (505-1372 seconds)

ht = hot start transient (0-505 seconds)

The sequence of the cycle is illustrated as follows:

CVS-CH test

CT	s		10 MIN.	ht	
o	505	1372	SOAK	o	505
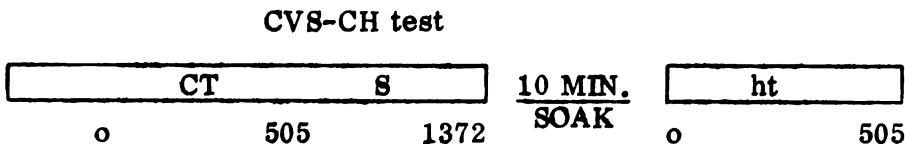
The CVS-CH fuel economy can be calculated from the fuel consumed for the three portions of the test as follows:

$$\text{CVS-CH (MPG)} = \frac{(7.5)(453.6)(6.18)}{.43F_{ct} + .57F_{nt} + F_s} \qquad \text{Eq. 2.8-2}$$

Where:

7.5	=	miles travelled during CVS-CH test
453.6	=	conversion factor, grams/pound
6.18	=	fuel density, pounds/gallon
F_{ct}	=	fuel used during cold start transient, grams
F_{ht}	=	fuel used during hot start transient, grams
F_s	=	fuel used during cold stabilized, grams
.43 & .57	=	factors derived from EPA test procedure

Based upon the 4-215 engine testing, it was reasonable to assume that the engine had reached steady-state hot conditions after the first 505 seconds. Therefore, the cold start fuel used could be added to the fuel used during hot start transient to yield the cold start transient fuel as follows:

$$F_{ct} = F_{ht} + \text{cold start fuel} \qquad \text{Eq. 2.8-3}$$

The CVS-CH fuel economy could therefore be calculated from CVS-HOT data by adding 43% of the engine warm-up fuel flow quantity to the fuel used during the hot start and cold stabilized bags.

The following table shows the calculations and results giving the amount of heat stored in the hot section of the 4-215 engine after reaching steady state conditions from 20°C ambient.

HEAT STORED IN 4-215 STIRLING ENGINE

	Volume (cm)^3	Density (g/cm^3)	Mass (kg)	C_p (J/kg°C)	T_1 (°C)	T2 (°C)	Q (kw-HR)
Heater Tubes	1075	8.23	8.85	540	750	730	.969
Cylinder & Reg. Ends	1034	8.23	8.31	538	700	680	.865
Cylinder & Reg. Walls	1642	8.23	13.51	542	375	355	.722
Regenerator Matrix	1124	8.23	3.52	542	375	355	.188
Preheater Matrix	5450	.72	3.92	1092	428	408	.485

HEAT STORED IN 4-215 STIRLING ENGINE

	Volume (cm)^3	Density (g/cm^3)	Mass (kg)	Cp (j/kg^{o}C)	T$_1$ (^{o}C)	T$_2$ (^{o}C)	Q (kw–HR)
Heater Head Insulation	7875	.192	1.51	1130	700	680	.322
Jacket Insulation	13596	.096	1.31	1130	426	406	.167
Preheater Cover & Other			10.0	460	150	130	.166

T$_1$ & T$_2$ = high and low values of the respective metal temperatures   3.88

Using these results, the heat-up fuel quantity can be calculated as follows:

Heat stored in engine	=	3.88 kW-hr
Heating value of fuel	=	43.9 kW-s/g
Assume heat system efficiency	=	0.90
The heat-up fuel required	=	$\frac{(3.88)(3600)}{(43.9)(.90)}$ = 354 g

Using these values, an example calculation for the 4-215 Stirling engine cold start penalty is as follows:

$$(.43) (354) = 152 \text{ g}$$

The above described cold start calculating procedure was added to the appropriate computer routines and used on a continuing basis in engine optimizations and fuel economy projections.

In an effort to identify potential fuel economy gains for the metro-highway driving cycle and during warm-up, an optimization was made having the metro-highway fuel economy as the function to be maximized. The cold start fuel penalty was included in this function in order to more fully account for the influence of this quantity on overall fuel economy.

Normally, the optimization process includes the possibility of specifying up to three (3) requirements to be met while maximizing the optimized function. For this case we picked full load power, and two (2) intermediate operating points specified by torque and speed. The speeds were selected as time weighted means of the speeds of 10 vehicle simulation speed/torque points for the baseline vehicle. The torques for each point were selected differently so that the resulting fuel flow at that speed-torque point would give the fuel consumption of the respective cycle when multiplied by the total cycle time as shown in the following table.

The selection of torque was based on the 4-215 engine map, and takes into account varying engine efficiency thus providing realistic values for the fuel consumption.

The three requirements for the optimization were:

CVS	— 114 Nm @ 1300 RPM	
Highway Torque	— 176 Nm @ 1700 RPM	} Indicated basis
Full Load Power	— 155 Kw @ 4000 RPM	

Fuel Consumed by 4-215 Engine for CVS-H and HWY Cycles

	CVS-H	HWY
4-215 Fuel Consumption — gram	1387	1410
Time — Seconds	1372	764
Fuel Flow Average — g/sec.	1.01	1.85
Weighted Mean Speed — RPM	1300	1700
Net Torque with Above Fuel Flow and Speed — Nm	57	120
Indicated Torque — Nm Based on 4-215 Accessories	114	176

[ ] Used in Optimization

The function to be optimized was developed as follows. The city (CVS) and highway fuel quantities were determined:

$$\text{City fuel consumption (CITYFU)} = \frac{QE(1) * 1372.}{.9 * 43.98 * 1000.} \qquad \text{Eq 2.8-4}$$

$$\text{Highway fuel consumption (HWYFU)} = \frac{QE(2) * 764.}{.9 * 43.98 * 1000.} \qquad \text{Eq 2.8-5}$$

Where QE (1) and QE (2) are the heats required for the city and highway speed/torque points respectively, .9 is the assumed burner system efficiency, 43.98 is the fuel heating value (kW-s/g), 1000 is for units conversion and 1372 and 764 are the respective cycle times (sec).

The cold-start penalty was added to the city fuel consumption to represent the CVS-CH fuel consumption:

$$\text{CHFUEL} = \text{CITYFU} + \text{FUEL (2)} \qquad \text{Eq 2.8-6}$$

Where FUEL (2) is based on the heater temperature at the highway speed/torque point. The miles per gallon for each cycle were then calculated.

$$\text{CITMPG} = 46.35/(\text{CHFUEL} * .002205) \qquad \text{Eq 2.8-7}$$

256

$$\text{HWYMPG} = 63.296/(\text{HWYFU} * .002205) \qquad \text{Eq 2.8-8}$$

The 45.35 and 63.296 factors represent the cycle miles times fuel density (lb/gal) and .002205 is the conversion from grams to pounds.

Finally, the function for the optimization was expressed as the M-H fuel economy.

$$F = \cfrac{1}{\cfrac{.55}{\text{CITMPG}} + \cfrac{.45}{\text{HWYMPG}}} \qquad \text{Eq 2.8-9}$$

This function, in conjuction with the two (2) intermediate load and full-load requirements, should be the best representation of the metro-highway fuel economy obtainable with the current optimization procedure and reasonable amount of computer time.

2.8.5.3 Results and Conclusions — An optimization of this type was run with the same constraints, engine length, engine diameter, materials, etc., as the fourth generation fuel economy assessment engine, 4-245 (see section 2.8.8). An engine map was made and the resulting fuel economy was actually slightly less than the 4-245 engine which was optimized by the "normal" part load technique (see Section 2.8.7).

The conclusion that can be made is that at this engine size and power nothing is to be gained by using the cold start penalty in the optimization. This is not to say that this procedure would not provide fuel economy gains in other engine and vehicle sizes or other engine configurations.

2.8.6 Heater Head Heat Flux

2.8.6.1 Summary — As part of the work originally outlined under the category of cycle analysis, an attempt was made to determine the effect of heater tube heat flux on metro-highway fuel economy. In this instance, heat flux is defined as the ratio of the total heat energy transferred to the working fluid to the total inside tube wall area.

The baseline engine used in this investigation was the original 4-215 engine with required accessories and drive. The vehicle simulation points mentioned in previous sections also remained unchanged.

2.8.6.2 Results and Conclusions — Initial plans called for reoptimizing the 4-215 engine at heat fluxes of 100,150, and 200 watts/cm^2, as compared to the baseline value of approximately 125 watts/cm^2. At flux levels at other than the baseline value the optimization program initially failed to produce convergent runs. After rewriting various routines to improve the linkage of heat flux to other cycle parameters, fully converged cases were obtained. However, the majority of the results obtained were judged to be of questionable value because the number of heater tubes and heater tube dimensions resulting were such that construction of the heater head would be next to impossible utilizing tubes with practical wall thicknesses, bend radii, etc.

Because of the seeming inability of the program to fully include the effects of heater tube heat flux, further effort on this subject was abandoned until such time as a more appropriate analysis technique could be developed and added to the existing routines.

2.8.7 Part-Load Optimization

2.8.7.1 Summary — With the information obtained from the regenerator heat conduction study, it was decided to revise the computer optimization program in order to bias the engine design at some intermediate operating point while still satisfying the full-load design conditions. Also included in this revised optimization was the reduced power required to match baseline vehicle performance (0-60 MPH time of 13.3 seconds at 4500 lb. IWC). In addition, the reoptimized engine was allowed to be as large as the base 4-215 engine, with the intention of realizing some of the benefits associated with lower specific power engines.

2.8.7.2 Analysis — The beginning points for starting the reoptimization were defined as follows:

P_{IND} = 146.5 kW (full load)

Length = 306 mm ⎫

O.D. = 428 mm ⎭ same as 4-215 engine*

$Tube_{Flux}$ = 125 W/cm^2

Top Water Temperature = 50°C

T_{ED} = 750°C (Heater tube inside wall temperature)

* See Figure 2.8-7 for explanation.

Figure 2.8-8 schematically shows a hypothetical engine speed/torque map indicating those points which were of interest in the part-load reoptimization. The definition of the points shown in figure are as follows:

Full Load (FL) = Point at which the engine maximum power and maximum allowable flux requirements are calculated.

Maximum Torque (MT) = Point of maximum engine torque, and characteristically the point of highest engine efficiency.

Metro-Highway (M-H) = Point representing a speed and torque weighted mean of the CVS-CH and HWY driving cycles. Its approximate location with respect to the torque converter stall and road-road curve is given in Figure 2.8-8.

Figure 2.8-9 is a representation of how the M-H composite point was calculated.

The procedure may not be statistically correct, but nevertheless it is a means by which to condense the total number of M-H points in order to arrive at some part-load point on which to optimize efficiency. For the 4500 lb. IWC vehicle under consideration, the results were:

Speed   =   1475 RPM

Torque   =   127 NM (Net)

    =   175 NM (Indicated)

As arranged, the optimization was conducted on indicated quantities.

Although the M-H composite point was substantially more representative of normal engine operation than either the MT or FL point, it was a poor point on which to solely base an optimization. Engine maximum power and heater tube flux had to be checked at the FL point. The MT point could be useful in designing an engine for steady-state operation only, if maximum overall efficiency was required at that point.

For the reoptimizations discussed here maximum engine power and flux were requirements to be calculated at the FL point, and engine efficiency was maximized either at MT or MH. Engine length was also a requirement in many cases, but was not dependent on where the optimization point was, depending only on geometry. Geometric fitting relations constraining engine outside diameter and length were also included in the reoptimization to insure that resulting engine dimensions were compatible and realistic. For the purpose of this series of reoptimizations, a fixed burner system efficiency of 86.5 percent was assumed, as well as equal heat transfer numbers for the first and second heater cage passes. These assumptions were valid only for the FL operating point, and were somewhat conservative at the MH or MT points.

Figure 2.8-10 summarizes those part-load reoptimization runs which resulted in the 4-247 engine design. Those parameters indexed with subscript 1 refer either to the MH or MT point, and those with subscript 2 refer to the FL point. An explanation of some of the other quantities in Figure 2.8-10 are as follows:

LOC_i	:	The location of that operating point;
$AREV_j = \%AREV_i$	:	The speed at operating point j was a constant percentage of the value of the speed at operating point i;
$PRM_j = PRM_i$	:	Mean engine pressure at point j equals the mean pressure at point i;
$AREV_i = V.$	:	Engine speed at point i is a variable quantity during the optimization;
$PRM_j = \dot{V}*PRM_i$	:	Mean pressure at point j equals mean pressure at i times a variable quantity;

η_i	:	The engine efficiency at point i, including safety factors of 5% and 2% on P_{ind} and QE respectively;
REQ	:	This indicates the number and nature of the stated requirements in effect during that particular reoptimization. For example:

KW_i — a power requirement

L — a length requirement

W/CMi^2 — a flux requirement

NM_i — a torque requirement;

CONV	:	When convergence is indicated, it represents the situation where the stated requirements are met within a certain degree of accuracy and the function to be optimized (maximized) cannot be improved.

For most of the runs summarized in Figure 2.8-10, an attempt was made to formulate a stable relationship between the full and part-load points. This amounted to expressing speed and pressure at the other point using several different techniques. Runs A through I used the approximate MT point of the engine on which to base the efficiency calculation, and runs J through M used the MH composite point. For runs F through M, the requirement for heater head flux at FL was "built-in" in such a way as to insure that a maximum flux would not exceed 125 w/cm^2. For the final runs, a torque requirement corresponding to the MH speed was added.

2.8.7.3 Results — Figure 2.8-11 shows the theoretical performance map of the 4-215 engine. Figure 2.8-12 gives the analytical projection for the 4-215 Stirling engine fuel economy. This can be compared to the projected fuel economy of the 4-247 engine listed in Figure 2.8-13. The reduced power and part-load optimization technique improved the projected fuel economy by 2.1 MPG.

The first part-load optimization showed the technique to be a particularly powerful tool in Stirling engine design for automotive application. Use of the part-load technique will tend to result in an engine better suited to perform efficiently in a specific application.

2.8.8 Fourth Generation Fuel Economy Assessment Engine — This portion of section 2.8 addressed three (3) main areas of interest regarding the fourth generation engine design. Included were the projected engine torque characteristics, engine optimization and design, and the effect of power reduction on engine characteristics.

2.8.8.1 Torque Requirement — Figure 2.8-14 depicts engine net torque vs. speed for the projected fourth generation engine for two (2) 0-60 MPH acceleration times. The following table gives the numerical values for the torque as well as the accel times.

Fourth Generation Engine Torque Requirements

Engine Speed	Engine Torque (ft/lbs) For 12.15 Sec. 0-60 MPH Acceleration-PB1111 Projected	Engine Torque for 12.60 Sec. 0-60 MPH Acceleration PB1111 Projected
600	302.4	202.4
1000	315.2	304.8
1500	308.4	298.2
2000	303.5	293.4
2500	285.7	276.4
3000	266.4	257.6
3500	245.9	237.7
4000	220.3	213.1
4500	192.9	186.5

Also shown in Figure 2.8-14 are the torque vs. speed characteristics of the current fourth generation engine design (4-247C) and the 1977 351M I.C. engine. It is evident that the current fourth generation engine falls short of the projected torque level.

A new optimization procedure was initiated to increase the power and meet the torque requirements shown in Figure 2.8-14. At the same time other changes, which will be discussed later, were incorporated. The new torque projections resulting from this optimization are given in the following table, and shown in Figure 2.8-15. The resulting engine has been designated the 4-245, and will be discussed in detail later.

Revised Fourth Generation Engine Torque Requirements

Engine Speed (RPM)	Engine Torque (ft-lbs) For 13.0 Sec. 0-60 MPH Acceleration-PB1111 Projected	Engine Torque (ft-lbs) For 13.5 Sec. 0-60 MPH Acceleration-PB1111 Projected
600	322.0	312.0
1000	331.2	326.0
1500	333.7	322.5
2000	317.4	307.6
2500	292.6	283.5
3000	365.1	256.9
3500	232.5	225.3
4000	197.0	190.0
4500	156.4	151.6

Vehicle 0-60 acceleration times may be altered by changing the first to second gear shift speed of the automatic transmission. With the 4-247 Stirling engine map, increasing the first to second gear shift speed would result in lower 0-60 MPH acceleration times (improve performance). However, with the shape of the current fourth generation Stirling engine curve (preliminary) it was found that the optimum 0-60 MPH acceleration shift speed was the same as that specified for the baseline vehicle.

261

2.8.8.2 Fourth Generation Engine — The basic assumptions included in the fourth generation engine design are as follows:

- Heater head diameter and overall heater head length — same as the 4-215;

- Preheater design — identical to the 4-215 except for thin wall core, and mechanically driven;

- Drive system — swashplate type, same concept as the 4-215;

- Seals — rollsocks;

- Hydrogen compressors — one, externally driven;

- Burner — same as the 4-215 (including operating conditions, e.g., 30% excess air, standard EGR curve, and 750°C inside heater tube wall temperature).

2.8.8.2.1 Analysis — From the full-load net power curve for the 351M engine, the maximum power developed was found to be 124kW at 4000 RPM. It was from this point that the indicated full-load power point for the new engine was established. Using auxiliary and accessory losses from previously designed engines, the total full-load loss for the new engine was estimated to be 52 kW. Hence, the new engine's indicated full-load power point, at 4000 RPM, was determined to be 52 + 124 = 176 kW.

This full-load indicated power requirement, combined with the part-load torque speed requirement (175 Nm at 1475 RPM) and the heater head length requirement (302 mm) became the basis for engine optimization runs designed to maximize the part load point efficiency.

After eight optimization runs, (all of which led to engines which met the above three requirements while maximizing part-load efficiency), a satisfactory engine design was attained. The resulting engine had a swept volume of 267 cm^3 per cylinder and a part-load indicated efficiency of 48.6%. Using the optimization information from the engine (now designated as the 4-267) an engine map was created yielding full-load power. Upon comparison of the full-load curves of the 4-267 and the 351M, it could readily be seen that the 4-267 was overpowered. Hence, a second series of optimizations based upon a scaled down version of the 4-267 engine's full-load torque curve was undertaken. Using the scaled down torque curve (a curve with a shape identical to that of the 4-267 4-267 but scaled down sufficiently to produce the vehicle performance desired) a new net power of 108 kW at RPM was found to be required. The new power of 108 kW translated to an indicated power of 155 kW. By using this value of 155kW as our new requirement for full-load power at 4000 RPM, (and keeping the other two requirements unchanged), two more optimizations were performed before finally achieving a satisfactory engine.

2.8.8.2.2 Results — The final engine resulted in a swept volume of 245 cm^3 per cylinder and a part-load indicated efficiency of 49.4%. Prior to creating an engine map, the heater tube fins were sized using the newly developed fin optimization routine. This routine used the burner program in an optimization

procedure enabling heater tube fin geometry to be optimized. The heater tube geometry that resulted was as follows:

Number of tubes:	16
Tube O.D.:	7.2 mm
Tube I.D.:	4.8 mm
Fin thickness:	.50 mm
Fin width:	9.65 mm
Fin length:	14.48 mm

Some of the engine's more important design parameters are summarized in the following table.

Fourth Generation Engine Design Parameters

Indicated Efficiency	(1475 RPM, 92.5 Kg/cm^2)	49.35%
Max. Power (net)	(3300 RPM, 200 Kg/cm^2)	114 kW (153 HP)
Max. Torque (net)	(1000 RPM, 200 Kg/cm^2)	444 Nm
No. of Cylinders		4
Swept Volume/Cylinder		245 cm^3
Heater Head Length		302 mm
Heater Head Diameter		428 mm
Piston Diameter		83.43 mm
Stroke		44.79 mm
No. of Cooler Tubes/Cylinder		830
No. of Heater Tubes/Cylinder		16
Max. Heater Tube Heat Flux		158 w/cm^2
No. of Regenerator/Cylinder		2
Regenerator Length		80.61
Regenerator Diameter		64.49 mm
Dead Volume		3.68% of swept at full load
		175% of swept at part load

Using the above information, as well as parameters relating to engine drive, etc., a complete engine map was generated and is shown in Figure 2.8-16.

Figure 2.8-17 shows the 4-245 engine's performance with respect to the torque requirements of a 4500 lb IWC vehicle having 0-60 MPH acceleration times of 13 and 13.5 seconds. Also shown is the current 4-215 engine performance.

Because of its higher power, the 4-215 curve lies above the other curves in the higher speed range.

The metro-highway fuel economy predicted for the 4-245 engine in a 4500 lb IWC vehicle was 21.75 MPG (see Figure 2.8-18). The fuel economy for the 4-215 in a 4500 lb IWC vehicle was 16.05 MPG, as is displayed in Figure 2.8-12. It should be noted that both of these M-H fuel economy numbers are theoretical results and are not representative of vehicle chassis roll tests. The substantial improvement of the 4-245 over the 4-215 can be attributed to the fact that the 4-245 incorporates the engine improvements contained in the analytical studies on fuel economy gains. These fuel saving improvements are classified as shown below:

Cycle Analysis

. Lower power requirement — the 4-245 engine was designed to have a maximum indicated power (155 kW) much lower than that of the 4-215 (189 kW).

. Thermal conduction loss reduction and part-load optimization — the indicated efficiency for the 4-215 was optimized at the full-load point rather than at a part-load point as was the case for the 4-245. It was found that by forcing the Stirling optimization to reduce regenerator heat conduction losses at part-load and sacrificing some full-load efficiency, gains in efficiency could be made at part-load in the driving cycle ranges.

. Aluminum cooler tubes — the cooler tubes for the 4-245 are aluminum, enabling lower hydrogen temperature, especially at full power, and thus slightly higher engine efficiency than could be previously obtained from the stainless steel tubes of the 4-215 engine.

. Dead volume — the optimization of the 4-245 included for the first time as an optimization variable, the selection of the amount of dead volume to be added to the compression space. (The addition of the proper amount of dead volume has been previously shown to increase efficiency. See section 2.6.)

Preheater System

. Thin wall preheater core — the 4-245 engine uses a thin wall material preheater core, resulting in higher burner system efficiency.

. Preheater core drive — 4-245 uses a mechanically driven core, rather than the previously used electrically driven design, which reduces the alternator load.

External Heat and Blower System — Blower drive ratio — In general, net efficiency of the 4-245 engine is higher than that of the 4-215. Hence, the 4-245 requires less fuel flow and air flow than the 4-215. This reduced air flow demand enables the use of a smaller blower drive ratio which results in reduced blower power consumption.

Accessories:

- Fuel pump — The 4-245 fuel pump is mechanically driven for reduced alternator load.

- Air assist pump — The 4-245 air assist pump is also mechanically driven.

- Alternator — The 4-245 uses a 60 Amp alternator (as opposed to the previously used 105 Amp).

- External compressor — The 4-245 engine incorporates use of an external compressor rather than two internal compressors per cylinder.

A detailed description of the accessory powers used in the fourth generation engine (4-245) analysis are as follows, where P = power in kW, and RPM = engine speed (see Figures 2.8-19 and 2.8-20 for plots of expressions):

1) Mechanically driven fuel pump   Eq 2.8-10

$$P = 1.43265\text{E-}06 + 1.15687\text{E-}06 \cdot \text{RPM} + 7.61263\text{E-}10 \cdot \text{RPM}^2$$
$$-3.23713\text{E-}13 \cdot \text{RPM}^3 + 6.52957\text{E-}17 \cdot \text{RPM}^4 - 3.78518\text{E-}21 \cdot \text{RPM}^5$$

2) Mechanically driven air assist pump   Eq 2.8-11

$$P = 3.57144\text{E-}05 + 1.12746\text{E-}05 \cdot \text{RPM} + 2.33729\text{E-}08 \, \text{RPM}^2$$
$$-1.44922\text{E-}11 \cdot \text{RPM}^3 + 3.36633\text{E-}15 \cdot \text{RPM}^4 - 2.72025\text{E-}19 \cdot \text{RPM}^5$$

3) Mechanically driven preheater   Eq 2.8-12

$$P = 52.8765 \cdot \text{RPM}^2 \cdot (3.1416) \cdot 1.224\text{E-}07$$

4) 60 Ampere alternator

   Car Accessory load = 44.5 Amps

   Engine electrical load: (similar to the latest 4-215 engine's electrical load)

Ignition box	1.5 Amps
Electronic control box	1.5 Amps
Hydraulic/electric governor	0.1 Amps
Fuel Safety valve	3.0 Amps
Safety relay	0.5 Amps
Vortair fuel metering electronics, fuel injectors	1.0 Amps
Accessory relay	1.0 Amps

Blower and EGR Throttle
valve control motor   0.4 Amps

Total engine electrical load   9.0 Amps

Total car and engine   =   44.5 + 9.0 = 53.5 Amps.

BLOWRAT = NBLPR/(RPM*100) where: Eq. 2.8-15
BLOWRAT = New blower drive ratio
NBLPR   = New reduced blower power, with

$$NBLPR = \begin{cases} = 4.75*(RPM/100) \text{ for } RPM \leq 1600 \\ = 13.29413 + 6.902467 \cdot \dfrac{RPM}{100} - .0873352 \cdot \dfrac{RPM^2}{100} \\ \quad + .0002823 \cdot \dfrac{RPM^3}{100} \text{ for } RPM > 1600 \end{cases}$$

Eq. 2.8-16

2.8.8.3 Full Load Power Reduction — The 4-245 engine (see preceding section) had a lower specific power than the 4-215 because the 2-245 engine was optimized at a lower maximum power than the 4-215 engine but with the total volume of the engine kept the same as the 4-215. Since the lower specific power and part-load optimization technique were both influencing the improved efficiency of the 4-245, it was of particular interest to evaluate the effect of the lower specific power alone.

2.8.8.3.1 Analysis — For evaluation of the lower specific power of the 4-245 compared to the 4-215, an optimization was carried out for an engine which had all the 4-245 features but was similar to the 4-215 in maximum power output. The only change was that the optimization utilized the part-load technique. The results of the optimization was an engine with 270 cm^3 displacement per cylinder designated the 4-270B are shown in Figure 2.8-21.

2.8.8.3.2 Results — The results of this study demonstrate that by employing all of the fuel saving refinements outlined for the 4-245 engine except reduced maximum power, a 0.4 MPG reduction in fuel economy is projected. Hence power reduction in the 4-215 size engine accounts for 0.4 MPG out of a total of 5.7 MPG.

It should be emphasized that the effect of specific power reduction for other sized engines may not follow the same trend.

2.8.9 Other Cycle Analysis Work

2.8.9.1 Summary — In addition to the preceding cycle analysis items, two (2) other main areas of investigation were included, covering the areas of heater head temperature scheduling and the 302 CID equivalent engine.

2.8.9.2 Temperature Scheduling — By outlining a control schedule that kept the Stirling engine operating at a heater tube inside wall temperature giving maximum efficiency at each load point, it was felt some potential gain in fuel economy could

be made. An analytical study was performed on the 4-215 Stirling engine to identify this gain. Some related testing was also performed on the actual engine; this was reported in section 2.1.

2.8.9.2.1 Analysis — Calculations of fuel flow for the 4-215 engine at the ten simulation points for hydrogen temperatures from 450°C to 850°C were made and are shown in Figure 2.8-22. The minimum fuel flow point moves lower because the conduction losses through the regenerator and cylinder walls represent a much larger proportion of the total losses at low loads. At low loads the conduction losses fall off faster, with decreasing temperature, than the semi-adiabatic cycle efficiency, and this results in a net increase in indicated cycle efficiency. Just the opposite is true at higher loads.

The optimum temperature schedule would pass through each speed/torque curve at minimum fuel flow. Within the 450°C-850°C range the resulting schedule would be Schedule A as shown on Figure 2.8-23. Based on this schedule and the cold start penalty associated with the highest temperature in the schedule a metro-highway fuel economy gain of .27 MPG over the 4-215 baseline (700°C constant hydrogen temperature) could be realized.

A more realistic schedule would be Schedule B as shown on Figure 2.8-23. This schedule varies the temperature through the minimum fuel flow points between 650°C-750°C, and results in a analytically predicted metro-highway fuel economy improvement of .14 MPG.

Maximum fuel economy using a constant temperature control (any vertical line on Figure 2.8-22) occurs at 700°C hydrogen temperature (approximately 750°C inside tube wall temperature). The fuel economy falls off either side of this point as shown in Figure 2.8-24. The fuel economy in Figure 2.8-24 includes the appropriate cold-start fuel penalty.

The reduction in fuel economy due to a temperature distribution that forced running 50°C below the maximum point would be .09 MPG and for 100°C below maximum the fuel economy decrease would be .27 MPG.

2.8.9.2.2 Results and Conclusions — Based on schedule A in Figure 2.8-23 and the cold-start penalty associated with the highest temperature in the schedule, an M-H fuel economy gain of .27 MPG over the 4-215 baseline (700°C constant hydrogen temperature) could be realized. However, a schedule of this range would not be entirely practical for two reasons. First, the inside tube wall temperature would be 900°C which would significantly shorten their life. Second, such a schedule would be difficult to maintain throughout transient engine operation.

2.8.9.3 302 CID Equivalent Engine — A preliminary investigation was made to check the effect of making certain components interchangeable with the 4-215 and to investigate changes in various parameters in a Stirling engine with approximately 302 CID IC engine performance (302 equivalent).

For this preliminary study, vehicle simulation points previously selected for a 4000 pound IWC vehicle with a C4 automatic transmission and 2.75 axle ratio were used.

267

2.8.9.3.1 Analysis — Using the method shown in Figure 2.8-9, the weighted mean of the cycle points was calculated to use as the part-load point for the 302 equivalent optimizations. The resulting part-load point was:

Speed	=	1550 RPM
Net Torque	=	122 Nm
Indicated Torque	=	167 Nm

The maximum power requirement was selected based on 302 engine performance. The requirement used for most of the optimizations were:

Speed	=	3600 RPM
Net Power	=	93 kW
Indicated Power	=	131 kW

2.8.9.3.2 Results — Figures 2.8-25 and 2.8-26 describe the results of the 4-215, the 4-245, and 302 equivalent optimized engines. A description of the objectives, unique features and constraints for each optimization is as follows:

4-215 — This engine was optimized at maximum power (4000 RPM and approximately 190 kW indicated) by Philips to meet 351 CID IC engine performance. The engine was sized to package in a 1975 Torino.

4-245 — This engine was optimized by the part-load technique with the same heater head length (302 mm), diameter (428 mm) and maximum mean pressure (200 atm) as used in the 4-215 engine. It also was designed to meet a 0-60 MPH performance of 13.3 seconds. Also, the part-load dead volume was allowed to vary but it was assumed to be switched off at full-load. This was the resulting fourth generation fuel economy assessment engine.

The following results for the 302 equivalent engine optimizations are referenced by alphabet characters to those listed in Figures 2.8-25 and 2.8-26:

A — This engine was optimized by the part-load technique at the part-load point and maximum indicated power requirement of 131 kW. The stroke and cylinder bore center distance was fixed to make the drive interchangeable with the 4-215 drive. Also, the heater head length was required to be the same as the 4-215 (302 mm), the diameter was constrained to 428 mm maximum and the full-load mean pressure was fixed at 200 atm. The part-load dead volume was allowed to vary.

B — This optimization was performed in essentially the same manner as the 4-245 engine but at the part-load point and maximum indicated power requirement of 141 kW. The heater head length was required to be the same as the 4-215, the diameter was constrained to 428 mm maximum and the full-load pressure was fixed at 200 atm. However, in this optimization the stroke and cylinder bore center distance were allowed to vary. Also, the part-load dead volume was allowed to vary.

C and D — Same as A and B, but the engine length was allowed to vary.

E and F — Same as A and B, except no add-on dead volume was allowed at part or full load.

G and H — Same as A and B, except the add-on dead volume had to be the same amount throughout the total operating range of the engine, i.e., no dead volume control.

I — Same as A, but the heater tube cage diameters were held the same as the 4-215 to make the preheater. The cooler was kept the same as the 4-215.

J and K — Same as A and B, except the maximum power requirement was taken at 4500 RPM instead of 3600 RPM.

L and M — Same as A and B, but the full-load pressure was allowed to vary.

N — Similar to case B but with the heater head temperature increased to 850°C.

O — The part-load optimization was done at idle conditions.

P — Engine optimized at reduced dimensions in an attempt to look at a scaled engine for packaging considerations.

Q — Similar to case I but at a reduced power level and a redefinition of the heater head insulation thickness and heater tube crossover connection.

R — Similar to case Q but with maximum pressure reduced to 150 atm.

S — Similar to case Q but heater head length reduced by 1.5 inches.

T — Similar to case Q but heater head length reduced by 1.5 inches and maximum temperature increased to 800°C.

U — Similar to case Q but shorter heater head length and maximum pressure reduced to 150 Atm. and max. temperature increased to 800°C.

V — Similar to case S but maximum pressure reduced to 150 atm.

To make preliminary projections for the 302 equivalent engine a map was made of optimization B using the same accessory curves as for the 4-245. Figure 2.8-27 shows a plot of WOT torque for the 302 IC and the preliminary 302 equivalent (4-228). As can be seen, the 302 equivalent is somewhat overpowered.

2.8.9.3.3 Conclusions — Optimization B provides a slight indicated efficiency advantage over the 4-245 due to the lower power required.

Making the 302 equivalent drive interchangeable with the 4-215 (optimization A compared to B) costs 0.8% in part load indicated efficiency (▲ 0.4 MPG). And making the preheater interchangeable and using the same cooler (optimiza-

tion I compared to A) costs an additional 0.5% in part load indicated efficiency (Δ 0.3 MPG).

This is a relatively small fuel economy penalty to pay for the added flexibility of interchangeability with 4-215 hardware.

The benefit of add-on dead volume which is closed off for maximum power can be seen by comparing optimizations A and B to E and F, respectively. This benefit is 1.1% in part load efficiency (Δ 0.5 MPG). Add-on dead volume without the switchover is of no benefit as can be seen by comparing optimizations E and F to G and H.

The improvement in part load indicated efficiency coming from additional length (optimizations C and D) is more than offset by the additional cold start penalty.

Also, there is no significant improvement as a result of changing the full-load speed point (optimizations J and K) or by varying the full-load pressure (optimizations L and M).

Case U has the advantage of good indicated efficiency at part load and a low cold start penalty. Whether the cylinder and regenerator housings can be designed to take advantage of the reduced pressure at 50°C higher temperature by reducing the wall thickness will require more detailed analyses. Because of the higher heater head temperature and the freedom to reduce thermal conduction losses, the resulting engine had thinner reg/cyl walls than Case R.

2.8.10 Cycle Analysis Conclusion — Using the part-load optimization in lieu of the previous maximum power optimization which was used on the 4-215 engine, significant fuel economy gains were projected for the driving cycles. Included in the fuel economy improvement was the effect of reducing the maximum power level from 179 HP to 153 HP for the required performance in a 1977 4500 lb. IWC vehicle. Based upon the input from cycle analysis and other sections, a fourth generation fuel economy assessment engine (4-245) resulted. The 4-245 engine showed a theoretical improvement of 5.7 MPG over the baseline 4-215 engine on the M-H composite cycle. Of this 5.7 MPG improvement, 3.34 MPG was directly credited to cycle analysis and the improvements in the computer optimization. The remaining 2.36 MPG improvement is the result of work in other areas which could be theoretically incorporated into an engine map. Other engine or cycle improvements beyond those included in the 4-245 engine projection can be additive to the 5.7 MPG as an incremental improvement.

270

METRO-HIGHWAY FUEL ECONOMY SUMMARY FOR 4-270 ENGINE PREPARED ON 2 DEC 1977
BASED ON ENGINE MAP DATA FILE W270.02 AND M-H DATA FILE MH27045A (4500 LB. INC VEH.)

THESE RESULTS ARE BASED ON A VEHICLE ENGINE WITH STEERING AND FAN LOSSES INCLUDED

M-H PT	SPEED RPM	TORQUE NM	POWER KW	PRESS ATM	FUEL G/S	CITY SEC	CITY GRAM	Z TOT CITY	HWAY SEC	HWAY GRAM	Z TOT HWAY	ICARE
1	360.000	67.800	2.698	41.163	0.436	292.560	127.696	10.073	3.000	1.309	0.119	<
2	600.000	128.800	8.093	57.756	0.749	215.480	161.493	12.739	12.270	9.196	0.835	<
3	750.000	101.700	7.987	48.767	0.785	491.610	385.832	30.434	51.460	40.388	3.669	<
4	900.000	216.900	20.442	86.533	1.460	169.860	248.050	19.566	32.190	47.008	4.270	<
5	1000.000	-6.800	-0.712	15.739	0.442	43.000	19.017	1.500	93.000	41.130	3.736	<
6	1100.000	155.900	17.958	66.622	1.396	33.880	47.292	3.730	292.890	408.836	37.140	<
7	1200.000	318.600	40.036	123.706	2.640	57.490	151.749	11.970	43.620	115.138	10.459	<
8	1350.000	176.300	24.924	75.199	1.858	68.130	126.619	9.998	235.570	437.806	39.771	<

TOTAL CVS-H FUEL CONSUMPTION = 1267.7481 GRAMS
CVS-H FUEL ECONOMY = 16.5809 MPG
COLD START FUEL PENALTY = 166.0000 GRAMS
TOTAL CVS-CH FUEL CONSUMPTION = 1433.7481 GRAMS
CVS-CH FUEL ECONOMY = 14.6612 MPG
TOTAL EPA HWY FUEL CONSUMPTION = 1100.8103 GRAMS
EPA HWY FUEL ECONOMY = 26.0769 MPG

HWAY
====
* TOTAL H-H FUEL ECONOMY = 18.2579 MPG *

CITY
====
TOTAL POSITIVE ENGINE WORK = 5.416 HP-HR
TOTAL NEGATIVE ENGINE WORK = -0.011 HP-HR
NET ENGINE WORK = 5.405 HP-HR
NET OVERALL EFFICIENCY = 26.024 PCT.

HWAY
====
TOTAL POSITIVE ENGINE WORK = 5.235 HP-HR
TOTAL NEGATIVE ENGINE WORK = -0.025 HP-HR
NET ENGINE WORK = 5.210 HP-HR
NET OVERALL EFFICIENCY = 28.892 PCT.

Figure 2.8-1   Metro-Highway Fuel Economy Summary

4-270 Stirling Engine (2500 RPM)
4500 lb. IWC Vehicle
2.0 Axle Ratio
C4 Automatic Transmission (2.46, 1.46, 1.00 gear ratios)
60 K Torque Converter (13" Dia.)
Front Transmission Pump
No Accessories
VSIM Computer Program

Simulation Point	Engine Speed (RPM)	Engine Torque (ft-lb)	CVS-H Time (s)	EPA-HWY Time (s)
1	380	50	292.56	3.0
2	600	95	215.48	12.27
3	750	75	491.61	51.46
4	900	160	169.86	32.19
5	1000	-5	43.0	93.0
6	1100	115	33.88	292.89
7	1200	235	57.49	43.62
8	1350	130	68.13	235.57

Figure 2.8-2   Fourth Generation Low Speed Vehicle Simulation Points

METRO-HIGHWAY FUEL ECONOMY SUMMARY FOR 4-204 ENGINE PREPARED ON 2 DEC 1977
BASED ON ENGINE MAP DATA FILE W204.01 AND M-H DATA FILE NM215.45 (4500 LB. INC VEH.)

THESE RESULTS ARE BASED ON A DYNAMOMETER ENGINE WITH STEERING AMP FAN LOSSES EQUAL TO ZERO

M-H PT	SPEED RPM	TORQUE NM	POWER KW	PRESS ATM	FUEL G/S	CITY SEC	CITY GRAM	Z TOT CITY	HIWAY SEC	HIWAY GRAM	Z TOT HIWAY	ICASE
1	600.000	53.180	3.341	41.902	0.475	384.700	182.820	15.553	10.500	4.990	0.404	4
2	800.000	40.700	3.410	35.892	0.517	202.800	104.789	8.915	5.100	2.635	0.213	4
3	900.000	-6.780	-0.639	14.102	0.339	115.000	39.032	3.321	56.000	19.007	1.537	2
4	1000.000	67.840	7.104	47.931	0.734	184.700	135.552	11.532	11.400	8.367	0.677	4
5	1100.000	108.540	12.503	67.929	1.027	202.400	207.838	17.682	13.200	13.555	1.096	4
6	1300.000	156.020	21.240	92.875	1.523	120.600	183.640	15.623	20.300	30.911	2.500	4
7	1600.000	203.510	34.098	119.910	2.289	37.800	86.518	7.361	32.800	75.074	6.071	4
8	1700.000	108.540	19.323	70.304	1.512	58.000	87.715	7.462	311.000	471.542	38.133	4
9	1800.000	217.080	40.919	129.119	2.733	25.300	69.136	5.882	33.600	91.817	7.425	4
10	2000.000	122.110	25.575	79.258	1.926	40.700	78.387	6.669	269.300	518.663	41.944	4

```
TOTAL CVS-H FUEL CONSUMPTION = 1175.4263 GRAMS
            CVS-H FUEL ECONOMY =   17.8832 MPG
        COLD START FUEL PENALTY =  161.3000 GRAMS
TOTAL CVS-CH FUEL CONSUMPTION = 1336.7263 GRAMS
           CVS-CH FUEL ECONOMY =   15.7253 MPG
TOTAL EPA HWY FUEL CONSUMPTION = 1236.5600 GRAMS
           EPA HWY FUEL ECONOMY =   23.2141 MPG
```

* TOTAL M-H FUEL ECONOMY = 18.3758 MPG *

CITY
====
```
TOTAL POSITIVE ENGINE WORK =  4.793 HP-HR
TOTAL NEGATIVE ENGINE WORK = -0.027 HP-HR
         NET ENGINE WORK =  4.766 HP-HR
NET OVERALL EFFICIENCY = 24.748 PCT.
```

HWAY
====
```
TOTAL POSITIVE ENGINE WORK =  6.010 HP-HR
TOTAL NEGATIVE ENGINE WORK = -0.013 HP-HR
         NET ENGINE WORK =  5.997 HP-HR
NET OVERALL EFFICIENCY = 29.603 PCT.
```

Figure 2.8-3   Metro-Highway Fuel Economy Summary

273
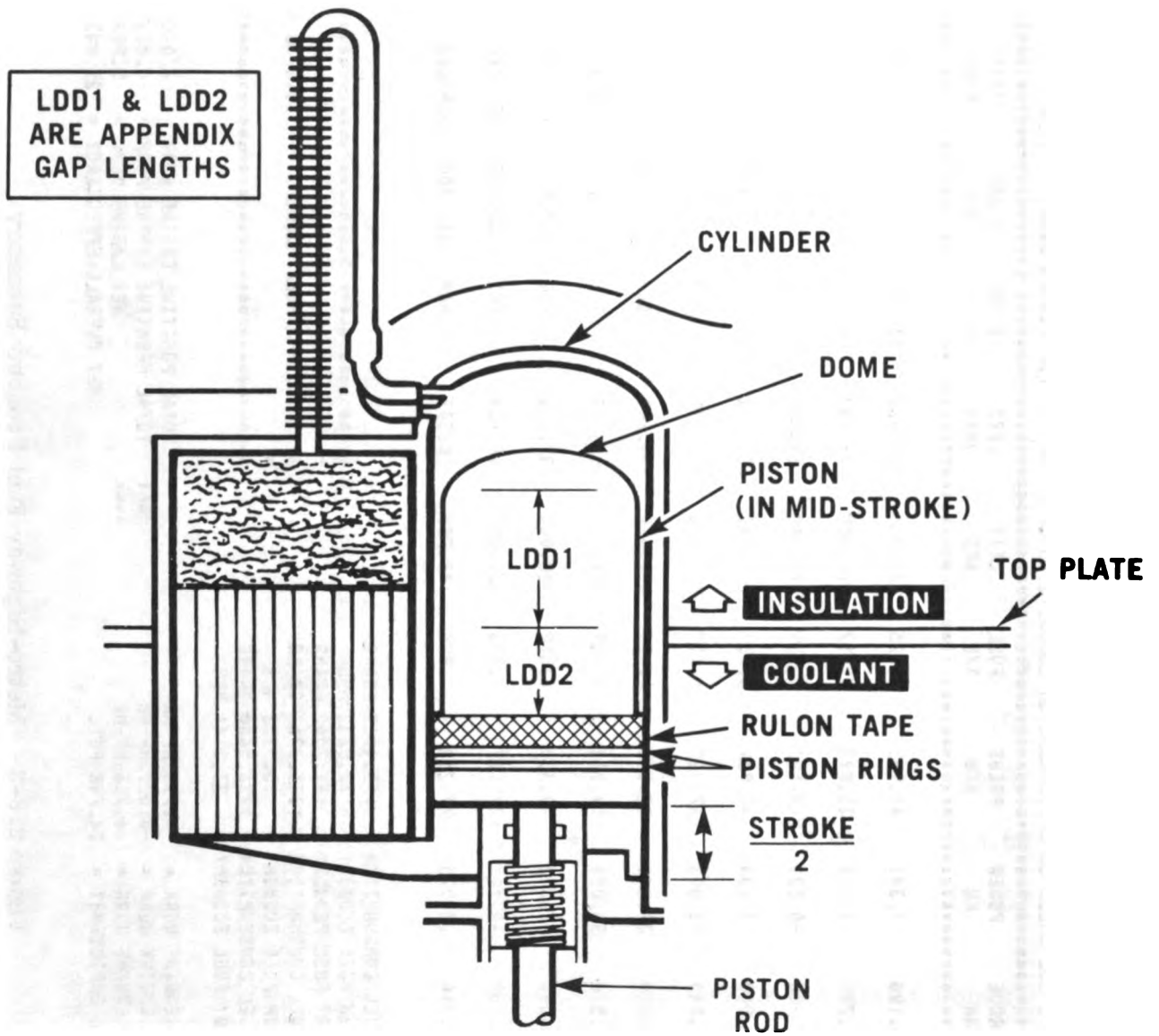
Figure 2. 8–4   Appendix Gap Length Diagram
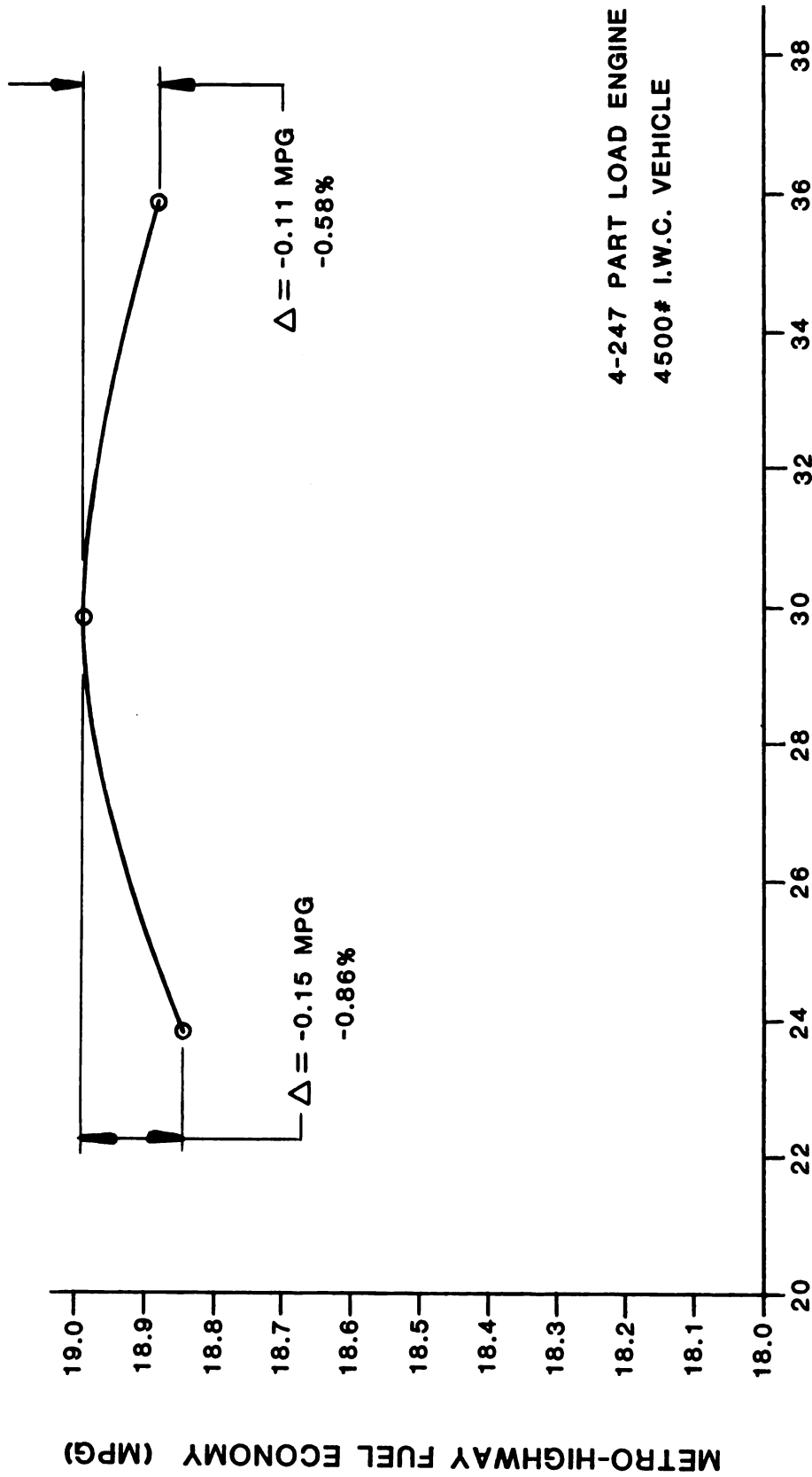
Figure 2.8-5   Metro-Highway Fuel Economy vs. Appendix Gap Length
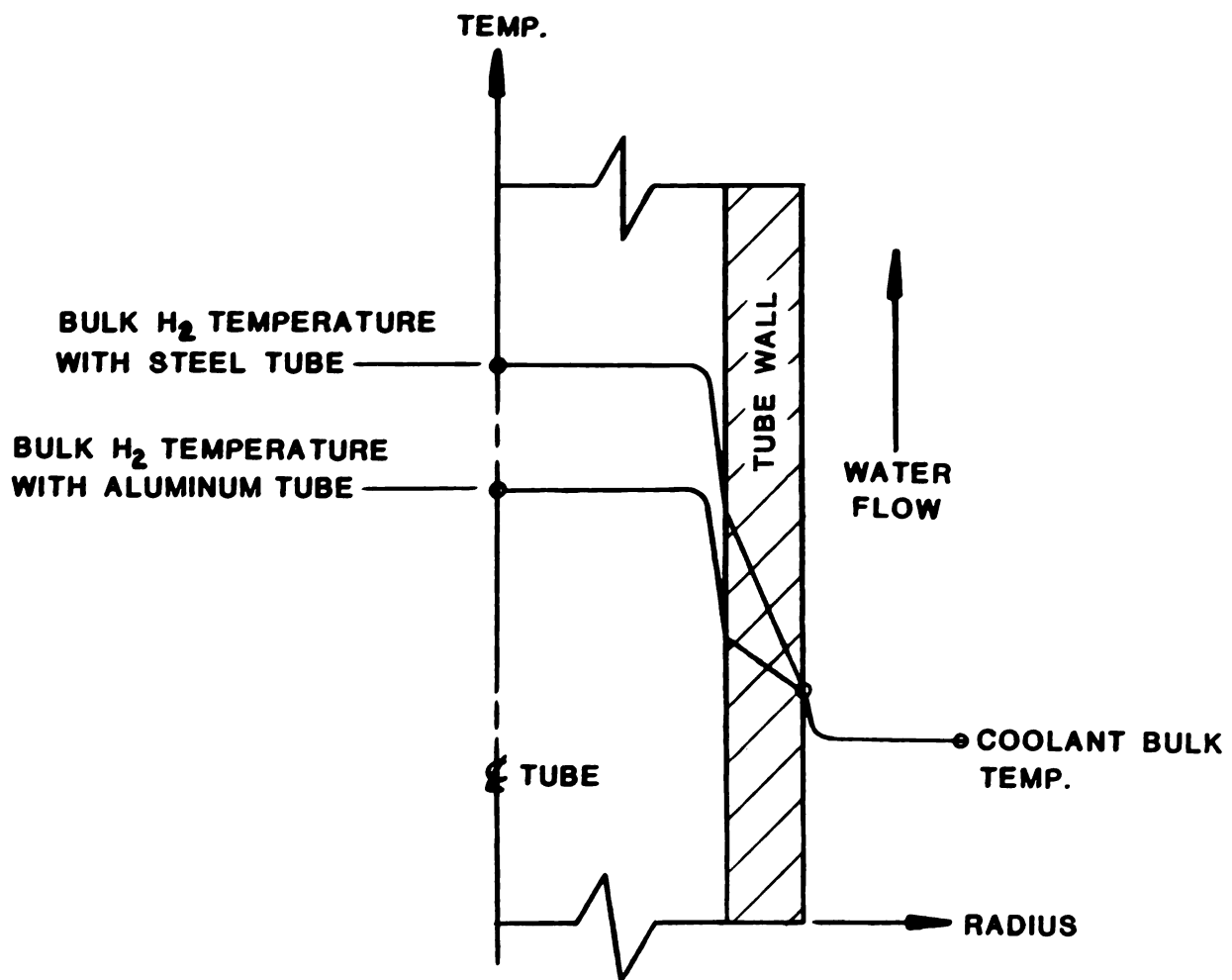
Figure 2.8-6 Temperature Effects of Cooler Tube Heat Conductivity
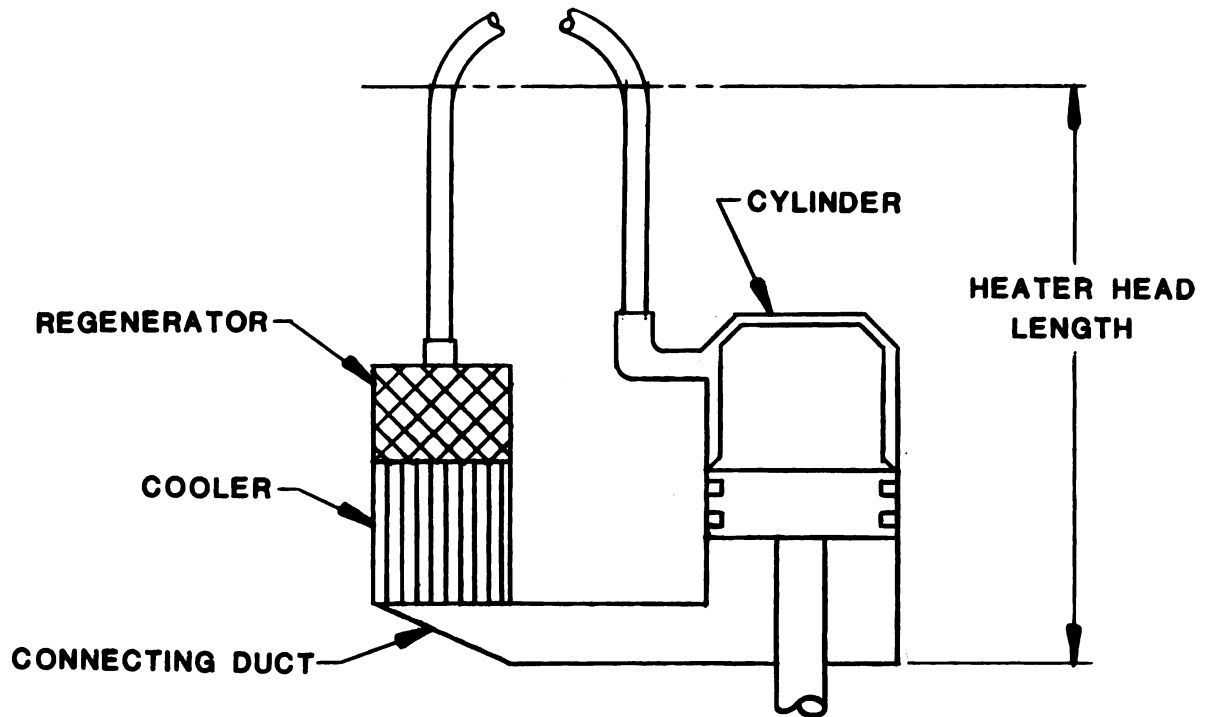
For our purposes, the heater head length is defined as the distance, measured parallel to the engine center line, from piston BDC to the point of tangency between the heated portion of the 1st pass heater tubes and the crossover length from 1st to 2nd pass.
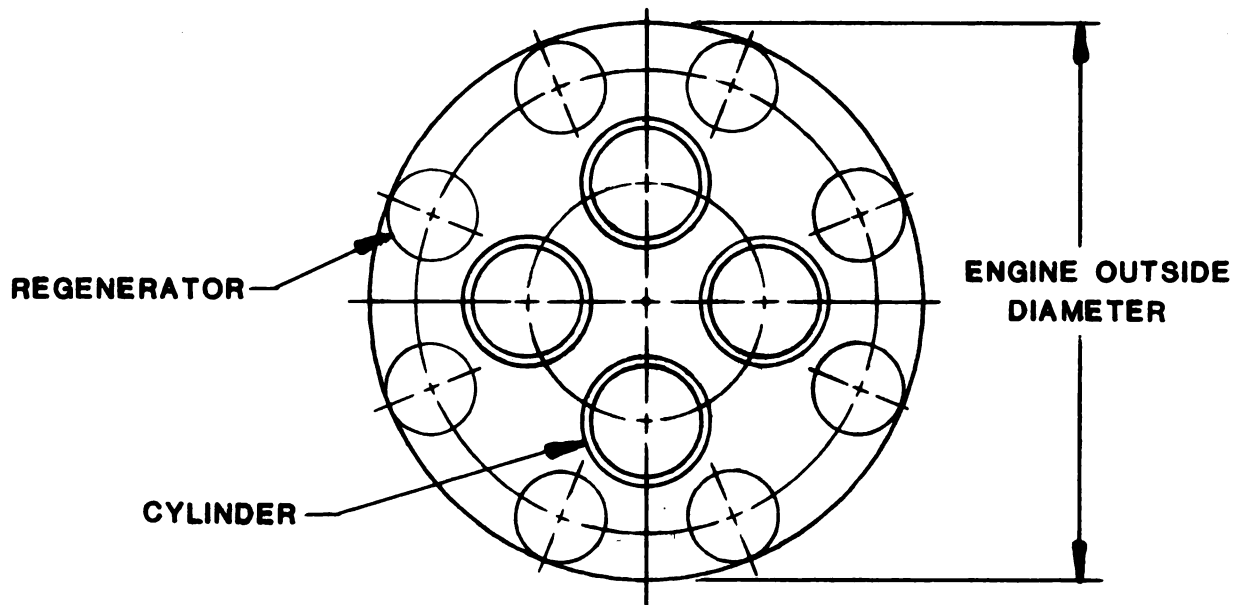
Maximum engine outside diameter is measured tangent to the regenerator housings. This parameter is handled internally in the optimization procedure.

Figure 2..8-7 Description of Engine Length and Engine O.D. Parameters
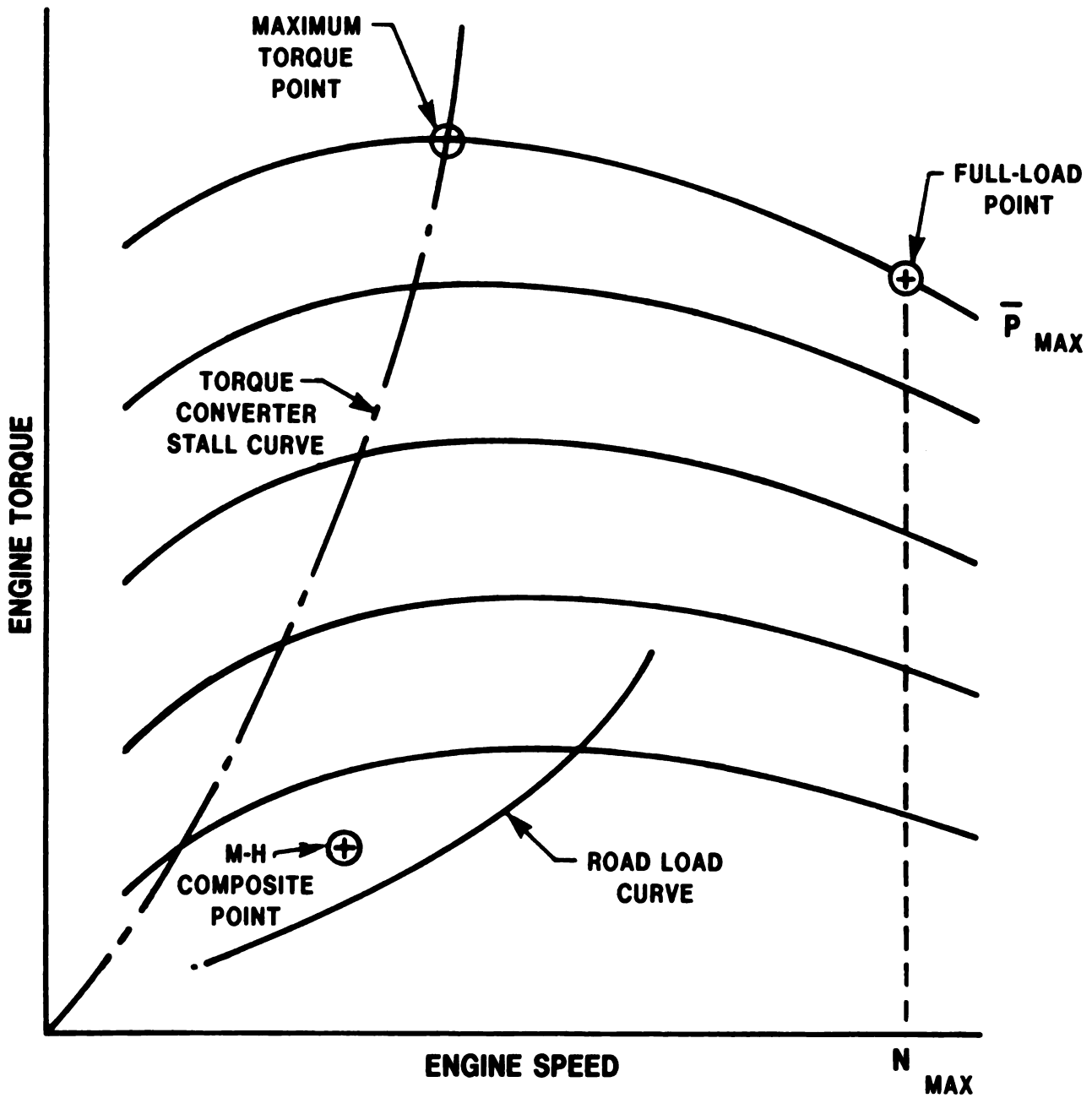
Figure 2. 8-8   Possible Design Points Considered in Part Load Optimization
Study
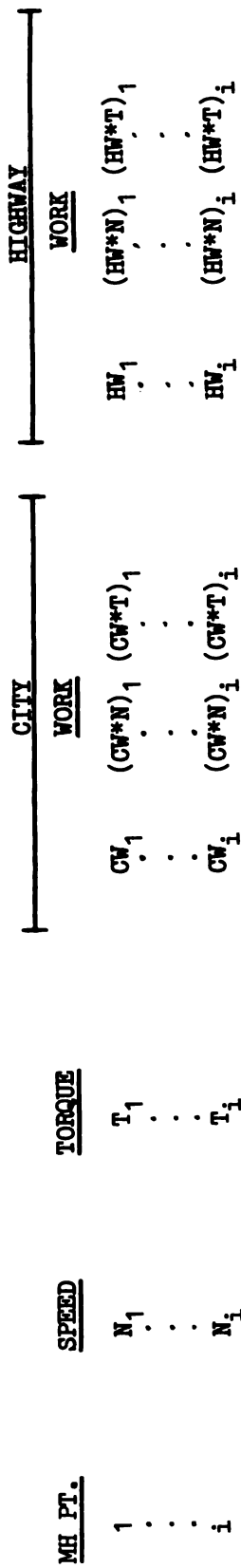
$$\text{SPEED} = \left[\frac{\sum_{j=1}^{i}(CW*N)_j}{\sum_{j=1}^{i}(CW)_j}\right] * 0.55 + \left[\frac{\sum_{j=1}^{i}(HW*N)_j}{\sum_{j=1}^{i}(HW)_j}\right] * 0.45$$

$$\text{TORQUE} = \left[\frac{\sum_{j=1}^{i}(CW*T)_j}{\sum_{j=1}^{i}(CW)_j}\right] * 0.55 + \left[\frac{\sum_{j=1}^{i}(HW*T)_j}{\sum_{j=1}^{i}(HW)_j}\right] * 0.45$$

MH PT.	SPEED	TORQUE	CITY WORK		HIGHWAY WORK	
1	N_1	T_1	CW_1	$(CW*N)_1$ $(CW*T)_1$	HW_1	$(HW*N)_1$ $(HW*T)_1$
.	.	.	.	.	.	.
i	N_i	T_i	CW_i	$(CW*N)_i$ $(CW*T)_i$	HW_i	$(HW*N)_i$ $(HW*T)_i$

Figure 2.8-9   M-H Composite Point Calculations

279

RUN DATE	A 6/28	B 7/1	C 7/7	D 7/12	E 7/13	F 7/14	G 7/15	H 7/18	I 7/19	J 7/20	K 7/21	L 7/25	N 7/27
LOC_1	MT	MT	MT	MT	MT	MT	MT	MT	MT	MT	MT	NH	NH
$AREV_1$	$\$ AREV_2$	1050.	1050.	$\$ AREV_2$	1250.	1250.	1250.	$\$ AREV_2$	$\$ AREV_2$	1475.	1475.	1475.	1475.
PRM_1	200.	200.	200.	PRM_2	PRM_2	PRM_2	PRM_2	PRM_2	PRM_2	80.	80.	V.	V.
TED_1	750.	750.	750.	750.	750.	750.	750.	750.	750.	750.	750.	750.	750.
η_1	47.4	46.9	38.7	38.	42.5	47.8	46.2	45.8	43.8	45.2	45.	45.1	45.6
LOC_2	FL	FL	FL	FL	FL	FL	FL	FL	FL	FL	FL	FL	FL
$AREV_2$	V.	V.	V.	V.	4000.	4000.	4000.	4000.	3000.	4000.	4000.	4000.	4000.
RPM_2	200.	200.	200.	V.	V.	V.	V.	V.	V.	$V.*PRM_1$	$V.*PRM_1$	$V.*RPM_1$	$V.*RPM_1$
TED_2	750	750.	750.	750.	750.	750.	750.	750.	750.	750.	750.	750.	750.
η_2	38.5	36.6	26.7	38.	36.8	39.5	36.5	40.5	41.2	44.8	37.	42.2	42.9
REQ_x	kW_2	kW_2	kW_2	kW_2	kW_2	L	L	L	L	L	L	L	L
REQ_y	-	-	W/cm_2^2	W/cm_2^2	W/cm_2^2	kW_2	kW_2	kW_2	kW_2	kW_2	kW_2	kW_2	kW_2
REQ_z	-	-	-	L	L	-	-	-	-	-	-	Nm_1	Nm_1
CONV.	NO	YES	NO	NO	NO	NO	NO	YES	YES	YES	YES	NO	YES

Figure 2.8-10   Part-Load Reoptimization Summary

280
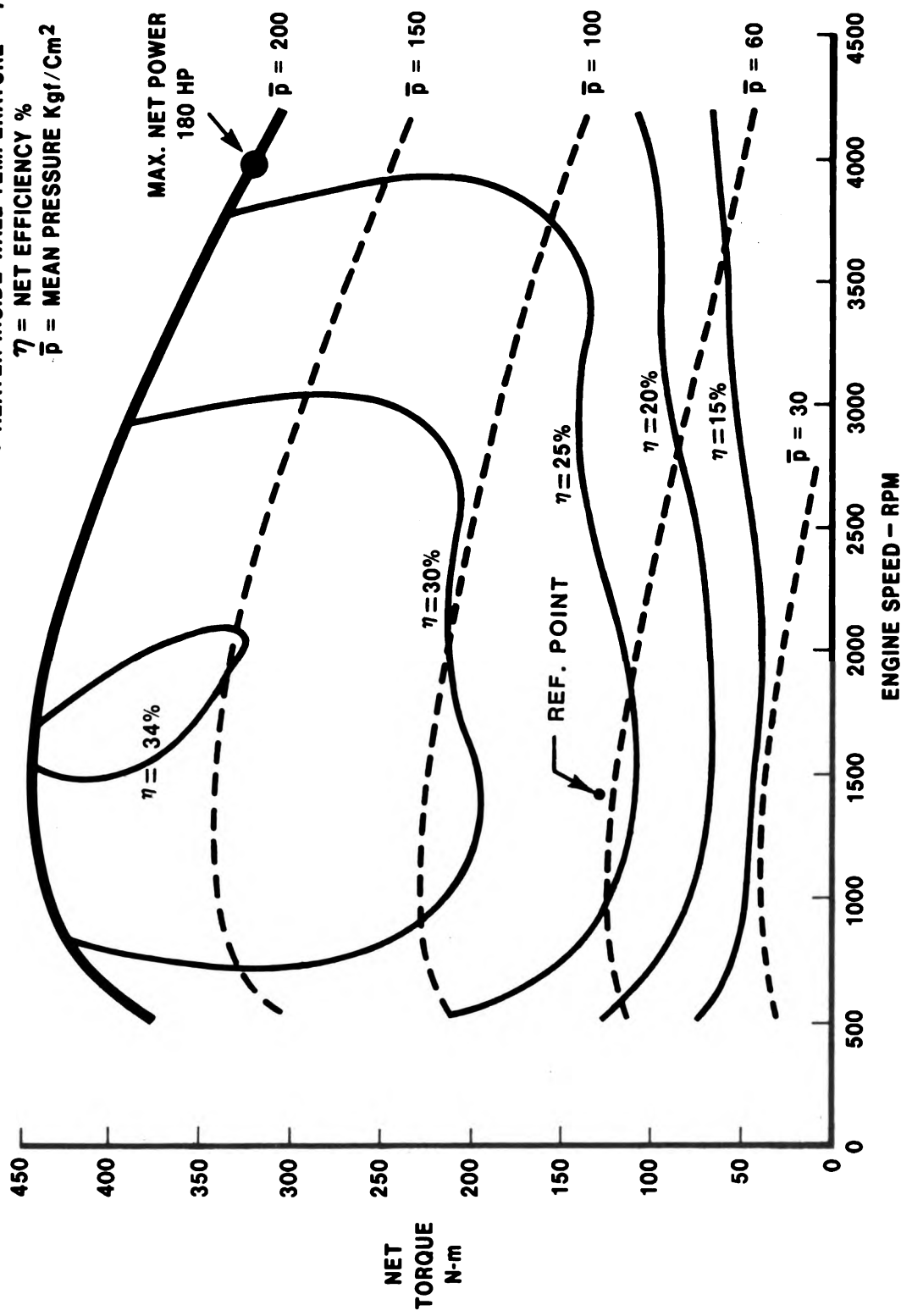
Figure 2.8-11   Performance Map 4-215 Stirling Engine

281

Metro-Highway Fuel Economy Summary For 4-215 Engine Prepared On 24 AUG 1978 BY T. DUNLAP
BASED ON ENGINE MAP DATA FILE TDENBLVT AND M-H DATA FILE MM2.5-10 (4500 LB. IUC VEH.)
THESE RESULTS ARE BASED ON A DYNAMOMETER ENGINE WITH STEERING AND FAN LOSSES EQUAL TO ZERO

M-H PT	SPEED RPM	TORQUE NM	PGWER KW	PRESS ATM	FUEL G/S	CITY SEC	CITY GRAM	Z TOT CITY	HIWAY SEC	HIWAY GRAM	Z TOT HIWAY	BSFC W/HPHR
1	600.000	53.200	3.343	33.015	0.552	362.338	199.881	14.406	10.253	5.656	0.401	0.977
2	800.000	40.700	3.410	27.997	0.598	272.141	162.643	11.723	5.235	3.129	0.222	1.037
3	900.000	-6.800	-0.641	12.092	0.410	74.000	30.325	2.186	52.000	21.310	1.511	0.
4	1000.000	67.830	7.100	37.120	0.842	167.184	140.773	10.146	29.131	24.529	1.740	0.702
5	1100.000	108.500	12.498	51.490	1.160	185.672	215.290	15.516	32.763	37.989	2.694	0.549
6	1300.000	155.900	21.224	69.614	1.706	147.190	251.097	18.097	45.847	78.212	5.547	0.476
7	1600.000	203.400	34.080	90.239	2.583	58.349	150.701	10.861	72.734	187.854	13.322	0.449
8	1700.000	108.500	19.316	54.332	1.733	57.496	97.615	7.179	331.356	574.091	40.713	0.531
9	1800.000	216.900	40.885	97.123	3.087	36.123	111.530	8.038	76.840	237.243	16.825	0.447
10	2000.000	122.000	25.552	61.528	2.226	11.509	25.622	1.847	107.842	240.082	17.026	0.516

TOTAL CVS-M FUEL CONSUMPTION = 1387.4964 GRAMS
CVS-M FUEL ECONOMY = 15.1499 MPG
COLD START FUEL PENALTY = 148.9000 GRAMS
TOTAL CVS-CH FUEL CONSUMPTION = 1536.3964 GRAMS
CVS-CH FUEL ECONOMY = 13.6816 MPG
TOTAL EPA HWY FUEL CONSUMPTION = 1410.0952 GRAMS
EPA HWY FUEL ECONOMY = 20.3573 MPG

* TOTAL M-H FUEL ECONOMY = 16.0501 MPG *

Figure 2.8-12   Metro-Highway Fuel Economy Summary

Metro-Highway Fuel Economy Summary For 4-247 Engine Prepared On 24 AUG 1978 BY T. DUNLAP
BASED ON ENGINE MAP DATA FILE TDEN247C AND M-H DATA FILE MH2.5-10 (4500 LB. IWC VEH.)
THESE RESULTS ARE BASED ON A DYNAMOMETER ENGINE WITH STEERING AND FAN LOSSES EQUAL TO ZERO

M-H PT	SPEED RPM	TORQUE NM	POWER KW	PRESS ATM	FUEL G/S	CITY SEC	CITY GRAM	Z TOT CITY	HIWAY SEC	HIWAY GRAM	Z TOT HIWAY	BSFC N/HPHR
1	600.000	53.200	3.343	40.109	0.444	362.338	160.936	13.489	10.253	4.554	0.363	0.786
2	800.000	40.700	3.410	34.522	0.498	272.141	132.774	11.129	5.235	2.554	0.203	0.847
3 *	900.000	-6.800	-0.641	14.096	0.314	74.000	23.221	1.946	52.000	16.317	1.300	0.
4	1000.000	67.800	7.100	45.820	0.705	167.184	117.839	9.877	29.131	20.533	1.636	0.588
5	1100.000	109.500	12.498	64.789	1.004	185.672	186.379	15.622	32.763	32.888	2.620	0.475
6	1300.000	155.900	21.224	88.632	1.517	147.190	223.296	18.716	45.847	69.553	5.542	0.423
7	1600.000	203.400	34.080	115.120	2.328	53.349	135.845	11.386	72.734	169.335	13.492	0.404
8	1700.000	108.500	19.316	68.744	1.537	57.496	88.393	7.409	331.356	509.419	40.587	0.471
9	1800.000	216.900	40.885	124.559	2.812	36.123	101.582	8.514	76.840	216.083	17.216	0.407
10	2000.000	122.000	25.552	77.838	1.983	11.509	22.626	1.913	107.842	213.684	17.041	0.459

TOTAL CVS-H FUEL CONSUMPTION = 1193.0914 GRAMS
CVS-H FUEL ECONOMY = 17.6184 MPG
COLD START FUEL PENALTY = 165.1300 GRAMS
TOTAL CVS-CH FUEL CONSUMPTION = 1358.2214 GRAMS
CVS-CH FUEL ECONOMY = 15.4764 MPG
TOTAL EPA HWY FUEL CONSUMPTION = 1255.1205 GRAMS
EPA HWY FUEL ECONOMY = 22.8708 MPG

****
* *
* TOTAL M-H FUEL ECONOMY = 18.1115 MPG *
* *
****

Figure 2.8-13   Metro-Highway Fuel Economy Summary

283
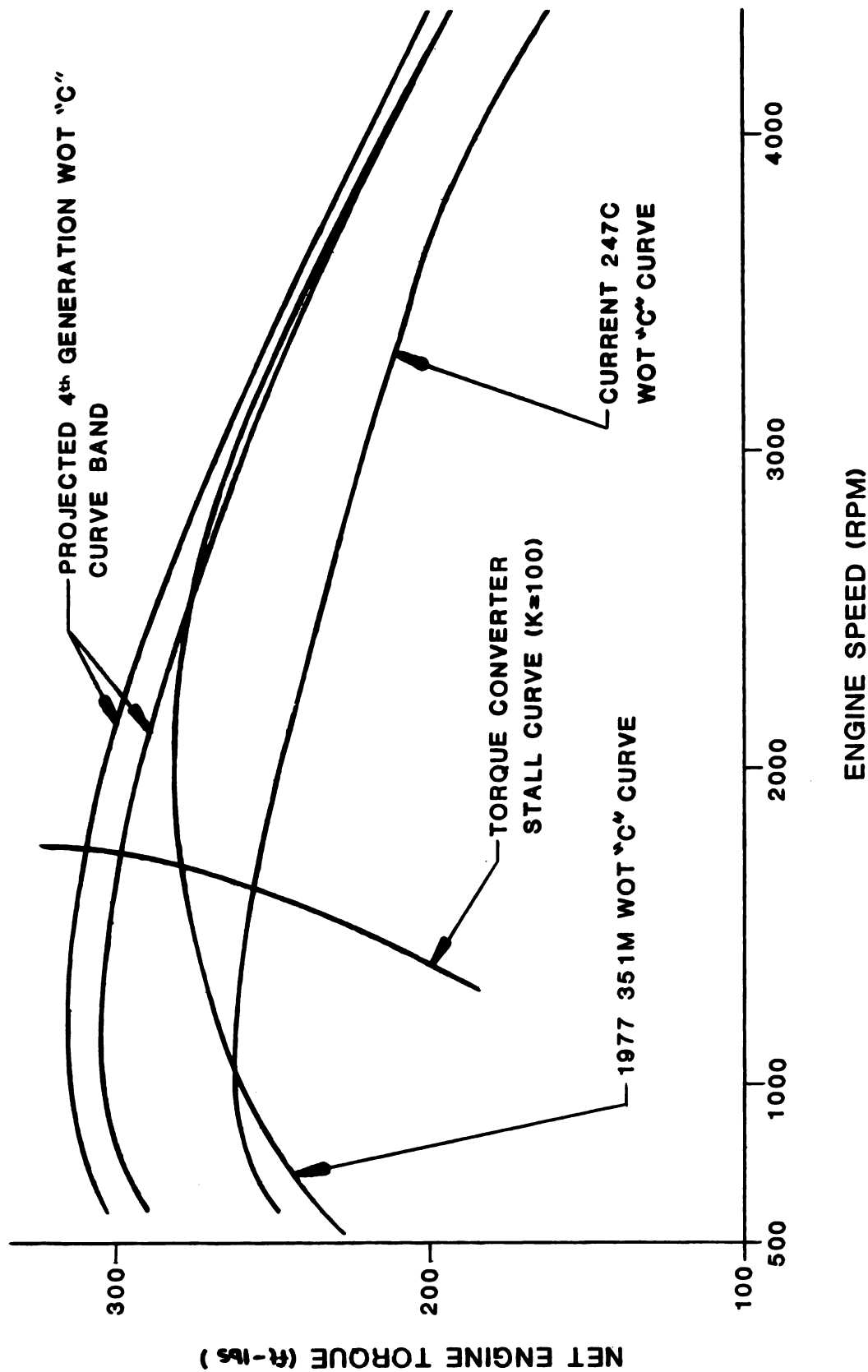
Figure 2. 8-14   Engine Net Torque vs. Engine Speed
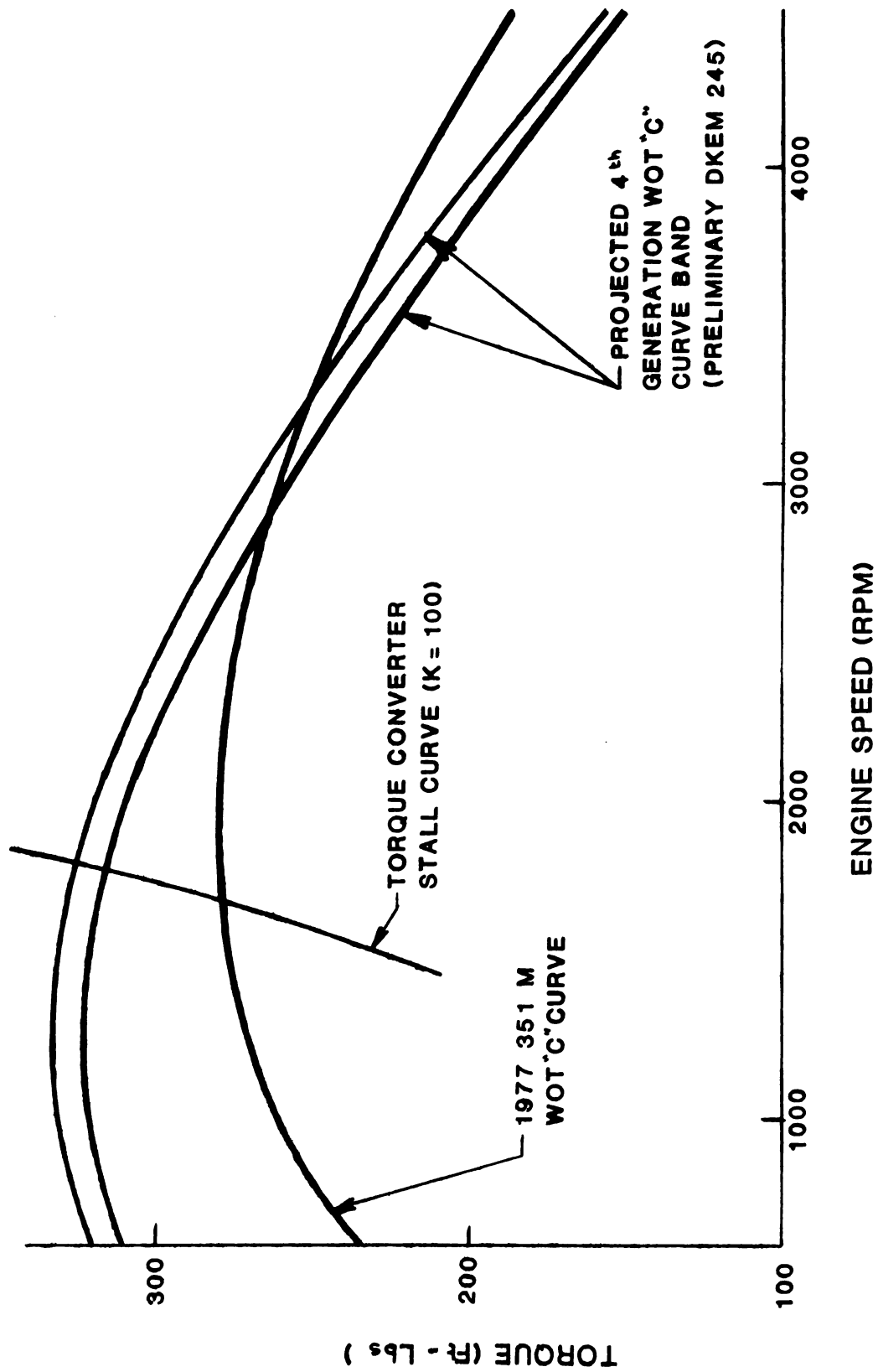
Figure 2.8-15   Graphs of Engine Net Torque vs. Engine Speed
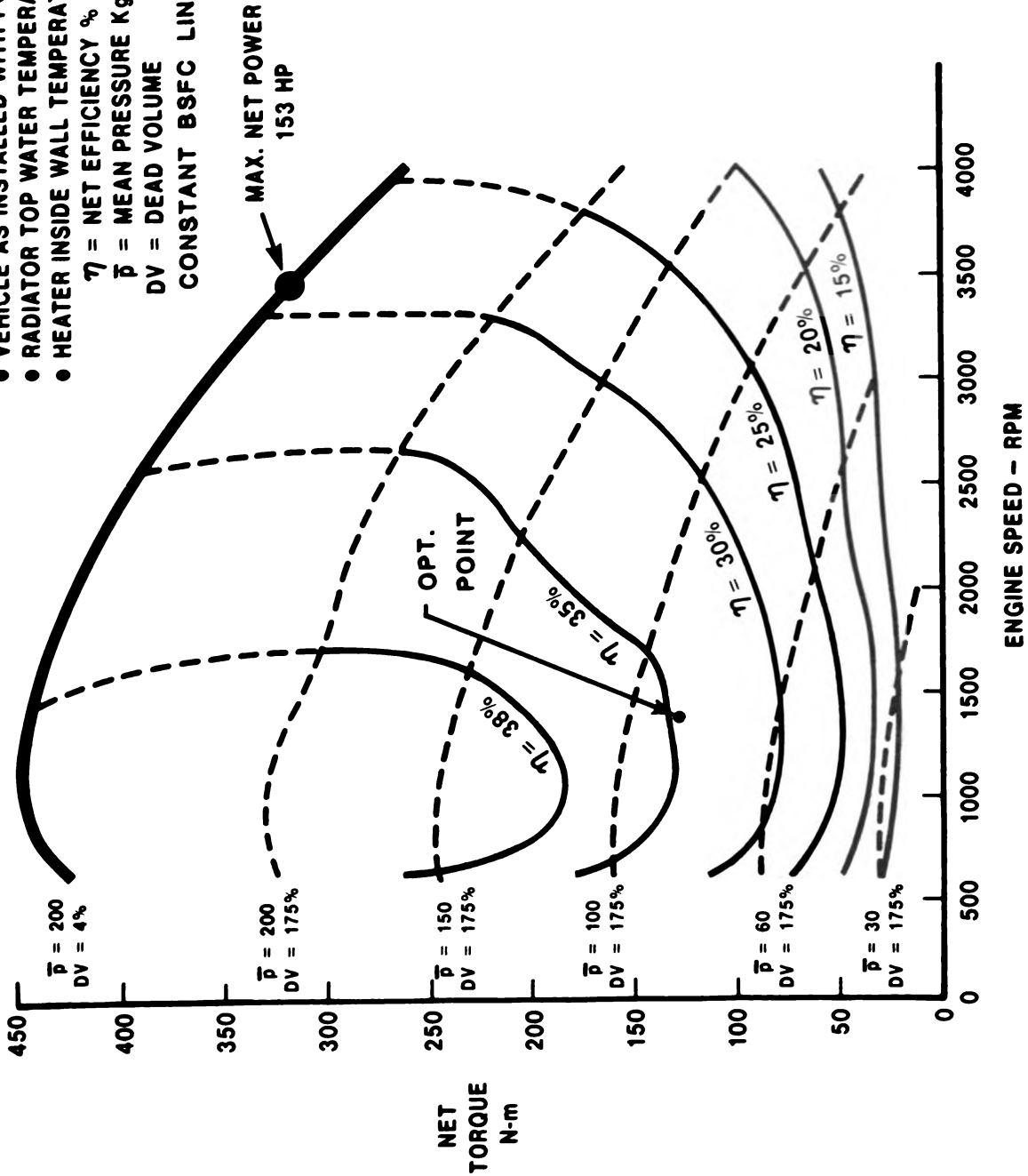
Figure 2.8-16   Performance Map 4-245 Stirling Engine

(FOR A 0 TO 60 MPH ACCELERATION OF A 4500 LB. VEHICLE IN 13.0 TO 13.5 SECONDS)

A-TORQUE FOR 13.0 SECONDS
B- 4-245 FULL LOAD TORQUE
C-TORQUE FOR 13.5 SECONDS
D-4-215 FULL LOAD TORQUE

ENGINE SPEED (RPM)

NET TORQUE (N·M)
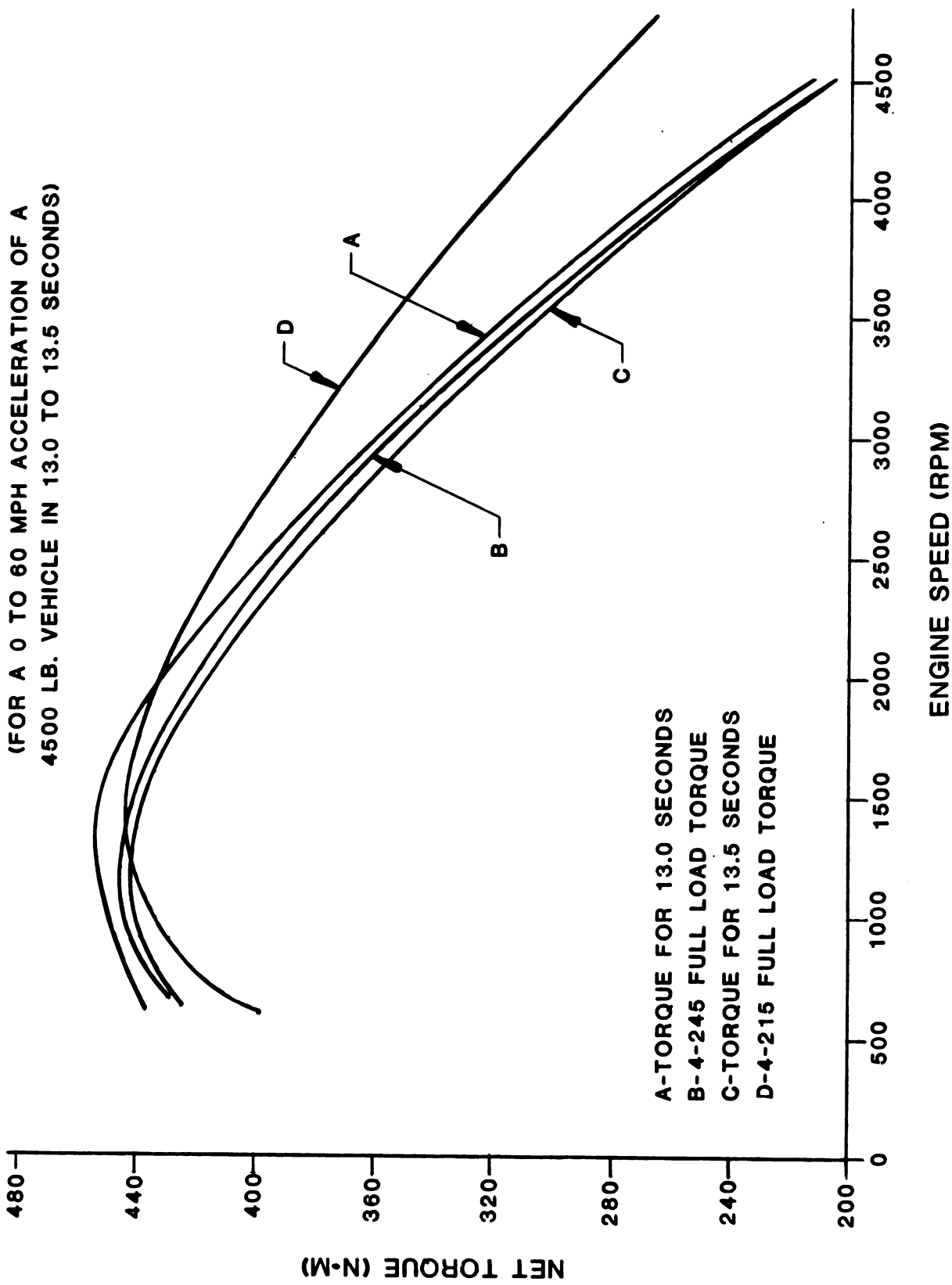
Figure 2.8-17   Engine Torque vs. Engine Speed

Metro-Highway Fuel Economy Summary For 4-245 Engine Prepared On 24 AUG 1978 BY T. DUNLAP
BASED ON ENGINE MAP DATA FILE DKEM245C AND M-H DATA FILE MH2.5-10 (4500 LB. IWC VEH.)
THESE RESULTS ARE BASED ON A DYNAMOMETER ENGINE WITH STEERING AND FAN LOSSES EQUAL TO ZERO

M-H PT	SPEED RPM	TORQUE NM	POWER KW	PRESS ATM	FUEL G/S	CITY SEC	CITY GRAM	% TOT CITY	HIWAY SEC	HIWAY GRAM	% TOT HIWAY	BSFC M/HPHR
1	600.000	53.200	3.343	36.357	0.330	362.338	119.559	12.450	10.253	3.383	0.319	0.584
2	800.000	40.700	3.410	30.643	0.353	272.141	95.982	9.995	5.235	1.846	0.174	0.612
3 *	900.000	-6.800	-0.641	7.212	0.183	74.000	13.512	1.407	52.000	9.495	0.896	0.
4	1000.000	67.500	7.100	46.089	0.550	167.184	91.904	9.571	29.131	16.014	1.511	0.458
5	1100.000	108.500	12.498	68.835	0.820	185.672	152.186	15.848	32.763	26.854	2.533	0.388
6	1300.000	155.900	21.224	97.043	1.276	147.190	187.742	19.551	45.847	58.478	5.516	0.356
7	1600.000	203.400	34.080	129.105	2.007	58.349	117.117	12.196	72.734	145.990	13.771	0.349
8	1700.000	108.500	19.316	75.978	1.285	57.496	73.866	7.692	331.356	425.698	40.155	0.394
9	1800.000	216.900	40.885	141.864	2.459	36.123	88.833	9.251	76.840	188.963	17.824	0.356
10	2000.000	122.000	25.552	88.660	1.701	11.509	19.574	2.038	107.842	183.415	17.301	0.394

```
TOTAL CVS-H FUEL CONSUMPTION =  960.2739 GRAMS
       CVS-H FUEL ECONOMY     =   21.8900 MPG
       COLD START FUEL PENALTY =  161.2900 GRAMS
TOTAL CVS-CH FUEL CONSUMPTION = 1121.5639 GRAMS
       CVS-CH FUEL ECONOMY    =   18.7421 MPG
TOTAL EPA HWY FUEL CONSUMPTION = 1060.1363 GRAMS
       EPA HWY FUEL ECONOMY   =   27.0773 MPG
```

****
* TOTAL M-H FUEL ECONOMY =   21.7558 MPG *
****

Figure 2.8-18   Metro-Highway Fuel Economy Summary
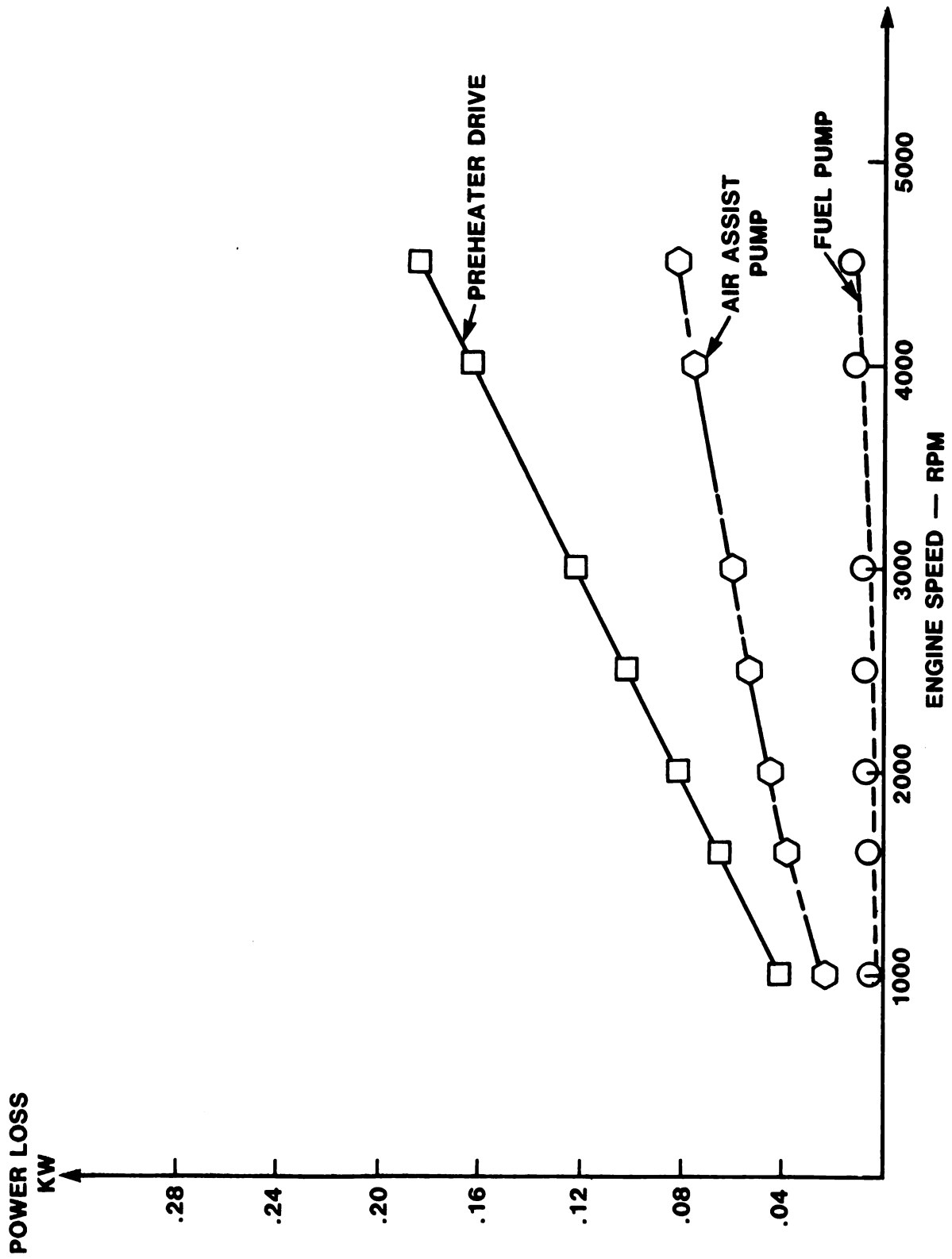
Figure 2.8–19   Engine Accessory Power Losses – Preheater Drive Air Assist Pump and Fuel Pump
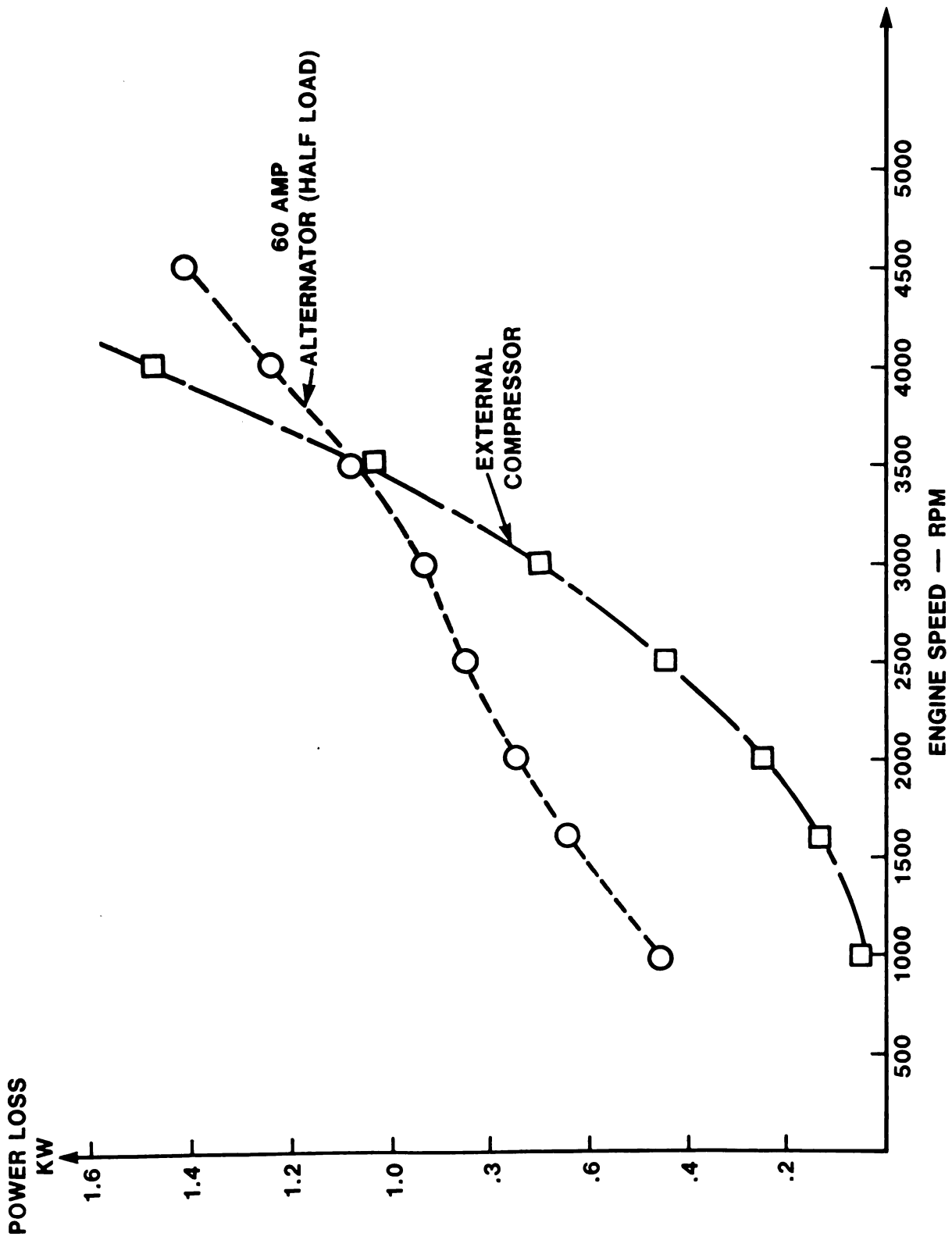
Figure 2. 8–20   Engine Accessory Power Losses – Alternator and External Compressor

290

Metro-Highway Fuel Economy Summary For 4-270 Engine Prepared On 11 SEP 1978 BY KAB270
BASED ON ENGINE MAP DATA FILE DKEM270 AND M-H DATA FILE MH2.5-10 (4500 LB. IUC VEH.)
THESE RESULTS ARE BASED ON A DYNAMOMETER ENGINE WITH STEERING AND FAN LOSSES EQUAL TO ZERO

M-H PT	SPEED RPM	TORQUE NM	POWER KW	PRESS ATM	FUEL G/S	CITY SEC	CITY GRAM	Z TOT CITY	HIWAY SEC	HIWAY GRAM	Z TOT HIWAY	BSFC W/HPHR
1	600.000	53.200	3.343	32.526	0.341	362.338	123.436	12.600	10.253	3.493	0.324	0.603
2	800.000	40.700	3.410	27.475	0.363	272.141	98.799	10.085	5.235	1.901	0.176	0.630
3 *	900.000	-6.800	-0.641	6.555	0.193	74.000	14.284	1.458	52.000	10.038	0.931	0.
4	1000.000	67.800	7.100	41.120	0.561	167.184	93.749	9.570	29.131	16.335	1.515	0.467
5	1100.000	108.500	12.498	61.147	0.833	185.672	154.746	15.796	32.763	27.306	2.532	0.395
6	1300.000	155.900	21.224	86.002	1.294	147.190	190.526	19.449	45.847	59.345	5.503	0.361
7	1600.000	203.400	34.080	114.212	2.036	58.349	118.774	12.124	72.734	148.056	13.730	0.353
8	1700.000	108.500	19.316	67.769	1.308	57.496	75.191	7.675	331.356	433.333	40.185	0.401
9	1800.000	216.900	40.885	125.453	2.497	36.123	90.206	9.208	76.840	191.884	17.794	0.361
10	2000.000	122.000	25.552	79.137	1.731	11.509	19.921	2.033	107.842	186.660	17.310	0.401

```
TOTAL CVS-H FUEL CONSUMPTION =   979.6317 GRAMS
        CVS-H FUEL ECONOMY =      21.4575 MPG
      COLD START FUEL PENALTY =  164.1900 GRAMS
TOTAL CVS-CH FUEL CONSUMPTION = 1143.8217 GRAMS
        CVS-CH FUEL ECONOMY =     18.3773 MPG
TOTAL EPA HWY FUEL CONSUMPTION = 1078.3504 GRAMS
      EPA HWY FUEL ECONOMY =      26.6200 MPG
```

```
*********************************
*                               *
*  TOTAL M-H FUEL ECONOMY  =  21.3526 MPG  *
*                               *
*********************************
```

Figure 2.8-21   Metro-Highway Fuel Economy Summary
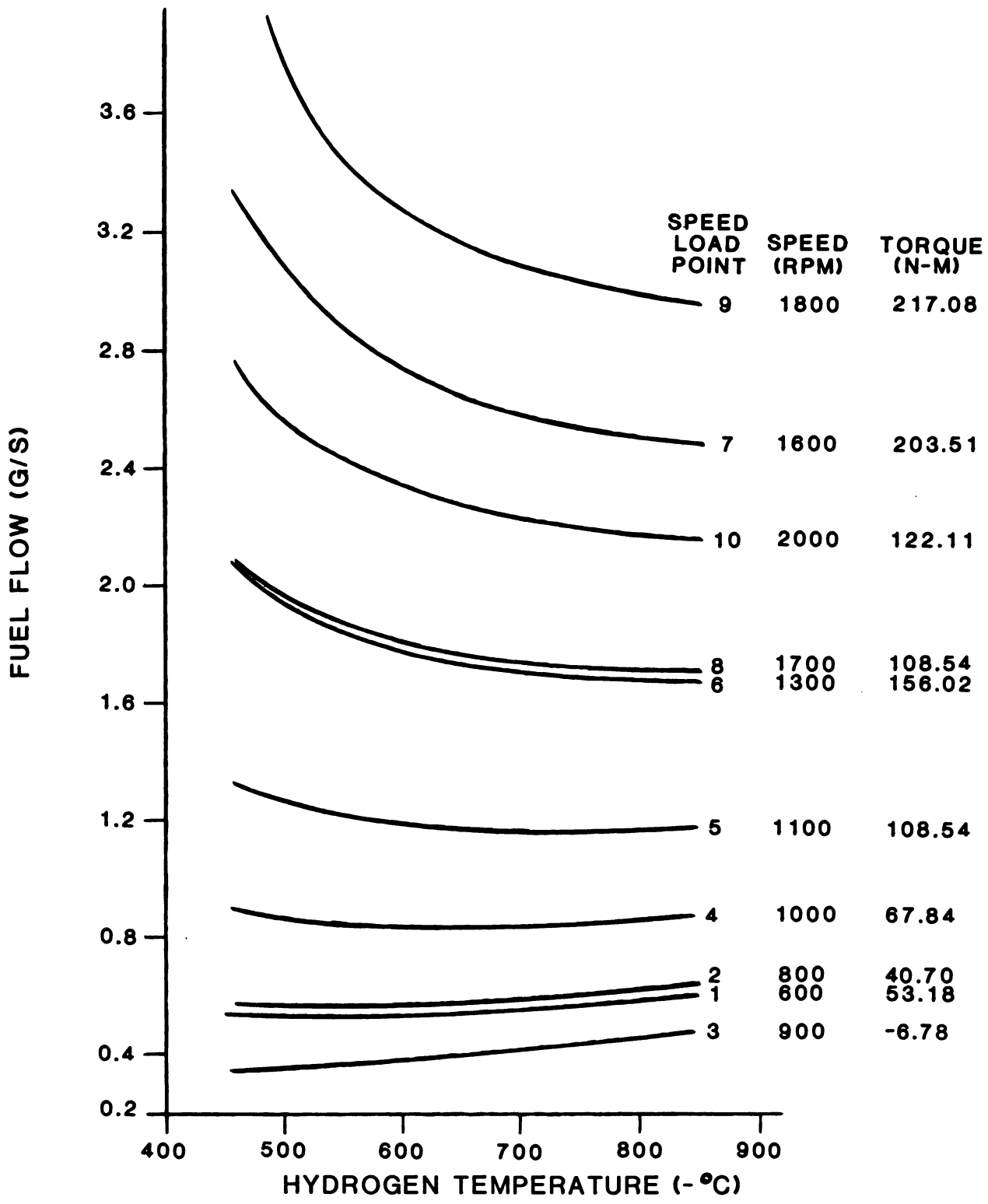
Figure 2.8-22   Fuel Flow vs. Hydrogen Temperature Constant Speed Load –
4-215 Engine
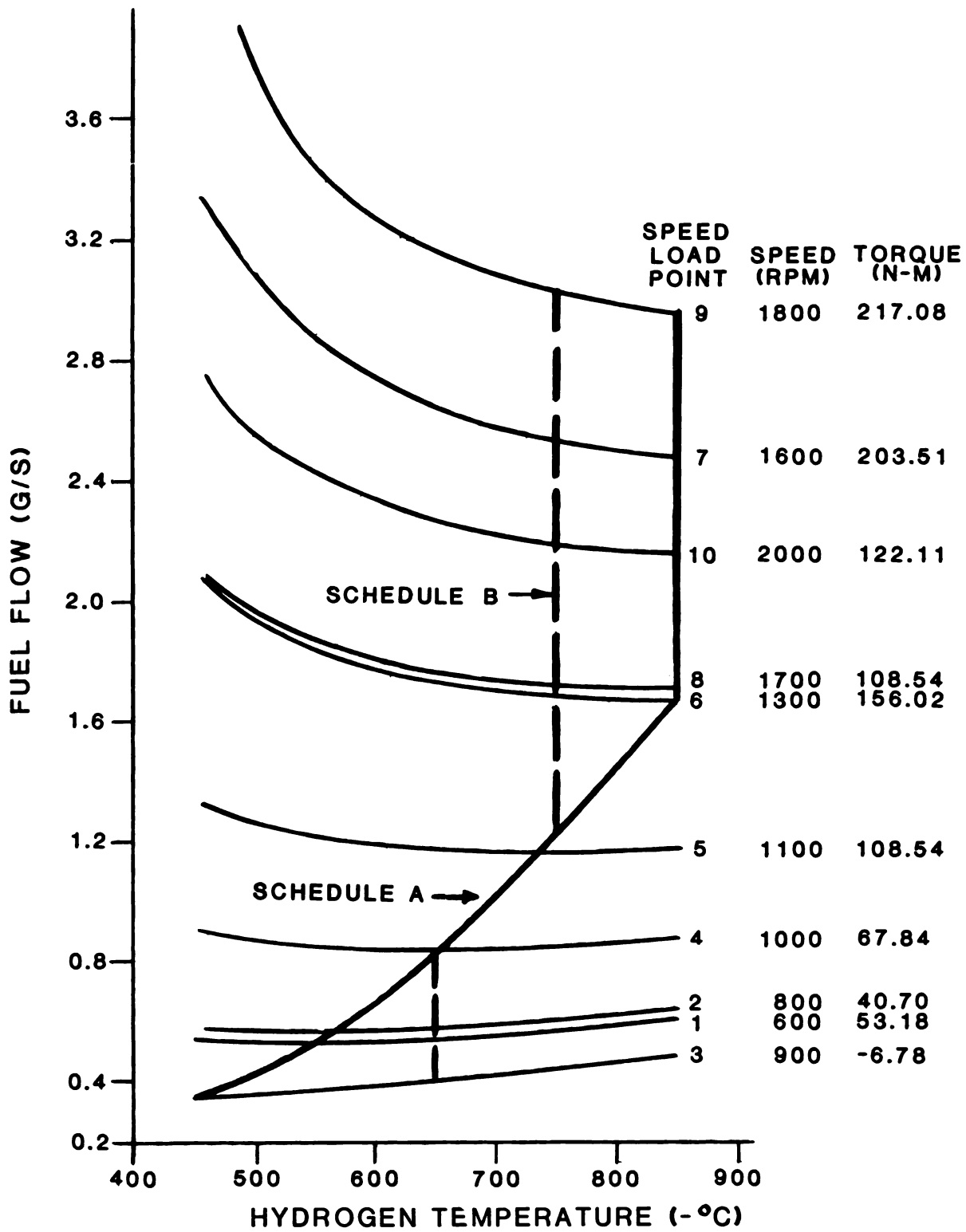
Figure 2.8-23   Fuel Flow vs. Hydrogen Temperature Constant Speed Load –
4-215 Engine
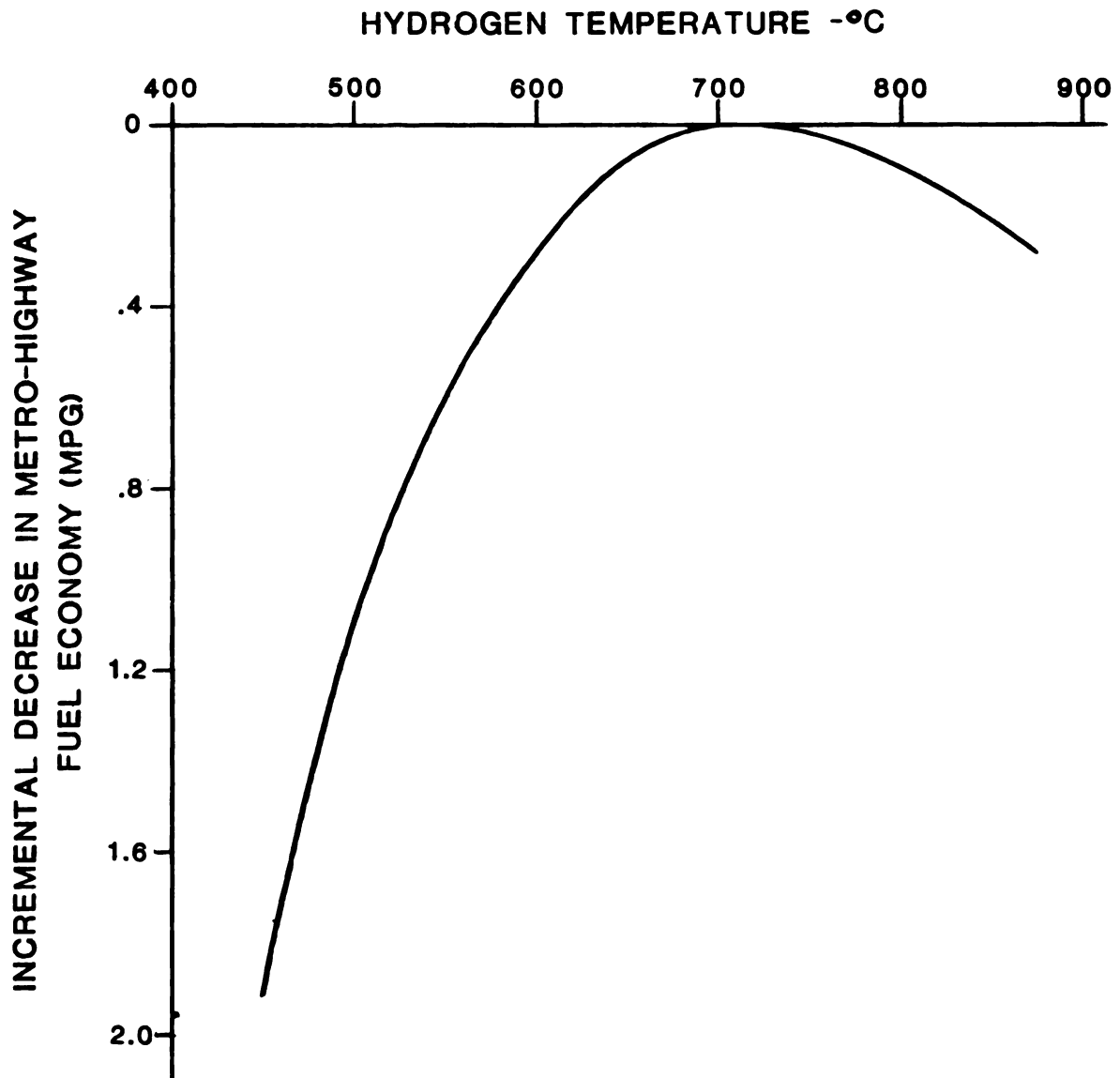
Figure 2.8-24   Decrease in Metro–Highway Fuel Economy vs. Hydrogen Temperature
(Constant Control Temperature)

VARIABLE NAME	DESCRIPTION	UNITS	4-215	2-245	A	B	C	D	E	F	G	H	I	J	K	L	M
			Baseline Engine Optimized at Full Load	Fourth Generation Fuel Economy Assessment Engine	Interchangeable With 4-215 Drive – Height Requirement	Drive Configuration Allowed to Float – Height Requirement	Interchangeable With 4-215 Drive – Height Allowed to Vary	Drive Configuration Allowed to Float – Height Allowed to Vary	Interchangeable With 4-215 Drive – No "Extra" Dead Volume – Height Requirement	Drive Configuration Allowed to Float – No "Extra" Dead Volume – Height Requirement	Interchangeable With 4-215 Drive – Dead Volume Varied But No Switchover – Height Requirement	Drive Configuration Allowed to Float – Dead Volume Varied But No Switchover – Height Requirement	Interchangeable With 4-215 Drive, Preheater and Cooler – Height Requirement	Interchangeable With 4-215 Drive – Maximum Power Point at 4500 RPM – Height Requirement	Drive Configuration Allowed to Float – Maximum Power Point at 4500 RPM – Height Requirement	Interchangeable With 4-215 Drive – Variable Full Load Pressure – Height Requirement	Drive Configuration Allowed to Float – Variable Full Load Pressure – Height Requirement
HEIGHT	Heater Head Length	mm	302	303	302	303	336	376	302	303	302	302	302	302	302	302	302
OD	Engine OD	mm	428	428	409	424	413	426	420	425	413	425	428	415	422	422	424
VO	Reference Volume	cm³	218	245	216	228	218	251	218	234	218	241	218	218	226	218	228
DC (1)	Bore	mm	73.0	84.4	72.8	80.4	73.0	77.1	73.0	76.6	73.0	77.0	73.0	73.0	77.2	73.0	76.4
STROKE	Stroke	mm	52.0	44.8	52.0	44.9	52.0	53.9	52.0	50.8	52.0	51.6	52.0	52.0	48.3	52.0	49.7
DCLC	Cylinder Pitch Circle	mm	160.0	179.1	160.0	173.8	160.0	168.0	160.0	167.3	160.0	168.0	160.0	160.0	168.3	160.0	167.7
RSP	Swash Plate Radius	mm	85.0	89.5	85.0	86.0	85.0	84.0	85.0	83.6	85.0	84.0	85.0	85.0	84.1	85.0	83.9
ASP	Swash Plate Angle	deg	17.0	14.0	17.0	14.5	17.0	17.8	17.0	16.9	17.0	17.1	17.0	17.0	16.0	17.0	16.5
FLUX	Heater Flux (Avg)	w/cm²	138	148	138	133	137	135	130	136	135	133	129	151	154	145	142
PDSAD1 (1)	Dead Volume-Part Load	%	6.61	175.0	124.9	144.8	127.6	175.8	3.68	3.68	75.0	30.6	125.3	95.3	122.9	95.7	135.0
PDSAD (2)	Dead Volume-Full Load	%	6.61	3.68	3.68	3.68	3.68	3.68	3.68	3.68	75.0	30.6	3.68	3.68	3.68	3.68	3.68
PAREV (1)	Part Load Speed	RPM	1475*	1475	1550	1550	1550	1550	1550	1550	1550	1550	1550	1550	1550	1550	1550
	Part Load Ind. Torque	Nm	175*	175	167	167	167	167	167	167	167	167	167	167.0	167.0	167	167
PAREV (2)	Maximum Power Speed	RPM	4000	4000	3600	3600	3600	3600	3600	3600	3600	3600	3600	4500	4500	3600	3600
	Maximum Ind. Power	kW	189	155	131	131	131	131	131	131	131	131	131	129.7	129.7	131	131
FUEL	Cold Start Penalty	gm	148.9	161.3	151.7	157.7	159.6	173.0	157.2	160.6	154.7	161.4	159.7	158.0	157.4	166.9	160.7
PPRM (2)	Full Load Pressure	kg/cm²	200	200	200	200	200	200	200	200	200	200	200	200	200	221	207
	Part Load Ind. Eff.	%	41.03*	49.35	48.66	49.47	48.90	49.68	47.61	48.33	47.70	48.32	48.13	48.78	49.27	48.59	49.07
	Maximum Power Ind. Eff.	%	40.27	38.67	42.09	41.17	41.70	40.06	43.47	43.16	42.98	43.21	42.06	38.40	37.05	42.37	41.78

* Optimized at Maximum Power

Figure 2.8-25 Comparison of Optimizations

VARIABLE NAME	DESCRIPTION	UNITS	N	O	P	Q	R	S	T	U	V
	UNIQUE FEATURES OF OPTIMIZATION		Similar to Case B, = p max - 200 atm, T - 850°C, - Higher temperature	= p max - 200 atm, T - 750°C, - Idle OPTIMIZATION	= p max - 200 atm, T - 750°C, - Scaled engine (.84)	Similar to Case I, = p max - 200 atm, T - 750°C, - Reduced power to 120 kW	Similar to Case I, = p max - 250 atm, T - 750 C, - Reduced press. to 150 atm	Interchangeable With 4-215 Drive, = p max - 200 atm, T - 750 C, - max power point at 3000 RPM	Interchangeable With 4-215 Drive, = p max - 200 atm, T - 800 C, - Max Power Point at 3000 RPM	Interchangeable With 4-215 Drive, = p max - 150 atm, T - 800 C, - Max Power Point at 3000 RPM	Interchangeable With 4-215 Drive, = p max - 150 ATM, T - 750 C, - Max Power Point at 3000 RPM
HEIGHT	Heater Head Length	mm	302	302	254	302	302	264	264	264	264
OD	Engine OD	mm	428	376	350	428	428	404	396	387	400
VO	Reference Volume	cm³	204	184	168	218	218	225	215	239	259
DC (1)	Bore	mm	83.6	79.4	75.8	73.0	73.0	74.3	72.5	76.6	79.7
STROKE	Stroke	mm	37.2	37.0	37.3	52.0	52.0	52.0	52.0	52.0	52.0
CCLC	Cylinder Pitch Circle	mm	179.3	172.1	165.7	160.0	160.0	160.0	160.0	160.0	160.0
RSP	Swash Plate Radius	mm	89.6	86.1	82.9	85.0	85.0	85.0	85.0	85.0	85.0
ASP	Swash Plate Angle	deg	11.7	12.2	12.7	17.0	17.0	17.0	17.0	17.0	17.0
FLUX	Heater Flux (Avg)	w/cm²	126	162	125	140	140	141	139	141	141
PDSAD (1)	Dead Volume-Part Load	%	119.4	402.2	173.9	109.8	185.3	111.4	98.6	225.0	235.9
PDSAD (2)	Dead Volume-Full Load	%	3.68	3.68	3.68	3.00	3.00	3.00	3.00	3.00	3.00
PAREV (1)	Part Load Speed	RPM	1550	600	1550	1550	1550	1550	1550	1550	1550
	Part Load Ind. Torque	Nm	167	53	167	167	167	167	167	167	167
PAREV (2)	Max. Power Speed	PRM	3600	3600	3600	3600	3600	3600	3600	3600	3600
	Max. Ind. Power	kW	131	131	131	120	120	121	121	120	121
FUEL	Cold Start Penalty	gm	173.0	129.3	97.7	156.9	135.2	136.6	139.3	125.0	125.9
PPRM (2)	Full Load Pressure	kg/cm²	200	200	200	200	150	200	200	150	150
	Part Load Ind. Eff	%	51.77	36.59	46.41	47.73	46.99	47.27	48.16	48.88	47.92
	Max. Power Ind. Eff.	%	45.86	37.01	34.75	40.80	41.28	41.15	43.11	41.26	39.99

Figure 2.8-26   Comparison of Optimizations

296
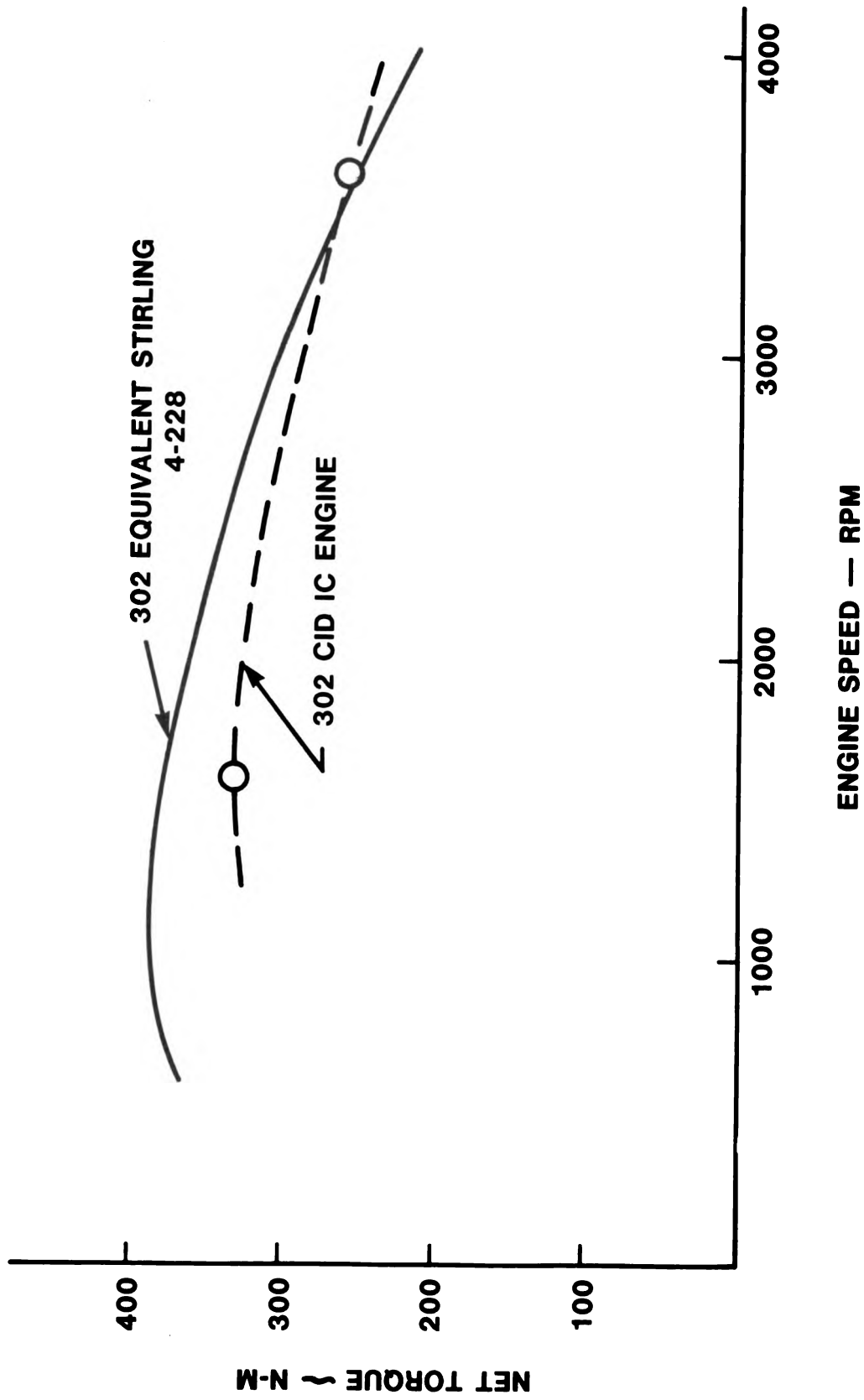
Figure 2.8-27   WOT Torque for Preliminary 302 Equivalent

297

2.9 Other Fuel Improvements

2.9.1 Summary — The objective of this section was to identify and assess the magnitude of potential fuel economy improvement areas not previously covered under any of the current program sections. When these improvements were considered viable, studies were conducted and placed into the proper areas.

Work required for this section was specified as the need arose and the assessed fuel economy improvements were based on estimates or theoretical analysis. When a proposed idea was considered ready for investigation, it was moved to its applicable section. At this point the assessed fuel economy improvement was also transferred to the applicable section, lowering the fuel economy estimate of this section. Accordingly, when new concepts were added to this section, the fuel economy improvement estimate of this section was increased.

The opportunities listed under Other Fuel Economy Improvements were individually reported on the Fuel Economy Assessment chart (refer to section 2.11). The rationale for improvement opportunities with fuel savings equal to or less than 0.10 MPG was based in most cases on a non-investigated estimate. It was assumed that a real, but unknown, maturity improvement existed in engine efficiency with the development of these concepts. Improvement opportunities in this category are listed as follows:

- Decreased air cleaner pressure drop (.02 MPG);

- Accessory drive starting energy requirements (.02 MPG);

- Burner development (0.10 MPG).

Improvement opportunities, based on estimates or theoretical analyses which resulted in a fuel savings greater than 0.10 MPG (with the exception of Reduction of Engine and Accessory Inertia) are discussed in the following sections:

2.9.2 Analysis — In-depth investigations of the improvement potential in the following areas were performed:

- Reduction of Engine and Accessory Inertia.

- Methods to Reduce Conduction Losses.

- Fuel-Off during H_2 Overtemperature.

- Higher Heater Head Mean Temperature.

- Powertrain Matching.

Following is a detailed description of the work performed in each area.

2.9.2.1 Reduction of Engine and Accessory Inertia — An analysis was performed to determine the effect of a reduction in the rotating inertia of the Stirling engine on fuel economy over a typical M-H driving cycle. To do this it was assumed that the effective moment of inertia of the engine could be re-

duced by 30% by redesigning the blower impeller, swashplate, etc.

A computer program called VSIM (Vehicle Simulation) was used to calculate the time allotted to various speed-load points to simulate the M-H driving cycle for both the baseline and "lightened" engines. These time intervals and speed-load points were then used as input to another program, ECONCALC, which calculates the expected fuel economy of a vehicle using the engine in question. The results of this calculation indicated the reduction in engine inertia would increase the M-H fuel economy by only 0.003 MPG because the engine inertia was very small compared to the total vehicle inertia.

In view of the insignificant improvement in fuel economy, no attempt was made to predict the improvement in vehicle performance which could be expected. Instead, it was assumed that no improvement in M-H fuel existed due to a reduction in engine and accessory inertia.

2.9.2.2 Methods to Reduce Conduction Losses — Engine mapping techniques were applied to theoretical data generated by the N.V. Philips computer program to determine the effect of cylinder and regenerator-cooler housing heat losses (Figure 2.9-1) on M-H fuel economy. The calculations indicated that the M-H fuel economy would increase from 15.8 to 20.9 MPG (32%) for a 4-215 Stirling engine installed in a 4500 lb. IWC vehicle, provided that all heat losses from the cylinder and regenerator-cooler walls to the engine coolant were prevented. Although it was impossible to achieve a maximum gain of 32% in M-H fuel economy, it was practical to initiate design studies directed toward reductions in heat losses from the cylinder and regenerator-cooler housing walls to the engine coolant. This study was divided into two (2) categories to include the reduction of heat loss through thinner housing walls and the application of thermal insulation.

2.9.2.2.1 Thin Walls — A theoretical analysis aimed at reducing the heat conduction losses from the heater head to the engine coolant was conducted. Changes in length of the cylinder and regenerator walls were not included; only changes in wall thickness were made as follows:

	4-245 Standard Wall Thicknesses (mm)	Thin Wall Thicknesses (mm)
Regenerator	7.68	3.840
Cylinder @ Top	9.59	4.795
@ Midpoint	8.68	4.340
@ Bottom	7.93	3.965

The use of thinner walls would have the following effects:

a) Reduction of heat losses to the engine coolant during fully-warm engine operation.

b) Reduction of stored heat losses to the engine cold-start operation (engine would reach operating temperature faster).

The theoretical analysis indicated that a metro-highway fuel economy improvement of 1.02 MPG and 0.35 MPG (gasoline) would be achieved for fully-warm and cold-start operation respectively.

It is also recognized that thinner housing walls will reduce the engine's structural strength. No stress analysis has been performed during Task I. By way of comparison, however, it has been estimated that the present 4-215 Stirling engine housing walls are designed to a factor of safety of approximately four (4), and with thin walls (1/2 thickness) the factor of safety is considered to be two (2). It is for this reason that an individually assigned confidence level of 20% rather than the arbitrarily assigned confidence level of 40% for theoretical analysis has been assigned to this incremental fuel economy improvement.

2.9.2.2.2 Insulation — The effect of adding a thermal insulating material to reduce heat conduction losses from the cylinder and regenerator-cooler housing walls to the engine coolant was analyzed for the 4-245 Stirling engine. It was assumed in this analysis that the thickness of cylinder and regenerator-cooler walls was reduced (1/2 thickness) and that the insulating material was 1/16" (1.588 mm) thick with a thermal conductivity of 0.090 Btu/hr-ft$^{\circ}$F (0.158 watts/m-$^{\circ}$C). The estimated improvement in M-H fuel economy for the 4-245 Stirling engine was found to be 0.50 MPG. A split heater head design concept would be required in order to incorporate an insulation material. One such design has been developed by USS for use in the P-40 Stirling engine (Figure 2.9-2). In this design, an insulating material is not presently used but this type of design is one model amenable to the use of insulation techniques in future Stirling engines.

2.9.2.3 Fuel-Off During H_2 Overtemperature — From a continuous measurement of gas (H_2) temperatures recorded during vehicle operation over the CVS (city) and EPA-HWY (highway) driving cycles, it was determined that the overtemperature set point controller caused fuel flows during vehicle deceleration to be reduced to 0.4 g/s for 190 sec. over the city driving cycle and 40 sec. over the highway driving cycle. If the fuel flow had been shut off during the overtemperature periods, instead of being reduced to 0.4 g/s, there would have been a projected fuel savings of 76 g (city) and 16 g (highway). A summary of the baseline fuel economy calculations and the adjusted fuel economy calculations with the fuel shut-off is reported as follows:

4-215 Stirling Engine Baseline Data

4500 lb. Vehicle

	CVS-H	CVS-C/H	EPA-Hwy	M-H
Fuel (grams)	1350.3685	1500.2685	1445.6557	
Fuel Economy (MPG)	15.57	14.01	19.86	16.15

4-215 Stirling Engine Revised Data with

Fuel Shut Off - 4500 lb. Vehicle

	CVS-H	CVS-C/H	EPA-Hwy	M-H
Fuel (grams)	1274.3685	1424.3685	1429.6557	
Fuel Economy (MPG)	16.50	14.76	20.08	16.76

IMPROVEMENT = 0.61 MPG

The M-H fuel economy incremental improvement opportunity was calculated to be 0.61 MPG. It was also determined from the temperature record that energy was added to the hydrogen working gas during vehicle decelerations. For the times stated above the temperature continued to rise even though the fuel flow rate was reduced to 0.4 g/s. Therefore, it was assumed that energy losses from the engine also existed as follows during fuel-off decelerations:

1. Heat transfer from the walls to the H_2 gas.

2. Heat transfer from the regenerators to the H_2 gas.

3. Heat transfer from the walls of the cylinder and regenerator-cooler to the engine coolant.

These losses were not analyzed to determine a net gain in fuel savings with the fuel shut-off.

It was assumed, nevertheless, that the optimum fuel economy improvement potential was in the range of 0.61 MPG M-H. A confidence level of 20% was assigned to this improvement. Further analyses and test would be required to determine what effect energy losses from the engine have on the calculated improvement in fuel economy during fuel-off decelerations.

2.9.2.4 Higher Heater Head Mean Temperature — An investigation was made of the cycle efficiency improvement that would be obtained by increasing the heater head temperature 100°C from 750°C to 850°C. The analysis was done by optimizing a Stirling engine of the 302 engine equivalent full load power with an arbitrary 100°C increase in heater head temperature. The results from the optimization showed a 2.4% indicated efficiency improvement at maximum power compared to a baseline 302 equivalent Stirling engine. It was projected that this efficiency increase would translate into approximately a 1.0 MPG improvement over the M-H driving schedule.

302

2.9.2.5 Powertrain Matching — The torque characteristics of the Fourth Generation (4-245) Stirling engine differed from the torque characteristics of the 351M internal combustion engine. Powertrain components used as standard equipment for the baseline vehicle were compatible with the 351M internal combustion engine. With a torque converter more compatible with the Stirling engine and a fuel efficient automatic transmission, the M-H fuel economy of the baseline vehicle with the 4-245 Stirling engine installed was projected by the TOFEP computer program to be increased by 2.62 MPG. Using these optimized powertrain components in the baseline vehicle when the 351M internal combustion engine was installed caused an increase in M-H fuel economy of 2.22 MPG. Accordingly, with the optimized powertrain, an increase of 0.40 MPG was projected for the 4-245 Stirling engine over the 351M internal combustion engine. The complete description of the optimized powertrain was the same as the baseline vehicle with the 351M internal combustion engine and the standard equipment powertrain (i.e., a 0-60 MPH acceleration time of 13.3 seconds).

2.9.3 Conclusions and Recommendations — The total incremental fuel economy improvement opportunity for Other Fuel Economy Improvements (section 2.11) ranged from a minimum of 1.20 MPG to 4.02 MPG (gasoline). This improvement represented approximately 13% of the total improvement opportunity for the Fourth Generation Stirling engine. Of the improvement opportunities discussed, the most promising areas included:

a. Methods to reduce conduction losses (1.37 MPG).

b. Higher heater head mean temperatures (1.0 MPG).

c. Powertrain matching (0.40 MPG).

These opportunities represent approximately 10% of the total improvement opportunity for the Fourth Generation Stirling engine.

It is recommended that future programs to develop a Fourth Generation Stirling engine include in their content provisions for active studies of at least the most promising areas reported. In particular, further studies of design methods to reduce heat conduction losses to the engine coolant should include analyses covering static strength, endurance strength and creep rupture strength of the metal cylinder and regenerator-cooler housing walls at elevated temperatures. Hydrogen gas containment as affected by thin metal wails and insulated joints should also be investigated during this study.
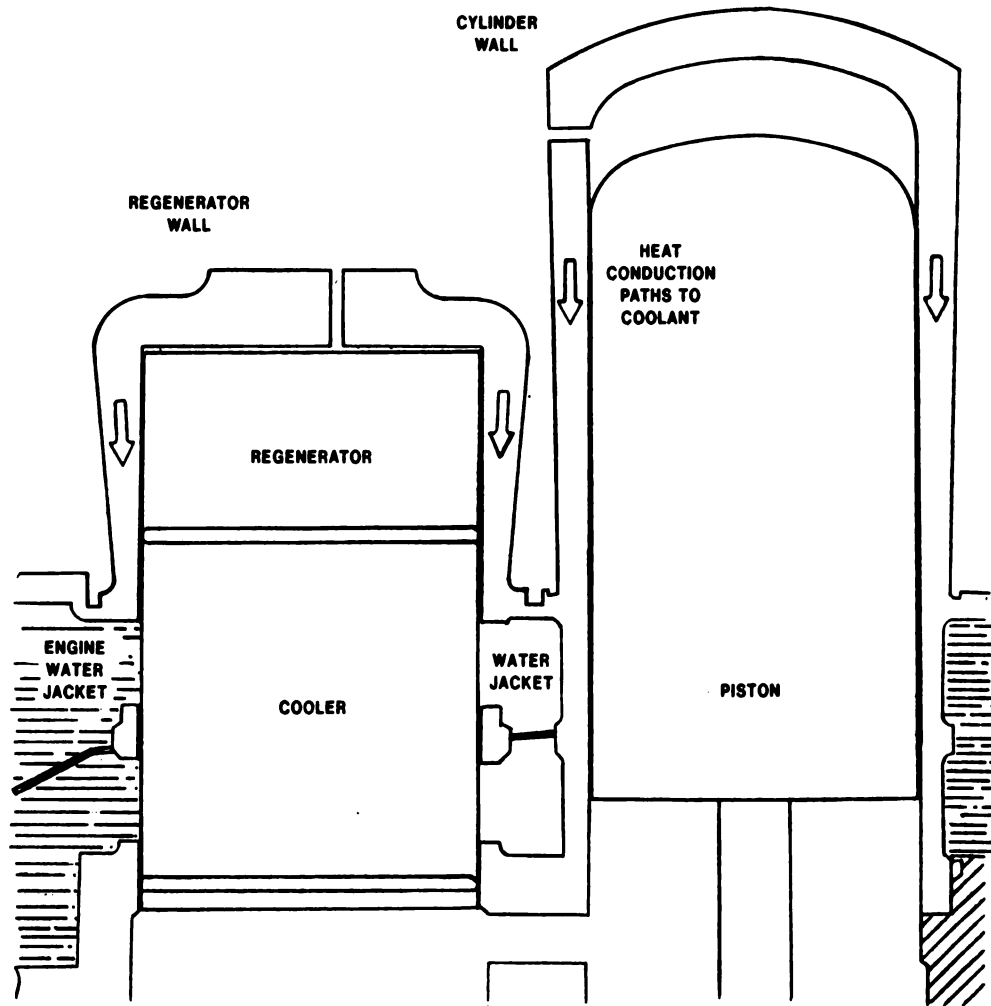
Figure 2.9-1   Integral Heater Head - N. V. Philips Co. - 4-215 Engine
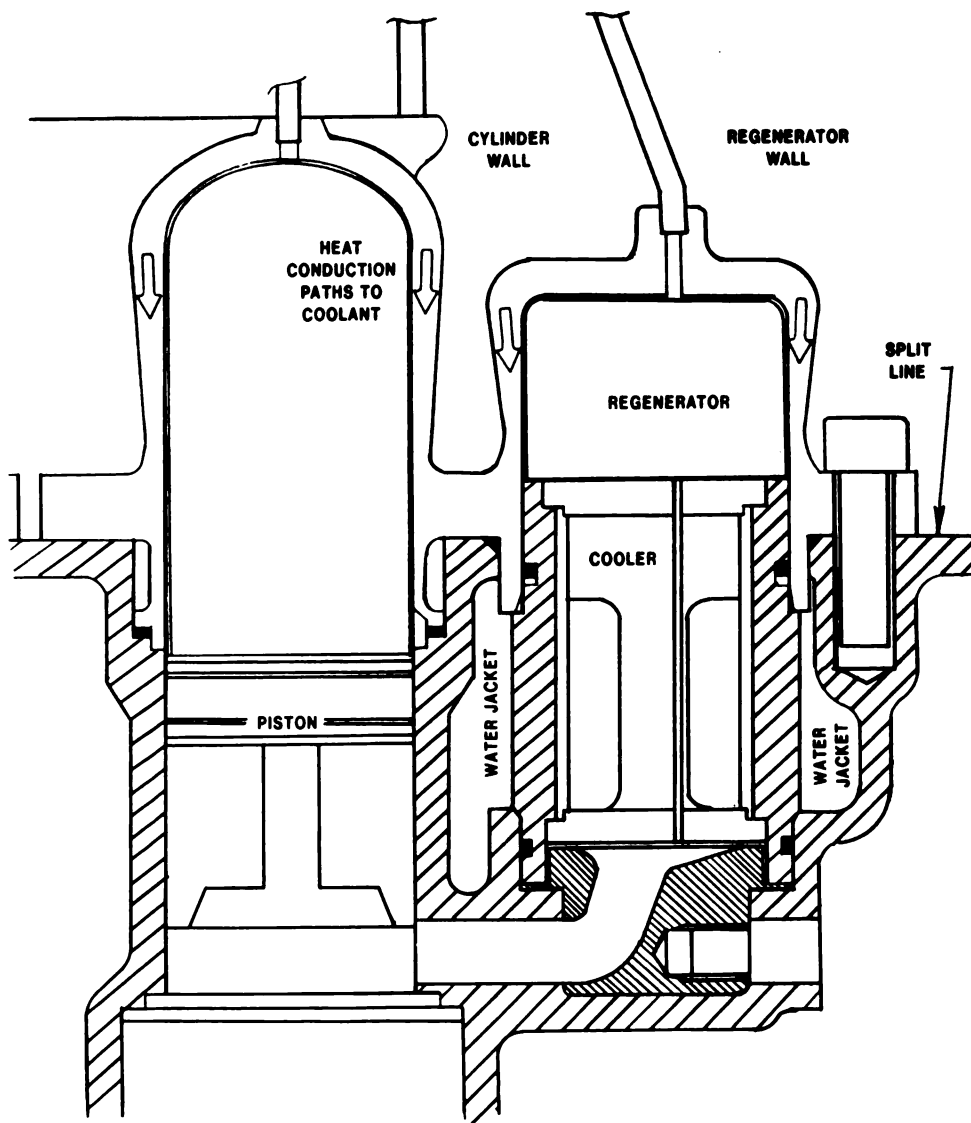
Figure 2.9-2   Split Heater Head – United Stirling of Sweden – P40 Engine

2.10 Cooling System Analysis

2.10.1 Summary — The objective of this effort was to identify and quantify the fuel economy gain opportunities related to the engine cooling system.

The principal areas of investigation within the 4-215 Stirling engine cooling system were divided into water-side and air-side opportunities, and the following were selected as the most promising for further study:

a. Heat conduction losses from the cylinder and regenerator housing walls to the coolant;

b. Coolant flow losses within the water jacket;

c. Coolant distribution around hydrogen cooler tubes:

d. Radiator air-side fin effectiveness.

The only improvement opportunity studied analytically was the reduction in heat conduction losses from the cylinder and regenerator housing walls to the engine coolant. The remaining areas required experimental development of models. Coolant flow model studies were planned within the Alternate Engines Research Department, while developments in designs with experimental air side fin geometries were followed within the Ford Motor Company for potential application with the Stirling engine.

The work performed in this section was in the following areas:

> Heat Conduction Losses
> Coolant Flow Losses
> Hydrogen Cooler Tubes
> Radiator Fin Development

Computer programs referred to in this section are described in section 5.3.

2.10.2 Heat Conduction Losses — Engine mapping techniques were applied to theoretical fuel flow data generated by the N.V. Philips computer program to determine the effect of cylinder and regenerator-cooler housing heat losses on M-H fuel economy. Analysis revealed that the theoretical upper limit of improvement would approach 5.1 MPG when all heat losses from the housings were prevented. Practical methods to reduce heat losses to the coolant were then studied under Cooling System Analysis and Cycle Analysis with the fuel economy improvement opportunities reported in section 2.9. With the application of insulated thin cylinder and regenerator-cooler housing walls, analysis revealed a maximum improvement opportunity of 1.87 MPG.

2.10.3 Coolant Flow Losses — It was estimated that a fuel economy improvement opportunity of 0.04 MPG could be realized through a reduction in water pump power consumption by improving water pump efficiency and/or reducing coolant flow losses within the Stirling engine water jacket.

With the present design, the 4-215 Stirling engine water pump efficiency is 53%

while current production water pumps range up to 40%. The TOFEP computer program was used to determine the fuel economy improvement opportunity for a 60% efficient Stirling engine water pump. The results indicated that an improvement opportunity of 0.03 MPG existed and, as such, it was decided that during Task I an improvement of this magnitude did not justify a project on water pump development to hopefully achieve a relatively high static efficiency of 60%.

An improvement in fuel economy through a reduction in water pump power consumption was also possible when coolant flow losses were reduced. Improvements in coolant distribution through the eight (8) parallel paths leading to and away from the regenerator-cooler tube bundles would not only reduce water jacket flow losses but would also permit an improved thermal balance of the hydrogen gas in the cylinders. A visual examination of the water jacket configuration revealed that improvements in coolant distribution and flow pressure drop were possible through experimental evaluations of and modifications to the coolant flow regimes in transparent plastic models. Locally low coolant flow velocities in critically-cooled regions of the water jackets would be detected with an optical velocimeter tracking micron-sized rheoscopic trace particles entrained in the coolant. Experimental in-clay modifications within the transparent models would then be applied to correct locally poor flow conditions. In some instances of extremely complicated flow conditions, high speed photography would be introduced to examine coolant behavior. Static pressure taps would be installed at key locations to determine the reduction in local flow losses due to improved design features as well as the overall reduction in pressure loss across the entire water jacket system.

A transparent plastic model of the main and secondary water jacket for the 4-215 Stirling engine was designed and built. These flow models are shown in Figures 2.10-1 thru 2.10-4. The models were designed for ease of assembly and disassembly to permit rapid in-clay modifications within the jackets. An existent closed circuit water flow facility was located for test of these models within Engineering and Research Staff, Ford Motor Company. These models were not evaluated during Task I, the Fuel Economy Assessment Program, due to a lack of manpower but were scheduled for developmental study under Task VII, Sub-System and Component Development in 1979-1980 with application directed toward the Second Generation Stirling engine cooling system.

2.10.4 Hydrogen Cooler Tubes — Each of eight (8) regenerator-cooler housings within the 4-215 Stirling engine contains a bundle of hydrogen gas filled tubes which are cooled in two-pass flow configuration by the engine coolant. Although the Philips cycle analysis computer program (section 5.3) assumes a uniform coolant flow distribution across each of the eight (8) tube bundles, an examination of the housing port openings and containing walls in relation to the tube bundle suggests that up to 10% of the tubes are located in regions of locally-low coolant velocities. In order to improve the design of the housing and tube bundle array it was decided to evaluate and correct the coolant flow regime using a two-dimensional large size transparent plastic model. The development and test of this model was scheduled under Task VII, Sub-Systems and Component Development, which was scheduled for 1978-1979.

2.10.5 Radiator Fin Development — The largest thermal resistance in the heat

transfer path from the engine coolant to air is on the air-side of the radiator and is due to the relatively poor film coefficient of heat transfer. In order to improve the performance of radiators, the air-side surface area is optimized with extended (fin) surfaces, and the fin geometry is configured to minimize the build-up of a fluid boundary layer on the surface. Experimental studies to develop improved fin geometries are in progress within the Ford Motor Company, and as improved designs would have become available, they would have been evaluated for application with the radiator for the Second Generation Stirling engine.

Radiators tested with improved fin designs have a higher heat rejection rate per unit of air flow pressure drop, i.e., Colburn Number/Fanning Friction factor ratio. This improvement in performance leads to lower coolant temperatures within the engine water jacket and, as a result, increased engine thermal efficiency. However, if it is desired to maintain the coolant temperature at a given design level, the power consumption of the engine cooling fan may be reduced. In order to assess the fuel economy improvement opportunity with reduced fan power consumption, an analysis with the TOFEP vehicle simulation computer program was conducted. In this analysis the fan power was arbitrarily set equal to one-half of the present level and, for comparison, set equal to zero. The results indicated that an improvement of 0.09 MPG would be achieved when the fan power consumption was reduced to one-half of the present level, and 0.19 MPG when the fan was removed. A 10% reduction in fan power was estimated to result in a fuel economy improvement opportunity of 0.02 MPG.

The TOFEP computer program was also used to determine the fuel economy improvement opportunity with reduced cooling system weight through improved design and/or material substitution. It was determined that a reduction of 10 lb. in the weight of the cooling system resulted in an improvement opportunity of 0.01 MPG.

Conclusion — It was estimated that a fuel economy improvement opportunity of 0.06 MPG would be achieved for the Fourth Generation Stirling engine through design improvements in the internal and external engine cooling system.

Main Water
Jacket Model

Secondary
Water Jacket
Model
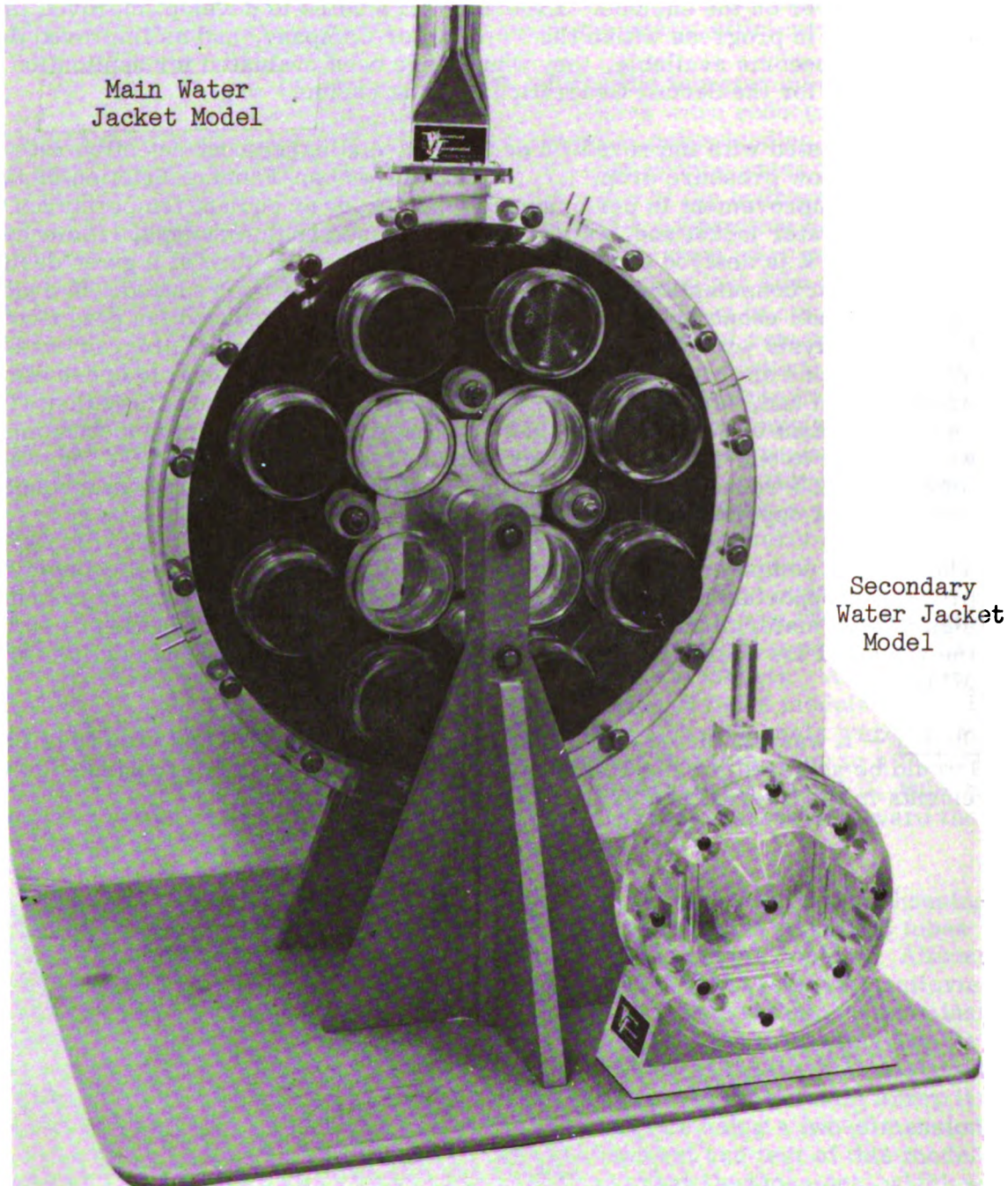
Figure 2.10-1   4-215 First Generation Stirling Engine - Transparent Plastic Water
Jacket Models

AUTOMOTIVE STIRLING ENGINE DEVELOPMENT PROGRAM

4-215 FIRST GENERATION STIRLING ENGINE

TRANSPARENT PLASTIC WATER JACKET MODEL
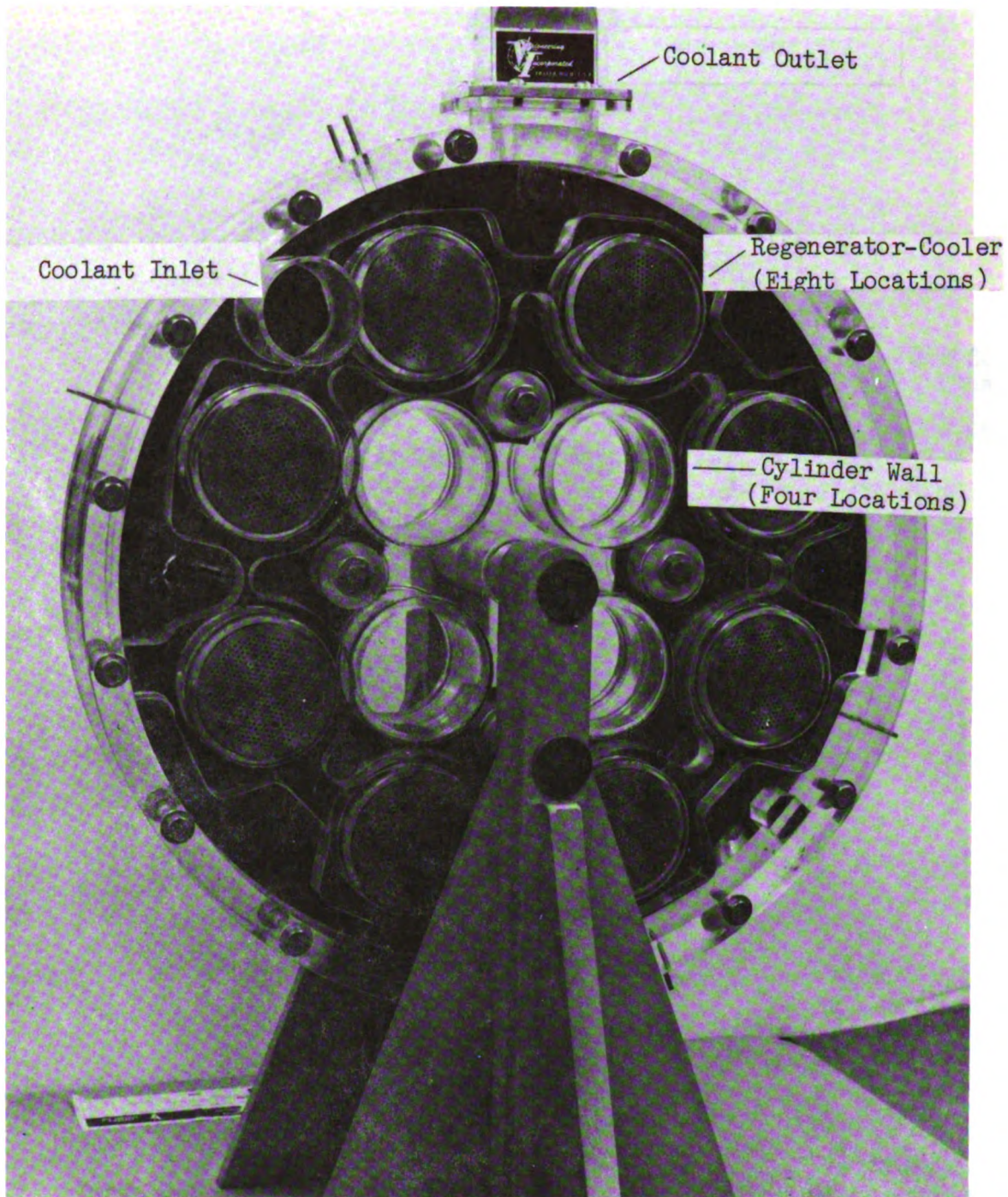
Figure 2.10-2   Main Water Jacket Front View

AUTOMOTIVE STIRLING ENGINE DEVELOPMENT PROGRAM

4-215 FIRST GENERATION STIRLING ENGINE

TRANSPARENT PLASTIC WATER JACKET MODEL
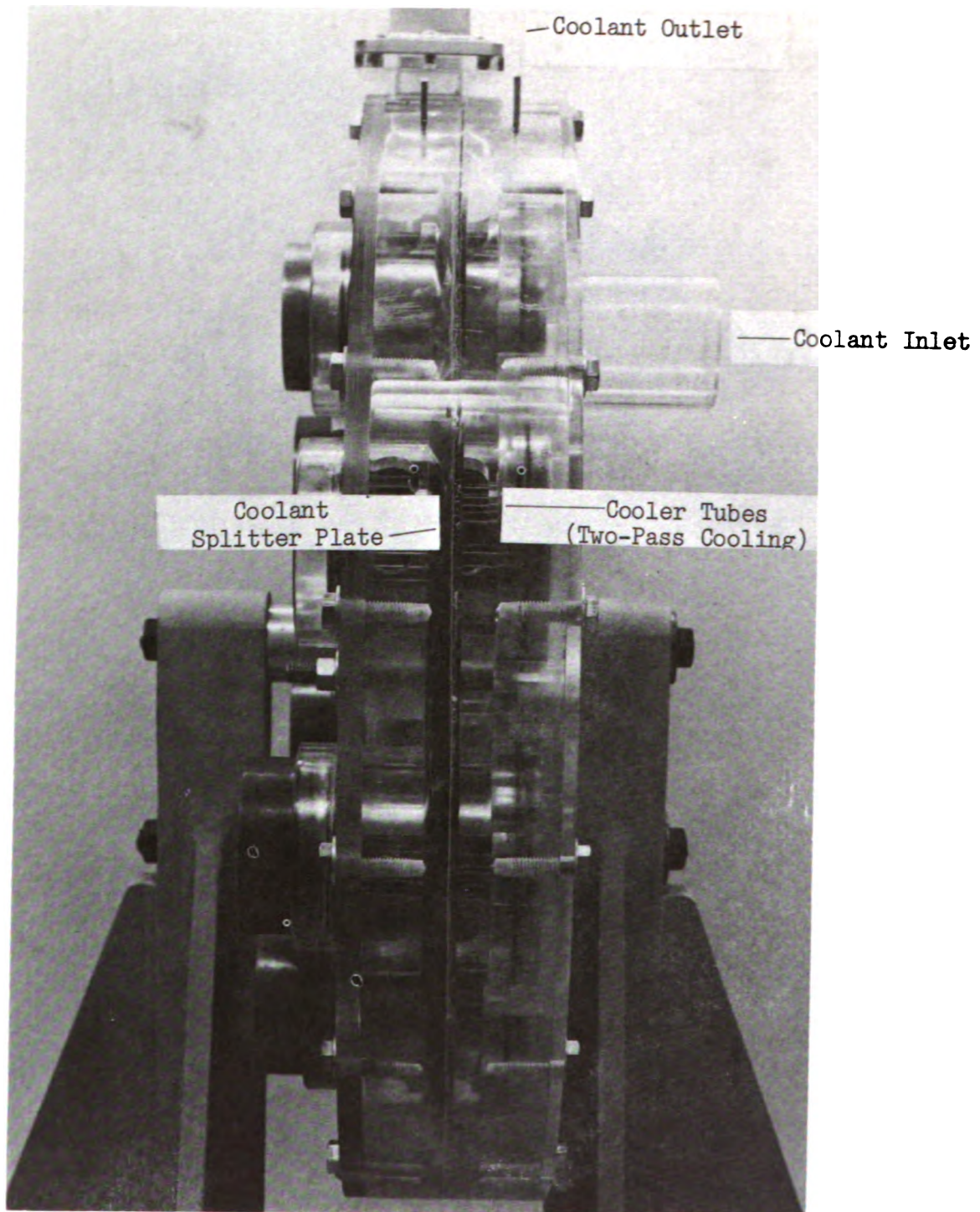
Figure 2.10-3   Main Water Jacket Side View

AUTOMOTIVE STIRLING ENGINE DEVELOPMENT PROGRAM

4-215 FIRST GENERATION STIRLING ENGINE

TRANSPARENT PLASTIC WATER JACKET MODEL
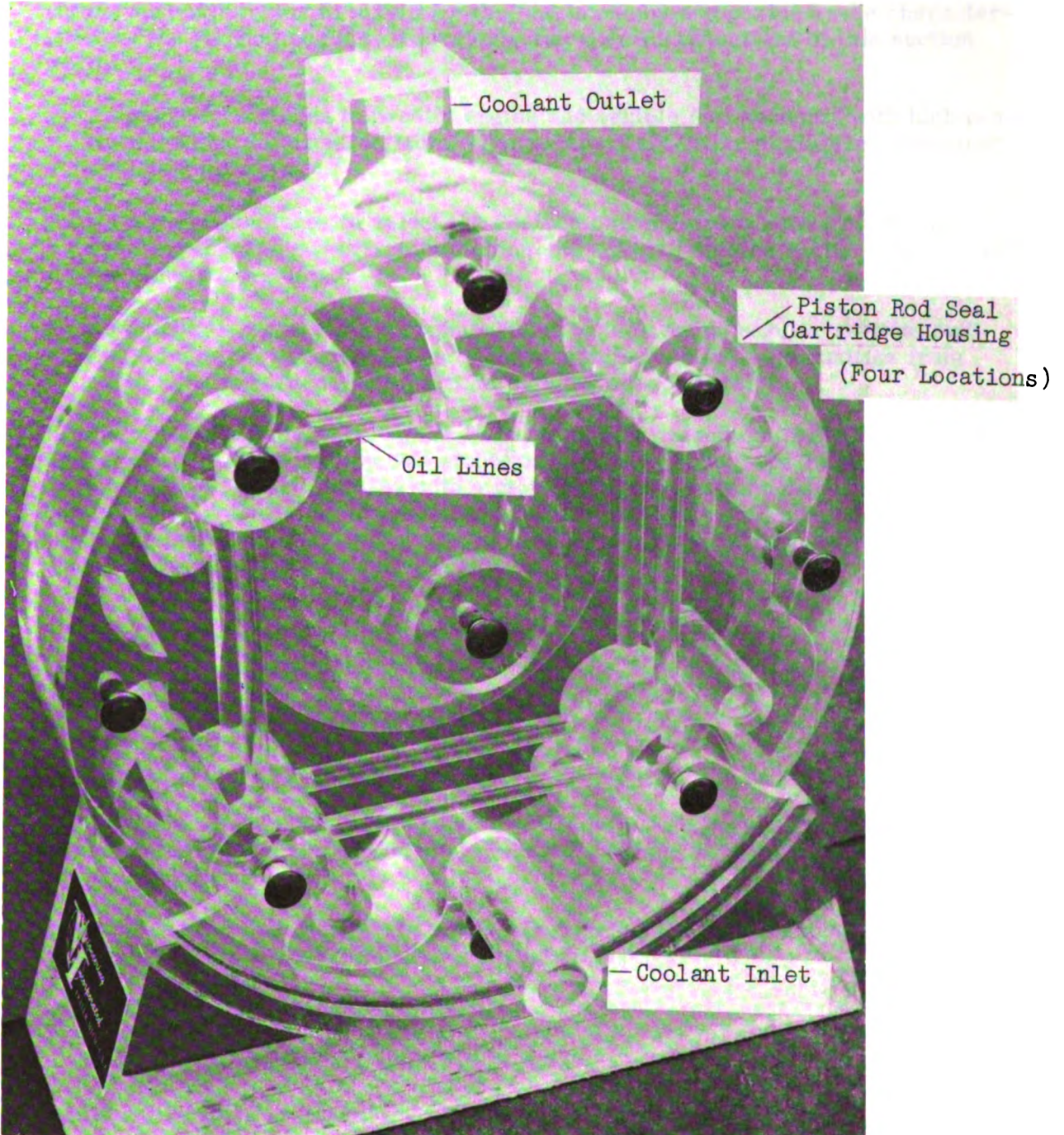
Figure 2.10-4   Secondary Water Jacket

2.11 Fuel Economy Analysis

2.11.1 Summary — The objective of this section was to predict engine and vehicle fuel economy characteristics at higher confidence levels, using information acquired from the results of work in other areas and from established Stirling engine computer modeling programs. In addition, analyses were to be conducted to help select other powertrain parameters such as torque converter, transmission gear ratios, and axle ratios to maximize the fuel economy and performance characteristics of the Stirling engine. Therefore, the specific objectives of this section were:

a. To perform analyses to predict engine and vehicle fuel economy with high confidence using information from other sections and from established computer modeling programs;

b. To perform analyses to select the desired parameters which optimize fuel economy through powertrain matching and tradeoff studies at the various vehicle simulation points.

c. To establish a reporting technique which would permit regular reviews and would track the progress of fuel economy improvement opportunities from early low confidence levels to final high confidence levels.

Task I, Fuel Economy Assessment, was originally presented to ERDA (DOE) on February 4, 1977. The task was structured to provide both the Federal government and Ford Motor Company with a more accurate assessment of the ultimate fuel economy potential of a passenger car Stirling engine with near-term technology. The intent of the program was to identify systems and components to provide the following functional objectives:

	Stirling	Baseline
Emissions (gm/mi, HC/CO/NO$_x$)	0.4/3.4/0.4	1.5/15/2.0
Fuel Economy (gasoline) (MPG, M-H)	20.2	15.5
Performance (sec., 0-60 MPH time)	13.3	13.3

The baseline was a 1977, 4500 pound car with a 351-2V engine and automatic transmission at 49 state emission calibration. (Refer to Figure 2.11-1 for complete description.)

Analysis showed that there were two primary areas for fuel economy improvement for the 4-215 First Generation Stirling engine.

a. Modifications to the cycle itself

b. Reduction of friction and parasitic losses

Realistically, only an estimated 1/3 of friction and parasitic losses could be reduced. Therefore, most of the future gains would have to be made by modifications to the 4-215 Stirling engine cycle.

Projections supported by preliminary calculations, which included some mapping technology, indicated the following potential fuel economy gains were achievable from improvements to the 4-215 First Generation Stirling engine:

Reduced friction and parasitic losses	2.0 MPG
Improved cycle parameters	2.9 MPG
Phase I 4-215 Stirling engine objective	15.7 MPG
Total (Fourth Generation)	20.6 MPG[1]

[1] 0.4 MPG over the Fourth Generation Stirling powered automobile M-H economy objective of 20.0 MPG.

A detailed summary of the estimated fuel economy improvements follows:

Fuel Economy Improvements Supported by Rig and Dynamometer Test and Development Work

• Mapping and optimization	0.4
• Burner system development	0.2
• Preheater development	0.3
• External heat blower system development	0.1
• Power control development	0.9
• Air fuel control development	0.2
Sub-total	2.1

Fuel Economy Improvements Supported by High Confidence Level Calculations

• Engine drive system study	0.2
• Cycle analysis	2.1
• Cooling system development	0.5
Sub-total	2.8
TOTAL	4.9
Phase I 4-215 Stirling Engine Objective	15.7
Projected Capability of Fourth Generation Engines	20.6 MPG [1]

[1] Projected capability is 0.4 MPG more than objective of 20.2 MPG. These

estimates were based upon a preliminary detailed analysis conducted prior to initiation of the Task I Work Plan. Upon completion of the Task I program, it was expected to substantiate the above information at a high level of confidence.

All computer programs referred to in this section are described in section 5.3.

2.11.2 Procedure — The procedure of evaluating alternate engine fuel economy potential and associated confidence level permits a consistent approach in the projection of M-H fuel economy. The Fuel Economy Assessment Chart is used to report improvement opportunities in M-H fuel economy due to improved design features of the engine. A particular improvement opportunity may be based on either an estimate, theoretical analysis, component test or engine dynamometer test.

The Fuel Economy Assessment Chart (See Figure 2.11-2) details individual improvement opportunities, the types of evaluation completed, the types of evaluation planned, the individual as well as overall confidence levels, and the total fuel economy improvement opportunity over a defined baseline vehicle fuel economy.

Arbitrary confidence levels of 20%, 40%, 60%, and 80% have been defined on the chart for estimates, theoretical analysis, component test, and engine dynamometer test respectively. Fuel economy projections are reported along with an overall confidence level on the final page of the chart. The chart also identifies the type of fuel economy evaluations planned for a particular improvement opportunity with open boxes. Shaded boxes indicate the types of fuel economy evaluations not planned within the scope of the study. In some cases large open boxes are present where a number of small improvement opportunities will be evaluated collectively.

2.11.2.1 Fuel Economy Assessment — The incremental metro-highway fuel economy opportunities reported on the Fuel Economy Assessment Chart are based on the application of engine mapping techniques to theoretically generated or test-developed engine fuel flow data. Engine mapping points are a select number of steady-state operating conditions conducted at a stabilized temperature which, when combined, simulate the transient operation of vehicle over the EPA city (CVS-HOT) and highway (HWY) driving schedule. Each of the selected mapping points is assigned a percentage of the total time for the vehicle to complete either the city or highway schedule such that the total work done at the mapping points is equal to the total work done during actual transient operation. Engine mapping points are expressed in terms of engine speed/load points and the time that the vehicle spends at each speed/load point is referred to as a time-weighting factor.

A computer program, VSIM, is used to obtain the selection of appropriate engine mapping speed/load points. A second program, TIME, is used to determine the city and highway time weighting factors of the vehicle. Road-load characteristics, powertrain parameters, and accessory loads are required as input data to the VSIM program, and engine speed/load points are required as input data to the TIME program. The results from one set of calculations for a 1977 LTD II are presented in Figure 2.11-3. Typical input information required for the VSIM program is described in Figure 2.11-1.

A computer program, ECONCALC, has been written to interpolate fuel flow

317

rates from an engine map once the speed/load points and time-weighting factors have been determined. The program then applies a cold-start correction factor to the computed city (CVS-HOT) fuel economy. The M-H fuel economy is subsequently computed as a weighted harmonic mean average of the city (CVS-COLD/HOT) and EPA highway fuel economy (Figure 2.11-4). The equations used to calculate M-H fuel economy are presented in Figure 2.11-5.

A correction factor to adjust the city (CVS-HOT) fuel economy for engine cold-start operation is included in all projections of M-H fuel economy.

The corrected value is a prediction of the city (CVS-COLD/HOT) fuel economy. This correction factor is determined through a comparison of a number of CVS-HOT and CVS-COLD/HOT fuel economy evaluations of the vehicle chassis roll dynamometer. A theoretical analysis of engine cold-start fuel penalty has also been made and the result is in good agreement with vehicle chassis roll test evaluation. The cold-start penalty used in the ECONCALC computer program is conveniently based on theoretical analysis in order that theoretical engine models in various sizes may be evaluated for M-H fuel economy.

In addition to VSIM and TIME, a computer program entitled TOFEP is also used to predict vehicle fuel economy. Unlike VSIM and TIME, TOFEP does not require the use of vehicle simulation points but rather integrates the fuel consumed second-by-second as the vehicle model is "driven" over the EPA city and highway driving schedules. This program is used to compare the performance as well as the fuel economy for a number of engines and powertrains under study without resorting to vehicle simulation mapping techniques. The TOFEP computer program results have also been compared to the VSIM/TIME/ECONCALC program results for a select number of cases and the results are discussed elsewhere in this report.

2.11.2.2 Confidence Level — The term "Confidence Level," described in this procedure, is not the same as the classical, statistical confidence level. As used in this paper, the meaning has the connotation of a "weighting factor" which describes how confident we feel about our published data, i.e., not too confident with estimates (20%) and very confident with vehicle test data (100%). The rules to establish "confidence levels" for calculations of incremental improvements in M-H fuel economy have been developed in order that a consistent approach is used by all personnel.

Arbitrary "confidence levels" are defined as follows:

Confidence Level	Definition	Required Document
.2	Estimated values	Rationale
.4	Theoretical analysis using mapping technology but not based on proven correlations with hardware tests	Analysis
.6	Results of component test using mapping technology but not based on proven correlations with engine	Test results

318

Confidence Level	Definition	Required Document
	dynamometer data	
.7	Theoretical analysis using mapping technology and based on proven correlations from hardware tests	Proven correlation and analysis
.8	Results of engine dynamometer tests based on mapping technology	Test results and analysis

The present overall confidence level of incremental fuel economy improvements is defined as follows:

$$CL_o = \frac{\sum_{i=1}^{n} \left(CL_i \times MPG_i \right)}{\sum_{i=1}^{n} \left(MPG_i \right)} \qquad \text{Eq 2.11-1}$$

Where:

CL_o = Overall confidence level of present incremental fuel economy improvements

CL_i = Sub-sub-task incremental fuel economy improvement confidence level

MPG_i = Sub-sub-task incremental fuel economy improvement

n = Number of incremental fuel economy improvements reported on the Fuel Economy Assessment chart

The expected overall confidence level of incremental fuel economy improvements at the end of Task I, Fuel Economy Assessment, is determined as follows:

1. Shift the present incremental fuel economy estimates to the last planned phase of study, i.e., relocate from the estimate column to the dynamometer test column as an example.

2. Calculate the expected overall confidence level.

2.11.3 Fuel Economy Assessment

2.11.3.1 Method of Analysis — The Fuel Economy Assessment Chart was de-

319

veloped to establish a method by which the progress of Stirling engine fuel economy improvement opportunities could be tracked and periodically reviewed throughout the one (1) year Fuel Economy Assessment Program. Individual confidence weighting factors were assigned to each improvement opportunity on the chart in order to determine the overall confidence level in the published fuel economy projections for the 4-245 Fourth Generation Stirling engine installed in the baseline vehicle (4500 lb (IWC) 1977 Ford LTD II). Refer to section 2.8 for a description of the 4-245 engine.

Fuel economy projections of the Fourth Generation Stirling-powered automobile (SPA) were obtained by adding the fuel economy improvement opportunities reported on the Fuel Economy Assessment Chart to the hardware-proven fuel economy for the 4-215 First Generation baseline SPA. In order to establish the fact that the improvement opportunities are truly additive, all opportunities were screened to insure that "double-counting" of a given opportunity did not exist.

Since steady-state dynamometer engine projections of vehicle M-H fuel economy were not equal to actual transient vehicle chassis roll dynamometer test results, a vehicle fuel economy range from 12.9 MPG to 14.0 MPG based on vehicle chassis roll results was established for the First Generation SPA (Stirling-powered automobile). (Reference 2.11-1) In addition to the establishment of First Generation SPA fuel economy based on vehicle test data, each improvement opportunity was reported in terms of a minimum to maximum range where the maximum fuel economy improvement represents the optimum improvement opportunity for the Fourth Generation SPA. The predicted M-H fuel economy range for the 4-245 Fourth Generation engine was, therefore, based on the addition of the minimum 4-215 First Generation SPA fuel economy (12.9 MPG) to the minimum improvement opportunities and the addition of the maximum 4-215 First Generation SPA fuel economy (14.0 MPG) to the maximum improvement opportunities.

In addition to the minimum/maximum Fourth Generation SPA M-H fuel economy opportunities, a confidence-weighted fuel economy opportunity is also reported on the Fuel Economy Assessment Chart. The confidence-weighted opportunity was determined by first multiplying each maximum fuel economy opportunity by the assigned confidence-weighting factor (if the assigned weighting factor was less than 0.7) and, then, adding the weighted and unweighted fuel economy opportunities to the maximum First Generation baseline SPA fuel economy (14.0 MPG).

2.11.3.2 Fuel Economy Results — The overall objective at the beginning of the one (1) year Fuel Economy Assessment Program was to establish with a high degree of confidence the capability of the Fourth Generation Stirling engine to achieve a 30% greater M-H fuel economy (20.2 MPG) over the current and comparable internal combustion engine (15.5 MPG) in a 4500 lb (IWC) vehicle equipped with an automatic transmission.

It has subsequently been determined upon completion of the one (1) year assessment program that the Fourth Generation 4-245 Stirling engine fuel economy potential in a 4500 lb. (IWC) vehicle ranges from a minimum of 21.4 MPG to a maximum of 28.1 MPG (Figure 2.11-2). This range represents an improve-

320

ment from 38% to 81% over the base fuel economy of 15.5 MPG M-H (Figure 2.11-6). The overall confidence level to achieve 28.1 MPG is 52% and the overall confidence level to achieve 20.6 MPG is 76% as reported in Figure 2.11-2. A summary of the month-by-month change in the projected Fourth Generation SPA fuel economy during Task I is chronologically reported in Figure 2.11-7 for reference.

2.11.3.3 Conclusions — The original objective of the one (1) year Fuel Economy Assessment Program to determine the near-term and longer range fuel economy improvement opportunities for the Fourth Generation Stirling engine in a 4500 lb (IWC) vehicle has been met. This determination was made at a 0.4 NOx level and was supported by systems and component test work and analysis to the extent that a relatively high confidence in the improvement opportunities was achieved.

The original objective to achieve at least a 30% improvement potential in EPA M-H fuel economy compared to the equivalent 1977 spark-ignition engine powered automobile calibrated to the 49 state emission standards, utilizing identical fuels and at identical inertia weight classifications and performance levels has been exceeded. It has been determined that the maximum fuel economy opportunity for the 4-245 Fourth Generation Stirling-powered automobile is 28.1 MPG with a confidence level of 52%. This maximum fuel economy opportunity represents an improvement of 81% over the 1977 base vehicle M-H fuel economy of 15.5 MPG. It has also been determined that the minimum fuel economy opportunity of 21.4 MPG and the confidence-weighted opportunity of 23.1 MPG for the 4-245 Fourth Generation Stirling-powered automobile exceeds the original M-H fuel economy objective of 20.2 MPG.

2.11.4 Computer Analysis

2.11.4.1 Analytical Approach - During Task I, projections of M-H fuel economy and performance were made using the Ford developed PB1111, VSIM, TIME, ECONCALC and TOFEP computer programs. These projections were made primarily to determine the incremental changes in M-H fuel economy and performance associated with planned engine or vehicle changes.

These computer programs were also used in powertrain matching studies, engine sizing studies and in the development of engine mapping points used for dynamometer testing.

2.11.4.2 Analytical Results

Mapping Points - An accurate, consistent vehicle description is required to ensure accuracy in computer program projection and to ensure validity in computer program comparisons. One of the first items accomplished during the Task I effort was to obtain an accurate definition of the powertrain, tires, and pertinent vehicle parameters which were needed to comprise a complete description of the 4500 lb. IWC 1977 LTD II baseline vehicle (refer to Figure 2.11-1).

With an accurate description of the baseline vehicle, the VSIM and TIME computer programs were used to develop engine mapping points and time weighting factors in the manner previously discussed. The engine mapping points and

time weighting factors selected for the baseline 1977 LTD II 4500 lb. IWC vehicle are presented in Figure 2.11-3.

The engine mapping points were used to specify the speeds and torques used for dynamometer testing and could be used to obtain projections of M-H fuel economy from dynamometer test data. In engine testing these mapping points were the engine operating conditions of speed and torque at which steady-state fuel flows were measured. These steady-state fuel flows were in turn used to analytically project vehicle fuel economy with the equations reported in Figure 2.11-5.

The engine mapping points were also used to obtain theoretical projections of M-H fuel economy in the ECONCALC computer program with the aid of theoretically-generated engine maps as previously discussed.

Performance and Economy Comparisons - Performance and M-H fuel economy comparisons were made during Task I for simulated installation of the 4-215, 4-247, and 4-245 Stirling engines in the baseline 4500 lb. (IWC) vehicle. (Refer to Section 2.8 for description of 4-247 and 4-245 engines.) Also, performance and M-H fuel economy calculations were performed for the 351M internal combustion engine installed in the baseline vehicle in order to provide a basis for comparison.

The 4-215 Stirling engine represents the baseline First Generation Stirling engine. The 4-247 Stirling engine represented initial attempts at derating the power of the 4-215 engine to obtain an engine with torque characteristics similar to the torque characteristics of the 351M internal combustion engine. The 4-245 Fourth Generation Stirling engine also represents an engine which has had a derating to torque characteristics such that is was similar to the performance achieved with a 351M internal combustion engine.

Since two computer programs (PB1111 and TOFEP) were used to obtain projections of vehicle performance, the results of these two programs may be compared. For purposes of comparison, the 0-60 MPH wide-open throttle (WOT) acceleration times are presented in Figure 2.11-8. A review of the data in this figure shows that good agreement exists between the PB1111 and TOFEP computer programs in projecting vehicle performance. It is important to note the following: a final summary of performance data on 1977 vehicles (Reference 2.11-2) reported that the average 0-60 MPH acceleration time for a 4500 lb. (IWC) LTD II equipped with a 351M internal combustion engine was 13.3 seconds. It is seen from Figure 2.11-8 that PB1111 and TOFEP agree closely in their projections of 0-60 MPH acceleration time for all vehicle/engine combinations but that for the 351M internal combustion engine projection the predicted time was between 12.4 and 12.6 seconds, which was substantially less than 13.3 seconds. Accordingly, it was assumed during Task I that a PB1111 or TOFEP projection for 0-60 MPH acceleration time of between 12.4 and 12.6 seconds corresponded to a test track 0-60 MPH acceleration time of 13.3 seconds.

Sizing of Fourth Generation Engine - As previously discussed, the 4-215 First Generation Stirling engine has higher torque/power characteristics than the 351M internal combustion engine. This, in turn, caused the 4-215 Stirling powered baseline vehicle to have a projected 0-60 MPH acceleration time which

was faster than necessary. Accordingly, part of the Task I effort was directed towards the development of a Fourth Generation Stirling engine which had torque/ power characteristics which were similar to those of the 351M internal combustion engine. To obtain the required torque characteristics for the Fourth Generation Stirling engine, a linear scaling factor was applied to the torque vs. engine speed curve of a Stirling engine which had been optimized under part-load operating conditions (See Section 2.8.7). The final result was the 4-245 Fourth Generation Stirling engine. From Figure 2.11-8 it is seen that the 0-60 MPH acceleration time of the 4-245 Fourth Generation Stirling engine is projected to be approximately the same as is projected for the 351M internal combustion engine.

Figure 2.11-9 presents a comparison of the fuel economies projected for the various engines installed in the baseline vehicle. A review of the results presented in this figure shows that relatively good agreement exists between the ECONCALC and TOFEP computer programs in projecting EPA M-H fuel economies. In the worst case (4-245 Stirling engine), the difference between the ECONCALC and TOFEP computer projections was 0.38 MPG (1.8%).

Powertrain Optimization — The standard equipment used in the powertrain of the baseline 4500 lb IWC Ford LTD II includes a C-4 automatic transmission, an axial torque converter and a 2.5 rear axle ratio. The final effort of Task I was to optimize the Fourth Generation 4-245 Stirling engine in lieu of using the powertrain defined with the 351M internal combustion engine. In performing this optimization, the performance and fuel economy characteristics of all current production torque converters were evaluated in relation to their use with a Stirling engine. From this part of the evaluation, the use of torque converter D7DP-A2A (curve no. T8245) provides the optimum fuel economy savings over the standard torque converter. Also, the C-4 automatic transmission was replaced with the fuel efficient FIOD (Ford Integral Overdrive) transmission.

With the use of the optimized powertrain, the fuel economy of the baseline vehicle equipped with the 4-245 Stirling engine was projected to increase by 2.67 MPG M-H. When the optimized powertrain was simulated in the 351M internal combustion powered baseline vehicle, the increase in M-H fuel economy was projected to be 2.22 MPG M-H. Therefore, an increase of 0.45 MPG M-H was projected for the optimized package in the baseline vehicle with the 4-245 Stirling engine over the 351M internal combustion engine.

It should be noted that performance effects of varying the rear axle ratio were included in this study. This study showed that the rear axle specified as standard equipment for the baseline vehicle (2.5) is the best selection for use in the optimized powertrain.

It should also be noted that with the new powertrain the performance of the baseline vehicle was projected to improve slightly by 0.083 seconds.

Reference Engine Study — This effort was concerned with a Stirling engine designed to be the performance equivalent of a Ford 302 internal combustion engine. This reference engine was designated as the 4-248 Stirling engine, and for this study a different baseline vehicle was selected which has a lower inertial weight class than the original baseline vehicle (4500 lb. IWC). The characteristics of this new, updated 4000 lb. IWC reference engine baseline vehicle are described in

Figure 2.11-10. The projected performance and economy of the 4-248 Stirling engine and the 302 internal combustion engine are compared in Figure 2.11-11 for the updated Reference Engine baseline vehicle.

A review of the data in this figure shows that a 4-248 Stirling engine is projected by the TOFEP computer program to have a minimum improvement potential of 7.62 MPG in M-H fuel economy over the 20.0 MPG M-H fuel economy projected for the 302 internal combustion engine when installed in the Reference Engine 4000 lb. IWC baseline vehicle.

It should be noted that for either the 4-248 Stirling engine or the 302 internal combustion engine installed in the Reference Engine baseline vehicle, the projected 0-60 MPH acceleration time is the same (i.e., 13.0 seconds).

2.11.5 Conclusions and Recommendations — The data presented in Figure 2.11-8 demonstrates that the PB1111 and TOFEP computer programs closely in projecting the 0-60 MPH acceleration times of the baseline vehicle equipped with a 351M internal combustion by approximately 0.8 seconds. Test data for the baseline vehicle equipped with a 351M internal combustion engine reports that the 0-60 MPH acceleration time is 13.3 seconds while TOFEP and PB1111 project a 0-60 MPH acceleration time between 12.4 and 12.6 seconds.

The data presented in Figure 2.11-9 demonstrates that the TOFEP computer program and the VSIM/TIME/ECONCALC computer programs agree closely in projecting the M-H fuel economy of the baseline vehicle with the various Stirling engines installed. The maximum difference between the TOFEP and VSIM/TIME/ECONCALC projections in M-H fuel economy is 0.38 MPG (1.8%).

A review of the data given in Figure 2.11-9 shows that, in projecting the change in M-H fuel economy associated with engine changes in the baseline vehicle, reasonably good agreement exists between the TOFEP and VSIM/TIME/ECONCALC computer programs. For example, VSIM/TIME/ECONCALC projects an increase in M-H fuel economy of 5.71 MPG for the Fourth Generation (4-245) Stirling engine over the 4-215 Stirling engine while TOFEP projects an increase in M-H fuel economy of 6.33 MPG for this same engine change.

Powertrain optimization of the 4500 lb. (IWC) 1977 Ford LTD II baseline vehicle with a 4-245 Stirling engine installation increases M-H fuel economy by 2.67 MPG. Use of the optimized powertrain in conjunction with a 351M internal combustion engine causes a projected increase in M-H fuel economy of 2.22 for the baseline vehicle. Accordingly, the 4-245 Stirling engine offers a projected increase of 0.45 MPG in M-H fuel economy over the 351M internal combustion engine powered base line vehicle equipped with an optimized powertrain. Performance of the baseline vehicle with the optimized powertrain and the 4-245 Stirling engine installed, as measured by 0-60 MPH acceleration time, improved over the projected performance of the baseline vehicle with the standard powertrain and the 351M internal combustion engine powered baseline vehicle equipped with an optimized powertrain. Performance of the baseline vehicle with the optimized powertrain and the 4-245 Stirling engine installed, as measured by 0-60 MPH acceleration time, improved over the projected performance of the baseline vehicle with the standard powertrain and the 351M internal combustion engine by 0.083 seconds.

In the powertrain optimization studies contained in this report, the torque converters evaluated were all current production torque converters. Preliminary studies of torque converters planned for future production are projected by the TOFEP computer program to be more fuel efficient than the current production torque converters, and are also projected by the TOFEP computer program to provide better vehicle performance than do current production torque converters. Accordingly, it is recommended that additional powertrain optimization studies include evaluation of those fuel efficient torque converters currently planned for future production.

The Reference Engine study discussed in this section projects that for the same performance level (0-60 MPH acceleration time = 13.0 seconds), a 4-248 Stirling engine will have a minimum improvement potential of 7.62 MPG in M-H fuel economy over the 20.6 MPG M-H fuel economy projected for the 302 internal combustion engine when these engines are installed in the Reference Engine study 4000 lb. IWC baseline vehicle.

2.11.6 References

2.11-1   "Stirling Engine Feasibility Study of an 80-100 HP Engine and of Improved Potential for Emissions and Fuel Economy," Final Report, Ford Motor Company, November, 1977 (prepared for the U. S. Department of Energy, Division of Transportation Energy Conservation).

2.11-2   "Final Summary of Specifications and Performance Data on 1977 Ford-Built and Competitive Models," Inter-Office Communication, Car Product Development Group, Ford Motor Company, R. C. Heathfield, July 8, 1977.

VEHICLE DATA

Model	1977 LTD II 4-Door Sedan
Inertial Weight Class (IWC)	4500 lbs.
Performance Weight	4721 lbs. total (when equipped with a Stirling engine)
	4671 lbs. total (when equipped with a 351M engine)
Weight on Driving Wheels	2055 lbs.
Projected Frontal Area	23.4 ft^2
Drag Coefficient	0.62
Center of Gravity Height	20.5 in.

TRANSMISSION DATA

Type	C4 Automatic Transmission

Gear Ratios:

1st. Gear	2.46
2nd. Gear	1.46
3rd. Gear	1.00

Drive Shaft Speed
Shift Points:

3-2 Down Shift	2081 RPM
2-1 Down Shift	1031 RPM
1-2 Up Shift (WOT)	1575 RPM
2-3 Up Shift (WOT)	2439 RPM
3-1 Down Shift (WOT)	390 RPM

TORQUE CONVERTER DATA (Source: Transmission Division, Ford Motor Company)

Type	T-8302 (Axial)
Size	12 in.
Torque/Speed Ratio	1.96 @ stall conditions
Capacity Factor	100 @ stall conditions

Figure 2.11-1   1977 LTD II Vehicle and Engine Descriptive Data

ENGINE DATA

4-215 Stirling Engine	Engine Map: "TDEMBLVT"
4-245 Stirling Engine	Engine Map: "DKEM245C"
351M Internal Combustion Engine	Engine Map: "7351MENG"

REAR AXLE DATA

Ratio   2.50

TIRES/WHEEL DATA

Tire Size	HR 78X15 (Radial Ply)
Inflation Pressure	24 psig
Track Dynomometer Inflation Pressure	45 psig
Rolling Radius	1.131 ft.
Wheel Assembly Inertia	157.5 lb.-ft.^{2} (4-Wheels)
Revolutions/Mile	743
Track Tire Rolling Resistance Coefficient	0.394
Dynomometer Tire Rolling Resistance Coefficient	1.06

ENGINE FUEL DATA

Type	XE-M4C-332-A
Specific Weight	6.18 lb/gal.

ROAD LOAD DATA $(F=a+bV+CV^2)$[a/]
Test Track for 4721 lb. vehicle
(351M Engine equipped):

a = 56.81   )
b = -0.19559   ) Generated from VSIM
c = 0.035407   )

Figure 2.11-1   1977 LTD II Vehicle and Engine Descriptive Data (Cont'd)

ROAD LOAD DATA (Continued)

Test Track for 4671 lb. vehicle
(Stirling engine equipped):

$$a = 57.633$$
$$b = -0.19559$$
$$c = 0.035407$$

) Generated from VSIM

Chassis Dynamometer for 4500 lb IWC: With A/C[b]

$$a = 52.427$$
$$b = 0.0250$$
$$c = 0.03936$$

[a] F=(Lb$_f$),   V=(MPH);   4500 lb (IWC) Vehicle

[b] 1977 EPA "Cookbook" PAU Setting: 14.0 HP

Figure 2.11-1   1977 LTD II Vehicle and Engine Descriptive Data (Cont'd)

Confidence Level: Low ▼ — High ▲

Sub-Task No.	Sub-Task Description	ERDA Proposal Estimate (1)	Estimate (Min)-(Max)	Theoretical Analysis (Min)-(Max)	Component Test (Min)-(Max)	Dynamometer Engine Test (Min)-(Max)	Vehicle Projection (Min)-(Max)
01	MAPPING & OPTIMIZATION (ERVIN)	.4					
	• Reduced EGR reqmts	.04				PTS-110	.15-.45
	• Reduced exh back pressure	.03				PTS-097	
	• Minimum air flow reqmts	.04				PEN-166	
	• Temperature scheduling	.27				.15-.45	
02	BURNER SYSTEM (REAMS)	.2					
	• Low pressure drop burner	.02	0-.02		PTS-121	PTS-121	0-.02
	• Improved heater head temperature distribution	.13		PEN-167 0	PTS-121		
03	PREHEATER (REAMS)	.3					
	• Engine driven preheater	.14		PEN-149 .14-.16	PTS-113 .14-.16		0.40-0.62
	• Thin wall material preheater core	.14		PEN-147 .23-.26/.04		PTS-119 .26-.44	
	• Reduced preheater leakage	.02	0-.02				
	• Seal friction reduction	.01	0				

Figure 2.11-2   Improvement Opportunities in Metro-Highway Economy

Confidence Level — Low ▼ ▲ High

Sub-Task No.	Sub-Task Description	ERDA Proposal Estimate (1)	Estimate (Min)-(Max)	Theoretical Analysis (Min)-(Max)	Component Test (Min)-(Max)	Dynamometer Engine Test (Min)-(Max)	Vehicle Projection (Min)-(Max)
04	ENGINE DRIVE SYSTEM (KANTZ)	.2		PEN-156			1.21-1.94
	• Crankshaft vs swashplate	.10		.55-1.10	PEN-185		
	• Accessory drive	.05	0-.08	PEN-183			
	• Engine drive for fuel & atomizing air pump	--		0.29-0.36	PEN-185 .19-.24		
	• Piston ring friction	--		PEN-143	PNS-104		
				PEN-138	0		
				.18-.24			
05	EXTERNAL HEAT AND BLOWER SYSTEM (KANTZ)	.1		PEN-178			0.26-0.38
	• Improved blower design	.04		.05-.11			
	• Improved blower drive	.05	0-.08	PEN-183			
	• Reduced air flow reqmts (ref. Sub-task 10)	--		PEN-179 .21-.27			
08	POWER CONTROL SYSTEM (KOSACHEFF)	.9					2.26-3.13
	• Alternate power control	--		PEN-159			
	• Reduce power losses of power control actuator need for fast transient response	--		.54-.74	0-.02		
	• Hydrogen compressor losses	.85		PEN-176 .35-.56		1.72-2.30	
	• Eliminate "short circuiting" power losses during decelerations	--		0-.03			
	• Hydrogen distributor friction	.05		0-.03			
	• Sealed piston dome	.05(2)		0-.01			

Figure 2.11-2 Improvement Opportunities in Metro-Highway Economy (Cont'd)

Sub-Task No.	Sub-Task Description	ERDA Proposal Estimate (1)	Estimate (Min)-(Max)	Theoretical Analysis (Min)-(Max)	Component Test (Min)-(Max)	Dynamometer Engine Test (Min)-(Max)	Vehicle Projection (Min)-(Max)
09	AIR/FUEL CONTROL SYSTEM (FENTON)	.2					0-.16
	• Low pressure drop A/F control	.04		0-.06			
	• Improved A/F control	.10	0-.10	PEN-154 0			
	• Reduce power loss of electronic power & control systems	—					
10	CYCLE ANALYSIS (REAMS)	2.1					3.01-3.34
	• Reduced power re-optimization	.63					
	• Reduced thermal losses	.16					
	• Modified appendix gap	.27	PEN-148				
	• H$_2$ cooler tube material	.12	3.01-3.34/70%				
	• Part load reoptimization	.63	PEN-140				
	• Reduce fuel loss used for engine warm-up	—		PEN-172 0			
	• Increased heater head heat flux	.16	0				

Confidence Level   Low ▼   High ▲

Figure 2.11-2   Improvement Opportunities in Metro-Highway Economy (Cont'd)

331

Confidence Level — Low ▼ ▲ High

Sub-Task No.	Sub-Task Description	ERDA Proposal Estimate (1)	Estimate (Min)-(Max)	Theoretical Analysis (Min)-(Max)	Component Test (Min)-(Max)	Dynamometer Engine Test (Min)-(Max)	Vehicle Projection (Min)-(Max)
14	OTHER FUEL ECONOMY IMPROVEMENTS (JONES)	–					1.30–4.02
	• Decreased air cleaner pressure drop	–	0–.02				
	• Accessory drive starting energy reqmts	–	0–.02				
	• Reduction of engine and accessory inertia	–		PEN-177 0			
	• Methods to reduce conduction losses (thin walls)	–		.30–1.37/20%			
	• Fuel off during H_2 overtemperature	–	0–.61				
	• Methods to reduce conduction losses (insulation)	–	.20–.50				
	• Higher heater head mean temperature			.50–1.00			
	• Powertrain matching		.20–.45/40%				
	• Burner improvement		0–.10				
15	COOLING SYSTEM (JONES)	.50					0–.06
	• Radiator fin improvement for lower pressure drop	–	0–.02				
	• W/P power reduction	–	0–.04				

Figure 2.11-2 Improvement Opportunities in Metro-Highway Economy (Cont'd)

	Estimate (Min)-(Max)	Theoretical Analysis (Min)-(Max)	Component Test (Min)-(Max)	Dynamometer Engine Test (Min)-(Max)	Vehicle Projection (Min)-(Max)
PHASE I CAPABILITY[3]	-	-	-	-	12.9-14.0
ERDA PROPOSAL ESTIMATE (1) 4.90	-	-	-	-	20.6
FOURTH GENERATION ENGINE TECHNOLOGY (4)	0.40-1.90	5.63-8.66	0.33-0.42	2.13-3.19	21.32-28.17 (6)
Confidence Level Weighting Factor	.20	.40	.60	.80	
Confidence Level of (5) Present Projections	53% to meet 28.2 MPG 76% to meet 20.6 MPG				
Confidence Level (5) at End of Task I	53% to meet 28.2 MPG 76% to meet 20.6 MPG				

Figure 2.11-2   Improvement Opportunities in Metro-Highway Economy (Cont'd)

Fuel Economy Assessment Chart References

(1) ERDA Proposal May 12, 1977 Volume II, Exhibit VII, page 5

(2) Estimate included in the Total of CYCLE ANALYSIS, No. 10

(3) Phase I Capability; 4500 lb. (IWC), 2.75 rear axle ratio, 12.7 sec. (0-60 time)
"Stirling Engine Feasibility Study of an 80-100 HP Engine and of Improved Potential
for Emissions and Fuel Economy", Ford Motor Company, November, 1977, Page 25.

(4) 1977 baseline vehicle; 4500 lb. (IWC), 2.50 rear axle ratio, 13.3 sec. (0-60 time)

(5) Confidence level based on upper limit (Maximum) incremental M-H fuel economy improvements

(6) Maximum opportunity based on 14.0 capability is estimated to be 28.1 MPG (M-H). The
confidence weighted opportunity is 23.1 MPG (M-H).

(7) PTS (Philips Test Summary) and PEN (Philips Engineering Nore) are internal independent
studies within the Ford Motor Company and are not available for general distribution.

Figure 2.11-2   Improvement Opportunities in Metro-Highway Economy (Cont'd)

334

```
1977 LTD II Vehicle
4500 lb. (IWC)
4-215 Stirling Engine
100K Torque Converter
C4 Automatic Transmission
2.50 Rear Axle Ratio
```

(I.) Included in Vehicle Simulation
Front Transmission Pump
Cooling Fan (Clutch Disengaged)
Power Steering Pump

(II.) Installed on Engine Dynamometer and Operating
Blower - 6.25:1 Drive
         - Modified Viscous Fan Clutch
Alternator - 50 AMP Constant Load

Mapping Point Number	Engine Speed (RPM)	Engine Torque (ft-lb)	Engine Torque (N-m)	With A/C[a] CVS-H Time (Sec)	With A/C[a] EPA-HWY Time (Sec)
1	600	39.2	53.2	362.3	10.3
2	800	30	40.7	272.1	5.2
3	900	-5	-6.8	74.0	52.0
4	1000	50	67.8	167.2	29.1
5	1100	80	108.5	185.7	32.8
6	1300	115	155.9	147.2	45.9
7	1600	150	203.4	58.3	72.7
8	1700	80	108.5	57.5	331.4
9	1800	160	216.9	36.1	76.8
10	2000	90	122.0	11.5	107.8

a/ Chassis dynamometer road load with A/C: $F = 52.427 + 0.025V + 0.03936V^2$

Figure 2.11-3   Dynamometer Engine Mapping Points
(Chassis Dynamometer Road Loads)

Metro-Highway Fuel Economy Summary For 4-215 Engine Prepared On 12 SEP 1978 BY O. SPROW
BASED ON ENGINE MAP DATA FILE TDEMBLVT AND M-H DATA FILE MH2.5-10 (4500 LB. IWC VEH.)
THESE RESULTS ARE BASED ON A DYNAMOMETER ENGINE WITH STEERING AND FAN LOSSES EQUAL TO ZERO

M-H PT	SPEED RPM	TORQUE NM	POWER KW	PRESS ATM	FUEL G/S	CITY SEC	CITY GRAM	% TOT CITY	HIWAY SEC	HIWAY GRAM	% TOT HIWAY	BSFC #/HP HR
1	600.000	53.200	3.343	33.015	0.552	362.338	199.881	14.406	10.253	5.656	0.401	0.977
2	800.000	40.700	3.410	27.997	0.598	272.141	162.663	11.723	5.235	3.129	0.222	1.037
3	900.000	-6.000	-0.641	12.092	0.410	74.000	30.325	2.186	52.000	21.310	1.511	0.
4	1000.000	67.800	7.100	37.120	0.842	167.184	140.773	10.146	29.131	24.529	1.740	0.702
5	1100.000	108.500	12.498	51.490	1.160	185.672	215.290	15.516	32.763	37.989	2.694	0.549
6	1300.000	155.900	21.224	69.614	1.706	147.190	251.097	18.097	45.847	78.212	5.547	0.476
7	1600.000	203.400	34.080	90.239	2.583	58.349	150.701	10.861	72.734	187.854	13.322	0.449
8	1700.000	108.500	19.316	54.332	1.733	57.496	99.615	7.179	331.356	574.091	40.713	0.531
9	1800.000	216.900	40.885	97.123	3.087	36.123	111.530	8.038	76.840	237.243	16.825	0.447
10	2000.000	122.000	25.552	61.528	2.226	11.509	25.622	1.847	107.842	240.082	17.026	0.516

TOTAL CVS-H FUEL CONSUMPTION   = 1387.4964 GRAMS
CVS-H FUEL ECONOMY   = 15.1499 MPG
COLD START FUEL PENALTY   = 148.9000 GRAMS
TOTAL CVS-CH FUEL CONSUMPTION   = 1536.3964 GRAMS
CVS-CH FUEL ECONOMY   = 13.6816 MPG
TOTAL EPA HWY FUEL CONSUMPTION   = 1410.0952 GRAMS
EPA HWY FUEL ECONOMY   = 20.3573 MPG

TOTAL M-H FUEL ECONOMY   =   16.0501 MPG

Figure 2.11-4   Metro-Highway Fuel Economy Summary

City Fuel Economy

$$\text{F.E. (CVS-H)} = \frac{7.5 \times 453.6 \times 6.18}{\sum\limits_{i=1}^{n} (m_{fu})_i}$$

$$\text{F.E.(CVS-C/H)} = \frac{7.5 \times 453.6 \times 6.18}{\sum\limits_{\substack{i=1 \\ \text{city}}}^{n} (m_{fu})_i + 0.43 \, (m_{fu})_{\text{warm-up}}}$$

Highway Fuel Economy

$$\text{F.E. (EPA-HWY)} = \frac{10.242 \times 453.6 \times 6.18}{\sum\limits_{\substack{i=1 \\ \text{HWY}}}^{n} (m_{fu})_i}$$

Metro-Highway Fuel Economy

$$\text{F.E. (M-H)} = \frac{1}{\dfrac{0.55}{\text{F.E.(CVS-C/H)}} + \dfrac{0.45}{\text{F.E.(EPA-HWY)}}}$$

Nomenclature

- i — Specific mapping point
- n — Number of mapping points
- F.E. — Fuel Economy (mpg)
- m_{fu} — Mass of fuel (g)

Figure 2.11-5   Engine Mapping Points – Calculations

AUTOMOTIVE STIRLING ENGINE DEVELOPMENT PROGRAM

	M-H Fuel Economy (MPG)	
	Minimum	Maximum
Present 4-215 Engine Capability[a]	12.9	14.0
Identified Opportunities for Improvement		
• Mapping and Optimization	+0.15	+0.45
• Burner System	+0.00	+0.02
• Preheater	+0.40	+0.62
• Engine Drive System	+1.21	+1.94
• External Heat & Blower System	+0.26	+0.38
• Power Control System	+2.26	+3.13
• Air/Fuel Control System	+0.00	+0.16
• Cycle Analysis	+3.01	+3.34
• Other Fuel Economy Improvements	+1.20	+4.02
• Cooling System	+0.00	+0.06
Fourth Generation Engine Technology	21.4	28.1
Baseline 1977 LTD II (351 CID Engine)	15.5	15.5
Projected Improvement Over Base	5.9	12.6
	(38%)	(81%)

a/ 4500 lb. (IWC), C4 Auto. Trans., 100k Torque Conv., 2.50 Rear Axle, 14.0 HP (PAU), 13.3 sec. (0-60 MPH time)

Figure 2.11-6   4th Generation Engine Fuel Economy Assessment

<u>TASK I</u>

Date of Issue	Maximum Opportunity 4th Generation[a]/ Engine Projections (MPG)	Confidence Weighted Opportunities (MPG)[c]/	Confidence Level (%)	
			Present	Expected
July 1977	22.00	-	27%	-
Aug. 1977	22.00	-	27%	52%
Sept. 1977[b]/	21.16	-	29%	54%
Oct. 1977	21.16	-	29%	54%
Nov. 1977	21.23	-	29%	54%
Dec. 1977	22.11	-	29%	54%
Jan. 1978	23.65	-	37%	54%
Feb. 1978	23.68	-	37%	53%
March 1978	23.69	-	40%	55%
April 1978	23.69	-	40%	55%
May 1978	26.33	-	44%	54%
June 1978	26.12	19.6	44%	53%
July 1978	27.75	20.7	46%	49%
Aug. 1978	26.00[c]/	20.6	46%	49%
Sept. 1978[d]/	28.12	23.1	52%	52%

<u>a</u>/ Phase I objective - 15.7 MPG
        DOE Proposal Estimate - 20.6 MPG

<u>b</u>/ Start of contract

<u>c</u>/ Based on the 4-215 at 14.0 MPG

<u>d</u>/ End of contract

Figure 2.11-7   Fuel Economy Assessment Chart - Monthly Summary

| Engine Type | Projected 0-60 MPH Acceleration Time (Sec.) | |
	PB1111	TOFEP
1977 351M	12.4	12.6
4-215 (Engine Map: TDEMBLVT)	11.4	11.4
4-247 (Engine Map: TDEM247C	14.9	15.2
4-245 (Engine Map: DKEM245C)	12.4	12.4

Figure 2.11-8   Baseline Vehicle Projected 0-60 MPH Acceleration Time (Test Track Road Load Conditions)

Engine Type	ECONCALC M-H	TOFEP M-H
351	N/A	14.69
4-215 (Engine Map: TDEMBLVT)	16.05	15.81
4-247 (Engine Map: TDEM247C)	18.11	18.21
4-245 (Engine Map: DKEM245C)	21.76	22.14

* Tr = Tire Rolling Resistance Coefficient

PAU = Chassis Dynamometer Power Absorber Unit

NOTE: It must be noted the above projections of a M-H fuel economy are not intended to accurately reflect the fuel economy potential of the Stirling engine because the fuel economy maps used are incomplete insofar as the incorporation of all engine changes to improve fuel economy.

Figure 2.11-9   Baseline Vehicle Projected Metro-Highway Fuel Economies (MPG) Chassis Dynamometer Road Load Conditions (Tr=1.06, PAU=14.0 HP)*

340

Vehicle Data

Inertial Weight Class (IWC)	4000 lb.
Performance Weight	4099 lb.
Weight on Driving Wheels	1777 lb.
Projected Frontal Area	24.4 ft^2
Drag Coefficient	.55
Center of Gravity Height	20.5 in.
Power Absorption Unit Setting	9.5 HP

Transmission Data

Type - FIOD
Gear Ratios:

1st. Gear	2.40
2nd. Gear	1.47
3rd. Gear	1.00
4th. Gear	0.67

Drive Shaft Speed (RPM)
Shift Points :

3-2 Down Shift (WOT)	2090
2-1 Down Shift (WOT)	890
1-2 Up Shift (WOT)	1600
2-3 Up Shift (WOT)	2650
3-1 Down Shift (WOT)	324
3-4 Up Shift (WOT)	3340
4-3 Down Shift (WOT)	3430

Torque Converter Data

Type	T-8331
Size	12"
Torque/Speed Ratio at stall	2.28
Capacity Factor at stall	138

Engine Data

120 HP Equivalent Stirling Engine (4-248)

Rear Axle Data

Ratio	2.73

Figure 2.11-10   Reference Engine 4000 lb. IWC Baseline Vehicle Descriptive Data

Tires/Wheel/Data

Tire Size	OFR-792
Dyno Inflation Pressure (psi)	45.0
Track Inflation Pressure (psi)	35.0
Rolling Radius (ft)	1.06
Wheel Assembly Inertia (lb.-ft^2)	132.0
Revolutions/Mile	792
Track Tire Rolling Resistance Coefficient	.394
Dynomometer Tire Rolling Resistance Coefficient	1.124

Figure 2.11-10   Reference Engine 4000 lb. IWC Baseline Vehicle Descriptive Data (Cont'd)

	TOFEP Projected 0-60 MPH Acceleration Time (Sec.)	TOFEP Projected M-H Fuel Economy (MPG)
302 Internal Combustion Engine	13.0	20.0
4-248 Stirling Engine Engine Map: Second Generation Demonstration Engine	13.0	27.62*

*   The above projection of M-H fuel economy is not intended to accurately reflect the fuel economy potential of the Stirling engine because the fuel economy map used is incomplete insofar as the incorporation of all engine changes to improve fuel economy.

Figure 2.11-11   Performance and Fuel Economy Comparison of 302 Internal Combustion Engine and 4-248 Stirling Engine for the Reference Engine Baseline Vehicle

342

3.1 Engine Durability Upgrade

3.1.1 Summary — The objective of this effort was to develop protective devices, checking procedures, and component changes to significantly improve the durability and reliability of the existing 4-215 Stirling engine. The strategy used to meet the objective was:

a. Establish failure analysis system in an attempt to prevent repetition of past failures.

b. Initiate component redesign where necessary to eliminate problem areas.

c. Check all components for any defect or possible defect prior to engine build.

d. Establish and use during each engine build a complete checking procedure.

e. Install and test on engine upgraded components after their development.

The introduction of a problem analysis system plus the analysis of failures which occurred prior to its conception resulted in hardware changes which substantially improved engine durability. These changes and the addition of rollsock seal protective devices allowed engine (3 X 17) to run 230 dynamometer hours without a major failure.

3.1.2 Work Performed

3.1.2.1 Seal Protection System — Since receipt of the engine from N. V. Philips in October 1975 it was apparent that the major source of failure on this engine was the rollsock sealing system (refer to Figure 3.1-1). The rollsock seal is a tube shaped polyurethane seal which separates the oil and hydrogen sides of the engine. This seal is shown schematically in the following figure.

ROLLSOCK SEAL FOR A PISTON ROD

GAS
ROLLSOCK
ROD
OIL
REGULATING VALVE
OIL PUMPING RING
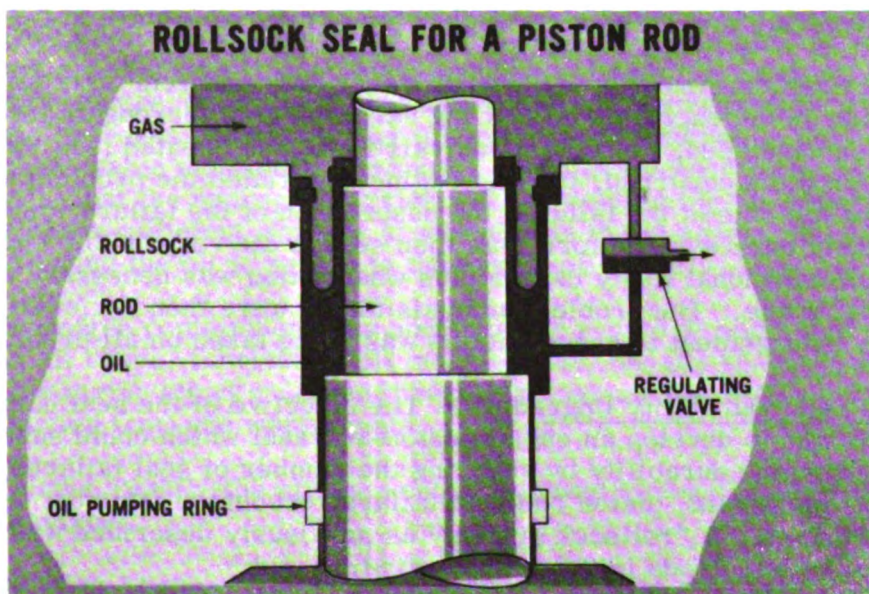
Mean engine cycle pressure of hydrogen is supplied to the gas side of the seal and varies between 14 atm and 200 atm during engine operation. The oil side is supplied with crankcase oil via the pumping rings which pump the oil to pressures within 3 to 5 atm of the gas side of the seal. A larger difference in pressure will rupture the rollsock and a zero pressure differential will allow scuffing of the rollsock on itself, resulting in its destruction. To help maintain this pressure differential, a rollsock regulator is attached which operates as follows:

If the oil pressure builds up beyond the present limit, oil is bypassed through the regulator and back to the crankcase. If the gas pressure exceeds the preset limit, hydrogen is dumped to the oil side of the rollsock to maintain the pressure differential. This hydrogen is then lost to the atmosphere through the engine breather cap. This problem occurred on every engine after 3 to 4 hours of running time because of degradation of the oil pumping rings and the failure to supply the desired oil pressure. To compensate for this inadequacy, an auxiliary oil pump was packaged on (and driven by) the engine. Because malfunctioning of the regulating valve itself was a large contributor to rollsock failures, and the fact that there was no capability within the system to account for a sudden loss of hydrogen, a rollsock protection system was added externally to the engine for protection (see Figure 3.1-2). A delta pressure transducer was added to monitor the pressure differential across the rollsock. This signal was sent to an electronic control box called the solenoid control. If the pressure differential dropped below 3 atm, solenoid number 2 opened, dumping nitrogen into the gas side of the rollsock at 2000 psi. Nitrogen was used to reduce the fire hazard associated with hydrogen. If the pressure differential continued to drop to 2 atm, solenoid number 1 would open and dump the oil from the oil side of the rollsock back into the engine oil sump. If the differential increased because of a malfunction of the rollsock regulator, and exceeded 6 atm, solenoid number 2 would open and dump hydrogen to the atmosphere until the differential pressure returned to 5 atm. In all cases, an alarm would sound in the control room to warn the operator of the problem and the engine would shut down. This system was activated on several occasions since its installation on August 3, 1977 and successively prevented a rollsock failure (refer to Figure 3.1-3).

3.1.2.2 Problem Analysis — To assure that each problem or failure that occurred either on the engine or on test rig hardware was thoroughly investigated and a solution developed, a problem analysis form was created (see Figure 3.1-4). When a problem occurred, the test engineer initiated the problem analysis form by listing the date of the failure, the description of the failure, and if known, some likely causes. The form was then sent to the responsible engineer who would add additional likely causes plus what action was necessary to determine the actual cause. The problem analysis forms were then reviewed on a monthly basis by management to assure action was being taken on all problems.

3.1.2.3 Seal Durability Upgrading — The objective of the seal durability upgrading task was to develop an engine piston-rod seal which could substantially improve the engine durability by reducing the number of seal failures. Prior to the Ford/DOE program, piston rod seal failures accounted for most 4-215 Stirling engine failures. A "rollsock system" as previously described was utilized for sealing the piston rods in the 4-215 engine.

The effort to improve the durability of the rollsock seal was limited to improving its static sealing capabilities during engine shutdown by adding a sliding seal check-valve. This was tested briefly in the test rig and was considerably more effective than the pumping ring in acting as a static seal.

3.1.2.3.1 Leningrader Sliding Seal — Developing improved piston rod seals was essential for short term engine testing as well as for the eventual Stirling engine success. Sliding seals were considered most promising for both the short and long term because they are less prone to catastrophic failures than rollsocks, do not require the pressure regulator, and are more adaptable to mass production techniques.

Initially, United Stirling's sliding seal design was adapted to the 4-215 and eventually three engines were built with these seals (see Figure 3.1-5). The system consisted basically of four sealing elements: a cap seal, two scraper rings, and a main sealing ring. The purpose of the cap seal was to eliminate pressure fluctuations in the seal cartridge, providing a relatively constant pressure which is lower than or equal to the pressure in the cylinder at all times. The cap seal restricts the flow of hydrogen from the cylinder into the seal cartridge. However, if left long, the pressure in the cartridge would approximate the mean cylinder pressure. This is prevented by the inclusion of a check valve in the hydrogen return line which allows gas to flow from the cartridge to the cylinder when the pressure in the cartridge exceeds that in the cylinder. Therefore, the cartridge pressure is maintained slightly above the minimum cycle pressure and there is constant circulation of hydrogen from the cylinder through the seal cartridge and back to the cylinder. The main seal ring is interference fitted over the hardened and polished piston rod. It is designed to take advantage of the pressure drop it causes to seal itself tightly around the rod. The seal is made of ceramic filled Teflon, and has cold flow ability which enables it to conform to the rod as it wears.

The scraper rings are located on either side of the main seal ring, and removes excess oil from the piston rod as it reciprocates. The oil which is removed from the rod flows with the hydrogen to a gas/oil separator in the hydrogen return line. This separator collects the mixture of oil and hydrogen from the cartridge. Oil droplets collect in the reservoir at the bottom, while the hydrogen passes through a demister and returns to the engine through the check valve mentioned previously. The demister condenses any oil vapor or mist that the hydrogen carries with it, completing the separation process. When a sufficient quantity of oil collects in the reservoir, a float valve opens, allowing the oil to return to the engine oil sump.

Hydrogen containment was adequate for engine development testing although, in all cases, lubrication oil migrated into the gas space in less than 40 hours. The major effort was then directed at redesigning the seal to improve oil exclusion from the working gas.

During Task I, the sliding seal design was revised to include the following features:

a. The Leningrader seal was moved closer to the piston rod guide bushing.

b. An oil drain was added to prevent build up of oil pressure on the Leningrader seal.

c. The oil scraper on the oil side of the Leningrader seal was removed to assure adequate lubrication of the seal.

d. The Rulon oil scraper was replaced with a Polyurethane lip type scraper.

e. An open path for oil around the scraper was eliminated.

f. The pressure drop across the scraper was eliminated so that the lip will remain in contact with the piston rod.

In addition, the seal design allows for the evaluation of different oil scraper designs by providing ample installation space. The redesigned seal is shown in Figure 3.1-6.

To evaluate the sliding seal performance two new test rigs were designed and built. The intent of the test rigs was to simulate the seal operating conditions in the engine. Both the cycle working gas pressure and the loading placed on the piston rods by the drive were considered when designing the test rigs. The first rig was intended for initial screening of candidate seals. It has a crankshaft drive mechanism and therefore does not duplicate the drive induced piston rod loads of the swashplate engine. It does, however, have pressure cycles of the proper magnitude so that the oil/gas separator can be used. The majority of the seal testing was performed on this rig. The second rig used a swashplate drive from the 4-215 engine and therefore reproduced the piston rod deflections as well as the pressure fluctuations which the seal experiences in the engine.

The first step in the test program was to check out the test rigs using the original sliding seal design, referred to as "baseline," shown in Figure 3.1-5. It was expected that if the rigs reasonably duplicated the actual engine conditions, oil would migrate to the gas space of the test rig. The baseline seals were first run on the crank drive fixture for 101 hours at 1000 RPM with a mean gas pressure of 851 psi. One cylinder had a film of oil in it. The inside of both cylinders were covered with a black powder which appeared to be carbon. United Stirling indicates that this powder is a mixture of carburized oil and filler material from the Rulon LD capseals. It is formed when a small amount of oil gets on a Rulon seal and inhibits the self-lubricating properties of the Rulon but is insufficient to lubricate the seal. Therefore, this powder is evidence of oil on the capseals. This, combined with a heavy oil film inside the seals on the "dry" side of the scrapers, indicated that the seal allowed oil into the gas space.

The baseline seals were also tested on the Swashplate Drive Rig during one of the shakedown runs of the fixture. They were checked after 25 hours at 1000 RPM and 700 psi mean pressure. An oil film was found in two of the four cylinders. This was the only run on the Swashplate Drive Rig. Flexing of the center section holding the seals caused one of the seal tubes to crack. A more rigid housing was designed, but could not be completed before the end of Task I.

346

The test rigs were determined to be valid indicators of seal performance because the baseline seals, known to be ineffectual in the engine, also proved to be inadequate for oil exclusion in the test rigs. The test program then was directed at finding a seal that would prevent oil contamination of the gas. All of the testing was done on the Crank Drive Test Rig due to durability problems with the Swashplate Drive Rig.

The new sliding seal design, shown in Figure 3.1-6, was then tested. The scraper used was a Type D-562 rod wiper made by Parker Seal, Figure 3.1-7. After 17 hours at 1000 RPM and 1050 psi mean pressure, enough oil had migrated past the seals to fill the gas passages. The test was repeated and the same result occurred after 6 hours. The scraper was found to be too small for the 15 mm piston rod and therefore the lip was not contacting the rod properly. Since the proper size scraper was not available, testing on Parker "D" seals was discontinued.

The next oil scraper tested was a Simrit type AUAS wiper which was available for 15 mm rods but required modification for installation within our seal cartridge (see Figure 3.1-7). After 100 hours at 1000 RPM and 1050 psi mean pressure, there was no evidence of oil in either cylinder of the fixture or on the "dry" side of the scraper inside the seal cartridges. Additional testing of the Simrit scrapers was delayed until commercial availability of the revised scraper could be established.

Samples and tooling were eventually ordered from Simrit Corporation but delivery was not expected before the end of Task I.

The next type of scrapers tested were "Polypak" seals made by Parker and they are also shown in Figure 3.1-7. Polypak seals are compression type seals that use an integral O-ring as a spring to hold the sealing lips in place. The seals were purchased in two materials, "Fluoromyte," a proprietary plastic, and "Molythane," an internally lubricated urethane. The Fluoromyte material has a lower coefficient of friction than urethane, and a higher temperature limit. The Fluoromyte seals were tested for 65 hours at 1000 RPM and 800 psi mean pressure with no indication of oil on a cotton indicator exposed to the gas space. An apparent interruption in the cooling water flow caused the gas space temperature to jump from 160°F to 240°F in fifteen minutes. The temperature was restored by increasing the coolant flow, but within two hours a large quantity of oil was found in the gas space. Inspection revealed that the scraping lips of the Polypak seals had overheated.

Subsequent tests conducted were on Polypak seals made from Molythane because it is a more elastic material and can better follow transverse piston rod motions. Two tests were run at 1000 RPM and 800 psi mean pressure for 100 hours. In both tests, one cylinder was free of any signs of oil either in the test cylinder or inside the seal cartridge on the "dry" side of the scraper. The second cylinder in both tests had a light film of oil in the "dry" portion of the seal cartridge and possibly in the test cylinder.

More severe tests were then performed on Polypak seals (1500 RPM and 1000 psi mean pressure or approximately an average of the CVS cycle operating conditions). The test continued until liquid oil was found in the gas space of

one cylinder after 495 hours of operation. Inspection of the other cylinder revealed only a film of oil.

The Rulon pumping ring shown in Figure 3.1-7 was also tested as a scraper. This device uses the action of the piston rod to pump oil from the "dry" side to the "wet" side of the scraper. Philips is currently evaluating such scrapers made of white metal. The test was run for 107 hours at 1000 RPM and 875 psi mean pressure. One cylinder had no indication of oil in the cylinder or the dry side of the cartridge, while the other had a film of oil in the cylinder and cartridge. Further evaluation of this scraper was not possible due to a lack of time in Task 1.

During Task 1, two oil scraper designs were found which substantially improved the oil containment capability of the piston rod seals when tested in the Crankshaft Drive Test Rig. They were the Polypak and Simrit type AUAS scrapers. (See Figure 3.1-8 for all test results.) Although their performance in the Swashplate Test Rig was not evaluated, their improved performance on the Compressor Drive Rig would indicate improved performance in the engine.

During the sliding seal test program, cap seals were wearing out in approximately 100 hours. Alternative designs were tested but wear continued to be unacceptably high. Wear has been less of a problem with the rollsock sealing system where the cap seals remain dry. Rulon LD material, from which the cap seals were made, apparently wears little with no lubrication or flooding lubrication but rapidly with trace lubrication.

3.1.2.3.2 Metal Scraper Oil Seal — Another rod seal design which has potential is an adaption of a Philips design (Figure 3.1-9) which has been successfully tested in a Rhombic drive displacer type Stirling engine. In this design, the high pressure gas seal is an "O" ring or a "T" seal which is lubricated with engine oil. On the high pressure side of the seal is a white metal scraper which is similar in operation to a pumping ring. The piston rod motion moves oil from the gas side of the scraper to the oil side. The scraper is radially compressed with high pressure oil to compensate for wear.

In tests, this scraper has allowed less than 1 gram of oil past per thousand hours of operation. Since the piston rods on the 4-215 Stirling engine tend to have more transverse motion than those in Rhombic drive engines, the seal has been mounted at the end of a flexible tube to allow it to follow the piston rod motions. A load of 8 kg causes the seal assembly to deflect about 0.1 mm, which is greater than the anticipated rod deflections. Parts for this seal were completed but no testing was accomplished because the Swashplate Seal Test Rig was not in service.

2.1.2.3.3 Analysis — Long term optimization of the trade-off between friction and leakage of the piston rod sliding seal requires analysis of the frictional power loss of the seal. The current sliding seal frictional power or heat generation rate as a function of mean pressure and RPM was calculated from the product of lubricated dynamic coefficient of friction, piston rod velocity, and radial contact force between the seal and piston rod as follows:

348

$$\dot{Q} = \text{work/time} = \text{force} \times \text{distance/time} = \mu \, F_n |V| \quad \text{Eq 3.1-1}$$

Where: $\dot{Q}$ = instantaneous rate of heat generation

μ = lubricated dynamic coefficient of friction $\approx .05$

$|V|$ = piston rod velocity magnitude (ft/min)

F_n = seal contact force normal to piston rod (lb f)

$$|V| = \frac{dX}{dt} = \frac{d(s/2 \ (1 - \cos w \ t)}{dt}$$

$$= w \, \frac{s}{2} \left| \sin w \ t \right| = .537 \times RPM \times \left| \sin wt \right| \quad \text{Eq. 3.1-2}$$

X = piston position (X = 0 @ TDC)

s = piston stroke = 52 mm

w = swashplate angular velocity

The radial contact force (F_n) was estimated from a force balance on the seal cross-section by making the following assumptions:

a. The reduction in force transmitted to the piston rod due to rigidity of the seal is negligible since the modulus of elasticity of the Rulon LD seal is much less than that of the steel piston rod.

b. Pressure drop across a sealing surface is linear. Gas pressure forces acting on the cross-section of the seal are then as shown in the following figure:
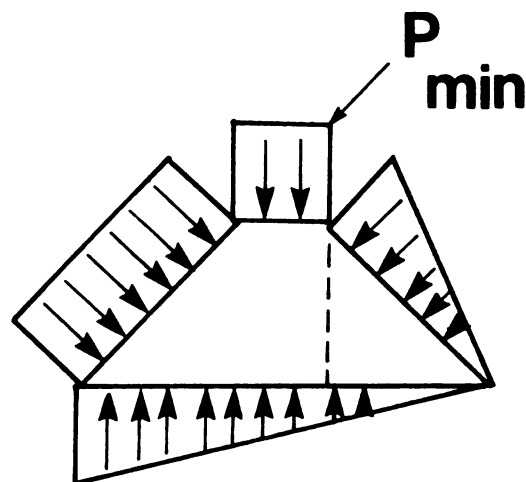
From the proceding figure and the seal geometry, the net radial gas pressure force (F_{RP}) acting on the seal cross-section is:

$$F_{RP} (\text{lbf}) = 2.97 \, P_{min} (\text{atm}) = 2.08 \, P_{mean} (\text{atm})$$

c. The contact forces exerted on the seal by the seal compression rings act perpendicular to the slanted surfaces of the seal. This assumption is shown schematically in the following figure, and is reasonable because the coefficient of friction of Rulon is low.
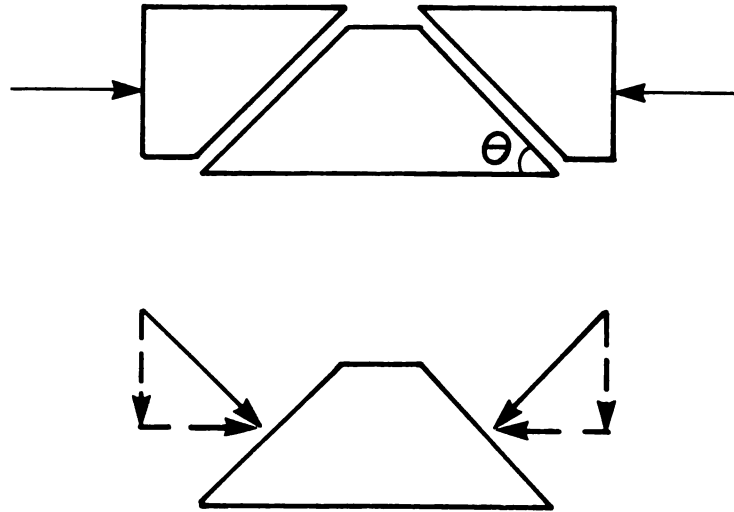
Referring to the preceding figures, the axial component of the contact force between the seal compression ring and the seal on the high pressure side of the seal is equal to the spring force alone, since P_{min} acts across the entire cross-section. From force equilibrium, the axial component of the contact force on the low pressure side of the seal is equal to the spring force plus the reduction in pressure force due to pressure drop across the seal, or about $1/2 \, P_{min}$ times the projected radial seal area. The radial components of the contact forces result in tensile hoop stresses in the seal compression rings and in a radial contact force between the seal and piston rod. Since the seal angle is equal to 45°, these radial components of the contact forces are equal to the axial components.

The radial force (F_{RC}) due to the contact forces between the seal and the seal compression rings is thus:

$$F_{RC} = 2 \times \text{spring force} + .47 \, P_{min} \times \text{projected radial seal area}$$

Eq. 3.1-3

$$F_{RC} (\text{lbf}) = 176 + 2.15 \, P_{min} (\text{atm}) = 176 + 1.5 \, P_{mean} (\text{atm})$$

The net radial contact force (F_n) between the seal and piston rod is thus:

$$F_n (\text{lbf}) = F_{RP} + F_{RC} = 176 + 3.58 \, P_{mean} (\text{atm})$$

The friction force required to withdraw the rod from the seal assembly as a function of pressure was measured and the calculated contact force is reasonable.

Sliding seal heat generation was then calculated as follows:

$$\dot{Q} = \mu F_n V \qquad\qquad \text{Eq. 3.1-4}$$

$$\dot{Q} \ (BTU/hr) = .05 \ x \ (176 + 3.58 \ P_{mean})(.537 \ RPM \ |sinw \ wt|)(60/778)$$

$$\dot{Q} \ (BTU/hr) = 2.07 \ x \ 10^{-3} \ x \ (176 + 3.58 \ P_{mean}) \ RPM \ |sin \ wt|$$

The average rate of heat generation $(\dot{Q}_{avg})$ is obtained by integrating $\dot{Q}$ over a cycle:

$$\dot{Q} \ avg \ (KW) \approx (3.87 \cdot 10^{-7})(176 + 3.58 \ P_{mean}) \cdot RPM \qquad \text{Eq. 3.1-5}$$

This equation is plotted on Figure 3.1-10 for various mean pressures and indicates excessive seal friction power loss is expected at high speed and load. The primary mode of heat rejection from the piston rod is by convection to the lubricating oil flowing between the rod and the rod guide bushing. Since the guide bushing is axially offset from the sliding seal, a temperature gradient would be expected along the piston rod, and would result in a varying rod diameter due to thermal expansion. Because the sliding seal and oil scraper must remain in contact with the rod to seal, a significant temperature gradient could result in less effective dynamic sealing, especially at high RPM.

Approximate modeling of the spatial heat generation and conduction along the rod and heat rejection from the rod indicated that the expected rod temperature gradient was not acceptable. The gradient along the travel of the sliding seal was then measured in the Sliding Seal Compressor Test Rig. A cross-section of the seal cartridge end of the rig is shown in Figure 3.1-11. Five thermocouples were routed through an axial hole in the rod and welded to the rod utilizing radial holes which were then plugged, as shown in the figure. The compressor was extended using plexiglass to provide space for a linkage which was attached to the big end of the connecting rod and used to guide and prevent excessive bending of the thermocouples. This is shown in Figure 3.1-12. Temperature vs. thermocouple location for various speeds and mean pressures is shown in Figure 3.1-13. Thermocouple #3 failed after a short time, but initial data indicated that this temperature was slightly below the linearly interpolated temperature derived from temperatures #2 and #4. Rod temperatures increased with increasing speed and mean pressure. The total temperature difference (or mean temperature gradient) between thermocouples #1 and #5 increased with increasing speed but remained approximately constant with increasing mean pressure. The maximum temperature difference measured was $84^{\circ}F$, corresponding to a variation in rod diameter of about .0003 inch. A plot of temperature difference shows approximately linear variation with RPM. Linear extrapolation to 4000 RPM results in a temperature difference of about $225^{\circ}F$, which corre-

sponds to about .001 inch variation in rod diameter. A change in rod diameter of this magnitude would probably adversely affect dynamic sealing.

The test rig does not exactly duplicate heat transfer conditions in the engine. In the engine, the end of the rod beyond the cap seal is exposed to relatively low velocity gas in the engine compression space, whereas in the test fixture it is exposed to higher velocity gas in the annulus around the rod (refer to Figure 3.1-11). Higher gas velocity causes increased heat transfer from this end of the rod which results in a lower rod temperature gradient. Increasing gas pressure also increases this effect. Evidence that this mode of heat transfer is not negligible is shown by the gradual reduction in the temperature difference between thermocouples #1 and #2 with increasing mean pressure at constant speed. Although this is somewhat speculative, it indicates that the temperature gradient could be greater in the engine than in the test fixture and would probably become larger with increasing pressure because of increased heat generation.

It should be noted that the temperature of the oil in the test rig was about 80°F, whereas the temperature of the oil in the engine is expected to be in the vicinity of 170°F. An increase in oil temperature should result in a direct increase in rod temperatures in order to maintain the temperature difference for heat rejection to the oil.

3.1.2.3.4 Recommendations

a. Oil scraper testing should be continued in order to establish oil seal durability.

b. Since the frictional power loss of the current sliding seal is excessive, the trade-off between friction and gas leakage should be investigated. Seal friction could be reduced by decreasing the spring force or by redesigning the seal with smaller cross-section.

c. The temperature gradient of the piston rod could be decreased by locating the rod guide bushing axially closer to the seal or by increasing the effective conductivity of the rod. A reduction in seal friction would also decrease the temperature gradient.

352

Failure	No. of Times *	Cause	Corrective Action
Rollsock	17	-7 Regulating Valve	- Control group
		-2 Attachment Knot	- Knot tied on opposite side of piston rod
		-2 Exterior Fitting	- Pressure check all fittings to 10,000 psi
		-1 Rollsock Retaining Thread Came Loose	- Use retaining clips
		-1 Cell Operator	
		-2 Rollsock Retainers Loose	
		-1 Rollsock Flaw	
		-1 Unknown	
Heater Head	4	Poor Manufacturing	Returned to Philips
Broken Compressor Plunger	1	Bad Heat Treat	New plungers installed
Engine Would not Run with Load	1	Crossheads Rubbing Swashplate	Concentric drive
Regenerator Cooler Leak	2	Flanges Bent	Flanges straightened and reinforced
Regeneator Cooler Leak	2	Bad "O" Ring	Sheared at Ass'y Sharp Edge
Pressure Valves Stuck Open	3	Metal Chips in Engine	New cleaning procedures, including sonic cleaning, oven drying, and special care
High Pressure Crankcase Leak	4	Bad braze	New ring brazed in crankcase in Dearborn
Major Failure	1	Front Crankcase Separated	Relieved stress concentrations and used through bolts and spacers in front crankcase
Low Oil Pressure	1	Missing plug	Installed plug
Internal Oil Leak	3	Sliding Seal Engines	Engine oil escaped through seal cartridge
Crosshead	3	Crosshead Retaining Groove Crosshead Bridge Broke	X-Rays taken. Sent to Bldg. 4 Materials Analysis to check broken parts

* Oct. 1975 to Oct. 1978

Figure 3.1-1   Summary of Engine Failures

ORIGINAL SYSTEM — BOLD LINES
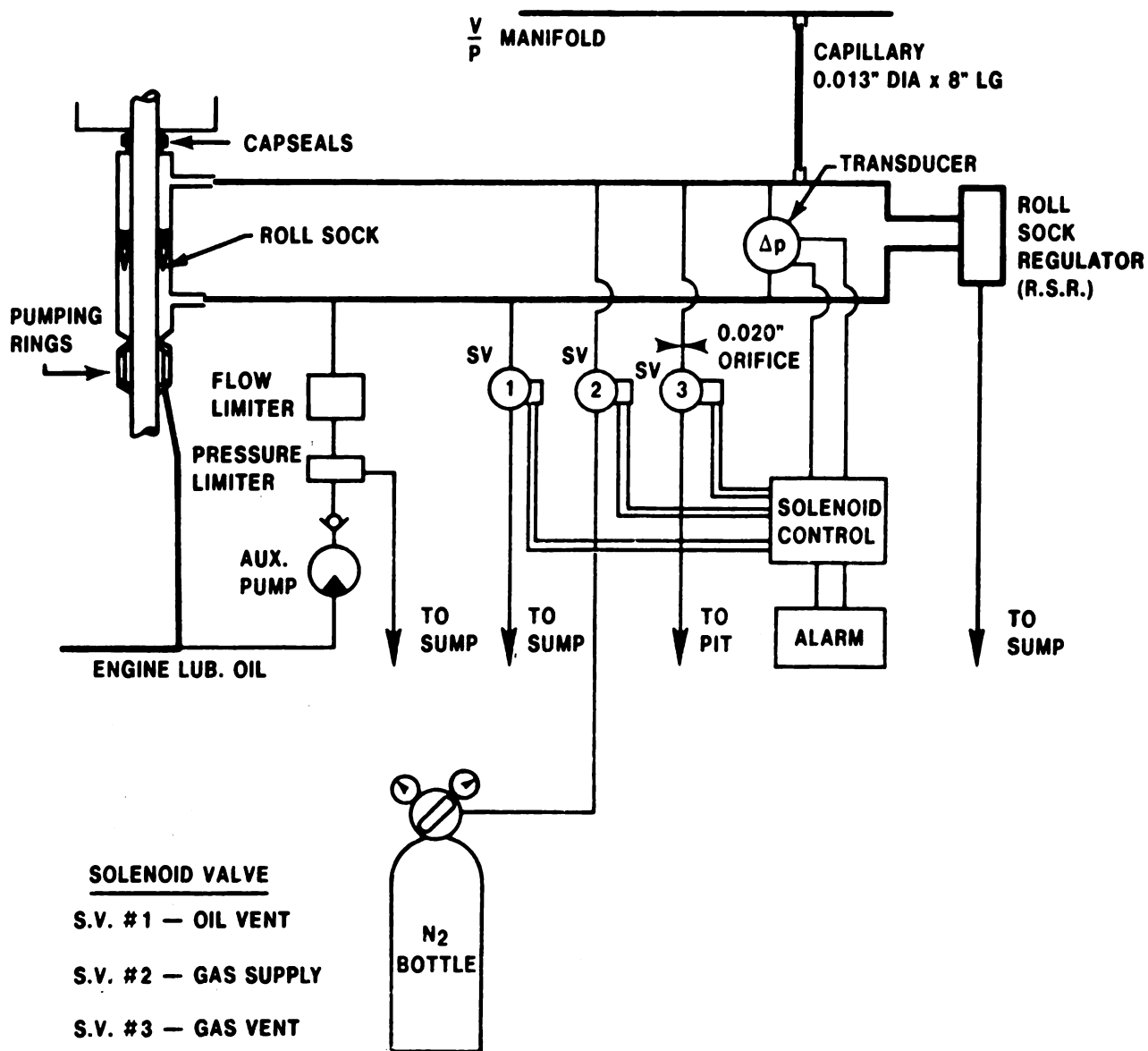
Figure 3.1-2   Rollsock Gas and Oil Circuitry with Protection Devices

354
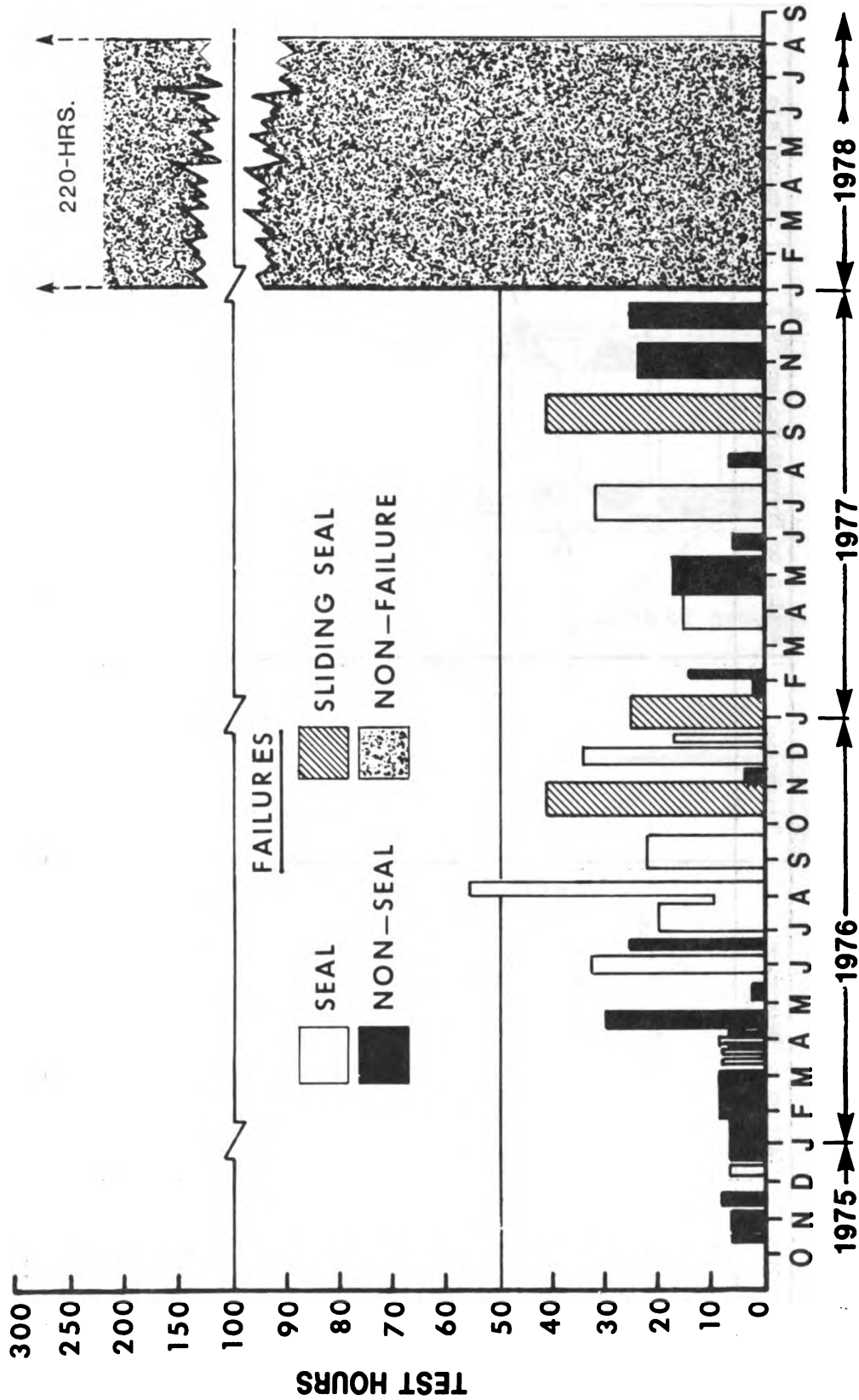
Figure 3.1-3   Stirling Engine 4-215 Test Hours Per Engine Build

355

Engine/Components: _____ Failure Report No.: _____

Date of Failure: _____ Ref. Reports: _____

Description of Failure:

Likely Causes	Action to Determine Real Cause	Diagnosis	Action to Prevent Failure	Status/Date

Closing Notes:

Figure 3.1-4   Problem Analysis Form
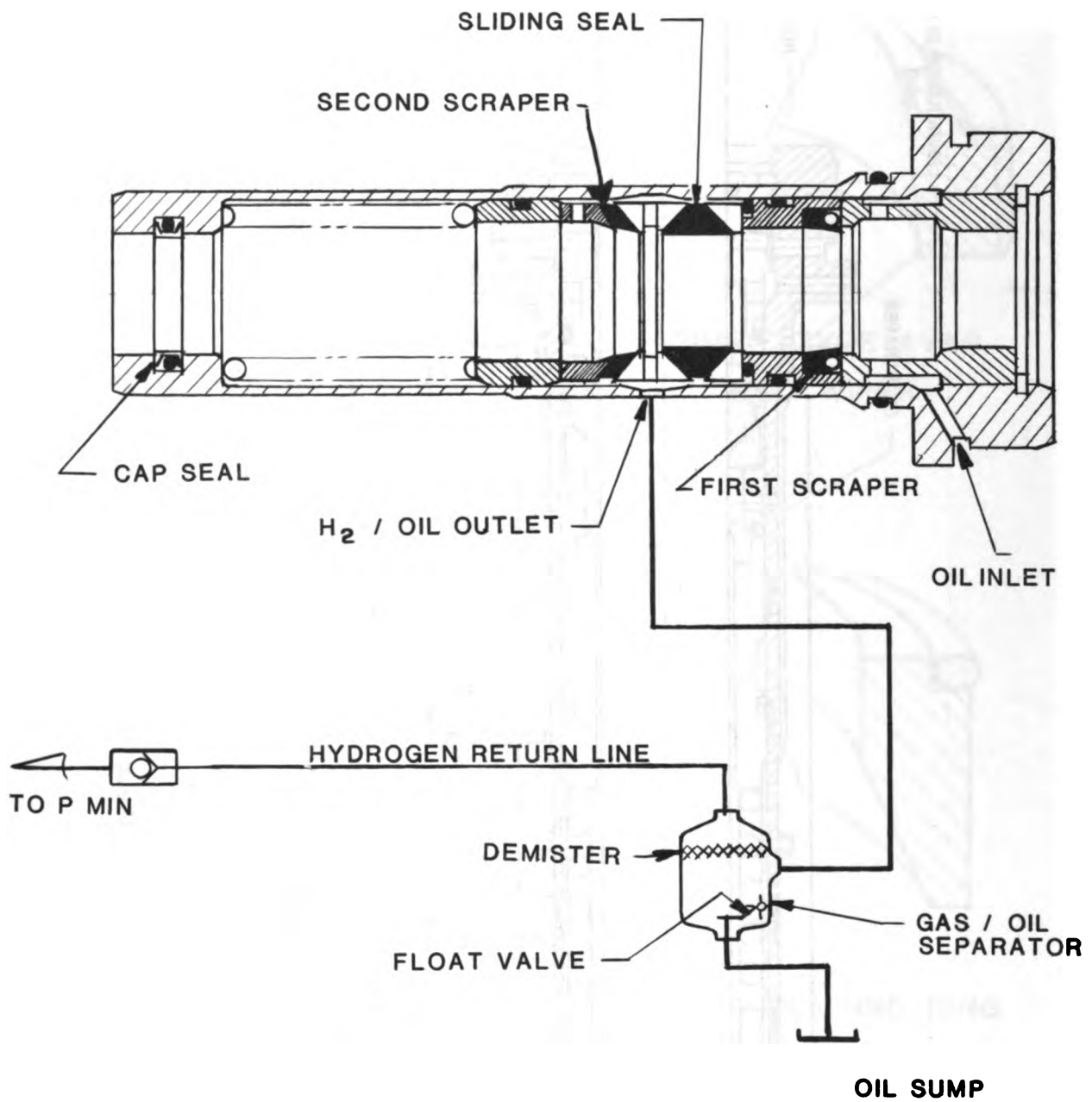
Figure 3.1-5   4-215 Sliding Seal System
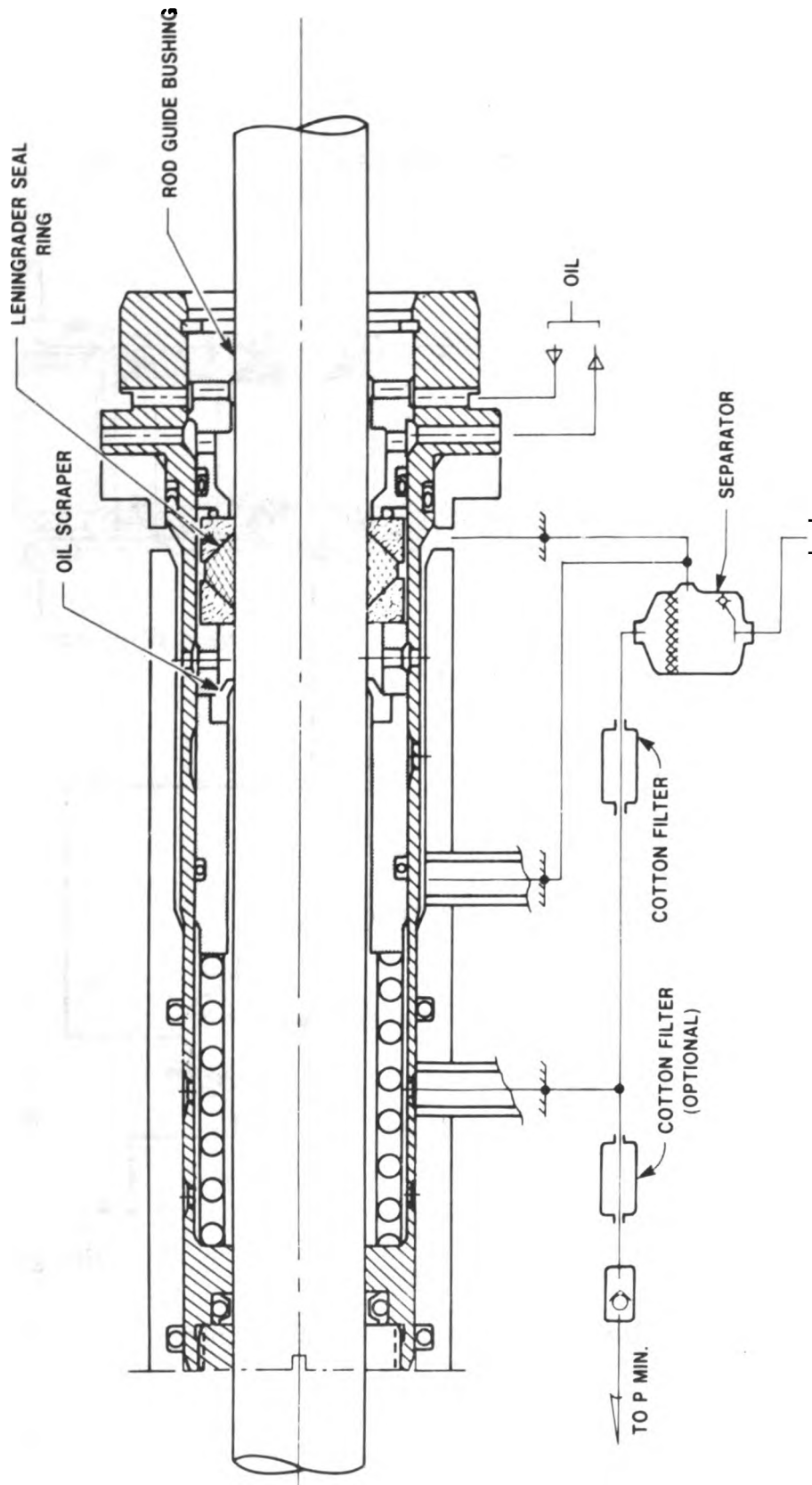
Figure 3.1-6 Sliding Seal Cartridge

358
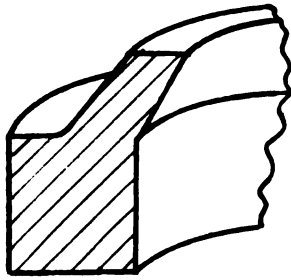
PARKER TYPE-D
WIPER RING
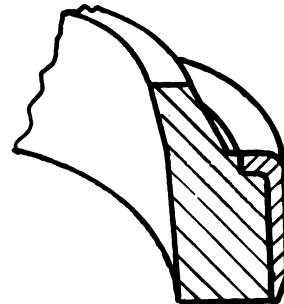
SIMRIT TYPE AVAS
ROD WIPER
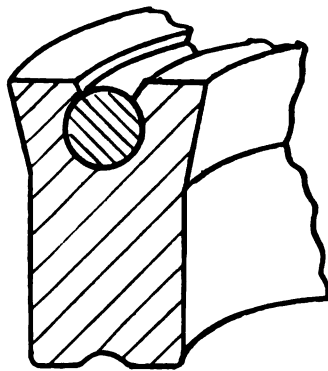
PARKER POLYPAK
SEAL
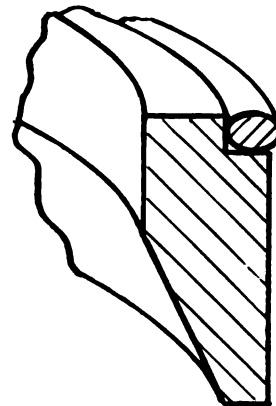
RULON PUMPING RING
SCRAPER

Figure 3.1-7   Oil Scrapers Tested

SEAL TYPE	SCRAPER	TEST RIG	SPEED (RPM)	P MEAN (PSI)	HOURS	OIL IN GAS	REMARKS
Baseline	Baseline	Crank Drive	1000	850	101	Yes	
Improved	Parker D	"	1000	1050	17	Yes	Large amounts of oil scraper wrong size for 15 mm shaft; See PTS-099
"	Parker D	"	1000	1050	6	Yes	See PTS-102; Scraper must be custom molded
"	Simrit	"	1000	1050	100	No	
"	Polypak (Fluoromite)	"	1000	800	65	Yes	Loss of coolant damaged scrapers; See PTS-103
"	Polypak (Molythane)	"	1000	800	100	Trace in One Cyl.	See PTS-105
"	Polypak (Molythane)	"	1000	800	100	Trace in One Cyl.	See PTS-107
"	Polypak (Molythane)	"	1500	1000	495	Yes	See PTS-108; Test was run until oil appeared in gas space
"	Rulon Pump. Ring	"	1000	875	107	Trace in One Cyl.	See PTS-109
Baseline	Baseline	Swashplate Drive	1000	700	25	Yes	Oil film found in two of four cylinders; Test was shakedown of Test Rig

Figure 3.1-8   Sliding Seal Test Results

HIGH PRESSURE
OIL LINE

SCRAPER PUMPING RING

H₂ GAS SEAL

GUIDE BUSHING

CROSS HEAD

HOUSING
ASSEMBLY
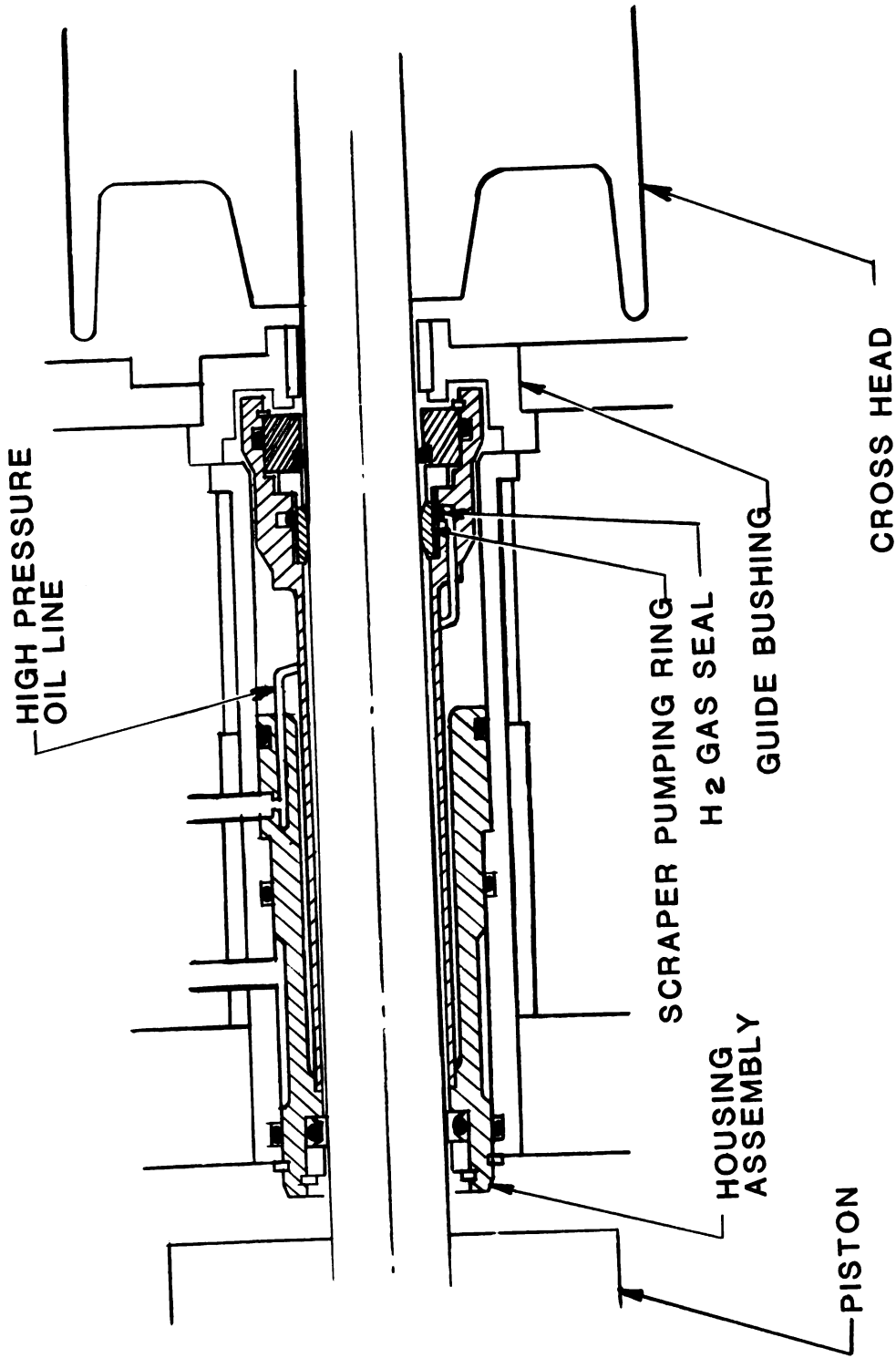
PISTON

Figure 3.1-9   White Metal Scraper Seal
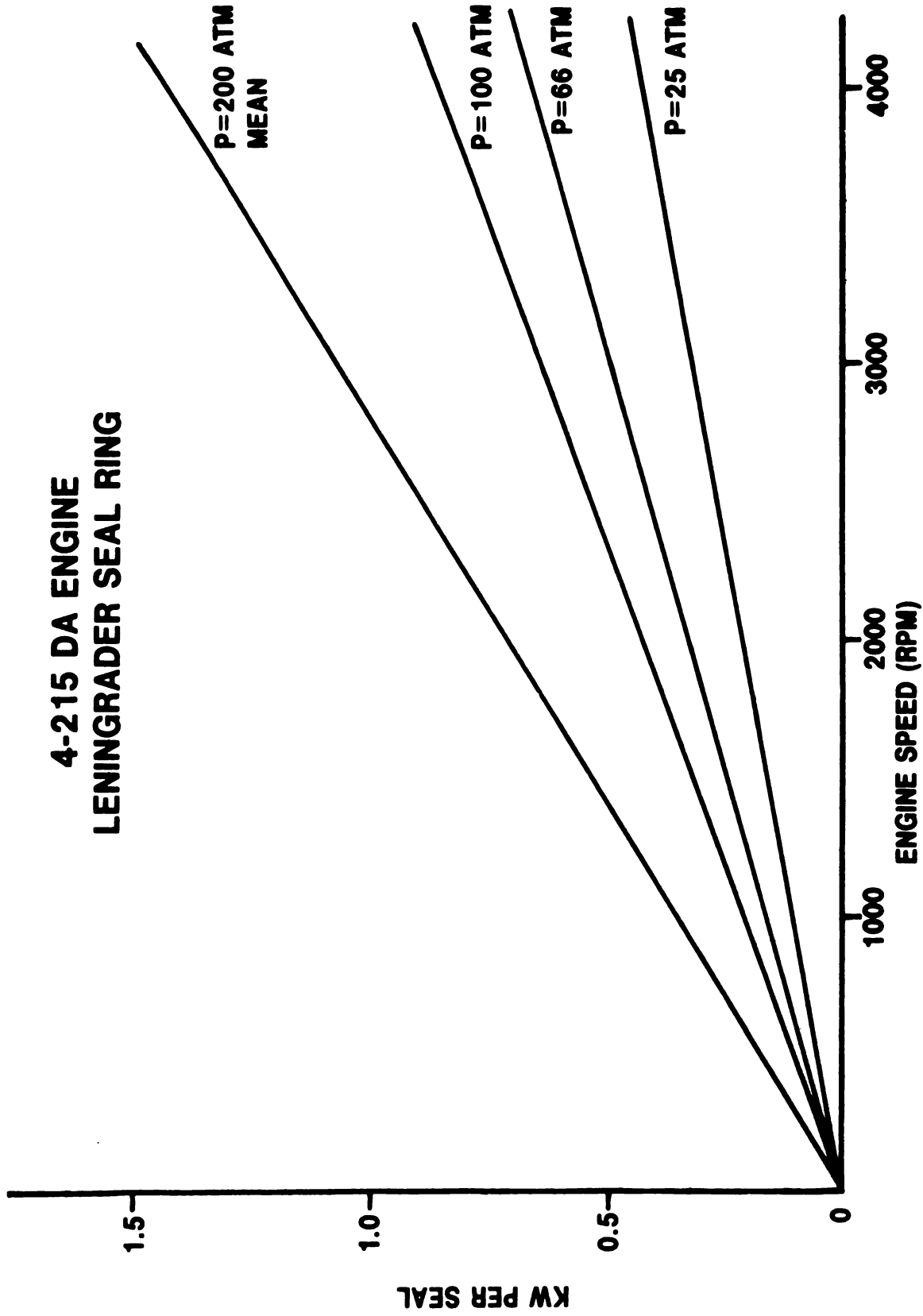
Figure 3.1-10 Sliding Seal Heat Generation

OIL INLET

OIL OUTLET

COOLING WATER IN

CAP SEAL

COOLING WATER OUT

THERMOCOUPLE

MAIN SEAL

#5

#4

#3

#2

#1

H₂ IN
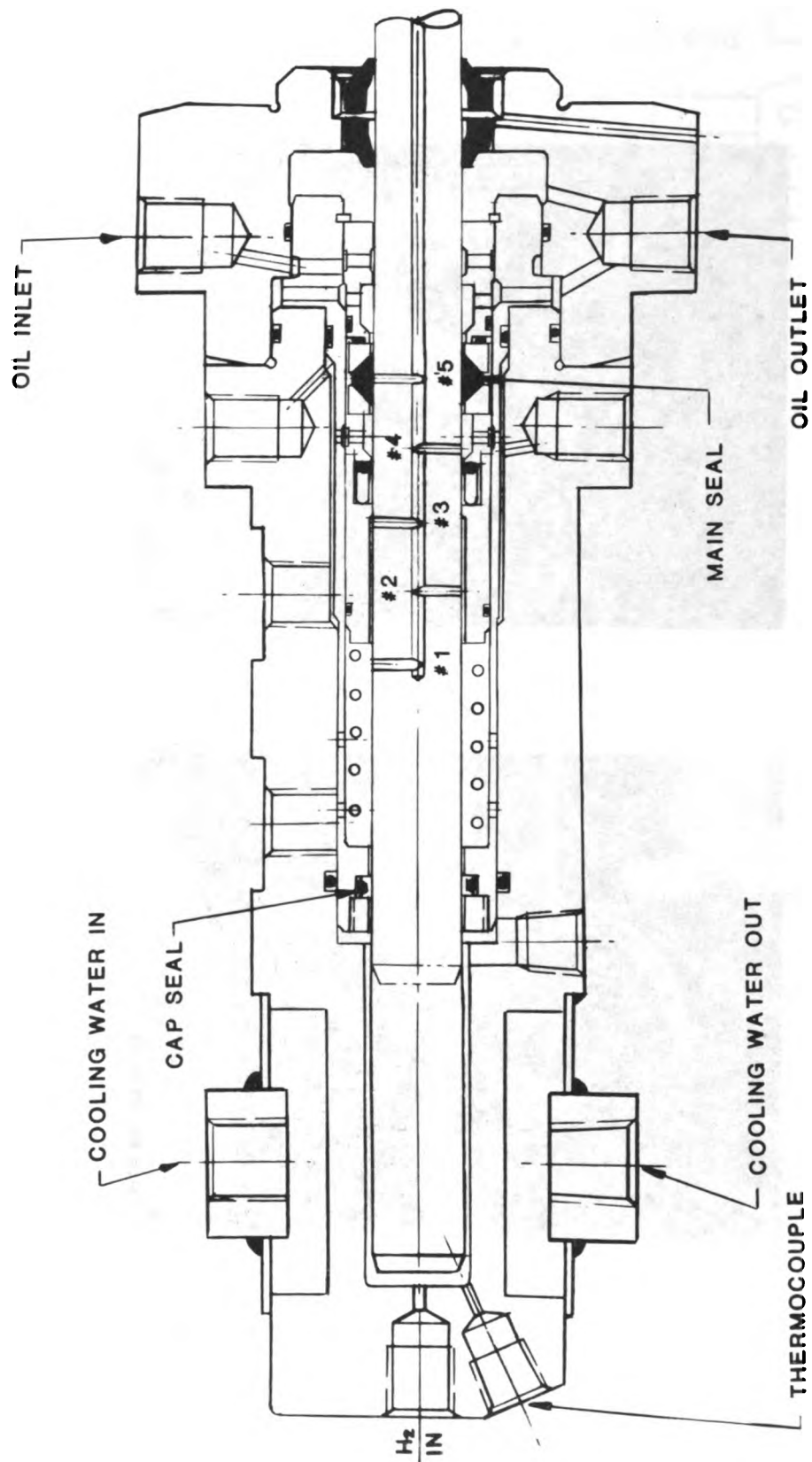
Figure 3.1-11   Cross Section of Sliding Seal Test Rig

363
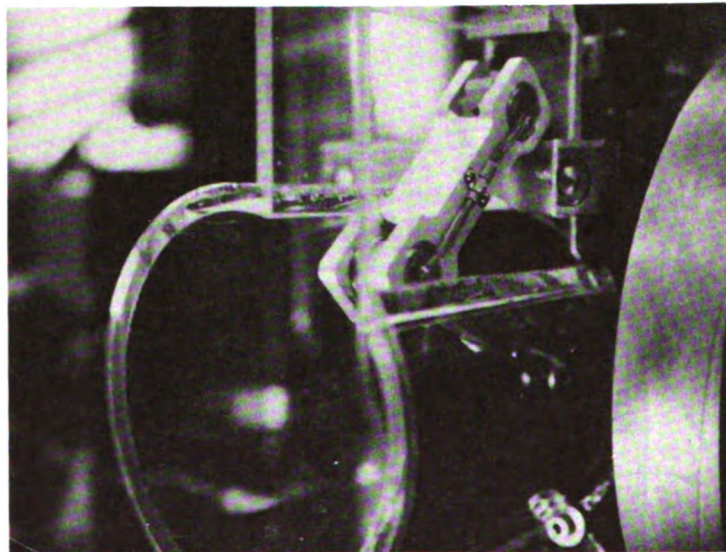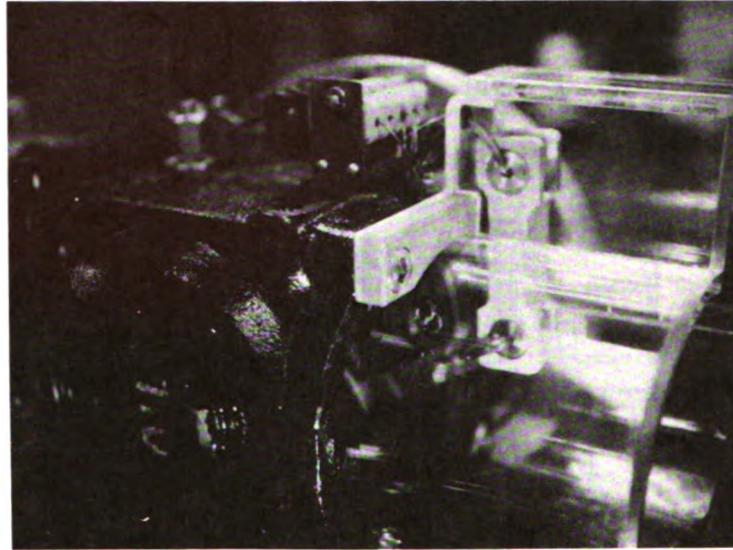
Figure 3.1-12   Compressor Test Rig Extension
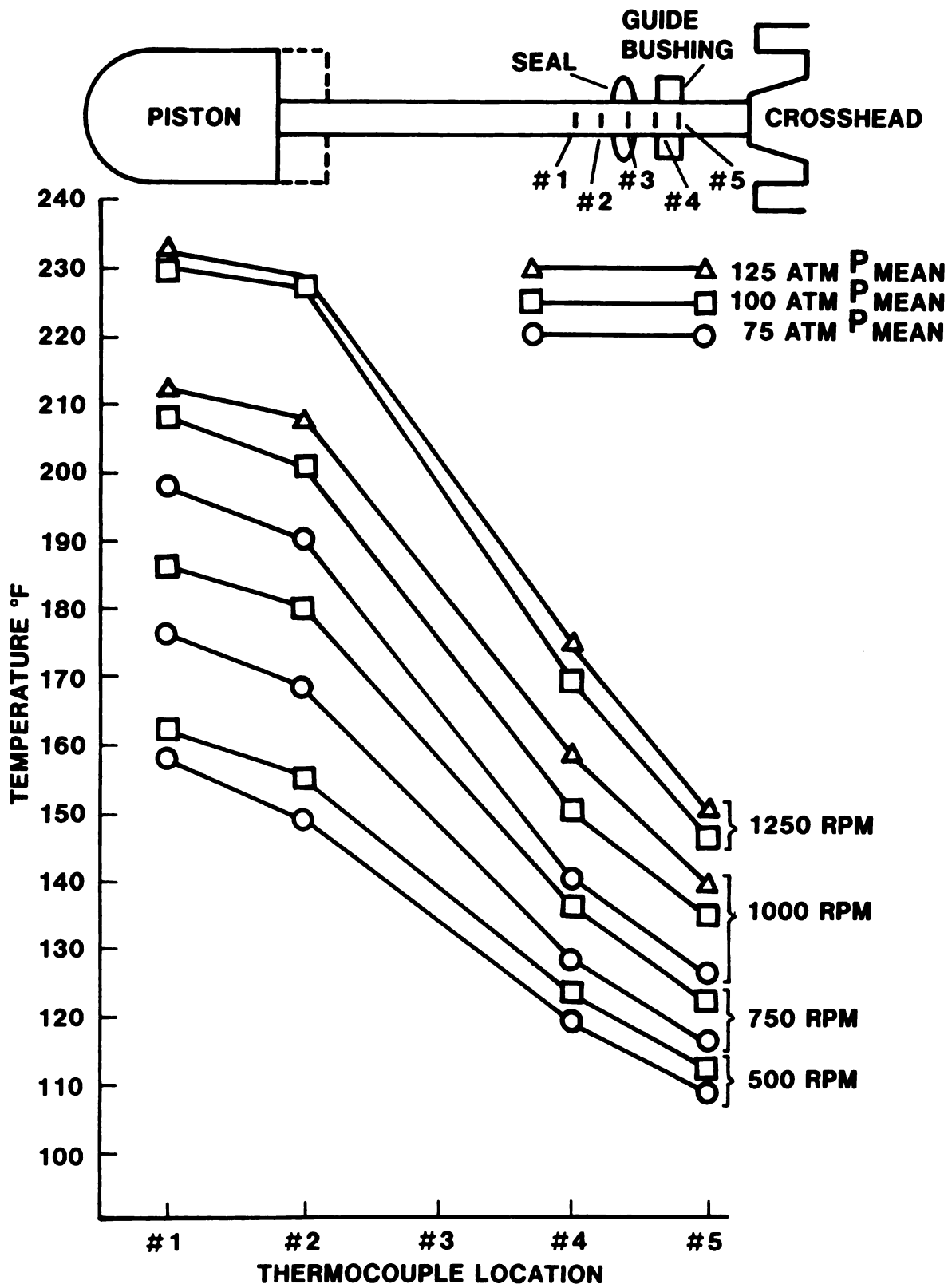
Figure 3.1-13   Piston Rod Temperature vs. Axial Location – 80°F Oil Temperature

3.2 Reference Engine

3.2.1 Summary — The objective of this sub-task was to provide designs of complete Stirling engine and vehicle packages which incorporate information from the other sub-tasks and new concepts which might improve the function of the Stirling engine. This engine design also served as the basis for incorporating the fuel economy improvements compiled in section 2.11.

The Reference Engine Design Task was intended to serve two functions:

1. To study alternative engine configurations in relation to vehicle engine compartments to determine whether some configurations other than the present barrel-shaped, swashplate drive design might package better in current (1979) and future passenger cars.

2. To study how new component designs might be packaged within the existing and alternative Stirling engines.

It was possible to package the present 4-215 Stirling engine in a 1975 Torino because engine compartments at that time were large enough to accommodate 460 CID engines and long hood styling was in vogue. Even with the large 1975 Torino engine compartment, some significant compromises were required because of the long nature of the engine and the high driveshaft center line associated with the swashplate drive engine.

The most accepted drive configuration for automotive internal combustion engines has been the single crankshaft with an in-line or vee cylinder arrangement.

With Stirling engines, the swashplate drive is currently an acceptable approach which lends itself reasonably well to front engine, rear wheel drive packages such as the Ford/Philips 4-215 swashplate drive engine in a 1975 Ford Torino. In-line cylinder arrangement Stirling engines have been demonstrated by N.V. Philips of the Netherlands, and a single crankshaft vee cylinder arrangement Stirling engine has been successfully tested by the United Stirling of Sweden.

Since future passenger vehicles will be more fuel and package efficient than those of the present and recent past, and will use more in-line 4 cylinder and V-6 engines, rather than in-line 6 cylinder and V-8 engines (including some front wheel drive vehicles), packaging a swashplate design Stirling engine will present some major packaging problem areas. Extended front ends result in weight (and therefore fuel economy) penalties as well as poor weight distribution. Increased transmission tunnel sizes cannot be tolerated in narrower vehicles because of encroachment on pedal clearance zones.

For production automotive applications, an engine with a compact single-heater head and a single combustion system is deemed necessary. This may best be accomplished by a double-crankshaft engine rather than a single-crankshaft vee cylinder configuration. Figures 3.2-1 and 3.2-2 illustrate this point.

3.2.2 Comparison on Double Crank vs Single Crank Vee Configuration — Figure 3.2-1 depicts some of the differences between the single-crank and the double-crank Stirling engines. The upper illustration shows that a vee angle of the cylin-

ders exists to provide clearance between the pistons and the necessary spread needed to form a symmetrical circular heater head. In the lower illustration, the distance between the two crankshafts permits the angle between the pistons to vary from positive (as in the vee arrangement) to zero or even negative as shown. This lends itself to a compact heater head. It may be noted that the crankshafts can be synchronized by gears or a timing chain which may permit several optional locations for the output shaft. This flexibility could be an advantage in difficult packaging situations or with front wheel drive applications.

Figure 3.2-2 shows another fundamental difference between the single-crankshaft and double-crankshaft arrangements. The upper illustration shows that cylinders B & D are spaced a distance "X" along the crankshaft axis from the heater head center. Cylinders A & C are spaced a distance "Y" and "Y" is greater than "X" because each connecting rod must have its individual crank throw. To achieve radial symmetry of the heater head (necessary for equal temperature distribution to each cylinder) cylinders A & C must be located a distance "X" perpendicular to the crankshaft axis and cylinders B & D a distance "Y" to the crankshaft axis.

The results of these two restrictions are that unequal vee-angles are required, and the encompassing heater head diameter is quite large.

In the lower illustration, all the cylinders can be spaced "X" distance along the crankshaft axis from the heater head center, however, this "X" distance is not a design limitation with a double-crankshaft engine. Because the "Y" dimension in the upper illustration is greater than the "X" dimension, the encompassing diameter of the double-crankshaft design is more compact than the single crankshaft vee-cylinder design.

Should a crankshaft-type Stirling engine be considered for a front wheel drive vehicle, the double crankshaft engine would be more compact laterally across the vehicle and therefore preferred to the swashplate design which would have to be packaged longitudinally in the engine compartment because of its length. Figure 3.2-3 illustrates schematically the similarities and differences between the double crankshaft and swashplate Stirling engines. The high pressure crankcase, heater head, rotary preheater and the burner systems are common to both engines. The differences occur in the output drive and accessory drive as noted:

. The double crankshaft output axis is at right angles to the piston axis while the swashplate drive output axis is parallel with the piston axis.

. The double crankshaft output speed may be geared up or down and there is flexibility in its location.

. The swashplate drive output has no inherent speed change flexibility and its location is fixed.

. The double crankshaft drive permits accessory drives from either or both ends of the crankcase whereas the swashplate drive accessory take-off locations are limited.

3.2.3 Package Studies — Most of the Reference Engine package studies were conceptual with the intent to optimize the engine design and placement within the en-

gine compartment for both current and long range vehicles. Detailed engine or package layout studies were not conducted for most of the studies and, therefore, fuel economy projections were considered premature at this time.

Figures 3.2-4, 5, 6, and 7 are sketches of swashplate Stirling engines in a 1979 Ford engine compartment. Figures 3.2-8, 9 and 10 are sketches of swashplate and double crankshaft engines in a future downsized vehicle. Major problem areas or open issues for each of the above package studies are listed on each of the figures.

The following preliminary Stirling engine package installation studies were completed during the Task I effort:

3.2.3.1 1979 Ford Vehicle Installation Studies:

1. 4-215 size swashplate Stirling engine in a 1979 Ford engine compartment. Conventional front engine rear wheel drive. See Figure 3.2-4.

2. Modified 4-215 (120 HP) swashplate Stirling engine in a 1979 Ford engine compartment. Conventional front engine rear wheel drive. See Figure 3.2-5.

3. Redesigned swashplate engine (based on 4-215 design) 120 HP 4-248 engine in a 1979 Ford engine compartment. Conventional front engine rear wheel drive. See Figure 3.2-6.

4. Scaled swashplate Stirling engine (120 HP) in a 1979 Ford engine compartment. Conventional front engine rear wheel drive. See Figure 3.2-7.

3.2.3.2 Future Downsized Vehicle Installation Studies:

1. Scaled 120 HP swashplate Stirling engine (based on the 170 HP 4-215 engine) longitudinal engine installation for a front wheel drive vehicle. See Figure 3.2-8.

2. Scaled 120 HP swashplate drive Stirling engine, transverse engine and transaxle installation for a front wheel drive vehicle with the engine either for or aft of the front wheels. See Figure 3.2-9.

3. Scaled 120 HP double crankshaft Stirling engine, longitudinal horizontal engine installation for a front wheel drive vehicle. See Figure 3.2-10.

The preliminary package studies listed above were made to get early visibility of major packaging problem areas. Detail layouts would undoubtedly reveal other less serious problem areas, but it would be premature at the current stage of the Stirling engine program to make detail layouts.

Complete accessory and/or auxiliary arrangements are not shown for the above figures because it was felt that this would not be a major problem area. However, rearrangement of engine accessories or auxiliaries, compared to the current 4-215 Stirling engine, may be necessary to simplify the present complex accessory drive and/or also to fit within the confines of future reduced engine compartment sizes.

3.2.4 Conclusions

1. Installation of a 4-215 size (170 HP) Stirling engine in a 1979 Ford engine compartment should not be considered because of the major packaging implications.

2. A modified 4-215 (120 HP) or redesigned 4-248 (based on the 4-215 design) Stirling engine could be packaged in a 1979 Ford engine compartment but each concept would present some significant packaging problems.

3. The most viable 1979 Ford swashplate Stirling engine package is with a scaled engine (120 HP) based on the 4-215 (170 HP) design. This scaled engine could be installed in a 1979 Ford engine compartment with the least vehicle modifications or compromises compared to the other swashplate engine designs.

4. Future passenger vehicles will be smaller than those of the present. Stirling engine configurations such as a double crankshaft design must be considered.

PISTON

(+) (+)

CROSSHEAD

SINGLE CRANKSHAFT

OUTPUT
SHAFT

DUAL CRANKSHAFTS

CLUSTER CONFIGURATION

PISTON

(−) (−)

CROSSHEAD

OUTPUT
SHAFT

DUAL CRANKSHAFTS

Figure 3.2-1   Crankshaft Comparison

SINGLE CRANKSHAFT

VEE CONFIGURATION

CRANK ₵

LARGE
ENCOMPASSING
HEATER HEAD
DIAMETER

DUAL CRANKSHAFTS

CLUSTER CONFIGURATION

CRANK ₵

CRANK ₵

SMALL
ENCOMPASSING
HEATER HEAD
DIAMETER
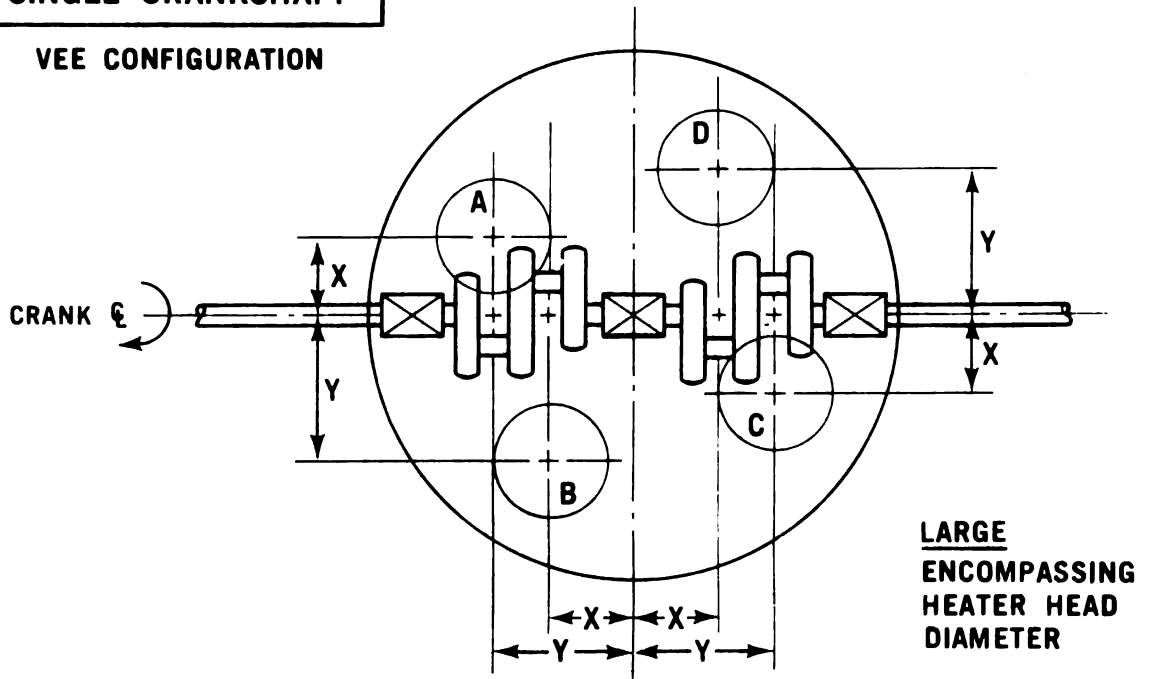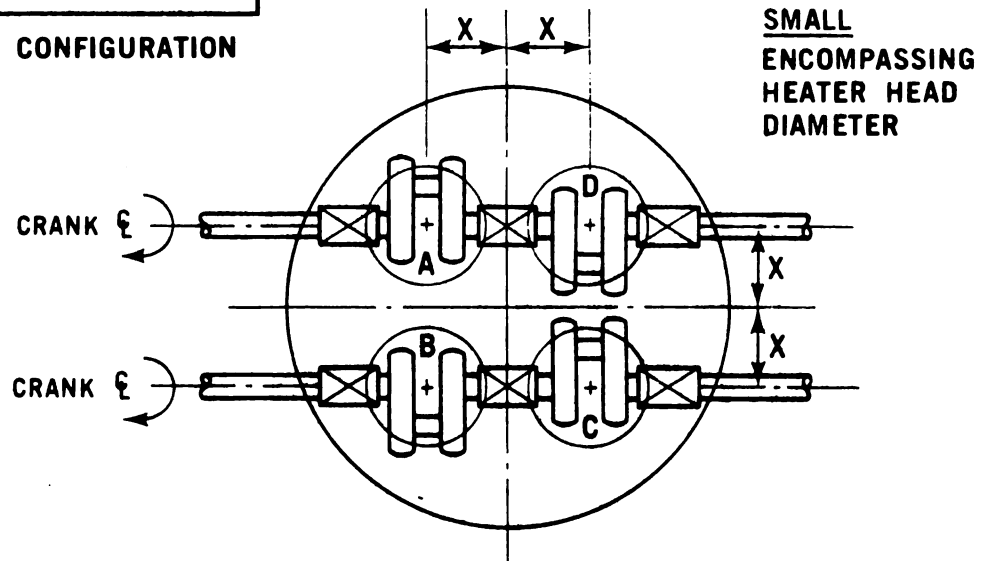
Figure 3.2-2   Heater Head Comparison
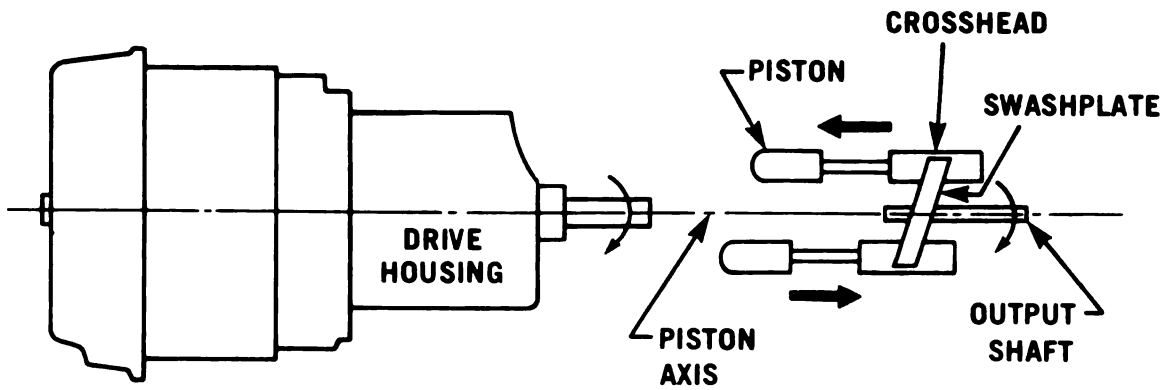
SWASHPLATE DRIVE
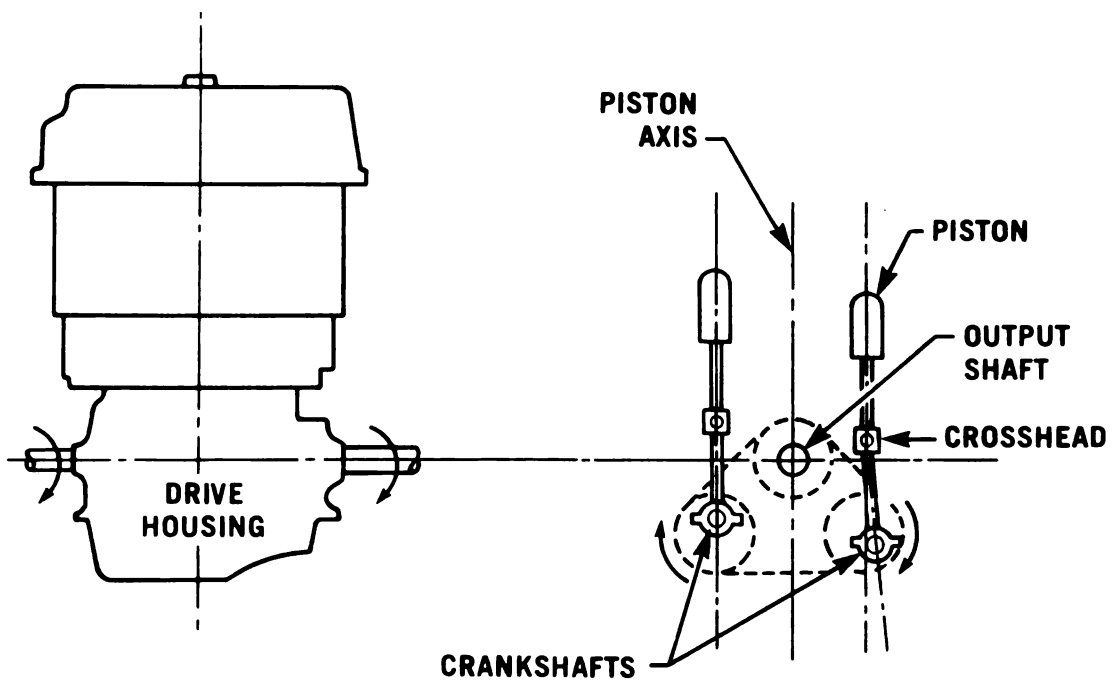
DUAL CRANKSHAFT DRIVE

Figure 3.2-3   Stirling Engine Comparison – Two Engine Configurations

9.0 IN.
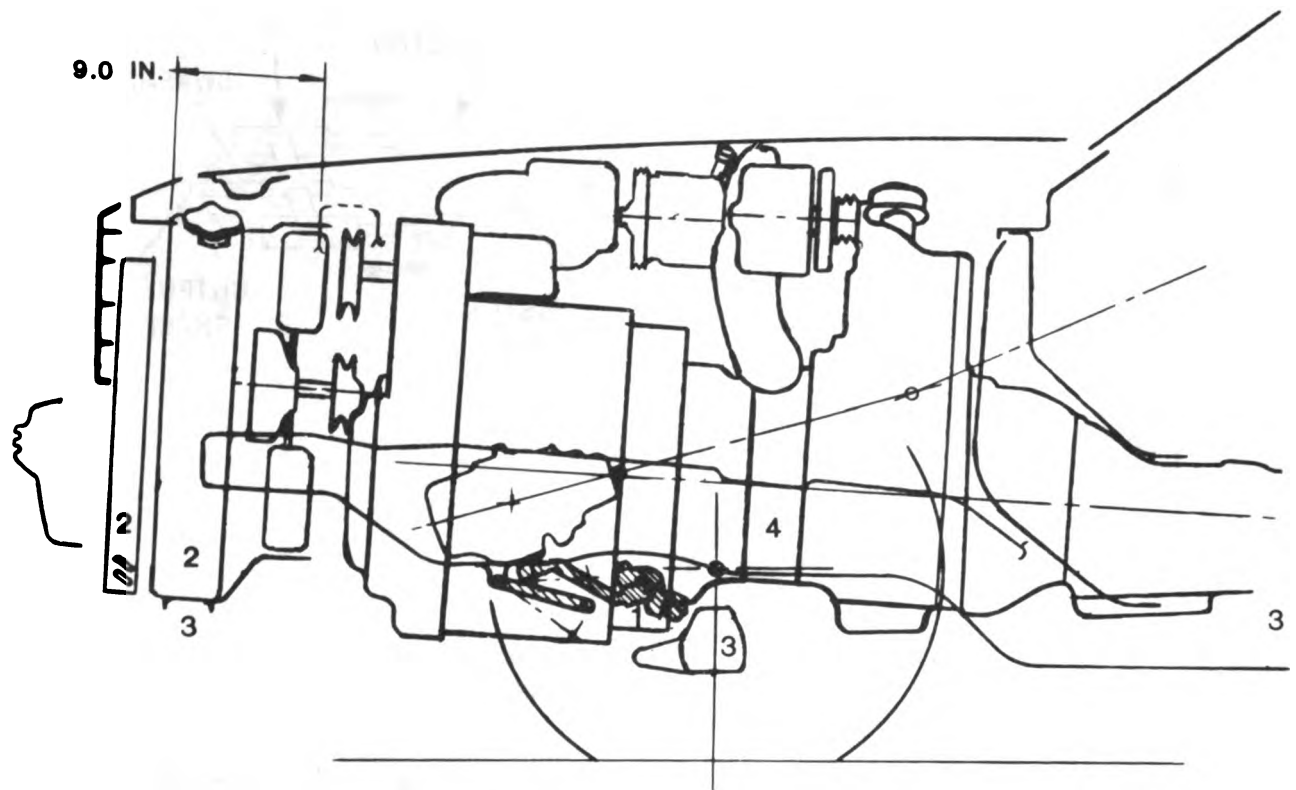
OPEN ISSUES

1. TOTAL INTERFERENCE WITH STEERING LINKAGE

2. STIRLING ENGINE RADIATOR AND CONDENSER 9 IN. FORWARD OF NORMAL 79 FORD POSITION (INTERFERENCE BETWEEN CONDENSER AND GRILL).

3. NEW NUMBERS 1, 2, AND 3 CROSSMEMBERS REQUIRED.

4. PROBABLE UPPER SUSPENSION ARMS REWORK.

Figure 3.2-4   4-215 Size Stirling Engine in a 1979 Ford Engine Compartment
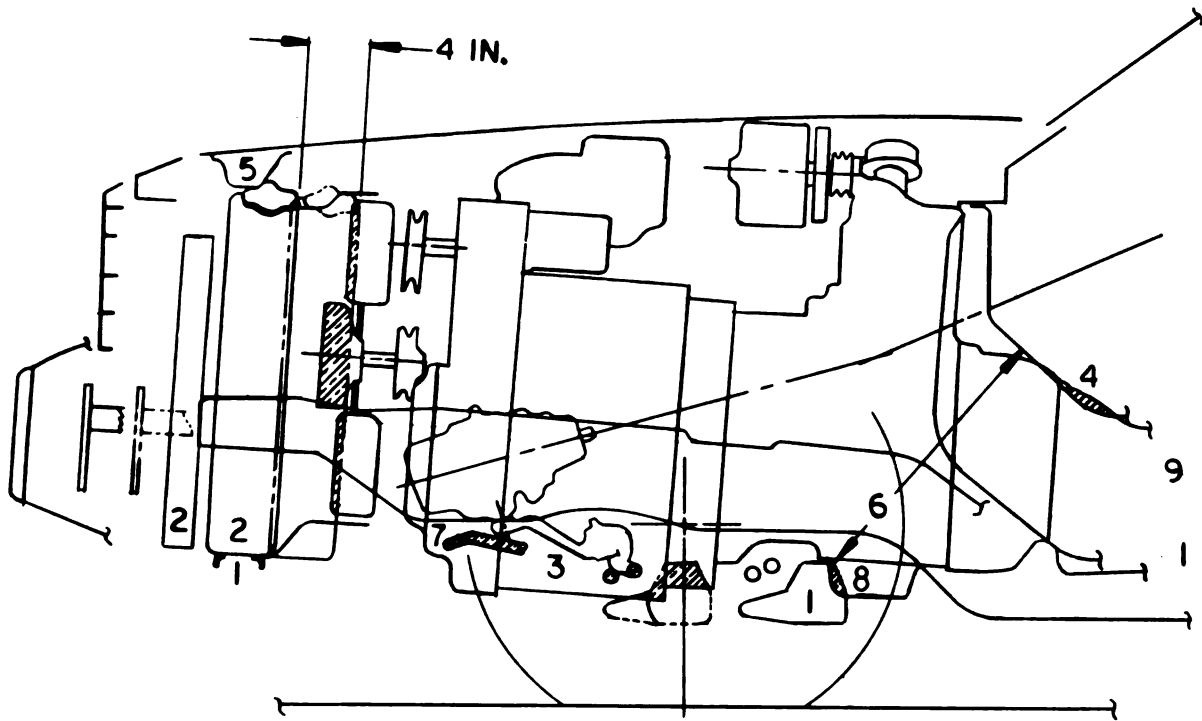
PACKAGE PARAMETERS

.ENGINE MOVED REARWARD 1.75 FROM

PREVIOUS PACKAGE. SEE FIG. 3.2-4

.ENGINE SHORTENED 3.5 IN.

.RADIATOR MOVED 4.00 IN. FORWARD

FROM NORMAL 1979 FORD POSITION

OPEN ISSUES

1. NEW NO. 1, 2 & 3 FRAME

   CROSSMEMBER

2. RADIATOR MOVED 4.0 IN. FORWARD

OPEN ISSUES (CONT)

3. REVISED STEERING LINKAGE

4. MODIFIED TUNNEL

5. NEW HOOD LATCH & SUPPORT

   MECHANISM

6. DECKING PROBLEM

7. NEW FRONT STABILIZER BAR

8. INTERFERENCE BETWEEN NO. 2

   CROSSMEMBER AND REAR CRANKCASE

   AND OIL PAN

9. REVISED (SHORTENED) DRIVESHAFT-NOT

   SHOWN

Figure 3.2-5   Modified 4-215 (120 HP) Stirling Engine in a 1979 Ford Engine
                Compartment
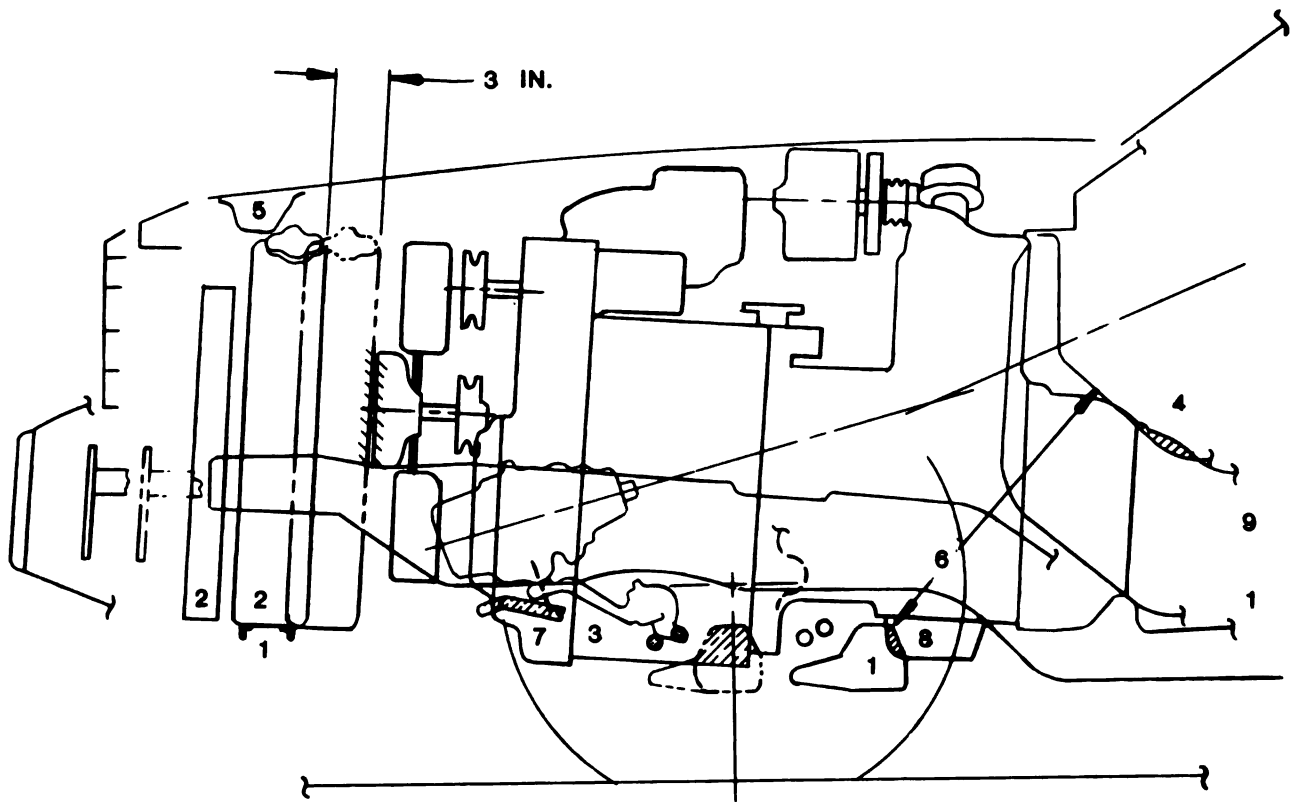
PACKAGE PARAMETERS

.ENGINE MOVED REARWARD 1.75 FROM
PREVIOUS PACKAGE. SEE FIG. 3.2-4

.ENGINE SHORTENED 5.0 IN.

.RADIATOR MOVED 3.0 IN. FORWARD
FROM NORMAL 1979 FORD POSITION

OPEN ISSUES

1. NEW NO. 1, 2, & 3 FRAME
CROSSMEMBER

2. RADIATOR MOVED 3.0 IN. FORWARD

OPEN ISSUES (CONT)

3. REVISED STEERING LINKAGE

4. MODIFIED TUNNEL

5. REVISED HOOD LATCH & SUPPORT
MECHANISM

6. DECKING PROBLEM

7. NEW FRONT STABILIZER BAR

8. INTERFERENCE BETWEEN NO. 2
CROSSMEMBER AND REAR CRANKCASE
AND OIL PAN

9. REVISED (SHORTED) DRIVESHAFT-NOT
SHOWN

Figure 3.2-6   Redesigned Engine (Based on 4-215 Design) 4-248 Engine in a 1979
Ford Engine Compartment
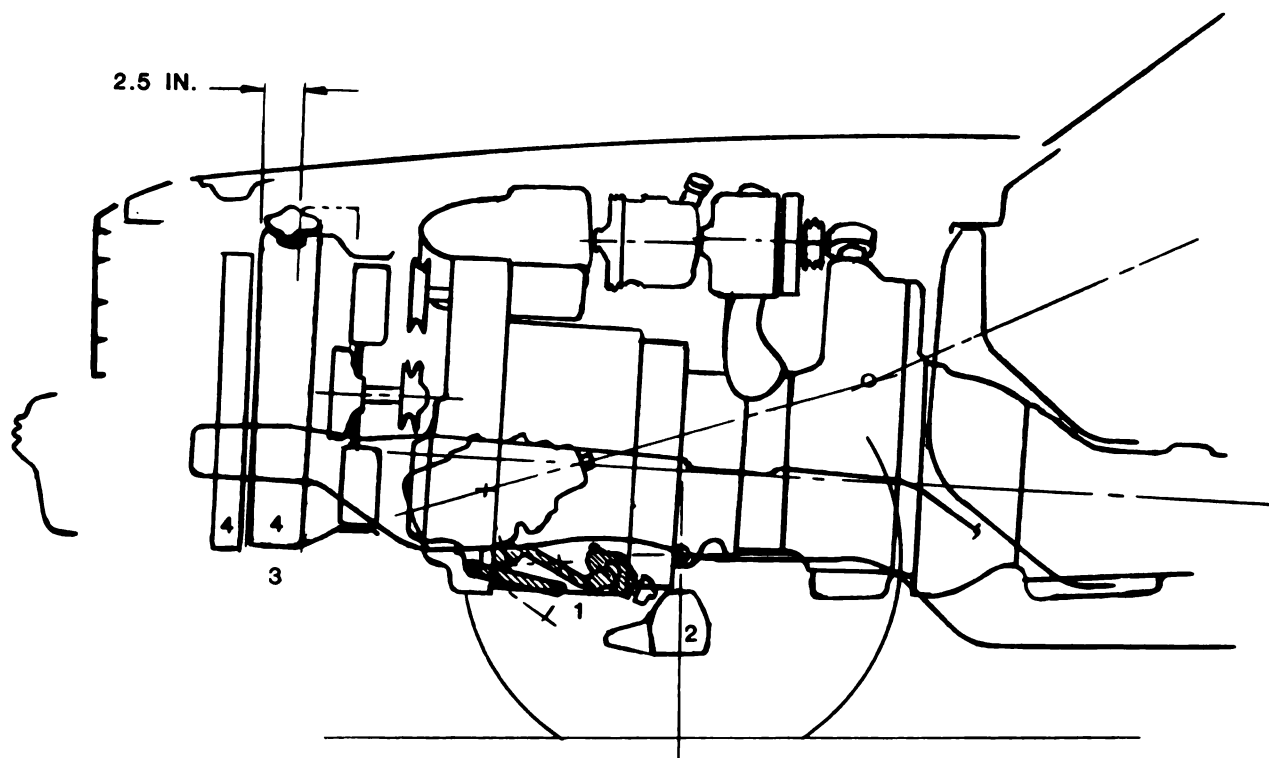
2.5 IN.

OPEN ISSUES

1. INTERFERENCE WITH STEERING LINKAGE.

2. NEW NUMBER 2 CROSSMEMBER.

3. POSSIBLE NEW NUMBER 1 CROSSMEMBER.

4. STIRLING ENGINE RADIATOR AND CONDENSER 2.5 IN. FORWARD OF NORMAL 1979 FORD POSITION

Figure 3.2-7   Scaled Stirling Engine (120 HP) in a 1979 Ford Engine Compartment

377

6.0 IN.

C ENG.

C TRANS.

1

2

SIDE VIEW

FRONT VIEW
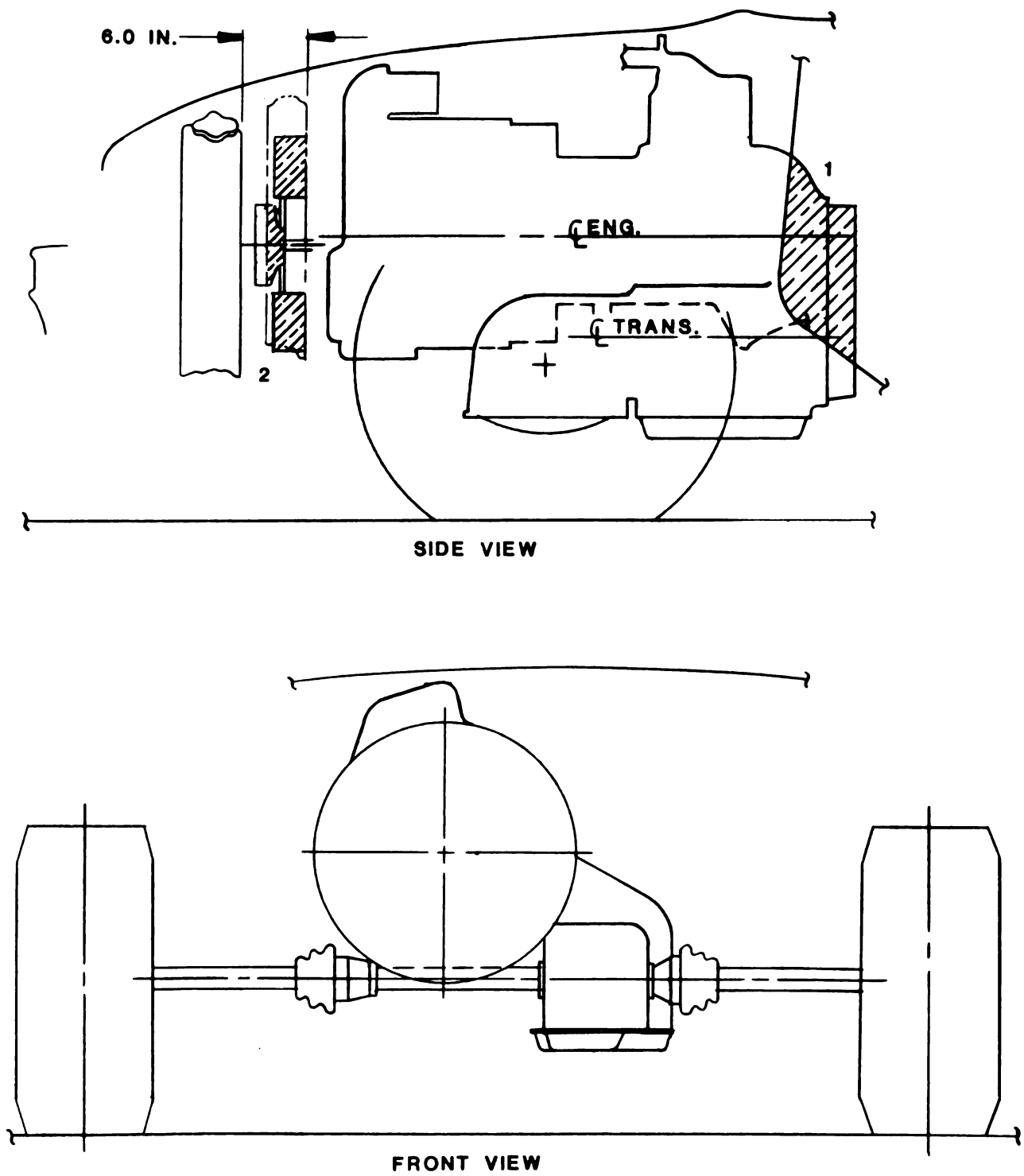
Figure 3.2-8   Scaled 120 HP Swashplate Drive Stirling Engine

PACKAGE PARAMETERS

.FUTURE SMALLER FRONT WHEEL DRIVE

.LONGITUDINAL ENGINE AND TRANSMISSION

.TRANSMISSION PARALLEL TO ENGINE

OPEN ISSUES

1. CONSIDERABLE INTRUSION INTO THE PASSENGER

   COMPARTMENT

2. RADIATOR MOVED FORWARD APPROXIMATELY 6.0 INCHES

Figure 3.2-8 Continued

ENGINE MOUNTED FORWARD OF WHEELS

ENGINE MOUNTED AFT OF WHEELS

SIDE VIEW

FRONT VIEW
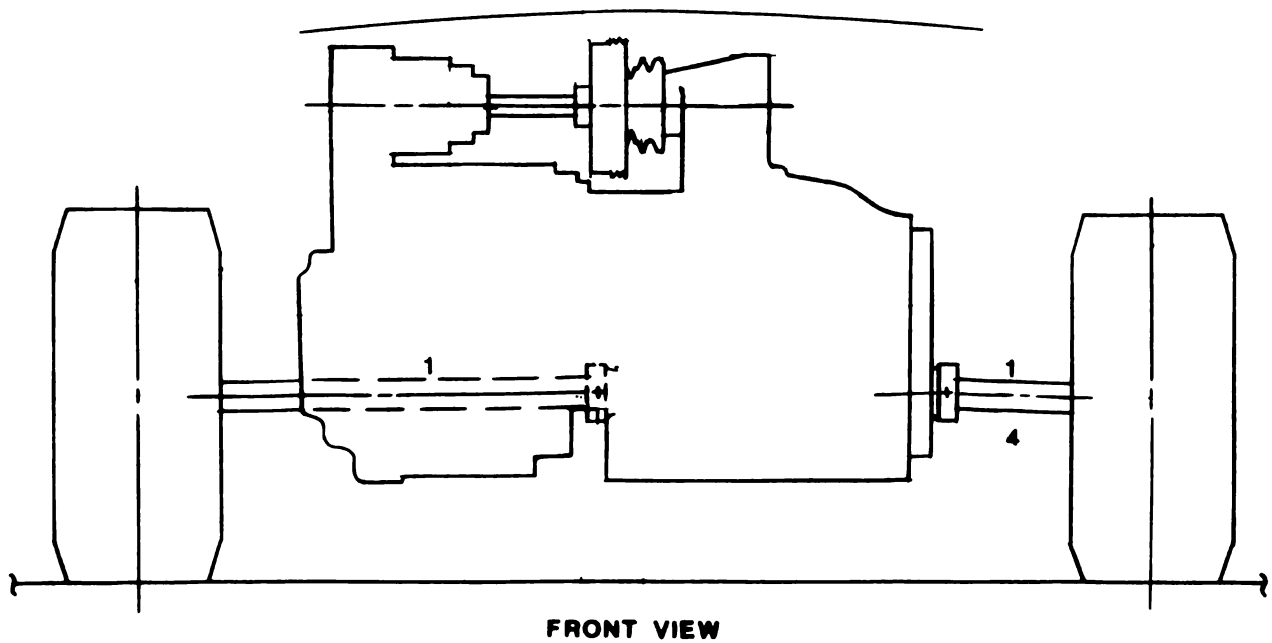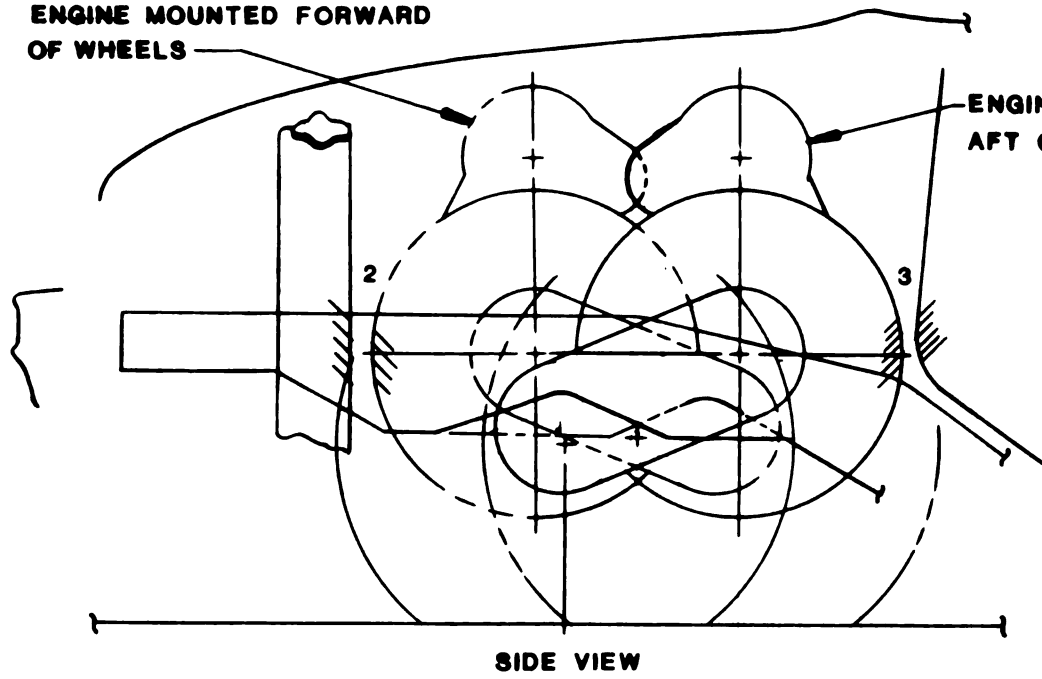
Figure 3.2-9   Scaled 120 HP Swashplate Drive Stirling Engine

PACKAGE PARAMETERS

.TRANSVERSE ENGINE AND TRANS/AXLE INSTALLATION FOR A

FUTURE (SMALLER) FRONT WHEEL DRIVE VEHICLE

.ENGINE AND TRANS/AXLE SHOWN BOTH FORE AND AFT OF

FRONT WHEELS

OPEN ISSUES

1. VERY UNEQUAL HALF SHAFT LENGTHS

2. SUBSTANDARD CLEARANCE BETWEEN RADIATOR AND

ENGINE BURNER SECTION WITH ENGINE MOUNTED FORWARD

OF THE FRONT WHEELS

3. SUBSTANDARD CLEARANCE BETWEEN DASH PANEL AND

ENGINE BURNER SECTION WITH ENGINE MOUNTED AFT OF

THE FRONT WHEELS

4. LEFT SIDE HALF SHAFT TOO SHORT

Figure 3.2-9   Continued

6.0 IN.

SIDE VIEW

FRONT VIEW
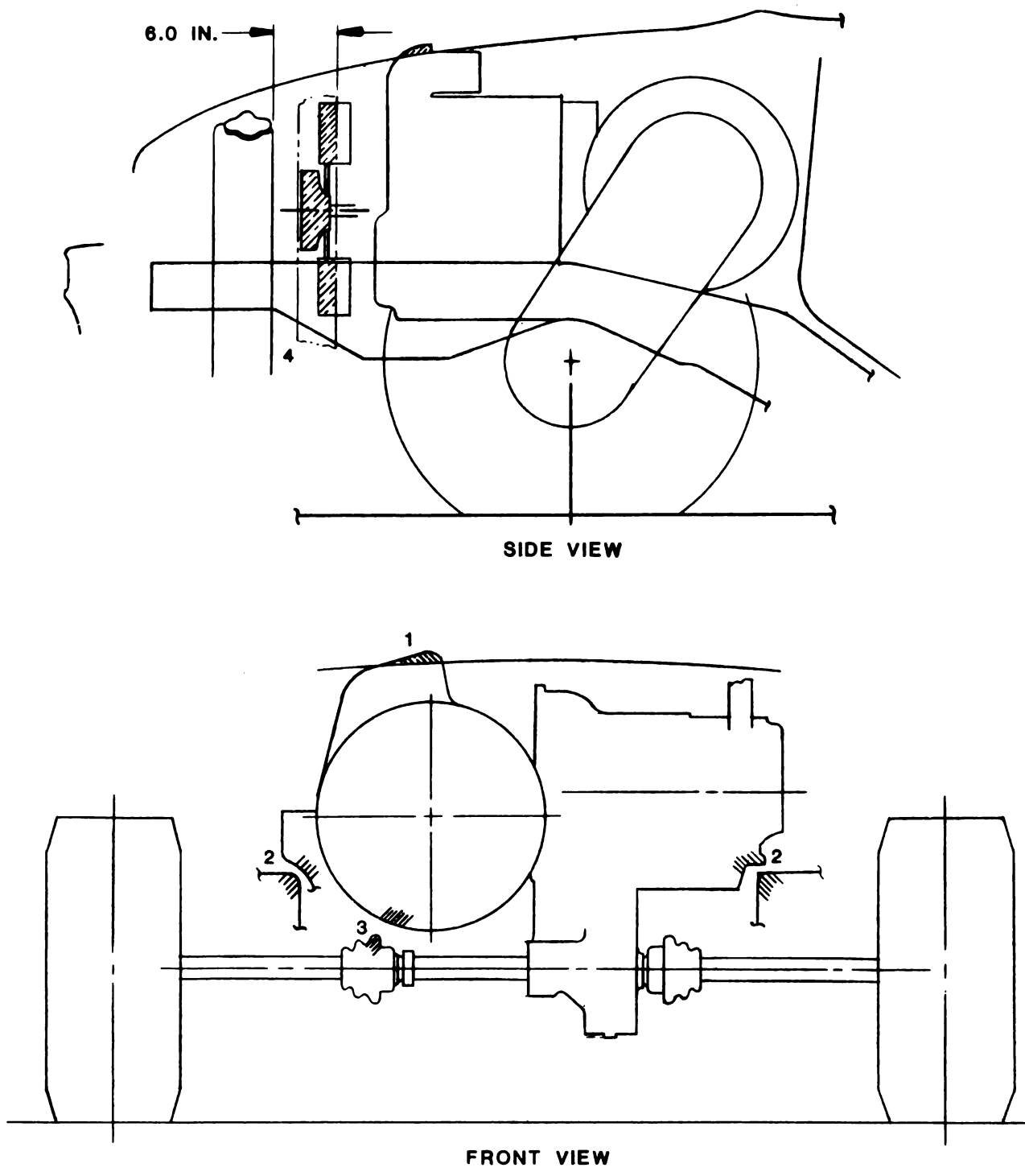
Figure 3.2-10   Scaled 120 HP Double Crankshaft Stirling Engine

PACKAGE PARAMETERS

.HORIZONTAL, LONGITUDINAL ENGINE

.TRANSVERSE TRANS/AXLE INSTALLATION FOR A FUTURE

SMALLER FRONT WHEEL DRIVE VEHICLE

OPEN ISSUES

1. INTERFERENCE BETWEEN PREHEATER AND HOOD

2. SUBSTANDARD CLEARANCE BETWEEN TRANSMISSION,

   ENGINE AND FRAME RAILS

3. SUBSTANDARD CLEARANCE BETWEEN HEATERHEAD

   AND CONSTANT VELOCITY JOINT

4. RADIATOR MOVED FORWARD FROM A NORMAL POSITION

   APPROXIMATELY 6.0 INCHES

Figure 3.2-10   Continued

4.1 Stirling Cycle Description

4.1.1 The Stirling Cycle

4.1.1 The Stirling Cycle — The Stirling engine is a machine in which the conversion of heat energy to work takes place through the alternate compression and expansion of a fixed quantity of working fluid, operating at a lower temperature during compression than expansion.

From the Carnot theorem in thermodynamics it is stated that heat engines operating between given temperature limits cannot be more efficient than a reversible heat engine operating between the same temperature limits. Under realistic pressure, temperature and volume limitations, the ideal reversible Stirling cycle is the most efficient, giving the highest work output per cycle. The following two figures depict the ideal Stirling cycle in terms of pressure — volume and temperature — entropy coordinates, respectively.
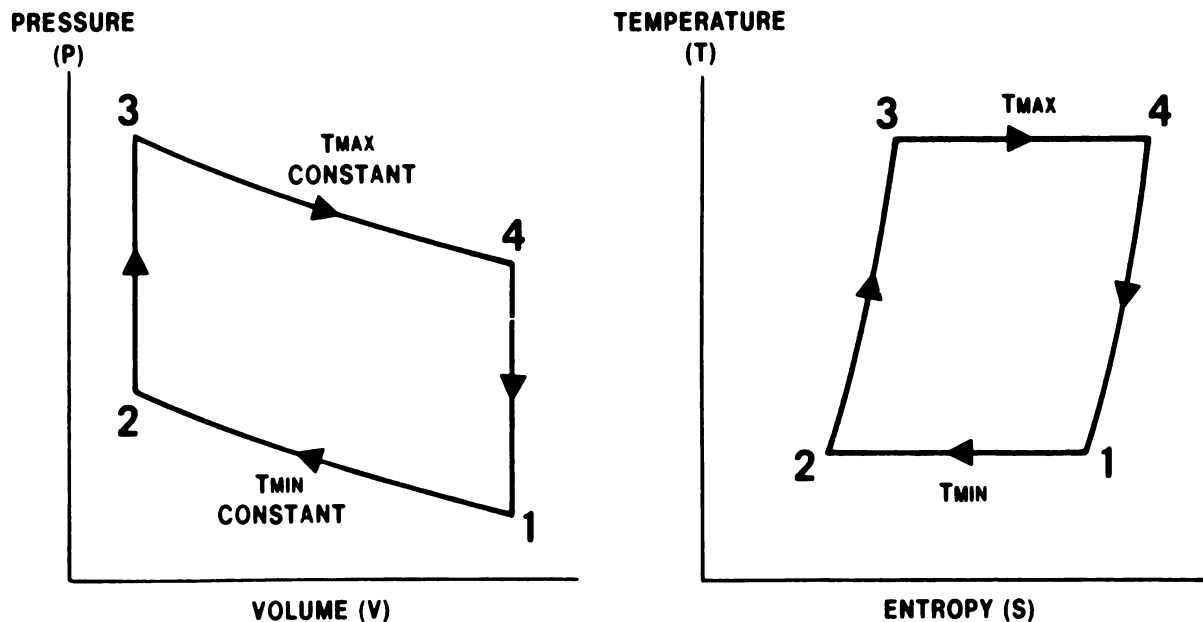
The distinctive features of the Stirling engine which set it apart from other heat engines are:

. The cyclic flow of the working fluid within the machine is achieved solely through geometric volume changes and without the use of intermittently-closed valves or ports.

. Thermal regeneration is accomplished via in intermittent flow heat exchanger, which stores a large portion of the heat of the working fluid after expansion and subsequently returns it to the working fluid after compression.

The physical operation of the Stirling engine can be explained with the aid of a simple two piston arrangement as shown in the following figure.
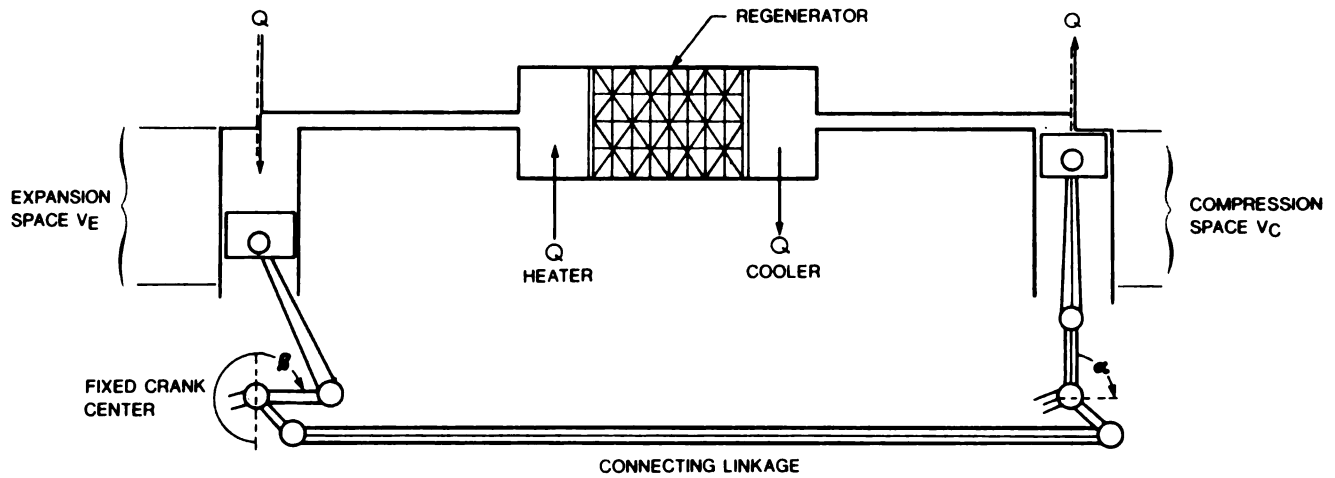
$\beta = 0$, $V_e = V_E$

$V_e = 1/2\ V_E\ (1 + \cos \beta)$

$V_c = 1/2\ V_c \left[1 + \cos (\beta - \alpha)\right]$

Two-piston mechanism illustrating the operation of a Stirling engine (Reference 4.1-1).

The direction of crank rotation is clockwise and the crank angle β is measured from the reference position where the expansion space volume V_e is maximum. The volume variation of the compression space $\bar{V}_c$ with respect to the crank angle β lags behind that of V_e by the angle α as determined by the connecting linkage. Values for α usually lie between 45° and 135°, with 90° being near optimum. Clearly, both cranks could be on the same shaft and displaced by the angle α. As the crank rotates, the total volume of the system, $V_t = V_e + V_c + V_D$, varies from V_{min} to V_{max} according to the relation

$$V_t = 1/2\left\{ V_C\ \left[1 + \cos(\beta - \alpha)\right] \right.$$

$$\left. + V_E\ \left[1 + \cos \beta\right] \right\} + V_D$$

where V_D is the dead volume (which includes the volume of heater tubes, cooler, regenerator, and connecting passages). Written in terms of the geometric engine parameters $\delta = V_D/V_E$ and $\zeta = V_C/V_E$, Eq. (1) becomes

$$V_t = (V_E/2)\left\{ \zeta\ \left[1 + \cos(\beta - \alpha)\right] \right.$$

$$\left. + \cos \beta + 2\ \delta\ + 1\right\}$$

providing that the motion of the piston can be adequately represented by simple harmonic expressions.

The variation of the total working space volume V_t with crank angle β as determined from Eq. (2) with $\alpha = 90^{\circ}$, $\zeta = 1$, and $\delta = 1$ is shown in the following figure.
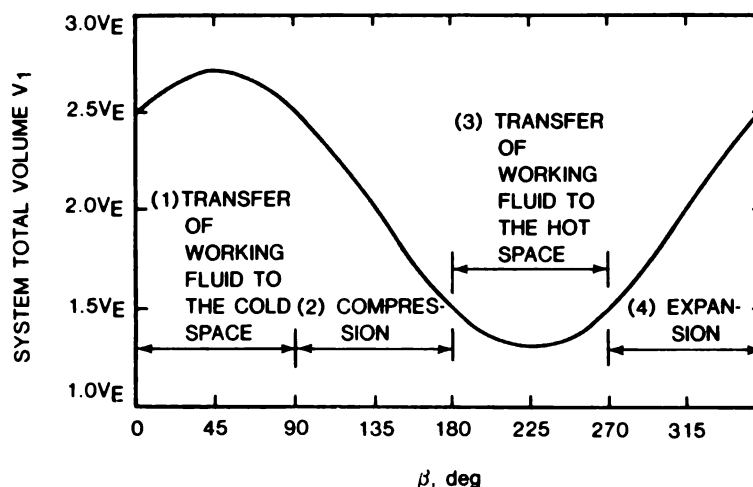
Variation of total working space volume with crank rotation angle β

with $\zeta = 1$, $\bar{\delta} = 1$, and $\alpha = 90^{\circ}$ (Reference 4.1-1).

The maximum working space volume $V_t = 2.71 \, V_E$, occurs at $\beta = 45^{\circ}$, and the minimum, $V_t = 1.29 \, V_E$, occurs at $\beta = 255^{\circ}$. The volume changes which occur within the expansion and compression spaces are phased such that the working fluid is located primarily in the hot space of the engine as the total working space volume increases and, conversely, located primarily in the cold space of the engine as the total working volume decreases. Therefore, one revolution of the crankshaft produces a sequence of four processes which are not distinctly separate but which, nevertheless, can be identified. As shown in the preceding figure, the four processes are:

(1) A transfer of the working fluid from the hot space through the heater, regenerator, and cooler to the cold space, which occurs with a relatively small change in total working space volume.

(2) A compression process occurring with the working fluid located primarily within the cold space and the adjacent cooler.

(3) A transfer of the working fluid from the cold space through the cooler, regenerator, and heater to the hot space, with a relatively small change in the total working space volume.

(4) An expansion process occurring with the working fluid located primarily within the hot space and the adjacent heater.

The work output of the engine is produced during the expansion process which occurs during each revolution of the crankshaft.

These four processes comprising the ideal Stirling cycle have been embodied in a variety of mechanical arrangements. However, two basic types of mechanisms, the piston-displacer and the two-piston, are most prominent in terms of developmental effort expended. These will be discussed in the following sections:

4.1.2 The Piston-Displacer Engine — The basic configuration of the piston-displacer engine is shown in the following figure. The cylinder of a piston-displacer engine is divided into a hot expansion space and cold compression space. The power piston executes reciprocating motion within the lower or cold portion of the cylinder, while the displacer executes reciprocating motion in the upper or hot portion of the cylinder.
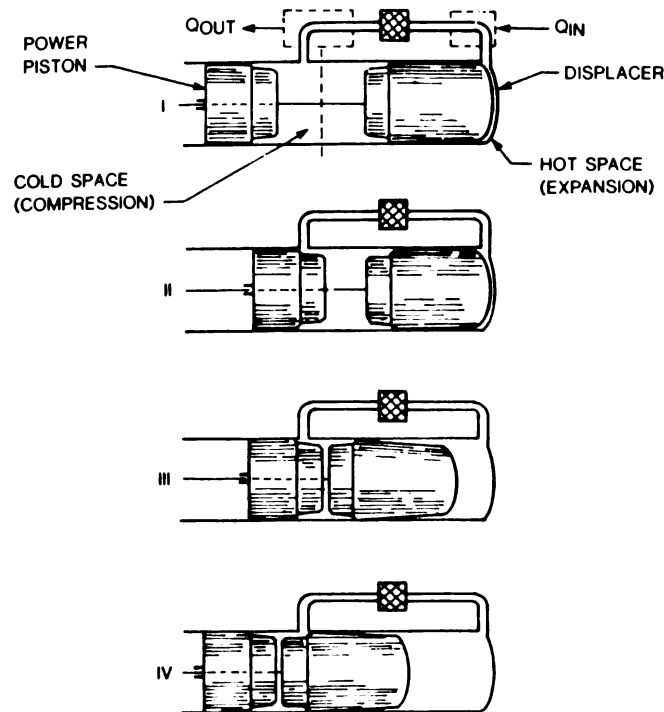

Piston displacer diagram showing Stirling cycle: I. Piston at bottom dead center. Displacer at top dead center. All gas in cold space. II. Displacer remaining at top dead center. Piston has compressed gas at lower temperature. III. Piston remaining at top dead center. Displacer has shifted gas through cooler regenerator and heater into hot space. IV. Hot gas expanded. Displacer and piston have reached bottom dead center together. With piston stationary, displacer now forces gas through heater, regenerator and cooler into cold space, thus re-attaining situation I. (Reference 4.1-1)

388

The displacer piston does not necessarily make a gas tight seal with the cylinder wall. Also, the external gas flow passages (consisting of the heater, regenerator and cooler) are designed so that the pressure difference across the displacer is quite low as the working fluid is shuttled between the hot and cold spaces. The relative motion of the piston and displacer is such that the sequence of positions I, II, III, and IV is obtained. The four processes comprising the Stirling cycle are executed as the piston and displacer move through these positions.

4.1.3 The Two-Piston Engine — The single acting two piston engine has been previously described in this section.

A more compact version of the two-piston engine may be constructed by utilizing double-acting (DA) piston/cylinder arrangements, with expansion occurring on one side of the piston and compression on the other. An arrangement which gives the necessary phase lead of the expansion space, when DA cylinders are interconnected as shown in the following figure, was invented at Philips, as reported by Rinia (Reference 4.1-2).
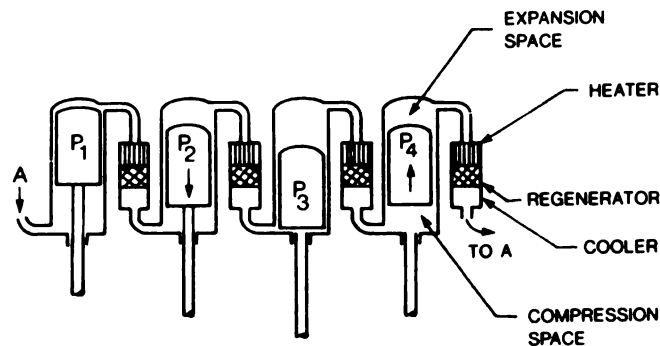
The Philips Rinia arrangement for two-piston type double-acting

Stirling engines (Reference 4.1-2).

The Rinia (Philips) arrangement requires multicylinder engines, which are expensive for laboratory test work. Further, the Rinia engine is more complex fluid-dynamically and thermodynamically, making it more difficult to optimize for high efficiency. However, with the more sophisticated understanding of the Stirling engine processes developed during the years of work on rhombic drive engines, the problems with DA engines are yielding to renewed developmental effort.

A four cylinder Rinia engine with $a = 90^\circ$ may be constructed in either an in-line crankshaft drive or a circular-swashplate drive configuration. The latter configuration is of particular interest since it packages quite compactly.

The DA-Rinia cylinder arrangement may also be used with the cylinders arranged in a V-configuration. In such an engine the angle between the cylinders forming the V can provide proper phasing if the connecting rods of a cylinder pair are connected to the same crankshaft throw. Of course, a crankshaft similar to an in-line four may also be used but the V arrangement provides more compact packaging than an in-line engine.

389

4.1.4 References

4.1-1   Jet Propulsion Laboratory report, "Should We Have A New Engine?" JPL SP 43-17 Volume II, pages 6-1 to 6-46. Copyright 1975, JPL, California Institute of Technology.

4.1-2   Rinia, H., "New Possibilities for the Air-Engine," Philips Gloei-lampenfabrieken, Paper No. 1684, 1946 or Proceedings, Koninklijke Nederlandsche Akademie van Wetenschappen, pg. 150-155, Feb. 1946, (published in English).

4.2 4-215 Engine Description

4.2.1 Background — The 4-215 Stirling engine is a four-cylinder, double acting (DA) swashplate drive engine having a displacement of 215 cc/cyl. This displacement is referred to as "swept volume". The functional objectives governing the original engine as designed by Philips are as follows: (Reference 4.2-1)

Criteria	Objective
Emissions (HC/CO/NOx)	0.41/3.4/0.4 grams/mile
Fuel economy at 16°C (60°F) ambient temperature - city/suburban test route - steady speeds 30-70 mph.	25% better than base line average 21.8 mpg
Performance with test weight of 2230 kg (4919 lbs): 0 - 60 mph	12.7 sec.
Warm-up (from key-on to drive away)	15 sec.
Driveability	6.0 (jury rating)
Weight	Base line plus 50 lbs.
Noise level (SAE J986)	70 decibels
System recharge period	One year

Base line: 1975 Ford Torino — California Emissions

A four-cylinder double-acting (DA) swashplate drive engine was selected as the basic design because it best fulfilled the constraints of vehicle packageability, weight, and fuel economy better than other engine configurations.

The number of cylinders, bore, and stroke were selected so that the resultant swept volume would be adequate for the power and speed requirements of the Torino vehicle, without modifications to the existing transmission. The indicated power objective of 177 kW included an estimate of 127 kW brake and 50 kW friction and accessories.

With these power, speed and geometry requirements, an engine optimization was undertaken, resulting in the basic engine data given as follows:

Number of cylinders	4
Number of cooler/regenerator units	8
Bore	73 mm (2.87 in)

Stroke	52 mm (2.047 in)
Working fluid	hydrogen
Maximum net power	127 kW (170 hp) at 4000 rpm
Maximum net torque	428 Nm (360 ft. lb.) at 1350 rpm
Maximum mean working fluid pressure	20 N/mm^2 (2844 psi)
Heater-head temperature	750°C (1382°F)
Cooling-water temperature	64°C (146°F)

Basic 4-215 Engine Data   (Reference 4.2-1)

A cross-sectional drawing of the original design 4-215 engine is shown in Figure 4.2-1. The engine on test is shown in Figure 4.2-2. As engine testing and hardware experience proceeded, many changes were made in the original design, as has been discussed in previous sections of this report.
Based on engine and component testing basic data has been gathered which, together with computer generated information, results in the following economy and performance map for the base 4-215 engine.
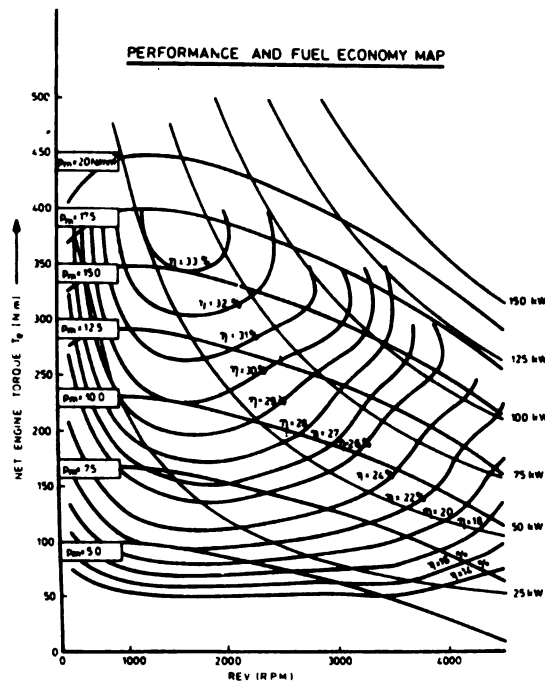

Fuel economy map - 4-215 D.A. engine   (Reference 4.2-1)

4.2.2 Engine Design

4.2.2.1 Heater Head — The basic heater head is composed of:

- Four cylinder bores;

- Eight chambers (bores) for the regenerator-coolers;

- Heater tubes - two rows with the outer row finned, 88 total

- Eight regenerator-coolers units.

By grouping the four cylinders around a central axis, the heater tubes which connect the cold side of one cylinder to the hot side of the adjacent cylinder via two intermediate regenerator-coolers also can be clustered in a cylindrical cage. The cylindrical heater tube cage configuration allows a single burner to serve all four cylinders. The heater head is shown in the following illustration.
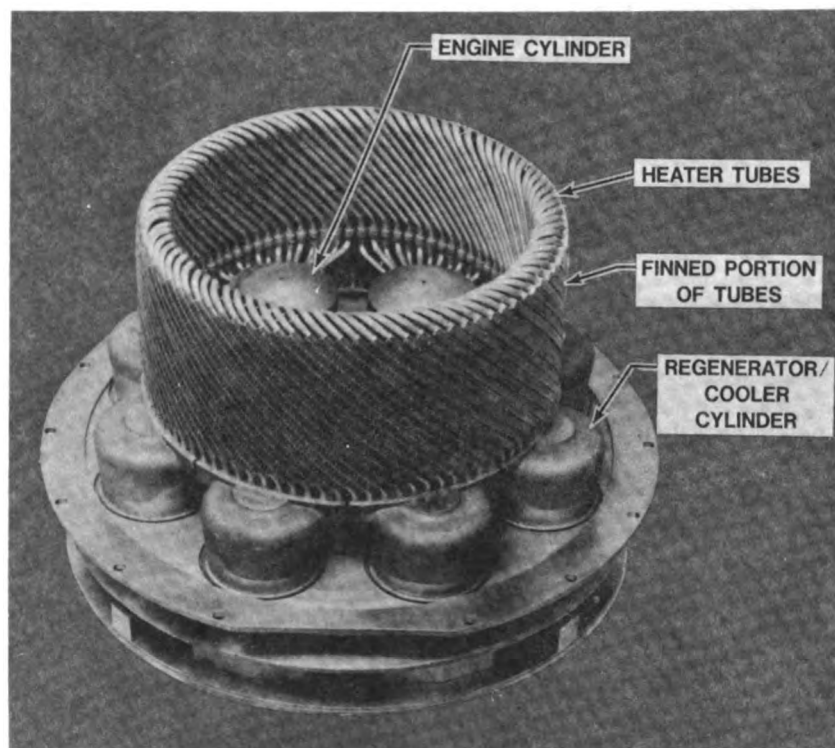
STIRLING ENGINE HEATER HEAD

The heater tube cage of the 4-215 engine is designed to be flexible to allow for tube growth and relative motion during operation. Multimet tubing was used based on

393

Digitized by Google

past experience and because of its compatibility with the brazing cycle used during the heater head fabrication.

The cast material for the cylinders and regenerator housings had to satisfy the following requirements:

- impermeability and immunity to hydrogen gas under pressure,

- structural stability at temperatures of up to 750°C (1382°F),

- compatibility with the brazing process used during assembly of the heater head,

- good resistance to oxidation.

To satisfy these demands CRM-6D, an iron-based carbide-strengthened steel developed by Chrysler, was chosen. Investment casting of CRM-6D proceeded without difficulties. CRM-6D was found to pose no problems during brazing, once the correct brazing cycle had been defined.

Each cooler-regenerator unit is comprised of a bundle of stainless-steel tubes 1.8 mm (0.0709") in diameter, having a wall thickness of .45 mm (0.0177"), attached to the regenerator portion consisting of closely packed stainless steel gauze screens. Wire diameter, thermal conductivity, heat capacity, etc. of the regenerators must be carefully chosen to provide optimum performance.

4.2.2.2 Air Preheater — Being an external combustion engine, the Stirling engine combustion process occurs in a separate burner assembly, and heat is transferred
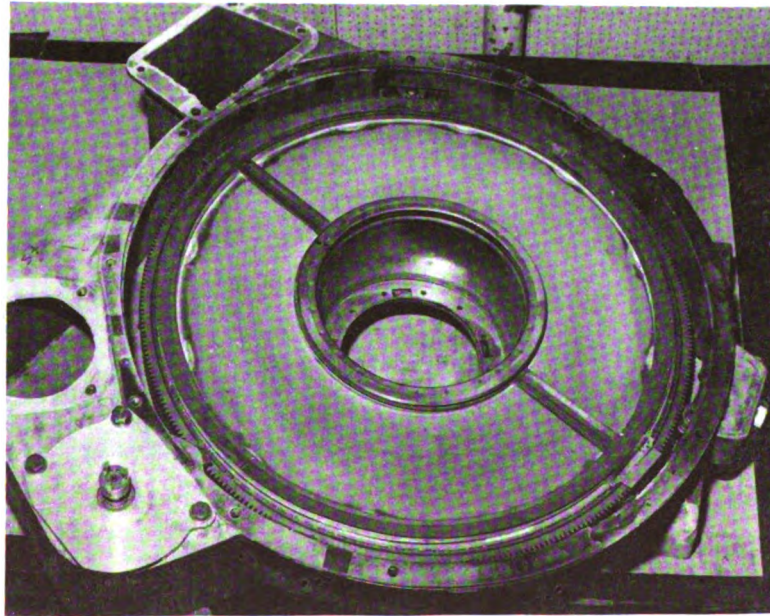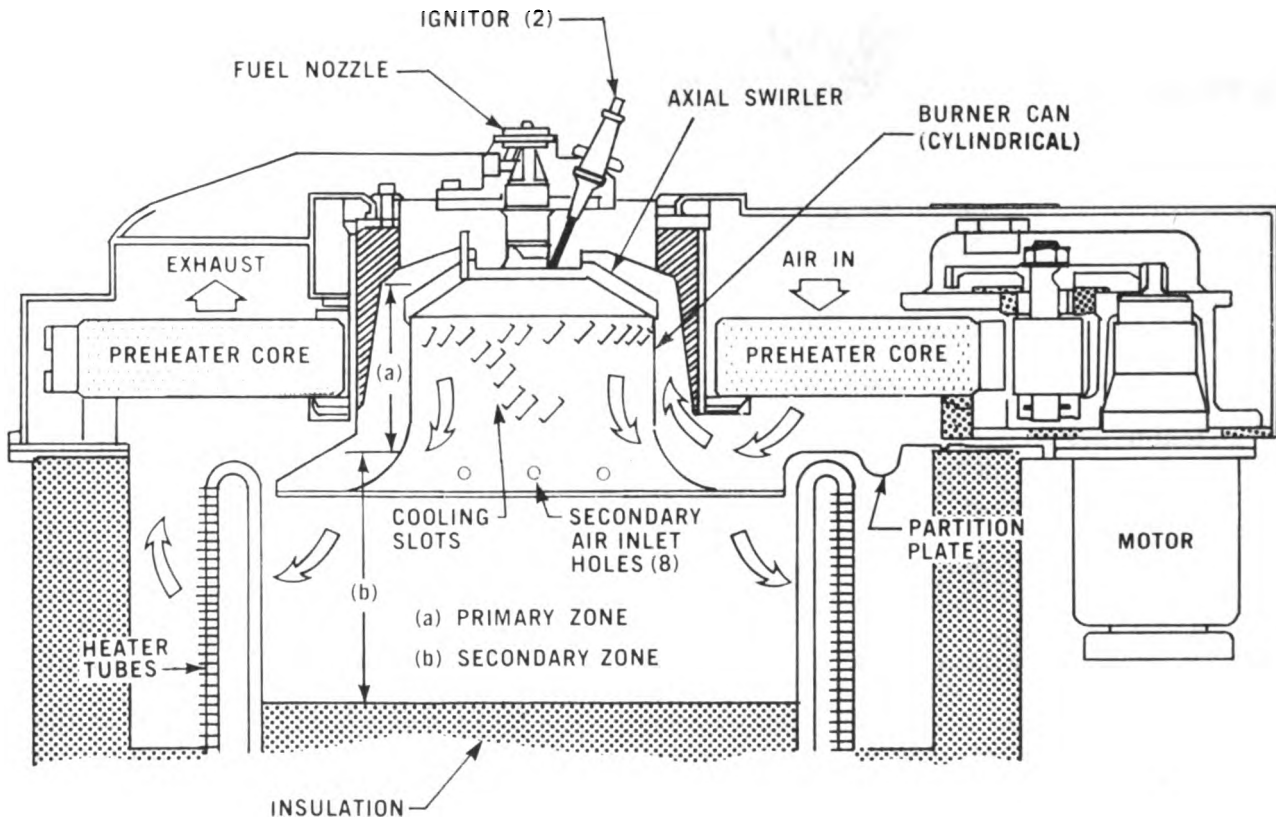

4-215 Stirling Engine Preheater Assembly
(Reference 4.2-1)

to the working fluid through the heater tubes. The present 4-215 heater head can transfer only a little more than half of the energy of the fuel to the working fluid. Thus, without a recovery system, approximately 45% of the energy of the fuel would be lost to the atmosphere. Besides the advantage of increased fuel economy, the recovery system, or preheater as it is called, results in a lower outer surface temperature of the engine, and allows the exhaust system to be made from less expensive materials.

In the design of the 4-215 engine, use is made of porous, rotating ceramic disc, originally developed for gas turbine application. The preheater assembly is shown in the preceding illustration.

The ceramic disc is 40 mm (1.575") thick and is driven by an electric motor at a constant speed of 8 RPM. Analysis of the stresses within the core was performed with a computer program developed by Ford to ensure that the core would exhibit acceptable life without rupture. To date we have not experienced problems with the preheater core and after initial modifications, seals have also proved to be satisfactory.

4.2.2.3 Burner — The 4-215 engine combustion system is comprised of a burner can, an air-assisted atomizing fuel nozzle, and an ignitor, as shown in the following illustration.

4-215 STIRLING ENGINE
BURNER-PREHEATER CROSS SECTION

The 4-215 combustion system utilizes a continuous type combustion process and functions similarly to other continuous combustion systems, such as those in gas turbine and Rankine cycle engines. The levels of unburned hydrocarbons (HC) and carbon monoxide (CO exhaust emissions from a continuous combustion system are inherently low, resulting in a high combustion efficiency. Exhaust gas recirculation (EGR) is used to control nitrogen oxides (NO_x) to acceptable levels.

Combustion system flow tests conducted in a water flow rig showed that an acceptable flow pattern could be realized with a conical burner can, rather than the original cylindrical can. The following picture shows this conical combustor.
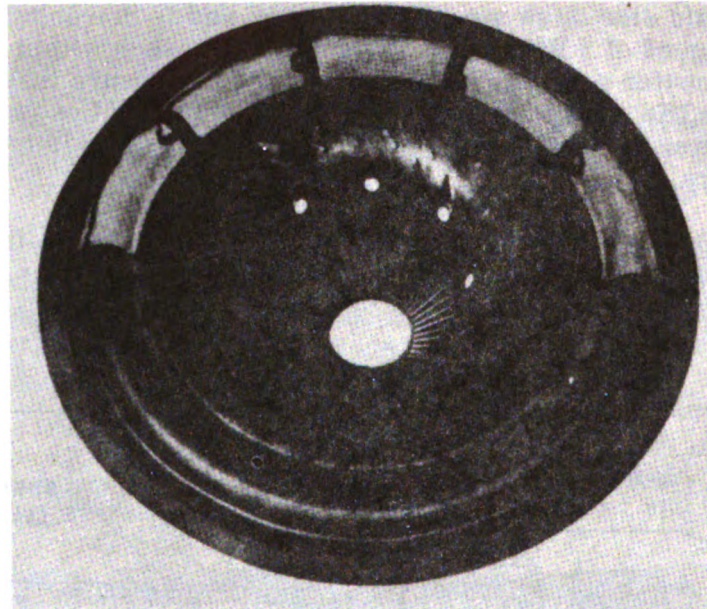

4-215 Engine Conical Burner (Reference 4.2-1)

Inside the conical can an internal recirculation is set up by a 48-blade swirler in conjunction with the conical shape of the burner, as shown in the following illustration.

4.2.2.4 Mechanical Drive System — As mentioned previously, the basic engine configuration is a four cylinder double acting swashplate design. Each piston in a double acting engine serves both as a power piston and a displacer piston for the adjacent cylinder.

The swashplate drive mechanism consists of a thick disk which is mounted on the output shaft of the engine, and oriented at a fixed angle with respect to the centerline of the shaft. The swashplate is surrounded by four crossheads evenly spaced around its periphery and oriented so that their centerlines are parallel with the centerline of the mainshaft. The crossheads straddle the swashplate and convert the reciprocating motion of the pistons to rotary motion.

396
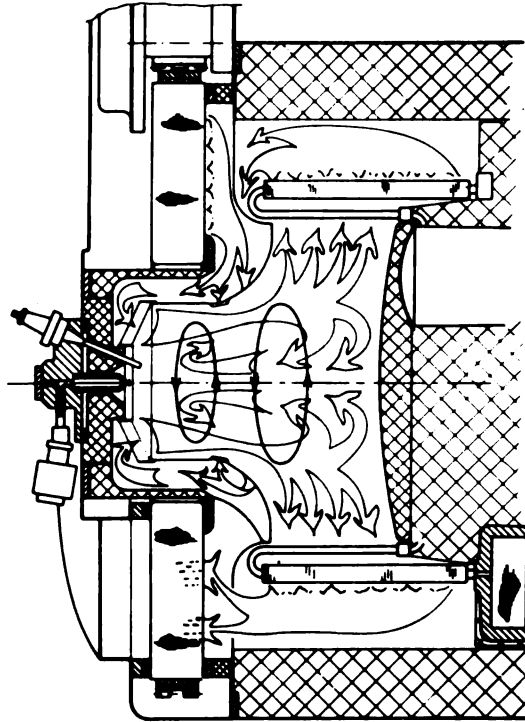
4-215 Burner Circulation (Reference 4.2-1)

The following picture shows the basic components making up the swashplate drive.
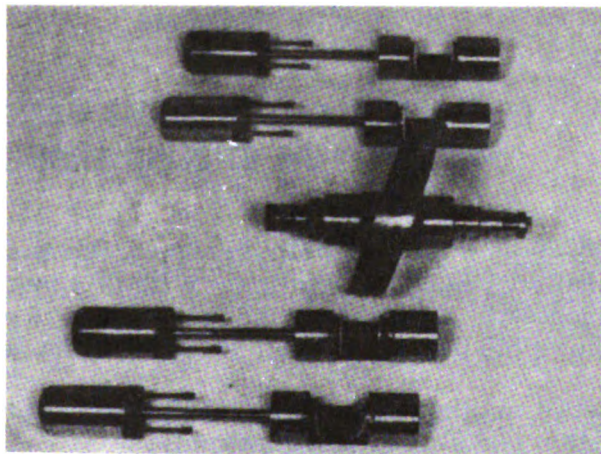
4-215 Swashplate Drive Components
(Reference 4.2-1)

It was noted after running the 4-215 engines that the crossheads were worn at the crosshead bridge edges which had contacted the outer diameter of the swashplate. This wear, plus the initial use of parts which had greater than desired clearances between the crosshead bridge and swashplate, contributed to excessive engine

noise. The noise originated from the crossheads striking the swashplate because reversing torsional loads were exerted on the crossheads due to its design, wherein the slider bearings were eccentric to it. This problem plus others necessitated a redesign to a concentric drive arrangement, as shown in the following figure.
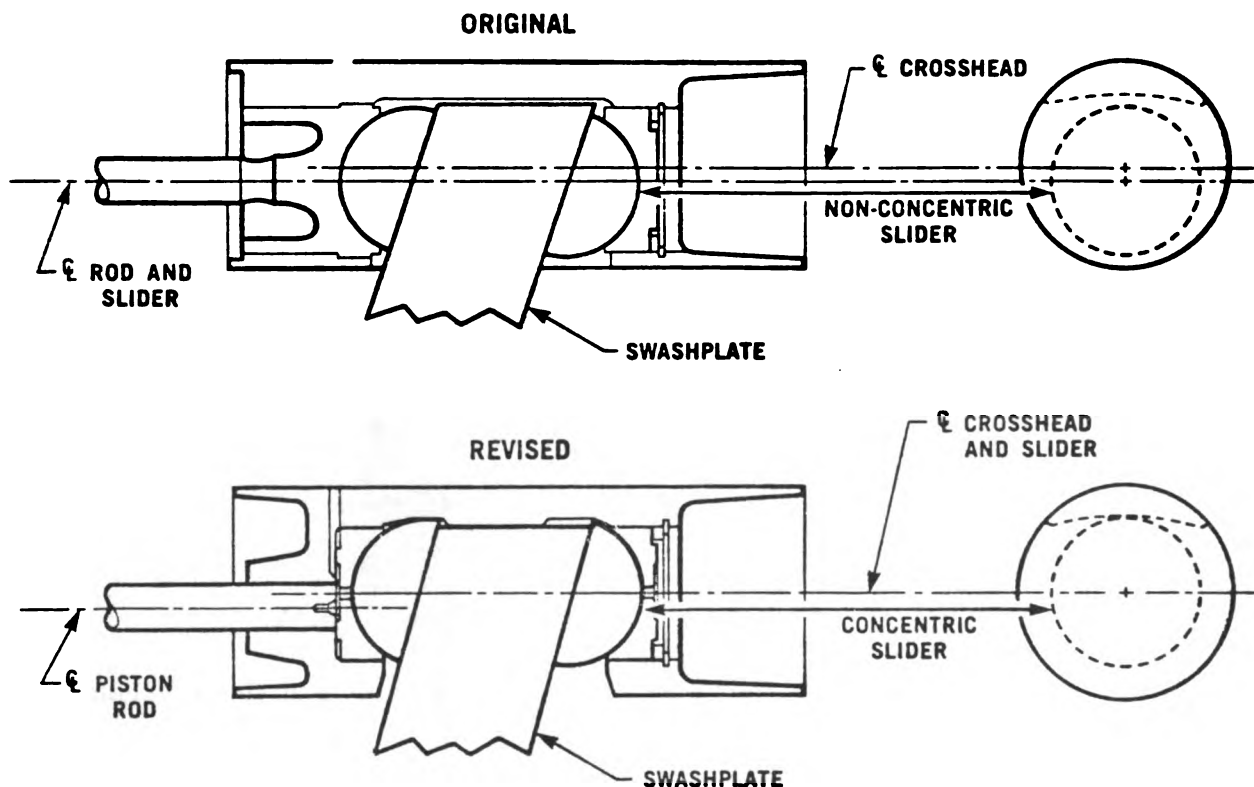

COMPARISON OF CROSSHEAD DESIGNS FOR THE 4-215 STIRLING ENGINE

4.2.2.5 Sealing System — As originally designed, the piston rods are sealed with four "rollsock" seals developed by Philips. With this system, a rolling rubber diaphragm is supported by oil to withstand the high cycle pressures. The following illustration shows the basic elements in the rollsock sealing system.

As explained in detail in other sections of this report, work was also carried out on an alternate piston rod sliding seal assembly.

4.2.3 Summary — More detailed descriptions of each of the areas discussed in this section can be obtained by referring to the appropriate section in part 2 of this report. Air/Fuel control, temperature control and power control techniques are all covered in greater detail in those sections.

WORKING FLUID
ROLLING DIAPHRAGM
ROD
OIL
OIL PUMPING RING
REGULATING VALVE
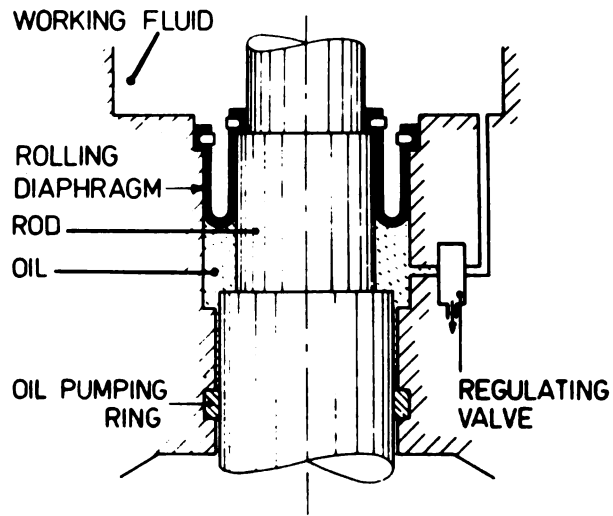
4-215 Rollsock Sealing System
(Reference 5.2-1)

4.2.4 References

4.2-1   Van Giessel, R., and Reinink, F., "Design of the 4-215 D.A. Auto-
motive Stirling Engine," Paper 770082 presented at the 28 Feb. — 4
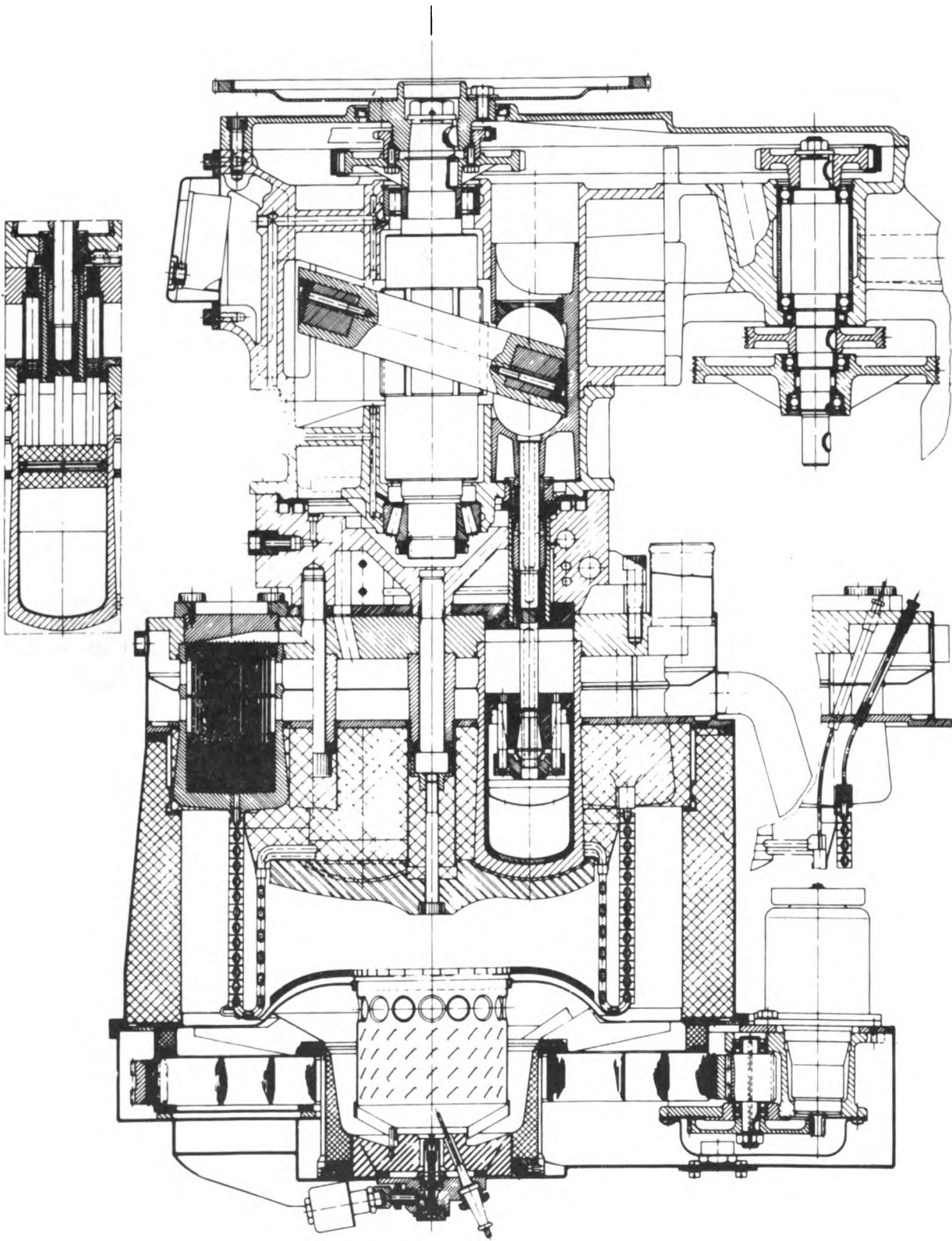Mar. 1977 SAE meeting, Detroit, Michigan.
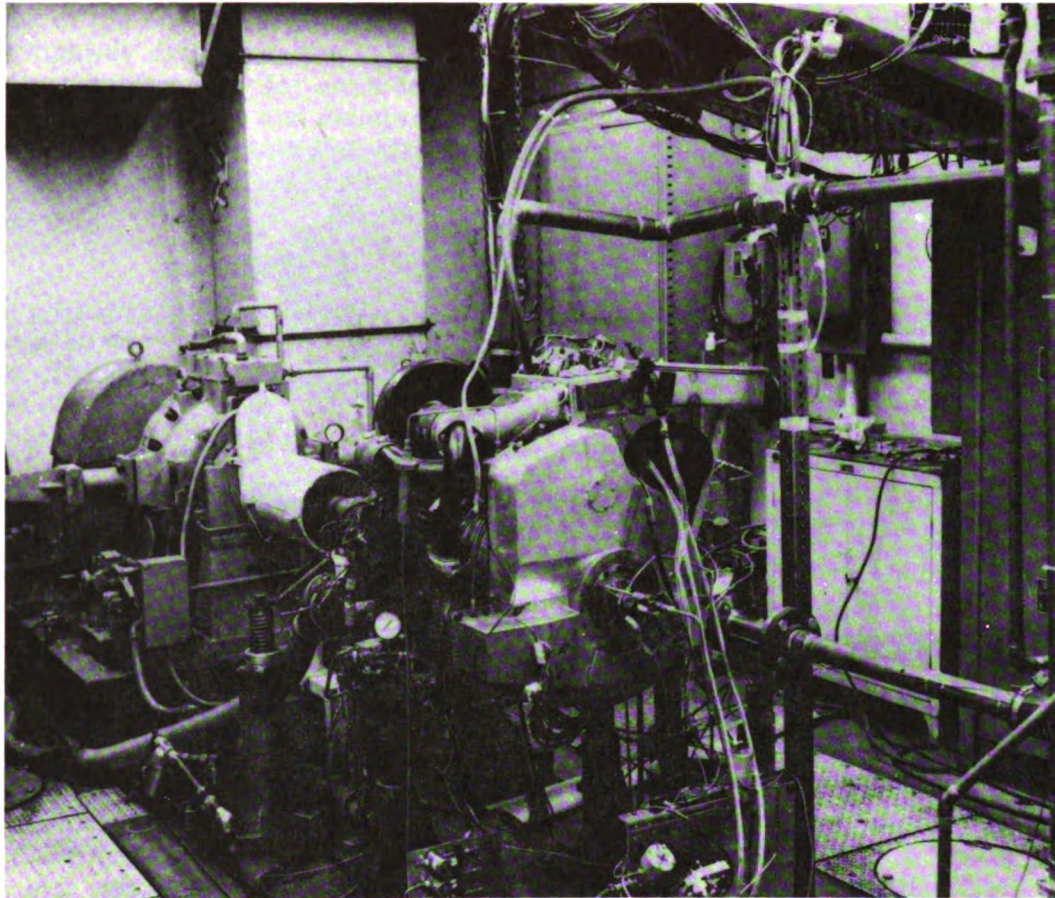
Figure 4.2-1   Cross Section of the 4-215 D. A. Design

Figure 4.2-2   First Installation of the 4-215 Stirling Engine in a
Dynamometer Cell in the U.S.A.

① ACCELERATOR PEDAL INPUT TO ELECTRONIC CONTROL BOX (ECB)

② ECB REGULATES POSITION OF POWER CONTROL ACTUATOR

③ ACTUATOR OPENS AND CLOSES WORKING GAS CONTROL VALVES

④ FOR ACCEL. ACTUATOR OPENS INLET CONTROL VALVE TO INCREASE H_2 PRESSURE WITHIN ENGINE

⑤ DURING DECEL. ACTUATOR OPENS RETURN VALVE AND COMPRESSOR PUMPS H_2 FROM ENGINE TO RESERVOIR, DECREASING PRESSURE

DECEL.
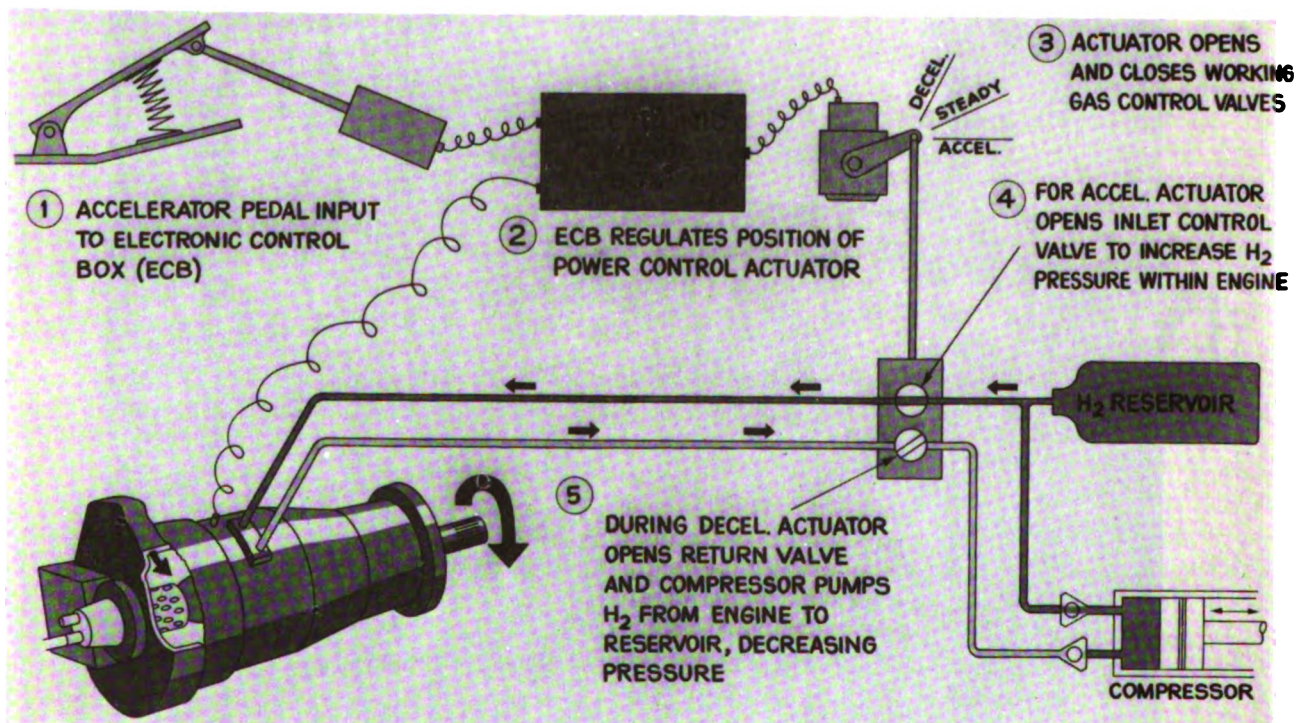STEADY
ACCEL.

H_2 RESERVOIR

COMPRESSOR

Figure 4.2-3   Schematic of Working Gas Control System

4.3 Computer Program Description — Many computer programs were used throughout
the course of this study. Those originally developed by N. V. Philips and USS are con-
sidered proprietary, requiring the description of those programs to be somewhat limited.

4.3.1 Ford Program PB1111 — This program projects performance parameters for
a specified engine/vehicle combination. Basically, this calculation is made by deter-
mining the torque available to accelerate the vehicle at various increments of vehicle
speed. Output computations from PB1111 include projected 0-60 MPG acceleration
time, maximum vehicle speed, and quarter mile acceleration time as well as other,
lesser used parameters which characterize vehicle performance.

4.3.2 Ford Program VSIM — The (vehicle simulation) program is used to obtain
estimates of the engine torques and speeds required to power a vehicle over the EPA
city and highway driving cycles. The VSIM computer program obtains this projec-
tion by first determining for each second of operation the torque required on the driv-
ing wheels to accelerate and decelerate the vehicle over the EPA highway and city
driving cycles. Next, the VSIM computer program translates the required driving
wheel torques into required engine torques by adjusting for drive line inefficiencies
and engine accessory loads. The output from the VSIM computer program is a listing
of the required engine torques and speeds for each second of operation.

From the VSIM output a matrix of engine speeds, torques, and the time spent at each
speed/torque condition is plotted. From this "time density matrix" it is possible to
determine those engine speeds and torque conditions which recur most frequently dur-
ing the driving cycles (i.e., which engine speed/torque conditions are most heavily
time weighted).

In performing engine dynamometer fuel economy testing it is not feasible to determine
fuel flows for each of the hundreds of engine torque and speed combinations that occur
during the driving cycles. Accordingly, engine dynamometer testing is performed at
a much smaller number of steady-state engine speed and torque conditions. For the
Stirling Engine Program, ten (10) steady-state engine speed and torque conditions
were selected on the basis of the time density matrix output from the VSIM computer
program. These ten (10) steady-state engine torque and speed conditions were then
used for engine mapping, and also to obtain computer estimates of M-H fuel economy.

4.3.3 Ford Program TIME — The TIME computer program is used to obtain esti-
mates of the time that would be required at each of the preselected steady-state engine
speed and torque points in order to accurately simulate the engine work required over
the EPA city and highway driving cycles. It is important to note that the TIME pro-
gram does not select which engine speeds and torques are to be used for engine map-
ping. Instead, the selected ten (10) engine speed/load mapping points were used as
input data to the TIME computer program. The estimates of time spent at each of the
ten (10) preselected steady-state speed-load points are termed "time weighting fac-
tors."

4.3.4 Ford Program ECONCALC — This program uses the time weighting factors
generated from the TIME computer program and the speed/load points selected with
the aid of the VSIM computer program to calculate M-H fuel economies. This calc-
ulation is made by entering a computer-generated engine map of net torque, speed,
and fuel flow with the ten (10) preselected speed/load points and then interpolating
within the map to determine the fuel flow at each condition. The time spent at each

403

engine mapping point, as determined by TIME, is then multiplied by the fuel flow at each speed/load point to obtain a projection of fuel economy over the EPA city (CVS-HOT) and highway driving cycles. Lastly, in obtaining a M-H fuel economy value, a cold-start fuel penalty is applied to the city (CVS-HOT) fuel economy by the ECON-CALC computer program.

This program also had the capability of modifying any accessory loss or mechanical friction value contained in the original engine map in order to determine what effect a change in that value had on fuel economy. In this way, the contribution to overall fuel economy of a reduction in engine friction by 15%, for example, could rapidly be determined.

4.3.5 Ford Program TOFEP — This computer program calculates both vehicle performance and fuel economy. TOFEP performance calculation are made in the same manner as previously described for the PB1111 computer program. The performance data output of the TOFEP computer program is the same as that obtained from the PB1111 computer program. However, TOFEP calculations of fuel economy are performed in a more sophisticated manner than the VSIM/TIME/ECON-CALC technique for obtaining projections of M-H fuel economy.

In lieu of obtaining a M-H fuel economy value by using a steady-state approximation to transient engine operating conditions (speed/load mapping points and time weighting factors) the TOFEP computer program computes the required engine torque speeds and fuel consumed for each second of the EPA city and highway driving cycles, sums the fuel consumed, and then calculates the EPA city (CVS-HOT) and highway fuel economies. The TOFEP computer program, however, does not calculate a cold-start fuel penalty which is required to obtain a M-H fuel economy. Instead, the cold-start fuel penalty and the M-H economy must be calculated separately when the TOFEP computer program is used.

4.3.6 N. V. Philips Optimization Program — The cycle optimization procedure has the capability of optimizing the design of a new engine concept arrived at from preliminary design investigations, or reoptimizing a particular design after a significant change in one or more components, or following an update of the basic analytic treatment of the cycle.

For a given set of input data, the optimization procedure will calculate the "best" engine for a particular steady-state operating point. This optimization is achieved by maximizing one of several possible quantities, such as indicated power or efficient, torque, etc. In addition to the one quantity being maximized, up to three requirements can be specified. For example, one could seek a maximum efficiency while specifying a certain value for power and engine height.

The main routine used during an engine optimization is the basic cycle analytic program developed by N. V. Philips, described more fully in the following sub-section. In arriving at an optimized engine, this routine may be called hundreds of times. The optimization procedure includes the capability of using up to 20 variable quantities on which to base the optimization. That is, up to 20 separate quantities can be varied until an engine is found which satisfies the optimization criteria. Only one (1) output quantity may be optimized.

Input for the optimization program consists of fixed data (similar to that used to per-

form a single analytic calculation) and data which is allowed to vary between fixed boundaries. The quantities which will be held constant during an optimization must be determined beforehand from preliminary engine design considerations.

Since the possibility exists that the 20 variable quantities may be different from one optimization to the next, provisions have been made to allow a re-formulation of the relationship among each of the 20 possible variables and the optimized function.

4.3.7 N. V. Philips Analytic Program — This is the main routine used in the optimization program, steady-state engine calculations, and the generation of complete engine maps. It has the capability of evaluating the Stirling cycle only and does not consider the complete engine assembly or specific components. The program analyzes the engine on a per-cylinder basis, and is useful in assessing the effects of dimensional changes, operational changes, and modifications to the analytic models within the program. Calculations are performed beginning with a semi-adiabatic engine model simulating engine operation. The model assumes that the temperatures in all volumes of the engine are isothermal, except the swept volumes in the expansion and compression spaces, and the volumes of the connecting ducts. The temperatures of these volumes, plus some smaller volumes near these spaces, are considered to behave adiabatically.

4.3.8 United Stirling Simulation Program — Unlike the closed-form solution technique employed in the Philips analytic program, the approach used in the USS cycle simulation program is to describe the state of the working gas by a set of time-dependent differential equations which are then numerically integrated. This program can account for varying heat exchange, wall temperatures, and can be adapted for investigating power control system operation.

4.3.9 Ford Program FCDVAREA — This computer program studies the gas flow through a valve connecting the main Stirling cycle to a control dead volume, as shown in the following figure.

CONTROL DEAD VOLUME

CONNECTING VALVE

CYCLE PRESSURE VARIATION
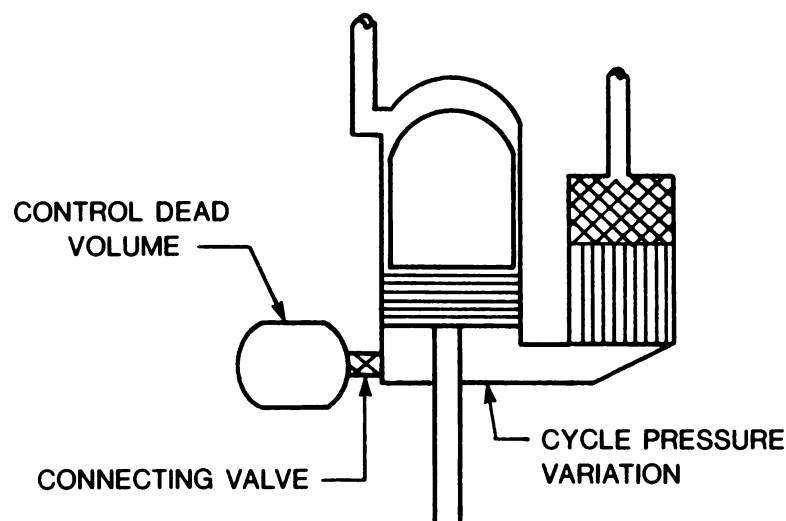
Calculations in the program are based on discrete crank angle increments, at the beginning of which both the pressure difference across the valve and the mean cycle pressure are assumed known. The program includes relationships which determine the instantaneous cycle pressure and the quantity of gas in the cycle. At the beginning of each calculation increment, all information concerning the gas flow is known and assumed constant throughout that increment.

4.3.10 Ford BURNER Program — The Ford - developed BURNER program calculates those quantities associated with the external combustion system only, including fuel, EGR, air, and exhaust gas mass flows, temperatures and flow losses. The calculations are carried out for a steady-state operating point and assume constant heater tube inside wall temperatures on both the inner and outer heater tube passes.

Also included in the calculations are estimates of engine radiation and convection losses (in order to adjust fuel flow in accordance with cycle requirements), and pre-heater heat transfer characteristics. Fin tip temperatures are also available, and in many cases those temperatures are the controlling factor in final tube design.

1. Report No. NASA CR-159836	2. Government Accession No.	3. Recipient's Catalog No.
4. Title and Subtitle AUTOMOTIVE STIRLING ENGINE DEVELOPMENT PROGRAM		5. Report Date March 1980
		6. Performing Organization Code
7. Author(s) Ernest W. Kitzner		8. Performing Organization Report No.
		10. Work Unit No.
9. Performing Organization Name and Address Ford Motor Company Dearborn, Michigan 48121		11. Contract or Grant No. EC-77-C-02-4396
		13. Type of Report and Period Covered Contractor Report
12. Sponsoring Agency Name and Address U.S. Department of Energy Office of Transportation Programs Washington, D.C. 20545		14. Sponsoring Agency Code Report No. DOE/NASA/4396-4

15. Supplementary Notes

16. Abstract

This report details the Task I accomplishments of the jointly funded Ford /DOE Automotive Stirling Engine Development Program. This task was directed at achieving 20.6 MPG (gasoline) fuel economy for a 4500 lb inertia weight Stirling engine powered passenger car. The report discusses results of engine testing and design, power control, fuel economy projections, and component design and development.

17. Key Words (Suggested by Author(s)) Automotive Stirling engine; Fuel economy; Stirling engine design; Stirling engine component development	18. Distribution Statement Unclassified - unlimited STAR Category 85 DOE Category UC-96		
19. Security Classif. (of this report) Unclassified	20. Security Classif. (of this page) Unclassified	21. No. of Pages 405	22. Price* A18